NATIONAL CENTER FOR EARTHQUAKE
ENGINEERING RESEARCH
State University of New York at Buffalo

PROCEEDINGS
from the
SYMPOSIUM ON SEISMIC HAZARDS, GROUND MOTIONS, SOIL-LIQUEFACTION AND ENGINEERING PRACTICE IN EASTERN NORTH AMERICA

October 20-22, 1987

Edited by: K.H. Jacob

Technical Report NCEER-87-0025

December, 1987

This Symposium was conducted at the Sterling Forest Conference Center, Tuxedo, New York and was partially funded by the National Science Foundation under Grant No. ECE 86-07591.

NOTICE

This report was prepared by the National Center for Earthquake Engineering Research (NCEER). Neither NCEER, associates of NCEER, its sponsors, nor any person acting on their behalf:

a. makes any warranty, express or implied, with respect to the use of any information, apparatus, method, or process disclosed in this report or that such use may not infringe upon privately owned rights; or

b. assumes any liabilities of whatsoever kind with respect to the use of, or for damages resulting from the use of, any information, apparatus, method or process disclosed in this report.

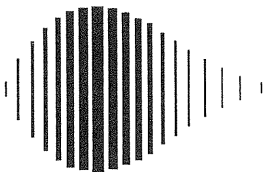

PROCEEDINGS
from the
SYMPOSIUM ON SEISMIC HAZARDS, GROUND MOTIONS, SOIL-LIQUEFACTION AND ENGINEERING PRACTICE IN EASTERN NORTH AMERICA

held at the
Sterling Forest Conference Center,
Tuxedo, New York
on
October 20-22, 1987

Technical Report NCEER-87-0025

Edited by: Klaus H. Jacob[1]
December, 1987

NCEER Contract Number 86-6011

NSF Master Contract Number ECE 86-07591

1 Senior Research Scientist, Lamont-Doherty Geological Observatory

NATIONAL CENTER FOR EARTHQUAKE ENGINEERING RESEARCH
State University of New York at Buffalo
Red Jacket Quadrangle, Buffalo, NY 14261

Preface

We have been fortunate that during this century truly damaging earthquakes were rare in eastern North America and nearly absent in the eastern United States. Historic and geologic evidence, together with modern monitoring of lesser seismic activity, tell us however, that severely damaging earthquakes are likely to revisit, in fact, may be inevitable. One could strike tomorrow.

How prepared is modern society to cope with the occurrence and consequences of future damaging earthquakes? Where do we stand, particularly in the eastern urbanized areas of the U.S. and Canada, to protect ourselves against catastrophic damage from earthquakes? To what extent are the existing or recommended building codes sufficient and adequate to mitigate against earthquake hazards? Are these codes properly adhered to? How much has been done to adopt suitable building codes? Are there special circumstances in the eastern and central U.S. whereby engineering solutions against hurricanes can help to mitigate against earthquakes? How do we strengthen the existing building stock? Do we understand the occurrence of earthquakes in time and space, and the nature, level, and attenuation of seismic ground motions, and the effects on soils and soil-structure interaction in the environments typical of eastern geologic conditions to realistically assess the future seismic hazards?

These are some of the nagging questions that this Symposium was convened to address. Every effort was made to stimulate cross-disciplinary communication between earthquake engineering, geotechnical, and earth-science experts during this event; in addition - we brought together academic researchers with practioners and representatives from the public and private sector. As a single event, this Symposium was successful as a starting point and cross pollinator. To bring these sowed seeds to fruition, we must now nurse the fledgling shoots which grow into complex tasks, with patience, systematic determination and persistence.

This Symposium is but one of several systematic efforts that NCEER is about to undertake to assure needed progress towards effective mitigation against earthquakes in the decades to come.

Klaus H. Jacob
Symposium Convenor
Palisades N.Y., December 1987

TABLE OF CONTENTS

Technical Papers

TOPIC 1: **Seismic Hazards Assessment vs. Engineering Practice**

TOPIC 2: **Tectonics and Seismicity of Eastern North America**

Appendices

Opening Address for the Symposium:

" SEISMIC HAZARDS, GROUND MOTIONS, SOIL LIQUEFACTION AND ENGINEERING PRACTICE IN EASTERN NORTH AMERICA"

Sterling Forest Conference Center, Tuxedo, N.Y., October 20-22, 1987.

Klaus H. Jacob
Lamont-Doherty Geological Observatory of Columbia University
Palisades N.Y. 10964

Welcome to Sterling Forest! This Symposium was organized by NCEER, the National Center for Earthquake Engineering Research, with several facts and goals in mind:

• (1) In its initial proposal NCEER made a strong committment to address eastern U.S. seismic hazards as one of its high-priority issues.

• (2) Past studies of eastern U.S. earthquake mitigation measures were largely aimed at nuclear powerplants. It seemed timely to review how some of the major results from these studies could be transferred to ordinary structures. In contrast to studies for nuclear facilities, to-date little effort in the eastern U.S. has gone into research and applications of earthquake mitigation measures for common structures and life lines such as bridges, dams, pipelines, transportation, energy distribution and communications systems; and especially for ordinary structures such as large public or private urban housing projects, residential homes, and commercial, government and industrial buildings and offices. NCEER wanted to provide a forum to discuss this new emphasis in research with experts from the earth sciences and earthquake engineering, and with representatives from the private and public sectors. This Symposium provides the vehicle to achieve this goal.

• (3) U.S. and Canadian approaches to earthquake hazards assessment and mitigation have been quite different, although the tectonic setting and economic/societal issues are remarkably similar across the border. This seemed a good opportunity to compare notes.

• (4) Eastern North America represents a relatively tectonically stable and geologically old, mid-plate region far away from the seismogenic belts along young, active plate boundaries such as those in California or Alaska. Seismic hazards in mid-plate regions are qualitatively and quantitaively distinct from those near plate boundaries. Recommended seismic building codes in the U.S. are strongly influenced by experience from highly seismic regions. Whether regions with moderate seismic hazards need specific code provisions appears unresolved and as the experts you are asked to address this question.

NCEER fully recognizes the past accomplishments in earthquake hazards reduction for the eastern U.S. through research efforts sponsored by the Nuclear Regulatory Commission (NRC), the Energy and Power Research Institute (EPRI), DOE and several National Laboratories. NCEER is equally aware of the progress made under the National Earthquake Hazards Reduction Program (NEHRP). A great deal of effort was put in by the U.S. Geological Survey, both through its internal program and

through its external program with leading earth science institutions, to understand the geologic-tectonic basis of the seismic hazards and to quantify it. The NSF has sponsored research within the academic community aimed primarily at the engineering aspect of this work.

There are, however, many serious gaps in data and knowledge. There are great uncertainties about the level, distribution and nature of earthquake hazards in the eastern U.S.; about the earthquake resistant properties (or lack thereof) of the existing, sometimes quite old building stock; and about the most economic engineering solutions to improve earthquake resistance of existing structures. The lack of some crucial data needed for hazards assessment in the East is well exemplified by the very fact that none of the previous efforts have lead to the gathering of significant amounts of useful strong-motion recordings for the eastern U.S. Farther north, our Canadian colleagues have not been much luckier, not withstanding the records obtained from the Nahanni earthquakes to be discussed in this meeting.

Seismic hazards in the eastern U.S.have been evaluated for some individual sites such as nuclear power plants and a few other critical structures. Seismic hazards maps exist, e.g. those produced by researchers from the USGS, which have been incorporated into national seismic building code recommendations such as ATC3-06, BSSC, and others. In contrast to California, this has not lead in the eastern and central U.S. to the adoption of locally and legally binding, State or Municipal Seismic Building Regulations. Boston, Massachusetts, is one of the few exceptions where a code has been adopted, although enforcing it apparently poses some difficulties. Large population areas such as New Jersey or New York State, and especially New York City, while seismically active have no formal seismic regulations for common structures, but may have some for hurricanes. This is in contrast to the seismic regulations imposed in the same states by the NRC for nuclear power plants. This contrast in public perception that nuclear facilities in the eastern U.S. need earthquake resistant designs, while structures in which we live or work do not, clearly calls for a long overdue reevaluation of the technical, economic, and public issues involved. Foremost, we must have a quantitative grip on the nature and level of present seismic risk to which modern society is exposed, in order to make meaningful compromises between reliable and economic engineering solutions.

NCEER decided to focus on mitigation of earthquake hazards to *existing, non-nuclear* structures, and in particular to lifelines, buildings, and other structures in urban population centers of the central and eastern U.S. To this end, NCEER and its investigators seek to quantitatively define and assess the earthquake hazards and to find systematic, modern engineering solutions that help to minimize future earthquake damage. NCEER also undertakes public education that advances the adoption of earthquake building codes, and fosters systematic introduction of new technologies and improved engineering practice. These are multifaceted goals; they need to be approached in distinct, systematic steps. One of these is to define the earthquake hazards in a form useful to engineers and decision makers. A common problem of the past has been that earth scientists and engineers did not communicate efficiently with each other. Hence, tasks that need scientific input from both disciplines were often poorly resolved. This communication gap needs to be overcome and this Symposium provides an opportunity to practice the necessary communication.

In this spirit, NCEER, decided to bring together a representative group of experts from earthquake engineering and the earth sciences. Many of you have been leading investigators in past earthquake hazards mitigation efforts for the eastern U.S. and

elsewhere. NCEER felt it was important that those not presently affiliated with NCEER meet with the handfull of new NCEER investigators that are now working on these pressing topics and will continue to do so for some years to come.

We have no illusions that NCEER as an organization, and NCEER investigators as individuals, will suddenly find magic solutions to the problems of eastern hazards mitigation that have been sought by others for some time. Compared to the past well-funded NRC and EPRI efforts, NCEER can pursue but a moderate set of tasks, and we must approach them in a well-planned systematic manner. NCEER can play an important catalytic role and can provide a new momentum at a crucial time when other efforts related to nuclear powerplant licensing are decreasing because of the lack of newly constructed plants. NCEER hopes that the existing momentum is redirected towards structures in urban concentrations in the East: It is there that earthquakes seem to pose a most poorly recognized risk and most eastern cities and their economies seem to be ill prepared for their effects.

This Symposium also serves to lay some ground work for the forthcoming, widely publicized conference on *"Earthquake Hazards and the Design of Constructed Facitlities in the Eastern U.S."* to be held February 24-26, 1988 in New York City. It will be jointly sponsored by NCEER, The New York Academy of Sciences, the Earthquake Engineering Research Institute and others. The little publicized Sterling Forest Symposium gives us the opportunity to develop a strategy for how to present complex and not fully resolved seismic hazards issues to the practicing engineering community. This community desperately needs executable design guidelines for earthquake-resistant construction of new structures and for rehabilitation of existing urban structures and facilities.

Let me close with a note on a subject that is of special concern to me. Some of you have been asked to come to this Symposium because for many years you have been making efforts, too many of them futile, to obtain high-quality on-scale seismic ground-motion recordings in the eastern parts of this continent. The few records from significant earthquakes that were obtained are badly needed to correctly estimate strong-motion characteristics for future earthquakes in eastern North America. NCEER, with your coopertion and with that of the USGS and others will make every effort to compile the most significant on-scale ground motion records for North America into a ground motion data base that will be made available to the public on optical disks. Some of you will soon receive a letter jointly drafted by Tom Hanks, myself and others that invites you to give your advice to this particular project. Please help to locate and contribute any precious ground motion records that may have been unavailable to the public until now. I hope you will cooperate in this long overdue effort to bring together a representative North American strong-ground-motion collection. Without it, strong-motion estimates for the eastern U.S. and eastern North America will remain largely speculative and unsubstantiated.

With this brief introduction I welcome you again to this Symposium. I anticipate it will be a success in that it will serve its many cross-disciplinary purposes. Good luck and may we have many challenging discussions!

TOPIC 1

Seismic Hazards Assessment vs. Engineering Practice

P. Basham: *Seismic Hazards Assessment and Seismic Codes for Eastern Canada*

D. M. Perkins and S. T. Algermissen: *Seismic Hazards Maps for the U.S.: Present Use and Prospects*

J. C. Stepp (Abstract only): *On Probabilistic Seismic Hazard Methodology for Critical Industrial Facilities in the Eastern United States*

J. P. Singh: *Current Trends in Seismic Zonation*

G. Nordenson: *Some Limitations of Current Seismic Codes for Eastern U.S. Earthquake Resistant Design*

M. Shinozuka: *Earthquake vs. Wind Risks to Buildings and Structures inthe Eastern U.S.*

C. Scawthorn: *Approximation of Earthquake Losses for a Major Earthquake near a Large Eastern U.S. Urban Center: Preliminary Results*

R. V. Whitman: *Thoughts re Seismic Building Code Requirements for ENAM*

SEISMIC HAZARDS ASSESSMENT AND SEISMIC CODES FOR EASTERN CANADA

P.W. Basham

Geophysics Division, Geological Survey of Canada,

1 Observatory Crescent, Ottawa K1A 0Y3

INTRODUCTION

New seismic zoning maps were completed in the early 1980s and incorporated into the 1985 edition of the National Building Code of Canada (NBCC; Associate Committee on the National Building Code, 1985). Despite difficulties - in defining earthquake source zones in many parts of the country, uncertainties about strong ground motion attenuation, and poor understanding of the near-source effects of large earthquakes - these zoning maps depict in a reasonable way the relative levels of seismic hazard across the country for purposes of earthquake-resistent design of common buildings. These zoning maps are intended to remain in force until 1995, unless there is a significant change in our understanding of seismic hazards in some region of the country, e.g., a recognized imminence of a large subduction earthquake affecting southwestern British Columbia.

Seismic codes for critical facilities are prepared by the Canadian Standards Association (CSA) and require more rigorous, site-specific assessments of seismic hazards. Standards are currently in effect for nuclear power plants (CSA, 1981a) and liquefied natural gas facilities (CSA, 1981b) and under development for offshore petroleum production structures (CSA, 1987).

For all of these seismic hazard codes and standards, the principal issue in eastern Canada is the interpretation of the potential for future large earthquakes in locations that have not experienced such earthquakes in historical time. Following a brief discussion of the 1985 zoning maps, I address this issue with respect to large earthquakes on the Paleozoic rift structures in the St. Lawrence and Ottawa valleys and on the Mesozoic rift structures along the passive eastern margin. The strong seismic ground motion produced by the 1985 Nahanni, Northwest Territories, earthquake is suggested as the best available example of what might be expected from a future moderate to large earthquake in eastern North America.

SEISMIC ZONING MAPS OF CANADA

The seismic zoning maps adopted for the 1985 edition of NBCC are shown in Figure 1. The development of these maps is described by Basham et al. (1982a, 1985) and the associated seismic design provisions required for NBCC by Heidebrecht et al.

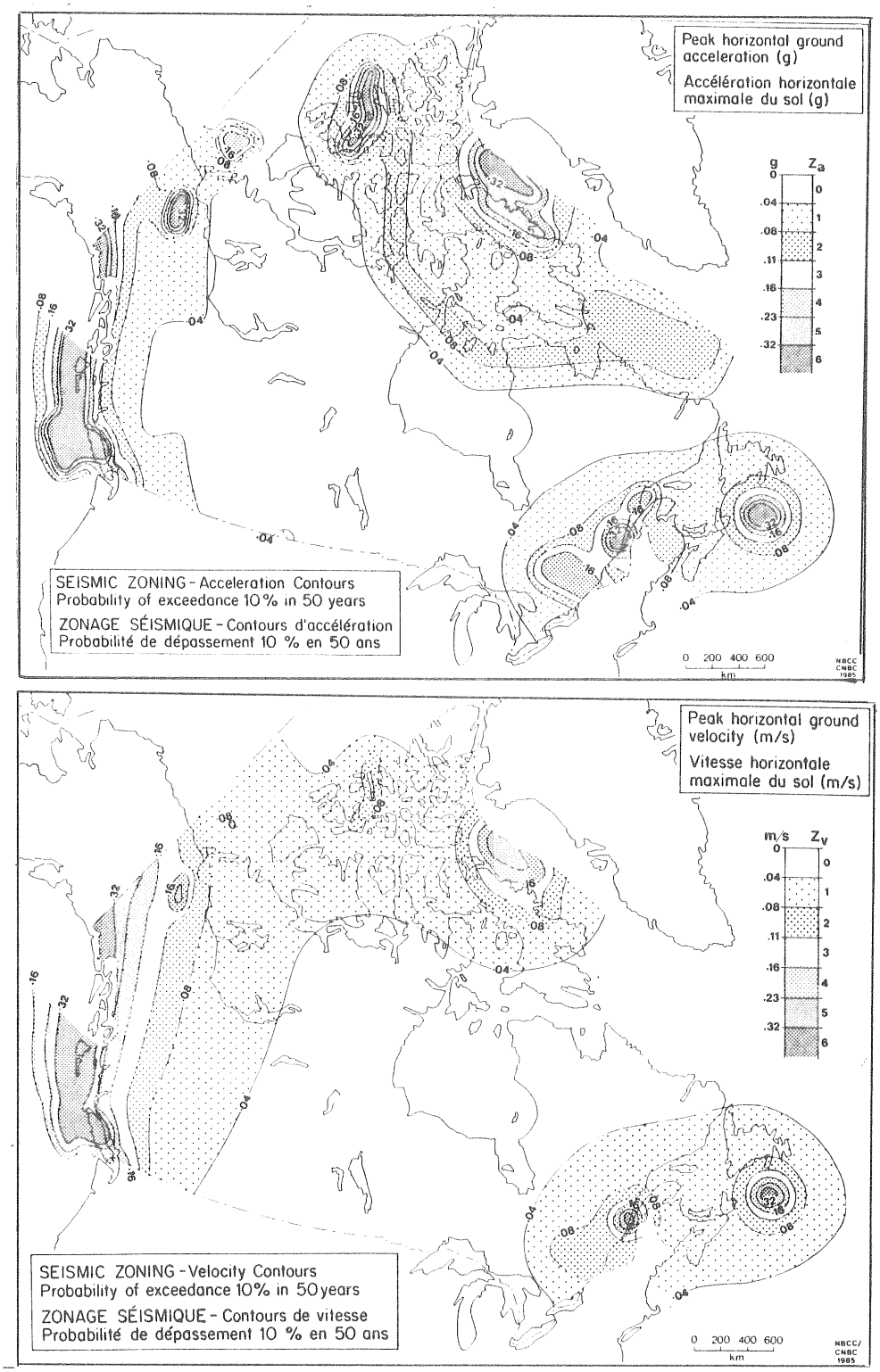

Figure 1. Seismic zoning maps of Canada adopted for the 1985 edition of the National Building Code. The peak horizontal acceleration (upper) depicts ground motion relevant to the design of small rigid structures; the peak horizontal velocity (lower) depicts ground motion relevant to the design of tall, flexible structures such as highrise buildings.

(1983). The zoning maps are based on the Cornell-McGuire method of probabilistic seismic ground motion estimation and used the earthquake source-zone model shown in Figure 2.

Although a number of large urban Canadian centers are in relatively high seismic hazard zones, no significant structures have been shaken at their seismic design levels or have experienced damage in recent decades. The NBCC design provisions for the higher hazard zones are based on engineering experience in places like California where similar types of buildings have been damaged in the past. For the higher hazard zones, these provisions provide what is considered to be an adequate degree of protection. They are also a calibration point for lower levels of seismic design. While the seismic ground motion probability level used for the maps can be considered somewhat arbitrary and is required only as a means of assessing relative hazard levels across the country, the probability adopted (10 per cent probability of exceedence in 50 years) is considered roughly appropriate to the design levels desired to prevent major collapse of buildings.

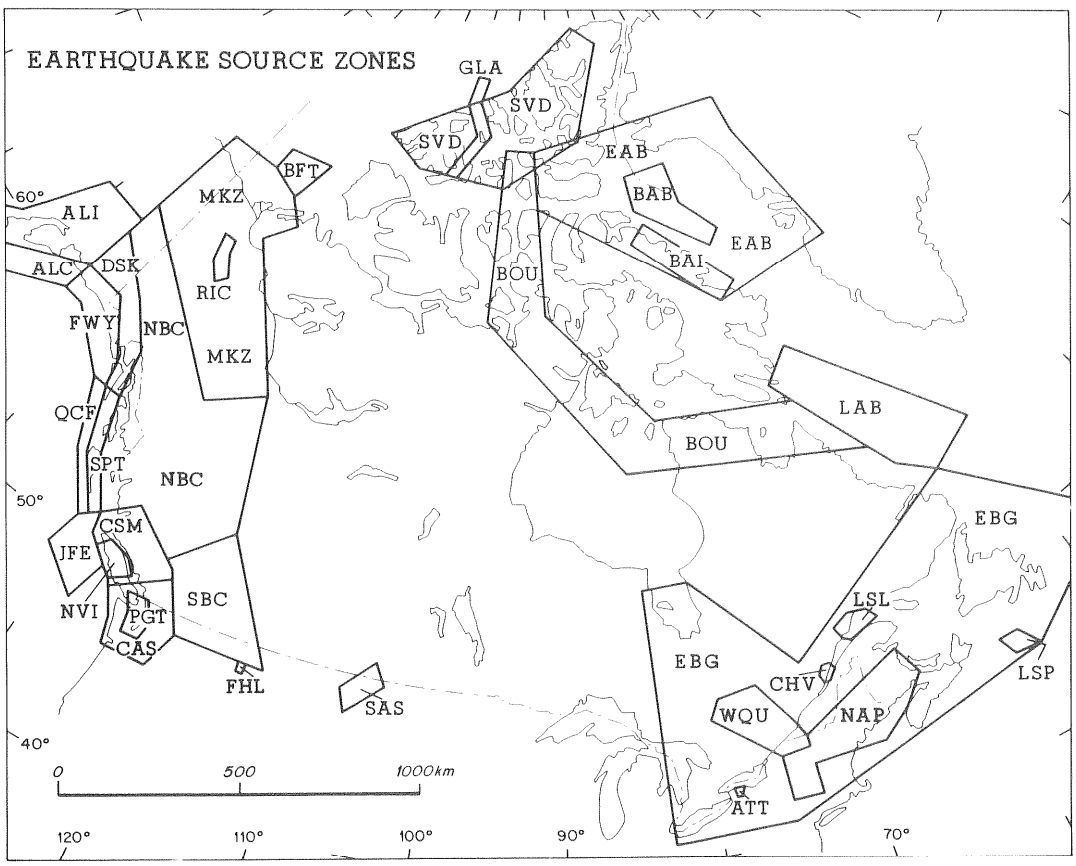

Figure 2. Thirty-two earthquake source zones used for probabilistic strong seismic ground motion estimates shown as seismic zoning maps in Figure 1. A detailed description of each source zone is given by Basham et al. (1982a).

In 1982, strong seismic ground motion estimates were made by Canadian and United States agencies on either side of the eastern Canada-U.S. border (Figure 3; Basham et al., 1982a; Algermissen et al., 1982). The U.S. ground motion estimates are adapted from the maps produced by Algermissen et al. (1982) and the Canadian estimates are those employed for the zoning maps shown in Figure 1, but contoured at the intervals used in the U.S. map.

Figure 3 shows some significant differences in seismic hazard estimation at the border, and a detailed investigation of the two hazard models used has revealed the principal reasons for these differences (see Basham et al., 1985). The Canadian estimates have been employed for the official national zoning maps, as described above, but these U.S. estimates have not. However, the differences noted in Figure 3 would not necessarily translate directly into equivalent differences in the design of buildings. To establish differences in design, it would be necessary to account for any differences in the seismic design provisions of the various codes that make reference to the ground motion estimates.

If the two agencies, USGS and GSC, repeated the hazard estimates today, they would no doubt differ somewhat from those shown, because of developments in our understanding of seismic hazards. In particular, although it is still far from adequate, a consensus appears to be developing on the most appropriate form of strong seismic ground motion attenuation in eastern North America (e.g. Boore and Atkinson, 1987).

However, there have been few advances in the past decade on the most crucial aspect of understanding the earthquake source zones, in particular the potential locations of future large earthquakes. It is the effect of these uncertainties that are discussed in the remaining sections of this paper.

CHARLEVOIX, THE MOST ACTIVE EARTHQUAKE SOURCE IN EASTERN NORTH AMERICA

The first earthquake listed in the historical earthquake catalogues of eastern North America (1534) probably occurred in the Charlevoix seismic zone in the St. Lawrence valley (CHV in Figure 2). Six large earthquakes have subsequently occurred in this zone, in 1638 (location somewhat uncertain), 1663, 1791, 1860, 1870 and 1925, all with estimated magnitudes of 6 or greater. The repetitive nature of these large earthquakes has made the Charlevoix zone the principal focus of earthquake prediction research in eastern Canada (Buchbinder et al., 1988). It is also the focus of the Geological Survey of Canada's eastern strong motion seismograph network (Weichert and Munro, 1987). A six-station seismic array has been in operation around the zone since 1977, and has produced the epicentral pattern of micro-earthquakes shown in Figure 4.

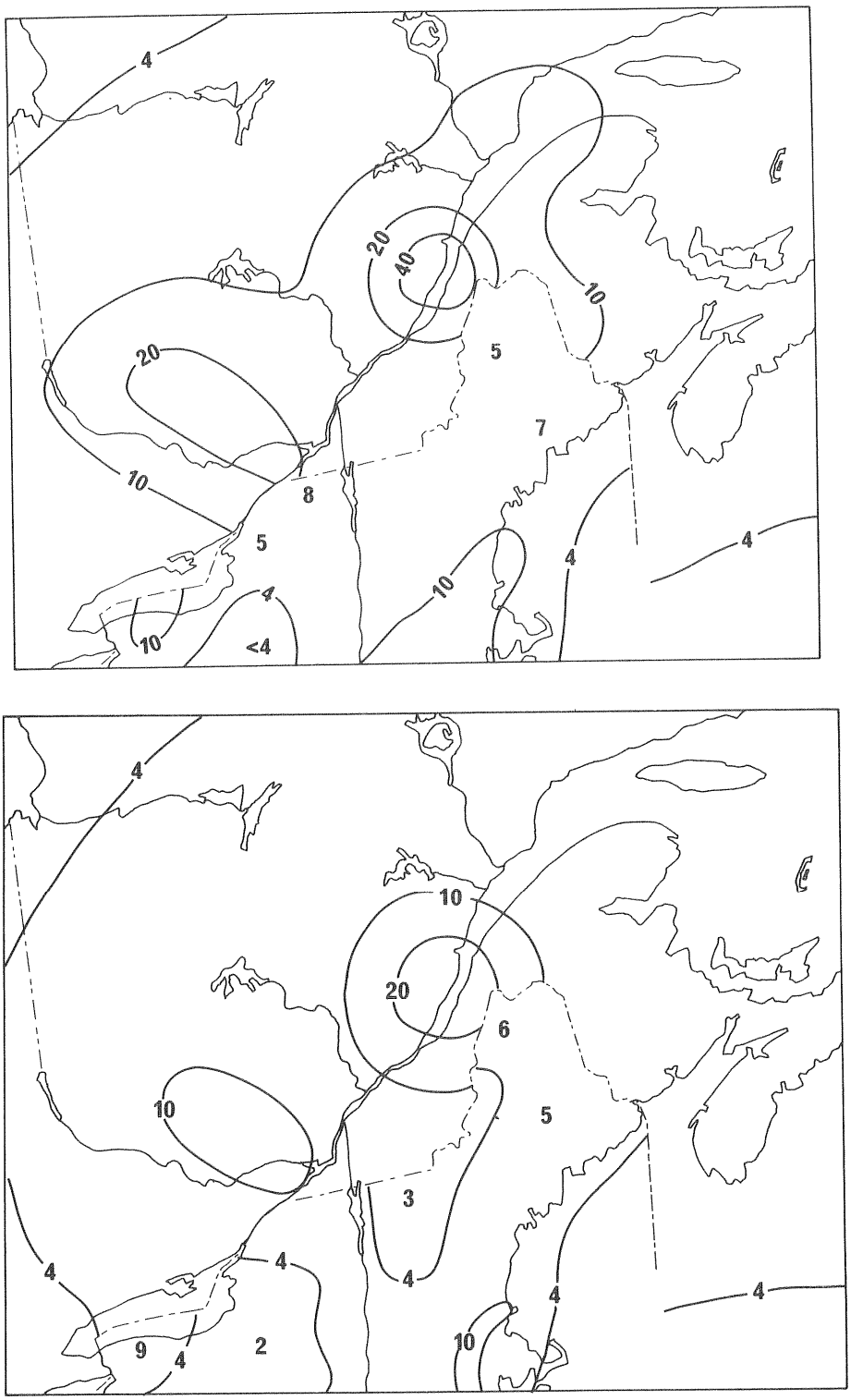

Figure 3. A comparison of peak horizontal acceleration (% g; upper) and peak horizontal velocity (cm/sec; lower) estimates with a probability of exceedence of 10 percent in 50 years in the region of the eastern Canada - U.S. border. After Basham et al. (1985).

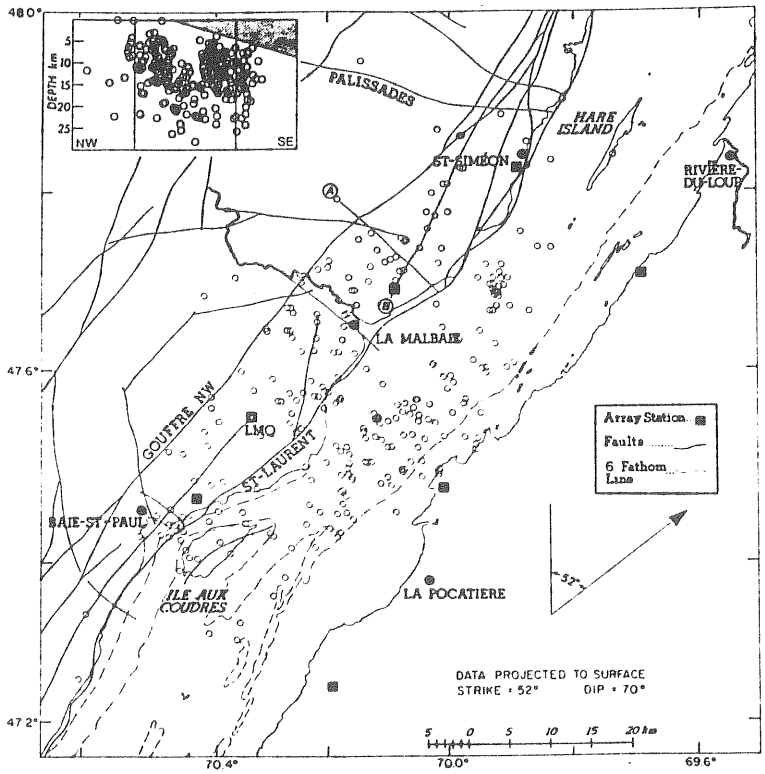

Figure 4. Charlevoix micro-earthquakes with hypocentres projected to the surface along the causative rift faults with strike and dip indicated in the legend. The inset is a NW-SE cross-section of the hypocentres to show their depth distribution. After Anglin (1984).

Stereo-pair plots produced by Anglin (1984) demonstrate that most of the micro-earthquakes are occurring on northeast-trending planes that dip to the southeast. A projection of the hypocenters to the surface along the postulated faults (as shown in Figure 4) suggests that the activity is confined between Paleozoic rift faults mapped on the north shore and a bathymetric feature near the river's south shore, which is assumed to be a river-bottom expression of a parallel rift fault. At Charlevoix, the rift structures have been complicated by a late Devonian meteorite impact that has caused the ring faults shown in Figure 4.

As shown in Figure 5, the Paleozoic rift faults extend along the entire length of the St. Lawrence River and northwestward up the Ottawa river valley. The high rates of the larger Charlevoix earthquakes would imply geological deformation on the rift faults that would amount to kilometers over a million years. Clearly, kilometers of uplift (if due to thrusting), or even kilometers of strike-slip motion, would have been recognized at Charlevoix, had they occurred. That they have not, we infer must be due to intermittent activity at Charlevoix and along the remaining rift system, perhaps with a time constant of thousands to hundreds of thousands of years.

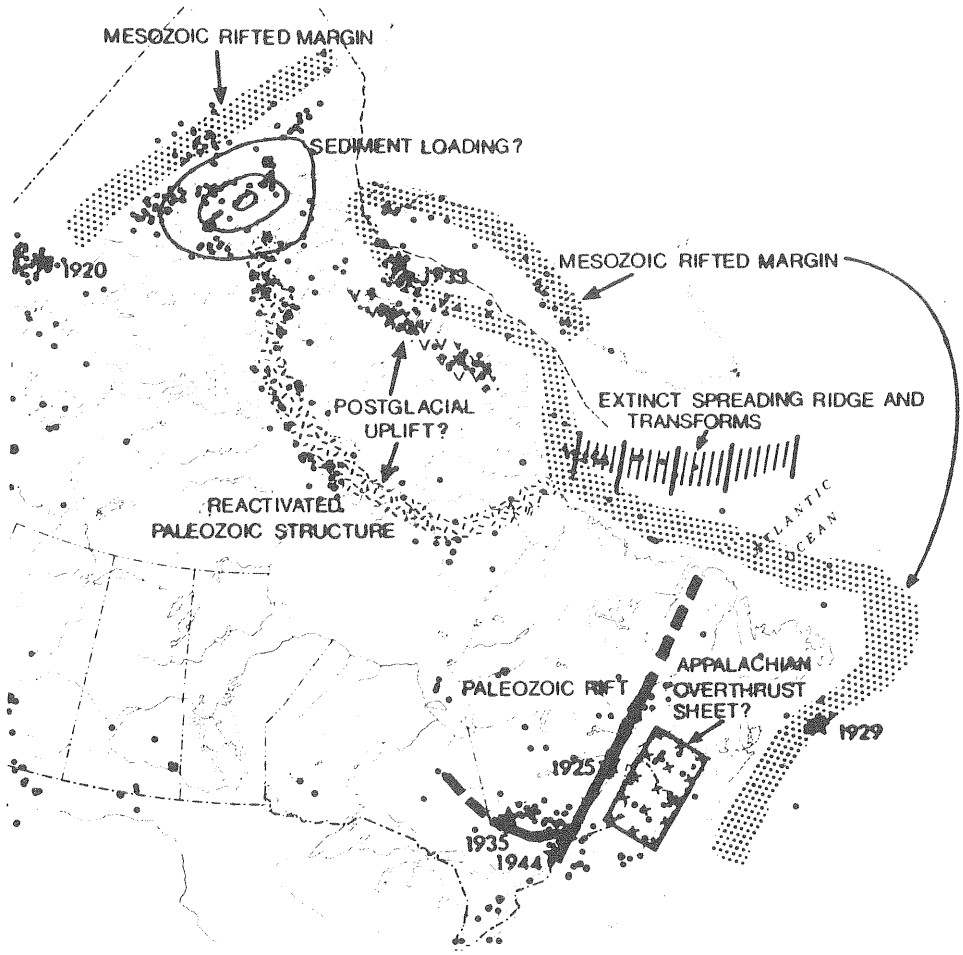

Figure 5. Earthquakes of eastern Canada M greater than 3.5, 1975-1985, and significant larger earthquakes during this century superimposed with a schematic representation of the extent of Paleozoic and Mesozoic rift faults, reactivated Paleozoic and Mesozoic structures and the Appalachian over-thrust sheet. After Adams and Basham (1988).

Are we near the end of an active Charlevoix episode? Do the smaller earthquakes further northeast in the lower St. Lawrence (Figure 5) represent the declining phase of a previous episode of large rift earthquakes, or the beginning of a new one? The seismic zoning maps (Figure 1) are intended to accommodate the near-source effects of a large earthquake in the Charlevoix zone because the repetitive nature of these earthquakes must be assumed to continue over the short term (e.g., 50 years), but they will not provide adequate design against a similar large earthquake elsewhere along the St. Lawrence and Ottawa valley rift system.

SINGLE LARGE EARTHQUAKES ON THE EASTERN CANADIAN CONTINENTAL MARGIN

A similar dilemma is posed by the individual large historical earthquakes along the eastern Canadian continental margin, beneath the Laurentian Slope off the Grand Banks south of Newfoundland in 1929 (magnitude 7.2) and beneath Baffin Bay in 1933 (magnitude 7.3) (Figure 5). The cause of the earthquakes along the margin and thus a rationale for their distribution has not been clearly established. Studies of stress from oil-well breakout data confirm that the margin is subject to the same northeast-directed compression as the rest of eastern North America. Many of the earthquakes along the margin probably occur along the ocean-continent transition on the deep-crustal rift faults formed during the opening of the Atlantic Ocean. Under the current compressive regime these faults would be reactivated as thrust or strike-slip faults. Clearly, however, the strain rates are very low, with only two magnitude 7 earthquakes along 5000 km of margin in historical time.

Marine geophysical and sediment sampling experiments on the 1929 earthquake submarine slump and turbidites (Figure 6) suggest that 1929-sized earthquakes are very infrequent at this location; they may have return periods of the order of 10,000 years. Other

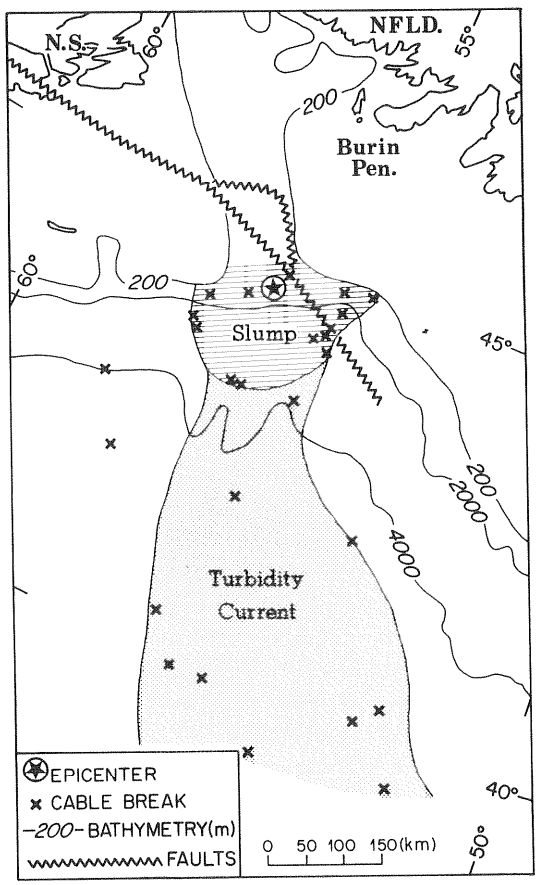

Figure 6. Submarine slump, turbidity current and cable breaks caused by the 1929, magnitude 7.2, Grand Banks earthquake.

prehistoric submarine slumps suggest that similar earthquakes may have occurred elsewhere along the margin in the past (e.g., Piper et al., 1985) but there has not yet been a systematic search for such slumps along the entire margin. The seismic zoning maps in Figure 1 are based on a model (Figure 2) that assumes that the Grand Banks and Baffin Bay earthquakes have a relatively high probability of recurring in the same locations during the next 50 years, but not elsewhere along the margin. The seismic hazards estimates that result from an alternative "state-of-ignorance" model are quite revealing.

The upper left panel of Figure 7 shows the eastern margin portion of the NBCC model in Figure 2; i.e., the large Grand Banks and Baffin Bay earthquakes are confined to the LSP and BAB source zones. The lower left panel of Figure 7 shows an alternative model that assumes that margin-rift earthquakes are equally likely along the entire margin. The magnitude recurrence relation for the source zone ESX is generated by accumulating all of the earthquakes that might be associated with the margin rift structures (Basham and Adams, 1983; Basham et al., 1983). The

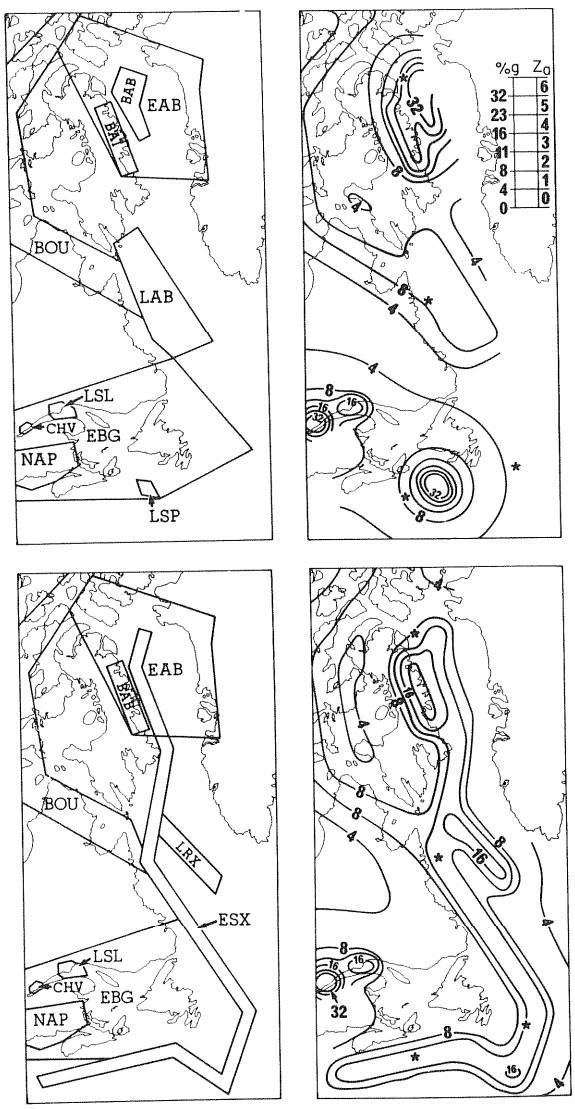

Figure 7. Eastern margin portion of the national earthquake source zone model (upper left) and an alternate model (lower left) that isolates the Labrador Ridge seismicity (LRX) and distributes the remaining seismicity evenly along the margin (ESX). The panels on the right show peak horizontal acceleration with a probability of exceedence of 10 percent in 50 years.

result, based on known historical seismicity, implies that ESX will experience about one magnitude 7 earthquake per thousand years per thousand kilometers of margin.

The resulting peak horizontal accelerations with a probability of exceedence of 10 percent in 50 years for the two margin models are shown in the right portion of Figure 7. The upper panel, the eastern portion of the acceleration zoning map shown in Figure 1, indicates small regions of zone 6 (acceleration greater than 0.32 g) in the areas of the historical magnitude 7 earthquakes. The lower panel shows the hazard distributed along the margin and, except for Baffin Bay which is influenced by earthquakes on Baffin Island, at no location along the continental shelf does the acceleration exceed 0.16 g.

These two models make very little difference to the hazard estimates on land, where the NBCC would apply, but they could have profound implications to, for example, petroleum production developments offshore. For the southeastern margin, the left panel suggests that the only hazard is in the region of the 1929 earthquake, which would likely preclude petroleum developments in that area. The right panel suggests that there is only moderate earthquake hazard at any location along the margin, at least when compared to the hazards of iceberg impact, which is a serious design consideration for petroleum production structures in this region (see CSA, 1987).

There is clearly a lack of confidence in the source zone models and hazard estimates along the eastern margin. The next magnitude 7 earthquake on the eastern margin is expected to occur in a region where moderate-probability hazard estimates will not accommodate its effects.

EXPECTED GROUND MOTION IN A FUTURE EASTERN EARTHQUAKE

In eastern Canada, no strong ground motion has yet been recorded in the near-source region of an earthquake larger than magnitude 5. Therefore it is necessary to rely on theoretical and empirical estimates of large-earthquake ground motions, or adopt ground motions from earthquakes elsewhere that most nearly match the assumed source properties of large eastern earthquakes.

The magnitude 6.8, 23 December 1985, earthquake in the Nahanni region of the northeastern Cordillera must be seriously considered as an appropriate "design earthquake" for the active seismic zones in the east (Wetmiller et al., 1987a, 1987b). The rupture was a shallow to mid-crustal thrust due to the same high horizontal compressive stresses that are predominant throughout eastern North America. The rupture within the high-velocity Paleozoic rocks and underlying Precambrian basement should have radiated seismic energy in the near-source region in a manner that does not differ significantly from that of the Canadian Shield or Appalachian terrains in the east.

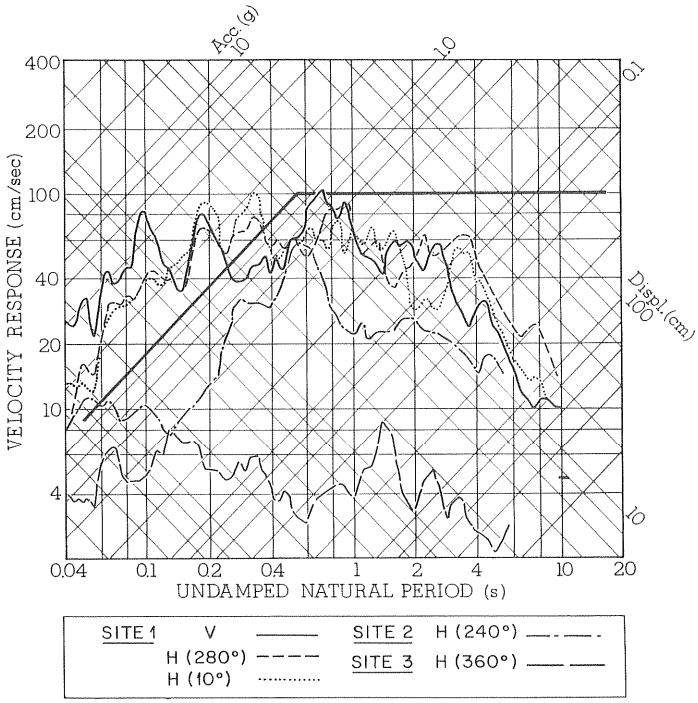

Figure 8. Five per cent - damped response spectra from the 23 December 1985 Nahanni strong motion records. Solid line is the nominal five per cent - damped design spectrum for a site in zone 6 of the 1985 NBCC seismic zoning maps.

The implications of this earthquake for eastern Canada have been discussed by Wetmiller et al. (1987b). They are summarized here with reference to Figure 8, which shows the five percent damped response spectra for three components of the site 1 strong ground motion and one horizontal component from each of sites 2 and 3.

The earthquake occurred in a source zone (MKZ in Figure 2; the epicentre is near the "Z" in MKZ) that had experienced no known historical earthquakes greater than magnitude 5. For purposes of the hazard model used for the zoning maps the MKZ source zone was assigned an upper bound magnitude of 6. The result was a seismic zonation of acceleration and velocity zone 1 for the Nahanni region (Figure 1). The fact that this earthquake significantly exceeded the assumed upper bound magnitude in the hazard model has significant implications for revised seismic zonation of the northeast Canadian Cordillera. These implications are beyond the scope of this paper, but we should take the Nahanni earthquake as a lesson on the potential for large earthquakes in other active zones that have experienced only moderate levels of historical seismicity.

In Figure 8 it can be seen that the three components of strong motion at site 1 exceed the NBCC design spectrum for zone 6 at structural response periods smaller than about 0.3 seconds. The response spectra for the site 2 and 3 records fall significantly below this design spectrum. Although a complete understanding of the site 1 records is not yet available (see D.H. Weichert in these Proceedings), it is clear that the extreme ground motions occurred over a small epicentral region.

The Nahanni strong motion records can be taken as representative of the near-source effects of a future large

Charlevoix earthquake; i.e., this is the kind of ground motion to be expected in the Charlevoix zone 6 region (Figure 1). An upper-bound magnitude of 7 was employed for the hazard model of the West Quebec zone (WQU in Figure 2), but, because of the dispersed nature of the seismicity, the resulting zonation was acceleration zone 4 and velocity zone 2. Hence, a Western Quebec earthquake near the upper-bound magnitude will exceed design levels if it occurs near a structure designed to NBCC specifications, as will a rogue earthquake elsewhere along the Paleozoic rift system discussed above.

These possibilities have always been explicitly accepted by seismic hazard specialists. Moderate-probability hazard estimates do not accommodate low-probability events such as the upper-bound earthquake in a diffuse seismic zone which occurrs directly under a particular site. More conservative codes and standards for critical facilities could accommodate the near-source effects of such earthquakes if society agreed that this degree of conservatism was necessary and was willing to pay the price of appropriate design.

CONCLUSIONS

Adequate earthquake source-zone models, and therefore hazard estimates, cannot be devised for earthquake source zones we do not understand. To overcome this difficulty, recent seismic hazards research projects by the U.S. Nuclear Regulatory Commission and the Electric Power Research Institute have employed "expert opinion" which results in multiple earthquake source-zone models, each assigned a probability that it is the "correct" interpretation of the earthquakes. In the treatment of a single large historical earthquake by this technique, shown hypothetically in Figure 9, the seismologists feel statisfied because they have included every possible explanation for the large earthquake. But, because each of the individual models includes the large earthquake, a computed hazard map will usually produce a peak in hazard at the known location of the historical earthquake, and significantly lower hazard elsewhere. This is not much of an improvement on an assumption that the next large earthquake will occur in the same location as the large historical earthquake, the model that was distrusted in the first instance and led to the need for expert opinion.

The real hazard, and therefore the real risk are often poorly represented by the hazard estimates and zoning maps we derive. With our current, primitive, level of knowledge in the east, earthquake hazard specialists would not be overly surprised if a large (magnitude 6.5 - 7) earthquake occurred at, or very near, say, Montreal or Boston. It is unlikely that current design codes accommodate such an earthquake. Have we made civil authorities in these cites adequately aware of this fact? Should we? Would they be unduly alarmed? Hopefully, answers to these types of questions can come from this symposium.

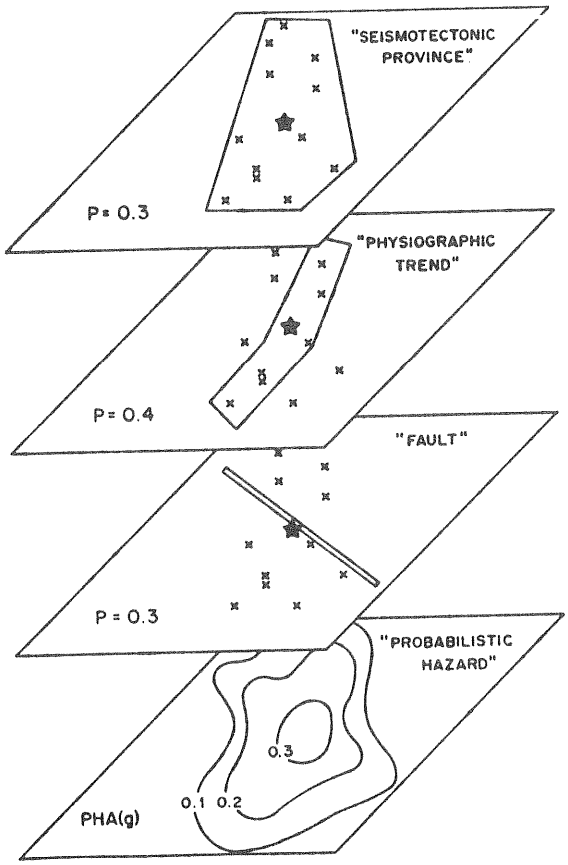

Figure 9. Hypothetical example of three source models for a single large historical earthquake in a region of moderate seismicity. P is the probability that the indicated feature is a correct interpretation of the large earthquake. The lower panel shows the computed hazard with a peak at the location of the large historical earthquake.

ACKNOWLEDGEMENT

I appreciate discussions with John Adams and Michael Berry on the issues dealt with in this paper.

REFERENCES

Adams, J., and P. Basham. The seismicity and seismotectonics of eastern Canada. In Geological Society of America "Decade of North American Geology", Volume GSMV-1, Neotectonics of North America (D.B. Slemmons, E.R. Engdahl, D. Blackwell, D. Schwartz and M. Zoback, Eds.), submitted, 1988.

Algermissen, S.T., D.M. Perkins, P.C. Thenhaus, S.L. Hanson, and B.L. Bender. Probabilistic estimates of maximum acceleration and velocity in rock in the contiguous United States. U.S. Geol. Surv. Open-File Rept. 82-1033, 99 pp., 1982.

Anglin, F.M. Seismicity and faulting in the Charlevoix zone of the St. Lawrence Valley. Bull. Seismo. Soc. Am., 74, 595-603, 1984.

Associate Committee on the National Building Code. National Building Code of Canada 1985, NRCC No. 23174; Supplement to the National Building Code of Canada 1985, NRCC No. 23178. National Research Council of Canada, Ottawa, 1985.

Basham, P.W., and J. Adams. Earthquakes on the continental margin of eastern Canada: need future large events be confined to the locations of large historical events? U.S. Geol. Surv. Open-File Rept. 83-843, 456-467, 1983.

Basham, P.W., J. Adams, and F.M. Anglin. Earthquake source models for estimating seismic risk on the eastern Canadian continental margin. Proc. Fourth Can. Conf. Earthquake Eng., Vancouver, 495-508, 1983.

Basham, P.W., D.H. Weichert, F.M. Anglin, and M.J. Berry. New probabilistic strong seismic ground motion maps of Canada: a compilation of earthquake source zones, methods and results. Earth Physics Branch Open-File Rept. 82-33, 205 pp., 1982a.

Basham, P.W., P. Morel-à-l'Huissier and F.M. Anglin. Earthquake risk at Gros Cacouna, Quebec, and Melford Point, Nova Scotia. Earth Physics Branch Open-File Rept. 82-2, 51 p., 1982b.

Basham, P.W., D.H. Weichert, F.M. Anglin, and M.J. Berry. New probabilistic strong seismic ground motion maps of Canada. Bull. Seismo. Soc. Am. 75, 563-595, 1985.

Boore, D.M., and G.M. Atkinson. Stochastic prediction of ground motion and spectral response parameters at hard-rock sites in eastern North America. Bull. Seismo. Soc. Am. 77, 440-467, 1987.

Buchbinder, G.G.R., A. Lambert, R.D. Kurtz, D.R. Bower, F.M. Anglin, and J. Peters. Twelve years of geophysical research in the Charlevoix seismic zone. Bull. Seismo. Soc. Am., submitted, 1988.

Canadian Standards Association. Ground motion determination for seismic qualification of CANDU nuclear power plants. CSA Standard CAN3-N289.2-M81, Canadian Standards Association, Rexdale, Ontario, 20 pp. 1981a.

Canadian Standards Association. Liquefied natural gas (LNG) - production, storage and handling. CSA Standard Z276-M1981, Canadian Standards Association, Rexdale, Ontario, 1981b.

Canadian Standards Association. General requirements, design criteria, environment and loads; Code for the Design, Construction and Installation of Fixed Offshore Production Structures. CSA Standard S471, Eighth Draft, Canadian Standards Association, Rexdale, Ontario, 1987.

Heidebrecht, A.C., P.W. Basham, J.H. Rainer, and M.J. Berry. Engineering applications of new probabilistic seismic ground-motion maps of Canada. Can. J. Civil Eng. 10, 670-680, 1983.

Piper, D.J.W., J.A. Farre, and A. Shor. Late Quaternary slumps and debris flows on the Scotian Shelf. Bull. Geol. Soc. Am. 96, 1508-1517, 1985.

Weichert, D.H., and P.S. Munro. Canadian strong motion seismograph networks. Proc. Fifth Can. Conf. Earthquake Eng., Ottawa, 647-654, 1987.

Wetmiller, R.J., R.B. Horner, H.S. Hasegawa, R.G. North, M. Lamontagne, D.H. Weichert, and S.G. Evans. An analysis of the 1985 Nahanni earthquakes. Bull. Seismo. Soc. Am., in press, 1987a.

Wetmiller, R.J., P.W. Basham, D.H. Weichert, and S.G. Evans. The 1985 Nahanni earthquakes: problems for seismic hazard estimates in the northeast Canadian Cordillera. Proc. Fifth Can. Conf. Earthquake Eng., Ottawa, 695-703, 1987b.

SEISMIC HAZARDS MAPS FOR THE U.S.: PRESENT USE AND PROSPECTS

by

D. M. Perkins and S. T. Algermissen
U. S. Geological Survey, Golden, CO 80014

ABSTRACT

The U. S. G. S. staff now in Golden has produced three generations of national seismic hazards maps since the mid 1960's. These maps, or adaptations of them, have been used in national building codes from 1969 to the present. Although the details of these representations of hazard in the eastern U. S. have shown continual evolution in size and orientation over this time, the overall impression is that the maps have remained quite similar.

This similarity in almost twenty years worth of national hazard maps is probably due to a subjective anchoring which attempts to balance the preservation of patterns of historical seismicity with conservative estimates of zones portraying the causal tectonics. Greater objectivity in such maps can be obtained by uncoupling the two concepts. We demonstrate results obtained by allowing radical interpretations in tectonics without regard to any constraint by historical seismicity. Most attempts to combine these estimates into a single map will result in a hazard map with too little geographic contrast in hazard. Greater contrast is obtained when one chooses to emphasize one tectonic hypothesis over the others or to leave the strict probabilistic format and use extreme estimates from all the maps.

We also demonstrate map results obtainable by various treatments of the historical seismicity without restraint imposed by zones representing any hypothetical tectonics. Unsatisfactory results are obtained unless location smoothing and magnitude smoothing are performed on the data. Useful maps appear with Gaussian geographic smoothing using standard deviations of 40 to 80 kms and magnitude smoothings which allow each epicenter to represent the potential for earthquakes of the full range of magnitudes possible. Subjectivity returns in choosing the best geographical smoothing parameter.

INTRODUCTION

The earliest national earthquake hazard maps were primarily a geometric partitioning of the United States according to the maximum intensities experienced historically. Progress since then has featured an

increasing reliance on tectonic principles to generalize from the seismic history to possible future earthquake locations, a focus on actual ground motion parameters, and the use of probability to incorporate seismic rate information into the regional comparison of hazard.

Since the last maximum-intensity based map by Algermissen [1969], two generations of national probabilistic ground motion maps have been produced and incorporated into national building standards. The first, published in 1976, was based primarily on the historical seismicity, generalized locally by source zones or source faults, and showed peak accelerations on rock, having a 10 percent chance of exceedance in 50 years [Algermissen and Perkins, 1976]. This map formed the basis for the seismic ground motion map used by the Applied Technology Council in their "Tentative Provisions for the Development of Seismic Regulations for Buildings" [Applied Technology Council, 1978).

The second-generation probabilistic map [Algermissen and others, 1982] provided both peak acceleration and peak velocity in order to provide estimates of ground-motion hazard for short- and long-period structures, respectively. These parameters were mapped at three different probability levels (10 percent chance of exceedance in 10, 50, and 250 years) to show relative levels of hazard which might be appropriate for building contents and equipment, ordinary buildings, and facilities providing critical services, respectively. Versions of the 50- and 250-year maps will be used in the forthcoming revision of the National Earthquake Hazards Reduction Program (NEHRP) "Recommended Provisions for the Development of Seismic Regulations for New Buildings," issued by the Federal Emergency Management Agency (FEMA) through the work of the Building Seismic Safety Council (BSSC) [Building Seismic Safety Council, 1985].

Work on a new, third-generation of national hazard maps has begun. New features include an algorithm permitting the representation of probabilistic source-zone boundaries, use of time-dependent occurrence models for characteristic earthquakes, inclusion of site response in the estimated ground motions, and regional, Q-based attenuations. The ultimate form of these maps has yet to be determined. In this paper we present the outcome of preliminary work exploring the variety of possible maps obtained by using new approaches to earthquake hazard estimation.

PAST EXPRESSION OF EASTERN HAZARD

The sequence of changes in the appearance of hazard on the east coast on these past maps is shown in figure 1. There are a few major differences. The size of the hazard zone shown around the Charleston, South Carolina, area varies, and the trend in hazard in New England changes from northwest-southeast to southwest-northeast. For the most

Figure 1. Eastern seaboard portion of seismic hazard maps. Left: Seismic risk zones [Algermissen, 1969]. Center: Probabilistic acceleration [Algermissen and Perkins, 1976]. Right: Probabilistic accelerations [Algermissen and others, 1982]. The latter two represent ground motions having a 90-percent probability of not being exceeded in 50 years.

part, however, the differences in the maps are not profound, suggesting there is a thematic linking in the manner in which such maps have been produced. We believe this linkage is the loose connection that has been maintained between expressing both the historical seismicity and the hypothetical tectonics that finds its expression in the eastern-U.S. seismicity.

In these maps its appears that the interpretation of the tectonics has not been allowed to stray far from one which merely re-expresses the main features of the historical seismicity, or, conversely, the generalization of the historical seismicity has not been allowed to be influenced by rather radical interpretations of possible driving tectonics. The maps have changed in response to only minor shifts in emphasis between tectonics and seismicity, while a rather strong linkage between the two is maintained. This linkage is a really a kind of subjective constraint, and accordingly the maps have sometimes been criticized as too subjective or opinionated.

One would suppose that deliberately breaking this linkage would provide more objectivity. In this paper we will present the results of recent studies in which this linkage has been deliberately broken. In the first case, tectonic interpretation has been allowed to govern the analysis completely, without constraint from the geographic form of the historical seismicity. In second case, the historical seismicity has been the basis of the interpretation, without constraint from possible tectonic interpretations. These approaches are rather startling, perhaps even offensive, but they can be fruitful, as we shall see.

MAPS DRIVEN BY TECTONICS ONLY

In the first study [Thenhaus and others 1987], each of several overall tectonic interpretations were imposed over the whole area under study and a hazard map was produced. Source zones were drawn in accordance with a particular overall tectonic interpretation. A Gutenberg-Richter fit to the overall seismicity of the study area produced an overall seismic rate, which was allocated among the individual constituent regional source zones according to a maximum likelihood fit to the historic seismicity experienced in the zones. The hazard maps from the various tectonic interpretations were compared with one another and with a map produced by applying the same procedure to the source zones of Algermissen and others (1982). Figure 2 shows several of the resulting maps along with a map using the source zones of Algermissen and others [1982], but with a seismicity treatment identical to that used for the tectonic models. The maps differ considerably, revealing that a large amount of variability has been suppressed by the method which links seismicity and hypothetical tectonics.

But how should one use this variety of hazard maps? The subjec-

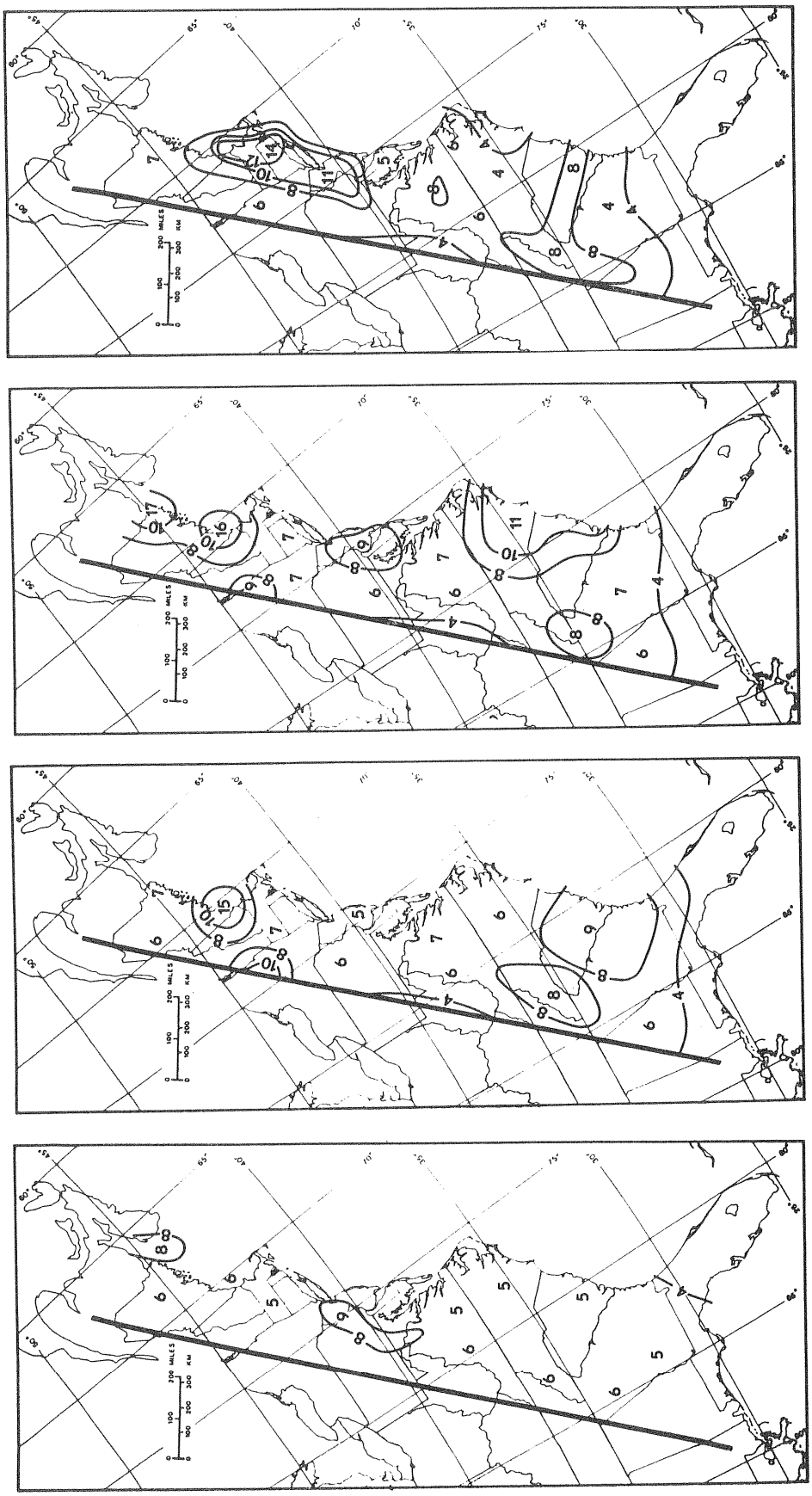

Figure 2. Probabilistic accelerations [Thenhaus and others, 1987] using seismic source zones drawn according to three different tectonic themes and (far right) using source zones from Algermissen and others [1982],

tivity we have been trying to avoid returns when it is necessary to decide which map to select or how to combine the results of several tectonic models. Suppose, for instance, one decides to weight each of the estimates equally. The result would be a map with values ranging from .06 g to .10 g. This is a relatively narrow range of values. There is too little contrast in hazard among the various sites, and perhaps the maximum hazard depicted is too low, although the process expresses the wide range of tectonic alternatives.

Suppose, instead, one chooses to depict the maximum hazard shown from among the various models as in the left-hand illustration in figure 3. Then the overall hazard values will be too high, implying an underlying seismic rate much higher than the historical rate, though by differing ratios, depending on the site.

As yet another alternative, one could combine the estimates, reflecting preferences among the models by combining the various hazard estimates using unequal weights. This is perhaps the most satisfactory option, but notice that subjectivity has come back into the picture. However, by putting subjectivity in at the *end* of the process, rather than at the beginning, one remains aware of the alternatives and achieves a result substantially different than by attempting a "best-estimate" single model at the beginning of the process.

MAPS DRIVEN BY SEISMICITY ONLY

What happens if we allow the process to be driven entirely by seismicity data? If one uses the historical earthquake data as seismicity input to the hazard mapping process, the result is a lumpy map, quite dependent on the historical magnitudes and locations (upper-left of figure 4). We have used an experimental program to explore how generalizing the historical data in location, magnitude, or both, affects the resulting hazard map. To generalize the location, we put a probability distribution on the historical epicenter, allowing the earthquake some likelihood of occurring in the vicinity of its original location. The resulting map becomes considerably smoother, but is still strongly dominated by the location of the historical large-magnitude earthquakes (compare the upper left and lower left of figure 4).

To generalize the magnitude, we replace the original magnitude with a Gutenberg-Richter distribution (exponential) from the minimum magnitude of interest to the maximum magnitude assumed. The resulting map removes the influence of the large-magnitude historical events, often revealing apparent structure not visible on the original map (upper right, figure 4).

As might be expected, if we generalize both location and magnitude,

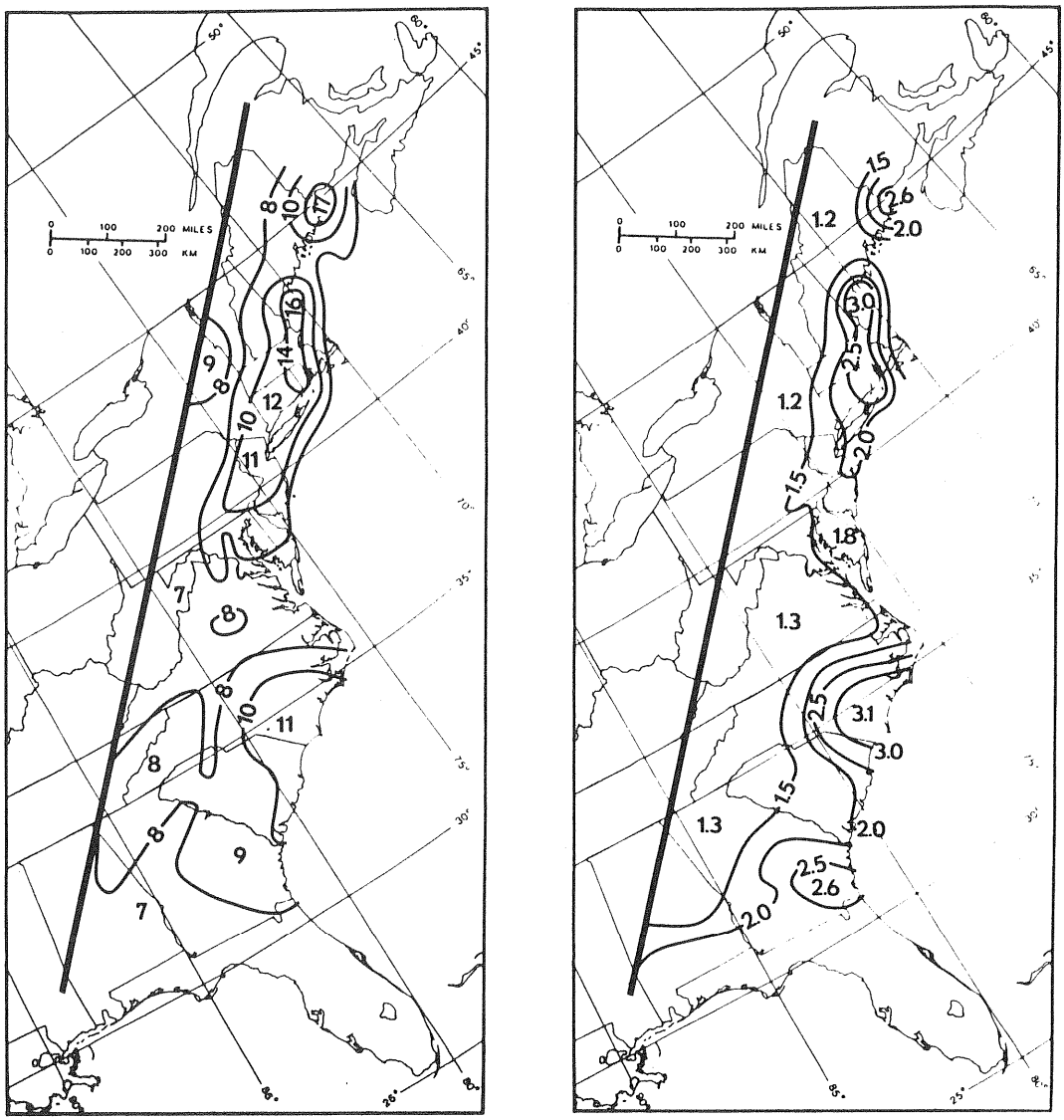

Figure 3. Left: Maximum probabilistic accelerations from all zonations considered. Right: Ratio of maximum probabilistic accelerations to minimum probabilistic accelerations at each site from all zonations considered. [From Thenhaus and others, 1987.] High ratios indicate sites benefiting most from research to impeach that tectonic principle which produces the maximum site probabilistic accelerations.

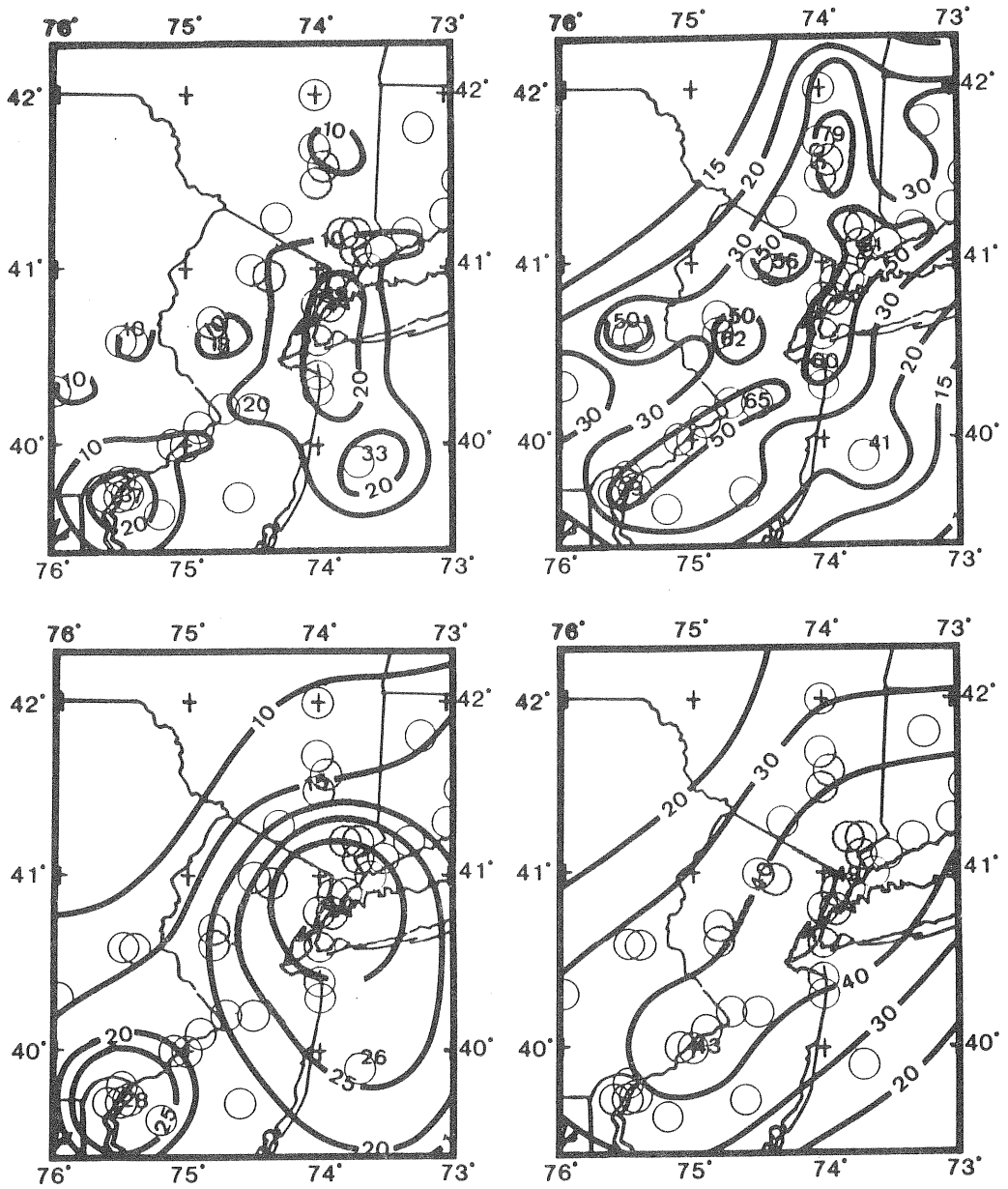

Figure 4. Probabilistic accelerations from historical seismicity. Upper left: Historical magnitudes and locations. Lower left: Historical magnitudes, but locations smoothed with Gaussian distribution and 40-km standard deviation. Upper right: Magnitudes have exponential distribution from $M_s = 4.0$–7.6; historical locations. Lower right: Magnitude and location both smoothed according to the given parameters.

we get a more conventional, smoother, more satisfactory map (lower right, figure 4). Generally, the broader the smoothing, the lower the hazard values and the less contrast in hazard from site to site. The most pleasing results, having good smoothness but retaining some detail, occur for smoothings with standard deviations of 40 to 80 km. As before, the element of subjectivity returns in the choice of what kind and what extent of generalization to perform, but the results do differ from those obtained by attempting an initial best estimate.

CONCLUSION

Judging from the variety of maps produced by attempting to force increased objectivity at the beginning of the hazard map process, there are a number of possible alternatives for future eastern U.S. hazard maps. This variety serves the useful purpose of demonstrating how uncertain is the seismic hazard for this region. Narrowing the range of alternatives will require substantial tectonic research. Meanwhile, the fashioning of seismic building code maps from among these alternatives will require considerable judgment and, hence, subjectivity, but this subjectivity will take place at the correct end of the process.

REFERENCES

Algermissen, S. T., 1969, Seismic risk studies in the United States: World Conference on Earthquake Engineering, 4th, Chilean Association for Seismology and Earthquake Engineering, Proceedings, Santiago, Chile, reprint, 20 p.

Algermissen, S. T., and Perkins, D. M., 1976, A probabilistic estimate of maximum acceleration in rock in the contiguous United States: U. S. Geological Survey Open-File Report 76-416, 45 p.

Algermissen, S. T., Perkins, D. M., Thenhaus, P. C., Hanson, S. L., and Bender, B. K., 1982, Probabilistic estimates of Maximum acceleration and velocity in rock in the contiguous United States: U. S. Geological Survey Open-File Report 82-1033, 99 p.

Applied Technology Council, 1978, Tentative provisions for the development of seismic regulations for buildings, National Science Foundation Publication 78-8, 505 p.

Building Seismic Safety Council, 1985, NEHRP (National Earthquake Hazards Reduction Program) recommended provisions for the development of seismic regulations for new buildings, Federal Emergency Management Agency Earthquake Hazards Reduction Series 17, 18, and 19, FEMA 95, 96, and 97/February 1986, 471 p. (in 3 vols.)

Thenhaus, P. C., Perkins, D. M., Algermissen, S. T., and Hanson, S. L., 1987, Earthquake hazard in the eastern United States: Consequences of Alternative Seismic Source Zones, Earthquake Spectra, v. 3, n. 2, p. 227–262.

ON PROBABILISTIC SEISMIC HAZARD METHODOLOGY FOR CRITICAL INDUSTRIAL FACILITIES IN THE EASTERN UNITED STATES

J. Carl Stepp
Electric Power Research Institute, Inc.
3412 Hillview Avenue
Palo Alto, California 94303

A methodology has been developed to assess probabilistic seismic hazard for critical facilities in the central and eastern United States. Key features of the methodology are the ability to assess hazard at the low probability levels required for critical facilities design and the incorporation of interpretation and data uncertainty in the hazard results. The methodology consists of systematic procedures to interpret earthquake sources and their seismicity parameters and to incorporate functions for the attenuation of seismic energy. The method is made flexible to be compatible with earth science interpretation procedures.

Interpretations of seismic sources is accomplished in two steps. First, a framework of tectonic features interpreted to be seismically active is developed and a structured procedure is provided to, assess the probability of activity of each based on the features physical characteristics, and associated geophysical data. Alternative seismic sources are derived from the tectonic framework. This permits the analyst maximum flexibility to express alternative interpretations, each with an assessed credibility. By the alternatives, the total uncertainty in seismic sources can be conveniently expressed.

To estimate rates of earthquake recurrence, the methodology makes maximum use of the historic earthquake data base. Procedures are provided to establish a uniform measure of earthquake size, to identify primary and secondary events, and to assess completeness in time, space and magnitude. The Poisson-exponential model is shown to be appropriate to estimate low probability hazard in low tectonic strain rate regions. The usual assumption of homogeneous seismicity within a source has been relaxed.

Uncertainty in seismic wave attenuation may be incorporated by use of alternative models, each with a specified weight. To express total scientific uncertainty, the methodology accepts alternative input interpretations developed by multiple interpreters. Procedures are developed to aggregate the hazard results from any number of interpretations to obtain a best-estimate hazard curve and its uncertainty.

CURRENT TRENDS IN SEISMIC ZONATION

J. P. SINGH
Geospectra, Richmond, California

HISTORICAL BACKGROUND

Trends in seismic zonation of the United States over the last two decades have changed considerably. The very first attempt of zonation of the United States was based on the maximum intensities experienced during historic earthquakes and the last of the maximum-intensity based maps was published by Algermissen in 1969.

A review of the state of seismic provisions in the early 1970's indicated that a more systematic approach to developing seismic design provisions applicable to the entire United States was desirable. As a result, the Applied Technology Council (ATC) undertook a coordinated program for formulating a comprehensive set of recommendations that could be used in the development of seismic provisions for the United States. The project was designated ATC-3 and was performed under a contract to the National Bureau of Standards (NBS) as a part of the cooperative Federal Program in Building Practice for Disaster Mitigation.

One of the key issues in this effort was to develop a more realistic definition of ground motion for design. Therefore, a major portion of the efforts to develop this Tentative Provisions centered around establishing the ground motion characteristics that might be expected at a site. The previous maximum-intensity (regardless of frequency of occurrence) based seismic zoning maps, were replaced with a probabilistic definition of ground motion. This kind of definition allows (a) realistic estimation of the likely ground motion intensities corresponding to a uniform probability of exceedence and (b) processing of the historical as well as geologic earthquake record. Information contained in geologic record is particularly valuable because it provides input for probabilistic analysis on the occurrence of earthquakes through periods of time many orders longer than the average repeat time of large earthquakes on individual faults and orders of magnitude greater than periods covered by historical records.

The uniform risk selected for the entire United States corresponded to a long recurrence interval of 475 years (an annual probability of 0.002 events/year or an event with 10 percent change of being exceeded in 50 years). The probabilistic maps for peak ground acceleration on rock corresponding to this criteria were developed by Algermissen and Perkins, 1976 and form the basis for the Seismic Ground Motion Map used by the ATC

in their "Tentative Provisions for the Development of Seismic Regulations for Buildings" (ATC publication ATC3-06, 1978).

Because the tall buildings are more vulnerable to long period motions, the ground motion mapping also considered the differences in attenuation with distance of high- and low-frequency motions. This was accomplished by introducing a pair of maps divided into seven areas of seismic intensity. One map gives the effective peak acceleration (A_A) and the other gives effective peak velocity related acceleration (A_V) on a county-by-county basis for the entire United States. The effective peak acceleration and effective peak velocity are related to the average spectral acceleration and velocity ordinates in the moderately-short and moderately-long period ranges, respectively. The values of A_A and A_V provide factors for constructing design response spectra. The relative magnitudes of A_A and A_V control the shape of the response spectra.

Local site effects were taken into account by the introduction soil factor, S, varying from 1 (for rock and firm sites) to 1.2 (for deep soil sites) to 1.5 (for soft soils and clays).

The 1985 National Earthquake Hazard Reduction Program (NEHRP) recommended provisions for the Development of Seismic Regulations for New Buildings and the 1985 Tentative Lateral Force Requirements developed by Structural Engineers Association of California (SEAOC), with minor changes, are a direct descendent of ATC3-06 (1978). The 1985 SEAOC Requirements with some minor revisions will become the 1988 Uniform Building Code.

In 1982, Algermissen and others, expanded the probabilistic ground motions estimates to include both peak acceleration and peak velocity at three different probability levels (10 percent change of exceedence in 10, 50 and 250 years), in order to provide estimates of ground motion hazard for short- and long-period structures, respectively. The 50- and 250-year maps will be included in the NEHRP revisions to "Recommended Provisions for the Development of Seismic Regulations for New Buildings".

CURRENT TRENDS

Recent studies related to seismic source zones; characteristic earthquake and slip rates; coefficient of an elastic attenuation; and interpretation of recorded strong ground motions have provided another surge into seismic zonation studies. This paper describs the variations in strong ground motions, in general, and long period motions, in particular as they relate to seismic zonation.

There is a growing consensus that peak ground acceleration and spectral shapes based on different categories of soil condi-

tions along (Seed et al, 1976a,b) are not sufficient to describe the characteristics of ground motion. This is based on evidence from recent recordings of earthquakes by strong motion instruments arrays installed in California, Taiwan and Mexico, that clearly show that the basic characteristics of waveforms are controlled by the characteristics of source and travel path and modified by local soil conditions (Singh, 1981, 1985, 1986). For a given soil condition, the characteristic of strong motion (peak ground acceleration (PGA), peak ground velocity (PGV), peak ground displacement (PGD), duration, spectral content, and time history) can vary significantly in one earthquake or different earthquakes for sites located near or far from the seismic source (Singh, 1985, 1986). Depending on the situation, the variation in ground motion due to source effects can overshadow the effect of local soil conditions or on the other hand, variations in ground motion due to local soil conditions can overshadow the effects of source. Such differences in ground motions, for a given soil condition, can be dramatic in different frequency bands depending upon the characteristics of the source and travel path. Therefore, it is important that these factors influencing the ground motion be properly considered in development of ground motion parameters and spectral shapes.

Examples of these variations in ground motion in the near field and far field are given below:

Near Field

In the near field, one of the effects of a moving source along the fault rupture is to cause a significant variation in the ground motion for a given soil condition. The variation results in part from: 1) enhancement of the long duration pulse called the "fling", which is related to the elastic rebound on the fault, and 2) compression of the duration of the strong shaking in the direction of rupture propagation. These effects of moving sources may be greater than the influence of local soil conditions.

Strong motion records from the October 15, 1979 Imperial Valley earthquake illustrate this variability in ground motion (see Figure 1). Figure 2 shows the plots of variations of near field PGAs, PGVs, PGDs and durations in the near field at a given distance from the source can easily vary by factors of 2 to 7. Figure 3 gives examples of variations in PGAs, PGVs, PGDs, and durations along the fault at 1 km from the source. From these examples, it is apparent that variations in ground motion in the near field are quite large and there is no consistent pattern among ground motion parameters at a given distance form the source and for a given soil condition.

Figure 4 shows the variations in V/A and AD/V^2 ratios (used to develop the design spectral shapes) along the fault at a dis-

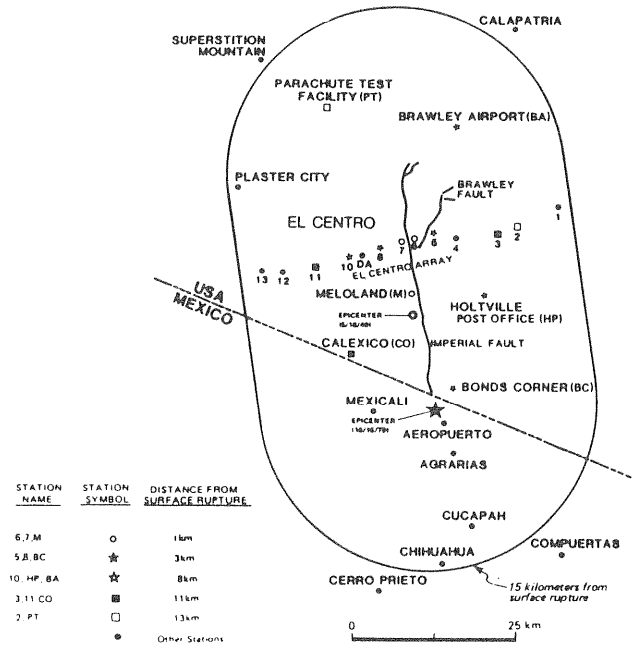

Figure 1. Map Showing Recording Stations in the Imperial Valley and Epicenters of 1940 (El Centro) and 1979 (Imperial Valley) Earthquakes.

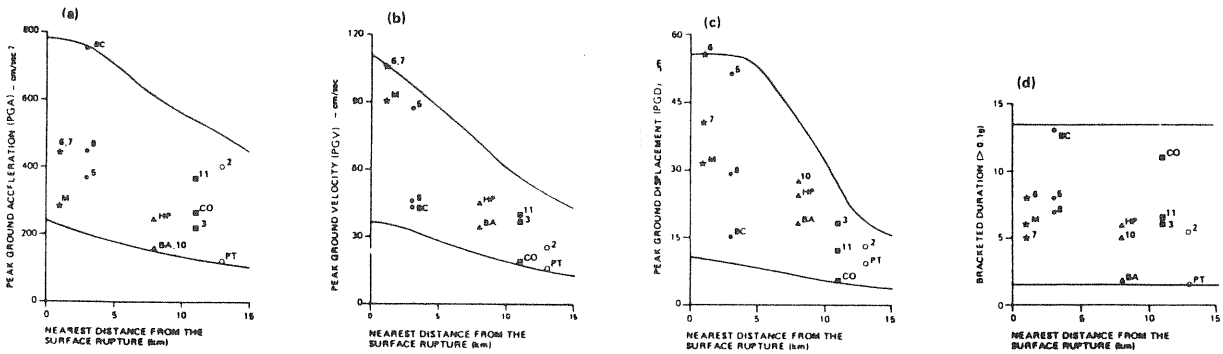

Figure 2. 1979 Imperial Valley Earthquake: Variations in PGA, PGV, PGD and Bracketed Duration with Distance from the Surface Rupture of Imperial Fault (230° Component).

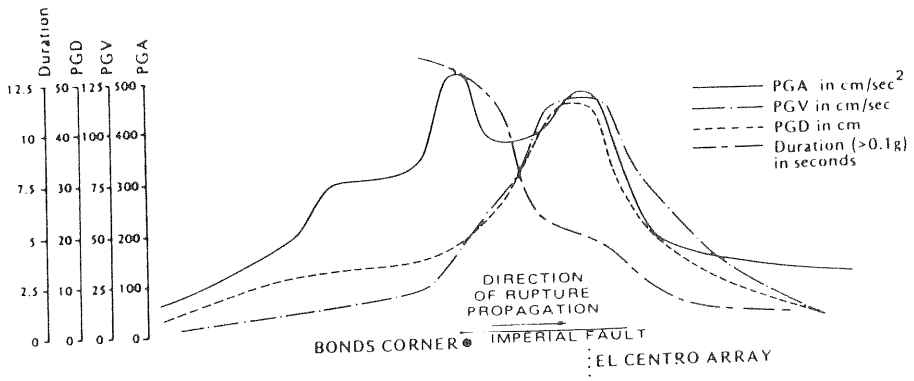

Figure 3. Attenuation Curves of PGA, PGV and PGD along the Fault at a Distance of 1 km.

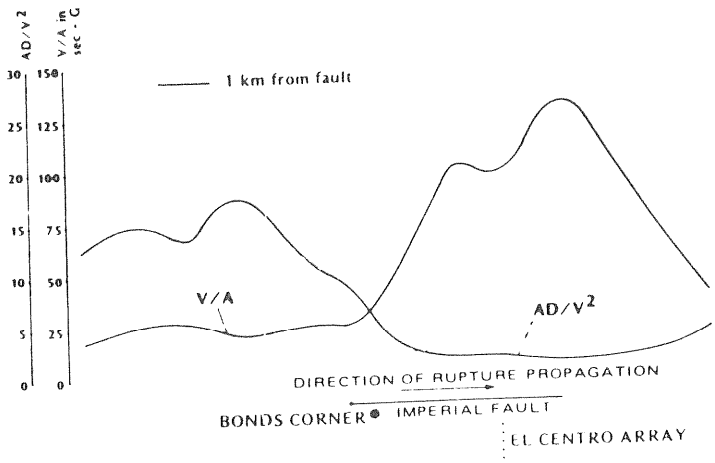

Figure 4 Variation of V/A and AD/V^2 Ratios along the Imperial Fault at a Distance of 1 km (230^o Component).

tance of 1 km. The V/A ratio varies from about 22 close to Bonds Corner to about 125 Close to El Centro Array. The AD/V^2 ratio for these two locations decreased from about 5.8 to 1.6. A reflection of the variation of V/A and AD/V^2 ratios on redistribution of spectral energy can be seen by comparing spectral amplitudes shown in Figure 5 for the 230^{o} horizontal component of Stations El Centro 7 and Bonds Corner.

For a given soil condition, the near field ground motion variations can be seen in the time domain as well. Figure 6 compares acceleration, velocity, and displacement time histories for Stations El Centro 7 and Bonds Corner. The shear wave portion of the record indicated on these traces shows quite clearly the effect of source directivity. The waves in the direction of rupture propagation are crowded together, producing a large-amplitude pulse called a "Fling" at Station El Centro 7. In contrast, the waves in the direction opposite to the direction of propagation produce a low-amplitude pulse at Bonds Corner.

An example of the effect of near field variations in ground motions on the inelastic response of a structure is shown by Anderson and Naeim (1984). They analyzed the response of a steel frame to two time histories having comparable PGAs - one from the 1979 Imperial Valley earthquake and the other from the 1940 El Centro earthquake (see Figure 7). From plots of computed maximum lateral displacement versus story level, also presented in Figure 7, it can be seen that the displacement produced by the 1979 earthquake time history is almost four times that produced by the 1940 earthquake time history. The differences in the response spectra, PGV, PGD, and durations for these time histories are also shown in Figure 7. The 1979 time history was recorded in the direction of the propagation and has much higher PGVs and PGDs and much lower durations compared to those of the 1940 time history, which was recorded in the direction opposite to the direction of propagation. This example clearly shows that the response of identical structures, equidistant from the earthquake source and sitting on identical soil conditions, could be significantly different because of variations in the ground motions produced by two different earthquakes of comparable size occurring on the same fault.

It is clear that the seismic source directivity has a strong effect on recorded ground motion and the observed damage and must be properly considered in interpreting strong motion records and in developing estimates of ground motion.

Far Field

In the far field, variations in ground motions can be seen from strong ground motions recorded by the SMART-1 strong motion array located near the City of Lotung in the highly seismic

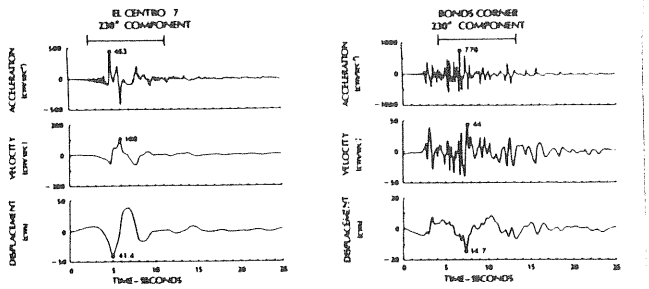

Figure 6 . Corrected Acceleration, Velocity and Displacement Records for Stations, Bonds Corner and El Centro 7 (230° component).

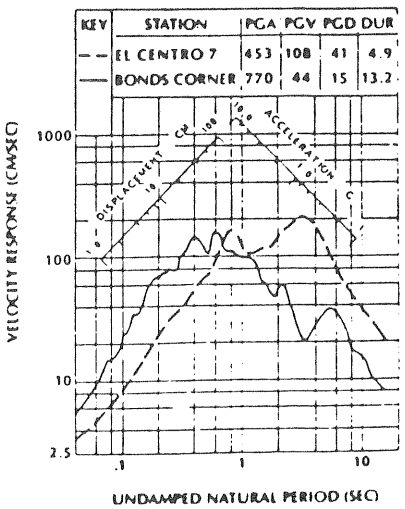

Figure 5 Comparison of Response Spectra for Stations El Centro 7 and Bonds Corner for 5 Damping (230° Component).

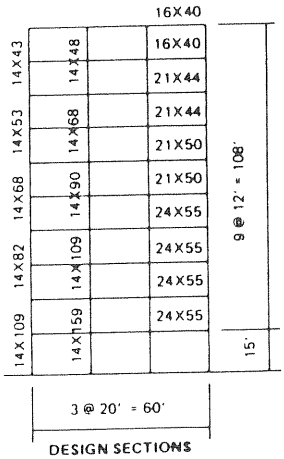

(a) Design Frame

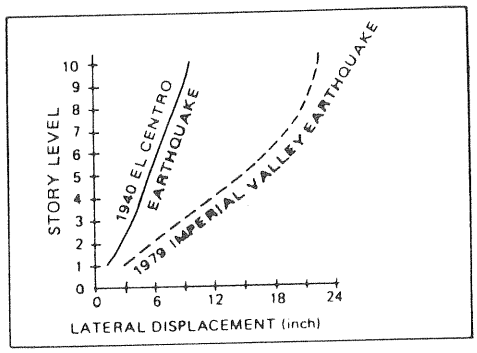

(b) Maximum Lateral Displacement

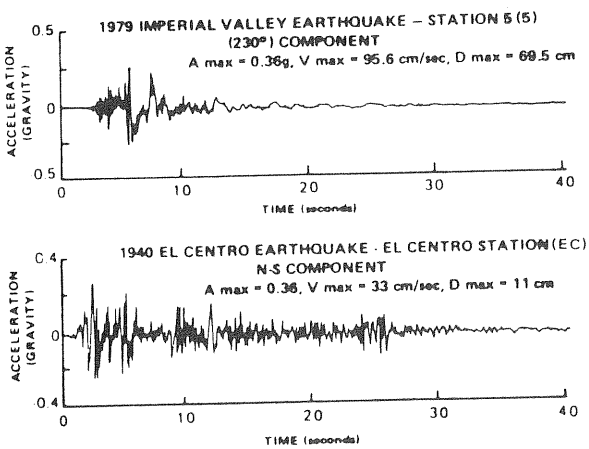

(c) Acceleration Time History

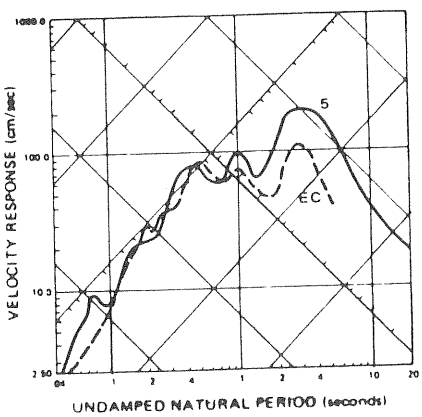

(d) Response Spectra

Figure 7 . An Example of Variations in Structural Response to Different Time Histories in the Near Field (Modified from Anderson and Naeim, 1984).

northeastern region of Taiwan (see Figure 8; for details of array, refer to Singh, 1985). Strong ground motion records obtained at the same site from different earthquakes have shown dramatically different time histories and response spectra for comparable levels of recorded PGAs. For illustration, we have used records from the 1981 and 1983 earthquakes. The locations of these two earthquakes and their epicentral distances, focal depths, and source mechanisms are summarized in Figure 8.

Because these events were recorded at hypocentral distances greater than 40 km, the variations in PGAs and the spectral content across the array were small for a given earthquake. In comparing spectral shapes for different events, therefore, it was considered appropriate to normalize the spectra to PGAs.

The mean of spectra obtained from all array stations for two earthquake are plotted on Figure 9. The spectrum for the 1981 earthquake shows a peak at approximately 0.25 seconds. The spectrum for the 1983 earthquake is quite different; the peak is broader and shifts to longer periods. The 1983 earthquake, which is larger, seems to have generated more long-period energy. These variations in spectral shape show that, for a given soil condition, the source mechanism and the size of the earthquake distinctly affect the shape of the response spectra.

The acceleration time histories for the 1981 and 1983 earthquakes recorded at Station I-03 of the SMART-1 array are plotted in Figure 10. The two acceleration time histories show very different motions, with substantially more long-period motions from the 1983 earthquake than from the 1981 earthquake.

The strong ground motions can significantly vary in the far field for a given soil condition. It is important that in interpreting or developing ground motions, the source effects be properly considered.

From the above examples, it can be seen that whether in the near or far field, it is very important to understand the long period motions. Therefore, the current trend is to (a) to define the ground motion in terms of equal probability spectral content based on source, travel path and local soil conditions and (b) map long period motions for seismic design of structures.

IMPLICATIONS TO SEISMIC DESIGN IN ENAM

It is well known that the seismic research in the ENAM has been driven by the needs of the nuclear industry. Therefore, a great importance has been given to studying the PGA and spectral

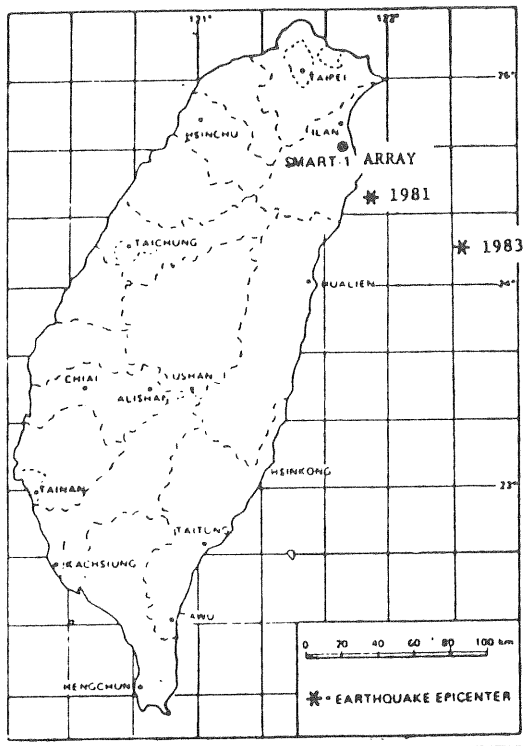

	Average PGA at SMART 1 ARRAY	M_L	M_s	EPICENTRAL DISTANCE (km)	FOCAL DEPTH (km)	SOURCE MECHANISM
1981	.24g	6.8	6.7	30	25	STRIKE SLIP
1983	.07g	7.2	6.7	82	44	STRIKE SLIP OBLIQUE

Figure 8 Information on Earthquake events in Taiwan.

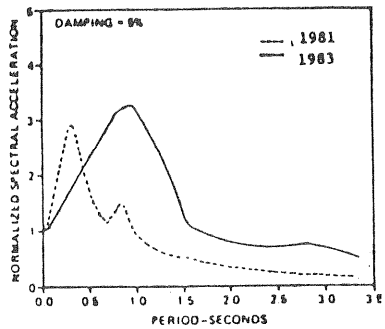

Figure 9 Comparison of Normalized Spectral Curves (Mean) for SMART-1 Array Stations for 1981 and 1983 earthquakes.

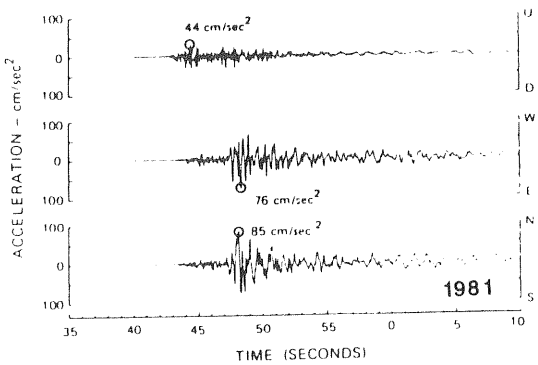

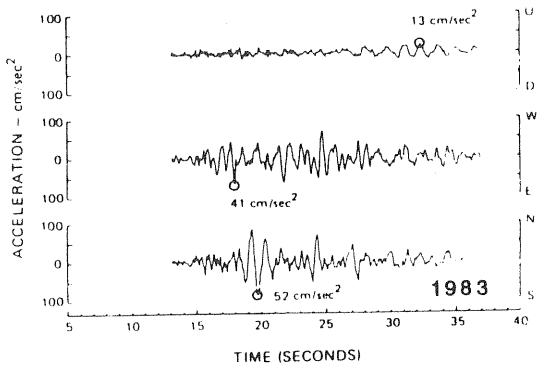

Figure 10 Comparison of Acceleration Time Histories from 1981 and 1983 Earthquakes Recorded at SMART-1 Array Station 1-03.

content in the high frequency range. Our immediate problem in the ENAM, on the other hand, is the enormous number of existing structures in the Metropolitan Areas with general lack of seismic design. Let us ask ourselves, "Is understanding the high frequency part of the ground motion sufficient to overcome the seismic design problem in ENAM?" Based upon my preceding discussions of the long period motions I would be inclined to say "No". I say that because the premise of most codes is "ductility" as a form of energy dissipation mechanism to prevent buildings from a collapse during a major earthquake that have been designed for a limited damage for moderate earthquakes.

The example by Anderson and Naeim shows that, for two time histories with similar accelerations, the one with higher long period motions puts much more demand on the structure. This means that the damage sustained by the structure for a given acceleration could vary widely depending upon the level of long period energy present in the ground motion. Therefore, (a) in preparing the loss estimates from earthquake damage and (b) in developing schemes for strengthening of existing structures in ENAM, it is extremely important that the nature and magnitude long period motions for the ENAM be properly understood.

REFERENCES

Algermissen, S. T., 1969, Seismic Risk Studies in the United States, Proceedings Fourth World Conference in Earthquake Engineering, Santiago, Chile, Volume A-1, PP14-27.

Algermissen, S. T. and Perkins, D. M., 1976, A Probabilistic Estimate of Maximum Acceleration in Rock in the Contigous United States, U. S. Geological Survey Open File Report 76-416.

Algermissen, S. T., Perkins, D. M., Thenhaus, P. C., Hansen, F. L., and Bender, B. C., 1982, Probabilistic Estimates of Maximum Acceleration and Velocity in Rock in the Contigous United States, U. S. Geological Survey Open File Report 82-1033.

Anderson, J. and Naeim, F., 1984, Design Criteria and Ground motion Effects on the Seismic Response of Multistory Buildings, Critical Aspects of Earthquakes Ground Motion and Building Damage Potential, ATC 10-1, Applied Technology Council.

Applied Technology Council, 1978, Tenative Provisions for the Development of Seismic Regulations for Buildings, Prepared by the Applied Technology Council, ATC 3-06.

NEHRP Recommended Provisions for the Development of Seismic Regulations for new Buildings, 1985, Federal Emergency Management Agency, Washington D. C.

Seed, H. B., Ugas, C., and Lysmer, J., 1976a, Site-Dependent Spectra for Earthquake-Resistant Design, Bulletin of the Seismological Society of America, vol. 66, no. 1, pp. 221-243.

Seed, H. B., Murarka, R., Lysmer, J., and Idriss, I. M., 1976b, Relationships of Maximum Accelerations, Maximum Velocity, Distance from Source and Local Site Conditions for Moderately Strong Earthquakes, Bulletin of the Seismological Society of America, vol. 66, no. 4, pp. 1323-1342.

Singh, J. P., 1981, The Influence of Seismic Source Directivity on Strong Ground Motions, Ph.D. Dissertation, University of California, Berkeley.

Singh, J. P., 1985, Earthquake Ground Motions: Implications for Designing Structures and Reconciling Structural Damage, Earthquake Spectra, vol. 1, no. 3.

Singh, J. P. (1986). "A Simple Method for Generating Synthetic Time Histories for Design of Base Isolation Systems," Applied Technology Council (ATC) Seminar on Base Isolation and Passive Energy Dissipation Devices, March 12-13, San Francisco, ATC-17.

SOME LIMITATIONS OF CURRENT SEISMIC CODES FOR EASTERN U.S. EARTHQUAKE RESISTANT DESIGN

Guy J. P. Nordenson
Ove Arup & Partners Intl. Ltd.
New York, New York

ABSTRACT

A number of seismic codes, including the Uniform Building Code (UBC), NEHRP/ATC Tentative Provisions and 1985 SEAOC Recommendations have been proposed for adoption throughout the United States. These codes include both national seismic zoning maps and detailing requirements keyed to the different zones. Both the underlying philosophy and the specific structural system qualifications have evolved from experience in the high seismic regions of the United States. In order to evaluate the advisability of adopting these seismic codes in moderate seismic zones (MSZ), this paper reviews some of the inherent limitations of these codes in their own context as well as in the context of MSZ seismicity and construction practices. The nature of Eastern U.S. seismic hazard is discussed with reference to recent site specific hazards evaluations of the New York City (NYC) area. The variation of peak horizontal acceleration with average return period as derived for NYC is contrasted to that implicit in the seismic codes. The validity for MSZ's of the response spectral shapes incorporated in the codes is also questioned in light of recent research. Finally several observations are presented on the possible resistance of construction systems typical of MSZ's which are not accounted for in the seismic codes.

INTRODUCTION

Seismic codes embody the minimum standards of practice accepted by the earthquake engineering profession and the public. Their purpose is to insure life safety and to a limited extent safeguard property. On the whole the codes have proven effective. However "earthquake performances have... shown that the resistance of buildings are not necessarily proportional to the code requirements under which they are designed" (Housner and Jennings [1982]). The fact that buildings designed in accordance with modern seismic codes have successfully withstood moderate to severe earthquakes may testify as much to the skill of the designers, the unaccounted-for overstrength of materials and contribution of non-structural elements, and the idiosyncrasies of local site effects, as to the impact of the code provisions themselves. The physical "constants" and analytical methods that are used in the code calculations cannot be considered to be accurately representative of actual physical behavior in the course of an earthquake. At most the values determined for mass, stiffness, building period, structural system "ductility" ratios and from these, base shear values and drift estimates are accurate to within factors of 2 to 4. Despite their substantial

benefits the seismic codes are not a sufficient condition for earthquake resistance.

It is suggested in the following that the seismic codes currently being proposed for national (U.S.) adoption (NEHRP/ATC 3-06 "Tentative Provisions for the Development of Seismic Regulations for Buildings" [1978] and the 1985 SEAOC Recommendations which have been approved for inclusion in the 1988 Uniform Building Code (UBC 88)) may not be appropriate for moderate seismic zones (MSZ) where design and construction practices as well seismicity are quite different from those in the highly seismic areas. The degree to which the codes are "coupled" to their context of origin is difficult if not impossible to establish. It is risky to transfer a code without its context or to extrapolate from the "logic" of the codes modifications to suit the conditions of MSZ's (e.g. the introduction of "ordinary" or "intermediate" ductile structural systems). If seismic codes are to be introduced in MSZ's they should be developed in the context of current local practice, and should:

1. Consider the unique characteristics of MSZ seismicity in the selection of acceptable annual risk, and of the corresponding peak horizontal acceleration and design response spectral shape.

2. Include structural systems, such as steel or RC frames with masonry infill, which have proven successful in testing and past earthquakes and are in common usage in MSZ's.

3. Coordinate seismic code requirements with provisions for resistance to extreme winds, progressive collapse or explosive effects.

LIMITATIONS AND BENEFITS OF CURRENT CODE-BASED EARTHQUAKE RESISTANT DESIGN

Implied Variability of Ground Motion

Both the NEHRP/ATC 3-06 and 1985 SEAOC Recommendations/UBC 88 seismic codes have based their zoning maps on contours of peak horizontal acceleration (PHA) values corresponding to a 90 percent probability of not being exceeded in 50 years. This is equal, assuming a Poisson distribution for earthquake events, to an average return period (ARP) of 475 years. The reciprocal of the ARP is the annual probability of exceedence, and is equal to 0.21 percent. Certain critical facilities are sometimes designed for PHA values derived for an ARP of 1000 years, or an annual probability of exceedence of 0.10 percent.

From the result of probabilistic seismic hazards analyses (e.g. Idriss [1985], Algermissen and Perkins [1982]) for

California, one can take the ratio of the design or code basis PHA to the largest values presented. For example Idriss [1985] presents results of hazards analyses for Los Angeles sites 10 km (Site B) and 78 km (Site A) from the southern San Andreas fault. Considering the contributions of all possible sources for each site he obtains a relation between PHA and ARP. At Site B the largest PHA shown is 0.70 g for an ARP = 800 years, and for Site A, PHA(max) = 0.70 g at ARP = 4000 years. The ratio of these maximum PHA values to PHA [ARP = 475 yrs] is 0.70/0.64 = 1.09 at Site B and 0.70/0.43 = 1.63 at Site A. If the Characteristic Earthquake Recurrence Model is used for the San Andreas fault the values for Site B change to: PHA [ARP = 475 yrs] = 0.40 and PHA(max), at ARP = 5000 yrs, is 0.70, for a ratio of 1.75. A similar comparison can be made using the results presented by Algermissen and Perkins [1982]. For the same Southern Californian location the ratio of PHA values for ARP = 2375 and 475 yrs is found to be 0.69/0.60 = 1.15. In general one finds from such simple exercises that for the highly seismic areas of California what one might call the "exceedence ratios" of maximum possible to code design basis PHA are on the order of 1.2 to at most 2.

The seismic codes use the PHA contours or derived zone factors to scale the design elastic response spectra which are in turn reduced by structural system response coefficients (e.g. the R of NEHRP/ATC 3-06 and Rw of 1985 SEAOC Recom./UBC 88) to obtain the base shear coefficients. The "absolute" upper bound on the exceedence of the PHA value used is implicitly included in the overall level of safety that follows from code-based designs.

The design elastic response spectra that are incorporated in the these seismic codes are based on the work of Seed et al [1976] using mostly the records from the 1971 San Fernando earthquake, M 6.2. The spectral ordinates in the long period range (T > 1.0 sec) reflect the energy content of this relatively large event.

Predicted vs. Actual Seismic Response of Code-designed Buildings

Bertero [1987] concludes, from an analysis of the response of buildings to the 19 Sept. 1985 Mexico City earthquakes, that:

> "The lateral strengths required by the building seismic codes were insufficient to cope with the severity of the response demanded by the ground motion that occurred in the zones of severe damage. The overall good performance of nearly 98.5% of the buildings in the zones of severe damage was due to the conservatism of Mexican designers and particularly to the added overstrength of the buildings as constructed, introduced by masonry infills."

The contribution of nonstructural elements, of structural elements not included in the design model (e.g. slabs as they both strengthen girders and couple frames and walls, see Aktan and Bertero [1987]) and the frequent overstrength of materials

above nominal design values can be expected to significantly affect the actual response of buildings in earthquakes in ways that are near impossible to predict from the code-based analyses. Housner and Jennings [1982] found, for example, that the response of 14 multistory RC frame buildings to the 9 Feb. 1971 San Fernando earthquake showed that "structures of this type can, on the average, be expected to resist base shears that are two to three times larger than the code design values without major structural damage."

The implication of such studies is that even thought the energy dissipating capacity, or "ductility" values, assigned to codified structural systems by the R or Rw coefficients are difficult to justify in terms of the structural behavior alone, there are contributing factors not explicit in the code, but part of the general design and constructional context, which play a significant role in supplying the total earthquake resistance of a building. There have been notable cases (Olive View Hospital, Imperial County Services building) of code designed buildings that have failed, testimony to the contribution of "good" design.

One can also point to structures that have successfully survived major earthquakes and would be forbidden by current standards. As related by Freeman [1932], the stiff steel frames, concrete encased and tightly infilled with unreinforced brick masonry, of the 315 ft. tall Claus Spreckels Building and the 240 ft. Chronicle Building, survived the 18 April 1906 San Francisco earthquake with minimal damage. More recently Klingner and Bertero [1978] and Brokken and Bertero [1981] have tested masonry (unreinforced and reinforced) infilled RC frames and found improvements in frame strength, stiffness and energy dissipating capacity that are significant and stable through several loading cycles. Since this construction is not uncommon both in older U.S. buildings and in other countries, it would be useful to develop simple analytical methods to analyze such "two-phased" structural systems, and include them in the codes.

Benefits of Code-based Earthquake Resistant Design

Among the "lessons from the San Francisco Quake of 1906" advanced by John R. Freeman in his seminal Earthquake Damage and Earthquake Insurance [1932] is that buildings and foundations should be "thoroughly tied together... so that the structure will oscillate as a whole." The 1927 Uniform Building Code, in a section devoted to "Bonding and Tying" required that "all buildings shall be firmly bonded and tied together as to their parts and each one as a whole in such manner that the structure will act as a unit." A designer applying the requirements of current seismic codes will specify the connection restraints and releases of cladding elements, size connection hardware to withstand the inertial loads from the cladding elements, analyze and design the horizontal floor diaphragms for the collection and transfers of inertial loads to and between the vertical resisting elements, analyze and design the main lateral load resisting system and review secondary systems for deformation

compatibility, design foundation elements to distribute the "reactions" and check for peak soil pressures due to overturning effects. In brief, follow a clear load path and explicitly design all elements and their links.

Similar procedures are typical of recommendations and codes for the design of structures to resist extreme wind, progressive collapse or blast effects. The British Standards [1985] for steel structures include a section on structural integrity with requirements for tying the structure together and "notional" inertial forces for which to design the ties. The purpose is to increase the building's resistance to progressive collapses of the sort that occurred at Ronan Point. Such code requirements further what one might call a "total design" approach which, by encouraging an explicit review of all elements and their connectivity for stability and nominal strength, substantially enhances the structure's toughness and redundancy. The magnitude of the forces used is not nearly as significant as the fact of the analysis itself.

MSZ SEISMICITY

Seismic Hazard

The understanding of eastern U.S. seismicity is severely limited by the short historical record, by the lack of any widely accepted hypotheses regarding the cause of intraplate earthquakes and by a paucity of data on recurrence and attenuation relationships. Nevertheless there has been progress recently in developing probabilistic seismic hazards evaluations that incorporate explicitly some of these uncertainties in their analysis. Statton et al [1986] have presented results for the New York City area which offer interesting comparisons to results obtained for the highly seismic regions. The variation of PHA, or zero-period acceleration, with ARP is shown in Table I.

Average Return Period (ARP) - years	Peak Horizontal Acceleration (PHA) - g
100	0.03
500	0.07
1,000	0.10
3,000	0.18
10,000	0.30
30,000	0.50

Table I - after Statton et al [1986]

The "exceedence ratios" of PHA values for large ARP's (say greater than 3,000 yrs) to the code design basis PHA for ARP = 500 yrs, are between 2.57 and 7.14, substantially greater than the values (1.2 to 1.75) determined for the Southern Californian sites considered above. For ARP = 475 and 2375 yrs, Algermissen and Perkins [1982] present PHA values of 0.12 and 0.30 respectively for the New York to Boston contour envelop. The corresponding exceedence ratio is 2.5 as against 1.15 for the Southern Californian comparison. The potential magnitude of exceedence of the design basis ground motion parameters is by these measures substantially greater in the New York area than in Southern California. In effect this is a reflection of the fact that large earthquakes occur less frequently in MSZ's.

Design Response Spectral Shapes

Boore and Atkinson [1987], Idriss [1985] and Joyner and Boore [1982] have presented relationship that permit the calculation of response spectral shapes as a function of epicentral distance and magnitude of earthquakes. Figures 1 and 2 show the ratio of spectral ordinates for response spectra calculated for M 5.5, 6.0, 6.5, and 7.0 to ordinates for the M 5.0 response spectrum shape. The spectral shapes are normalized to a zero period acceleration of 1.0 g. If one were to select as the code design basis earthquake a M 5.5 event then these results would suggest that the spectral shapes collected for M 6.0 or 6.5 events should be scaled down by factors on the order of 2.5 to 4.0.

Statton et al [1986] have suggested that the "standard" response spectral shape (e.g. Seed et al [1976]) be modified for use in New York City by reducing the spectral ordinates for periods over 1.0 sec. by half and interpolating for ordinate values between 0.3 and 1.0 sec.

IMPLICATIONS FOR EARTHQUAKE RESISTANT DESIGN AND SEISMIC CODES IN MSZ'S

The Commentary to the Recommended Lateral Force Requirements of the Structural Engineers Association of California [1980], as well as the Introduction to the NEHRP/ATC "Tentative Provisions for the Development of Seismic Regulations for Buildings" [1978], state that the objective of the seismic design codes is to provide buildings with the capacity to:

"1. Resist minor earthquakes without damage;

2. Resist moderate earthquakes without structural damage, but with some nonstructural damage;

3. Resist major earthquakes, of the intensity of severity of the strongest experienced in California, without collapse, but with some structural as well as nonstructural damage." SEAOC [1980]

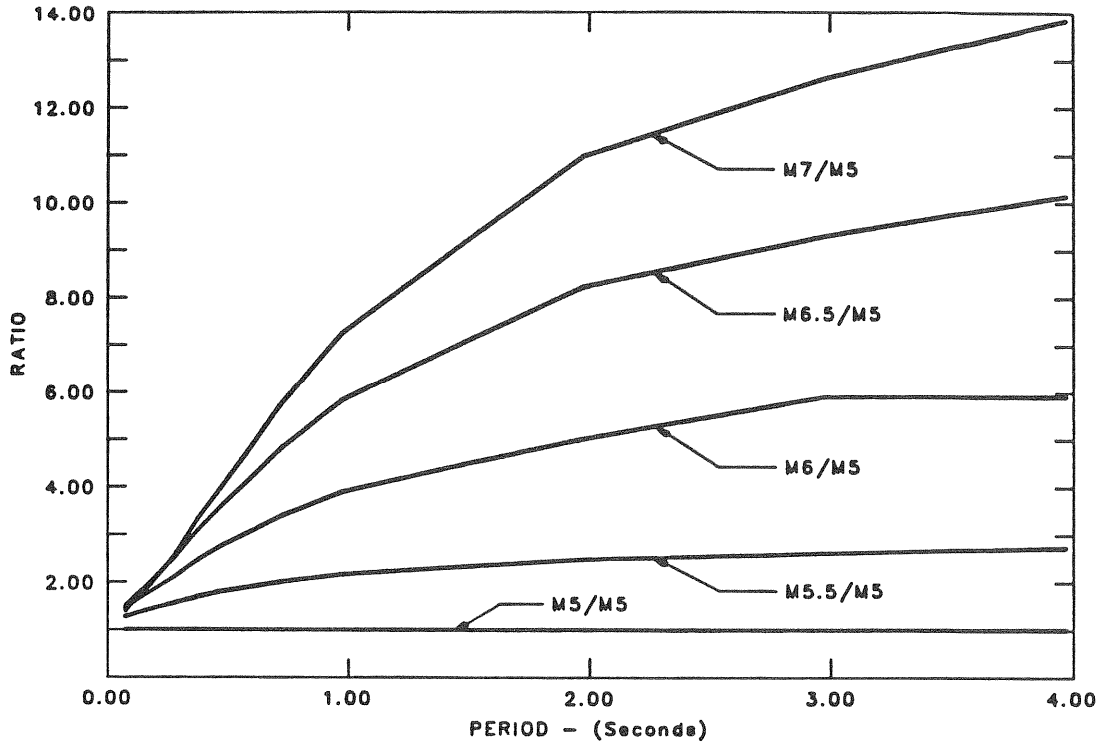

Figure 1 - Normalized Spectral Ordinate Ratios
(after Joyner and Boore [1982])

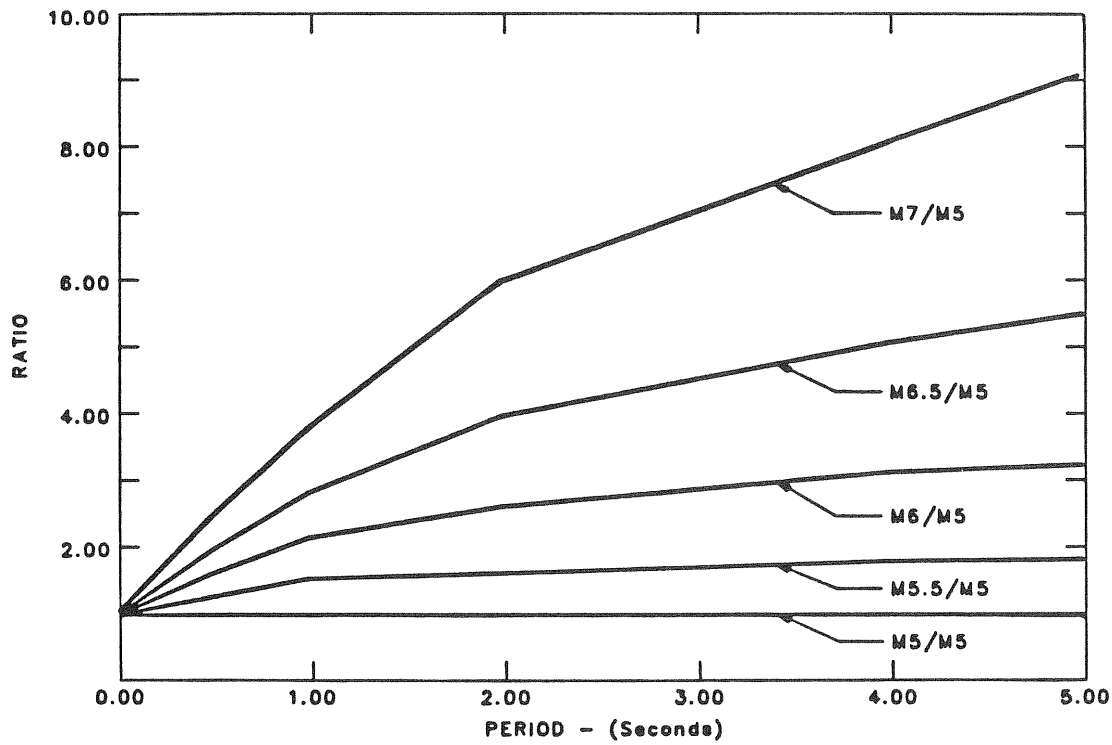

Figure 2 - Normalized Spectral Ordinate Ratios
(after Idriss [1985])

The code requirements are intended to provide for a balanced supply of structural strength and energy dissipating capacity that is sufficient to meet these objectives. The code specified base shear values, calculated from the dynamic characteristics of the elastic structural model, are used to find the stresses for which the structural elements are designed by allowable stress or load factor design methods. The detailing requirements included in the material sections of the codes are intended to provide for the energy dissipating capacity necessary to reconcile the elastic capacity provided to the actual demands of the earthquakes.

In light of the observations presented above a seismic code developed for MSZ's such as the New York City area would have to take into consideration the following:

1. Peak Acceleration and Design Response Spectrum. Select PHA on the basis of a lesser annual risk level (greater ARP) than has been used for the present seismic codes. This could be rationalized from an analysis of exceedence ratios or perhaps more effectively by reference to marginal rates of exceedence (i.e. slope or even curvature of the PHA - ARP curves). For the chosen annual risk (or ARP), estimate the appropriate response spectral shape to reflect the predominant magnitude contribution apparent from the hazards analysis. This should result in lower relative spectral ordinates in the long period range. It should be noted that there is at present a need for research on spectral shapes for MSZ's.

2. Bonding and Tying. Clear provisions should be included that aid the designer in visualizing the total building system and require nominal ("notional") tie forces for the design of all elements and their connections. More than any other requirement this will greatly improve the buildings' toughness.

3. Structural Systems. Since it appears possible that the MSZ code level base shear values could be exceeded by ratios far larger than is likely in the highly seismic areas, it seems prudent to provide for as much ductility or energy dissipating capacity as feasible. This suggests that the so-called "ordinary" or "intermediate" ductile system included in both the NEHRP/ATC 3-06 and 1985 SEAOC Recom./UBC 88 codes for the MSZ's are not appropriate. Rather the codes should include, with proper detailing requirements, the types of masonry infilled frame systems that are presently excluded but have historically worked well.

4. Non-structural Systems. A clear distinction should be made between non-structural elements whose failure would be life threatening (cladding and perhaps elevator guide rails etc.) or simply costly (e.g. mechanical equipment).

Presently perhaps the greatest hazard in MSZ's exist from parapets or unreinforced and unattached cladding (particularly masonry and precast concrete). These should be secured as part of the "bonding and tying" discussed above.

CONCLUSION

It is argued that current seismic codes should be carefully reviewed and probably modified before they are adopted in the MSZ's. On the one hand the effectiveness of the codes in the highly seismic zones is at least in part due to local design and construction practices that are not necessarily present in the MSZ's. In addition uncertainties regarding MSZ seismicity, particularly the difficulty in setting an upper bound, suggest a more cautious selection of acceptable ARP or annual risk. There is clearly a need for some seismic code provisions in MSZ's such as the New York City region. There is also a great need for research work that will help to refine some of the observations presented here. For an MSZ seismic code to be effective it must recognize its context and it should be part of an overall effort to improve the durability and toughness of our buildings.

BIBLIOGRAPHY

Structural Use of Steelwork in Building, Bristish Standard BS 5950, British Standards Institution, London, England, 1985.

Aktan, A.E. and V.V. Bertero, "Evaluation of Seismic Response of RC Buildings Loaded to Failure," Journal of Structural Engineering, v. 113, no. 5, pp. 1092-1108, May 1987.

Algermissen, S.T., D.M. Perkins, P.C. Thenhaus, S.L. Hanson and B.L. Bender, Probability Estimates of Maximum Acceleration and Velocity in Rock in the Contiguous U.S., U.S. Geological Survey, O/F Report 82-1033, 1982.

Bertero, V.V., "The Mexico Earthquake of September 19, 1985, Performance of Building Structures," Seminar, ASCE Met Section, 1987.

Boore, D.M. and G.M. Atkinson, "Stochastic Prediction of Ground Motion and Spectral Response Parameters at Hard-rock Sites in Eastern North America," Bulletin of the Seismological Society of America, v. 77, no. 2, pp. 440-467, April 1987.

Brokken, S.T. and V.V. Bertero, Studies on Effects of Infills in Seismic Resistant R/C Construction, Earthquake Engineering Research Center Report 81/12, University of California, Berkeley, CA, 1981.

Freeman, J.R., Earthquake Damage and Earthquake Insurance, McGraw-Hill Book Company, New York, 1932.

Housner, G.W. and P.C. Jennings, Earthquake Design Criteria, Earthquake Engineering Institute, Berkeley, CA, 1982.

Idriss, I.M., "Evaluating Seismic Risk in Engineering Practice," Proceedings of the Eleventh International Conference on Soil Mechanics and Foundation Engineering, A.A. Balkema, Accord, MA, pp. 255-320, 1985.

Joyner, W. and D.M. Boore, "Prediction of Earthquake Response Spectra," Proceedings of the 51st Annual Convention of the Structural Engineers Association of California, San Francisco, CA, 1982.

Klingner, R.E. and V.V. Bertero, "Earthquake Resistance of Infilled Frames," Journal of the Structural Division, v. ST6, pp. 973-989, June 1978.

Nordenson, G.J.P. and C.T. Statton, "Seismicity and Seismic Hazards in the New York City Area" Proceedings of the Third U.S. National Conference on Earthquake Engineering, Earthquake Engineering Research Institute, El Cerrito, CA, pp. 209-219, 1986.

Seed, H.B., C. Ugas and J. Lysmer, "Site-Dependent Spectra for Earthquake-Resistant Design," Bulletin of the Seismological Society of America, v. 66, no. 1, pp. 221-243, Feb. 1976.

Seismology Committee, Recommended Lateral Force Requirements and Commentary, Structural Engineers Association of California, San Francisco, CA, 1980 and 1985.

Statton, C.T., R.C. Quittmeyer and I.M. Idriss, Probabilistic Seismic Hazard Evaluation for George Washington Bridge, New York-New Jersey, Woodward-Clyde Consultants, Wayne, NJ, 1986.

EARTHQUAKE VS. WIND RISKS TO BUILDINGS AND STRUCTURES IN THE EASTERN US

M. Shinozuka*
Department of Civil Engineering
Columbia University
New York, NY 10027

1. INTRODUCTION

Conventional structures, in particular, low-rise buildings are usually designed according to provisions specified in building codes and standards such as the Uniform Building Code (UBC), Standard Building Code (SBC) and American National Standard ANSI A58.1. The code provisions are intended to achieve the satisfactory performance of buildings under loads imposed by the users or nature such as wind or earthquake. However, building codes usually employ simplified formulas in the provisions in order to facilitate the design process. For example, the equivalent static design forces are stipulated in building codes to represent the wind or seismic forces which are dynamic and random in nature. The United States are divided into several seismic zones to represent differing degrees of seismic hazards in these zones, and a typical peak ground acceleration (PGA) value is assigned to each zone. Furthermore, some building codes, e.g., New York City building laws, have provisions only for wind design without any provisions for aseismic design. Concern has been raised as to whether or not a building designed only for a wind load is safe under potential seismic hazards.

In the present paper, therefore, a study is carried out in order to examine the structural integrity of low-rise buildings located in the New York City area and designed to resist, the lateral forces generated by wind and earthquake. In the design and analysis of these buildings, appropriate provisions of ANSI A58.1-1982, ACI Code 318-83 and ATC 3-06 are used. The structural integrity is measured in terms of the limit state probability. While, as is well known, the accuracy and interpretation of such a probability is still open to discussion, it is used to provide a quantitative measure for comparing the extent of the risk which the structure is subjected to under different natural hazards; wind and earthquake in the present case.

2. DESIGN OF SHEAR WALL STRUCTURE

The building selected for this study is a five-story office building supposedly located in New York City. Figure 1 shows a

* The contents of this paper are primarily taken from "Natural Hazard Mitigation in Low-Rise Buildings" by M. Shinozuka, H. Hwang and H. Ushiba, presented at the US-Korea Seminar on Critical Engineering Systems, Seoul, Korea, May 11-15, 1987.

typical floor plan and section of the building. A reinforced concrete frame system is used to resist vertical loads, i.e., dead and live loads. The two reinforced concrete shear walls in the north-south direction as shown in Fig. 1 are used to resist all the lateral forces due to wind or earthquake loads in that direction. This paper focuses on the design and safety assessment of these two shear walls. The details of the design of the five-story office bulding are shown in Hwang et al. [1987].

Four types of loads, i.e., dead, live, wind and earthquake loads are considered to act on the building. The values of these loads used in the design, i.e., the design loads, are specified according to the American National Standard, Minimum Design Loads for Buildings and Other Structures (ANSI A58.1-1982). The analysis of a frame system due to dead and live loads follows a conventional procedure.

2.1 Wind Analysis

The wind pressure q_z, specified by ANSI A58.1-1982 is:

$$q_z = 0.00256\, k_z (IV)^2 \tag{1}$$

where V is the basic wind speed at a reference height of 10 m for exposure C. From the map of basic wind speeds in ANSI A58.1-1982, V = 80 mph for New York City for a return period of 50 years. The importance factor I is chosen to be 1.05 (Category I at hurricane ocean line). The velocity pressure coefficient k_z is varied with the height.

The design wind pressure P_z is determined by the following formula:

$$P_z = q_z G_h C_{p(W)} - q_h G_h C_{p(L)} \tag{2}$$

where G_h is the gust response factor at a height of h ft and q_h the wind pressure for a leeward wall and roof evaluated at mean roof height. For exposure B at 70 ft, $G_h = 1.36$. $C_{p(W)}$ and $C_{p(L)}$ are the wall pressure coefficients for the windward and leeward walls, respectively. In this case, $C_{p(W)} = 0.8$ and $C_{p(L)} = -0.5$. The design wind pressure P_z is plotted in Fig. 2. For convenience of design, the design wind pressure is converted into a concentrated lateral load acting at each floor level. The shear force and overturning moments due to these concentrated lateral loads can be determined and are shown in Fig. 2.

2.2 Seismic Analysis

The design base shear Q due to an earthquake is computed in accordance with ANSI A58.1-1982 as:

$$Q = ZIKCSW \tag{3}$$

where Q = total shear force at the base, Z = zone factor, I = im-

portance factor, K = building system factor, C = numerical coefficient, S = soil factor and W = total dead load of the building.

New York City is located in seismic zone 2 according to the map for seismic zones in ANSI A58.1-1982. In this study, however, zone 1 is also used in the design of the shear wall in order to evaluate the effect of seismic zones on the safety of buildings. For seismic zones 1 and 2, Z is 3/16 and 3/8, respectively. The importance factor I and building system factor K are determined to be 1.0. The value of C is determined by $C = 1/(15\sqrt{T})$ in which T is the fundamental period of the building in seconds. For shear walls, T can be computed by the following formula: $T = 0.05h_n\sqrt{D}$ where h_n is the building height from the base and D is the dimension of the building in a direction parallel to the applied seismic forces. For the building under consideration, h_n = 77 ft and D = 75 ft. On the basis of these data, T is 0.4445 sec and C is equal to 0.10.

In ANSI A58.1-1982, three types of soil are defined and denoted as S_1, S_2 and S_3. In this study, all three types of soil are considered. Thus, the soil factor S is 1.0, 1.2 and 1.5 for S_1, S_2 and S_3, respectively. Furthermore, the ANSI A58.1-1982 also specifies that the product of C and S need not exceed 0.14. Hence, in this study, for the soil type of S_3, CS is taken as 0.14 instead of 0.15. The base shears under various combinations of aseismic zone and soil conditions are also computed and tabulated in Table 1. The base shear is distributed over the height of the structure in accordance with

$$F_x = \frac{(Q-F_t)W_x h_x}{\sum_{i=1}^{n} W_i h_i} \tag{4}$$

where F_x = lateral force applied at level x, F_t = additional concentrated lateral force at top of structure, h_x, h_i = height from base to levels x or i respectively, W_x, W_i = weight located or assigned to levels x or i respectively and N = number of stories. According to ANSI A58.1-1982, F_t may be considered as zero when T is 0.7 seconds or less. In this case, T = 0.45 sec., thus F_t = 0. Given the lateral force, the shear force and overturning moment at each floor level can be determined. For seismic zone 2 and three soil conditions, the shear force and overturning moment for each shear wall are shown in Fig. 3. For seismic zone 1, the shear force and moment are one-half those shown in Fig. 3.

2.3 Design of Shear Wall

The shear wall is designed according to ACI Code 318-83, where the following design formulas are specified by ACI Code 318-83 to be used:

$$1.4D + 1.7L \tag{5a}$$

$$\phi R_n \geq \begin{cases} 0.75(1.4D + 1.7L + 1.7W) & (5b) \\ 0.9D + 1.3\,W & (5c) \\ 0.75(1.4D + 1.7L + 1.87E) & (5d) \\ 0.9D + 1.43E & (5e) \end{cases}$$

where D = dead load effect, L = live load effect, W = load effect due to wind (not to be confused with the W used for dead weight in Eq. 3), E = load effect due to earthquake, ϕ = strength reduction factor and R_n = nominal capacity.

However, the shear wall in this study is designed for wind and earthquake (zone 2 or 1) separately in order to compare the safety of the shear wall with respect to these two different types of natural hazard.

For wind load, the shear wall is designed according to Eqs. 5b or 5c. Since it is assumed that the end columns resist vertical loads and overturning moments, Eqs. 5b or 5c become:

$$\phi V_n \geq 1.3Q_W \tag{6}$$

where V_n = nominal shear capacity of the shear wall and Q_W = design shear force at the bottom of the shear wall. From Fig. 2, Q_W = 81.05 kips, and hence, $1.3Q_W$ = 105.4 kips.

The nominal shear capacity V_n specified by ACI Code 318-83 is

$$V_n = V_c + V_s \tag{7}$$

where V_c and V_s are the shear strength provided by concrete and reinforcement, respectively;

$$V_c = 2\sqrt{f'_c}\,td \qquad V_s = \frac{A_v f_y d}{s_2} \tag{8}$$

where f'_c is the compressive strength of concrete (f'_c = 3000 psi for this study) and f_y is the yield strength of the reinforcement. For the #3 and #4 rebars considered here, f_y = 40,000 psi. A_v is the area of horizontal shear reinforcement within each vertical distance s_2. t is the thickness of the shear wall and d = 0.8 ℓ_w in which ℓ_w is the length of the shear wall. Assuming the wall thickness is 5" and end columns have 22" x 22" cross-sections, then, the shear strength provided by concrete is 121.8 kips. The minimum horizontal reinforcement ratio ρ_h required by ACI 318-1983 is 0.0025. For one layer of #3 rebars (A_v = 0.11 sq.in) with yield strength f_y = 40,000 psi, the maximum spacing of s_2, i.e., $s_{2,max}$ to meet this minimum reinforcement requirement is $s_{2,max} = A_v/(t\rho_h)$ = 8.8". Hence, $s_{2,max}$ = 8" is used in Eq. 8. This produces a shear strength equal to 122.3 kips provided by steel reinforcement. Therefore, the nominal shear capacity of the shear wall V_n is 244.1 kips. The strength reduction factor ϕ for shear is 0.85 as specified in the ACI code. Thus, ϕV_n = 207.5 kips which is larger than the factored design shear 105.4 kips.

The design of a shear wall to wind load is summarized in Table 2.

The design formula for earthquake load is given by Eqs. 5d and 5e. Similarly to Eq. 6, Eqs. 5d and 5e become:

$$\phi V_n \geq 1.43\ Q_E \tag{9}$$

where Q_E is the design shear force due to earthquake at the bottom of each shear wall. The shear capacity for resisting earthquake forces is provided in the same way as the design for wind loads. The results are also summarized in Table 2.

3. PROBABILISTIC CHARACTERISTICS OF STRUCTURAL CAPACITY AND LOADS

The nominal structural capacity (resistance) and design loads are specified in building codes by simplified formulas. In reality, both structural capacity and loads are random in nature and also involve modeling as well as parameter uncertainty. However, in the present study, it is assumed that key parameters of the design, structural capacity and loads can be treated as lognormally-distributed random variables whose variability represents a combination of randomness and uncertainty. These assumptions are made for the reason that the current study is a preliminary analysis which intends to demonstrate how design parameters, loading conditions and resistance estimations can be combined for the evaluation of the limit state probability. While other limit states such as deformation ductility and/or absorbed energy may have to be considered, the limit state considered here is that related to the base shear, primarily for simplicity of analysis.

A log-normal variable X can be described by its median value $\tilde{X}$ and standard deviation β_X of $\ell n\ X$. If the coefficient of variation (COV) is not very large, say, less than about 0.4, β_X is approximately equal to its COV value.

3.1 Structural Capacity

The structural capacity is affected by the variations of material strength, structural geometry and workmanship. Ellingwood and Hwang [1985] estimate that the median shear capacity of a shear wall $\tilde{Q}_R^*$ is about 1.70 times the nominal capacity V_n and the COV is 0.18. On the basis of these findings, the capacity of the shear wall is summarized in Table 3.

3.2 Base Shear Due to Wind

The probabilistic model for the wind pressure P* is assumed as:

$$P^* = 0.00256\ C_p^* K_z^* G_h^* (V^*)^2 \tag{10}$$

where V* is the wind speed at the reference height of 10 m. From an analysis of the observation data (1947-1977) at LaGuardia Air-

port in New York City, Simiu et al. [1979] estimate that the annual extreme mean wind speed follows a Type I extreme-value distribution with expected value equal to 50.25 mph and standard deviation equal to 7.23 mph (COV = 0.14). In this study, it is assumed that the median value $\tilde{V}^*$ is the same as the mean, i.e., 50.25 mph and $\beta_V = 0.14$.

The statistics of C_p^*, K_z^* and G_h^* are described by Ellingwood et al. [1980]. The median values of these factors, $\tilde{C}_p^*$, $\tilde{K}_z^*$ and $\tilde{G}_h^*$ are taken to be 1.0 times the design values. Thus, $\tilde{C}_p^* = 1.3$, $\tilde{G}_h^* = 1.36$ and $\tilde{K}_z^*$ varies with height. In addition, $\beta_{Cp} = 0.12$, $\beta_{Kz} = 0.16$ and $\beta_{Gh} = 0.11$ are adopted for the study following Ellingwood et al. [1980].

The base shear Q_W^* due to wind is a product of the wind pressure and the exposed area of the building. The dimensions of the building are assumed to be deterministic. Thus, the variation of the base shear is the same as that of the wind pressure. The median value and COV of the base shear are, respectively, $\tilde{Q}_W^* = 28.7$ kips and $\beta_{QW} = 0.36$ according to the computations made by Hwang et al. [1987].

3.3 Seismic Base Shear

The total seismic base shear Q_{ET}^* is determined by the following expression in ATC 3-06.

$$Q_{ET}^* = \frac{1.2\, S^* W^*}{R^* (T^*)^{2/3}} A^* \tag{11}$$

In Eq. 11, A* is the annual extreme peak ground acceleration (PGA). The annual extreme peak ground acceleration is asumed to distribute in accordance with the Type II extreme-value distribution (Ellingwood et al. [1980]);

$$F_{A^*}(a) = \exp\left[-\left(\frac{a}{\mu}\right)^{-\alpha}\right] \tag{12}$$

The parameters μ and α are assumed to be $\mu = 0.0135g$ and $\alpha = 3.14$ for the New York area on the basis of a study by Hwang et al. [1984]. Equation 12 gives a COV of A* equal to 0.6255 and $\tilde{A}^* = 0.01517$. A* is also assumed to be log-normally distributed with the same median $\tilde{A}^* = 0.01517$ and $\beta_A = 0.5746$ corresponding to COV = 0.6255. The seismic hazard curve is obtained by plotting $1 - F_{A^*}(a)$ as a function of a. W* is the weight of the structure. Ellingwood et al. [1980] recommended that β_W be 0.10 and the median of $\tilde{W}^*$ be 1.05 times the design value. $1.2/T^{*2/3}$ is a factor for linear dynamic response amplification. Based on the data collected by Haviland [1976], the median of the period $\tilde{T}^*$ is taken to be 0.91 times the computed value and β_T is 0.34. R* is the response modification factor. The median value $\tilde{R}^*$ is assumed to be 7.0 and β_R is 0.4. Finally, the median $\tilde{S}^*$ of the soil factor S* is taken to be the same as the design value, which depends on the soil type. β_S is assumed to be 0.3 for all soil conditions.

From Eq. 11 and the property of the lognormal variable, the median of the total seismic base shear $\tilde{Q}^*_{ET}$ is:

$$\tilde{Q}^*_{ET} = \frac{1.2\ \tilde{S}^*\tilde{W}^*}{\tilde{R}^*(\tilde{T}^*)^{2/3}}\ \tilde{A}^* \tag{13}$$

For each shear wall, the median of the seismic base shear, $\tilde{Q}^*_E$, is equal to one-half of $\tilde{Q}^*_{ET}$. For soil types S_1, S_2 and S_3, Q^*_E is 20.2 kips, 24.2 kips and 30.3 kips, respectively. Furthermore, β_{QE} and β_{QET} are the same and, under the assumed independence of the random variables involved, can be determined by:

$$\beta_{QE} = \beta_{QET} = \left[\beta_S^2 + \beta_W^2 + \beta_R^2 + \left(\frac{2}{3}\right)^2\beta_T^2 + \beta_A^2\right]^{1/2} \tag{14}$$

Thus, β_{QE} is equal to 0.80.

4. SAFETY EVALUATION

The limit state probability is used as a measure of the safety of the shear wall. The limit state probability under earthquake load $P_{f,E}$ can be defined as

$$P_{f,E} = P_r\left(\frac{Q^*_R}{Q^*_E} \leqq 1\right) \tag{15}$$

Since both Q^*_R and Q^*_E are lognormally distributed, Eq. 15 becomes

$$P_{f,E} = \Phi\left[\frac{-\ln\left(\tilde{Q}^*_R/\tilde{Q}^*_E\right)}{\left(\beta^2_{QR} + \beta^2_{QE}\right)^{1/2}}\right] \tag{16}$$

where Φ is the standardized normal distribution function. Similarly, the limit state probability under wind load, $P_{f,W}$ is:

$$P_{f,W} = \Phi\left[\frac{-\ln\left(\tilde{Q}^*_R/\tilde{Q}^*_W\right)}{\left(\beta^2_{QR} + \beta^2_{QW}\right)^{1/2}}\right] \tag{17}$$

Furthermore, disregarding the joint occurrence probability of earthquake and severe wind, the total limit state probability P_f is approximated by

$$P_f = P_{f,E} + P_{f,W} \tag{18}$$

These limit state probability values are summarized in Table 4.

5. DISCUSSION

The limit state probability values summarized in Table 4 may be used primarily for comparative purposes. For example, it is

clear from Table 4 that, for the type of building and limit state considered, the seismic hazard appears to be more serious than the hazard imposed by wind, even when a zone 2 design is implemented. This conclusion obviously depends on the accuracy and credibility of the various assumptions made in the present study. Some of the more important factors that influence the probability values and therefore require further study are delineated below. (For details, see Hwang et al. [1987].)

(a) Limit state; (b) Seismic hazard curve; (c) Details of local wind pressure distribution for low-rise buildings; (d) Local geological and topographical particulars; (e) Effect of soil conditions represented by S_1, S_2 and S_3; (f) Dynamic interaction of building with others in vicinity; (g) Log-normal assumption; (h) Use of Eqs. 10 and 11, which are primarily devised for design, for estimation of actual forces; (i) Assumption that building frames provide vertical resistance. Also, (j) effects of possible torsional vibration of building.

6. CONCLUSIONS

Low-rise buildings located in the New York City area are subjected to potential natural hazards due to wind and earthquake. This work presents the results of a preliminary study where the safety of a low-rise shear-wall type building is evaluated in terms of the limit state probability. The limit state probability values are computed under various seismic and wind design conditions. The results indicate that the seismic hazard can by no means be disregarded for the type of building structure designed under the particular seismic hazard curve and annual extreme wind speed distribution assumed for the analysis. More importantly, the paper demonstrates how knowledge of different scientific and engineering disciplines can improve the various underlying assumptions in order to arrive at a more reliable safety evaluation. Similar results were also obtained for flat-slab structures by Hwang et al. [1987].

7. ACKNOWLEDGEMENT

This work was supported by Sub-contract Nos. SUNYRF-NCEER-86-3031 and 86-3033 under the auspices of the National Center for Earthquake Engineering Research under NSF Grant No. ECE-86-07591.

REFERENCES

American Concrete Institute, Building code requirements for reinforced concrete, ACI 318-83, Detroit, Michigan, 1983.

American National Standard Institute, Minimum design loads for buildings and other structures, ANSI A58.1-1982, New York, 1982.

Applied Technology Council, Tentative provisions for the development of seismic regulations for buildings, ATC3-06, Special Publication NBS SP 510, National Bureau of Standards, Washington, DC, 1978.

Ellingwood, B. and H. Hwang, "Probabilistic descriptions of re-

sistance of safety-related structures in nuclear plants," Nuclear Engineering and Design, Vol. 88, pp. 169-178, 1985.
Ellingwood, B. et al., Development of probability-based load criterion for american national standard A58, Special Publication NBS SP 577, National Bureau of Standards, Washington, DC, 1980.
Haviland, R., "A study of the uncertainties in the fundamental translational periods and damping values for real building," M.I.T., Cambridge, Massachusetts, 1976.
Hwang, H. et al., "Reliability assessment of Indian Point Unit 3 containment structure under combined loads," Structural Engineering in Nuclear Facilities, ASCE, Vol. 1, 1984, pp. 274-293.
Hwang, H. et al., "Assessment of code-designed structures under natural hazards," to be published as a National Center for Earthquake Engineering Research report, 1987.
International Conference of Building Officials, Uniform building codes, Whittier, California, 1982.
Simiu, E. et al., Extreme wind speeds at 129 stations in the contiguous United States, Building Science Series NBS BS 118, National Bureau of Standards, Washington, DC, 1979.
Southern Building Code Congress International, Standard building code, Birmingham, Alabama, 1985.

Table1 Seismic Base Shear

Earthquake	Seismic Zone	Soil Type	Total Base Shear *(kips)*
E - 2 - S_1	2	S_1	308.4
E - 2 - S_2	2	S_2	370.1
E - 2 - S_3	2	S_3	431.8
E - 1 - S_1	1	S_1	154.2
E - 1 - S_2	1	S_2	185.1
E - 1 - S_3	1	S_3	215.9

Table 2 Design of Shear Wall

Case	Loading	Wall Thickness (in)	Horizontal Reinforcement at bottom	Vc (kips)	Vs (kips)	$Vn = Vc + Vs$	ϕVn	$1.43Q_E$ or $1.3Q_W$
1	$E-2-S_1$	5	#3@7in	121.8	139.8	261.6	222.4	219.4
2	$E-2-S_2$	5	#3@5in	121.8	195.7	317.5	269.9	263.4
3	$E-2-S_3$	5	#4@7in	121.8	254.2	376.0	319.6	307.2
4	$E-1-S_1$	5	#3@8in*	121.8	122.3	244.1	207.5	109.7
5	$E-1-S_2$	5	#3@8in*	121.8	122.3	244.1	207.5	131.7
6	$E-1-S_3$	5	#3@8in*	121.8	122.3	244.1	207.5	153.6
7	Wind	5	#3@8in*	121.8	122.3	244.1	207.5	105.4

* Minimum reinforcement required by ACI 318-83.

Table 3 Distribution of Shear Wall Resistance

Case	Wall Thickness (in)	Horizontal Reinforcement at Bottom	V_n (kips)	$\tilde{Q}_R^* = 1.7V_n$ (kips)	β_{QR}	Distribution
1	5	#3@7in	261.6	444.7		
2	5	#3@5in	317.5	539.8		
3	5	#4@7in	376.0	639.2		
4	5	#3@8in	244.1	415.0	0.18	Lognormal
5	5	#3@8in	244.1	415.0		
6	5	#3@8in	244.1	415.0		
7	5	#3@8in	244.1	415.0		

Table 4 Annual Limit State Probability

Case	$P_{f,E}$	$P_{f,W}$	P_f
1	8.2×10^{-5}	3.9×10^{-12}	8.2×10^{-5}
2	7.5×10^{-5}	1.4×10^{-13}	7.5×10^{-5}
3	1.0×10^{-4}	5.0×10^{-15}	1.0×10^{-4}
4	1.1×10^{-4}	1.1×10^{-11}	1.1×10^{-4}
5	2.6×10^{-4}	1.1×10^{-11}	2.6×10^{-4}
6	7.1×10^{-4}	1.1×10^{-11}	7.1×10^{-4}
7		1.1×10^{-11}	

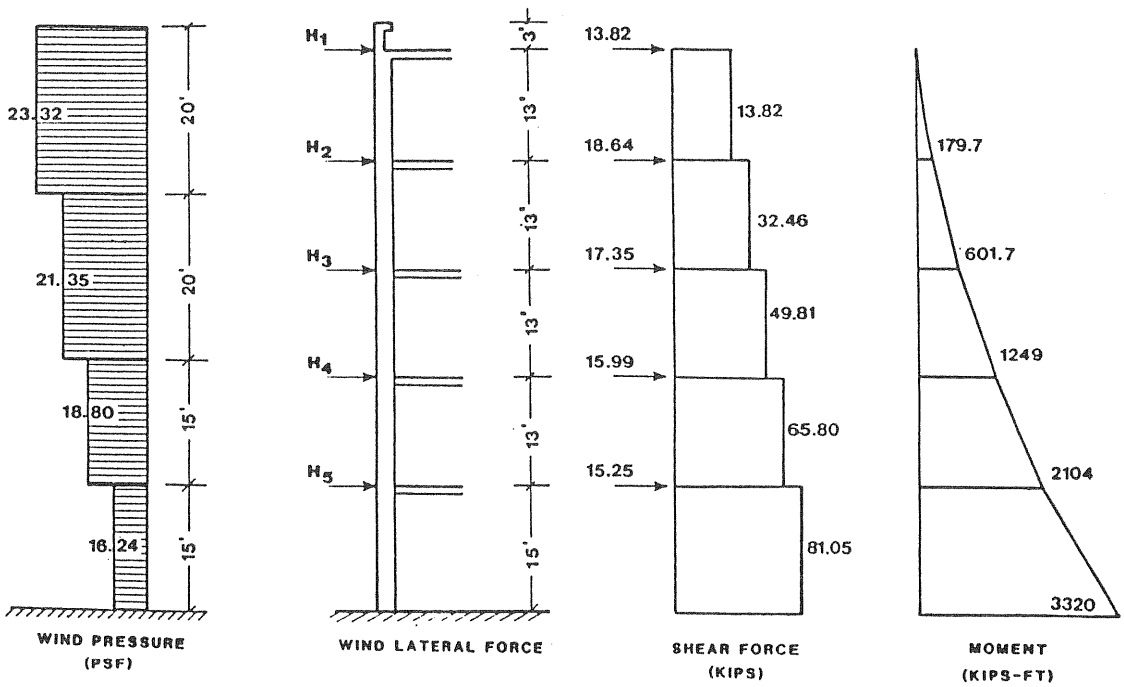

Fig. 2 Wind Pressure and Forces

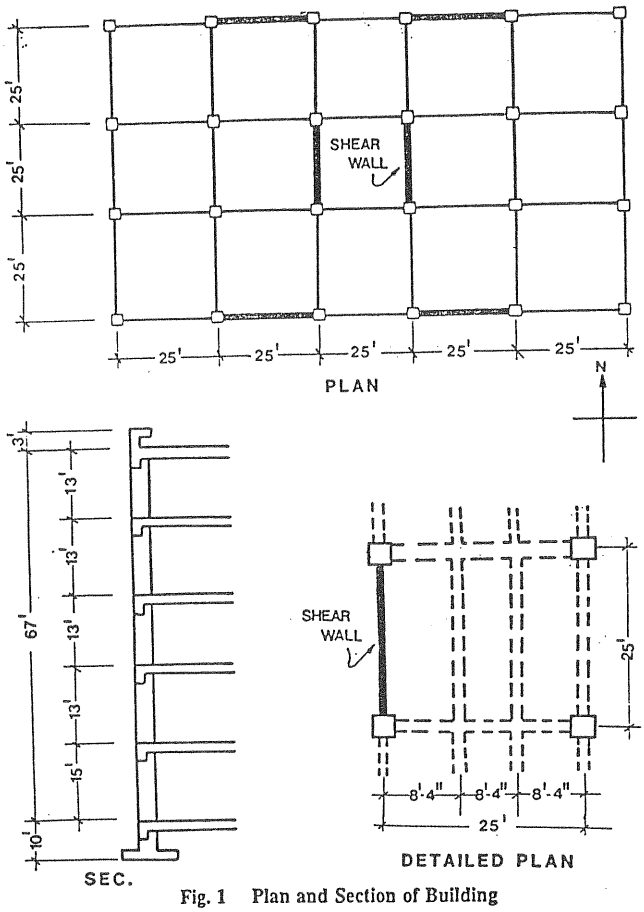

Fig. 1 Plan and Section of Building

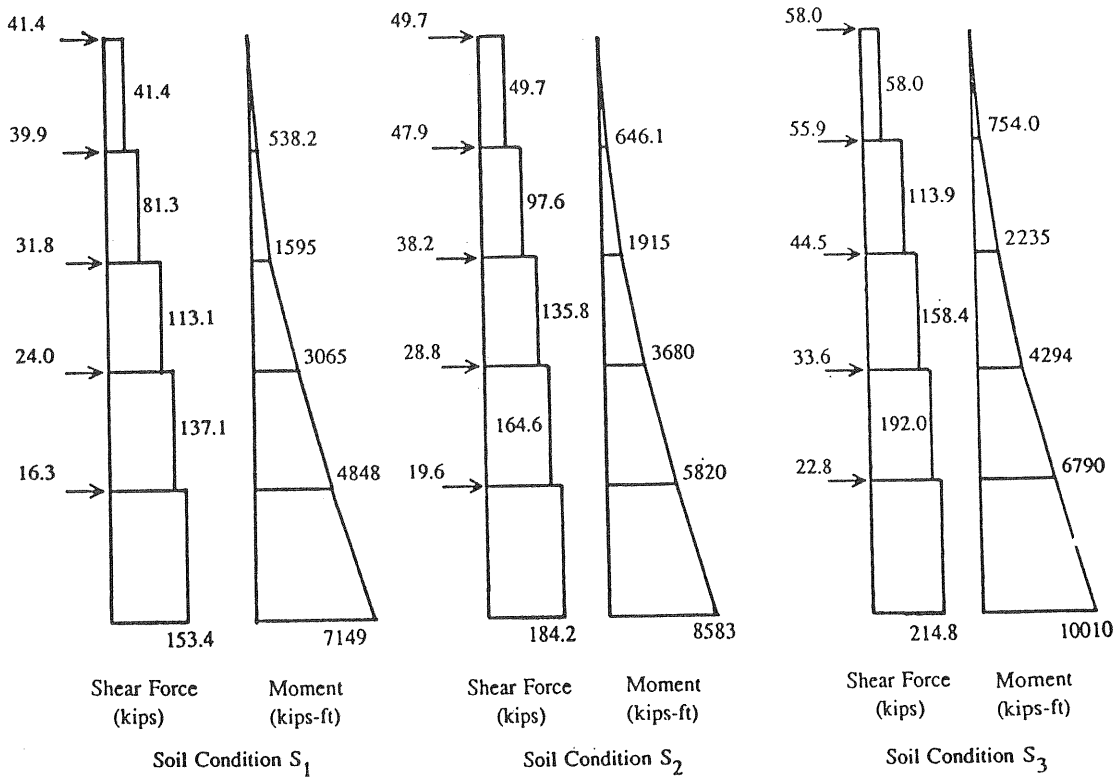

Fig. 3 Seismic Forces (Seismic Zone 2)

APPROXIMATION OF EARTHQUAKE LOSSES FOR A MAJOR EARTHQUAKE NEAR A LARGE EASTERN U.S. URBAN CENTER: PRELIMINARY RESULTS

Charles Scawthorn

EQE, Inc.
San Francisco CA 94105

While it has long been recognized that there exists the possibility of a moderate or even large earthquake in many areas of the eastern United States, the potential damage that might ensue from such an event has generally not been considered in many of these areas. An area of especial interest is the New York City area (NYC), due to its large size and global importance, and its general lack of seismic design. While the NYC metropolitan area is generally considered a low seismicity area (eg, UBC zone 1), earthquakes are not unknown in this area, and MMI VII have been observed in historical times (eg, the 18 December 1737 event, which caused chimneys to fall in NYC).

This paper reports preliminary results of work in progress to estimate the potential losses and building collapse were a moderate earthquake to occur in or near the center of the NYC metrolpolitan region. There are several steps involved in seismic damage estimation, including the determination of the seismic hazard, the estimation of the structures or building inventory at risk, and the estimation of the vulnerability of these structures to various levels of seismic shaking.

Building inventory for NYC has been estimated by Jones et al. Table 2 presents findings of that investigation, wherein numbers of buildings in Manhattan are cross-tabulated by height (number of stories) and total floor area. If a conservative value of $50 of a square foot of construction is employed, it can be seen that the building stock of Manhattan (as of 1972) is approximately valued at $136 billion. Information is presently at this time regarding detailed structural characteristics of this inventory, and has been estimated by the author based on his experience, Table 1. Using this breakdown and the data in Table 2, numbers of buildings by height and size can be estimated for each gross structural category, presented in Tables 2W (wood), 2RC (reinforced concrete), 2S (steel), 2RM (reinforced masonry) and 2URM (unreinforced masonry).

Very little experience exists and little investigation has been performed into the structural vulnerability of US non-California construction. The most extensive broad compilation to date of California construction seismic vulnerability is the recent investigation by the Applied Technology Council (ATC-13), which provides mean damage estimates and distributions thereon, for various types of construction

and levels of Modified Mercalli Intensity (MMI). Recently, an investigation into extending the ATC-13 data into regions of the U.S. beyond California has indicated that NYC construction seismic vulnerability may be very approximately estimated by increasing the mean damage levels of ATC-13 by about 60% (this is a preliminary result, to be confirmed).

Employing the building inventory of Tables 2 and the mean damage levels arrived at by adapting the ATC-13 data to NYC construction, by increasing mean damage levels by about 60%, mean NYC damage levels can be approximated, and are indicated in Tables 3. Also indicated therein are mean estimates of shaking only losses for Manhattan, were the structures thereon to be submitted to an average MMI VI or VII level of shaking. Examining MMI VI, we see that damage would break down approximately as follows:
«IPO,0»

SUMMARY SHAKING ONLY LOSSES FOR MANHATTAN GIVEN MMI VI
(Preliminary)

Construction	Damage ($ millions)
Wood	2
Steel	790
Reinf. Concrete	518
Reinf. Masonry	123
Unreinf. Masonry	295
TOTAL	$1,728

The total shaking loss of about $1.73 billion represents approximately 1.2% of the building value in Manhattan. The relatively high loss to steel construction relative to reinforced concrete construction is due to the fact that herein a high fraction of the building stock was assumed to be of steel. This derives from the fact that relatively few high-rise buildings in Manhattan are of concrete (herein, all buildings greater than 10 stories were assumed to be of steel, which almost certainly neglects some high-rise concrete buildings) and that the 11 and greater story height building category representes perhaps 40% of the value in Manhattan.

FUTURE WORK

This is the first report of work in progress. Seismic sources, soil distribution/microzonation, better approximation of the building inventory, and improved estimation of the building seismic vulnerability are all aspects which are necessary elements of a seismic damage estimation for the NYC metropolitan region. This data is presently being gathered and will be incorporated in a seismic damage estimation, to be reported on.

REFERENCES

ATC-13 (1985) Earthquake Damage Evaluation Data for California, C. Rojahn, Principal Investigator, Redwood City, CA.

Jones, B. et al (1976), The Estimation of Building Stocks and their Characteristics in Urban Areas, Cornell University, Ithaca, NY

TABLE 1: BUILDING STRUCTURE DOMINANT MATERIAL (Fraction, by Height)

(Estimated, for Manhattan)

Height (stories)	<-------- TOTAL --------> %WOOD	% RC	% STL	% RM	% URM	<-------- RESID. ------> %WOOD	% RC	% STL	% RM	% URM	<--- NON-RESID. ------> %WOOD	% RC	% STL	% RM	% URM
0															
1	0.00	0.50			0.50	0.1				0.9		0.5			0.5
2	0.10	0.39			0.51	0.1				0.9	0.1	0.4			0.5
3		0.25	0.07	0.15	0.53		0.1			0.9		0.3	0.1	0.2	0.4
4		0.15	0.02	0.12	0.70		0.1		0.1	0.8		0.3	0.1	0.2	0.4
5		0.15	0.05	0.12	0.68		0.1		0.1	0.8		0.3	0.2	0.2	0.3
6		0.10	0.06	0.12	0.72		0.1		0.1	0.8		0.1	0.4	0.2	0.3
7		0.22	0.24	0.20	0.34		0.2	0.2	0.2	0.4		0.3	0.4	0.2	0.1
8		0.31	0.31	0.34	0.05		0.2	0.2	0.5	0.1		0.4	0.4	0.2	
9		0.35	0.40	0.25			0.2	0.4	0.4			0.4	0.4	0.2	
10		0.35	0.50	0.15			0.3	0.5	0.2			0.4	0.5	0.1	
11-15		0.44	0.50	0.06			0.3	0.5	0.2			0.5	0.5		
16-20		0.40	0.55	0.05			0.4	0.5	0.1			0.4	0.6		
21-40		0.20	0.80				0.2	0.8				0.2	0.8		
41-60		0.09	0.91					1				0.1	0.9		
60+			1.00					1					1		
			1.00					1					1		

TABLE 2: MANHATTAN BUILDING INVENTORY (as of 1972)

TOTAL (RESIDENTIAL AND NON-RESIDENTIAL; ALL MATERIALS)

Height (stories)	<---------- FLOOR AREA (thous sq ft) ----------												
	0-1	2	4	6	10	15	25	50	100	500	1000	1000+	SUM
					NO. BLDGS								
0	329	261	986	147	361	133	38	13	16	17	6	4	2311
1	525	507	616	332	270	106	62	32	17	15		2	2484
2	178	534	560	360	341	172	208	111	40	24	2	1	2531
3	33	951	5216	549	386	193	176	122	57	38	1	2	7724
4	5	86	3986	3166	1358	303	252	174	79	57	2	2	9470
5		5	349	2675	6227	4092	1342	562	139	66	2	1	15460
6		1	22	57	440	1630	1850	1308	517	117	6	1	5949
7			2	4	47	191	241	313	122	52	3		975
8			1	1	4	37	55	166	94	51	3	3	415
9					1	4	46	200	141	48	4	2	446
10						3	27	97	124	79	4	2	336
11-15						3	42	354	844	860	56	17	2176
16-20						1	1	40	222	725	53	12	1054
21-40									1	4	10	2	17
41-60									3	60	30	42	135
60+										5		6	11
SUM	1070	2345	11738	7291	9435	6868	4340	3492	4634	2400	281	99	51494

(from Jones et al, 1976, Estim. of Bldg. Stocks and their Characteristics in Urban Areas, Cornell Univ., 1976)

TABLE 2S: MANHATTAN BUILDING INVENTORY (cont.)

(as of 1972, after Jones et al)

STEEL (RESIDENTIAL AND NON-RESIDENTIAL; ALL MATERIALS)

Height (stories)	<---------- FLOOR AREA (thous sq ft) ---------->												% STEEL
	0-1	2	4	6	10	15	25	50	100	500	1000	1000+	
	NO. BLDGS											SUM	
0													
1													
2	13	40	41	27	25	13	15	8	3	2		187	0.07
3	1	23	126	13	9	5	4	3	1	1		186	0.02
4		4	184	146	63	14	12	8	4	3		438	0.05
5			22	169	392	258	85	35	9	4		974	0.06
6			5	14	107	395	449	317	125	28	1	1441	0.24
7			1	1	14	59	74	96	37	16	1	299	0.31
8					2	15	22	66	38	20	1	1 165	0.40
9					1	2	23	100	71	24	2	1 224	0.50
10						2	14	49	62	40	2	1 170	0.50
11-15						2	23	194	462	470	31	9 1191	0.55
16-20						1	1	32	178	580	42	10 844	0.80
21-40									1	4	9	2 16	0.91
41-60									3	60	30	42 135	1.00
60+										5		6 11	1.00
SUM	14	67	379	370	613	766	722	908	994	1257	119	72 6281	

TABLE 2RC: MANHATTAN BUILDING INVENTORY (cont.)

(as of 1972, after Jones et al)

REINF. CONC. (RESIDENTIAL AND NON-RESIDENTIAL; ALL MATERIALS)

Height (stories)	<---------- FLOOR AREA (thous sq ft) ----------> 0-1	2	4	6	10	15	25	50	100	500	1000	1000+	SUM	% RC
					NO. BLDGS									
0	164	130	492	73	180	66	19	6	8	8	3	2	1151	0.50
1	203	196	238	128	104	41	24	12	7	6		1	960	0.39
2	44	132	139	89	85	43	52	28	10	6			628	0.25
3	5	141	773	81	57	29	26	18	8	6			1144	0.15
4	1	13	583	463	199	44	37	25	12	8			1385	0.15
5		1	35	268	623	409	134	56	14	7			1547	0.10
6			5	13	97	361	409	289	114	26	1		1315	0.22
7			1	1	14	59	74	96	37	16	1		299	0.31
8					1	13	19	58	33	18	1	1	144	0.35
9						1	16	69	49	17	1	1	154	0.35
10						1	12	42	54	35	2	1	147	0.44
11-15						1	17	142	338	344	22	7	871	0.40
16-20								8	44	145	11	2	210	0.20
21-40											1		1	0.09
41-60														
60+														
SUM	417	613	2266	1116	1360	1068	839	849	728	642	43	15	9956	

TABLE 2URM: MANHATTAN BUILDING INVENTORY (cont.)

(as of 1972, after Jones et al)

UNREINF. MASONRY (RESIDENTIAL AND NON-RESIDENTIAL; ALL MATERIALS)

Height (stories)	<-- FLOOR AREA (thous sq ft) --> 0-1	2	4	6	10	15	25	50	100	500	1000	1000+	SUM	% URM
					NO. BLDGS									
0	165	131	494	74	181	67	19	7	8	9	3	2	1160	0.50
1	269	260	316	170	139	54	32	16	9	8		1	1274	0.51
2	94	283	297	191	181	91	110	59	21	13	1	1	1342	0.53
3	23	669	3669	386	272	136	124	86	40	27	1	1	5434	0.70
4	3	59	2728	2167	930	207	172	119	54	39	1	1	6480	0.68
5		4	252	1929	4491	2951	968	405	100	48	1	1	11150	0.72
6			7	19	148	548	622	440	174	39	2		1999	0.34
7					2	9	11	15	6	2			45	0.05
8														
9														
10														
11-15														
16-20														
21-40														
41-60														
60+														
SUM	554	1406	7763	4936	6344	4063	2058	1147	412	185	9	7	28884	

TABLE 2RM: MANHATTAN BUILDING INVENTORY (cont.)

(as of 1972, after Jones et al)

REINF. MASONRY (RESIDENTIAL AND NON-RESIDENTIAL; ALL MATERIALS)

Height (stories)	<-- FLOOR AREA (thous sq ft) --> 0-1	2	4	6	10	15	25	50	100	500	1000	1000+	SUM	% RM
					NO. BLDGS									
0														
1														
2	26	79	83	53	50	25	31	16	6	4			373	0.15
3	4	118	647	68	48	24	22	15	7	5			958	0.12
4	1	11	491	390	167	37	31	21	10	7			1166	0.12
5		1	40	310	721	474	155	65	16	8			1790	0.12
6			4	11	88	326	370	262	103	23	1		1188	0.20
7			1	1	16	65	82	106	41	18	1		331	0.34
8					1	9	14	41	23	13	1	1	103	0.25
9						1	7	31	22	7	1		69	0.15
10							2	6	8	5			21	0.06
11-15							2	19	45	46	3	1	116	0.05
16-20														
21-40														
41-60														
60+														
SUM	31	209	1266	833	1091	961	716	582	281	136	7	2	6115	

TABLE 2W: MANHATTAN BUILDING INVENTORY (cont.)

(as of 1972, after Jones et al)

WOOD (RESIDENTIAL AND NON-RESIDENTIAL; ALL MATERIALS)

Height (stories)	<---------- FLOOR AREA (thous sq ft) ---------->												% WOOD
	0-1	2	4	6	10	15	25	50	100	500	1000	1000+	
	NO. BLDGS											SUM	
0													0.00
1	53	51	62	33	27	11	6	3	2	2		250	0.10
2													
3													
4													
5													
6													
7													
8													
9													
10													
11-15													
16-20													
21-40													
41-60													
60+													
SUM	53	51	62	33	27	11	6	3	2	2		250	

TABLE 3RC: ESTIMATED DAMAGE IN MANHATTAN, GIVEN MMI VI OR VII
(Preliminary, $ millions)

RC	<-- MMI VI -->		<---- MMI VII ---->	
	DAMAGE		DAMAGE	
	%	$mills	%	$mills
Height (stories)				
0	0.008	7	0.047	43
1	0.008	4	0.047	26
2	0.008	4	0.047	23
3	0.008	4	0.047	24
4	0.008	6	0.047	36
5	0.017	21	0.062	78
6	0.017	48	0.062	175
7	0.017	17	0.062	63
8	0.017	16	0.062	59
9	0.017	17	0.062	63
10	0.02	29	0.093	136
11-15	0.02	249	0.093	1159
16-20	0.02	92	0.093	429
21-40	0.02	1	0.093	5
41-60	0.02	0	0.093	0
60+	0.02	0	0.093	0
SUM		518		2317

TABLE 3S: ESTIMATED DAMAGE IN MANHATTAN, GIVEN MMI VI OR VII
(Preliminary, $ millions)

STL	<-- MMI VI -->		<---- MMI VII ---->	
	DAMAGE		DAMAGE	
	%	$mills	%	$mills
Height (stories)				
0	0.01	0	0.03	0
1	0.01	0	0.03	0
2	0.01	1	0.03	4
3	0.01	1	0.03	2
4	0.01	3	0.03	8
5	0.013	10	0.097	76
6	0.013	40	0.097	299
7	0.013	13	0.097	99
8	0.013	14	0.097	101
9	0.013	19	0.097	139
10	0.015	25	0.09	149
11-15	0.015	255	0.09	1532
16-20	0.015	279	0.09	1671
21-40	0.015	11	0.09	68
41-60	0.015	108	0.09	649
60+	0.015	11	0.09	65
SUM		790		4864

TABLE 3RM: ESTIMATED DAMAGE IN MANHATTAN, GIVEN MMI VI OR VII
(Preliminary, $ millions)

RM	<-- MMI VI --> DAMAGE %	$mills	<---- MMI VII ----> DAMAGE %	$mills
Height (stories)				
0	0.013	0	0.048	0
1	0.013	0	0.048	0
2	0.013	4	0.048	14
3	0.013	6	0.048	21
4	0.013	8	0.048	31
5	0.013	19	0.048	70
6	0.013	33	0.048	122
7	0.013	15	0.048	54
8	0.013	9	0.048	34
9	0.013	5	0.048	20
10	0.013	2	0.048	9
11-15	0.013	22	0.048	80
16-20	0.013	0	0.048	0
21-40	0.013	0	0.048	0
41-60	0.013	0	0.048	0
60+	0.013	0	0.048	0
SUM		123		456

TABLE 3URM: ESTIMATED DAMAGE IN MANHATTAN, GIVEN MMI VI OR VII
(Preliminary, $ millions)

URM	<-- MMI VI --> DAMAGE %	$mills	<---- MMI VII ----> DAMAGE %	$mills
Height (stories)				
0	0.013	12	0.048	45
1	0.013	9	0.048	33
2	0.013	15	0.048	56
3	0.013	33	0.048	122
4	0.013	48	0.048	179
5	0.013	119	0.048	440
6	0.013	56	0.048	207
7	0.013	2	0.048	7
8	0.013	0	0.048	0
9	0.013	0	0.048	0
10	0.013	0	0.048	0
11-15	0.013	0	0.048	0
16-20	0.013	0	0.048	0
21-40	0.013	0	0.048	0
41-60	0.013	0	0.048	0
60+	0.013	0	0.048	0
SUM		295		1089

THOUGHTS RE SEISMIC BUILDING CODE REQUIREMENTS FOR ENAM

Robert V. Whitman
Massachusetts Institute of Technology
Cambridge, Massachusetts 02139

INTRODUCTION

Along with many other engineers, I tend to regard the seismic provisions of building codes as the nation's first line of defense against the losses and suffering caused by large earthquakes.

Knowing the seismicity of an area, or how to perform dynamic analyses of buildings, certainly is important. However, this knowledge is of no avail unless it is put to use in design. Being able to predict an earthquake reliably, as to place, size and time, has the potential for saving life and limb (but perhaps not property damage and general disruption), but I believe it will be a considerable time before this potential is realized. Rescue and recovery operations save some lives and mitigate suffering, but earthquake-caused damage is a classic case of "...an ounce of prevention is worth [at least!] a pound of cure." This leaves, as the primary strategy for earthquake hazards mitigation, striving for safe buildings, structures and facilities - which at least seems to get us back to building codes.

At the same time, there are difficulties with the "building code approach". There are at least three troublesome points.

First, building codes do not ensure a safe building. Codes are imperfect; it is impossible to cover all situations. Provisions can be honestly misinterpreted. There are also engineers who, often at the urging of their clients, are adept at finding loopholes in the provisions of codes. It can be argued that codes are useless unless there is careful plans checking and review of calculations. While there is a point here, the conclusion is too extreme. It can also be argued that the knowledge and professionalism that come from education and experience are more important than the words in a code. While this too is a valid point, codes are the legal means for expressing the intent of governments in their function of protecting public safety - and thus it is essential that such codes be as clear and thorough as possible.

Second, the fine efforts to write seismic provisions in model codes are for naught unless the codes are adopted by states and cities (or by the Federal government in the case of

its own buildings). Most states within Eastern North America (ENAM) have either neglected to, or chosen not to, require seismic design in their building codes. (Some states have no structural building code requirement, and - despite nearly a decade of effort - the Federal government has not yet required attention to seismic design in all its buildings!) The pertinent question here is: To what extent is this because of ignorance or political expediency, or owing to a concern that the available recommended provisions in model codes are unreasonable or confusing? If the latter reason is a factor, it is of concern to us.

Third, seismic code provisions are aimed primarily at new construction. In principle they are applicable also when an existing building undergoes major renovation or addition or perhaps even change of occupancy. However, in Massachusetts at least, this requirement is almost automatically waived - on the basis that it is unreasonable to require an old building to be brought "up to code". Here is a problem that is, to a major extent, the result of a deficiency in our codes.

It is potentially possible for us to do something about the problems identified at the end of the previous two paragraphs, and the comments that follow are aimed at these points.

SHOULD THERE BE A MODEL CODE?

In several forums during 1986 (e.g. Ref. 5), I argued that there should be a single nationally-recognized set of model seismic design requirements. My thesis was that the country and the profession are not well-served by having different language in the model codes issued by the International Conference of Building Officials (ICBO) who have the Uniform Building Code (UBC), the Building Officials Conference of America (BOCA), the American National Standards Institute (ANSI), the Building Seismic Safety Council (BSSC) - plus others as well. I felt this breeded confusion, which the special interests opposing adoption of seismic requirements could exploit.

At my suggestion, the topic of having such a single nationally-recognized provision were the focus of a seminar in connection with the 1987 Annual Meeting of the Earthquake Engineering Research Institute (EERI). The lively discussion at that seminar confirmed my feeling that the California-based (or at least California-influenced) engineers who have constructed the existing codes really don't understand the earthquake problem in ENAM, and that many engineers from ENAM are not satisfied that the existing codes are reasonable for their needs.

In the end, the seminar caused me to alter my thinking. I still feel that it would be desirable to have only one set

of model code language for any one region of the country. However, I now feel that it may be best to have one such set of provisions for the most seismic parts of the country and a second set for the less seismic regions. In effect, I now question whether the strategy embodied in the California-originated code is the correct strategy for ENAM - and I suggest that it is time to rethink the strategy applicable to ENAM.

What I mean by strategy is illustrated by asking the question: What level of earthquake should be used as a basis for design? Another question in the same vein is: Is there an alternative to requiring that buildings be designed for specific earthquake forces? As will be discussed in the sections that follow, certain such strategies are implicit in the California-originated codes - and it is possible that these particular strategies inhibit the development of sound and acceptable practice in ENAM.

There is a question as to whether the division into ENAM and "Western-NAM" may be too simplistic. Perhaps the disinction should be between regions now zoned 3 and 4 vs. those designated as 0, 1, and 2. Such technicalities can be sorted out later. What I urge is that engineers and researchers from the less seismic regions look afresh at the strategies for seismic design requirements most suitable to these areas. Ideally, some day - after this new thinking has been carried to fruition - the requirements found appropriate for ENAM can be merged together with those for more seismic areas, back into a single nationally-recognized code.

WHAT LEVEL(S) OF EARTHQUAKE SHOULD BE USED FOR DESIGN?

The thinking in earthquake engineering for some time, as applied to most buildings, is that:

* There should be little or no yielding during an earthquake that can reasonably be expected during the life of the building.

* There may be yielding should an extremely large earthquake occur, but the building must remain stable once the earthquake ceases and there should not be life-threatening damage.

These are sound principles, and I have no quarrel with them. The difficulties arise when trying to define these two events, especially the "extremely large earthquake", more precisely.

While this thinking is behind the codes developed in California, the California-originated codes do not explicitly refer to two different design earthquakes. Rather a single set of lateral forces is prescribed together with requirements

upon detailing often referred to as ductility requirements. Experienced engineers in California believe that well-executed designs based upon these codes will meet the criteria stated above.

From time to time there have been explicit attempts to establish the principle of "two level design". The most notable such effort was an early study by the Applied Technology Council (ATC) in Ref. (2). I do not recall exactly how the two levels of ground shaking were defined, but the "extremely large earthquake" was the largest event thought possible in a region - what is often imprecisely called the "maximum credible earthquake". For the several regions of California considered in the ATC study, the two levels of ground shaking were not very different. While I do not remember the actual numbers, the ratio of peak accelerations used to charaterize the two events was typically 4:5. This means that in California there is a significant likelihood that the "maximum credible event" may occur during the life of a building.

This appraisal contrasts with the situation in most of ENAM. For example, in Boston the earthquake with a 50% probability of occurring during 100 years has an effective peak acceleration (EPA) of about 0.05g. By contrast, EPA's of 0.25g to 0.3g or even greater are suggested as the safe-shut-down earthquake for nuclear plants in the vicinity. This is a ratio of 1:5 to 1:6.

The contrast is represented graphically in Fig. 1, which was originally prepared for the ATC-3 study (3) and is repeated in the NEHRP recommended provisions. In this figure, the 0.4 contour represents the situation in California, while the 0.05 or 0.1 contours characterize much of ENAM. All this implies that:

* If the California-originated codes strike the proper balance for both levels of earthquake shaking,

* And if a building designed for the 0.1 contour in ENAM has the same margin of safety against an extremely large event as a building designed for the 0.4 contour in WNAM,

* Then the ENAM building may collapse during an extremely large event.

As will be discussed subsequently, this reasoning may be too simplistic, but it neatly illustrates the dilemma faced in transferring California-based strategies to ENAM.

Indeed, California engineers have frequently criticized use of probabilistic risk analysis for selection of design events in ENAM, saying that all buildings everywhere should be

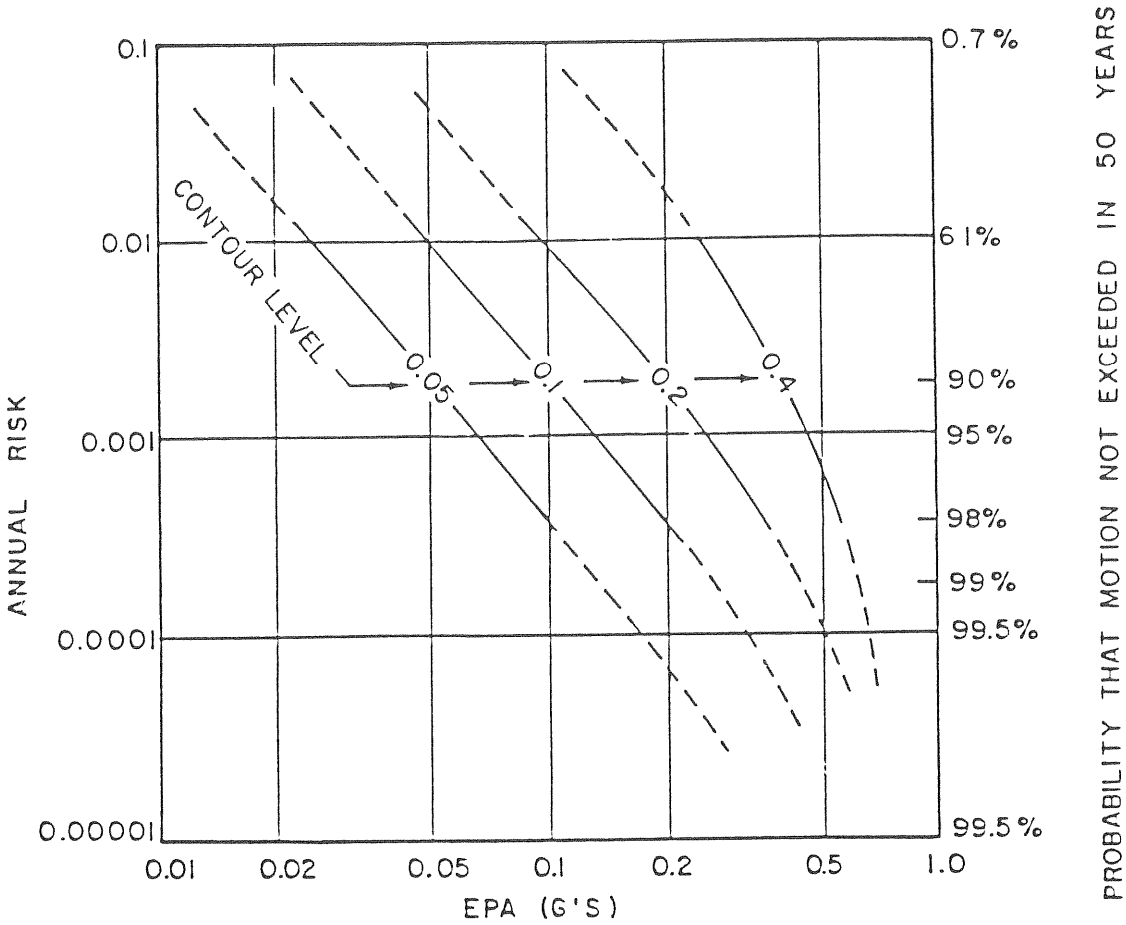

Figure 1. Annual risk of exceeding various levels of effective peak acceleration (EPA) for areas where the EPA with a mean recurrence interval is 500 years. (3)

able to come through the "maximum credible event", appropriate to the location of the building, without major structural failure. Aside from the problem of defining and pinning down "maximum credible events" within ENAM, any such event would certainly be larger than engineers and politicians in ENAM would consider reasonable as a basis for design.

Possible Strategies for ENAM

I do not have the answer as to what strategy should be followed in code provisions for ENAM, but I would like to suggest some possible alternates as a basis for discussion. First it is necessary, partially for the sake of brevity, to define some terms and symbols:

E_{mc}: The "maximum credible earthquake". To focus our thinking, I will arbitrarily assign a mean recurrence interval of 10,000 years to such an event. Hence $E_{mc}=E_{10,000}$.

E_{re}: The earthquake reasonably expected during the lifetime of a building. I will arbitrarily assign a mean recurrence interval of 100 years (E_{100}) to this event.

E_{md}: The maximum design earthquake. This is the earthquake for which we do not want buildings to suffer life-threatening structural (or non-structural) failures. The mean recurrence interval for this event is yet to be determined, but values such as 500 (E_{500}) to 2000 (E_{2000}) years have been suggested.

E_{ty}: The earthquake that brings a building to the threshold of yielding.

E_{tc}: The earthquake that brings a building to the threshold of collapse.

E_{mc} and E_{re} reflect the seismic hazard for an area, while E_{ty} and E_{tc} are characteristics of buildings. E_{md} is a choice to be made in writing a code.

Now some possible strategies may be defined. Fig. 1, with emphasis on the contours labelled 0.05 and 0.1, is the basis for the acceleration levels quoted in the following paragraphs.

Design not to collapse with E_{mc}: This strategy is characterized by $E_{tc}=E_{mc}$. This would be the most conservative possible design strategy. Effective peak accelerations might be on the order of 0.2 to 0.4g (and possibly higher in areas such as the New Madrid and Charleston areas). This would be a more severe criterion than currenly envisioned in, for example, the NEHRP-recommended provisions. If we think that

our lateral force and detailing requirements are such that $E_{tc}=4E_{ty}$, then E_{ty} is 0.05 to 0.1g - an event which is about E_{500} in ENAM. Thus it would be unlikely that there would be any earthquake-caused damage to buildings during a person's lifetime.

Design not to collapse with E_{500}: This strategy is characterized by $E_{tc} = E_{md}$ where $E_{md} = E_{500}$. This particular strategy is implied by what is written in the commentaries for the ATC3-06 and NEHRP recommended provisions, although this is too simplistic a view of these recommendations. Now there is a 10% probability that E_{tc} is exceeded during a 50-year period. This does not mean that all buildings designed to this strategy will collapse if an earthquake greater than E_{500} occurs, but rather that at least some life-threatening damage should be expected. Again using the rule-of-thumb that $E_{tc} = 4E_{ty}$, E_{ty} = 0.01g to 0.02g - events with a mean recurrence interval of about 20 years. Thus with this strategy some modest earthquake damage would be expected during a person's lifetime.

Design with $E_{ty} = E_{re}$ and $E_{tc} = E_{500}$: This is a possible example of a "two-level design". The probability of some damage during a 50-year period is now about 40% while that of major life-threatening damage remains, as above, at 10%. For the 0.1 contour of the ATC/NEHRP maps for effective peak acceleration (EPA), the EPAs for these two events are 0.05g and 0.10g respectively. Thus less ductility would be required than that usually associated with today's codes. To some extent this may be what we are achieving when we permit "semi-ductile" detailing in Zones 1 and 2 while requiring "ductile" concrete in Zones 3 and 4.

Design with $E_{md} = E_{2000}$ and $E_{ty} = E_{tc}/2$: This strategy keeps "Eastern" detailing but provides greater safety against yielding and collapse. For the 0.1 contour the EPA are 0.08g and 0.16g respectively, with associated exceedance probabilities of about 15% and 3%.

An Approach to Assessing the Strategies

There long has been talk about using loss estimation methodologies to guide the choice of a design earthquake. The engineers who wrote the seismic provisions for the Massachusetts code were provided information about the possible impact of E_{md} upon casualties, and claimed to have found this information of value to them (4). However, this approach has seldom been used, presumably because experienced earthquake engineers feel - no doubt with considerable justification - that their judgement is far more pertinent than the not-very-certain predictions of loss estimation studies. Perhaps the lesson is that the less the experience,

the greater the benefit of theoretical predictions of losses - and certainly we have scant actual earthquake experience in ENAM.

To carry out such a study of the implication of choosing different design earthquakes, it is necessary to have: (1) a probabilistic seismic hazard assessment; (2) relationships, for different qualities of construction, between intensity of ground motion and damage; and (3) relationships between level of damage and casualties. We cannot today claim that we know well the information required for any of these steps. However, we do have some reasonable, crude information, and our knowledge is not likely to increase significantly in the near future. Therefore we should plunge in and do the analyses.

I would suggest taking, as a start, the eastern seaboard. Seismologists should provide their current best estimate of the seismicity so that ground motion as a function of mean recurrence interval can be established at the locations of all major cities. Damage probability matrices should be estimated for a few types of construction, as a function of E_{tc} and E_{ty}. The damage vs. casualty tables in ATC-13 (3) may be used. An idealized inventory may be assumed, since at this stage we are talking about losses that would be associated with future construction. Once a computer program has been written to massage all such input, it will be a simple matter to investigate different alternatives and the influence of uncertainties in the input - always remembering that the aim is to provide information useful for decision making and not to make definitive predictions of what will actually happen.

IS THERE AN ALTERNATIVE TO LATERAL FORCE PROVISIONS?

The foregoing discussion addresses the choice of the lateral forces to be used for design. However, experienced earthquake engineers say that detailing and attention to connections are more important than analysis of forces. If so, perhaps we are missing the point by thinking too much about the choice of the design earthquake.

For Zones 0 and 1, existing codes already say it suffices to "tie the building together" and "provide sufficient strength in continuous load paths" - but a designing engineer is not given guidance as to what is adequate in this regard. Indeed, the codes finally succumb to saying that a designer must consider how certain force levels can be transmitted through the structure - which really gets back to using lateral forces but without the benefit of carefully described ductility requirements.

It would seem very useful if we could describe what is adequate in the way of details and connections without resorting to lateral forces. This is especially true when - as often is the case in ENAM - code seismic forces are less than code wind forces, a situation which leads some (many?) engineers to overlook the fact that small seismic forces are appropriate only when a building is provided with adequate ductility.

The problem, of course, is that there is now no good legal mechanism for ensuring that detailing and connections are adequate, other than prescribing forces to be resisted. For any one city or region it should be possible to develop a "handbook" of adequate detailing/connecting for common types of construction. This could come about by having designs and plans submitted to a group of experts who would pass on adequacy, and thus build up a "handbook" by experience. I think there is also a role for reduced scale testing on shaking tables, so as to learn what constitutes adequate tying-together. Once such a "handbook" is accepted by the professional community and building officials, buildings conforming to its provisions would be exempt from lateral force provisions.

THE PROBLEM OF EXISTING BUILDINGS

These thoughts bring me to the last and most important of the problem areas in codes: What to say and require concerning existing buildings which are potentially hazardous during earthquakes? Here I am convinced that the problem is not saying the right things in codes - although there have been several good attenpts at writing suitable language.

There are two problems: (1) when to require that a building be strengthened, and (2) how to prescribe adequate strengthening. Whatever is required must be balanced against the social need to keep available an economically-marginal or historically-important structure.

As to when to require strengthening, I do have an answer: Whenever there is a renovation that costs more than (say) 25% to 50% of the present value of the structure. I believe that useful upgrading of seismic resistance can be achieved at a cost that is lost within uncertainty in the total cost of such renovations.

The approach to prescribing adequate strengthening is either stating a level of lateral forces or of having available a handbook of approved detailing/tying for common types of construction. If the lateral force approach is used, the prescribed level should be less - I think 1/2 to 2/3 less - than that for similar new construction.

I believe we know enough to insert in codes reasonable provisions that will gradually bring about a significant improvement in existing buildings, and I urge that this effort be given high priority.

FINAL REMARKS

I have argued that engineers in ENAM should pause and ask whether the strategies for seismic design embodied in existing model codes are really right for their regions. One question is whether the mix of lateral forces and ductility requirements is best suited for the needs of ENAM. A second question is whether there are alternatives to focussing too much upon lateral forces.

This seems a good time to rethink these matters. The new generation of code requirements presaged by ATC-3 is now taking hold, and the new National Center for Earthquake Engineering Research is giving primary attention to ENAM. The task of rethinking and perhaps reshaping will not be easy, but it should and must be faced.

REFERENCES

1. Applied Technology Council (1974): An evaluation of a response spectrum response to seismic design of buildings (1975) Report ATC-2, Redwood City, CA. 270 pp.

2. Applied Technology Council (1978): Tentative provisions for the development of seismic regulation for buildings, Report ATC 3-06, NSF 7808, NBS Special Publication 510, Palo Alto, CA, 505 pp.

3. Building Seismic Safety Council (1986): NEHRP recommended provisions for the development of seismic regulations for new buildings, Part 1, Provisions, FEMA Earthquake Hazards Reduction Series 17, Washington, D.C. 129 pp.

4. Kringold, F. (1977): Seismic design decision for the Commonwealth of Massachusetts building code, Seismic Design Decision Report 32, M.I.T. Dept. of Civil Engineering CE R77-27.

5. Whitman, R.V. (1986): The prognosis for earthquake hazard mitigation, Proceedings 3rd National Conf. Earthquake Engineering, Vol IV (in press) Earthquake Engineering Research Institute.

TOPIC 2

Tectonics and Seismicity of Eastern North America

M. D. Zoback: *In Situ Stress, Crustal Strain and Seismicity in Eastern North America*

K. F. Evans: *Assessing Regional Potential for Induced Seismicity from Crustal Stresss Measurements : An Example from Northern Ohio*

J. Adams and P. Basham: *Seismicity, Crustal Stresses and Seismotectonics of Eastern Canada*

L. Seeber: *Problems in Intraplate Seismogenesis and Earthquake Hazard*

J. Armbruster and L.Seeber: *Seismicity and Seismic Zonation Along the Appalachians and the Atlantic Seaboard from Intensity Data*

J. Ebel: *The Seismicity of the Northeastern United States*

A. C. Johnston and S. J. Nava: *Seismotectonics of the Central United States*

G. A. Bollinger: *Seismotectonics of the Virginia and Eastern Tennessee Seismic Zones*

K. J. Coppersmith, A. C. Johnston and W. J. Arabasz: *Estimating Maximum Earthquakes in the Central and Eastern United States: A Progress Report*

D. Veneziano and L. Chouinard: *Local Models of Seismicity and Their Estimation*

In Situ Stress, Crustal Strain and Seismicity in Eastern North America

Mark D. Zoback
Department of Geophysics
Stanford University
Stanford, California 94305

Abstract

To better understand the physical processes controlling intraplate seismicity in eastern North America, three related types of investigations have been carried out over the past decade. First, numerous indicators of in-situ tectonic stress orientation have been compiled to understand the regional distribution of forces potentially responsible for large-magnitude earthquakes. Second, detailed measurements of in situ stress magnitude have been made in boreholes up to 1.5 km in depth in areas of known microseismicity. Third, analyses of historic crustal strain data have been carried out in several areas of microseismicity in an attempt to detect regions of localized crustal deformation. The results of these studies reveal several interesting features about the regional seismicity and allow us to constrain hypotheses responsible for the origin of the seismicity.

The compilations of tectonic stress orientation data indicate generally uniform tectonic stress orientations over most of central and eastern North America. These observed directions of maximum principal stress are consistent with predicted stress directions resulting from plate motion. This observation suggests that the predominant stress field responsible for seismicity in the region is of regional tectonic origin and not due to local sources. Thus, the localization of major earthquakes is primarily controlled by the occurrence of major faults and not local sources of stress. The second set of studies referred to above indicate that very high horizontal stresses exist in the upper ~1 km in many areas where high-velocity rocks are found near the surface. These large, shallow stresses may be responsible for widespread, low-magnitude seismicity and that the occurrence of such seismicity may have nothing to do with the potential for larger earthquakes to occur. Finally, studies have been undertaken to determine if zones of anomalously high crustal deformation could be found indicating areas where high rates of elastic strain accumulation was taking place. Localized zones with high rates of strain accumulation seem to be required to account for the occurrence of

repeated intraplate earthquakes over relatively short time periods in the New Madrid and Charleston areas. Although insufficient historical strain data were found in these two areas to determine if anomalously high rates of strain accumulation are occurring, evidence was found for high rates of strain accumulation in southern New York. Further measurements of the current strain field in this area are extremely important to either confirm or modify the implications of the historical data.

Introduction

During historic time earthquakes have occurred in essentially every state of the central and eastern U.S. and throughtout much of central and eastern Canada. Yet little is known about the stresses that cause these earthquakes, the faults the earthquake occur upon, or the rates of stress or strain accumulation. Recurrence rates for major earthquakes in central and eastern North America are several times as long as the historic record (Russ,1979; Obermeier and others, 1985). It is an unresolved question whether it is possible to evaluate seismic hazard from seismicity rates in the absence of a physical understanding of the earthquake generation process. This paper summarizes several efforts aimed at improving the physical understanding of earthquakes that occur in this region.

State of Stress in the Central and Eastern U.S.

Figures 1 shows a generalized stress map of the US and adjacent Canada. Figure 2 shows the quality-ranked data from which Fig. 1 was derived (both from Zoback and Zoback, 1988). The data come from *in situ* stress measurements at depth, well-resolved earthquake focal mechanisms, stress-induced wellbore breakouts, and several observations of fault slip. The latter are sites where evidence of post-Miocene faulting can be used to estimate stress directions because both the dip-slip and strike-slip components of motion can be constrained. With the exception of the gulf coast and continental margin, the state of stress in central and eastern US is compressive with strike-slip to reverse faulting observed essentially everywhere. Thus,

$$S_{Hmax} > S_{hmin} > S_v$$

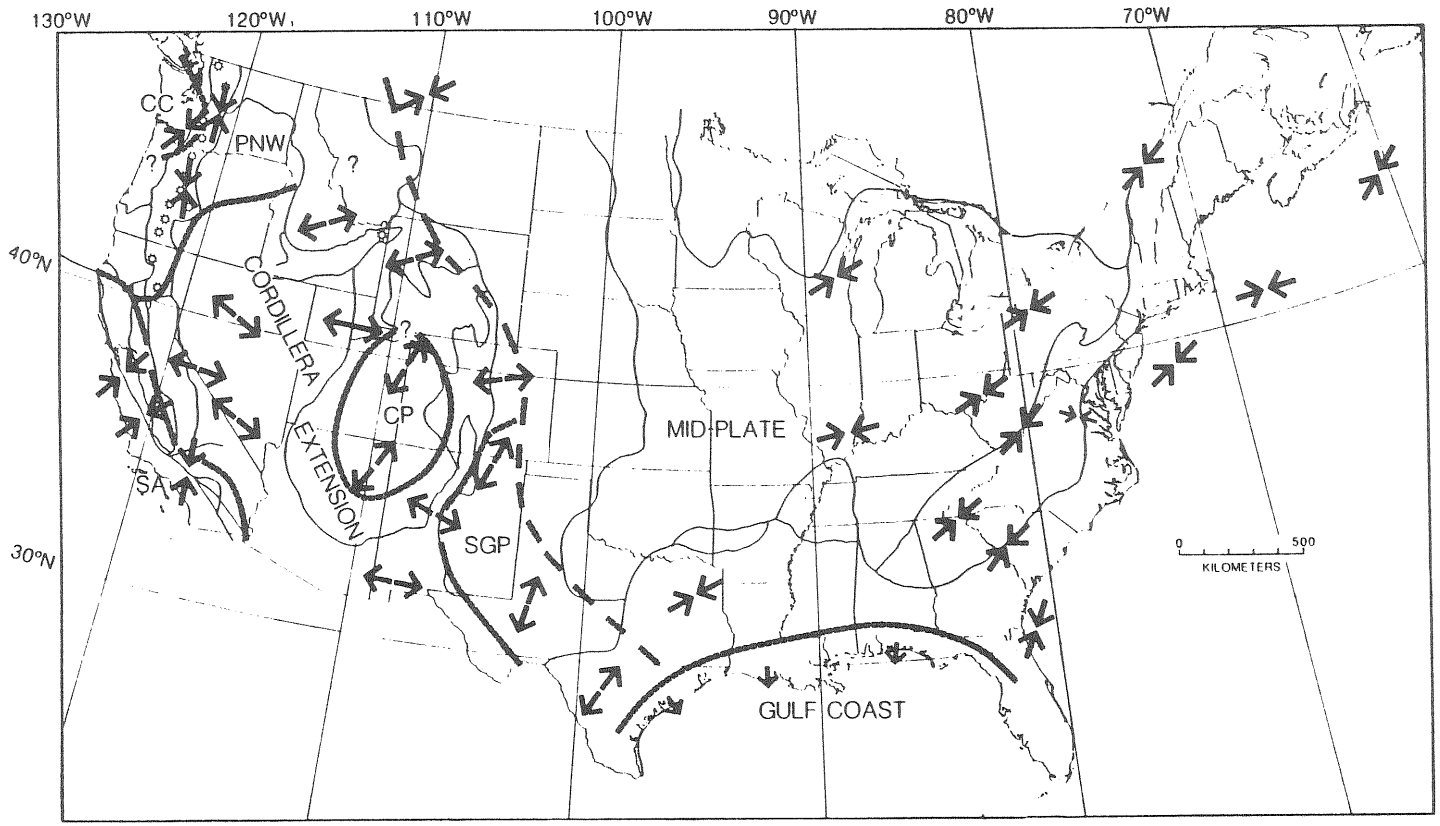

Figure 1- Generalized stress map of the United States. Inward-pointed arrows represent direction of maximum horizontal principal stress in areas of crustal compression (reverse and strike-slip faulting areas) and outward pointed arrows indicate direction of least horizontal principal stress in areas of crustal extension (normal and strike-slip faulting areas) (from Zoback and Zoback, 1988).

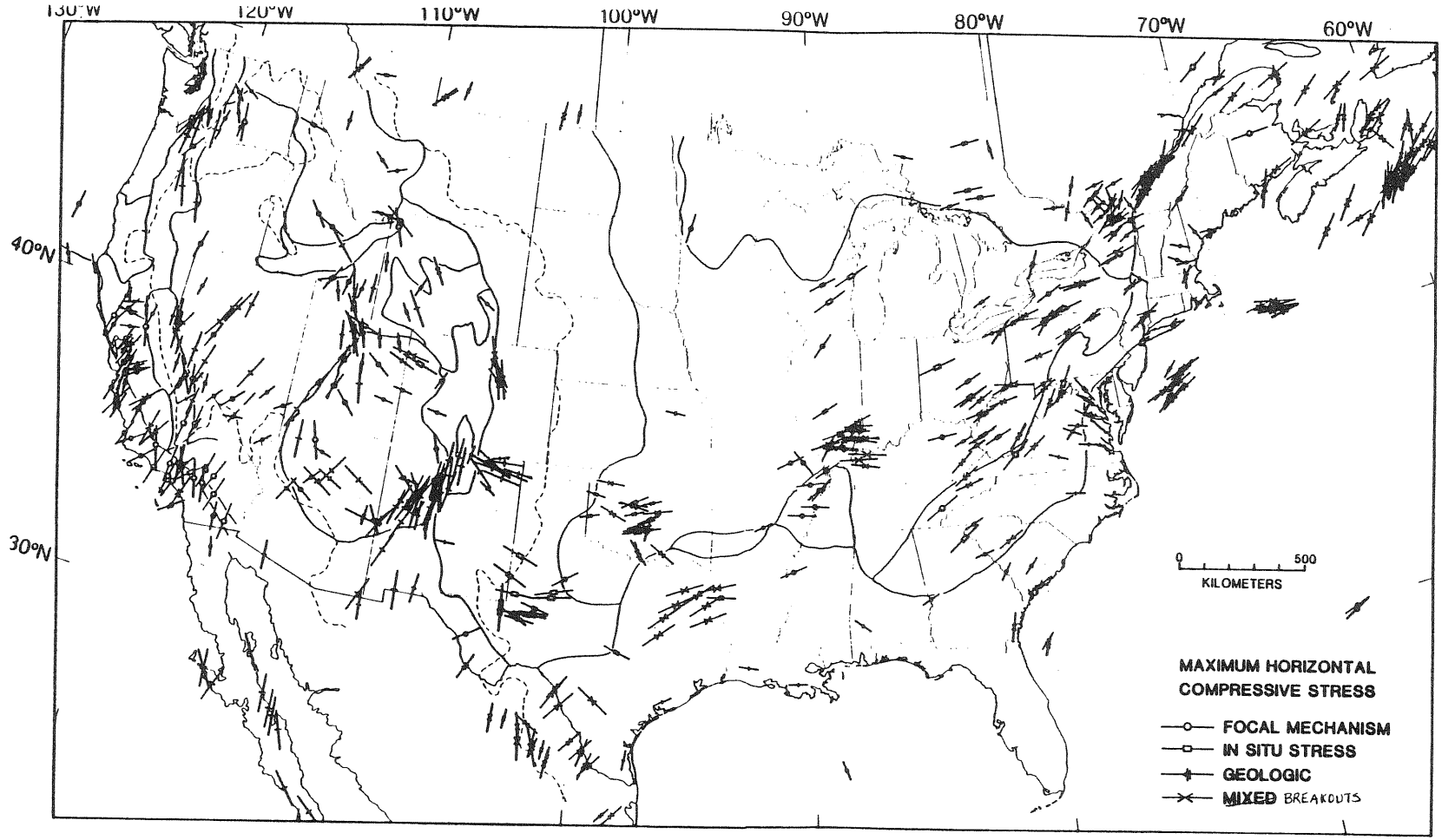

Figure 2- Map of directions of maximum horizontal principal stress direction gathered from a variety of sources. The different symbols represent the type of data and the lengths of the arrows indicate the data quality (from Zoback and Zoback, 1988).

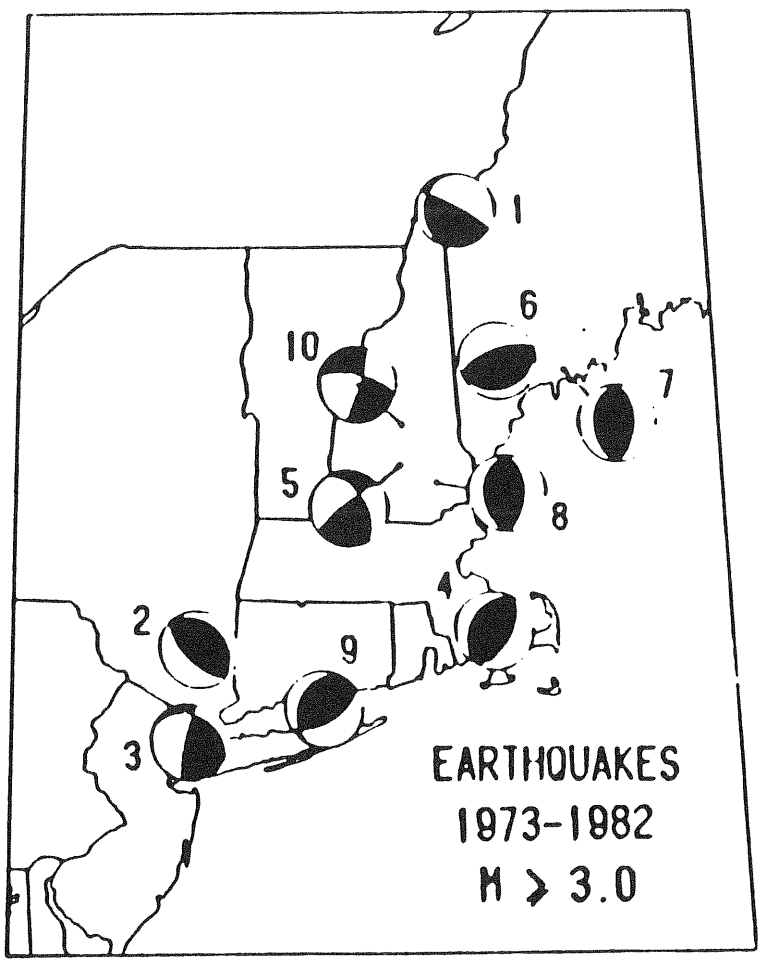

Figure 3- Relatively high quality earthquake focal mechanisms in New England (from Gephart and Forsyth, 1985).

The direction of maximum horizontal compression is generally ENE. This broad-scale and uniform stress field appears to be of plate-wide tectonic origin and is consistent with the theoretical directions of *push* from the mid-Atlantic ridge (Richardson and others, 1979) and absolute plate motion (these directions are essentially the same). On a plate-wide scale this stress field also seems to characterize most of central and eastern Canada Adams, 1987) and the western Atlantic ocean (Zoback and others, 1986).

Areas where the orientation of the stress field varies in the central and eastern US are also observed. Fault slip data in the mid-Atlantic states indicates a WNW direction of maximum horizontal stress. The reason for this is not understood and there are no contemporary stress indicators in the region to confirm whether or not this stress field is still active. Earthquake focal mechanisms in New England (Figure 3, as summarized by Gephart and Forsythe, 1985) show considerable variability in the orientations of the nodal planes and the P-axes (see also Pulli and Toksoz, 1981). This can be explained either in terms of true variations in stress orientation from area to area or that slip is occurring on pre-existing planes of weakness in a relatively uniform stress field.

Gephart and Forsythe preferred the latter possibility and suggested that the earthquakes represent slip on variably-oriented pre-existing zones of weakness and the observed slip could from a generally uniform NE to ENE compressive stress field. By a " pre-existing planes of weakness" it is not meant that earthquakes are simply occurring on pre-existing faults. Basically, the plane of weakness argument is that some faults in nature are much weaker than laboratory friction experiments would suggest and that faulting can occur on nearly any "weak" plane, even those striking nearly 90^{o} to the maximum principal stress (see Zoback and others, 1987). Thus, arguing that faulting occurs on planes of weakness basically suggests that faulting occurs in response to extremely low shear stresses, on the order of seismic stress drops, and that faulting can occur on planes with almost any orientation to the in situ stress field. In terms of classical Andersonian faulting theory and the Mohr-Coulomb failure criterion (Anderson, 1951; Jaeger and Cook, 1969), the stresses required to move pre-existing faults using laboratory-derived frictional coefficients are much greater than that referred to in the case of a pre-existing plane of weakness (Brace and Kohlstedt, 1980; Zoback and Healy, 1984) and that faulting is likely to occur only on those faults that are optimally-oriented to the stress field.

There is new evidence on the state of stress in New England that suggests that

focal mechanism variability in the region might be due to local variations in stress orientation and not due to the existence of planes of weakness. Observations of wellbore breakouts in ~1km deep holes near events 2, 8, and 9 indicate compressive stress directions that match the P-axes of the focal mechanisms surprisingly well. As this demonstrates that changes in the orientation of S_{Hmax} (of at least 45^{o}) actually do occur, it is not necessary to require that the earthquakes occur on pre-existing zones of weakness. In the section immediately below, evidence is presented that stress magnitudes measured in boreholes are consistent with magnitudes based on Mohr-Coulomb theory and laboratory-derived frictional coefficients. Additionally, in a subsequent section below, an argument based on stress observations near the San Andreas fault is presented that indicates that if pre-existing zones of weakness do exist, they must cause large variations in the orientations of the principal stresses (with respect to the surrounding regions). As such variations in the stress field are not observed in places such as New Madrid, Missouri and Charleston, South Carolina, there is no direct evidence to suggest that the earthquakes occur on pre-existing planes of weakness.

Stress Magnitudes at Shallow Depth

Using the hydraulic fracturing technique, in situ stress measurements have been conducted at a number of sites in the eastern US in seismically active areas. Measurements have been made in two ~1 km deep wells at Monticello South Carolina (Zoback and Hickman,1982), three 300-400 m deep holes in northeastern South Carolina (Zoback and others, 1986), in a 1.5 km deep hole in west central NY (Auburn) and in a 1 km deep hole in southeastern NY (Zoback and others, 1985). In each of these cases (except Auburn), the measurements were made in crystalline rock and in each of these cases (except Auburn), the shallow stress magnitudes are sufficiently high to cause reverse faulting on optimally oriented planes (see Fig. 4 from Kent Cliffs, N.Y.).

The most important question about these data is how deep do the critical stress magnitudes persist? In many cases, and at many other sites around the world (see Zoback and Healy, 1984) the critical stress magnitudes are generally restricted to shallow depths, shear stress does not increase markedly with depth below several hundred meters, and the deeper stress measurements do not imply incipient faulting. At Monticello, for example, both the stress measurements and the focal depths of the

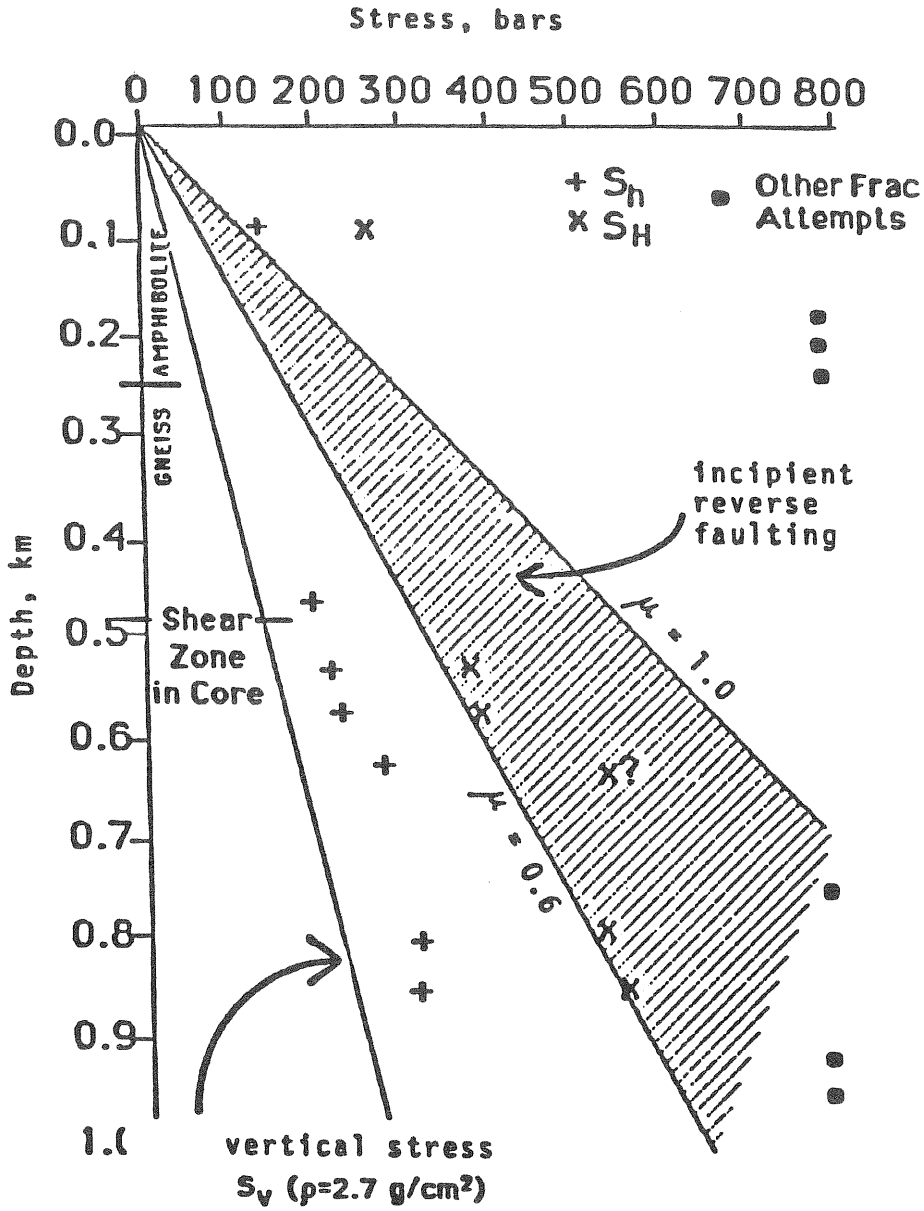

Figure 4- In situ stress measurements in the Kent Cliffs borehole. Different symbols represent least and greatest horizontal principal stresses and the hachured area indicates values for which the maximum principal stress is sufficiently greater than the vertical stress that well-oriented reverse faults would be potentially active (from Zoback and others, 1985).

earthquakes indicate that the majority of events are in the upper 1 km. As the stress orientations in these cases are consistent with regional orientations (see Fig. 5- Monticello is the data point in the middle of the state), it seems as if the near-surface horizontal stresses are either locally amplified, possibly by a process such as denudation, or that the horizontal stresses at shallow depth only seem to be high because the vertical stress is close to zero. In other words, a difference between S_{Hmax} and S_V of 20-30 MPa might be relatively insignificant at mid-crustal depth, but sufficient to cause reverse faulting in the upper few hundred meters. What this means is that it is possible that at least some, if not much, of the widely distributed seismicity in central and eastern U.S. and Canada might be of shallow origin and not particularly significant with respect to estimation of earthquake hazard associated with much larger magnitude events.

It is clear, however, that in many areas appreciable seismicity occurs at great depth in central and eastern North America and may be associated with a stress field that is capable of producing moderate to large magnitude earthquakes. In the section below, I argue that based on available evidence, such intraplate seismic zones do not seem to be controlled by localized "weakness" (as defined above) but instead, are zones of localized ductile strain in the mid- to lower crust.

Are Major Intraplate Seismic Zones Controlled by Crustal Weakness ?

For a variety of reasons the answer to this fundamental question appears to be probably not. First, unlike plate boundaries, stresses must be high in intraplate areas to support topography and flexure and about twenty cases of in situ stress measurements in intraplate areas around the world show high stress differences consistent with Mohr-Coulomb failure and "Byerlee" friction (see Brace and Kohlstedt, 1980; Zoback and Healy, 1984; Batchelor and Pine, 1986; Stephansson and others, 1986) While these measurements are relatively shallow (primarily in the upper 2 km), why have none of the measurements ever detected any "weak" crust?

Second, no viable mechanism has ever been proposed for generating weak zones within intraplate areas. Soft-inclusion (alkalic or serpentinized intrusive) models (Sykes, 1978; Kane, 1977; McKeown, 1982) do not hold up to careful correlations between seismicity and geology and deformation rates are too low to call on overpressure as along plate boundaries (see, for example, Dahlen and others, 1984).

Third, if a relatively small number of major weak zones did exist, wouldn't the

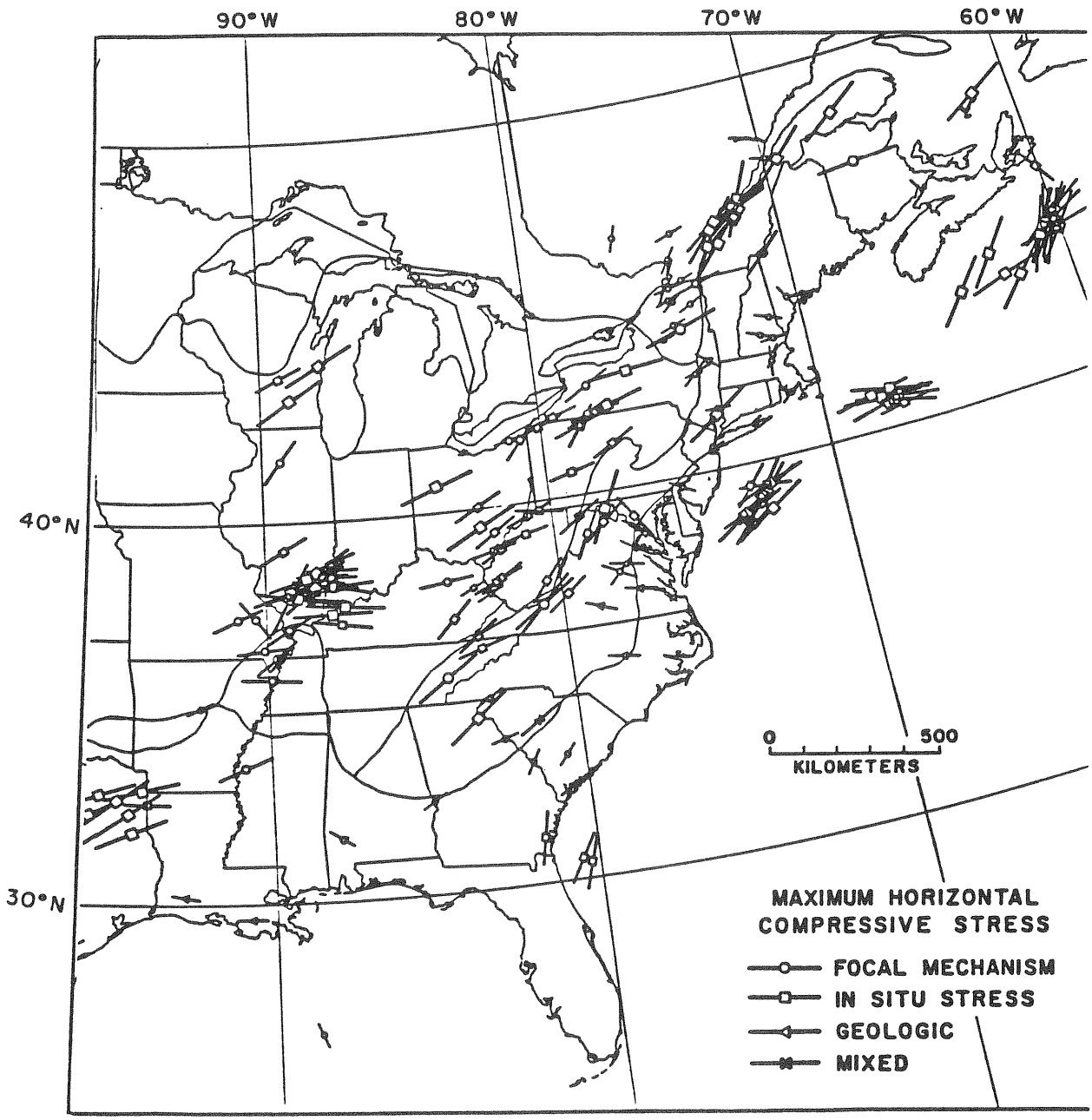

Figure 5- Stress map of the eastern U.S. (derived from Fig. 2).

intraplate deformation be concentrated only in the weak zones? How could you generate uniformly oriented stresses of sufficient magnitude over the entire plate that are sufficiently large in magnitude to cause widespread seismicity throughout the plate? If one argues that all the relatively moderate size earthquakes are occurring on faults which are weak, the first point above is violated.

Fourth, at New Madrid and Charleston, there seems to be evidence for recurrent activity in several intraplate seismic zones on the order of 1000 years (Russ,1979; Obermeier and others, 1985), simply allowing failure to occur at a lower stress level in one earthquake does not allow sufficient time to reaccumuate stress for another earthquake 1000 years later. In other words, the rate of stress (strain) accumulation must be anomalously high in these areas to explain the recurrence data. The stress level at which the faults fail (degree of weakness) is irrelevant with respect to the issue of recurrence.

Finally, in a recent paper (Zoback and others, 1987) we present evidence that the direction of maximum horizontal compression in western California is essentially perpendicular to the San Andreas fault (Fig. 6). We argue that because the San Andreas is so much weaker than the surrounding crust, the horizontal principal stresses must "refract" so as to minimize the shear stress on the fault. In other words, depending on the orientation of the maximum principal stress away from the fault, the direction of maximum compression near the fault must be either nearly perpendicular to the fault (as currently observed in central California), or parallel to the fault (as probably existed in central California prior to a plate motion change 4 my ago).

This argument relates directly to the issue of whether intraplate seismicity occurs along weak faults. If the fault zones along which the Charleston and New Madrid earthquakes occurred where extremely weak, one would expect the stress orientations in the epicentral zone to differ from the regional stress directions by as much as 40^{o}. In other words, if the shear stresses in the generally "strong" crust are sufficiently high as to cause regional seismicity, the principal stresses must rotate so as to result in relatively little shear stress on the "weak" fault planes, just as along the San Andreas (Fig. 7). The stress data shown in Figs. 5 and 2, do not show any significant stress rotation in these areas. In fact, the stress orientation in the Charleston area is remarkabl similar to that in the rest of South Carolina (as is the comparison between the stress orientation in the New Madrid seismic zone with that in the Illinois basin just to the north). In many other areas the data is regretably sparse and it is difficult to ascertain whether significant stress orientation changes occur, and if so, why. There

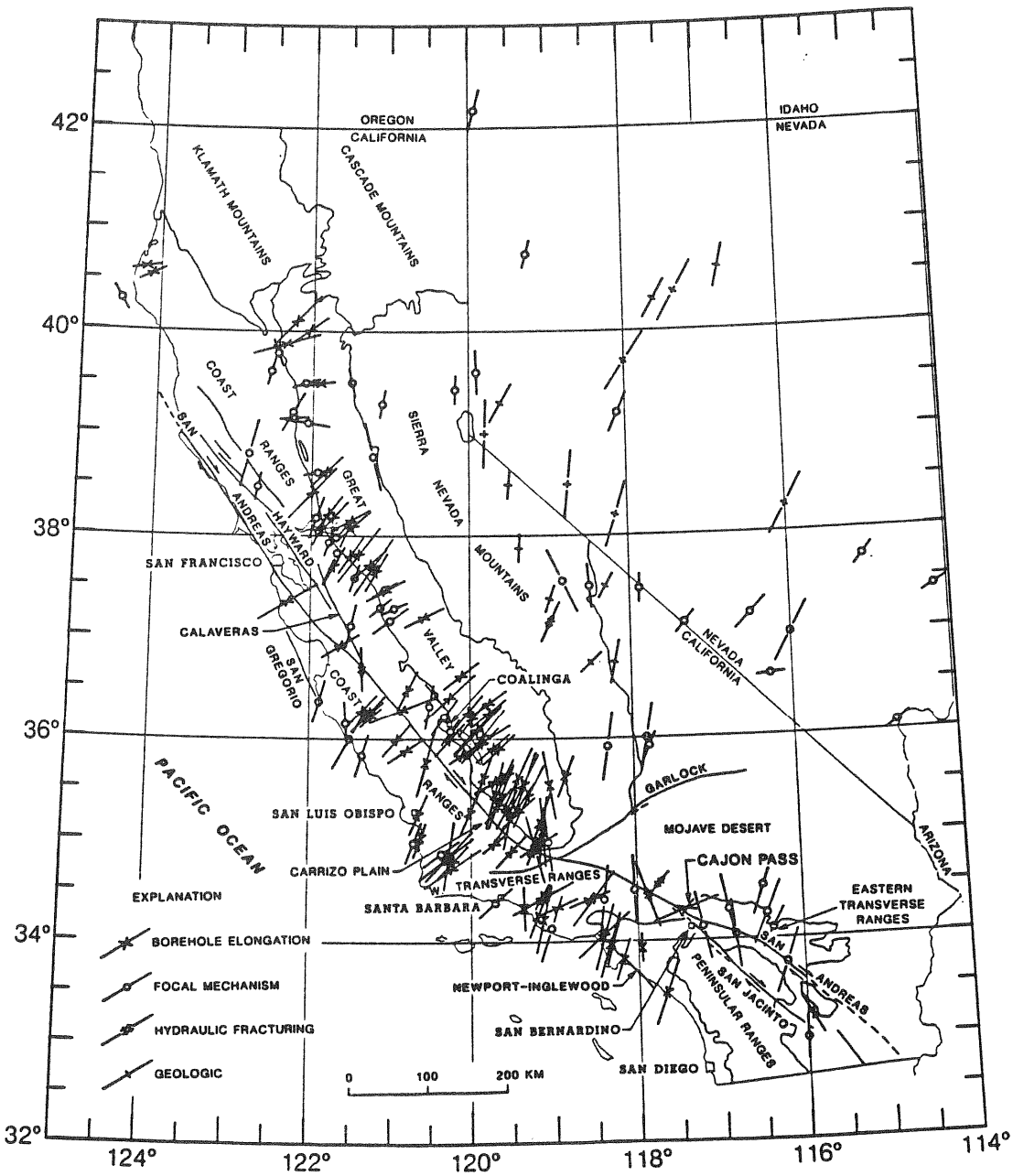

Figure 6- Directions of maximum principal stress in California. As in Fig. 2, the length of the arrows indicate the data quality and the symbol indicates the type of data (from Zoback and Zoback, 1987).

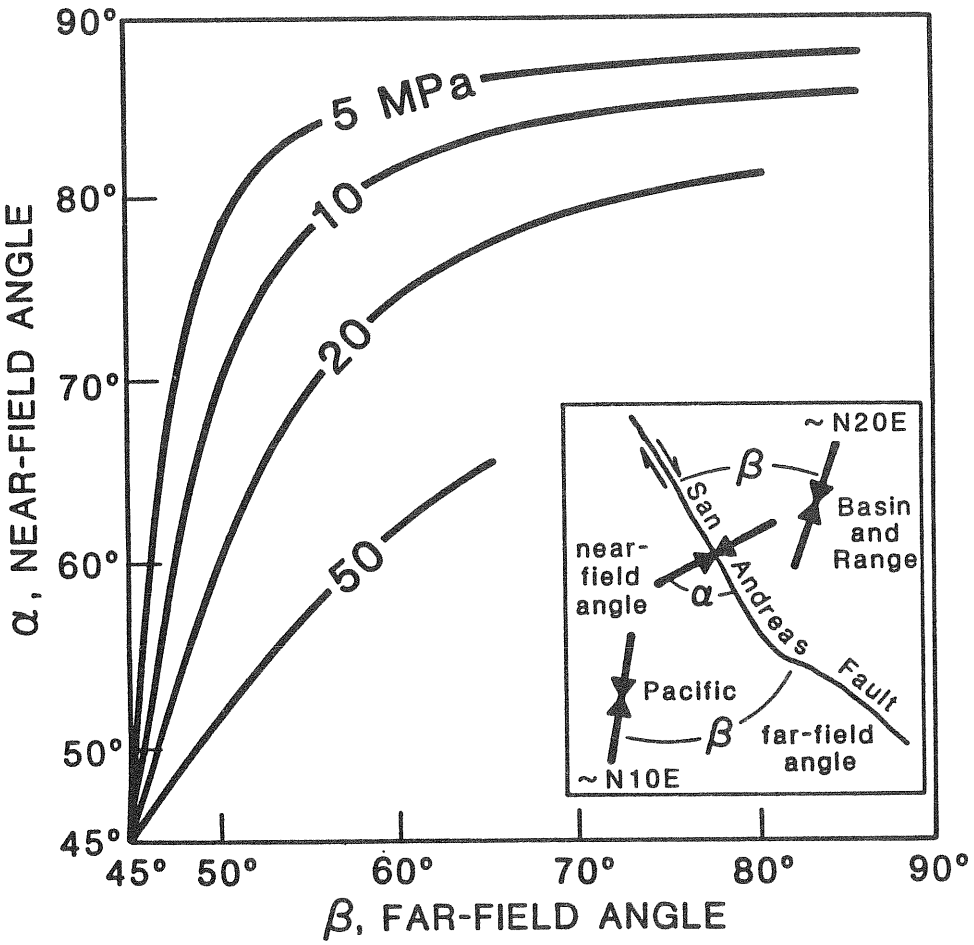

Figure 7- Orientation of maximum principal stress near a weak fault (i.e., one that can sustain appreciably less shear stress than the crust, in general) as a function of the orientation of the maximum principal stress to the strike of the fault (from Zoback and Zoback, 1987).

are many possible explanations for variations in stress orientations, some of which may be tectonic but many of which are data related (for example, a P-axes are only an approximation of S_{Hmax} directions and breakouts can be mis-interpreted on four-arm caliper surveys). Nevertheless, while there are numerous minor variations in stress orientation seen in the central and eastern U.S. , there does not seem to be evidence of major changes in stress orientation that would indicate the presence of major zones of crustal weakness. The consistent regional stress patterns in areas of known major earthquakes also argues strongly against major localized sources of stress being responsible for those earthquakes.

Crustal Strain Localization

As we know that there are areas of potentially catastrophic earthquakes that are currently aseismic and not revealed through either geology or geophysics (Charleston is the best known example) it is clearly uncertain whether seismic hazard can be adequately assessed through utilizing seismicity data and first-order geologic and geophysical discriminants. Zoback and others (1985a) take another approach and make the case that intraplate zones capable of producing major crustal earthquakes on a time scale on the order of 1000 years must be areas of localized ductile strain in the mid- to lower-crust and that such strain should produce detectable levels of geodetic strain, just as along the San Andreas fault.

Zoback and others (1985a) presented an analysis of repeated triangulation measurements in southern New York and western Connecticut that showed anomalously high strain rates whereas the surrounding region did not (Fig. 8, Table I). Two important aspects of this analysis is that the two areas of anomalously high strain rate (New York-Connecticut and western Long Island) showed similar directions of shear strain (although the rates were different) and when each of the two areas of anomalously strain rate were broken-up into seperate subsets of completly independent data, each subset of data reproduced the observed strain rate of the initial analysis (Table II).

Nevertheless, the statistical significance of this finding was later challenged by Snay (1986). Although Snay's analysis in large part just replicated the Zoback, Prescott, and Kruger results, Prescott, Zoback and Kruger (1987) argue that Snay's interpretation of the significance of the data was overly conservative. First, although Snay deleted a couple of the data points used redefined the standard error upward,

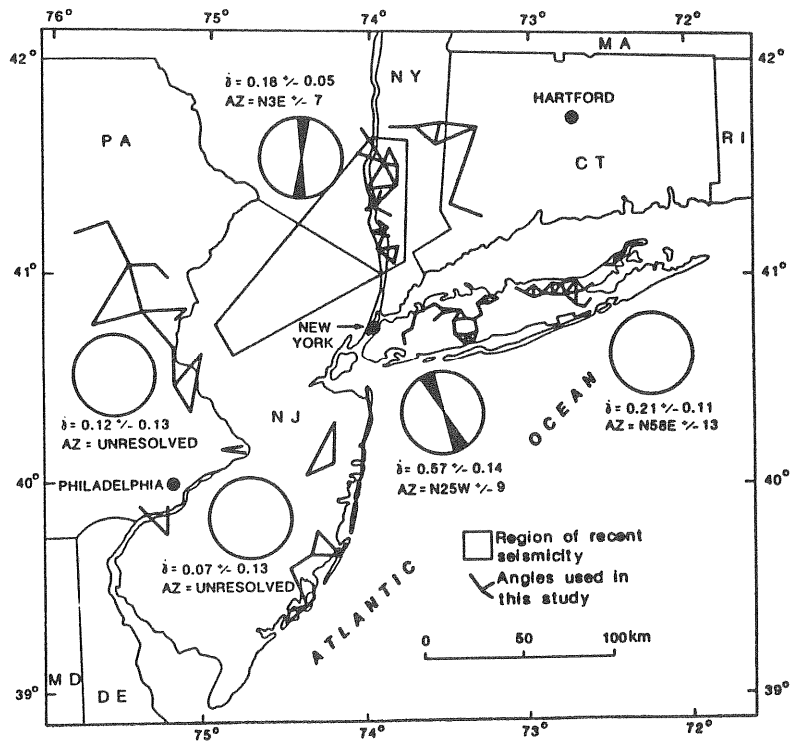

Figure 8- Five areas where shear strain has been computed from repeated triangulation measurements (angles are shown by solid lines). Only in the southern New York/western Connecticut and western Long Island areas were significant amounts of strain detected. In both areas the planes on which maximum shear occurs strike approximately N-S (from Zoback and others, 1985).

Table 1 Strain rate parameters on five groups separated according to the number of angles used in the analysis

Area	No. of angles	Dates of observations	$\dot{\gamma}_1$ (μrad yr^{-1})	$\dot{\gamma}_2$ (μrad yr^{-1})	$\dot{\gamma}$ (μrad yr^{-1})	Azimuth Ψ
New York–Connecticut	30	1862–1973	−0.02+/−0.04	−0.18+/−0.05	0.18+/−0.05	N3° E+/−7
Western Long Island	27	1932–1967	0.43+/−0.15	−0.37+/−0.15	0.57+/−0.14	N25° W+/−9
Eastern Long Island	31	1939–1967	−0.19+/−0.11	0.09+/−0.09	0.21±/−0.11	N58° E+/−13
Northern New Jersey	26	1931–1962	−0.05+/−0.16	0.04+/−0.14	0.07+/−0.13	N68° E+/−74
Eastern Pennsylvania	15	1885–1969	−0.06+/−0.20	0.10+/−0.18	0.12+/−0.13	N74° E+/−56

$\dot{\gamma}_1$, right-lateral shear strain rate on a NW–SE striking plane^{-1}, uncertainty is 1 s.d. $\dot{\gamma}_2$, Right-lateral shear strain rate on an E–W striking plane
$\dot{\gamma}$, Maximum shear strain rate. Azimuth, orientation of plane of maximum shear measured clockwise from the north.

Table 2 Strain rates of subsets of groups identified in Table 1

Subset	No. of angles	Dates of observations	γ	Ψ
New York–Connecticut	12	1862–1973	0.19+/−0.05	N2° E+/−8
New York–Connecticut	18	1932–1966	0.17+/−0.09	N7° E+/−15
West Long Island	8	1864–1948	0.62+/−0.23	N22° W+/−11
West Long Island	19	1932–1967	0.60+/−0.19	N18° W+/−11

TABLE III. Shear Parameters for Various Subsets of the Data Analyzed by *Zoback et al.* [1985] and *Snay* [1986].

Experiment	Number of Angles	$\dot{\gamma}$, μrad/yr	Ψ	σ_0
All repeated	30	0.184 ± 0.064(0.05)	N3°E ± 10°(7°)	1.40
All minus *D* and with *A* replaced	29	0.122 ± 0.057(0.046)	N3°E ± 13°(10°)	1.24
All minus *B*, *C*, and *D* and with *A* replaced	27	0.139 ± 0.051(0.046)	N2°W ± 10°(8°)	1.09
Zoback et al.'s subset I	12	0.192 ± 0.086(0.05)	N2°E ± 13°(8°)	1.59
Zoback et al.'s subset II	18	0.168 ± 0.121(0.09)	N7°E ± 20°(15°)	1.36

$\dot{\gamma}$ is the maximum right lateral shear strain rate. Ψ is the bearing of the axis of maximum right lateral shear. σ_0 is the ratio of the misfit standard error to the a priori standard error of the observations.

rows 2 and 3 of Table III (from Prescott, Zoback and Krueger, 1987) indicate that even by rejecting the data recommended by Snay, a strain rate of 0.1 to 0.2 μrad/yr on north-south trending planes is still observed (with the size of the signal exceeds two standard errors). Snay stated that such strain rates are still not statistically significant. While I do not agree with his view, the rates the were measured are surpisingly large and should be confirmed with dedicated measurements.

Intraplate strain rates must be quite low, but if earthquakes are recurring every ~1000 years the strain should be detectable. In most places there are excellent sets of historic triangulation data (that often go back into the 19th century) that can be used for reference, and using modern instrumentation such as Global Positioning System receivers, many of the old triangulation stations can be efficiently reoccupied. While it may take an appreciable amount of time to develop a crustal strain accumulation map of central and eastern North America, it's time to start. Such a map would present a true picture of long-term seismic hazard.

References

Adams, J., Canadian crustal stress data- a compilation to 1987, *Geol. Surv. Canada Open File Rep.*, in press, 1987.

Anderson, E.M., *The Dynamics of Faulting and Dyke Formation with Applications to Britain, 2nd ed.,* Oliver and Boyd, Edinburgh, 1951.

Batchelor, A.S. and R.J. Pine, The results of in situ stress determinations by seven methods to depths of 2500 m in the Carnmenellis granite, n *Proc. of Intl. Symp. on Rock Stress and Rock Stress Measurements, Stockholm, 1-3 September, 1986,* CENTEK Publ., Lulea, Sweden, 694 pp., 1986.

Brace, W.F. and D.L. Kohlstedt, Limits on lithospheric stress imposed by laboratory experiments, Jour. Geophys. Res., 85, 6248-6252, 1980.

Dahlen, F.A., J. Suppe and D. Davis, Mechanics of fold-and-thrust belts and accretionary wedges: Cohesive coulomb theory, *Jour. Geophys. Res., 89,* 10087-10101, 1984.

Gephart, J.W. and D.D. Forsyth, On the state of stress in New England as determined from earthquake focal mechanisms, *Geology, 13,* 70-76, 1985).

Jaeger, J.C. and N.G.W. Cook, *Fundamentals of Rock Mechanics,* 2nd ed., Methuen and Co., London, 1969.

Kane, M.F., Correlation of major eastern earthquake centers with mafic/ultramafic basement masses, in *Studies related to the Charleston, South Carolina Earthquake of 1886- A preliminary report,* U.S. Geol. Surv. Prof. Pap. 1028, 1977.

McKeown, F.A., Overview and dixcussion, in *Investigations of the New Madrid Missouri, Earthquake Region,* U.S. Geol. Surv. Prof. Pap. 1236, 1982.

Prescott, W.H., M.D. Zoback and S.W. Krueger, Comment on "Horizontal deformation in New York and Connecticut: Examining contradictory results from the geodetic evidence" by Richard Snay, *Jour. Geophys. Res., 92, 2805, 1987.*

Pulli, J.J. and M.N. Toksoz, Fault plane solutions for northeastern United States earthquakes, *Bull. Seis. Soc. Amer., 71,* 1875-1882, 1981.

Richardson, R.M., S.C. Solomon, and N.H. Sleep, Tectonic stress in the plates, *Rev. Geophys. Space Phys., 17,* 981-1019, 1979.

Snay, R. A., Horizontal deformation in New York and Connecticut: Examining contradictory results from geodetic evidence, *Jour. Geophys. Res., 91,*

12695-12702, 1986.

Stephansson, O., P. Sarkka, and A. Myrvang, State of stress in Fennoscandia, in *Proc. of Intl. Symp. on Rock Stress and Rock Stress Measurements, Stockholm, 1-3 September, 1986,* CENTEK Publ., Lulea, Sweden, 694 pp., 1986.

Sykes, L.R., Intraplate seismicity, reactivation of preexisting zones of weakness, alkaline magmatism, and other tectonism postdating continental fragmentation, *Rev. Geophys. Space Phys., 16,* 621-688, 1978.

Zoback, M.D. and M.L. Zoback, 1981, State of stress and intraplate earthquakes in the central and eastern United States, *Science, v. 213,* pp. 96-109.

Zoback, M.D. and S. Hickman, In situ study of the physical mechanisms controlling induced seismicity at Monticello Reservoir, South Carolina, *Jour. Geophys. Res., 87,* 6959-6974, 1982.

Zoback, M.D. and J.H. Healy,Friction, faulting, and in-situ stress. *Annales Geophysicae, 2*, 689-698, 1984.

Zoback, M.D., R.N. Anderson and D. Moos, In-situ stress measurements in a 1 km-deep well near the Ramapo fault zone, *EOS, 66,* p. 363, 1985.

Zoback, M.D., W.H. Prescott and S.W. Kruguer, Evidence for lower crustal strain localization in southern New York, *Nature, 317* (6039) 705-707, 1985a.

Zoback, M.D., D. Moos, B. Coyle, and R.N. Anderson, In-situ and physical property measurements in Appalachian site survey boreholes, *Amer. Assoc. Petrol. Geol. Bull., 70,* p. 666, 1986.

Zoback, M.D., M.L. Zoback, V. Mount, J. Suppe, J. Eaton, J. Healy, D. Oppenheimer, P. Reasenberg, L. Jones, C.B. Raleigh, I. Wong, O. Scotti, C. Wentworth, New evidence on the state of stress of the San Andreas fault system, *Science, 238,* 237-239, 1987.

Zoback, M.L. , S. Nishenko, R. Richardson, H. Hasegawa, and M.D. Zoback, Mid-plate stress deformation, and seismicity, in Vogt, P.R. and B.Tucholke, eds, *The Geology of North America, vol. M., The Western North Atlantic Region*, Geol. Soc. Amer., p. 297-312, 1986.

Zoback, M.L. and M.D. Zoback, Tectonic stress field of the continental U.S., in *Geophysical Framework of the Continental United States,* eds. L. Pakiser and W. Mooney, Geol. Soc. Amer. Memoir, in press, 1988.

Assessing regional potential for induced seismicity from crustal stress measurements: An example from northern Ohio

Keith F. Evans

Lamont-Doherty Geological Observatory of Columbia University, Palisades, NY 10964.

Summary

We use a Coulomb failure law to describe the strength of faults in a hydrostatically pore-pressured, faulted crust in which one of the principal stresses is vertical and increases linearly with depth. Within this framework we derive relations for the pore pressure increase above ambient required to induce failure at given depth on a favorably-oriented fault for arbitrary states of stress. We refer to this as the critical excess pressure. The stress state at a given depth is described by specifying the ratios of the greatest and least principal horizontal stresses to the vertical stress at that depth. The two stress ratio functions, $R_h(d)$ and $R_H(d)$, completely describe the stress state at depth provided the vertical stress gradient is known. We plot contours of pressure-to-failure per unit depth in R_h xR_H space. The contour values are a measure of the stability of the stress state and must be multiplied by depth to give the critical excess pressure. The value of the least stress ratio, R_h ($=S_h/S_V$), is found to be the dominant parameter influencing stability: stress states characterized by $R_h < 0.65$ are much more susceptible to failure through pore pressure increase than those for which $R_h > 0.65$. The value of R_H is of secondary importance.

To apply the analysis to hazard assessment we define an hazardous or 'unstable' stress state as one in which an induced pore-pressure increase of 8 MPa at the well bottom declining linearly to 2.5 MPa at 5 km results in failure throughout that depth range. This criterion is adopted to crudely simulate the disturbance to ambient pore pressure conditions that might result from prolonged injection at operational wellhead pressures in excess of 10 MPa. Making the assumption that the horizontal principal stresses increase linearly with depth we derive relations which delimit stable from unstable stress states as described in terms of four practically determinable stress parameters: the two stress ratios, $R_h[d']$ and $R_H[d']$, measured at the well bottom, d'; and the surface intercepts, b_h and b_H, of the linearized least and greatest horizontal stress profiles. The relative importance of each of these parameters in distinguishing stable from unstable stress states is evaluated given the different levels of effort required for their estimation. The results suggest they be ranked in decreasing importance as $R_h[d']$, b_h, $R_H[d']$, b_H. The depth d' should be as deep as practically possible. The determination of b_H is of questionable worth.

The analysis is applied to data which describe the variation of least stress ratio to 2 km depth in Paleozoic strata of northwestern Ohio to assess the predicted stability in a region where two suspected cases of induced seismicity have recently been reported. Least stress ratios of 0.65 ± 0.5 were determined for sandstones at 0.9 km and 2 km depth. No data on the value of R_H are available. Nonetheless, the analysis

shows that provided the greatest stress ratio in the sandstone overlying basement is 1.2 or greater, physically realizable stress states exist which are consistent with the available stress data and which result in failure to 5 km depth were the pore pressure at the well bottom to be raised to 8 MPa above hydrostatic and that at 5 km by as little as 1.0 MPa. Strike-slip focal mechanism solutions for earthquakes in the basement indicate the same orientation for maximum tectonic compression as is measured in the Paleozoic strata, and suggest R_H values which significantly exceed unity. Thus the available stress information suggest that the crust is close to failure, a conclusion that is supported by the history of seismicity in the area.

Introduction

The shear strength of rocks is efficiently reduced by increasing pore fluid pressure (Brace and Martin, 1968). Consequently, the injection of fluid at high pressure into deep boreholes may result in the triggering of earthquakes if the local state of stress of the crust is close to failure . Subsurface injection activity associated with waste disposal and secondary recovery of oil has increased substantially in the past decade and the trend is likely to continue. It has thus become important to devise methods for assessing on a regional basis the seismic hazard posed by this activity. An ideal strategy would be one that yields quantitative guidelines for the regulation of injection pressures in consideration of seismic hazard. Currently regulation is based only on aquifer protection. A promising approach in accord with this objective is to assess through stress measurements the proximity of the crust to failure conditions. Clearly the utility of the approach is dependent on the degree to which the strength attributes of the crust may be described in a given situation. The mechanical strength of the crust is a controversial question which touches on some fundamental issues such as the strength of faults as opposed to unfaulted bulk rock. For hazard mitigation purposes, however, it is justifiable to assume that a fault always exists in the orientation most suited to failure so that the strength of the crust is determined by the shear strength of the fault. Raleigh et al. (1972) have presented empirical evidence that a simple Coulomb failure criterion which presumes the effective normal stress acting on the fault is given by the total normal stress minus the pore pressure, may adequately describe the shear strength of faults. Within this framework, simple relations can be derived for predicting the pore pressure required to induce failure under arbitrary stress states. Using this approach, Raleigh et al. (1972) were able to successfully predict the pore pressure required to initiate microseismic swarm activity on a fault cutting the Rangely oil field in Colorado where the stresses acting on the fault at hypocentral depths were determined.

Given that a useful strength criterion is available, the practical question remains as to how one might recognise from practically realizable sampling of the *in-situ* stress field a stress state which is potentially hazardous in that it is extensively close to failure. Two aspects of this problem are addressed in this paper. The first is to develop relations which quantitatively describe in conceptually simple terms the 'degree of stability' of arbitrary crustal stress states in which one of the principal stresses is vertical. The measure of stability adopted is the pore-pressure in excess of hydrostatic which is required to initiate slippage on critically-oriented faults. We call this the critical excess pressure. The second aspect addresses practical constraints on the recognition of unstable stress states from necessarily limited sampling of the *in-situ* stress field. An 'unstable' stress state is taken as one in which a pore-pressure increase by 8 MPa at the well bottom linearly declining to 2.5 MPa at 5 km results in failure throughout that depth range. This criterion is adopted to

crudely simulate the disturbance to ambient pore pressure conditions that might result from prolonged injection operations. Injection pressures greater than 10 MPa in excess of hydrostatic are common and attenuation of this perturbation with depth can be anticipated. We shall assume that for practical reasons, stress measurements are limited to the sedimentary section penetrated by the prospective injection well, and hence that the deepest measurement lies above the crystalline basement which is the region whose stability is of greatest interest for hazard assessment. To accomodate this essentially economic constraint, it is necessary to make some assumption as to the manner in which stress magnitudes increase with depth. We assume that the principal stresses increase linearly throughout the depth range 1-5 km. With this assumption we examine the relative importance of various determinable stress parameters for identifying stress states which would suffer failure throughout this depth range for modest increases in pore-pressure. To illustrate the method we present an example pertaining to hazard assessment in northwestern Ohio which has recently hosted two suspected cases of induced seismicity.

Coulomb Friction

The simplest criterion that appears to reasonably describe the shear strength of intact rocks under shallow crustal crustal conditions is that due to Coulomb and is given by $t = m\, s_n + T_0$, where t and s_n are the (tensor) shear and normal effective stress components acting on the failure plane, m is the coefficient of internal friction and T_0 is the cohesive strength. The effective principal stresses, s_i, are related to total principal stresses, S_i, by $S_i = s_i + P_p$, where P_p is pore-pressure. Compression is taken positive. For rocks of isotropic strength, failure occurs on 'critically oriented' surfaces which lie in the S_1-S_3 plane at an angle $b = \tan^{-1}(-m^{-1})$ to the S_1 direction where S_1 and S_3 are the maximum and minimum principal total stresses (Jaeger and Cook, 1976). A major objection to the Coulomb fracture approach arises from the observation that the failure surface in most cases of induced seismicity can be identified with a pre-existing fault (Simpson, 1986). Hence the assumption of isotropic strength is not necessarily valid and the critical failure angle may not be realised (Sibson, 1985). A solution which is particularly acceptable for hazard assessment purposes is to assume that a critically oriented fault always exists and hence the values of m and T_0 that apply are those for frictional slippage on that fault. The Coulomb friction approach to estimating crustal strength was first suggested by Brace and Kohlstedt (1980) and is strictly valid where the crust is ubiquitously fractured on all scales and in all orientations so that the critical failure angle is realised. In the case where no frictional interface sub-parallel to a critical plane exists, an underestimate of crustal strength will result. The significance of the underestimate is controversial and touches on the fundamental issue of the shear strength of faults as opposed to unfaulted bulk rock, a question which may have no unequivocal answer (eg. Mount and Suppe, 1987). However, for the purpose of seismic hazard assessment, it would seem judicious to assume that a critically oriented fault is always present, since to show otherwise is generally difficult. The change to a friction criterion strictly requires that the cohesion be taken as zero, and that m now be identified with the coefficient of sliding friction, m_f, between the rocks in question. Byerlee (1968) has shown from laboratory sliding experiments that at confining pressures less than 200 MPa, the value of m_f is essentially independent of rock type and equal to 0.85. We shall adopt this value in all examples we present for focused discussion. However, given that some question remains as to the values of T_0 and m that are appropriate descriptors of fault zone shear strength, we shall formulate all

equations in terms of the general Coulomb strength law, $t = m\ s_n + T_0$, before reverting to the friction case in which $m = m_f = 0.85$ and $T_0 = 0$.

Representation of the Susceptibility of Arbitrary Stress States at Depth to Failure through Increased Pore Pressure

The familiar expression for failure of a Coulomb material, written in terms of the greatest and least principal total stresses, S_1 and S_3, is given by (eg Jaeger and Cook, 1976, p 97),

$$S_1 - S_3 = 2\{T_0 + m(S_3 - P_p)\}\{(m^2 + 1)^{0.5} + m\}, \qquad ...1$$

where P_p is the pore pressure and the effective stress law for shear failure given by $S_i = s_i + P_p$ is assumed. This may be reorganised to give,

$$^{c}P_p = S_3 - \frac{1}{\mu}\left\{\frac{S_1 - S_3}{2\left\{\left(\mu^2+1\right)^{0.5} + \mu\right\}} + T_0\right\}, \qquad ...2$$

which is the critical pore pressure, $^{c}P_p$, required to initiate shear failure at a point in the medium where the greatest and least principal total stresses are S_1 and S_3. For discussion of stress states it is useful to write equation 2 in terms of overburden-normalized stress magnitudes rather than absolute magnitudes. The overburden (vertical stress) is a convenient normalizing factor as it can be readily determined by integrating the density profile derived from borehole logs or seismic information. For simplicity we shall assume that density, r, is constant so that vertical stress, S_V, increases linearly with depth as rgd. We define the least and greatest stress ratios at depth, d, as,

$$R_h(d) = S_h(d) / S_V(d), \qquad ...3a$$
$$R_H(d) = S_H(d) / S_V(d). \qquad ...3b$$

Stress ratios afford a simple, readily conceptualized description of the stress state at depth. In the simple case where both horizontal principal stresses increase linearly with depth and extrapolate upward to intersect the free surface at zero stress, the stress ratio functions are two constants that, together with the vertical stress completely describe the entire crustal stress state. Generally, however, the stress ratios may vary with depth, although a first-order sense of the stress regime is readily conveyed by specifying their value at a given depth. In substituting for S_1 and S_3 in Equation 2, care must be taken in forming the correct association with the appropriate overburden-normalised principal stress components. For a *strike-slip* regime (ie. $R_h < 1 < R_H$) we have $S_1 = R_H S_V$ and $S_3 = R_h S_V$. For a *thrust* regime, however, S_3 is the vertical stress and hence the value of the associating stress ratio is unity (ie. $S_1 = (S_V/S_V)S_V$). Similarly for a *normal* regime, S_1 associates with a stress ratio of unity. Substituting Equations 3a/b into 2 gives, for the case of a *strike-slip* stress regime,

$$ {}^{c}P_p(d) = rgd\{ R_h(d)(1+f(m)) - R_H(d)f(m) \} + T_o/m , \quad ...4a $$

$$ \text{where } f(m) = (2m\{ (m^2+1)^{1/2} + m\})^{-1}. \quad ...4b $$

The cases of *normal* ($R_H < 1$) and *thrust* ($R_h > 1$) regimes are given by setting R_H and R_h respectively to unity.

For the case examined here, that of a frictional strength crust with $m = m_f = 0.85$ and $T_0 = 0$, permeated by a hydrostatically-pressured pore fluid of density r_f, Equation 4b gives $f(m) = 0.27$. If the stress ratios at depth, d, are $R_h(d)$ and $R_H(d)$, then the pore-pressure increase required to initiate frictional slippage at that depth, hereafter called the critical excess pore pressure, $D{}^{c}P_p(d)$, is given by

$$ D{}^{c}P_p(d) = d\, G(R_h, R_H), \quad ...5a $$

$$ \text{where } G = g\{ 1.27rR_h(d) - 0.27rR_H(d) - r_f\} . \quad ...5b $$

In Figure 1 we plot contours of the function G in R_h x R_H space for a mean overburden density of 2.6 gm/cc and a pore-fluid density of 1.0 gm/cc. The units of G are MPa/km. For a given depth at which the stress ratios are determined to be R_h and R_H, the pore pressure increase to initiate frictional sliding at that depth is obtained by multiplying the value of the G-contour at the R_H-R_h intercept by the depth in km. Thus the values of G are a measure of crustal stability expressed in terms of the fluid pressure increase required to induce failure. Negative values of G imply failure under hydrostatic pore pressure conditions and hence those stress states are not allowed. Smaller positive values denote stress states which are closer to failure and hence are more susceptible to induced seismicity. Clearly a least stress ratio of 0.55 implies near-failure conditions for all R_H. In fact, the smallest R_h value that a hydrostatically pressured crust can support (for $r = 2.6$, $m = 0.85$ and $T_o = 0$) is 0.52 at which point normal faulting occurs. Loci of critical excess pressure for suites of stress ratio pairs are shown as a function of depth in Figures 2a through 2d. R_h takes the values 0.6, 0.7, 0.8 and 1.0 in each successive figure for a variety of R_H values. These plots are not profiles since they do not presume the form of the *in-situ* stresses with depth. However, in the special case where both stress ratios are constant with depth, the loci then correspond to the vertical profiles of $D{}^{c}P_p$ for the crustal stress states defined by the R_h, R_H pair. This special case demands both S_h and S_H increase linearly with depth and extrapolate upward to intersect the surface at zero stress. Later we consider the effect of non-zero surface intercept. Two results are immediately apparent from Figures 1 and 2. Firstly, stress states where $R_h \leq 0.6$ are generally much more sensitive to failure through increased pore pressure than are stress states characterized by $R_h \geq 0.7$. Consider for example the special case of constant stress ratios. If $R_H = 1.3$, a ubiquitous 5 MPa increase in pore pressure will induce failure down to 7.4 km for $R_h = 0.6$, which compares with 2.2 km for $R_h = 0.7$. The second result of note is that sensitivity is largely determined by the value of R_h rather than R_H. Thus knowledge as to whether the least stress ratios at depth below

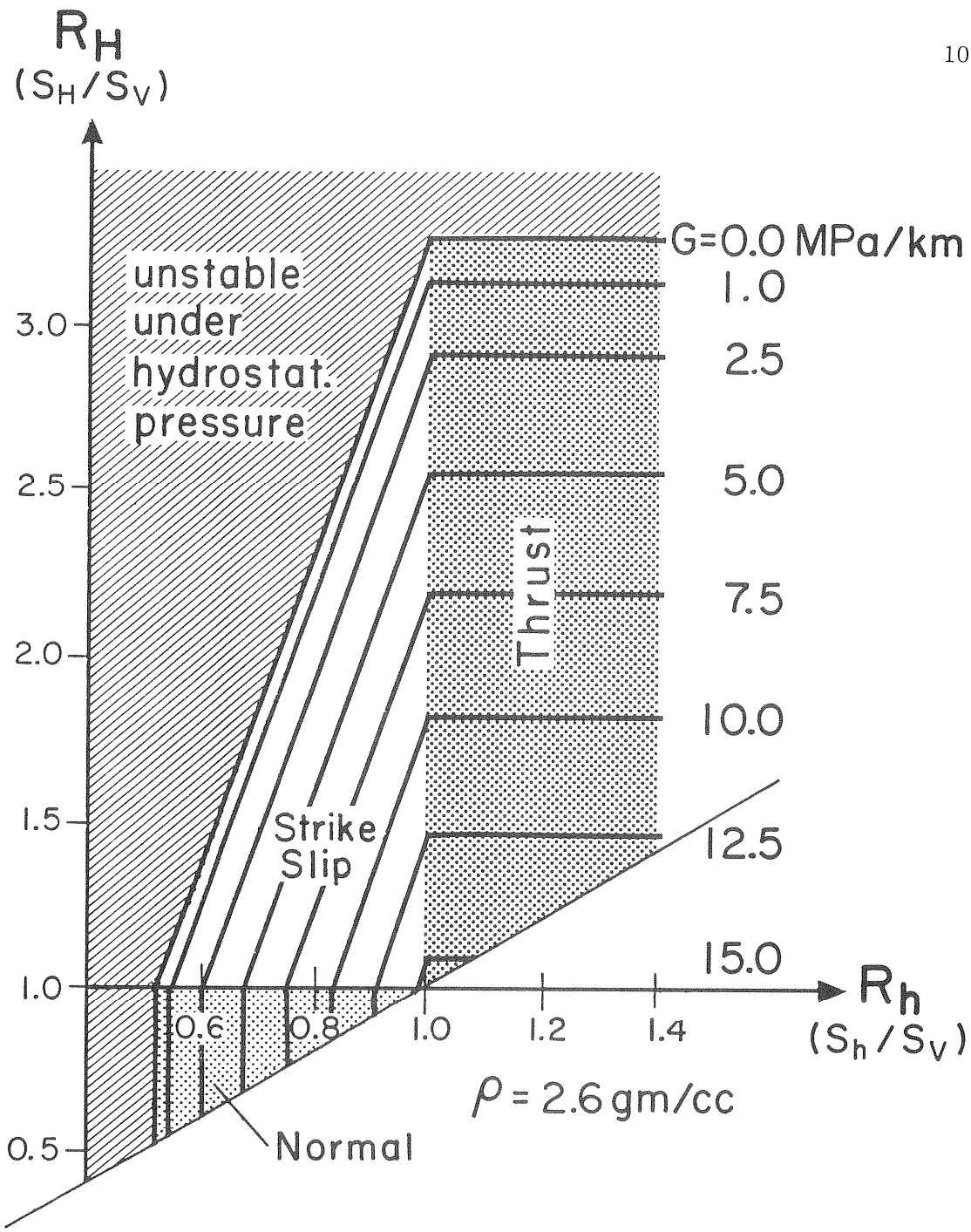

Figure 1 Contours of the critical pressure parameter, G, in stress-ratio space. The values of the two stress ratios define the stress state at a point in a medium in which one principal stress is vertical. Regions corresponding to the Ansersonian faulting categories are shown for convenience. It is assumed that vertical stress increases linearly with depth as 25.5 MPa/km. The value of the G-parameter at a point in R_h x R_H space gives the pore pressure gradient in excess of hydrostatic that is required to induce slippage on favorably-oriented frictional interfaces of friction coefficient 0.85. Multiplying this G value by depth in km gives the critical excess pressure at that depth for that crustal stress state defined by the R_h, R_H pair. Thus G is a measure of crustal stability, and the contours define crustal stress states of equal susceptibility to failure through pore pressure increase. Regions which are unstable under hydrostatic pore pressure are hatchured. The diagonal line forming the bottom boundary to admissible stress states arises from the semantic constraint that $R_H \geq R_h$.

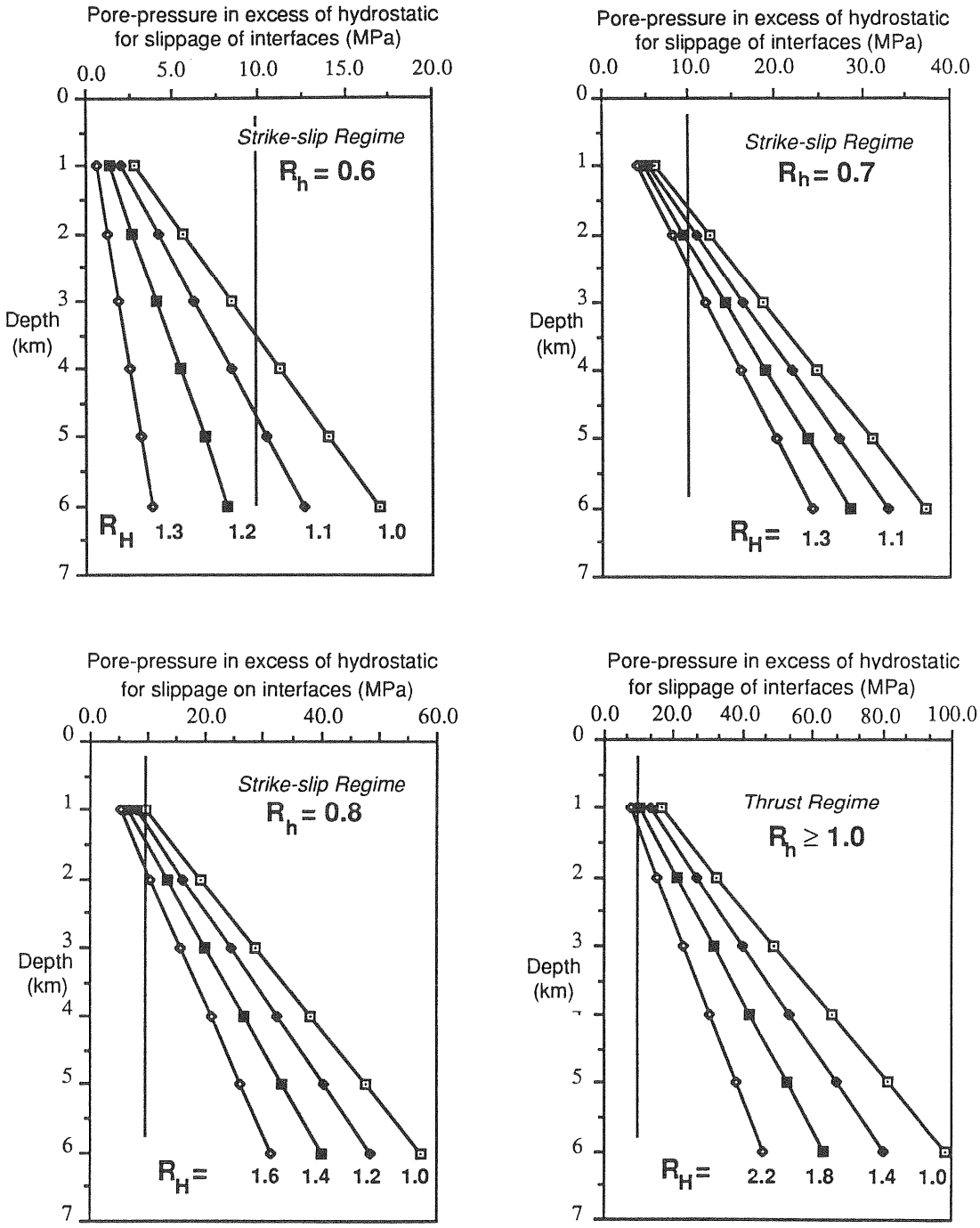

Figure 2: Critical excess pressure as a function of depth for various combinations of R_h and R_H. The slopes of the failure lines correspond to the values of G inferred from Figure 1. Clearly a stress state characterized by a least stress ratio of 0.6 is more prone to failure through increased pore-pressure than where $R_h \geq 0.7$. In the special case where the stress ratios are the same at all depths, the failure lines may be taken as defining depth profiles of excess pressure for failure.

a prospective well are less than, or greater than 0.65 is far more important for evaluating the potential for inducing failure at depth than is the corresponding determination of R_H. This is fortunate; for estimates of S_h are more readily obtained through measurement than those of S_H and are subject to less uncertainty.

Identification of Potentially Hazardous Linear Stress Regimes by Stress Measurement

Definitions and Assumptions

From the viewpoint of seismic hazard assessment, there is clearly much to be gained from knowledge of the approximate stress ratio values that apply to the crust below a prospective fluid injection well (or reservoir for that matter). Direct measurement of the stress profiles is possible throughout the section penetrated by the well but is impractical below the intended well bottom. As this is the region whose stability is of greatest concern, the stress ratios here must be estimated through extrapolation of the stress trends established above well bottom. In this section we evaluate the importance of various practically determinable stress parameters in facilitating the recognition of hazardous stress regimes. A stress state is considered unstable and therefore hazardous if its corresponding critical excess pressure profile is everywhere less than a linear threshold function which takes a value of 8 MPa at the well bottom and 2.5 MPa at 5 km depth. That is, a pore-pressure increase of 8 MPa at the well bottom linearly declining to 2.5 MPa at 5 km results in failure throughout that depth range. This criterion is based on typical surface injection pressures in excess of 10 MPa, and the anticipation of attenuation of the pressure disturbance with depth. It should be emphasised that although the criterion as defined constitutes a sufficient condition for failure on a scale equivalent to at least a moderate sized earthquake, it is not a necessary condition since it does not consider dynamic effects. The primary assumption we make is that throughout the depth range 1-5 km, both S_h and S_H increase linearly with depth as,

$$S_H(d) = a_H d + b_H \quad , \qquad ...6a$$

$$S_h(d) = a_h d + b_h \quad , \qquad ...6b$$

where a_i and b_i are constants. We take 1 km as the upper limit of linearity to exclude from consideration the complexities of the near-surface stress regime. The lower limit of 5 km is somewhat arbitrary. We assume that the deepest stress measurement available is at the depth of the well bottom, d', and yields point stress ratio determinations, $R_h[d']$ and $R_H[d']$, where brackets indicate measured values. This is a pivotal measurement in as much as it is 'closest to the heart of the matter'. Equations 6a/b can be expressed in terms of these pivotal stress ratios as,

$$S_H(d) = S_V R_H[d'] - b_H \{ (d/d') - 1 \} \quad , \qquad ...7a$$

$$S_h(d) = S_V R_h[d'] - b_h \{ (d/d') - 1 \} \quad , \qquad ...7b$$

which are the preferred form of the stress characterisation equations for substitution into Equation 2. The constants b_h and b_H are the surface intercept values of the linear S_h and S_H profiles and are zero for the special case of depth independent stress ratios discussed previously. We emphasize that stress measurements conducted near the surface itself do not generally yield reliable estimates of b_H and b_h as they

are heavily influenced by near-surface processes and topography. They must be estimated through extrapolation of the trends defined by conducting stress measurements at deeper points along the borehole. Substituting Equations 7a/b into 2 gives the general expression for the critical pore pressure under *strike-slip* stress conditions,

$$^{c}P_p(d) = rgd\{ R_h[d'](1+f(m)) - R_H[d']f(m) \} - ((d/d') - 1)\{ b_h(1+ f(m)) - b_H f(m) \} + T_o/m \quad ...8$$

The cases of *normal* and *thrust* stress regimes are this time obtained by setting $R_H[d'] = 1$; $b_H = 0$ for *normal*, and $R_h[d'] = 1$; $b_h = 0$ for *thrust*.. Care must be exercised in applying equation 8 to ensure that the correct form is used, especially where a change of regime occurs at some depth. In that case two forms must be used to cover each regime separately. For the case of interest of a frictional strength crust for which $m = m_f = 0.85$ and the undisturbed pore pressure is hydrostatic, the critical excess pressure at depth d is given by,

$$D^{c}P_p(d) = d\ G[R_h[d'], R_H[d']] - ((d/d') - 1)\{ 1.27b_h - 0.27b_H \}, \quad ...9$$

where G is given by equation 5b evaluated at depth d'. The first term can be recognized as defining the critical excess pressure profile that would apply were the stress ratios constant with depth (and equal to their value measured at d'). This would be the best estimate of the $D^{c}P_p$ profile given only knowledge of the principal stress magnitudes at the well bottom . The second term is a correction which utilizes the additional information of the surface intercepts, b_h and b_H. Its value increases in proportion to the vertical distance from the deepest stress measurement at which point it is zero. The forms of these two terms are illustrated in Figure 3 for the example where the *in situ* horizontal stress profiles are such that the least and greatest stress ratios determined at the bottom of a hypothetical 2 km deep well are 0.8 and 1.76 respectively, and the surface intercepts are $b_h = 9.2$ MPa and $b_H = 0$. These stress ratios imply G[2 km] = 4.0 MPa/km. The sum of the G[2 km] term and the correction term gives the critical excess pressure profile associated with the stress state. This profile is less than the threshold pressure at all depths from the well bottom to 5km and hence the stress state is hazardous. Note that the stress ratios that apply at 5 km depth are R_h(5 km) = 0.68 and R_H(5 km) = 1.76. Hence from Equation 5b, G(5 km) = 0.1 MPa/km which implies that failure conditions at 5 km depth are met for a pore pressure increase of 0.5 MPa. Inspection of the form of the correction factor in Equation 9 shows that, in keeping with previous results, the least horizontal stress offset, b_h, exerts a much stronger influence on the predicted critical excess pore pressure than does b_H . Henceforth for clarity we take $b_H = 0$.

Importance of Surface Intercept

To illustrate the importance of determining the least-stress surface-intercept we plot in Figure 4 combinations of G and b_h values which describe hydrostatically-stable stress states that become unstable when the pore-pressure field is disturbed in

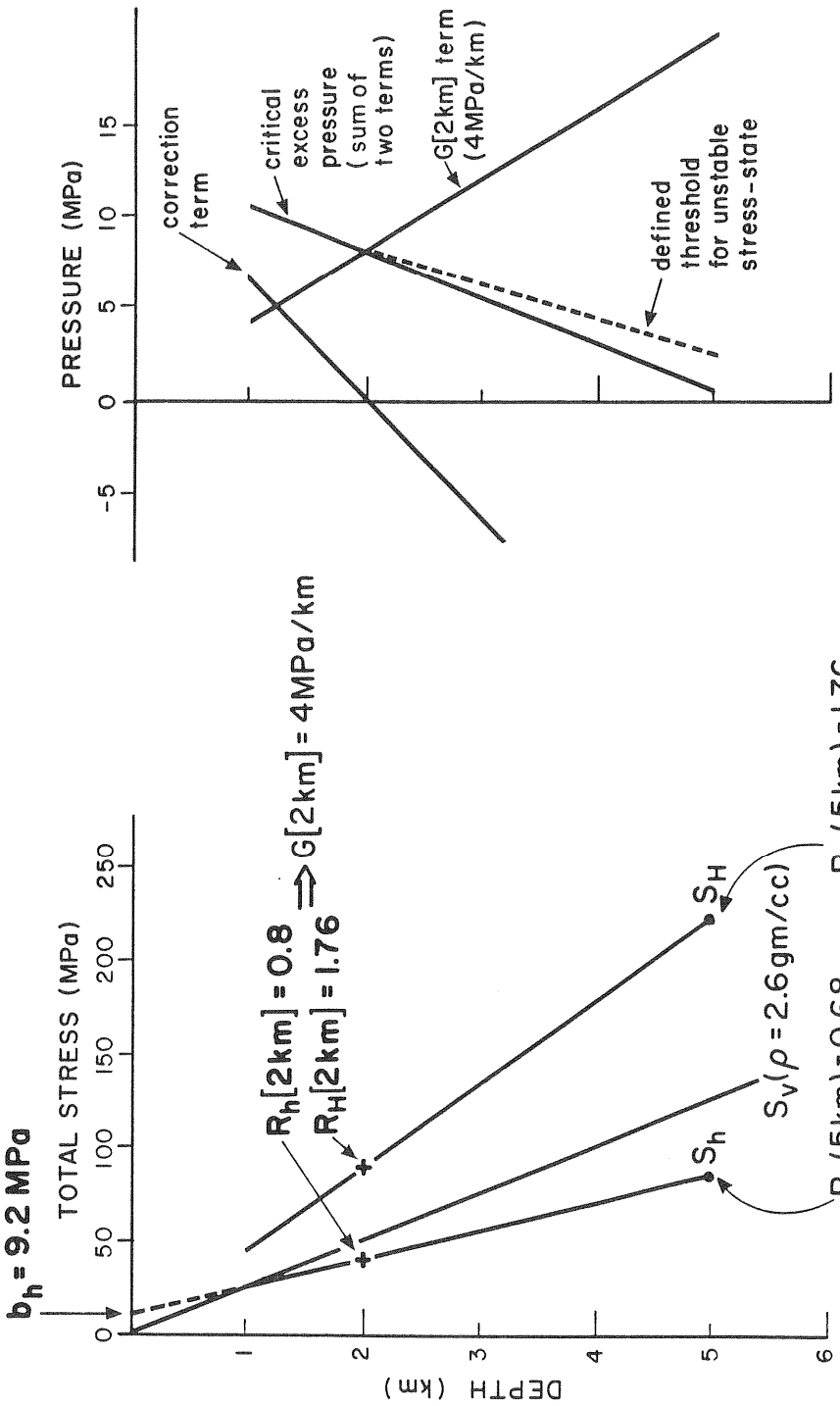

Figure 3: Example of a *strike-slip* stress state defined by least and greatest stress ratio values at 2 km depth of 0.8 and 1.76 respectively and surface intercept values of b_h= 9.2 and b_H = 0. The corresponding critical excess pressure profile (and the two terms of which it is the sum) are shown in the rightmost plot. The stress state is stable under hydrostatic pore pressures but becomes unstable everywhere in the depth range 1-5 km when the pore pressure is increased by the amount indicated by the dashed line.

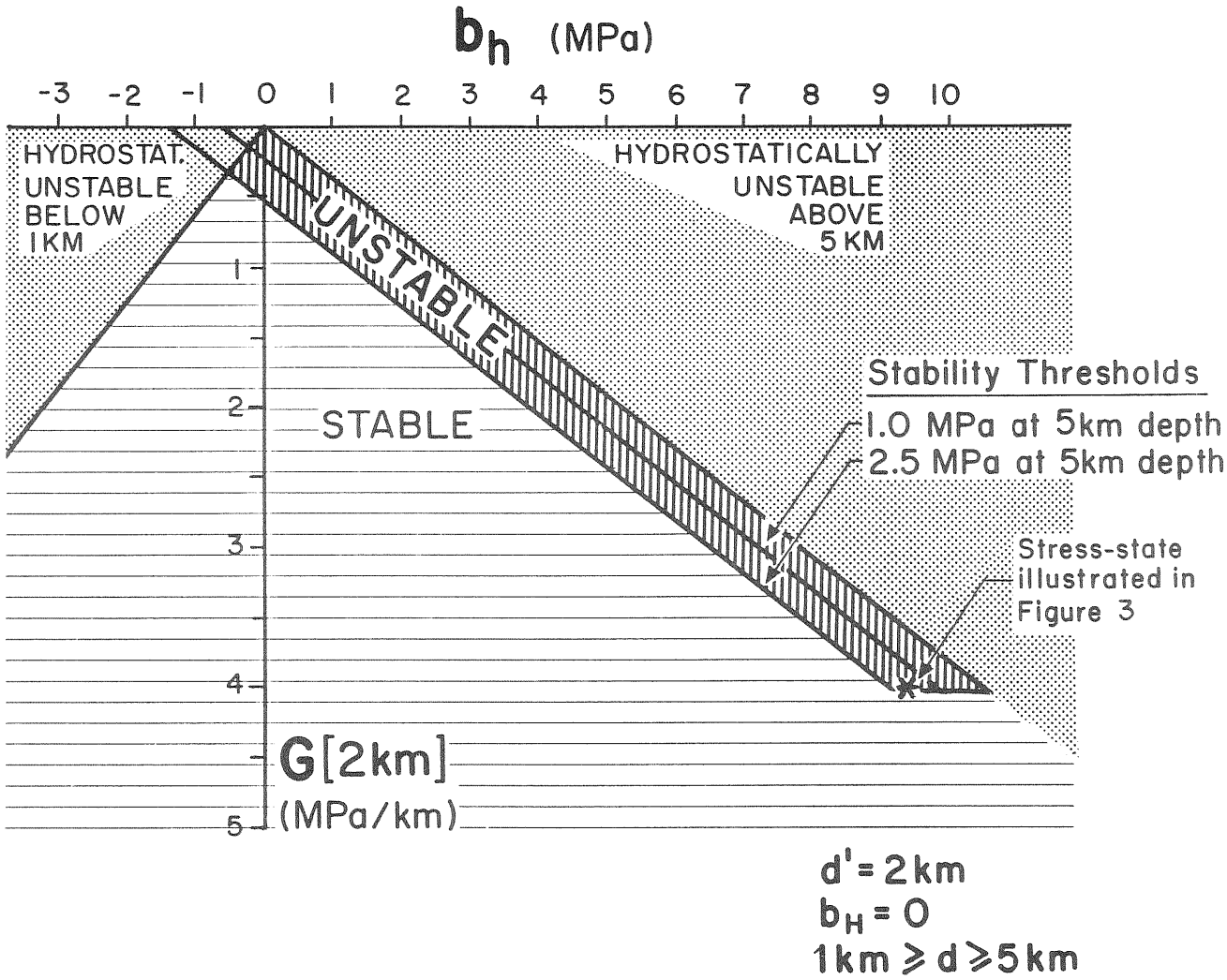

Figure 4: Stability field for allowable combinations of the stability factor G inferred at 2 km depth and the S_h surface intercept b_h. The value of b_H is taken as zero. Combinations in the stippled area are hydrostatically unstable somewhere in the depth range 1-5 km and hence are not allowable. The vertical hatchuring denotes combinations for which slippage is predicted everywhere in the depth range 1-5 km if the pore pressure is increased above hydrostatic by 8 MPa at 2 km linearly declining to either 1 or 2.5 MPa at 5 km as shown.

a manner that might reasonably result from injection well activity (ie. is raised by the amount of the threshold function shown in Figure 3). The specific case considered assumes a well depth of 2 km; hence the values of G define pairs of values of R_H and R_h that would be measured at that depth (Figure 1). Taking $b_H = 0$ and $d' = 2$ km, Equation 9 can be written,

$$G[2\ km] = d^{-1} \{ D^c P_p(d) + 1.27((d/2) - 1)\ b_h \} . \qquad ...10$$

The condition for stability at the well bottom, given by $D^c P_p(2\ km) \leq 8$ MPa, is satisfied for all $G[2\ km] \geq 4$ MPa/km. This is independent of the value of b_h since the correction term in Equation 10 is zero at the well bottom.

The condition for stability at depth d = 5 km given by $D^c P_p(5\ km) \leq 2.5$ MPa implies a stability threshold given by $G[2\ km] = 0.5 + 0.381 b_h$. This relation is plotted in Figure 4 where it delimits stable from unstable stress states. We also show the stability threshold that would apply for an instability criterion in which the critical excess pressure for failure at 5 km is 1 MPa.

Also indicated in Figure 4 are the disallowed stress states which are hydrostatically unstable somewhere in the depth range $1 \leq d \leq 5$ km. The condition for hydrostatic stability, $D^c P_p(d) \geq 0$, together with Equation 9 requires that in the prescribed depth range, b_h and G satisfy the relation,

$$d\ G\ [d'] - 1.27\ b_h\ (\ (d/d') - 1\ ) \geq 0 . \qquad ...11$$

For a well depth $d' = 2$ km, tensile (negative) values of b_h must satisfy the condition $G[2\ km] \geq -0.635\ b_h$ in order that hydrostatic stability be maintained up to 1 km depth. For compressive b_h the condition $G[2\ km] \geq 0.38\ b_h$ must be satisfied in order that solutions be realizable down to a depth of 5 km.

The domain of instability in the sense of our definition is identified in Figure 4 by the vertical hatchuring. An important result is that <u>all</u> physically realizable stress regimes for which $b_h < -1$ MPa are stable. This result is robust and is not altered appreciably by specifying that linearity holds only up to 1.5 km. Thus the stabilizing effect of tensile b_h is considerable. To illustrate the destabilizing effect of compressive b_h we note that extreme stress states which appear most stable from the 2 km stress measurement but which are, in fact, prone to failure are characterized by values of G[2km] which approach 4 MPa/km. The stress state depicted in Figure 3 are one suc example where $R_h[2\ km] = 0.8$ and $R_H[2km] = 1.76$ (Equation 5b and Figure 1). This limiting case requires that $b_h > 9.2$ MPa for failure to 5 km, a value which is high but not unreasonable. Thus what might appear to be a stable stress state from first order inspection of the high value of R_h at 2 km depth may in fact be unstable if the values of $R_H[2\ km]$ and b_h are sufficiently large.

The principal stress profiles shown in Figure 3 are noteworthy in that the corresponding critical excess pressure decreases with depth. Pine and Batchelor (1984) have reported a negative critical pressure gradient in granite at Rosemanowes

Quarry, UK and noted that negative critical excess pressures tend to favour downward migration of shear failure. Since shear failure results in enhanced conductivity of the fracture due to interface mismatch (self-propping), downward migration of fluid pressure will be promoted which in turn will further assist downward shearing. During a monthlong 10^5 m^3 injection of water into a 2 km deep well at Rosemanowes Quarry, microseismic emission was observed to migrate downwards to 3.5 km depth but not upwards (Batchelor et al., 1983). Downward shearing thus provides a mechanism of enhanced downward propagation of elevated pore pressure. Attendant microseismic emission would not necessarily be evident unless special provision was made for its detection.

Practical Implementation

The preceding analysis is based on the assumption that the principal stress magnitudes and ambient pore pressure increase linearly with depth below 1 km. To implement the analysis the quantities r, $R_h[d']$, $R_H[d']$ and b_h must be determined. All may be estimated at modest expense from measurements conducted in the prospective well. The mean density, r, may be obtained from well logs or deeper seismic information. The values of the two stress ratios at the well-bottom, $R_h[d']$ and $R_H[d']$, are crucial and should be estimated by conducting at least two 'scientific quality' hydrofracture stress measurements in an open-hole section at well-bottom. This is the only essential measurement that may interfere with common completion practice of running casing to total depth. A profile of S_h from which b_h can be derived (and the assumption that stresses increase linearly with depth evaluated evaluated) may be obtained by conducting a series of hydrofracturing stress measurements through perforations in cased portions of the hole which can later be cemented. The hydrofracture technique when applied to cased holes appears to yield satisfactory estimates of S_h (Warpinski, 1983) but fails for S_H. Indeed, there is no proven technique available as yet for obtaining estimates of S_H in cased holes. To estimate S_H requires a section of open hole free of natural fractures, and the estimation of b_H requires a series of S_H determinations at different depths. Thus, although the analysis can be improved from knowledge of b_H, the benefits are small in comparison to the additional effort and expense involved.

An example of hazard assessment in northern Ohio

On January 31 1986, a magnitude 5 earthquake occurred in the vicinity of Chardon, some 15 km south of the Perry Nuclear Power Plant near Cleveland Ohio. Focal mechanism and aftershock studies suggest that right-lateral strike-slip rupture occurred between 2-7 km depth on a near vertical NNW-SSE striking plane within the crystalline basement (Wesson et al., 1986). The area is located near the northwestern fringe of the Appalachian basin (Figure 5a) where the Paleozoic sedimentary cover, thickening to the SE, is approximately 2km thick (Figure 5b). This is illustrated in Figure 5b which presents a cross-section along profile B-B' of Figure 5a. The cross section is based upon a currently unpublished interpretation of seismic reflection profiles by R. Beardsley of Columbia Natural Resources, Charleston, WV. Some 10 km south of the epicenter are located several class 1 waste disposal wells which inject into the Cambrian Mt. Simon Formation, a low permeability (millidarcies) sandstone which immediately overlies the Precambrian basement (Figure 5b). Typical injection rates are 0.3 m^3/min and result in bottom hole pressures of the order 10 MPa in excess of hydrostatic . A cumulative volume of

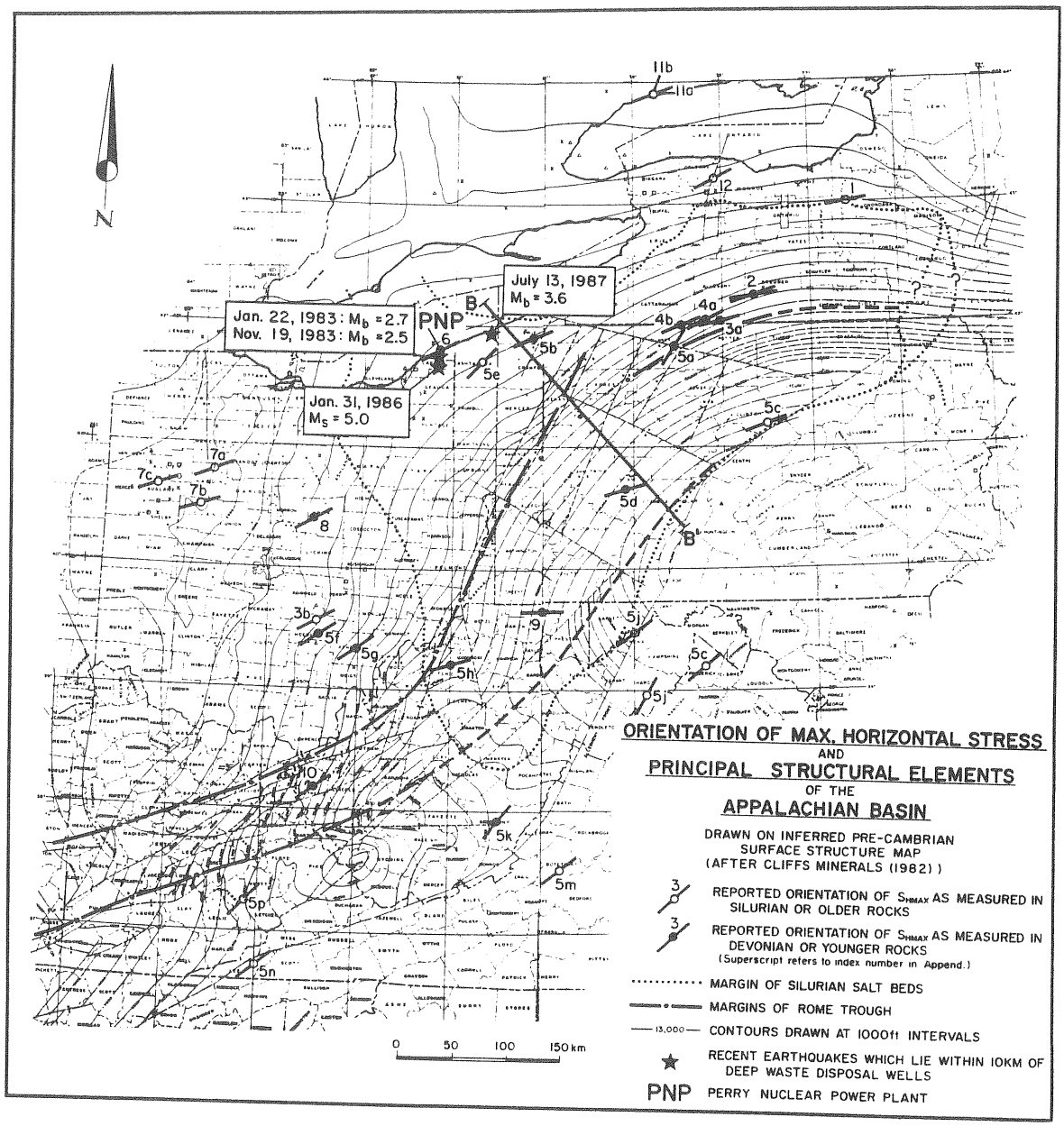

Figure 5: a) Orientation of maximum horizontal stress in the Appalachian basin as determined from hydrofracture and borehole-breakout observations (reproduced from Evans and Engelder (1987)). Distinction is made between measurements made in the Devonian (or younger), and (Silurian) or older sections. Also shown are the margins of the Silurian salt beds and the Cambro-Ordovician Rome Trough.

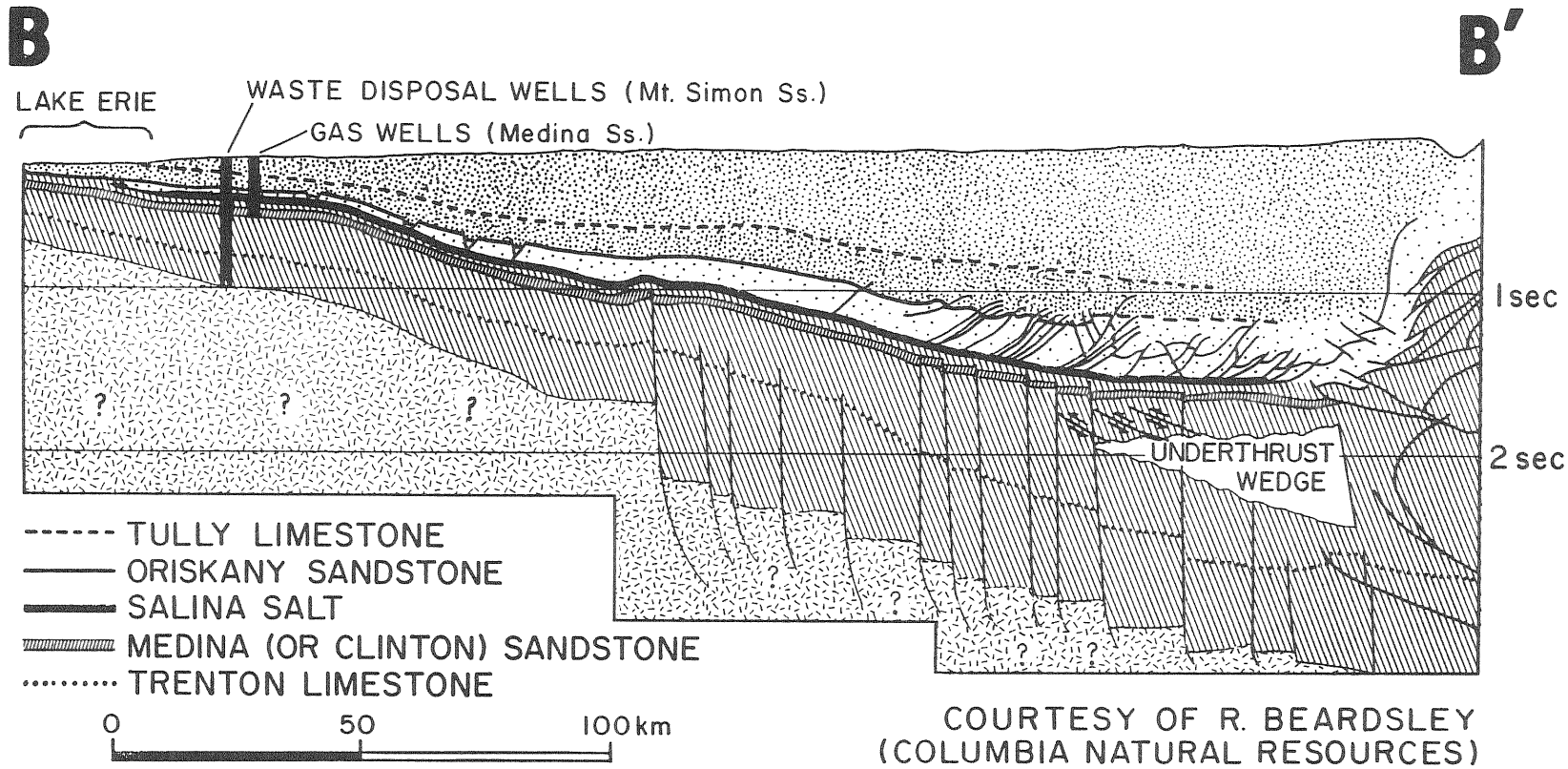

Figure 5: b) Cross section along profile B-B' of Figure 5a showing key stratigraphic horizons. Based on seismic reflection profiles interpreted by and reproduced courtesy of R. Beardsley (Columbia Natural Resources). Depth is indicated in two-way travel time (1 sec ≈ 2.25 km for the Paleozoic sediments).

10^6 m^3 has been injected since 1971. Nicholson et al. (1987) have discussed the possibility of a causal relationship between the January 31st, 1986 earthquake and the injection activity.

A further suspected case occurred on July 13th 1987 near Ashtabula on the shore of Lake Erie close to the Ohio/Pennsylvania state line. There, the epicenter of a magnitude 3.6 earthquake was located less than 1 km distant from a class 1 waste disposal well which had been injecting fluid at a surface pressure of 10 MPa into the Mt. Simon sandstone immediately above basement for the previous 15 months. Aftershock studies suggest that left-lateral strike-slip slippage occurred on an E-W trending vertical plane, and was limited to the upper kilometer or so of the basement (Armbruster et al., 1987). The last earthquake located in Ashtabula County occurred in 1857 (Weston Geophysical, 1979) whereas the historic record for the Chardon region shows a higher incidence of activity with magnitudes 4-5 being not uncommon. This history of seismic activity, which predates the advent of injection operations, demonstrates that, locally at least, the crust is close to failure conditions. The sense of slippage in the Chardon and Ashtabula earthquakes, and in all regional events for which a focal mechanism solution is available, suggests that the stress state in the basement is *strike-slip* and that the direction of maximum compression is approximately NE-SW. The orientation of maximum compression inferred from wellbore breakouts or induced hydraulic fracture orientation in the overlying Paleozoic rocks of the basin is shown in Figure 5a (after Evans and Engelder, 1987). Although a slight tendency to follow the structural trends of the basin can be seen, the inferred orientation of maximum compression in the Paleozoic sediments is consistent with that inferred the basement. The same orientation of compression is found over much of the Eastern U.S. (Figure 6, from Zoback and Zoback, 1987) and is thought to result largely from the push of the mid-Atlantic ridge which is seemingly transmitted across the continantal margin (Sbar and Sykes, 1973).

To impliment a stability analysis for northwestern Ohio requires information as to the magnitude of the stresses from which stress ratios can be calculated. Recently, Evans and Engelder (1987) presented maps of least stress ratios measured at various stratigraphic horizons in the Paleozoic strata of the area in question. These maps are well suited to examining stability in the area of suspected induced seismic activity. The data are derived largely from commercial hydrofracturing operations performed through casing and hence only R_h at the depth of the treatment is determined. However, as data are available from several stratigraphic levels, b_h may also be estimated. The mean overburden gradient for the Paleozoic section is 2.7 gm/cc and hence we assume a vertical stress gradient of 26.5 MPa/km. Evans and Engelder's map for the Silurian section is reproduced in Figure 7. A similar map for Cambrian rocks prepared as part of this study is shown as Figure 8. The index to the Cambrian data is presented as Appendix A of this report (see Evans and Engelder (1987) for the index to Silurian data points). Owing to the somewhat coarse method of measurement, the non-systematic error associated with the individual data values is about ± 0.05, or about 7%. However, the dominant source of systematic error that may affect the collective data is due to potential elevation of the fracture-normal total stress arising from formation pore pressure increases during the fracturing operation itself. The effect would be to increase the instantaneous shut-in pressure (ISIP) above the 'undisturbed' value of the least principal stress and thereby result in an overestimate of R_h. Hence the mean values of R_h inferred from the data as a whole may, if anything, be too high. The vast majority of the Silurian data points are obtained in the widespread Clinton/Medina sandstone which typically lies a few hundred meters below the extensive salt deposits of the Upper Silurian Salina Group

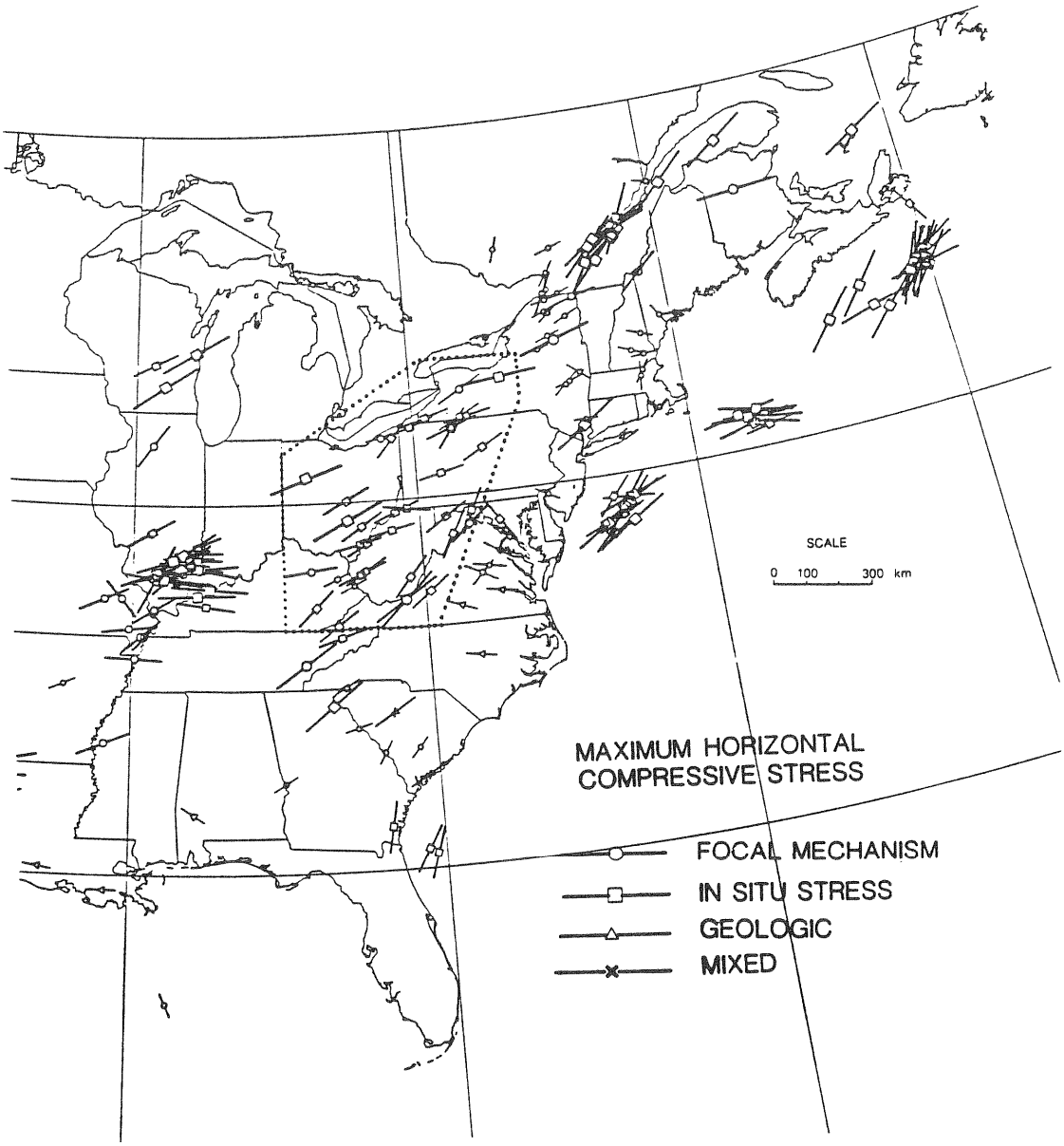

Tectonic stress field of the Eastern Continental U. S.
from M. L. Zoback and M. D. Zoback, in GSA Memoir " Geophysical Framework of the Continental United States, 1987.

Figure 6: Orientation of maximum horizontal stress in the Eastern U.S. as determined from a variety of crustal stress indicators sampling shallow and seismogenic depths (reproduced courtesy of Mary Lou Zoback, U.S.G.S., Menlo Park, CA). The field of view of Figure 5a is indicated.

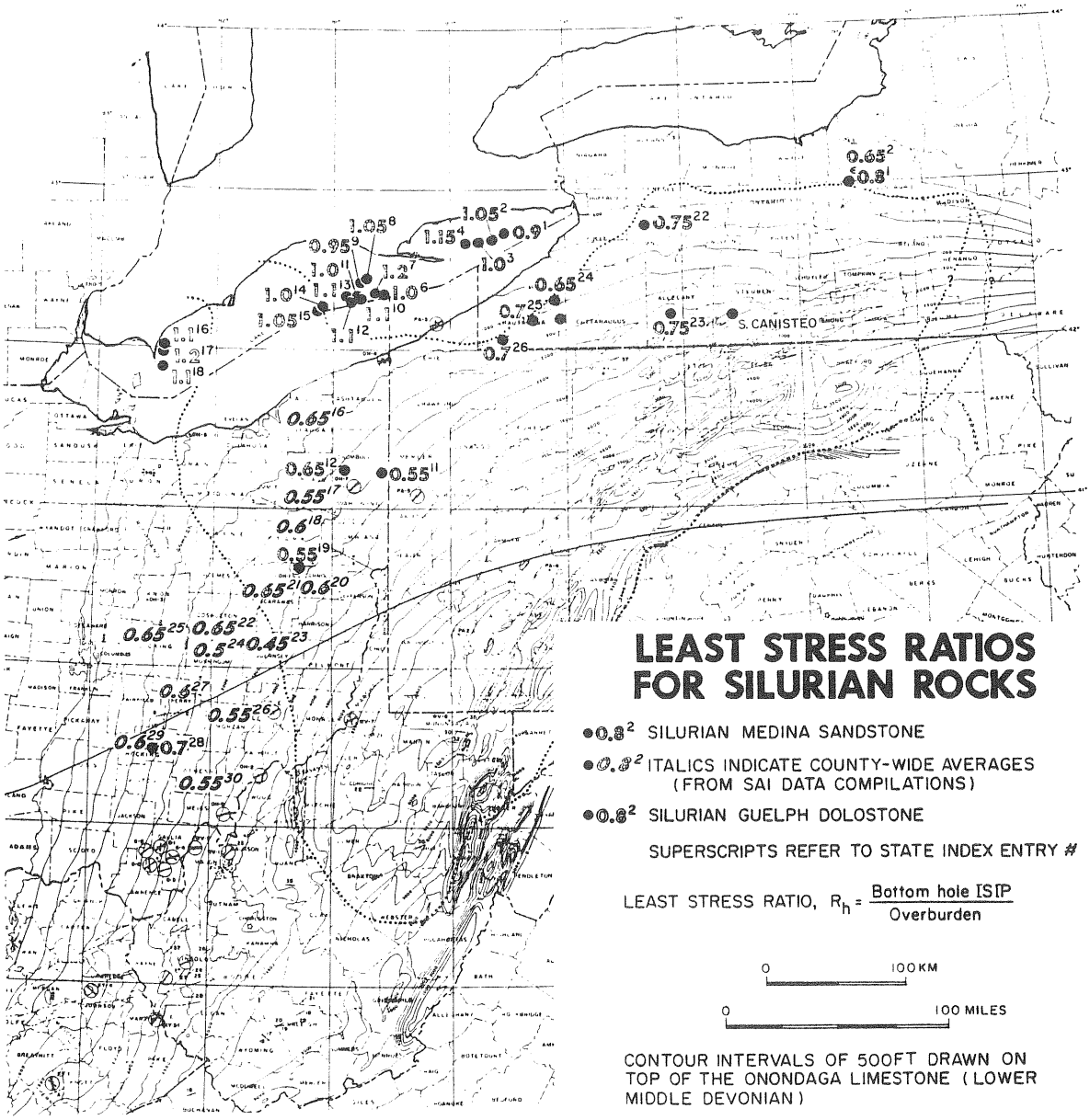

Figure 7: Map of least stress ratios measured in Silurian rocks underlying the salt.

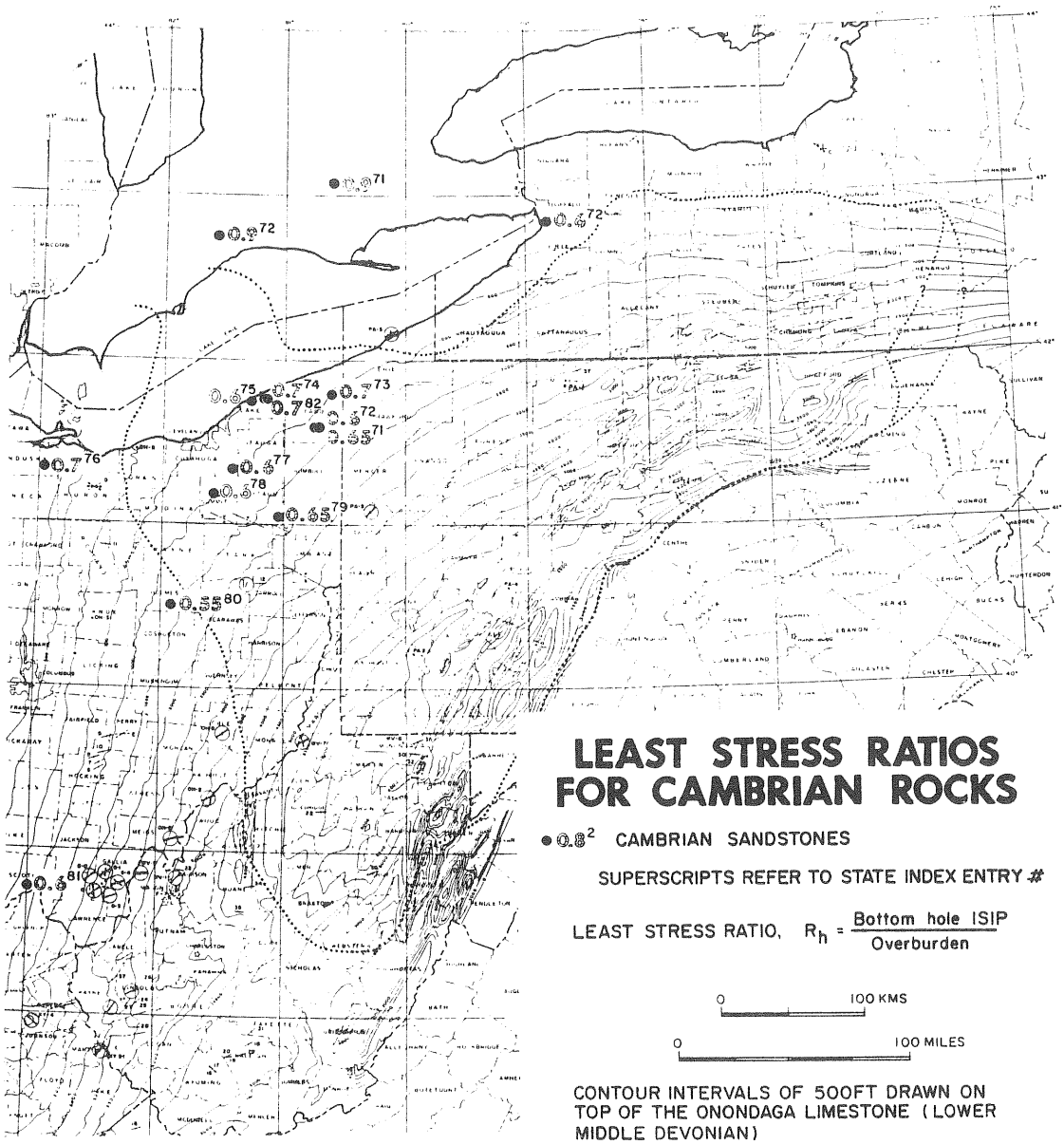

Figure 8: Map of least stress ratios measured in Cambrian rocks overlying the basement.

(Figures 5a/b). The low strength of the salt serves to mechanically decouple the Devonian strata from the underlying section (Figure 5b) and gives rise to a discontinuity in horizontal stress (Evans, 1987). For this reason we exclude from consideration stress ratios determined in strata above the salt. The data show that least stress ratios at the stratigraphic level of the Medina are remarkably uniform across the basin fringe region and indicate a slight tendency toward higher values in the north. This tendency becomes pronounced north of the southern shore of Lake Erie which may in part be due to shallowing of the formation to the north (its depth at the international boundary is ~ 300 m). In the southern Lakeshore region which includes the areas of recent seismicity, the Medina is ~900 m deep, and values of R_h[0.9 km] in the range 0.6-0.7 appear to be appropriate. The Cambrian data are largely derived from hydrofracture and completion tests performed on waste disposal wells completed in the Mt. Simon sandstone immediately above basement. These data indicate a very similar pattern with fairly constant least stress ratios south of Lake Erie of R_h [2 km] = 0.6 - 0.7 increasing northward in Canada. As the estimation error is of the order of ±0.05 it is uncertain whether the lateral variations in stress ratio are real, or whether they reflect scatter about a constant value of 0.65 which applies to both the Silurian and Cambrian formations. We consider both possibilities. Ambient pore pressures in this section are typically found to be approximately hydrostatic.

For a constant least stress ratio equal to 0.65 the stability analysis is particularly simple, for then b_h is zero. From Equation 10 (or Figure 4) we find that for b_h =0, unstable stress states (for 2.5 MPa threshold at 5 km) are given by $0.5 \geq G[2\ km] \geq 0$. Equation 5b shows that for R_h = 0.65 and r = 2.7 gm/cc this would be satisfied by $R_H > 1.62$ (note that Figure 1 applies for r = 2.6 gm/cc).

To provide some sense of the robustness of this result we also consider the two extreme cases, illustrated in Figure 9, which are marginally consistent with the data. These are given by: R_h[0.9km] = 0.6, R_h[2km] = 0.7 ; and R_h[0.9 km] = 0.7, R_h[2 km] = 0.6. The S_h surface intercepts implied by these values are b_h = -4.3 and +4.3 MPa respectively. The most 'stable' case is defined by R_h[2 km] = 0.7, b_h = -4.3 MPa which Figure 4 shows is stable in the sense of our definition for all possible values of R_H[2km]. The least stable extreme case is defined by R_h[2 km] = 0.6, b_h = 4.3 MPa. Taking b_h = 4.3 MPa, Equations 10 and 11 suggest allowable unstable states are given by $2.15 \geq G[2\ km] \geq 1.65$ (see Figure 4). For R_h[2 km] = 0.6, this corresponds to $1.22 \geq R_H[2\ km] \geq 1.15$ (Equation 5b; Figure 1). If a 1 MPa critical excess pressure is used to define the instability threshold at 5 km, then $1.85 \geq G \geq 1.65$ implying $1.22 \geq R_H \geq 1.19$, which is not greatly different.

Discussion

The preceding analysis shows that if indeed the inferred stress profiles may be linearly extrapolated into the basement, unstable stress states are found for reasonable levels of maximum horizontal stress. To invalidate this conclusion it would be necessary to accept that least stress ratios increase with depth from 0.6 at the level of the Medina to 0.7 in the sandstone immediately above basement. Although this is strictly within the margin of error for an individual measurement, it is not supported by the statistics of the data set as a whole. It does serve to demonstrate, however, the sensitivity of the analysis technique to the precision of comparitively shallow data which are implicitly extrapolated to depth. In implementing hazard assessment

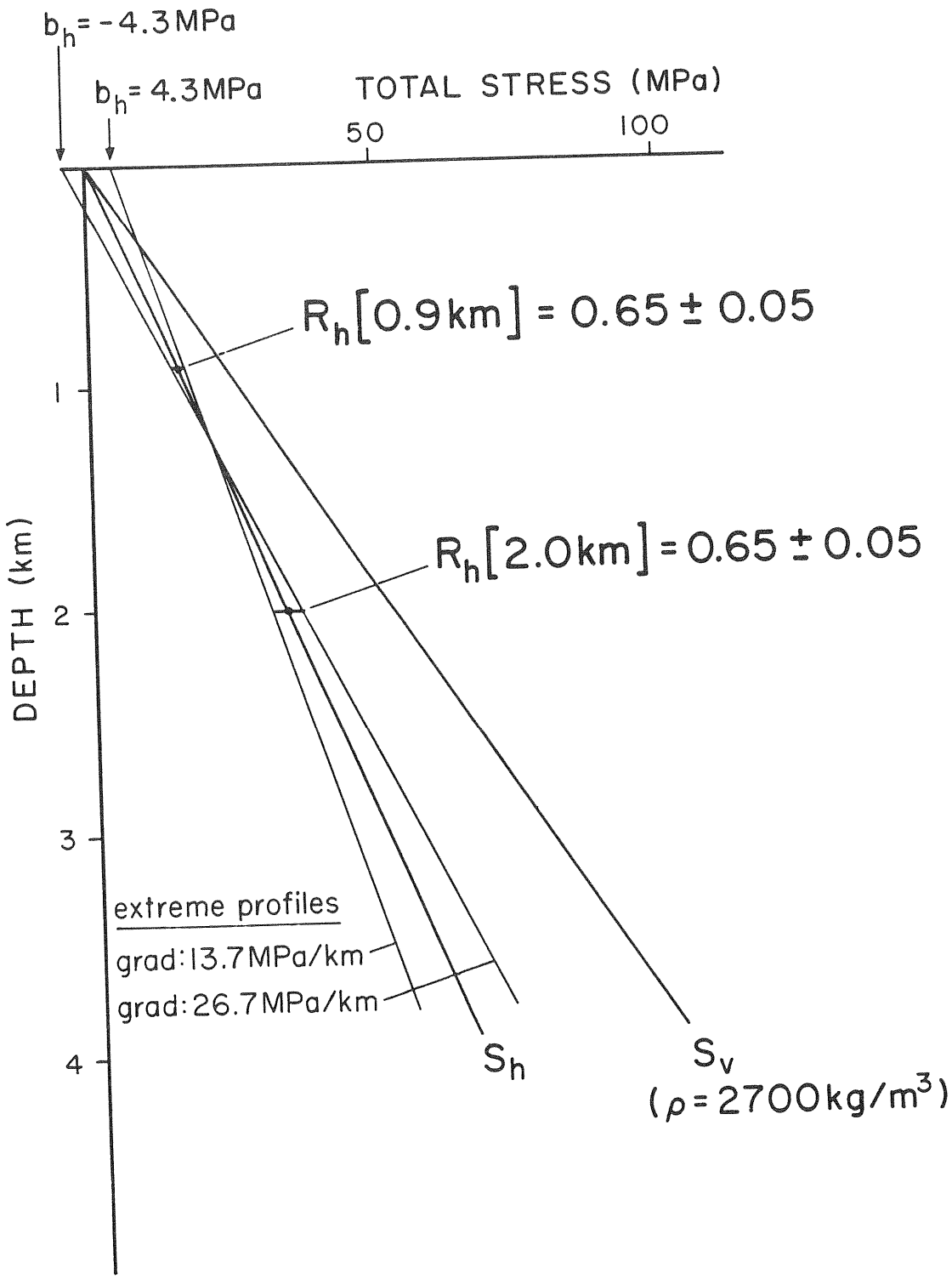

Figure 9: Stress profiles considered in the Coulomb friction stability analysis for northern Ohio.

schemes of this sort which are based on extrapolation, the objective must be to determine whether potentially unstable states of stress which are consistent with the constraining stress data exist, rather than to show that marginally stable states can also be found. Thus we conclude that provided the greatest stress ratio in the sandstone overlying basement is 1.2 or greater, a physically realizable stress state exists which is consistent with the available stress data and which would result in failure to 5 km depth were the pore pressure at the well bottom to be raised to 8 MPa above hydrostatic and that at 5 km by as little as 1.0 MPa.

The analysis of the potential for induced seismicity in northwestern Ohio could be greatly improved in two ways. Firstly, the precise value of R_H in the sandstone overlying basement is uncertain as no careful measurements have been conducted in the area. Nicholson et al. (1987) suggest values in the range R_H[2 km] = 1.0-1.25 based upon the breakdown pressure of ~40 m sections of open hole but this result may be in error due to the possible presence of natural fractures. Research quality hydrofracture measurements in this interval could certainly remove what is a major uncertainty. The second improvement would address what is perhaps the single most important question affecting the utility of the technique in general: the assumption of linearity and in particular, the validity of extrapolating stress trends established in the Paleozoic sedimentary strata downward into the crystalline basement. The consistency between the orientation of maximum compression in the basement as inferred from focal mechanism solutions and that in the Paleozoic strata demonstrates that the same tectonic stress field is dominant in both. However, our understanding of what governs the magnitude of stress in rocks is far too poor to be of help in reasoning the likelihood that stress magnitudes are continuous across the unconformity, or otherwise. Certainly at some level of precision one might anticipate variations in horizontal stress resulting from mechanical property contrasts or perhaps lithologic history. The presumption here is that at depths greater than 1 km these effects are second order although this remains to be determined. The stress ratio maps presented in Figures 7 and 8 suggest that stress magnitudes in the Paleozoic section (below the salt) increase linearly with depth and are reasonably well behaved in terms of lateral variability. Linkage of this result to the stress regime in the basement would have implications not only for the assessment of crustal stability in northwestern Ohio but for the applicability of the technique in general since it would further our fundamental understanding of crustal mechanics. To provide this linkage, hydrofracture stress measurements penetrating at least several hundred meters into basement at several sites in northwestern Ohio would certainly be useful.

Conclusion

An explicit relation is derived for the pore pressure increase above ambient hydrostatic levels required to induce slippage on a favorably-oriented Coulomb-strength interface at depth, d, under arbitrary states of stress. Stress states are described in terms of least and greatest stress ratios which are respectively the least and greatest horizontal total principal stress magnitudes normalized to the overburden. These are denoted as R_h (d) and R_H(d).

The single most important stress parameter determining the pore pressure increase for failure at a point at depth is the least stress ratio at that depth. The dependence on the value of greatest stress ratio is minor in comparison.

Evaluation of practical constraints imposed upon the recognition of hazardous stress states from depth-limited sampling of the *in-situ* stress field shows that the

determination of least horizontal stress (S_h) trend with depth is important, particularly where the deepest stress measurement is shallower than 2 km. Determination of the trend of S_H with depth, although useful, does not greatly influence the predicted propensity for failure and hence, in view of the problems it poses to well completion practice, is of questionable worth. The determinable stress parameters ranked according to utility in distinguishing stable from potentially unstable stress states are $R_h[d']$, b_h, $R_H[d']$ where d' should be as deep as practically possible. Estimation of this suite of parameters requires several open-hole hydrofracture stress measurements at the well bottom to adequately define $R_h[d']$ and $R_H[d']$, and a series of possibly cased hole hydrofracture measurements at various depths to define the trend of least horizontal stress with depth and hence determine the surface intercept, b_h, through upward extrapolation.

Data defining the variation of least stress ratio to 2 km depth in Paleozoic strata of northwestern Ohio were used to assess predicted stability in a region where two suspected cases of induced seismicity have recently been reported. No data on the value of R_H are available. Nonetheless, the analysis shows that provided the greatest stress ratio in the sandstone overlying basement is 1.2 or greater, physically realizable stress states exist which are consistent with the available stress data and which result in failure to 5 km depth were the pore pressure at the well bottom to be raised to 8 MPa above hydrostatic and that at 5 km by as little as 1.0 MPa. Strike-slip focal mechanism solutions for earthquakes in the basement indicate the same orientation for maximum tectonic compression as is measured in the Paleozoic strata, and suggest R_H values which significantly exceed unity. Thus the available stress information suggest that the crust is close to failure, a conclusion that is supported by the history of seismicity in the area.

Acknowledgements

This work was supported by the National Center for Earthquake Engineering Research. I thank R. Beardsley of Columbia Natural Resources for permission to use the unpublished cross-section shown in Figure 5b. I also thank Klaus Jacob for encouraging this work. John Beavan, Chris Scholz and David Simpson provided critical reviews which improved the manuscript. L-DGO contribution #4224.

Symbols

a_h : gradient of the linearized least horizontal principal stress profile (MPa/km)

a_H : gradient of the linearized greatest horizontal principal stress profile (MPa/km)

b_h : surface intercept of the linearized least horizontal principal stress profile(MPa)

b_H : surface intercept of the greatest horizontal principal stress profile (MPa)

g : acceleration due to gravity (9.81 m/sec^2).

$S_i(d)$: 'i' component of principal total stress at depth d (MPa).

$S_i[d']$: 'i' component of principal stress measured at depth d' (MPa).

$s_i(d)$: 'i' component of principal effective stress for shear failure (MPa).

P_p : pore pressure (MPa).

T_o : cohesion in Coulomb failure law (MPa).

m : co-efficient of internal friction in Coulomb failure law.
m_f : coefficient of sliding friction.

$^{c}P_p(d)$: critical pore pressure for Coulomb failure (MPa).

$D^{c}P_p(d)$: critical pore pressure in excess of hydrostatic for Coulomb failure (MPa).

r : mean overburden density (gm/cc).
r_f : 'hydrostatic' fluid density (gm/cc).
$R_H[d']$: maximum stress ratio determined at depth d'.
$R_h[d']$: minimum stress ratio determined at depth d'

References

Armbruster, J. G., Seeber, L. , and K. F. Evans, The July 1987 Ashtabula earthquake (M_b = 3.6) sequence in northeastern Ohio and a deep fluid injection well, Seis. Soc. Am. (Eastern Section), St. Louis, MO, October 7-9, 1987.

Batchelor, A.S., Baria, R. and K.Hearn, Monitoring the effects of hydraulic stimulation by microseismic event location: a case study, SPE Paper # 12109, presented at 58th Ann. Tech. Conf. and Exhib. of SPE, San Francisco, CA, 1983.

Brace, W.F. and R.J. Martin 3rd, A test of the law of effective stress for crystalline rocks of low porosity, Int. J. Rock Mech. Min. Sci., 5, 415-426, 1968.

Brace, W.F. and D.L. Kohlstedt, Limits on lithospheric stress imposed by laboratory experiments, J. Geophys. Res., 85, 6248-6252, 1980.

Byerlee, J.D., Brittle-ductile transition in rocks, J. Geophys. Res., 73, 4741-4789, 1968.

Cliffs Minerals Inc., Analysis of the Devonian shales in the Appalachian basin, Final Report to contract De-AC21-80MC14693, Morgantown Energy Technology Center, Volumes 1 and 2, Morgantown, West Virginia, 1982.

Evans, K.F. and J.T. Engelder, A study of stress in Devonian shales of the Appalachian Plateau, Final Report to USDOE under contract DE-AC21-83MC20337, Morgantown Energy Technology Centre, Morgantown WV., 1987.

Evans, K.F., In-situ stress discontinuity across the Appalachian Plateau decollement, late abstract in Trans. Am. Geophys. Union, Spring Meeting, Baltimore, MD, 1987.

Jaeger J.C. and N.G.W. Cook, Fundamentals of Rock Mechanics, 2nd Edition, Science Paperbacks #12, John Wiley and Son, New York, 1976.

Nicholson, C., Roeloffs, E. and R.L. Wesson, The northeastern Ohio earthquake of January 31st, 1986: Was it induced?, Bull. Seis. Soc. Am., in press, 1987.

Mount, V. S., and J. Suppe, State of stress near the San Andreas fault: implications for wrench tectonics, Geology, in press, 1987.

Pine R.J. and A.S. Batchelor, Downward migration of shearing in jointed rock during hydraulic injections, Int. J. Rock Mech., Min. Sci. & Geomech. Absr., 21, 249-263, 1984.

Raleigh, C. B., Healy, J. H., and J. D. Bredehoeft, 1972, Faulting and crustal stress at Rangely. Colorado, in Flow and Faulting, Am. Geophy. Union Monograph Series #16.

Sbar M. L., and L. R. Sykes, Contemporary compressive stress and seismicity in Eastern North America: An example of intra-plate tectonics, Geol. Soc. Am. Bull., 84, 1861-1882, 1973.

Sibson, R. H., A note on fault reactivation, J. Struct. Geol., 7, 751-754, 1985.

Simpson, D. W., Triggered earthquakes, Ann. Rev. Earth and Planet. Sci., 14,21-42, 1986.

Waller, R. M., Turk, J. T., and R. J. Dingman, Potential effects of deep-well waste disposal in Western New York, U.S. Geological Survey Professional Paper #1053, 1978.

Warpinski, N.R., An investigation on the accuracy and reliability of *in-situ* stress measurements using hydraulic fracturing in perforated, cased holes, Proc. 24th US Symp. on Rock Mech., Texas A and M Univ., College Station, TX, June, 1983.

Wesson R.L. and C. Nicholson, Studies of the January 31st, 1986 northeastern Ohio earthquake, USGS Open File Report 86-331, 1986.

Weston Geophysical Corp., Evaluation of local seismicity around the Perry nuclear power plant site, Appendix D to Site Characterization Study, submitted to The Cleveland Electrical ans Illuminating Co., 1979.

Zoback, M.L. and Zoback, M.D., Tectonic stress field of the Continental U.S., in Geophysical Framework of the United States, ed., L. Pakiser and W. Mooney, G.S.A. Memoir, in press, 1987.

Appendix A

Explanation to Cambrian Least Stress Ratio Map Index

The listing is sectioned into states and each state has its own numerical index sequence.

The format of each datapoint is as follows:

Index #) County (Township) : Well name : Depth of fluid injection in meters (Formation)
Fracturing fluid, Liquid volume injected (m^3) : Flush fluid : ISIP at surface : Stress Ratio

Stress Ratio, R_h, is calculated from the formula,

$$R_h = \frac{ISIP + \left\{9.81 \times 10^{-3} \times d \times \rho_{flush}\right\}}{9.81 \times 10^{-3} \times d \times \rho_{over}}$$

where

ISIP is the instantaneous shut-in pressure measured at the surface in MPa,

r_{flush} is the density of fluid (gm/cc) in the wellbore at the time of shut-in,

r_{over} is the density of overburden which was usually taken as equal to 2.7 gm/cc (from well logs).

d is the depth of the injection interval in meters.

also

$ISIP_{b-h}$ is the instantaneous shut-in pressure measured at the fractured interval.

INDEX TO STRESS RATIO MAP FOR CAMBRIAN ROCKS

CANADA: ONTARIO (ONSHORE)

71) Oxford (Gobles) : Desloovere #1 : 889-892 m (sandstone)
Crude Oil, 97 m^3 : Crude Oil (0.9 gm/cc) : ISIP = 13.8 MPa : R_h = 0.9

72) Middlesex (N.Willey) : A.I.S. Resources : 1086-1089 m (sandstone)
Crude Oil, 59 m^3 : Crude Oil (0.9 gm/cc) : ISIP = 15.9 MPa : R_h = 0.9

NEW YORK

71)Cayuga (Aubern) : Microfrac stress test in Geothermal well: 1482 m: (Theresa ss)
(see Hickman et al., 1985) : $ISIP_{b-h}$ = 30.6 MPa : R_h = 0.8

71) Erie (Lackawana) : Bethlehem Steel WPL#1 : 1158-1311 m (Potsdam ss.)
Acid/Bkdown, 8 m^3 : Water : ISIP = 6.9 MPa : R_h = 0.6
Injection test reported by Waller et al. (1978) : ISIP = 7.4 MPa : R_h = 0.6

OHIO

71) Ashtabula (New Lime) : Parobeck T-2 : 2142-2161 m (Mt. Simon ss)
Brine, 351 m^3 : Brine (1.17 gm/cc) : ISIP = 12.1 MPa : R_h = 0.65

72) Ashtabula (New Lime) : Lautanen : 2131-2160 m (Mt. Simon ss)
Acid/Bkdown, 4 m^3 : Brine (1.17 gm/cc) : ISIP = 8.3 MPa : R_h = 0.6
Brine, 410 m^3 : Brine (1.17 gm/cc) : ISIP = 10.7 MPa : R_h = 0.65

73) Ashtabula (Denmark) : Universal Energy : 2058-2136 m (Mt. Simon ss)
Water/Bkdown, 11 m^3 : Water : ISIP = 18.1 MPa : R_h = 0.7

74)Lake (Perry) : Calhio #1 : 1814-1851 m (Mt. Simon ss)
Water gel, 196.8 m^3 : Water : ISIP = 15.9 MPa : R_h = 0.7

75)Lake (Painsville) : Brine injection well LM #1 : 1779-1806 m (Mt. Simon ss)
Water gel, 186.7 m^3 : Water : ISIP=9.0-13.8 MPa :R_h =0.55-0.65

76)Sandusky (Clyde) : Chemical Waste Mgmt #2 : 853-890 m (Mt. Simon ss)
Versagel, 257.4 m^3 : brine (r = 1.18 gm/cc) : ISIP = 5.7 MPa : R_h = 0.7

77)Summit (Twinsberg) : #5 Deephole : 2140-2174 m (Mt. Simon ss)
Acid/Bkdown, ? m^3 : Water : ISIP = 13.8 MPa : R_h = 0.6

Water, 694 m^3	: Water	: ISIP = 16.8 MPa	: R_h = 0.65
78)Summit (Northampton)	: #2 Northampton	: 2122-2173 m (Mt. Simon ss)	
Water, 84 m^3	: Water	: ISIP=11.4 MPa	: R_h = 0.6
Water, 385 m^3	: Water	: ISIP=13.3 MPa	: R_h = 0.6
79) Portage (Deerfield)	: Viking Resources	: 2606-2652 m (Mt. Simon ss)	
Brine, 779 m^3	: Brine (1.08 gm/cc)	: ISIP = 16.3 MPa	: R_h = 0.65
80) Holmes (Killbuck)	: Ohio Oil Gathering #1	: 1647-1676 m (Mt. Simon ss)	
Brine, 246 m^3	: Brine (1.18 gm/cc)	: ISIP = 5.5 MPa	: R_h = 0.55
81)Scioto (Haverhill)	: U.S. Steel Disposal #1	: 1682-1694 m (Mt. Simon ss)	
Acid/Bkdown, ? m^3	: Water	: ISIP = 8.3 MPa	: R_h = 0.6
Water, 117 m^3	: Water	: ISIP=9.0 MPa	: R_h = 0.6
82)Lake (Perry)	: Calhio #2	: 1826-1862 m (Mt. Simon ss)	
Water gel, 196.8 m^3	: Water	: ISIP = 16.5 MPa	: R_h = 0.7
83)Sandusky (Clyde)	: Chemical Waste Mgmt #6	: 853-890 m (Mt. Simon ss)	
Versagel, 242.1 m^3	: brine or water	: ISIP = 6.4 MPa	: R_h = 0.7

SEISMICITY, CRUSTAL STRESSES AND SEISMOTECTONICS OF EASTERN CANADA

John Adams and Peter Basham
Geophysics Division, Geological Survey of Canada
1 Observatory Crescent, OTTAWA K1A 0Y3, CANADA

INTRODUCTION

Eastern Canada - Canada east of the Cordillera, and extending north from the United States border to the Arctic Ocean - comprises about two-thirds of the stable craton of the North American plate. Much of this large area appears to be substantially aseismic, however it contains several zones of intense seismicity.

Within the southern part of the continental region, seismicity is clustered in four zones. In three of these zones — western Quebec, Charlevoix, and the lower St. Lawrence — most of the earthquakes are occurring at depths of 5 to 25 km within the Grenville basement, apparently chiefly through reactivation of a Paleozoic rift fault system along the St. Lawrence and Ottawa rivers. The fourth zone, the northern Appalachians, includes the Miramichi earthquakes of 1982, which represent shallow thrust faulting in a sheet of rocks that have been thrust over the older basement.

Along the eastern margin of the continent, the seismicity includes the 1929 M7.2 Grand Banks and 1933 M7.3 Baffin Bay earthquakes. These and smaller earthquakes appear to be concentrated at the ocean-continent transition, perhaps by reactivation of the Mesozoic rift faults created when the North Atlantic was formed. In the Labrador Sea, earthquakes are associated with the extinct spreading ridge and its associated transform faults.

In Arctic Canada, continental earthquakes occur on Baffin Island, along an arcuate band between the Boothia and the Ungava peninsulas, and in the Sverdrup Basin. The Baffin and Boothia-Ungava earthquakes are spatially associated with steep gradients in the postglacial uplift rate, suggesting that they may represent differential uplift. The Sverdrup earthquakes represent deformation beneath a thick accumulation of sediments. Along the Arctic Ocean margin, earthquakes appear to be concentrated where thick sediments have loaded the rifted transitional and oceanic crust.

In the present paper we briefly discuss the regional seismicity and seismotectonics as it is currently understood, proceeding from southeast to east to northeast before summarizing our inferences about the causes of earthquakes in eastern Canada. All the earthquakes in eastern Canada appear to be occurring within a regional stress field dominated by northeast to east compression, and most large earthquakes have occurred near Paleozoic or younger structures, i.e. places where the continent has been most recently weakened.

SOUTHEASTERN CANADA

Western Quebec A significant cluster of earthquakes occurs in the Grenville Province of the Canadian Shield, dominantly in western Quebec but extending into eastern Ontario across the Ottawa River. An earthquake with magnitude about 6 occurred at or near Montreal in 1732 and during this century earthquakes of M6.2 occurred near Temiscaming, Quebec, in 1935 and M5.6 near Cornwall, Ontario, in 1944.

For the last four decades all earthquakes have been M4.3 or less and most have been located in the centre of the cluster, about 100 km north of the Ottawa River. In detail (Fig. 1), the seismicity appears to occur in two bands. The first band, trending slightly west of northwest, lies along the Ottawa River and includes the Timiskaming, North Gower (1983), Cornwall and Montreal earthquakes. The second band trends slightly north of northwest and extends from Montreal to the Baskatong Reservoir, about 200 km north of Ottawa. Recent monitoring by the ECTN shows the gap between the two bands is reasonably well defined by an absence of earthquakes at the northwestern end; however near the St. Lawrence River the two bands merge.

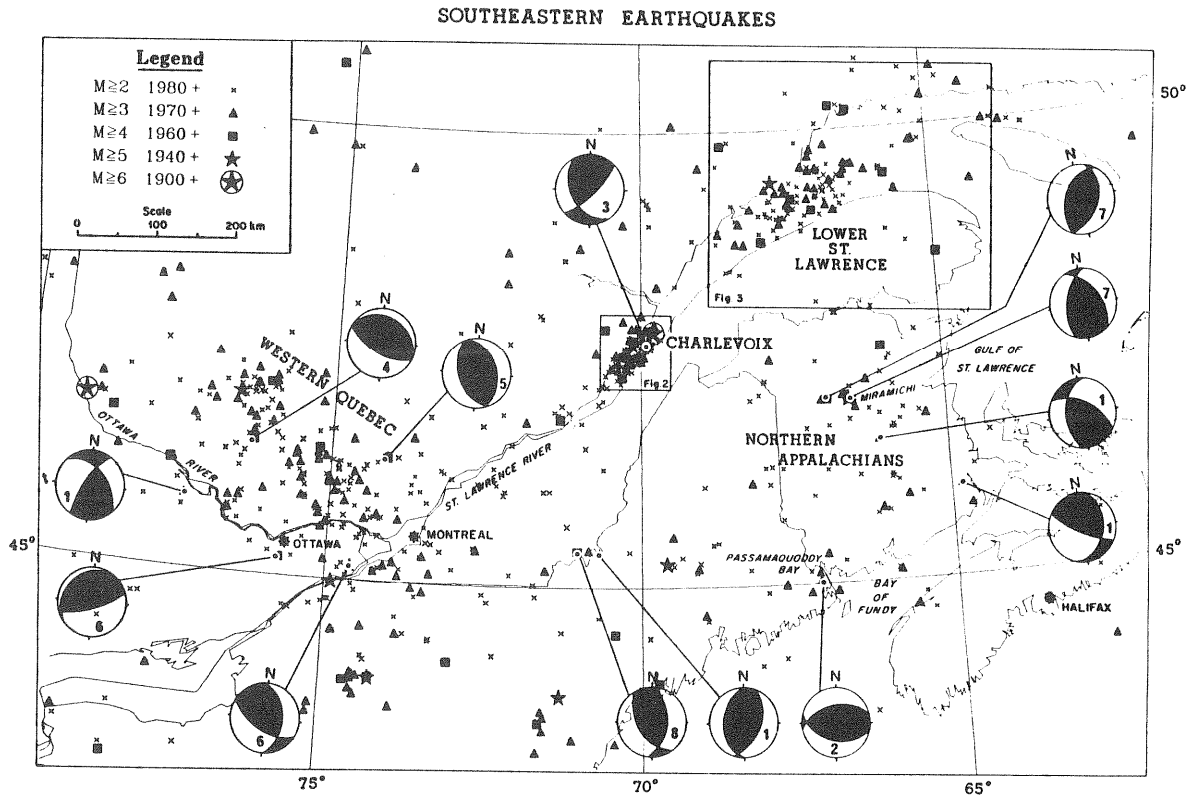

Figure 1. *Seismicity of southeastern Canada (legend shows the magnitude/time period criteria for the earthquakes shown), with representative focal mechanisms from the following sources: 1: Adams et al., 1987; 2: Ebel, 1985; 3: Hasegawa and Wetmiller, 1980; 4: Horner et al., 1978; 5: Horner et al., 1979; 6: Wahlstrom, 1987; 7: Wetmiller et al., 1984; and 8: Yang and Aggarwal, 1981.*

Field monitoring of aftershock sequences has provided good estimates for the focal depth of some earthquakes, and these together with some approximate depths computed from the ECTN network suggest most earthquakes lie between 5 and 20 km. Focal mechanisms have been determined for about 40 earthquakes in the zone, and a representative selection is shown on Figure 1. Almost all mechanisms have near-horizontal P-axes, and represent mainly thrust earthquakes. This evidence for high horizontal compression is confirmed by other evidence for regional stresses in eastern Canada (Hasegawa et al., 1985; Adams, 1987). Although the regional stress field appears to have the compression axis in the northeast to east octant, the P-axes for some of the western Quebec earthquakes are distinctly different.

Forsyth (1981) has shown that the earthquakes in the first band, including the larger historical earthquakes, may be associated with rift faults along the Ottawa River that were last active in the Paleozoic. The rift faults are part of a large structure that extends from the Ottawa Valley and from rifts along Lake Champlain, down the St. Lawrence River (Kumarapeli, 1985), and in related structures, through southern Labrador to the Labrador Sea. Other related structures may extend from Timiskaming northwest to Kapuskasing, Ontario. Assigning an origin to the second band of seismicity has proved less easy, but it may be related to the passage of a hot spot 120 m.y. ago.

Charlevoix. The Charlevoix zone is historically the most active in eastern Canada with at least five earthquakes of magnitude 6 or greater (1663, 1791, 1860, 1870, and 1925). Hypocentres located by a 6-station local network since the mid 1970's demonstrate that most earthquakes are confined to a zone that is about 80 km long by 35 km wide (Fig. 2),

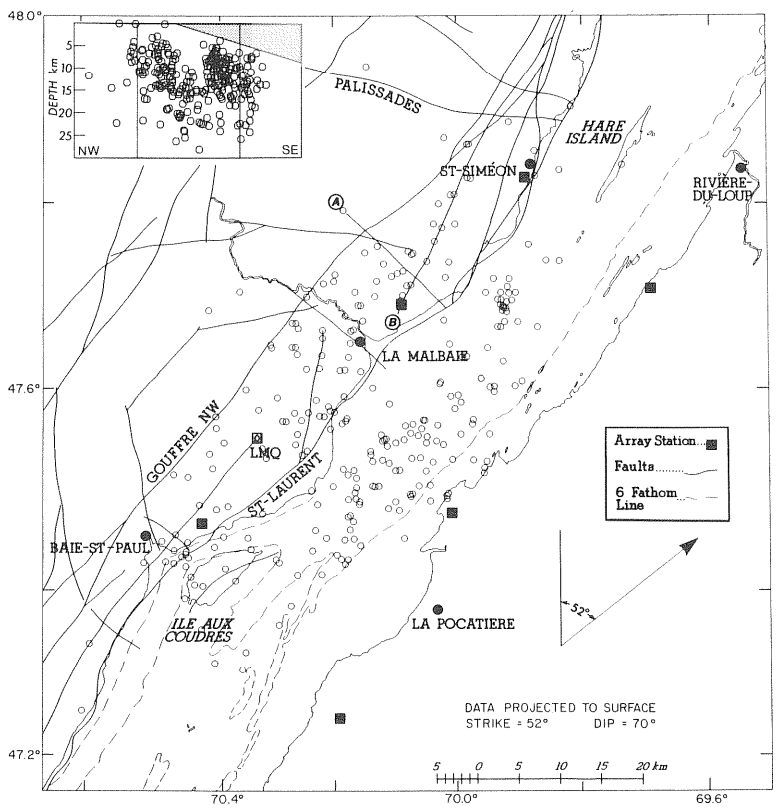

Figure 2. *Microearthquakes in the Charlevoix area (Anglin, 1984). In order to show their relation to the mapped surface faults, the epicentres have been migrated to the surface up the dip of the regional rift faults. The inset is a NW–SE cross-section of the hypocentres to show their depth distribution relative to the Paleozoic wedge (shaded).*

mainly under the St. Lawrence River (Anglin, 1984). Earthquake focal depths are well-determined for the past 10 years of microearthquakes, and are mostly between 5 and 25 km (Fig. 2 inset). Paleozoic sediments that crop out on the south shore are only a few kilometres thick, and so all the activity is occurring within the Precambrian basement (unshaded area on Fig. 2 insert). Stereo plots produced by Anglin (1984) demonstrate that most of the microearthquakes are occurring on northeast-striking planes that dip to the southeast. A projection of the hypocentres to the surface along the postulated faults (Fig. 2) suggests the activity is confined between mapped Paleozoic rift faults on the north shore and a bathymetric feature near the river's south shore. Further, the earthquakes do not extend downriver beyond the cross-cutting Saguenay graben faults.

Charlevoix, the Ottawa River, and the lower St. Lawrence seismic zones all lie along the same rift system. However, at Charlevoix the rift structures have been complicated by a late Devonian meteorite impact that caused ring faults and distributed fracturing (seen on Fig. 2). Considerable attention is being paid as to whether the earthquakes at Charlevoix occur because of the associated impact structure (in which case the seismicity could be considered to be localized and unlikely to occur elsewhere) or whether the earthquakes just happened to be coincident with the impact (in which case other parts of the rift fault system could become similarly active). Because other meteorite craters in Canada are not seismically active, because the earthquakes extend downriver beyond the impact structure, and because the hypocentral trends suggest reactivation of the rift faults, current opinion is that the impact structure is not the controlling factor in the seismicity.

Lower St. Lawrence. Similar to the Charlevoix zone, the Lower St. Lawrence earthquakes also lie mainly under the St. Lawrence River and may involve the old rift faults. The record of felt earthquakes extends back a 100 years at most in this sparsely populated area, and none is likely to have been much larger than M5. Despite the lack of known larger earthquakes, the zone has rates for magnitude 3 – 4 earthquakes similar to the more confined Charlevoix zone. Epicentre maps prepared by Smith (1962, 1966) show scattering of earthquakes extending onto the north and south shore. Relocation of some of these early epicentres has affirmed that most actually occurred under the river (Fig. 3). Reliable estimates of earthquake depth have been obtained for two earthquakes recorded by the Yellowknife array, 30 degrees to the northwest. Phases interpreted as pP and sP gave depths of 19 km and 21 km. Other earthquakes for which approximate depths have been computed from the ECTN network lie mostly between 10 and 20 km. Like the Charlevoix earthquakes, this places them within the Grenville basement and well beneath the onlapping St. Lawrence platform and the overthrust Appalachian sedimentary rocks.

Focal mechanisms have been derived for seven earthquakes (Adams et al., 1987); they have P-axis orientations only slightly less variable than at Charlevoix, and also indicate mostly thrust faulting in response to compression from the eastern quadrant. Significantly, five of the mechanisms have a common plane that strikes parallel to the river and dips to the southeast. Taken together, the northeast-striking focal planes, the position of the

larger earthquakes relative to the coastline, and the distribution of the smaller earthquake epicentres strongly suggest that the Paleozoic rift faults are the chief active structure.

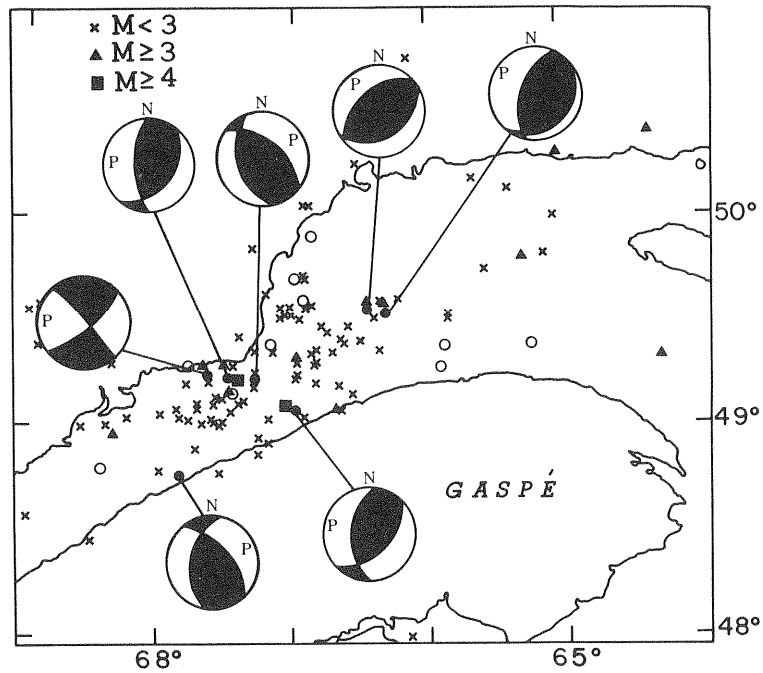

Figure 3. *Lower St. Lawrence seismicity, 1981-1987. Large open circles represent relocated epicentres of M3.5 to M4.8 earthquakes from the period 1944-1968 (Sharp and Adams, unpublished work, 1987). Focal mechanisms shown are those derived by Adams et al. (1987).*

Northern Appalachians. The northern Appalachian region, which includes most of New Brunswick and which extends into New England, is a zone of relatively uniform seismicity. Significant earthquakes include those near Passamaquoddy Bay on the New Brunswick/Maine border in 1817 (M4.8), 1869 (M5.2), and 1904 (M5.7), near Moncton in 1855 (M5.2) (Leblanc and Burke, 1985), and at Miramichi in 1982. Within New Brunswick there is an apparent concentration of earthquakes in the Miramichi Highlands and near Passamaquoddy Bay. Available focal mechanisms (some are shown on Fig. 1) represent dominantly thrust faulting, all but the one at Passamaquoddy Bay in response to northeast- to east-directed compression.

The Miramichi earthquakes, because of their size, and numerous aftershocks have been unusually well studied. The 9 January 1982 mainshock M5.7 occurred as a thrust with rupture up-dip on a west-dipping plane. A magnitude 5.1 aftershock occurred 3.5 hours later, probably on the lower northern portion of this plane. On 11 January, a M5.4 ruptured (probably up dip) a conjugate east-dipping plane and was followed by an intense aftershock sequence. Finally the 31 March M5.0 occurred as a repeat rupture on the upper northern portion of the west-dipping plane (Wetmiller et al., 1984; Basham and Adams, 1984). Although trenches were dug to locate a surface rupture, none was found, suggesting that the near-surface vertical offset was distributed over a zone several hundred metres wide and not confined to a single plane.

Although geological and geophysical investigations have confirmed that all the earthquakes occurred within a single granodiorite pluton, they provided no strong reason as to

why the earthquakes occurred at the Miramichi site. If Miramichi-type earthquakes occurred regularly at the site, more surface evidence for thrusting, such as a degraded fault scarp, would be expected. Therefore, despite considerable effort, we do not understand why the earthquakes occurred where they did, and have no evidence that they occur often at the Miramichi site. Thus we must consider that Miramichi-sized earthquakes could occur anywhere in the Northern Appalachian zone.

While aftershocks of the Miramichi and Trousers Lake earthquakes were shallow, all less than 9 km, earthquakes near Passamaquoddy Bay are deeper, perhaps 10 - 16 km. The northern Appalachian seismicity is thus significantly less deep than the earthquakes at Charlevoix, perhaps reflecting the lower mechanical strength of the lower crust in the young Appalachian belt (Hasegawa, 1986, Fig. 9). The shallow depths may indicate that the earthquakes are confined to the rocks above a shallow, sub-Appalachian detachment zone such as has been found beneath the Appalachians of the United States. If this were the case, it might mean that the Miramichi earthquakes nucleated on the detachment and ruptured upwards to the surface, while the Trousers Lake earthquake may have occurred on the detachment itself.

Southeastern Continental Margin. Although poorly monitored and little studied, the seismicity of the southeastern margin of Canada is clearly higher than that at many comparable passive margins (Fig. 4). The description that follows is condensed from Adams (1986).

About half of the earthquakes off the southeastern continental margin occur in the Laurentian Slope seismic zone, site of the M7.2 "Grand Banks" earthquake of 1929 (Fig. 4). This earthquake caused a large submarine slump and consequent tsunami that killed 27 people on the south coast of Newfoundland. The larger historical earthquakes, and many recent smaller earthquakes, have been systematically relocated and found to lie within a 100 km E-W by 35 km N-S box at the mouth of the Laurentian Channel. In addition to the 1929 earthquake and its immediate aftershocks, there have been four M5 earthquakes since 1951, the most recent in 1975. The elongation of the seismic zone, and the location of the 1929 epicentre at the eastern end are consistent with the hypothesis that current earthquakes could represent belated aftershocks of the 1929 earthquake. If so, the earthquake appears to have ruptured westwards along a fault about 70 km long (Adams, 1986).

Outside of the Laurentian Slope zone, scattered earthquakes occur northeast of Newfoundland and seaward of Nova Scotia. A trend of seismicity follows the Laurentian Fan south from the Laurentian Slope zone. Off Nova Scotia the revisions and new earthquakes on Fig. 4 suggest that the transition from oceanic to continental crust is active, though not currently at a very high level. Elsewhere, the transition is too poorly monitored to show if it is active at the low level we can detect off Nova Scotia.

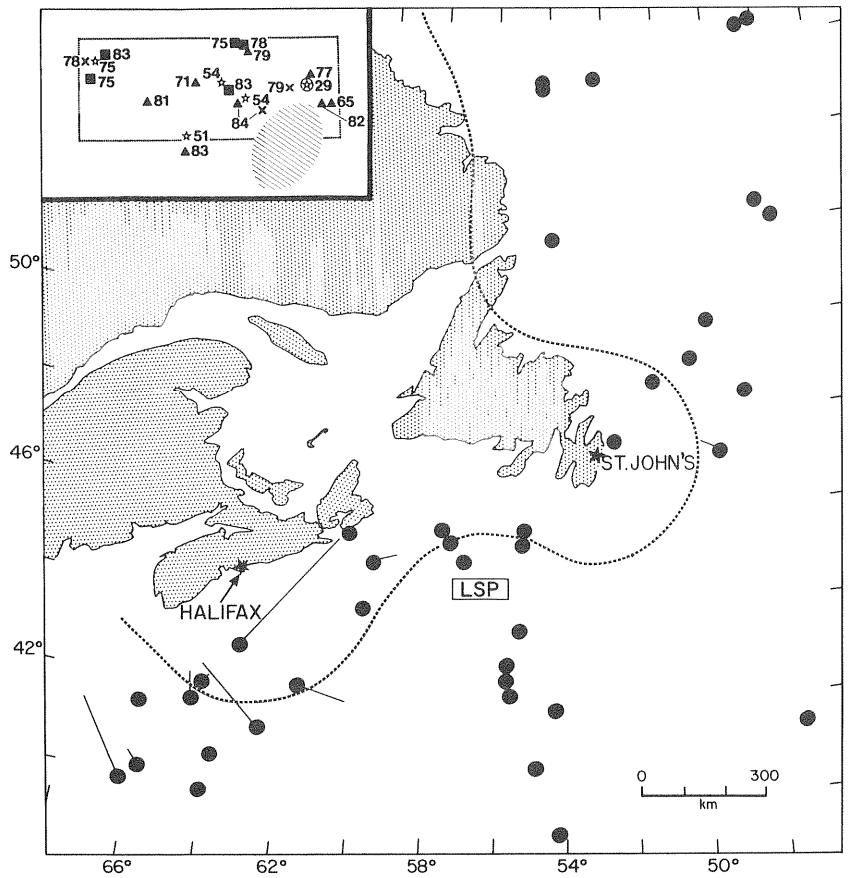

Figure 4. *Seismicity of the the southeastern margin (after Adams, 1986). Inland of the dotted line, M3.5 and larger earthquakes are thought to have been completely detected and located since 1983. Dots represent preliminary locations determined by Wahlstrom and Adams (in prep), and in some cases represent a substantial improvement over the current catalogued epicentre. For such earthquakes the "tails" join the catalogue location to the revised location. Dots with plus signs are newly discovered earthquakes. Magnitudes of the earthquakes are not distinguished. Box marked "LSP" encloses the many earthquakes near the epicentre of the 1929 "Grand Banks" earthquake. Inset shows in detail the seismicity of the box with the number identifying the year of the earthquake and the symbol the magnitude using the same scale as Figure 1. The striped ellipse indicates the approximate location of two microearthquakes recorded by ocean bottom seismometers in 1983.*

The cause of earthquakes along the eastern margin and thus a rationale for their distribution has not yet been established. Studies of stress directions from oil well breakout data (Podrouzek and Bell, 1985) confirm that the margin is subject to the same northeast-directed compression as the rest of eastern North America. While some studies have indicated local areas of near-surface faulting (e.g. Orpheus Graben off Nova Scotia), many of the earthquakes along the margin probably occur along the ocean-continent transition on

the deep-crustal rift faults formed during the opening of the Atlantic Ocean. Under the current northeast compression regime these normal faults would be reactivated as thrust or strike-slip faults.

As the numbers, location, and nature of the offshore earthquakes are poorly understood, Basham and Adams (1983) produced a speculative model that suggests rare large earthquakes can occur along the whole margin, using the pervasive Mesozoic rift faults as the causative structure, with a rate of about one M7 earthquake per thousand years per thousand kilometres of margin. This model implies that inactive parts of the margin are merely quiescent, and that recent earthquakes in active regions like the Laurentian Slope represent belated aftershocks that will diminish over the next century without producing another M7 earthquake. That such large earthquakes may have occurred in the past is suggested by prehistoric submarine slumps elsewhere along the margin.

Southeastern Background Seismicity. Some scattered seismicity lies in less intense clusters outside of the seismic zones discussed above, so we briefly mention these, once again moving from west to east. The shield areas of Ontario and Quebec show very low seismicity except for earthquakes near Cochrane and Iroquois Falls in northern Ontario, which may lie on an extension of the Ottawa-Timiskaming rift structure towards Kapuskasing. Further north, the earthquakes near southern James Bay have an unknown origin. A cluster of small earthquakes in the Burlington/Niagara Falls area of Ontario is poorly understood, but in part is believed to represent very shallow stress release. Earthquakes near Quebec City may lie on the St. Lawrence rift system. Earthquakes extending from Sept-Iles across easternmost Quebec and southern Labrador may also lie on structures related to the St. Lawrence rift system.

NORTHEASTERN CANADA

We continue our discussion of eastern Canadian seismicity and seismotectonics by proceeding northward along the continental margin of the eastern Arctic, inland to the northeastern portion of the Canadian Shield, northward into the Arctic archipelago, completing the picture with a brief discussion of the Arctic Ocean margin (Fig. 5).

Labrador Sea. The known seismicity of the Labrador Sea includes six earthquakes in the magnitude 5.0 to 5.6 range since 1934. The most recent moderate earthquake was M4.8 in 1986. There are older reports of felt earthquakes from fishing villages along the Labrador coast as early as 1809 (Staveley and Adams, 1985). These older events likely occurred offshore, and may have been of quite large magnitude (Basham and Adams, 1983).

The Labrador Sea is a product of seafloor spreading, and Srivastava and Tapscott (1986) have identified a central ridge and associated fracture zones from seismic and gravity profiles and linear magnetic anomalies. Seismicity can be associated with the central ridge and the associated fracture zones, as shown by some joint epicentre determinations. There is a

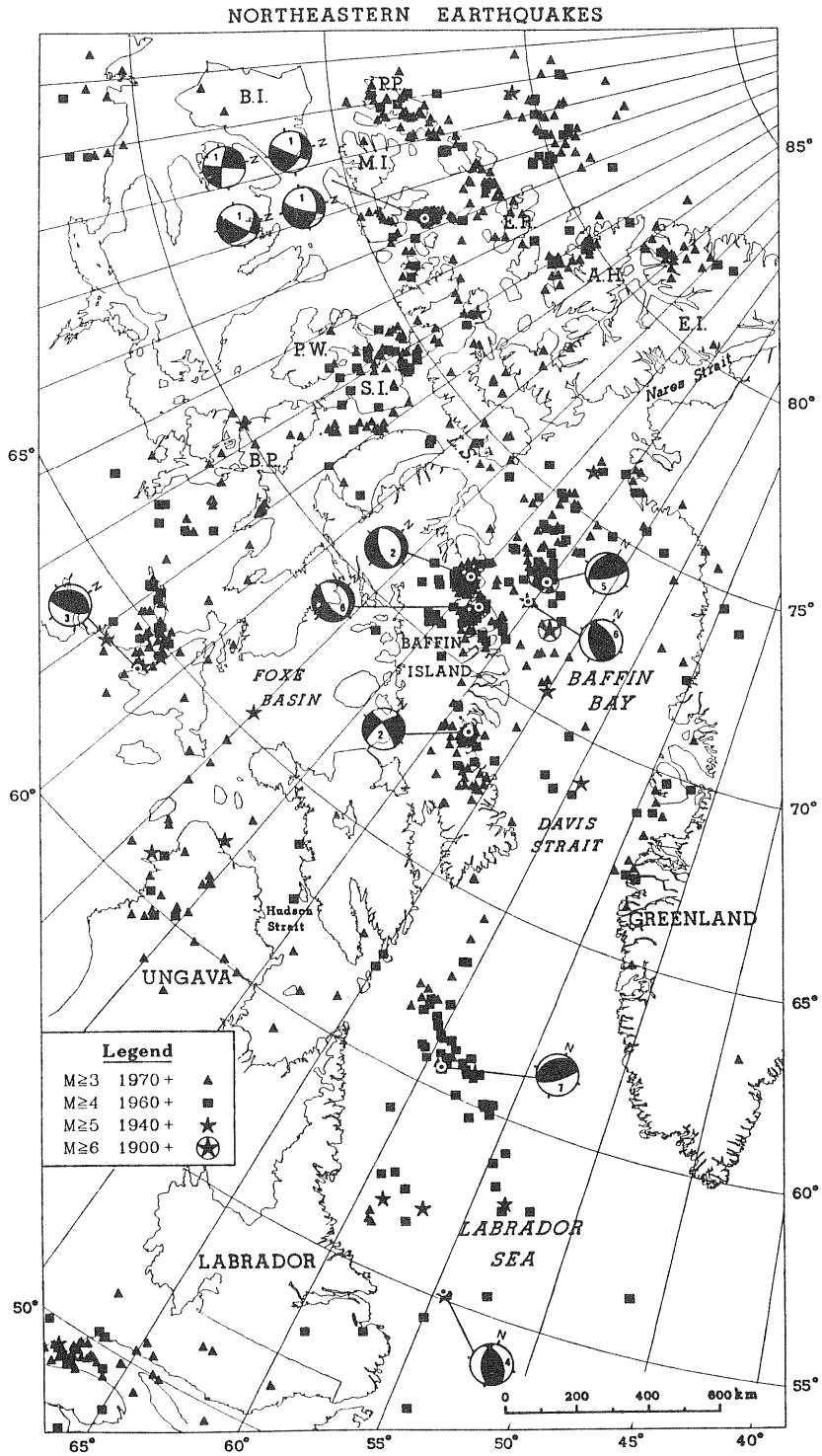

Figure 5. *Seismicity of northeastern Canada (legend shows the magnitude/age criteria for the earthquakes shown), with all available focal mechanisms, from the following sources: 1: Hasegawa, 1977; 2: Hashizume, 1973; 3: Hashizume, 1974; 4: Hashizume, 1977; 5: Sleep et al., 1987 6: Stein et al, 1979; and 7: Sykes and Sbar, 1974. Geographic features are identified by initials as follows: AH: Axel Heiberg Island, BI: Banks Island, BP: Boothia Peninsula, EI: Ellesmere Island, ER: Ellef Ringes Island, LS: Lancaster Sound, MI: Melville Island, PP: Prince Patrick Island, PW: Prince of Wales Island, SI: Somerset Island.*

separate trend of seismicity following the continental margin off Labrador that we associate with pre-existing faults beneath the rifted continental margin. North of the point where the ridge and margin seismicity merge, the region of Davis Strait is less sesimically active, at least at current detection levels (M about 3.5).

Baffin. The largest earthquake known to have occurred in northern Canada was the M7.3 event in Baffin Bay in 1933. This earthquake had aftershocks as large as M6.5, and M6 events have since occurred in the bay in 1945, 1947 and 1957. Precise boundaries for the Baffin Bay seismicity are difficult to define on the basis of geological and geophysical evidence, but there seems to be a clear separation between the activity in the bay and that on Baffin Island. Sleep et al. (1987) have established a focal depth of 10 km for the 1933 event (a correction to the 65-km depth estimated by Stein et al. (1979)) and 24 km for a 1976, M5.4 further south in the bay. Although there is evidence for seafloor spreading and an extinct spreading centre in the deep central region of Baffin Bay, there is little or no seismic activity in this region and the seismicity is confined almost exclusively to the landward side of the 2 km bathymetric contour in the northwestern segment of the bay that outlines the thick sedimentary sequence (Basham et al., 1977).

The highly active seismicity on Baffin Island appears to be confined to the coastal region and is concentrated in the regions of Buchan Gulf and Home Bay with a possible gap between these two regions. All available evidence on focal depths suggests the earthquakes are shallow. In contrast to the thrust faulting in Baffin Bay, the island earthquakes show normal faulting (Fig. 5), which is rare for eastern Canada. Stein et al. proposed a model for the entire passive margin of eastern Canada with thrust faulting seaward of the 1000 m isobath and normal or strike-slip faulting for more landward events as due to Pleistocene deglaciation reactivating faults remaining from the rifting. Sleep et al. developed this model further for the Baffin region, suggesting that the recent removal of surface loads by glacial erosion and by deglaciation is the major source of local stress that produces flexure of the lithosphere, and is comparable in magnitude to and superimposed on the compressional stress in the North American plate due to Mid-Atlantic Ridge spreading.

Boothia-Ungava. Basham et al. (1977) recognized an arcuate band of seismicity that extends southward from the Boothia Peninsula, across northern Hudson Bay, the Ungava Peninsula, and eastward through Hudson Strait, connecting with the northern end of the Labrador Sea. With the centre of postglacial uplift over Foxe Basin and a high differential rate of uplift on northeastern Baffin Island, they speculated that the Baffin Island-Foxe Basin block is responding independently to postglacial uplift, and may be decoupled from the rest of the Shield to the southwest along the arc of seismicity. The Boothia uplift, which has been geologically active from the Paleozoic to the Cretaceous (Okulitch et al., 1986), continues to be seismically active at present.

Sverdrup Basin. Most of the remaining seismicity in the Canadian Arctic archipelago can be spatially associated with the Sverdrup Basin, a 1000 km long northeast-southwest regional depression (between Melville and Ellef Ringnes islands) in which the sedimentary rocks reach thicknesses of 10 km. The seismicity is characterized by intense swarms. Because

of the swarm-like nature of the seismicity and the short instrumental observation period (25 years), it is unlikely that all potentially active regions of the basin have been identified. A feature running through the basin that shows some geological and geophysical correlation with the highest levels of seismicity is the Gustaf-Lougheed Arch (Forsyth et al., 1979; Basham et al., 1982). This arch is a structurally significant feature visible in the Bouguer anomaly contours that divides the western Sverdrup Basin into two separate sub-basins.

The focal mechanisms for the four largest earthquakes in the Byam Martin Channel swarm (M 5.1-5.7), while dominantly strike-slip, show some deviatoric tension at depths from 9 km (near the base of the sedimentary rocks) to 31 km (Fig. 5). This suggests that there may remain a small component of tension similar to that responsible for the opening of the Arctic Ocean Basin (Forsyth et al, 1979).

Arctic Ocean Margin. The seismicity along the Arctic Ocean margin offshore of the Canadian Arctic archipelago is concentrated in distinct clusters in the Beaufort Sea and northwest of Ellef Ringnes Island, with only very scattered activity elsewhere (Hasegawa et al., 1979; Forsyth et al., 1987). The largest earthquake, M6.5, occurred in the Beaufort Sea in 1920; elsewhere along the margin no events larger than about M5 are known.

The rifted margin was formed in early Cretaceous time when northern Alaska rotated anticlockwise away from Arctic Canada. The ocean-continent transition is characterized by a zone of negative magnetic anomalies that extend from the Beaufort Sea to north of Ellesmere Island. A series of elliptical free-air gravity anomalies lie over major sedimentary depocentres. Forsyth et al. (1987) have recently provided the following interpretation of the seismicity. The zone of rift faults separating continental and oceanic crust is inferred to lie immediately seaward of the magnetic lows. Although four major elliptical gravity anomalies lie along the margin, significant seismicity is associated with them only where the shelf break extends distinctly seaward of the magnetic low; i.e. where the sediments have prograded over more oceanic crust. This suggests that earthquakes occur on the rift faults chiefly where the oceanic or transitional crust is loaded by sediments.

SUMMARY

We summarize our conclusions regarding the causes of seismicity in eastern Canada on Figure 6. Almost all the significant earthquakes in the continental part of southeastern Canada can be spatially and probably causually associated with the Paleozoic rift system along the St. Lawrence, the chief exceptions being the northern band of seismicity in the Grenville terrain of western Quebec, and the seismicity in the Appalachian terrain to the southeast. To a first approximation, the continent-wide stress field is uniform, represents compression from the east-northeast quadrant, and causes thrust or thrust/strike-slip earthquakes (Fig. 7).

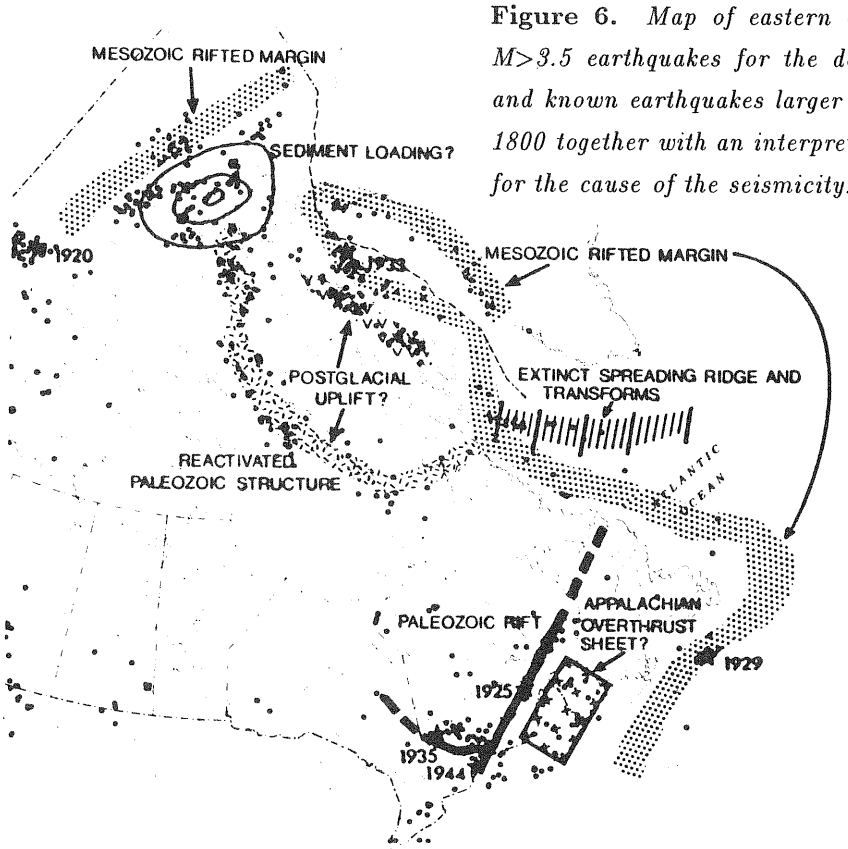

Figure 6. *Map of eastern Canada showing M>3.5 earthquakes for the decade 1975-1985 and known earthquakes larger than M5.5 since 1800 together with an interpretative framework for the cause of the seismicity.*

The earthquakes along the eastern continental margin are mainly related to the Mesozoic rift faults formed during the opening of the Atlantic, while those in the mid Labrador Sea are related to the extinct spreading ridge and its transform faults. The same structures extend into northern Baffin Bay where the earthquakes may also be partially related to stresses induced by deglaciation. The passive Arctic Ocean margin has a comparable ocean-continent transition to the Atlantic margin but it appears to be seismically active mainly where it has been recently loaded by thick sediments.

It is therefore clear from the above discussion and Figure 6 that most of the larger earthquakes can be associated with the rift systems that surround or break the integrity of the North American craton. By contrast, the largest earthquakes in the unbroken craton (in Canada, but outside the seismic zones discussed above) are probably not much larger than 5.

Coppersmith et al. (1987) have come to similar conclusions from a study of world-wide earthquakes in "stable continental interiors". They found that 71 percent of the seismicity of stable continental interiors was associated with imbedded continental rifts and continental passive margins (one-sided rifts). Further, all of their 17 M7 or larger earthquakes are strongly associated with the imbedded rifts or passive margins.

Both the Paleozoic and the Mesozoic rift systems in eastern Canada are continuous features, many thousands of kilometres long. Despite their continuity and the uniform stress field, the rift systems are only sporadically active, showing seismicity in clusters – as

at Charlevoix and the lower St. Lawrence - or single large earthquakes – such as the "Grand Banks" earthquake.

In each case there is a lack of geological evidence for continual activity at present rates. We, like many others, have been confounded by the high levels of seismic activity at Charlevoix relative to other places in eastern Canada. At such high rates (M7 every few

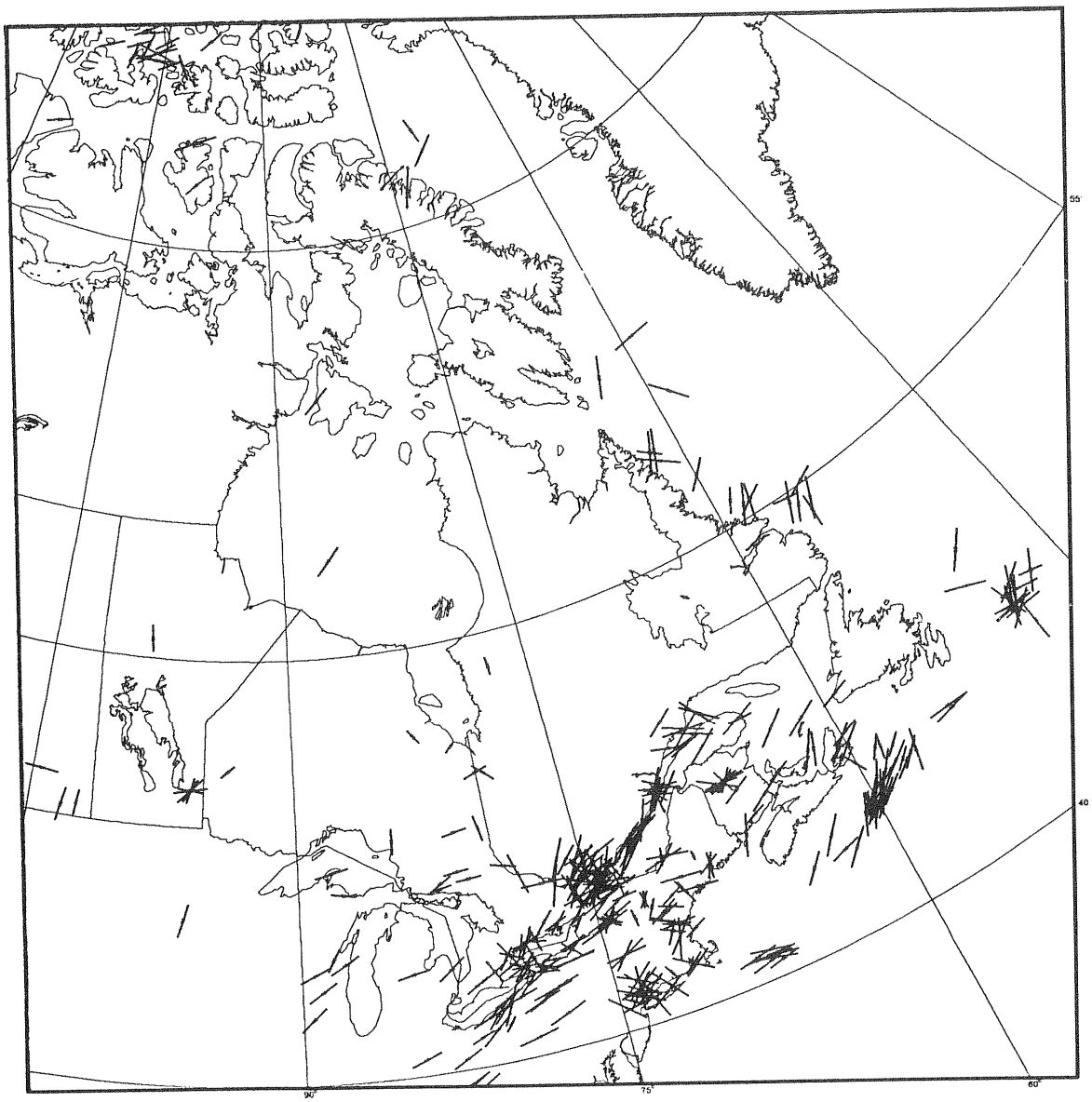

Figure 7. *Map of crustal stress data for eastern Canada and the adjacent United States as compiled by Adams (1987). Directions of relative compression and relative extension are shown by inward and outward pointing arrows respectively. Length of arrow is proportional to perceived data quality. Data are compiled from various sources and methods of stress determination including earthquake focal mechanisms, oilwell breakouts, and hydraulic fracturing experiments.*

hundred years), the implied rates of geological deformation would amount to kilometres over a million years. Clearly kilometres of uplift (if due to thrusting), or even kilometres of strike-slip motion, would have been recognized at Charlevoix, had they occurred. That they have not, we infer, must be due to intermittent activity at Charlevoix and along the remaining rift system, perhaps with a time constant of thousands to hundreds of thousands of years.

For single large earthquakes such as the "Grand Banks", a similar argument can be made for intermittent activity on comparable time scales. This leads to a dilemma for hazard estimates that need to be made for low levels of probablility: will the next large earthquake occur in a recognized seismic zone or not?

ACKNOWLEDGEMENTS

Concepts discussed in this paper will be more fully documented in our contribution to the seismicity part of the Geological Society of America's "Decade of North American Geology" volume on Neotectonics. The volume will accompany the DNAG seismicity map of North America, and is scheduled for publication in 1988 or 1989. We thank our colleagues in the Geophysics Division for their comments.

REFERENCES

Adams, J., Changing assessment of seismic hazard along the southeastern Canadian margin: Proceedings, Third Canadian Conference on Marine Geotechnical Engineering, St. John's Newfoundland, 11-13 June, 1986. p. 41-53, 1986.

Adams, J., Canadian crustal stress database – a compilation to 1987: Geological Survey of Canada Open File Report 1622, 130 pp, 1987.

Adams, J., Sharp, J., and Stagg, M., New earthquake focal mechanisms for eastern Canada: Geological Survey of Canada Open File Report, in preparation, 1987.

Anglin, F.M., Seismicity and faulting in the Charlevoix zone of the St. Lawrence Valley: Bulletin of the Seismological Society of America. v. 74, p. 595-603, 1984.

Basham, P. W., and Adams, J., Earthquakes on the continental margion of eastern Canada: need future large events be confined to the locations of large historical events?: United States Geological Survey Open File Report 83-843, p. 456-467, 1983.

Basham, P.W., and Adams, J., The Miramichi, New Brunswick earthquakes: near-surface thrust faulting in the northern Appalachians: Geoscience Canada. v. 11, p. 115-121, 1984.

Basham, P.W., Forsyth, D.A., and Wetmiller, R.J., The seismicity of northern Canada: Canadian Journal of Earth Sciences. v. 14. p. 1646-1667, 1977.

Basham, P.W., Weichert, D.H., Anglin, F.M., and Berry, M.J., New probabilistic strong seismic ground motion maps of Canada: a compilation of earthquake source zones, methods and results: Earth Physics Branch Open File 82-33. 202 p, 1982.

Basham, P.W., Weichert, D.H., Anglin, F.M., and Berry, M.J., New probabilistic strong seismic ground motion maps of Canada: Bulletin of the Seismological Society of America,. v. 75, p. 563-595, 1985.

Coppersmith, K.J., Johnston, A.C., and Arabasz, W.J., Methods for assessing maximum earthquakes in the central and eastern United States: E.P.R.I. Research Project 2556-12, Working Report, Electric Power Research Institute, Palo Alto, California, 1987.

Ebel, J.E., A study of seismicity and tectonics in New England: United States Nuclear Regulatory Commision, NUREG/CR-4354 RA, 88 pp, 1985.

Forsyth, D.A., Characteristics of the western Quebec seismic zone: Canadian Journal of Earth Science. v. 18 p. 103-119, 1981.

Forsyth, D.A., Mair, J.A., and Fraser, I., Crustal structure of the central Sverdrup Basin: Canadian Journal of Earth Sciences. v. 16. p. 1581-1598, 1979.

Hasegawa, H.S., Focal parameters of four Sverdrup Basin, Arctic Canada, earthquakes in November and December of 1972: Canadian Journal of Earth Sciences: v. 11. p. 2481-2494, 1977.

Hasegawa, H.S., Seismotectonics in eastern Canada, an overview with emphasis on the Charlevoix and Miramichi regions: Earthquake Notes, v. 57, p. 83-94, 1986.

Hasegawa, H.S., Adams, J., and Yamazaki, K., Upper crustal stresses and vertical stress migration in eastern Canada: Journal of Geophysical Research. v. 90. p. 3637-3648, 1985.

Hasegawa, H.S., and Wetmiller, R.J.,The Charlevoix earthquake of 19 August 1979 and its seismo-tectonic envronment: Earthquake Notes. v. 51, p. 23-37, 1980.

Hashizume, M., Two earthquakes on Baffin Island and their tectonic implications: Journal of Geophysical Research. v. 78. p. 6069-6081, 1973

Hashizume, M., Surface wave study of earthquakes near northwestern Hudson Bay, Canada: Journal of Geophysical Research, v. 79, p. 5458-5468, 1974.

Hashizume, M., Surface-wave study of the Labrador Sea earthquake, 1971 December: Geophysical J.R. Astronomical Society. v. 51. p. 149-168, 1977.

Horner, R.B., Stevens, A.E., Hasegawa, H.S., and Leblanc, G., Focal parameters of the July 12, 1975, Maniwaki, Quebec, earthquake-an example of interplate seismicity in eastern Canada: Bulletin of the Seismological Society of America. v. 68. p.619-640, 1978.

Horner, R.B., Wetmiller, R.J., and Hasegawa, H.S., The St. Donat, Quebec earthquake sequence of February 18-23, 1978: Canadian Journal of Earth Sciences. v. 16. p. 1892-1898, 1979.

Kumarapeli, P.S., Vestiges of Iapetan rifting in the west of the northern Appalachains: Geoscience Canada. v. 12 p. 55-59, 1985.

Leblanc, G., and Burke, B.S., Re-evaluation of the 1817, 1855, 1869, and 1904 Maine-New Brunswick area earthquakes: Earthquake Notes. v 56, p. 107-123, 1985.

Okulitch, A.V., Packard, J.J., and Zolani, A.I., Evolution of the Boothia uplift, Arctic Canada: Canadian Journal of Earth Sciences. v. 23. p. 350-358, 1986.

Podrouzek A.J., and Bell, J. S., Stress orientations from wellbore breakouts on the Scotian Shelf, eastern Canada: Geological Survey of Canada Paper 85-1B, p. 59-62, 1985.

Sleep, N.H., Kroeger, G., and Stein, S., Canadian passive margin stress field inferred from seismicity: Journal of Geophysical Research, in press, 1987.

Smith, W.E.T., Earthquakes of eastern Canada and adjacent areas 1534-1927: Publications of the Dominion Observatory, v. 26, p. 271-301, 1962.

Smith, W.E.T., Earthquakes of eastern Canada and adjacent areas 1928-1959: Publications of the Dominion Observatory, v. 32 p. 87-121, 1966.

Srivastava, S.P., and Tapscott, C.R., Plate kinematics of the North Atlantic: The geology of North America, v. M, The Western North Atlantic Region, Geological Society of America. p. 379-404, 1986.

Stein, S., Sleep, N.H., Geller, R.J., Wang, S.C., and Kroeger, G.C., Earthquakes along the passive margin of eastern Canada: Geophysical Research Letters. v. 6, p. 537-540, 1979.

Staveley, M. and Adams, J., Historical seismicity of Newfoundland: Earth Physics Branch Open File 85-22, 73 pp, 1985.

Sykes, L.R., and Sbar, M.L., Focal mechanism solutions of intraplate earthquakes and stresses in the lithosphere. in Kristjansson (ed.) Geodynamics of Iceland and the North Atlantic area, D. Reidel, Dordrecht, p. 207-224, 1974.

Wahlstrom, R., Focal mechanisms of earthquakes in southern Quebec, southeastern Ontario, and northeastern New York with implications for regional seismotectonics and stress field characteristics: Bulletin, Seismological Society of America, v. 77, p. 891-924, 1987.

Wetmiller, R.J., Adams, J., Anglin, F.M., Hasegawa, H.S., and Stevens, A.E., Aftershock sequences of the 1982 Miramichi, New Brunswick, earthquakes: Bulletin of the Seismological Society of America: v. 74. p. 621-653, 1984.

Yang, J.P., and Aggarwal, Y.P., Seismotectonics of northeastern United States and adjacent Canada: Journal of Geophysical Research. v. 86. p. 4981-4998, 1981.

PROBLEMS IN INTRAPLATE SEISMOGENESIS AND EARTHQUAKE HAZARD

Leonardo Seeber

Lamont-Doherty Geological Observatory of Columbia University, Palisades N. Y. 10964

ABSTRACT

Detailed hypocentral distribution in three aftershock zones of Mb = 4 to 5 main shocks and characteristics of preexisting structural features that seem to control the geometry of some zones of seismicity are considered in an effort to make geologic data more pertinent to the study of intraplate seismogenensis and to earthquake hazard in the eastern U.S. The main results are: 1. Ruptures can be sharply delineated by the aftershocks and they are smaller than expected when scaled to moments according to criteria based on data from plate boundaries. Thus, high stress drops should be expected and the criteria for determining maximum earthquakes on the basis of fault dimensions may have to be revised, i.e., small faults may be capable of damaging earthquakes; 2. Earthquakes can be generated by preexisting faults that show no detectable accumulated displacement of pre-Cenozoic markers. Thus, recency-of-faulting criteria to evaluate fault capability may not be applicable in intraplate regions. The combination of significant seismicity and low accumulated strain on individual faults suggests a model where faults are rooted in an elastic rather than ductile substratum; 3. Two broad zones of seismicity, in the central Adirondacks and in the northern Piedmont, are correlated with pre-Mesozoic shear zones. This correlation is not likely to result from reactivation because these features are now exposed at their formerly ductile deformation level and are probably healed, and because earthquakes along the seismic zones are generated by faults at large angles to the ancient ductile faults. Thus, zones of epicenters aligned with preexisting faults may not be taken as evidence that these faults are capable. Seismicity without reactivation along ancient faults may result from stress concentration stemming from ductile and brittle response juxtaposed along these features. A better understanding of intraplate neotectonics can be expected to allow a much expanded use of geologic data in the study of seismicity and the estimate of earthquake hazard.

INTRODUCTION

Engineers designing structures must rely on proven principles; in contrast, seismologists investigating geologic processes have the privilege of proposing, testing and discarding erroneous hypotheses. This difference in approach may be in part responsible for difficulties in communication. Propositions that are only working hypotheses for seismologists, may be given undue credit by engineers. This is particularly likely in the eastern U.S. where the state of knowledge on seismogenesis is rather primitive. In this

paper I wish to discuss recent results that raise questions regarding some long-standing assumptions, to only allude at possible solutions, and to offer a provocative reminder that basic properties of intraplate seismogenesis are still poorly understood.

SEISMICITY VERSUS GEOLOGIC SLIP RATES

The relation between seismicity and displacement on specific faults has been the main guiding principle in the western U.S., but it is particularly problematic in the eastern U.S. No historic earthquake in the East has been associated with a surface rupture on a fault. The major Holocene surface slip event recently recognized on the Meers fault in Oklahoma is prehistoric and is not marked by current seismicity nor by evidence of significant accumulated neotectonic displacement(e.g., Luza et al, 1987).

The two major earthquake sequences in the eastern U.S., in New Madrid, Mo., 1811-1812 and in Charleston, S.C., 1886 were centered in areas capped with flat-laying sediments. Subsurface investigations in these areas have revealed a remarkable absence of significant structural features in layers as old as Mesozoic (e.g., Stewart, 1986; Hamilton et al., 1983). This lack of accumulated vertical deformation is in contrast with the abundance of secondary near surface deformation associated with mobilization of unconsolidated sediments resulting from liquefaction (e.g., Obermeier et al, 1985).

In the lower Coastal Plain of South Carolina, secondary deformation has been associated with the widespread liquefaction event triggered by the 1886 earthquake, and to other distinct previous events, inferred to be related to prehistoric earthquakes similar to the one in 1886. In both New Madrid and Charleston, paleoseismic data suggest a repeat time of about a millennium for events similar to the historic ones. The faults that generated these historic and prehistoric events have only weak constraints on size and location. Thus, it was possible to account for the low rates of geologic deformation on any single steeply-dipping fault by either distributing the seismicity and related moment-release rate on many different faults (Wentworth and Mergner-Keefer, 1983; Anderson, 1986) or by generating it on a shallow-dipping fault or detachment (Behrendt et al., 1981; Seeber and Armbruster, 1981).

Recent results from the northeastern U.S. also raise the issue of low geologic rates of deformation. In these cases these rates pertain to specific faults which are known to be seismogenic and steeply dipping. The 1983 Goodnow earthquake in the central Adirondacks (Ms=5.3) ruptured a NNW striking fault dipping steeply to the west, according to first motions and to the distribution of aftershocks (Figures 1 and 2). The 1.5 km wide circular rupture is centered at a depth of about 8 km. The surface extrapolation of this inferred rupture nearly coincides with the 15 km long Catlin Lake Lineament (Isachsen and McKendree, 1977). Detailed geologic investigation has revealed a concentration of fractures along this lineament, including slickensided surfaces parallel to the lineament (Figure 3). The data suggest that the topographic lineament and the 1983 rupture are both related to a brittle fracture zone or fault that reaches the surface.

The detailed structural data also indicate, however, that Grenville age markers cannot be laterally displaced across the fracture zone along the Catlin Lake lineament by more than a few tens of meters, if at all (Figure 3). In this and other respects, then, the Catlin Lake fracture zone resembles the "zero-displacement faults" described by Isachsen et al. (1981). The age of these brittle features is not well constrained, but McLelland and Isachsen (1980) argue that they must be old, possibly Precambrian, on the basis of their relation to ductile structures of Grenville age. Thus, relatively old faults with an insignificant amount of accumulated displacement may generate significant earthquakes.

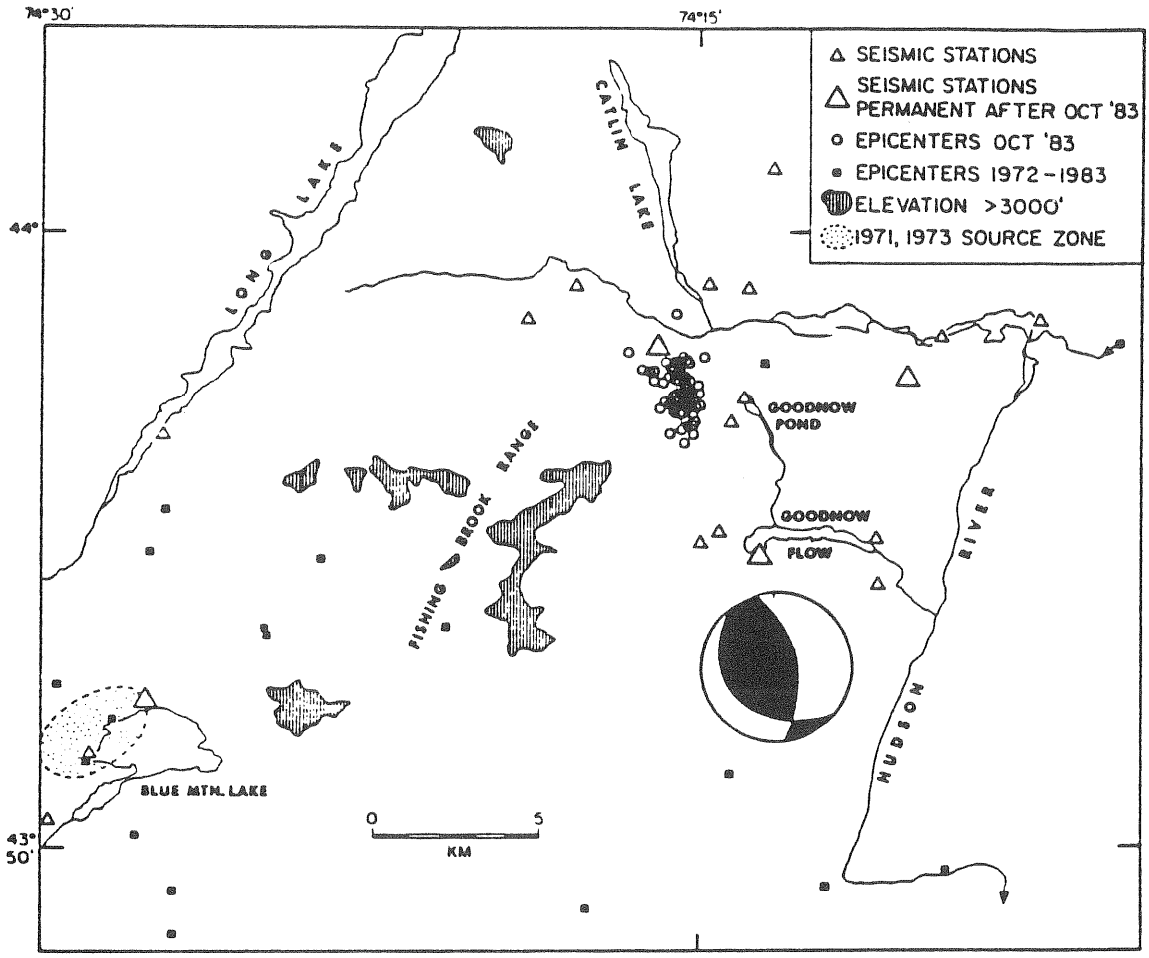

Figure 1. Blue Mountain Lake - Goodnow area of the Central Adirondacks. Three sets of epicenters are indicated: aftershocks of the 1983 Goodnow earthquake (October 7-29,1983; open circles; data from the temporary seismic stations shown); epicenter zone of the 1972-73 Blue Mt. Lake swarms (stippled area); 1972-83 epicenters located by the regional seismic network (filled squares). Long Lake, Catlin Lake and the Hudson River mark geomorphic features that reflect zones of fractures, possibly brittle faults. The north-northeast trend is dominant in the morphology of the Central Adirondacks, but the north-northwest trend seems to reflect the seismogenic faults.

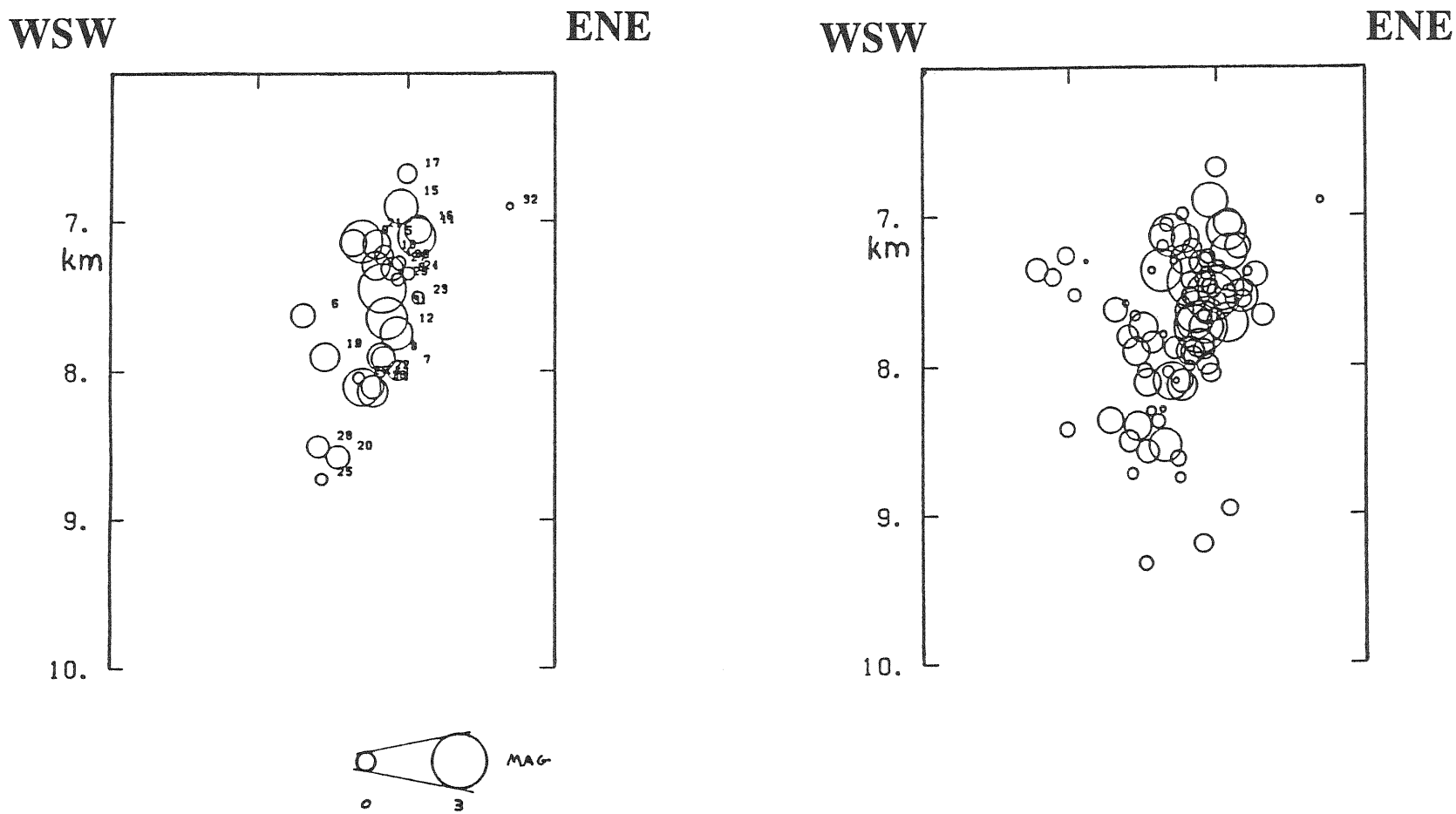

Figure 2A. Aftershocks of the 1983 Goodnow earthquake. Vertical section perpendicular to strike (see Figure 1). Section on the left shows aftershocks during the first week only. Section on the right shows aftershocks during the first month. Note growth of seismic zone on antithetic fault.

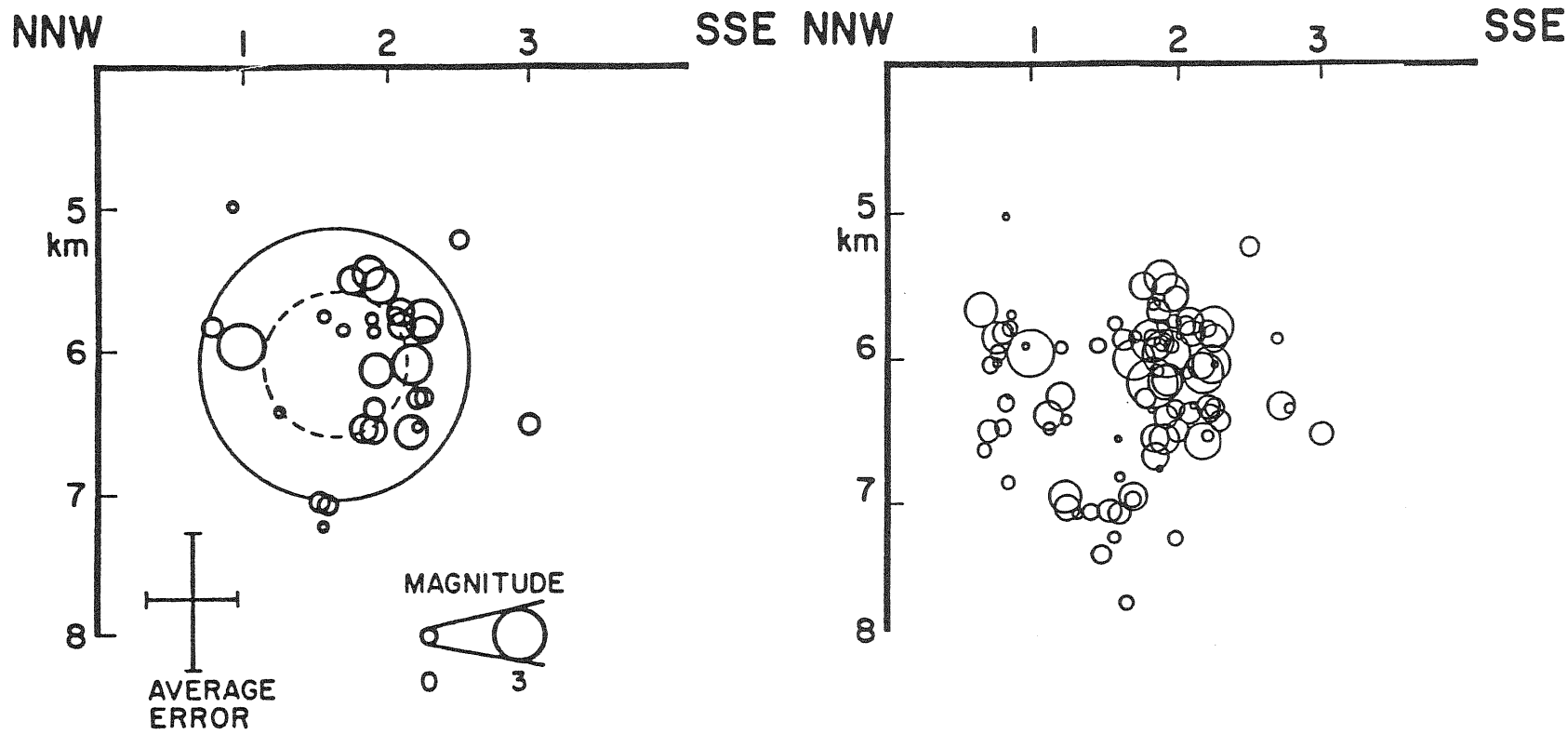

Figure 2B. Aftershocks of the 1983 Goodnow earthquake. Obliquely dipping section, parallel to the inferred rupture surface. Section on the left shows aftershocks during the first week only. Section on the right shows aftershocks during the first month. Circles cover the range in values for the dimension and depth of the rupture inferred from a moment-tensor inversion (from Nabelek and Suarez, this volume). Note annular pattern defined by aftershocks. This annulus probably defines the outer edge of the rupture. Compare with Figure 9.

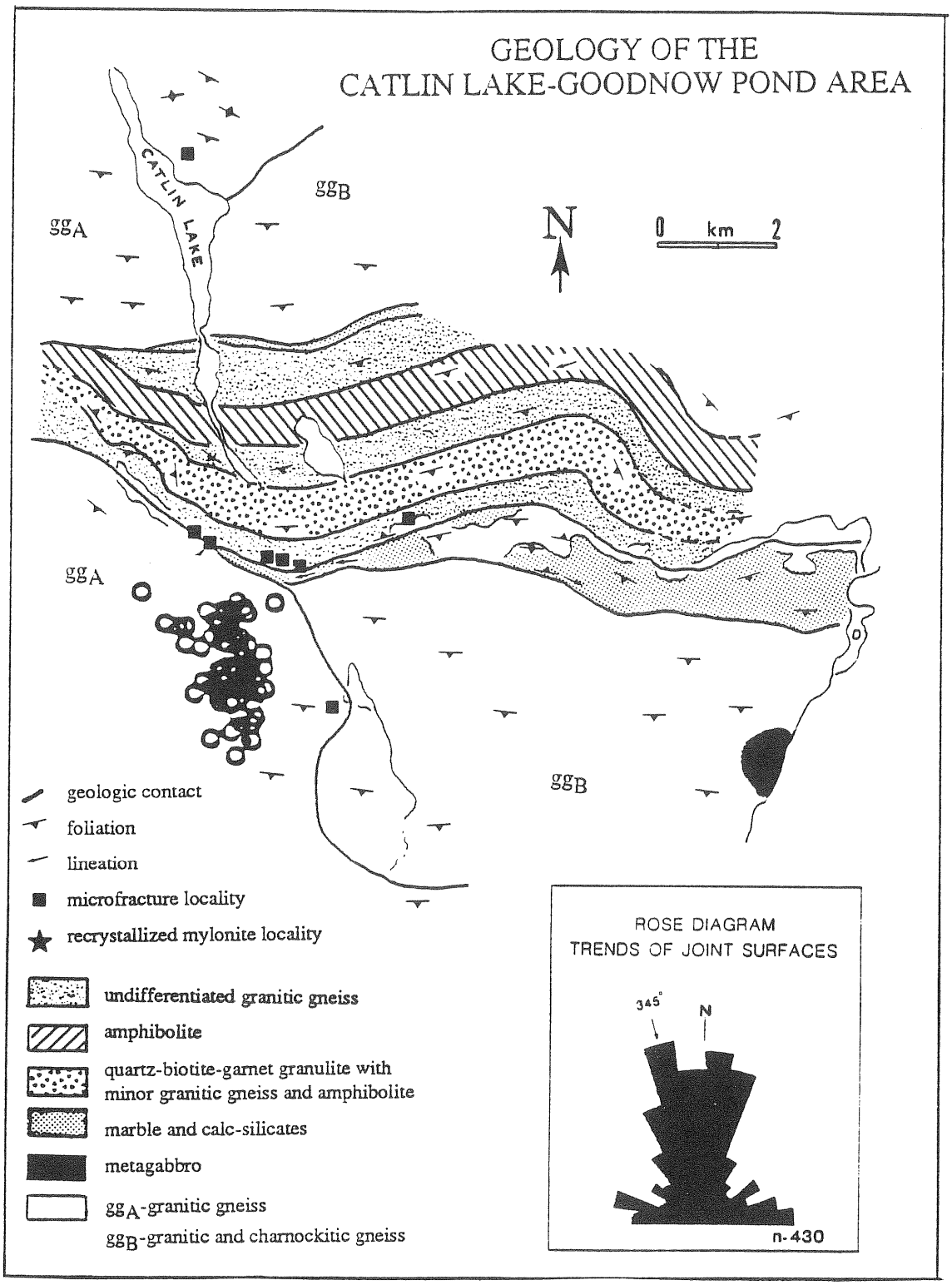

Figure 3. Ductile and brittle structural features in the epicentral area of the 1983 Goodnow earthquake (circles delineate aftershock epicenters). Surface extrapolation of the rupture falls approximately along the Catlin Lake lineament which is delineated by a narrow 10 km long valley and is marked by a pronounced fracture set (inset). Slickensided surfaces parallel to the inferred rupture and microfractures are concentrated at the intersection of the lineament with the marble layer. Although this lineament has many of the characteristics of a brittle fault, no displacement of the Grenville structures can be detected. The resolution is better than 50 meters.

A close spatial correlation was also found between a mapped fault, the Dobbs Ferry fault, and the inferred rupture of the 1985 Westchester earthquake (Mblg=4). Aftershocks and first motions suggest a small subvertical rupture with left-lateral motion and centered about 5 km deep (Figure 4). Detailed surface data for the Dobbs Ferry fault are still lacking, but a map compiled by Leo Hall (Nick Ratcliffe, personal communication, 1986) show early Paleozoic features cut by this fault with no significant displacement (Figure 5).

The Dobbs Ferry fault is part of a set of northwest striking brittle faults in the Manhattan Prong thought to be of Mesozoic age. The 125th Street fault in Manhattan is one of these faults. Subsurface studies of this fault reveal a thick breccia zone suggesting large accumulated slip. The northwestern portion of this fault, however, shows little displacement of the Jurassic age Palisades sill, and no recognizable vertical displacement of the Cretaceous erosional surface above the sill. In contrast, if the set of NW faults with a total seismogenic surface of 500 km^2 are considered to be the source of an event like the one in the Adirondacks in 1983 (average slip 30 cm; rupture area 1.5 km^2) every century (i.e., the events in 1884, 1783, and 1737), these events alone would account for a displacement rate of about 10 meters per million years, or 1/2 km since the Cretaceous. This back-of-the-envelope calculation for the inferred slip rate does not consider the contribution to the moment release from smaller events, like the one in 1985, and from possible larger events.

The data for the 1986 Ohio earthquake (Ms=5.0) and related seismicity present another case of a seismogenic fault with evidence of little accumulated displacement. The aftershocks and first motions for this event suggest a small (1x1 km) vertical rupture with right slip centered at a depth of about 5 km (Figure 6). The inferred rupture is aligned with a major linear aeromagnetic feature which strikes NNE and can be followed for at least 50 km. Many of the other epicenters in northeastern Ohio fall within error estimates of this feature (Figure 7). Aeromagnetic data reflects primarily rock type in the Precambrian basement. The feature in question is expressed as a boundary between domains with different magnetic signature and is probably a major Precambrian fault marking a tectonic boundary. The earthquake data suggest that this feature is reactivated, at least locally, in the current tectonic regime.

About two km of flat-lying Paleozoic sediments cap the basement in northeastern Ohio. These sediments can serve as a marker for vertical displacement since early Paleozoic. An effort to detect any such displacement using the abundant subsurface data from wells in the 1986 epicentral area has been unsuccessful so far (Mike Hansen, personal communication, 1986). Once again, then, there is evidence for a major preexisting fault, a Precambrian feature in this case, that is seismogenic, but shows no sign of displacement accumulated during this reactivation.

Detailed data on recent Mb=4 to 5 earthquakes in the northeast U.S. suggest that even for these relatively small events, ruptures are often located on faults which can be recognized from other data. Some of these faults, however, appear to have little or no accumulated slip. An important practical implication of these results is that lack of recent movement along a fault is not necessarily an indication of low earthquake potential on that fault. Recency of movement, then, is a proven criterium for fault capability in interplate zones such as the Western U.S., but it is not a reliable criterion in intraplate areas.

The commonly accepted classical model for intraplate tectonics is analogous to models for interplate deformation. This model has a brittle surface layer, the seismogenic upper crust where deformation is concentrated on discrete faults and discrete slip events.

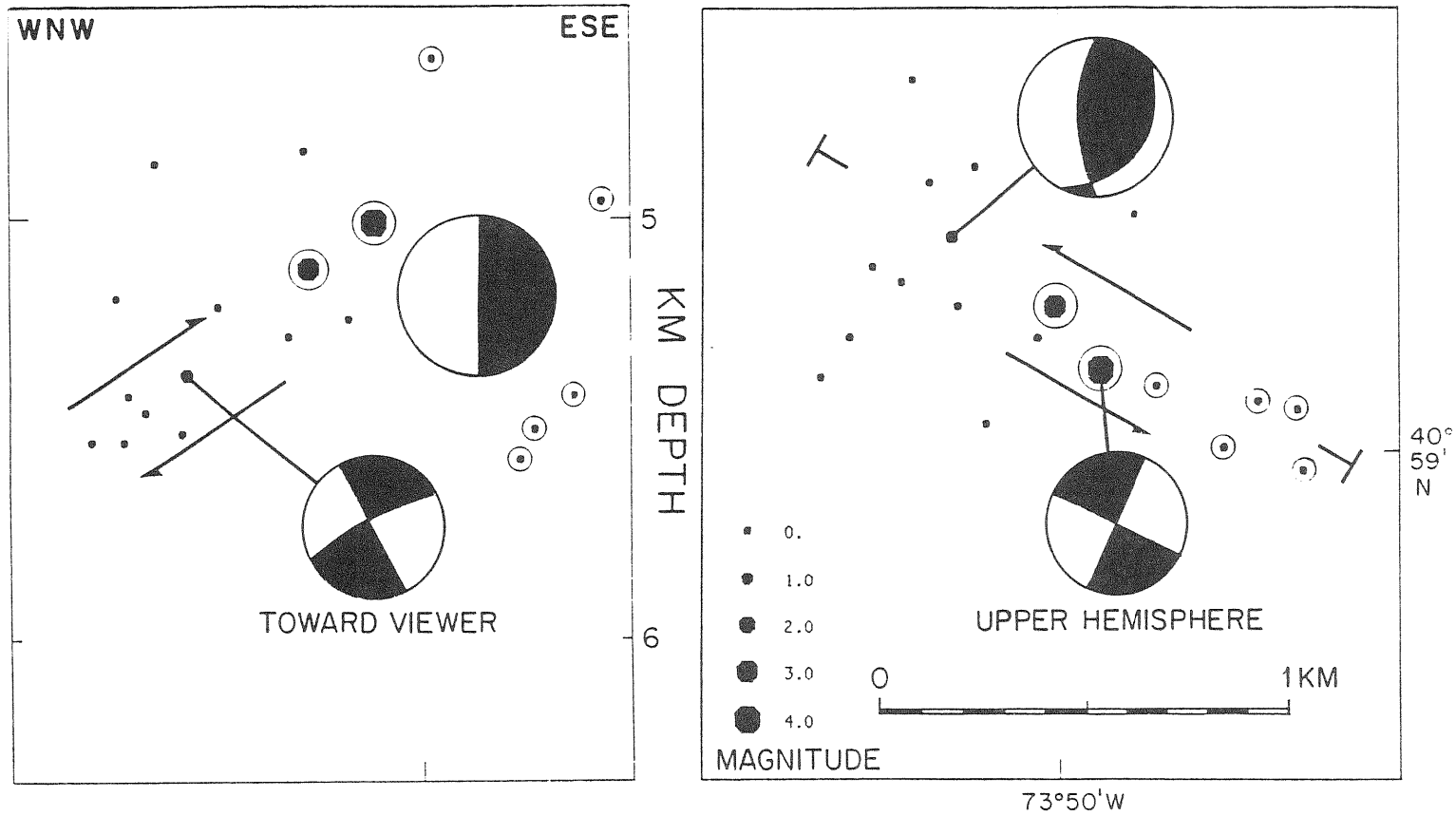

Figure 4. Aftershocks of the 19 October 1985 Westchester Co. earthquake: the right frame is a map view, the left frame is a vertical section parallel to the inferred rupture. Circled hypocenters occurred during the first week; the other hypocenters occurred later. Aftershock and first-motion data constrain the rupture to be vertical, strike northwest, and to be left-lateral. The distribution of early aftershocks suggest that the rupture is about 3/4 of a km across. Comparison with figures 2, 4 and 9 reinforces this conclusion.

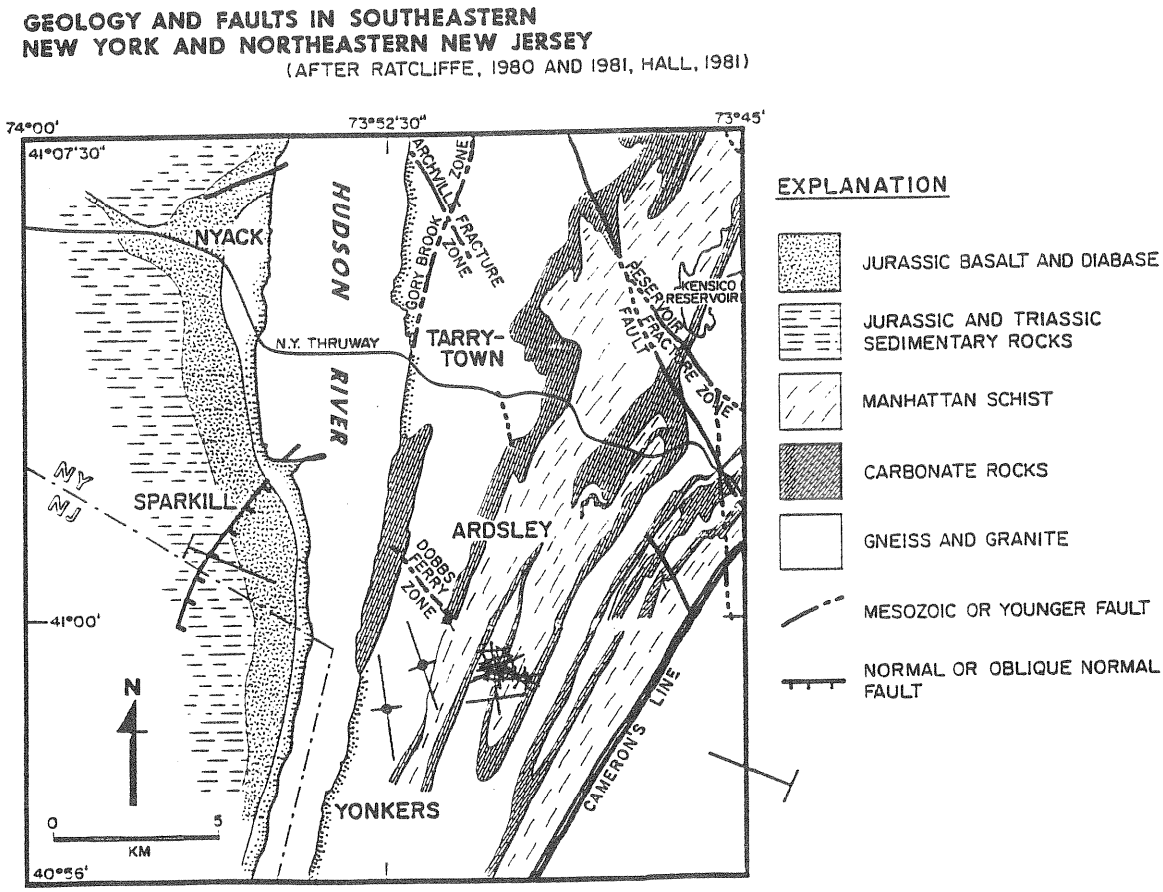

Figure 5. Geologic map of parts of the Newark Basin (west of Hudson River) and of the Manhattan Prong in the epicentral area of the October 19, 1986 Westchester Co. earthquake. The northwesterly striking main rupture is marked by the tight cluster of aftershocks (crosses indicate possible location errors). The Dobbs Ferry fault is aligned with the rupture. Most other brittle faults in the Manhattan Prong have the same trend.

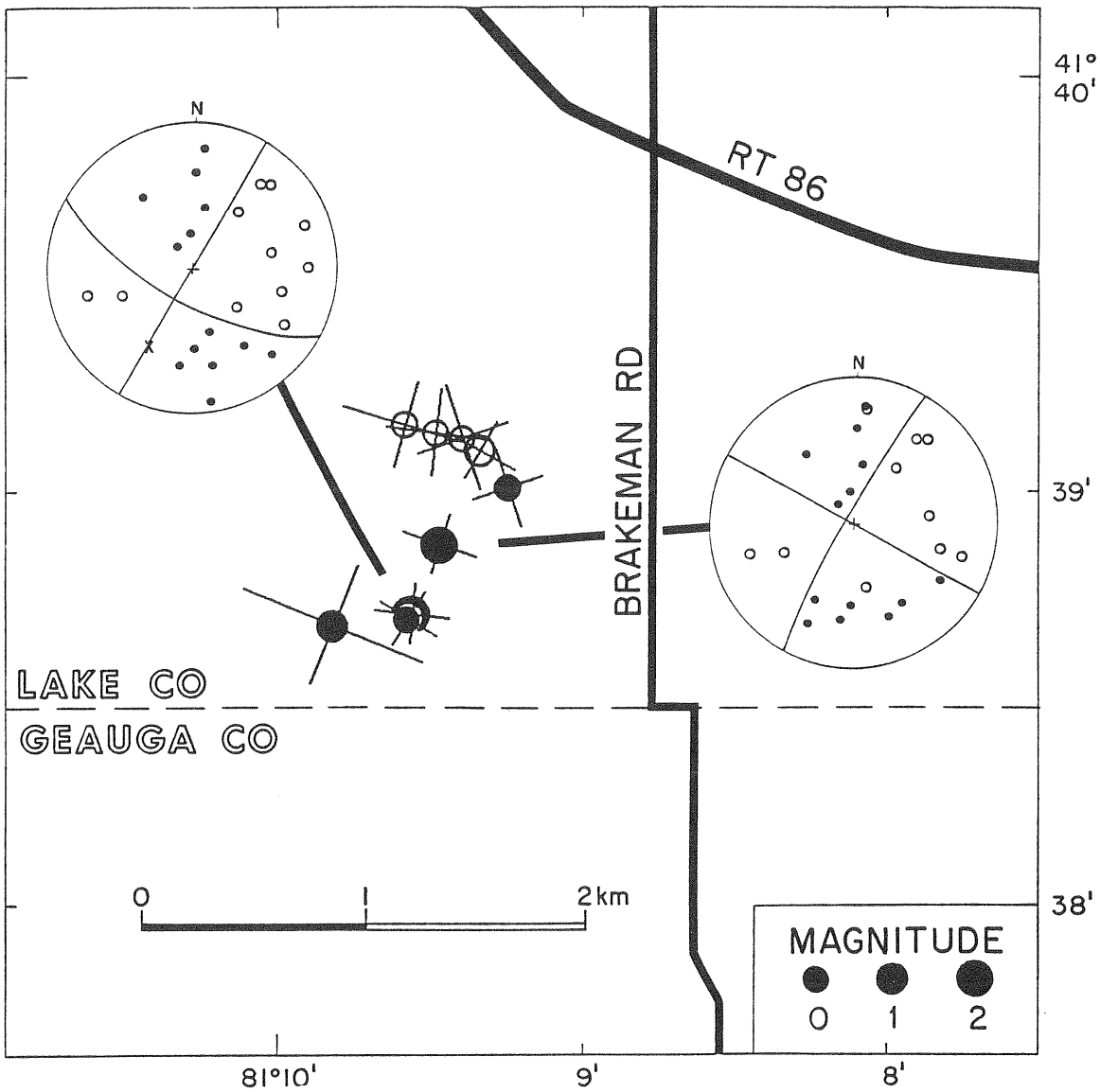

Figure 6A. Epicenters for the nine aftershocks of the January 31, 1986 chardon, Ohio earthquake for which reliable data are available. These data are from temporary seismic stations operated by many institutions. Filled circles indicated aftershocks during the first week of the sequence. Hypoinverse error bars are shown.

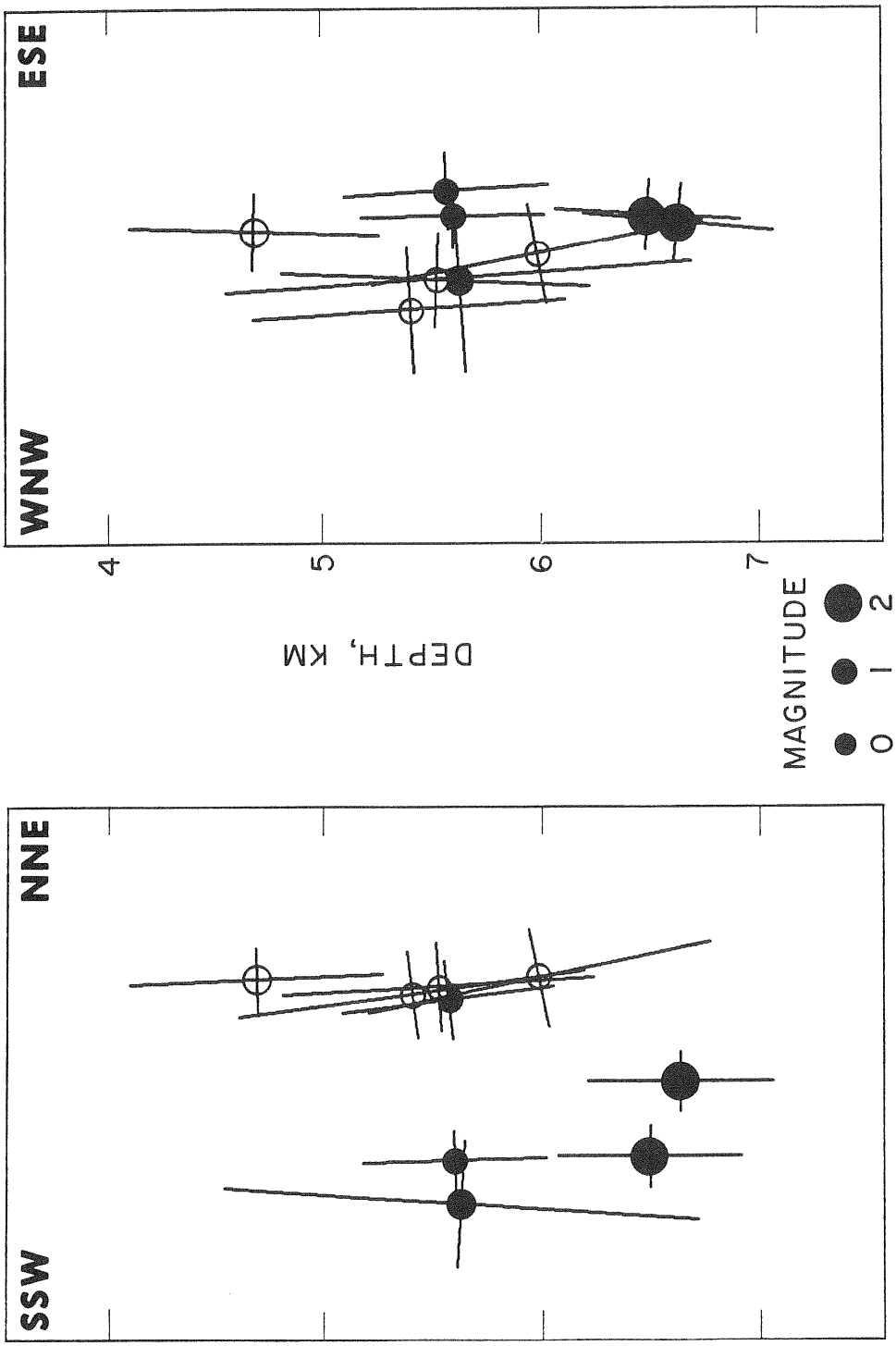

Figure 6B. Perpendicular vertical sections with hypocenters for the nine aftershocks shown in Figure 6A (same symbols). These sections are parallel (left) and perpendicular (right) to the inferred rupture.

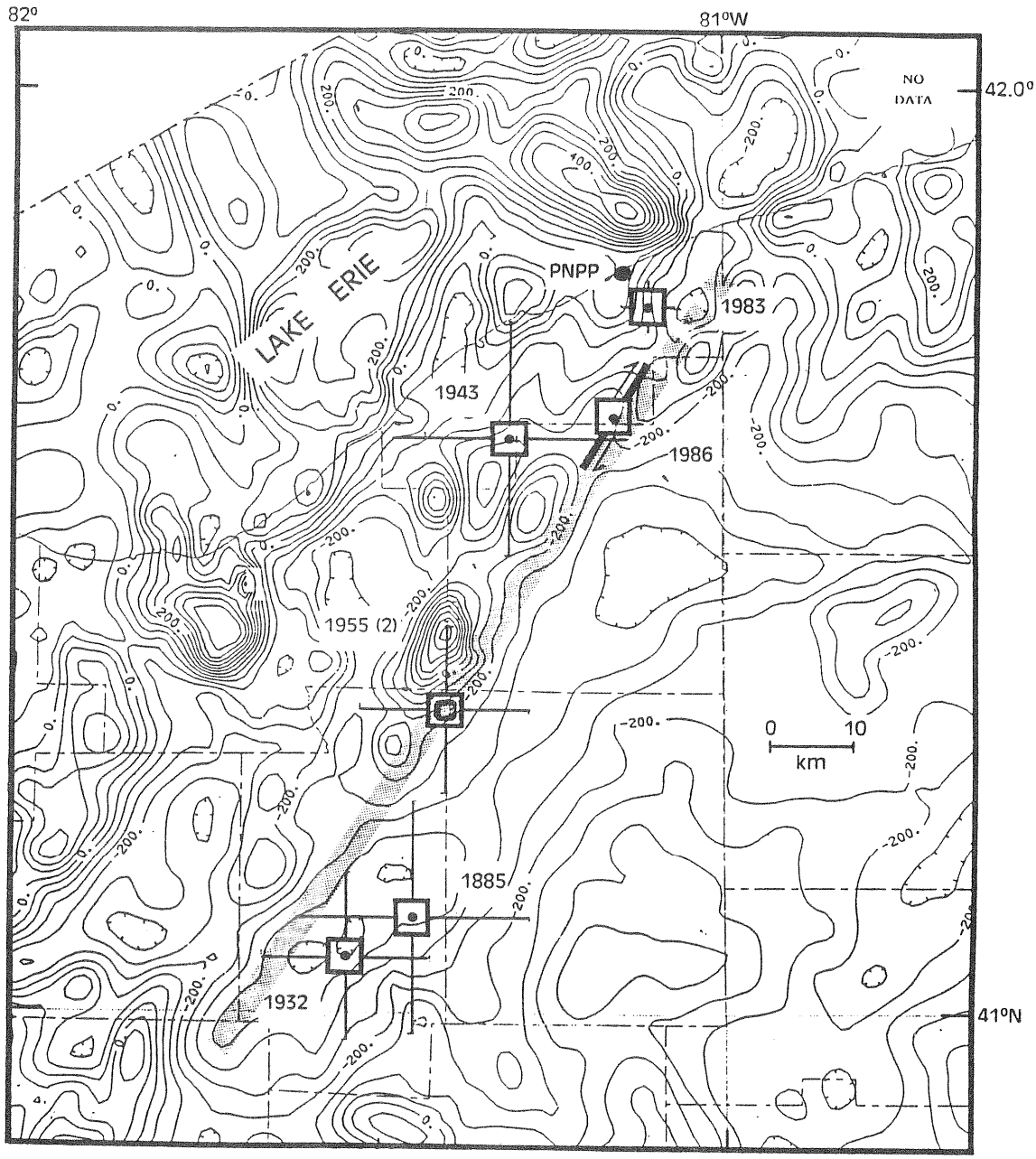

Figure 7. Epicenters of the most prominent known earthquakes and residual total magnetic map (from Hildebrand and Kucks, 1984) for the area of northeastern Ohio centered on the 1986 Chardon earthquake. Strike of the rupture and sense of motion are shown with the 1986 epicenter. The other epicenters (Western Geophysical, 1979, 1986; U.S. Geological Survey, 1986) are the better determined (uncertainties ≤16 km) within 50 miles of the Perry nuclear power plant (PNPP) and maximum Modified Mercalli intensity ≥IV or magnitude Mb≥3. Note that the main earthquakes known from this area appear to be spatially associated with a major linear boundary in the aeromagnetic data (shaded zone). The 1986 rupture is also on this boundary and is parallel with it. From Aggarwal, 1987.

The brittle layer lies above a ductile layer, where deformation is diffuse and aseismic. In the "ductile root" model the rate of deformation is governed primarily by the response of the ductile layer and is dependent on the level of stress. Tectonic stress seems to be uniform over major portions of plates and is inferred to derive from large scale and long term phenomena, such as push from the ridges or drag at the bottom of the lithosphere, that would tend to make a given stress field long-lasting, even in geologic terms. In view of the results discussed above, then, a ductile root model may not be easily reconciled with the low accumulated slip and the relatively high seismicity on at least some faults in the eastern U.S.

In an alternative intraplate model proposed here, the bulk behavior of the seismogenic layer, or parts thereof, remain elastic when subjected to tectonic stresses. Confined in this strong elastic layer are faults, zones of weakness (or stress concentration; see below). These faults are decoupled from the underlying ductile layer and are rooted in material experiencing only elastic deformation ("elastic root" model; Figure 8A). At an equilibrium state, which can be at any level of regional tectonic stress below the strength of the elastic layer, this layer is not deforming and the shear stress across the weak faults is low, possibly as a result of failure. If the regional stress changes, the strong layer deforms elastically. Shear stress on the weak faults, then, is likely to rise and possibly result in failure. It is conceivable that a rise in regional stress would cause slip on a weak fault and a subsequent drop in that stress would cause slip in the opposite direction on the same fault. Thus, weak faults may slip in different directions at different times responding to changes in stress. If the stress level tends to fluctuate, these faults could slip back and forth, experience large amount of slip and develop a thick gauge layer, but they would not accumulate much net displacement.

The elastic root model can account for the high ratio between seismicity rate and geologic displacement on some faults. In this model, the level of seismicity should depend on the rate of change of stress, radically altering the relation between tectonic stress and earthquake hazard. According to this model, stress localized on a weak fault and resulting strain may be drastically different, even in opposite directions, than the regional stress. This characteristic can be exploited to test the "elastic" model. The "elastic" and the "ductile" models are not exclusive. Both can apply, each at different scales or on different portions of the intraplate region (e.g., Figure 8A).

RUPTURES DELINEATED FROM DISTRIBUTION OF AFTERSHOCKS

A close spatial correlation between ruptures and aftershock zones has been demonstrated for ever smaller ruptures, as location uncertainties have continued to decline. By considering both hypocentral locations and first-motions, it has been possible to differentiate aftershocks that occur on the main rupture, the aftershocks proper, from aftershocks occurring beyond the limits of the rupture and on other faults. Moreover, particularly well constrained aftershock zones suggest a tendency for the aftershocks to populate the perimeter of the rupture, leaving the central part of the rupture relatively unpopulated. This characteristic is also instrumental for identifying the rupture from the aftershock distribution. These characteristics of aftershock zones have been illustrated by recent intermediate magnitude events in California (e.g., Figure 9).

Results from detailed studies of recent aftershock sequences of relatively small events in the northeastern U.S. suggest relationships between ruptures and aftershock zones that resemble the one observed for larger events in California. Figures 2,4, and 6

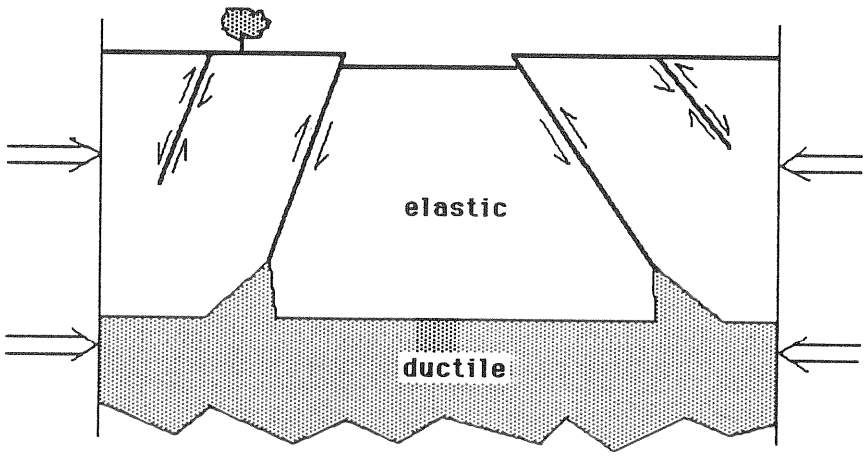

Figure 8A. Some faults cut through the elastic layer and reach the ductile layer. The accumulated displacement on these faults will reflect the amount of distributed strain in the ductile layer ("ductile root" model). Other faults are confined within the elastic layer ("elastic root" model). These faults will not accumulate significant displacement. If they are weak, shear stress across them will be dissipated by slip. After equilibrium is reached, renewed slip will occur if the tectonic stress changes. A decrease in the level of stress may cause slip on these weak faults opposite to the one expected from the regional stress. The rate of slip and, possibly, seismicity on such faults depends on the rate of change of the stress.

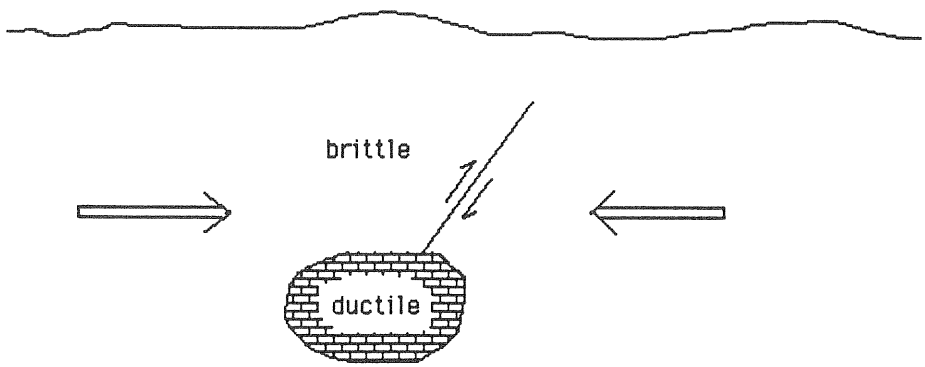

Figure 8B. A rock body that responds to stress with ductile deformation (e.g., calcitic marble buried several km below the surface), imbedded in an elastic medium (e. g., gneiss). At the equilibrium state the ductily deforming rock sustain little or no stress. The load is transferred to the surrounding rock. The concentration of stress around the ductile rock may be responsible for a concentration of seismicity.

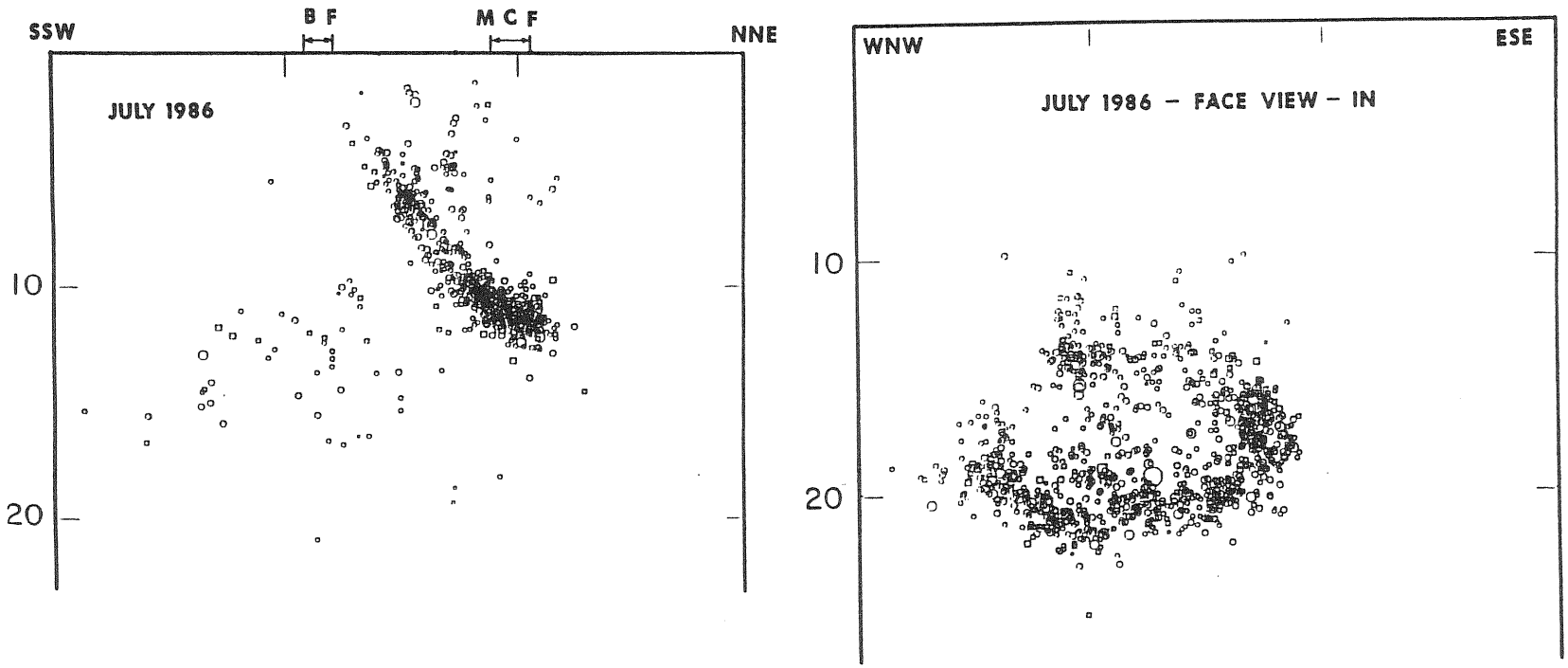

Figure 9. Aftershocks of the July 7, 1986 North Palm Spring earthquake (Ms=5.9) on the Banning fault in southern California. The vertical section on the left is perpendicular to the strike of the rupture. The section on the right is tilted and parallel to the inferred rupture plane. Note the concentration of aftershocks around the perimeter of the rupture. Note also that some of the "aftershocks" are not located on the rupture. Data from the Caltech/USGS network; relocation by Doug Given.

show the aftershock zones of the 1983, 1985 and 1986 earthquakes (discussed above) viewed in sections parallel to the inferred ruptures (i.e., the ruptures are viewed face on). An anular distribution of the seismicity can be clearly recognized for the 1983 sequence. A similar pattern may then be seen in the other two events. In each case, the anular pattern is the only active feature in the early part of the sequence. Subsequent aftershocks show a tendency for activity spreading to other faults as the sequence progresses. These results are significant in terms of the mechanics of the aftershock process, but also in terms of earthquake hazard analysis since they show that ruptures of small intraplate earthquakes can be resolved from detailed aftershock studies.

The rupture areas inferred from the aftershock distributions appear to be roughly circular with diameters of 1.5 km, 0.8 km, 1.0 km, for the events in 1983, 1985 and 1986, respectively. These ruptures are surprisingly small, significantly smaller than predicted by the Nuttli (1983) relation between moment and rupture size for the eastern U.S. One direct implication for earthquake hazard estimates is that the fault dimension - maximum earthquake relation may need to be altered toward larger earthquakes. Another one is that stress-drops may tend to be higher for earthquakes in the East than for earthquakes in the West (Scholz et al., 1986).

SEISMICITY ALONG PREEXISTING FAULTS: ZONES OF WEAKNESS OR STRESS CONCENTRATION?

Geologic data are relatively abundant and easily acquired. An understanding of the relation between seismicity and structural features inherited from previous orogenies may greatly expand the use of geologic data to infer characteristics of the seismicity. Much has been said about the reactivation of preexisting features that may have the tendency to persist as zones of weakness (e.g., Ratcliffe et al., 1986), but progress has been generally hampered by insufficient data. Steady improvement in this situation may be now reaching the critical level for new insights. For example, the data for northeastern Ohio in Figure 7 illustrate a case of possible reactivation of a Precambrian fault in the current stress regime. Similar correlation between preexisting faults and seismicity has been proposed for the New Madrid seismic zone.

Figures 10 and 11 show two broad seismic zones related spatially to ancient structural features in the central Adirondacks and in the northern Piedmont, respectively. The Central Adirondacks seismic zone follows Precambrian structural trends, and probably the locus of a major structural boundary. Exhumation has now brought to the surface the ductile deformation level of Precambrian (Grenville) deformation. Similarly, the seismic zone along the southeast side of the Newark Basin is centered along the Martic - Camerons line, a lower Paleozoic suture, also exhumed at the formerly ductile deformation level. The geometry of faulting along each of these zones has been resolved for several events, including the 1983 and 1985 events discussed above (Figures 1 through 7). In all these cases, the inferred seismogenic faults strike at large angles to the trend of the seismic zones and to the preexisting features along these zones. Reactivation, then, does not seem to apply in these cases. A similar relation between the overall trend of the seismicity, Precambrian structure, and seismogenic faults is found in eastern Tennessee (Johnston et al., 1985)

If seismic zones can be associated with preexisting faults by a process other than reactivation, the length of these zones and the related faults lose their connotation in terms of the maximum possible length of a rupture in that zone. It is possible, moreover, that these apparently inactive preexisting faults are associated with seismicity because they are

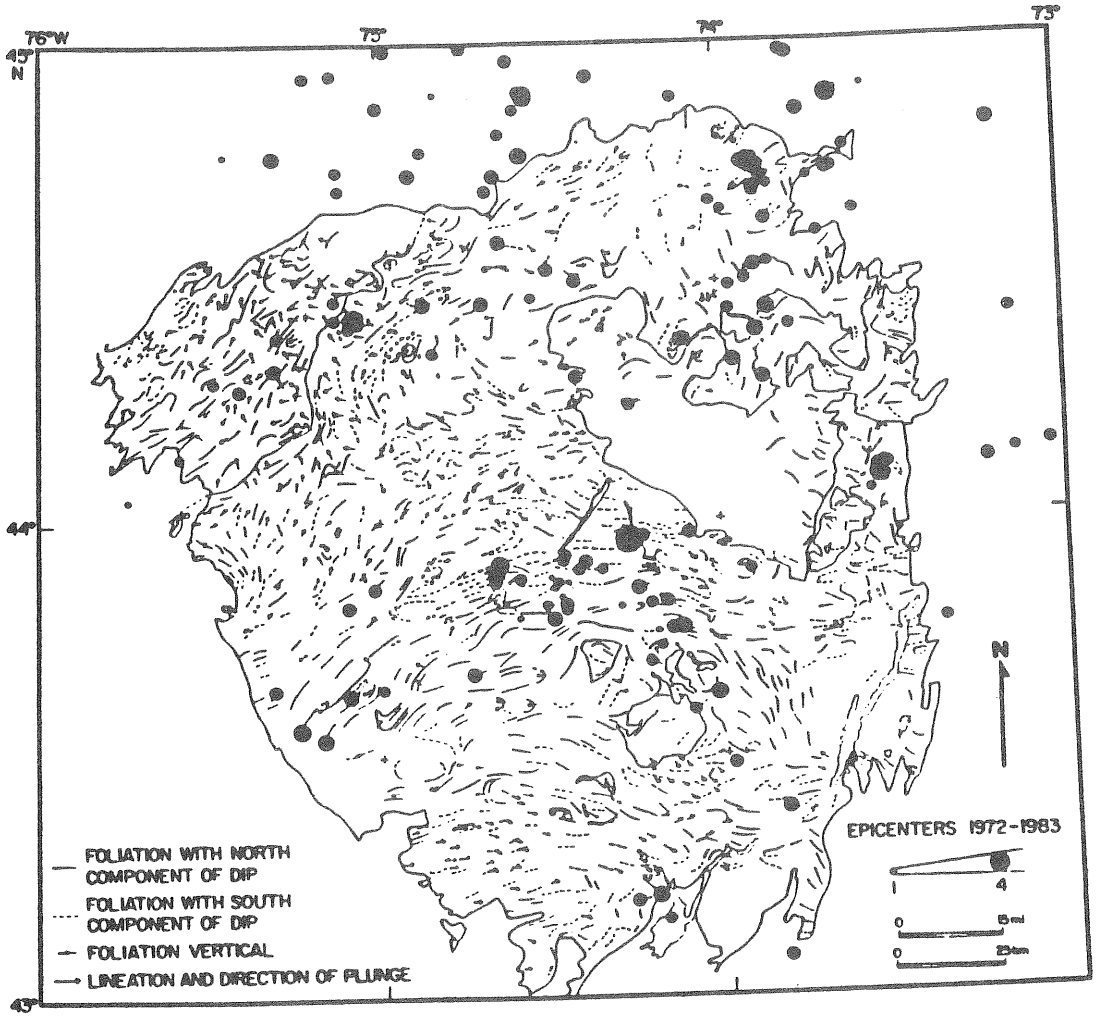

Figure 10. Epicenters from the New York State Seismic Network, 1972-1983 (black dots) superimposed on foliation and lineation data extracted from the 1:250,000 N.Y. State geologic map (Isachsen and Fisher, 1970). Two arcuate belts of seismicity in the central and northwestern Adirondacks are related to Precambrian (Grenville) structural trends. Large domains where dips of foliation have either a north or a south component can be recognized; boundaries between these domains may be tectonic. The seismic zone in the central Adirondacks, which contain the Goodnow and Blue Mt. Lake epicentral areas (Figure 1), is associated with a foliation-dip boundary.

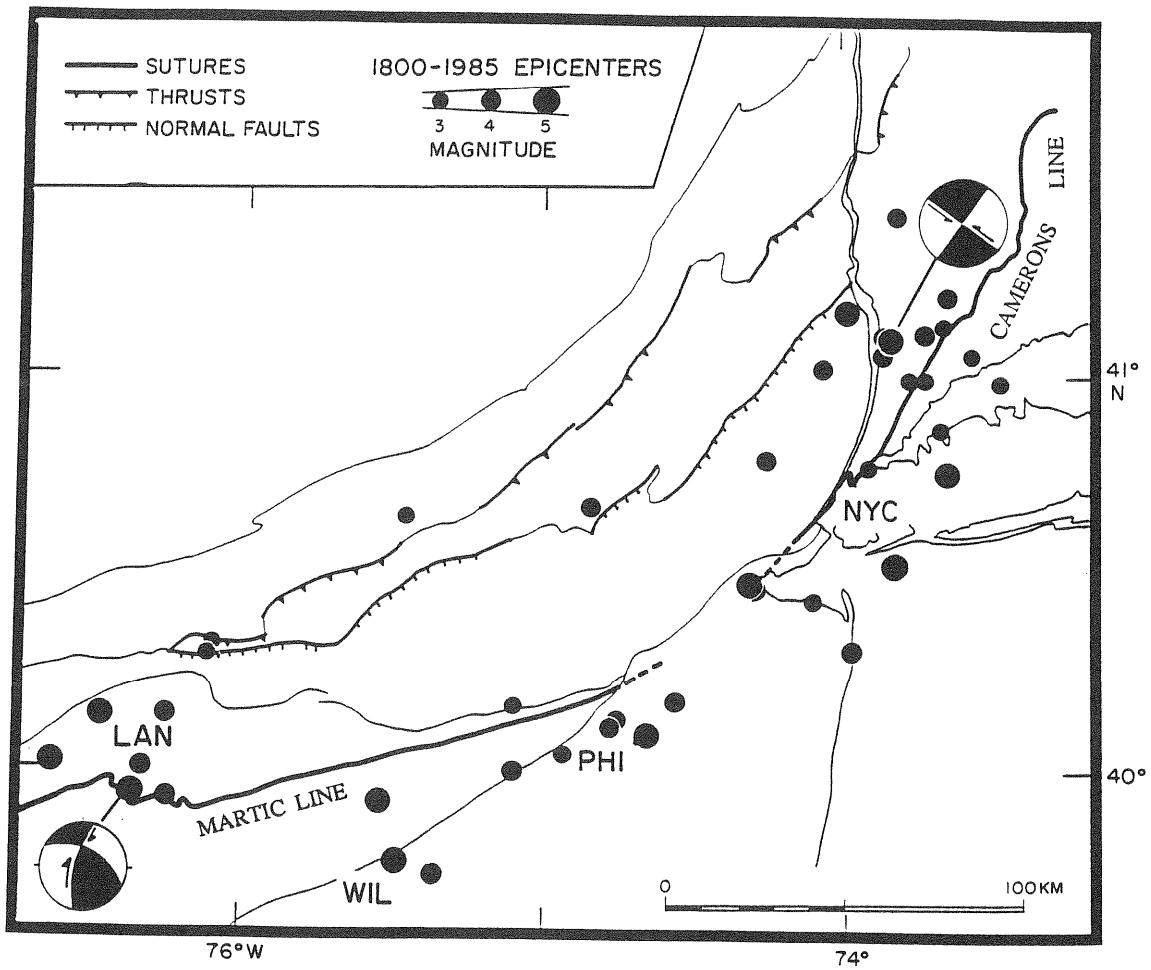

Figure 11. Epicenters of significant earthquakes (felt-area magnitudes Mfa≥3) in the area of the Newark Basin during almost two centuries. Most of the epicenters fall in a broad belt on the southeast side of the basin centered along the Martic-Camerons line, an early Paleozoic suture. The ruptures in the two most recent events on this map, the Lancaster (LAN) event in 1984 and the Westchester Co. event north of New York City (NYC) in 1985, were resolved from aftershock data and found to be at large angles to the trend of the belt. Balloons represent fault-plane solutions for these events (upper hemispheres); arrows indicate the fault plane and the sense of slip. Faulting in few smaller events have trends similar to the ones in 1984 and 1985. Reactivation of the Martic-Camerons line cannot be the cause of the spatial association between this feature and the seismic belt.

zones of stress concentration, rather than zones of weakness. This working hypothesis is inspired by the probable association of some of these structural features with deeply buried calcitic marble.

At a few km of burial, calcitic marble is expected to deform ductily. Ductile deformation of rock volumes imbedded in an elastic environment, would tend to lower the stress in the ductile rock and concentrate stress in the surrounding elastic rock (Figure 8B). This concentration of stress would probably raise locally the potential for earthquakes. Thus, earthquake potential would generally be raised along an ancient structural feature responsible for juxtaposing rocks with contrasting ductile and brittle rheologies within the appropriate depth range. These features may typically be deeply rooted thrusts at convergence boundaries along which calcitic sediments have been deeply buried. If stress concentration can be related to lithologic contrast and to preexisting structural features, geologic data could then play a much greater role in characterizing seismic zones.

Acknowledgements

This paper greatly benefited from reviews by Klaus Jacob and John Armbruster. The work was supported by NRC 04-85-111-02 and by NCEER 86-1014 and NCEER 87-1303.

References

Aggarwal, Y.P., Seismicity and tectonic structure in Northeastern Ohio: Implications for earthquake hazard to the Perry Nuclear Power Plant, Report to Ohio citizens for responsible Engery, Inc., 28 pp., March 1987.

Anderson, J.G., Seismic strain rates in the central and eastern United States, Bull. Seis. Soc. Amer., 76, 273-290, 1986.

Behrendt, J.C., R.M. Hamilton, H.D. Akerman, and V.J. Henry, Cenozoic faulting in the vicinity of the Charleston, South Carolina 1886 earthquake, Geology , 9, 117-122, 1981.

Hamilton, R.M., J.C. Behrendt, and H.D. Ackerman, Land multichannel seismic-reflection evidence for tectonic features near Charleston, South Carolina, U.S. Geol. Surv. Prof. Pap., 1313I, 18, 1983.

Hildenbrand, T.G., and R.P. Kucks, Residual total intensity map of Ohio, Map GP-961, U.S. Geol. Survey, Reston, VA, 1984.

Isachsen, Y.W., and D.W. Fisher, Geologic map of New York (scale 1:250,000), New York State Museum map and chart series 15, 1970.

Isachsen, Y.W., and McKendree, W.G., Preliminary brittle structure map of New York, 1:250,000 N.Y.S. Museum Map and Chart Series 31A, 1977.

Isachsen, Y.W., Geraghty, E.P., and R.W. Weiner, Fracture domains associated with a Neotectonic basement-cored dam - The Adirondack Mountains, New York, in Gabrielsen and others, eds., Proc. Fourth Internat. Conf. on Basement Tectonics, Oslo, Norway, 287-305, 1981.

Johnston, A.C., D.J. Reingold, and S.I. Brewer, Seismotectonics of the southern Appalachians, BSSA, 75 (N1), 291-312, 1985.

Luza, K.V., R.F. Madole, and A.J. Crone, Investigation of the Meers fault in southwestern Oklahoma, NUREG/CR-4937, U.S. Nuclear Regulatory Commission, Washington, D.C., 55, 1987.

McLelland, J., and Y.W. Isachsen, Structural synthesis of the southern & central Adirondacks: A model for the Adirondacks as a whole and plate tectonics interpretation, G.S.A. Bull, 91, Part II, 208-292, 1980.

Nabelek, J., and H. Suarez, this volume.

Nuttli, O.W., Average seismic source - parameter relations for midplate earthquakes, BSSA,73, 519-535, 1983.

Obermeier, S.F., G.S. Gohn, R.E. Weems, R.L. Gelinas, and M. Rubin, Geologic evidence for recurrent moderate to large earthquakes near Charleston, South Carolina, Science, 227, 408-411, 1985.

Ratcliffe, N.M., W.C. Burton, R.M. D'Angelo, and J.K. Costain, Low angle extensional faulting, reactivated milonites, and seismic reflection geometry of the Newark basin margin in eastern Pennsylvania, Geology, 14, 766-770, 1986.

Scholz, C.H., C.A. Aviles, and S.G. Wesnousky, Scaling Differences between large intraplate and interplate earthquakes, Bull. Seism. Soc. Am., 76, 65-70, 1986.

Seeber, L., and J.G. Armbruster, The 1886 Charleston, South Carolina earthquake and the Appalachian detachment, J. Geophys. Res., 86, 7874-7894, 1981.

Stewart, R.M., Review of geological, geophysical, and seismological data relevant to seismotectonics of the Charleston, South Carolina area (abstract), Earthquake Notes, 57, 16, 1986.

Wentworth, C.M., and M. Mergner-Keefer, Regenerate faults of small Cenozoic offset: probable earthquake sources in the southeastern U.S., USGS Prof. Pap., 1313S, 18, 1983.

SEISMICITY AND SEISMIC ZONATION ALONG THE APPALACHIANS AND THE ATLANTIC SEABOARD FROM INTENSITY DATA

by

John G. Armbruster and Leonardo Seeber

Lamont-Doherty Geological Observatory, Palisades, N. Y. 10964

ABSTRACT

Over most of the historic period for the eastern U.S., seismicity is parameterized from intensity data. Accuracy, uniformity and completeness of the earthquake catalog can be substantially improved by a systematic approach where new intensity data are retrieved from archival documents, primarily by systematic searches of newspapers, and where these data are analyzed by MACRO, an algorithm that yields source parameters from intensity data. MACRO fits these data with a prescribed geometry of intensity fall-off from the epicenter and calculates epicenter coordinates and magnitudes with error estimates. This parameterization procedure also generates residuals for each intensity point. When combined, sets of residuals for all the solutions provide information on the distribution of seismic site response. We are reexamining historic seismicity along the Appalachians and the Atlantic Seaboard concentrating at first on areas of special interest, but aiming for a revised catalog for that entire area. Some of the results are: 1. The 1886 Charleston, S.C., earthquake was followed by a widespread and intense aftershock sequence that mimics the current spatial distribution of seismicity. During the 19th century before the event, however, seismicity in the mesoseismal area was low, except for immediate foreshocks. This result suggests non-stationarity at the time scale of the historic period. Thus, the pattern of seismicity from the historic catalog may be a snapshot view of a changing pattern and future large events may occur in areas of low historic seismicity; 2. The rate of intensity fall-off from epicenters (IFR) tends to vary widely, even for earthquakes with similar locations and similar maximum intensity. Nevertheless, regional variations in IFR can be detected. Hypocentral depth and attenuation are probably the most important factors affecting IFR; 3. An azimuth dependence of IFR is detected for many earthquakes. Along the Appalachians, axes with lower IFR tend to be oriented along structural trends. This result suggests structurally controlled attenuation anisotropy. A scaling relation between intensity and instrumental data needs to be developed in order to interpret quantitatively IFR in terms of attenuation; 4. Intensity residuals show systematic patterns which correlate with both cultural and geologic factors. A tentative correlation is found between negative residuals (observed intensities lower than predicted) and Mesozoic basins, and between positive residuals and population centers.

INTRODUCTION

Earthquake data from felt and damage reports in the eastern U.S. provide unique information on both source parameters and seismicity, and on the type of adverse effects that can be expected in specific environments and from specific earthquakes.

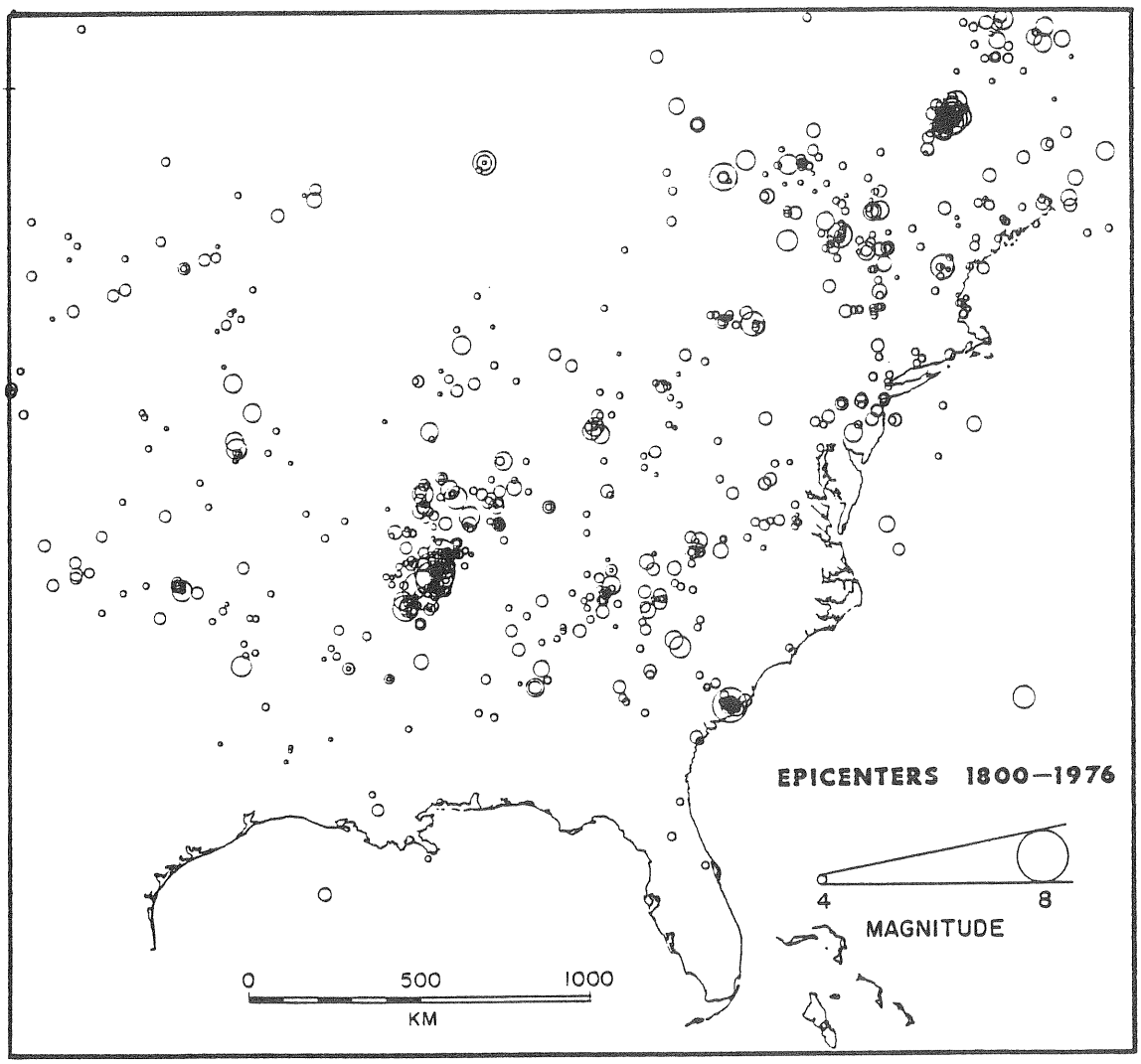

Figure 1A. Seismicity in the eastern U.S. and southeasten Canada (NRC catalog; Barstow et al., 1981). Seismicity is not randomly distributed, but tends to be clustered leaving broad regions with low seismicity. Do structural features control the pattern of seismicity?What elements in this pattern are stationary and what elements are time dependent?

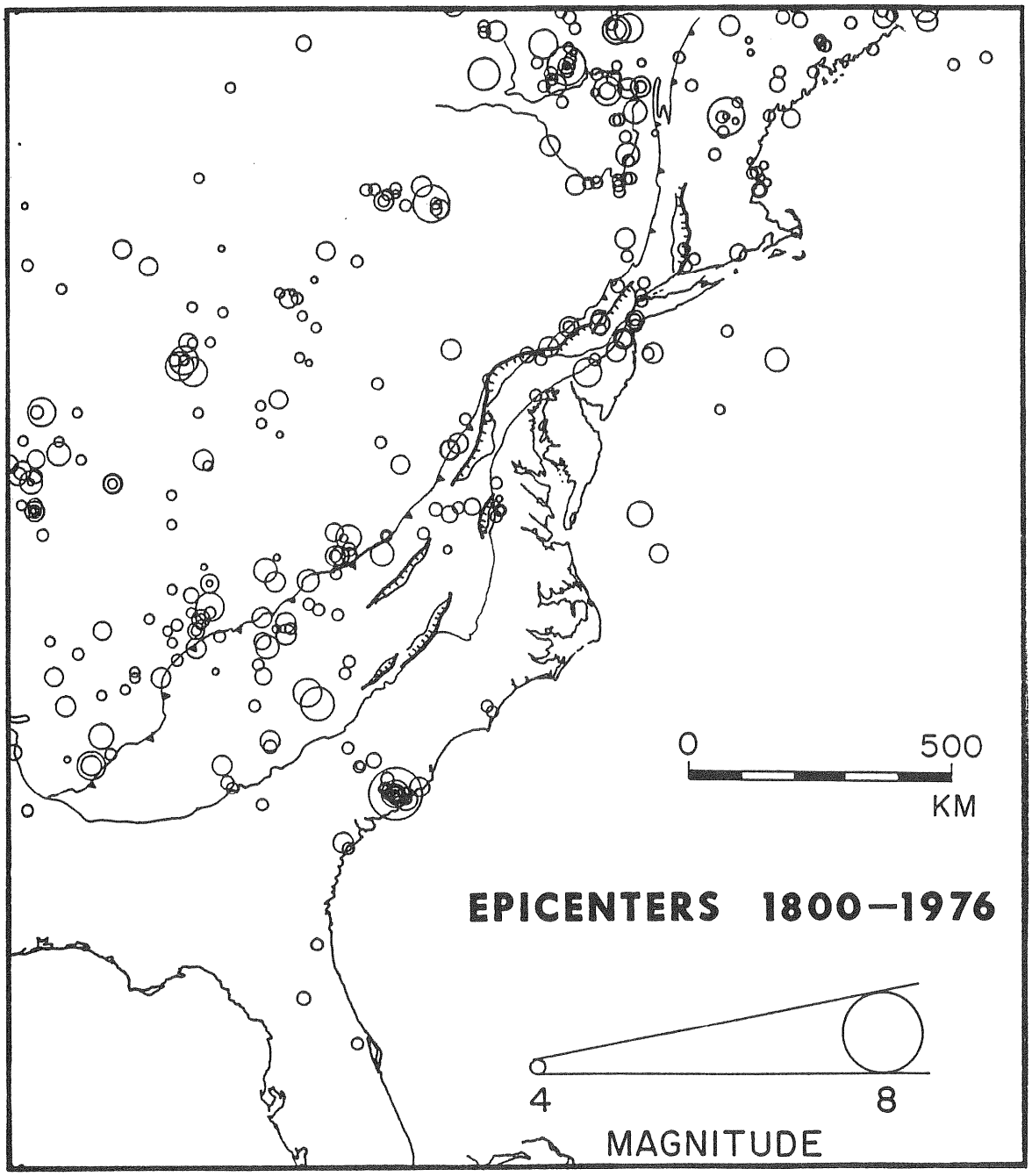

Figure 1B. Seismicity along the Appalachians and the Atlantic seaboard of the U.S. (same data as Figure 1A) and some of the main geologic features (from southeast to northwest: Fall Line, Mesozoic rift basins, western limit of the crystalline sheet in Paleozoic thrusts, Precambrian shield in the Adirondacks). Seismicity is spatially related to structural features in some areas, but it is not associated with similar features in other areas.

Macroseismic data provide earthquake information for the length of the historic period, 200-300 years, whereas instrumental data that could yield more reliable source parameters for small felt events are only available during the last 20-50 years. Most of the known large earthquakes in the eastern U.S., which are significant from the engineering point of view, are characterized either exclusively or primarily from intensity data.

The current earthquake catalog (e.g., Barstow et al, 1981; Coppersmith et al., 1986) is essentially a patchwork of various compilations that vary substantially in reliability and completeness, particularly for the period preceding the systematic collection of intensity data by the Federal Government starting in 1928 (U. S. Earthquakes; NOAA Earthquake effect File, Coffman and Angel, 1983). In contrast, a systematic search of archival material, such as newspapers, can produce a relatively continuous and uniform coverage of the seismicity. From such a compilation it is then possible to evaluate the temporal and spatial distribution of seismicity. A systematic search consists of a continuous scan that uncovers the events and a specific search that optimizes the coverage for each of these events. Recent archival searches have generally produced valuable new data (e.g., Weston Obs. for New England; Nuttli for central U.S.; Seeber and Armbruster, 1987 for southeastern U.S.).

A reliable and systematic procedure that extracts earthquake parameters and other information from macroseismic data is probably as important as the data themselves (see below). This paper discusses results from a study of seismicity along the Appalachians and the Atlantic Seaboard based on a reexamination of intensity data involving both new data and a new analytical procedure. The results are pertinent to several aspects of the problem of estimating earthquake hazard. The main concerns here will be: 1. The spatial distribution of seismicity and its relation to preexisting structural features; 2. The temporal distribution of seismicity and the issue of stationary versus changing patterns of seismicity; 3. Attenuation of seismic waves and its dependence on azimuth and hypocentral depth; 4. The pattern of intensity residuals and seismic zonation.

MACRO: a Model for Intensity Patterns

Many procedures have been adopted to derive earthquake parameters from intensity data. They generally involve subjective judgement and are non-systematic, contributing to bias in the catalog. There is an obvious need for a systematic procedure for parameterizing intensity data. MACRO is an attempt in that direction. It is an algorithm that models the intensity field by solving for epicenter coordinates, magnitude and other parameters relative to the shape of this field (Armbruster and Seeber, 1987). In its simpler form, MACRO assumes a circular pattern of intensity falling off linearly from the epicenter. Elliptical intensity patterns with non-linear fall-off are now being considered for events where the data are sufficient to constrain more complicated models. Station corrections based on population density are also being considered in the new version of MACRO.

Spatial Distribution of Seismicity

Epicentral maps derived from reexamined intensity data tend to show less scatter and better defined seismic zones than previous maps of historic seismicity, for a variety of reasons. Epicenters and magnitudes of historical earthquakes have often been assigned on the basis of location(s) and level of the maximum intensity. In contrast, magnitude is determined by MACRO on the basis of felt area (felt-area magnitude, Mfa). Mfa reflects the moment more directly than maximum intensity which is a function of

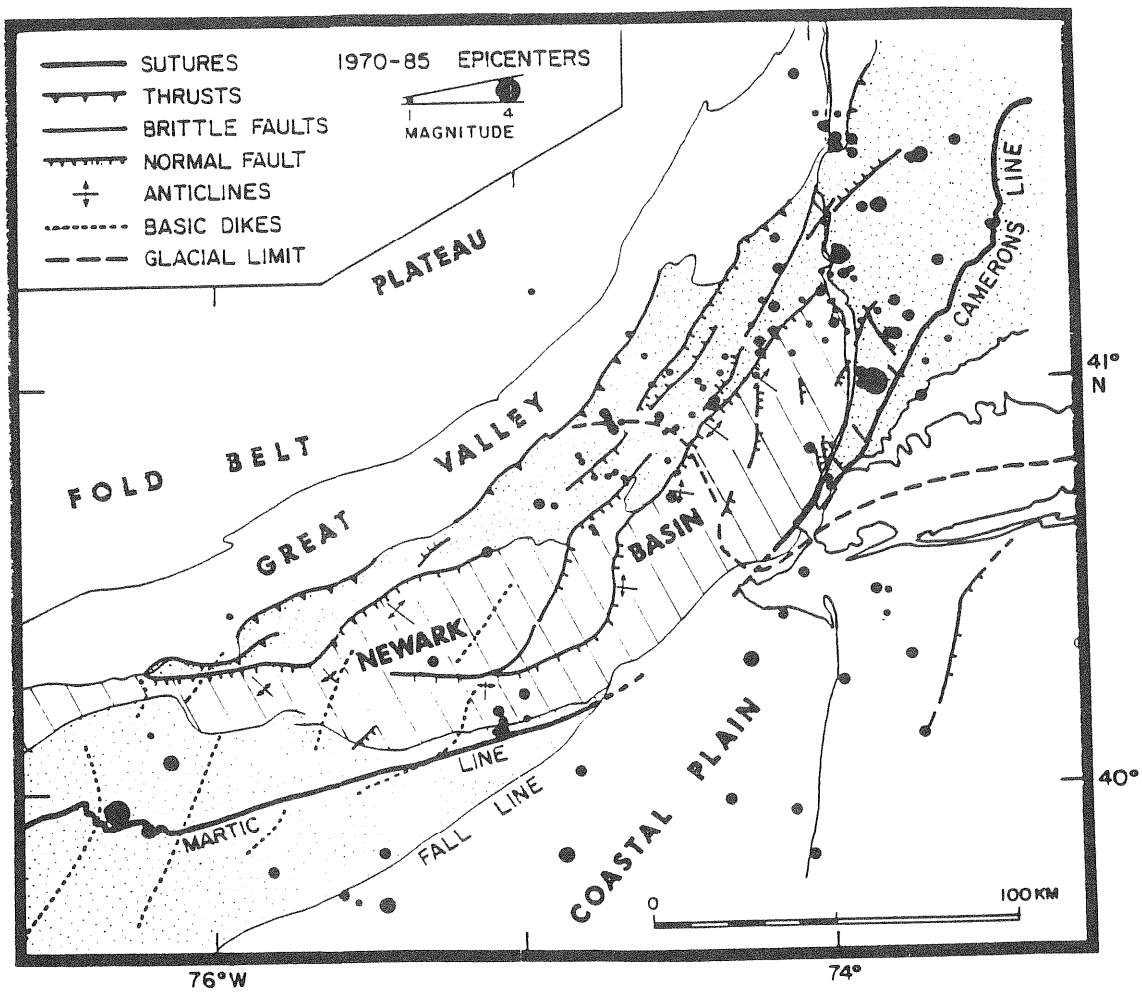

Figure 2A. The Newark Basin seismic zone viewed in 15 years of data accumulated by the Northeast Seismic Network. This map is dominated by small events because of the high sensitivity of the network and the short sample. Most of these events appear to be concentrated in the Hudson Highlands and along the trace of the Ramapo fault, the southeast-dipping border fault of the basin. Very few events, however, occur below the basin, along the subsurface extension of this fault.

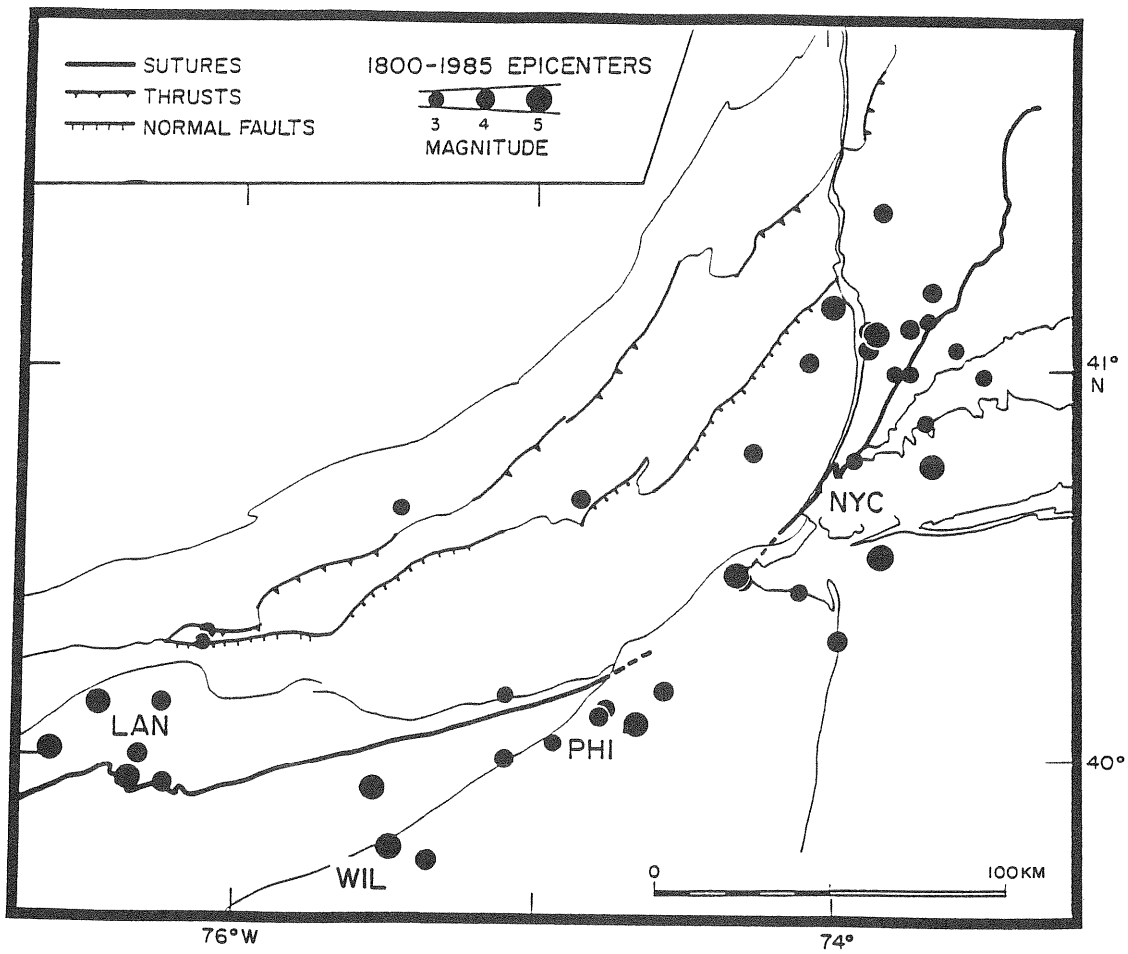

Figure 2B. The Newark Basin seismic zone viewed in a compilation of reexamined historic data analyzed by MACRO. Only events with magnitudes Mfa ≥ 3 are shown. Most of the larger earthquakes are concentrated along a broad belt that follows the Martic/Cameron's Line, an early Paleozoic suture along the southeastern side of the basin. This belt is centered on major metropolitan areas. The difference between the short and low-magnitude sample in figure 2A and the long sample with larger magnitudes in this figure may stem from differences in the distribution of magnitudes and/or from temporal changes in the spatial distribution and emphasizes the importance of long data samples.

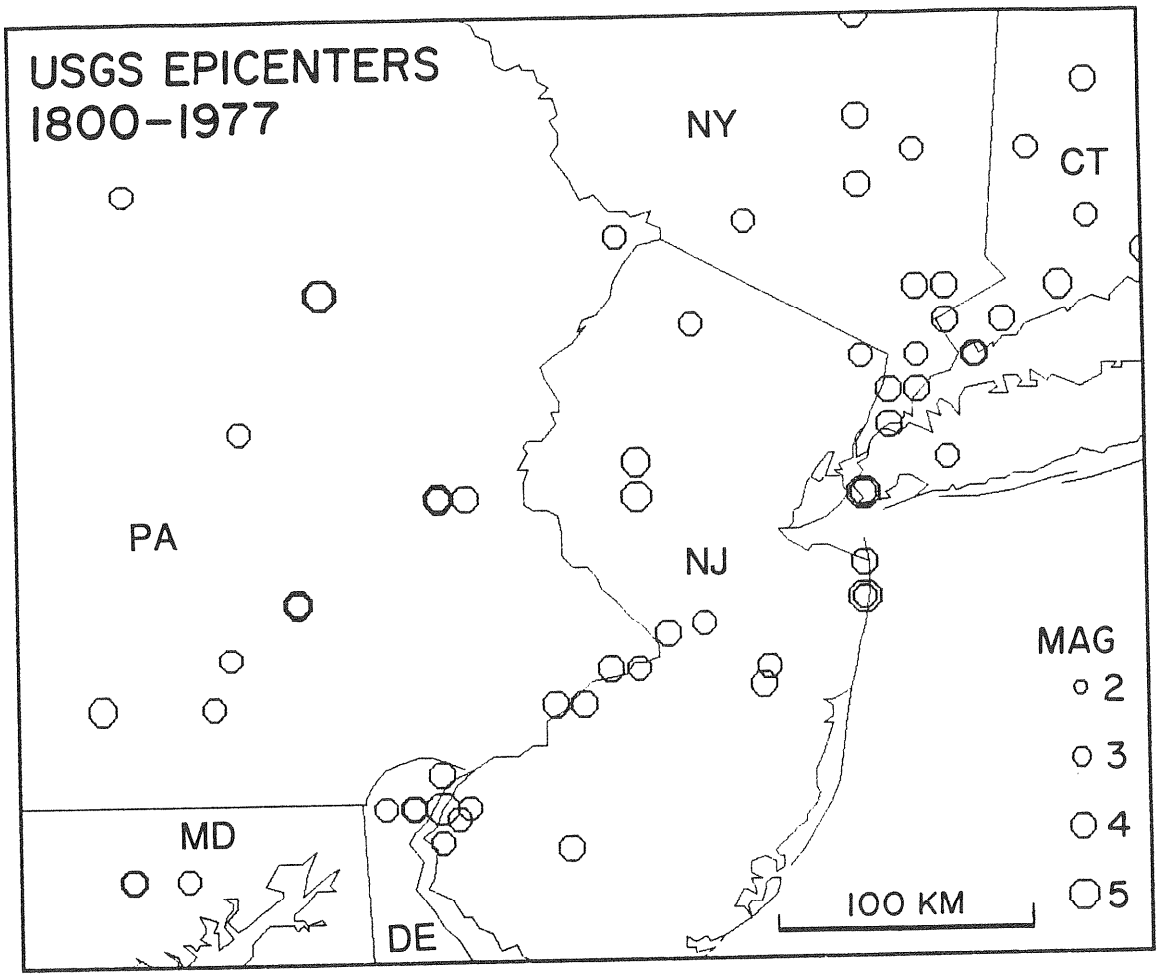

Figure 3. The Newark Basin seismic zone from the USGS catalog. Earthquake size is determined from maximum intensity. Many of the epicenters on the northwest side of the map are not earthquakes, but are mine collapses or artificial explosions.

moment, but also of other independent factors, such as hypocentral depth and data-coverage of the mezoseismal area. Both the level and spatial distribution of intensity are being considered in a more refined magnitude-determination algorithm. Thus, the application of MACRO tends to scale the earthquakes according to their tectonic significance and properly deemphasizes small shallow events with high maximum intensities and small felt areas. Moreover, a substantial portion of events listed as earthquakes are found to be quarry blasts, mine collapses and other non earthquakes, or induced earthquakes, and can be eliminated from a listing that wishes to emphasize tectonic events. Finally, the accuracy of locations are often substantially improved by more complete data and by a method that considers all these data in epicenter determinations.

The improved coverage of historical seismicity in the eastern U.S. shows many well defined seismic zones separated by areas where seismicity is low or absent. This uneven and complex distribution of seismicity is enhanced by displaying only the larger events, for example the ones with Mfa≥3 (Figure 1). Along the Appalachians and Atlantic seaboard of the U.S., epicenters are concentrated in northeastern and in southern New England including the offshore areas, in the Adirondacks, around the Newark Basin, in central Virginia, in western Virginia (Giles Co.), in eastern Tennessee, and in southwestern South Carolina and northern Georgia. Several of these seismic zones are found to correlate spatially with geologic provinces and prominent structural features. This correlation, however, is not systematic because only part of these geologic features are correlated with seismicity. The Newark Basin, for example, is associated with a prominent zone of seismicity, but the Gettysburg Basin and other Mesozoic basins are not. The Piedmont is active in South Carolina and Virginia, but is not active in North Carolina. The feather edge of the crystalline overthrust sheet is active in the Hudson Highlands and in the southern Blue Ridge, but not elsewhere along the Appalachians. Similarly, the authochthonous basement is active in the Adirondacks and in eastern Tennessee , but it is not active along the central Appalachians.

The revised earthquake data show that preexisting structural features often control the spatial distribution of seismicity. Detailed correlation with small-scale features is deciphered from recent instrumental data, whereas seismic zones defined by historical epicenters are spatially correlated with large-scale features. Recent results suggest that the mechanical basis for this correlation may be more subtle than simple reactivation of preexisting faults that persist as zones of weakness in the crust. The prominent zone of seismicity on the southeastern side of the Newark Basin, for example, is broadly correlated with Cameron's Line and the Martic Line which are interpreted as an early Paleozoic suture between proto North America and exotic terranes (Figures 2A, 2B and 3). While these major features strike northeast, recent aftershock sequences show that seismogenic faults along this zone tend to strike northwest, antithetic to Appalachian trends (e.g., The Ardsley, 1985 earthquake; Seeber, this volume). The spatial correlation between seismicity and the suture does not appear to be caused by renewed motion on this suture in the current stress regime, i. e., not by reactivation. In an alternative model, old tectonic boundaries are the locus of high stress, rather than low strength, as a result of lithologic contrast across them. The seismicity resulting from this stress may be on secondary faults, while the major tectonic boundary causing the stress concentration is itself inactive. Thus, preexisting structures may play a role in intraplate neotectonics both as zones of weakness and as stress concentrators.

Temporal Distribution of Seismicity

Generally, the pattern of seismicity derived from recent short-term instrumental data resembles the pattern of seismicity derived from long-term samples of historic data.

This similarity has been considered evidence that seismicity is time-stationary so that the future distribution of seismicity can be inferred directly from the historic distribution. Some changes in the pattern of seismicity, however, have been detected. The most prominent is the change associated with the 1886 Charleston, S.C. earthquake. The reexamination of intensity data from the southeastern U.S. has demonstrated that the burst of aftershocks that followed immediately the 1886 main shock established a pattern of seismicity that has subsided in level, but has persisted in shape to the present, and is known as the South Carolina-Georgia seismic zone. But, the distribution of seismicity in the same area is markedly different for at least 80 years before 1886, with a pronounced lack of seismicity in most of the area forthcoming aftershock zone, including the 1886 epicentral area (Figure 4). Thus, the large earthquake in 1886 coincided with a pronounced and long lasting change in the pattern of seismicity.

The low level of seismicity in the 1886 epicentral area before that event is of particular concern in light of the widely adopted stationary model to infer the spatial distribution of earthquake hazard from historic data. A more complex model is suggested by the spatial pattern of seismicity which is patchy, and yet is locally correlated with structural features of a continental scale. Major earthquakes with repeat times in the thousands of years may set off long lasting "aftershock" sequences. In the historic snap-shot view of seismicity, these sequences may appear as stationary active areas. In a view of the seismicity over a period substantially longer than the repeat times of the large events, seismicity would appear continuous along the structural belts. In such a model , the probability of a large event may be higher in areas of temporarily low seismicity.

Rate of Intensity Fall Off and Hypocentral Depth

Maximum intensity and felt area are only weakly related. For a given maximum intensity, felt area and the rate of intensity fall off (IFR) can vary through a wide range of values (e.g., Figure 5). Although source spectrum and rupture kinematics can affect the IFR, the strongest independent factor is probably hypocentral depth. Preliminary results as well as early work (e.g., Karnik, 1969) suggest that crude hypocentral depth constraints may be obtained from intensity data. Regional variations in IFR (Figure 6) may reflect both changes in the seismogenic depth range and in attenuation. A comparative study of intensity and instrumental data is necessary to scale IFR in terms of hypocentral depth and to separate depth and attenuation effects.

Anisotropic Attenuation Controlled by Structural Trends

If sufficient intensity data are available (at least 20 points), MACRO fits these data with an elliptical cone, in a space where horizontal dimensions are latitude and longitude and the vertical dimension is intensity. In this case, besides epicentral coordinates, felt area, and maximum intensity, the free parameters include azimuth and relative size of axes for the elliptical cone, adding up to a total of six parameters to be determined from the data. In many cases the extra parameters improve the fit considerably because the shape of the intensity distribution is indeed elongated rather than circular.

The shape of the intensity distribution is to some degree affected by the distribution of sampling points. This is obviously the case when the earthquake is centered near a coastline. For some of the early events, sampling points are available exclusively along a communication and population corridor. Even after eliminating the cases where the intensity distribution is obviously biased, however, many of the intensity patterns are still clearly elongated (Figure 6). Moreover, in the Appalachians and Atlantic seaboard the

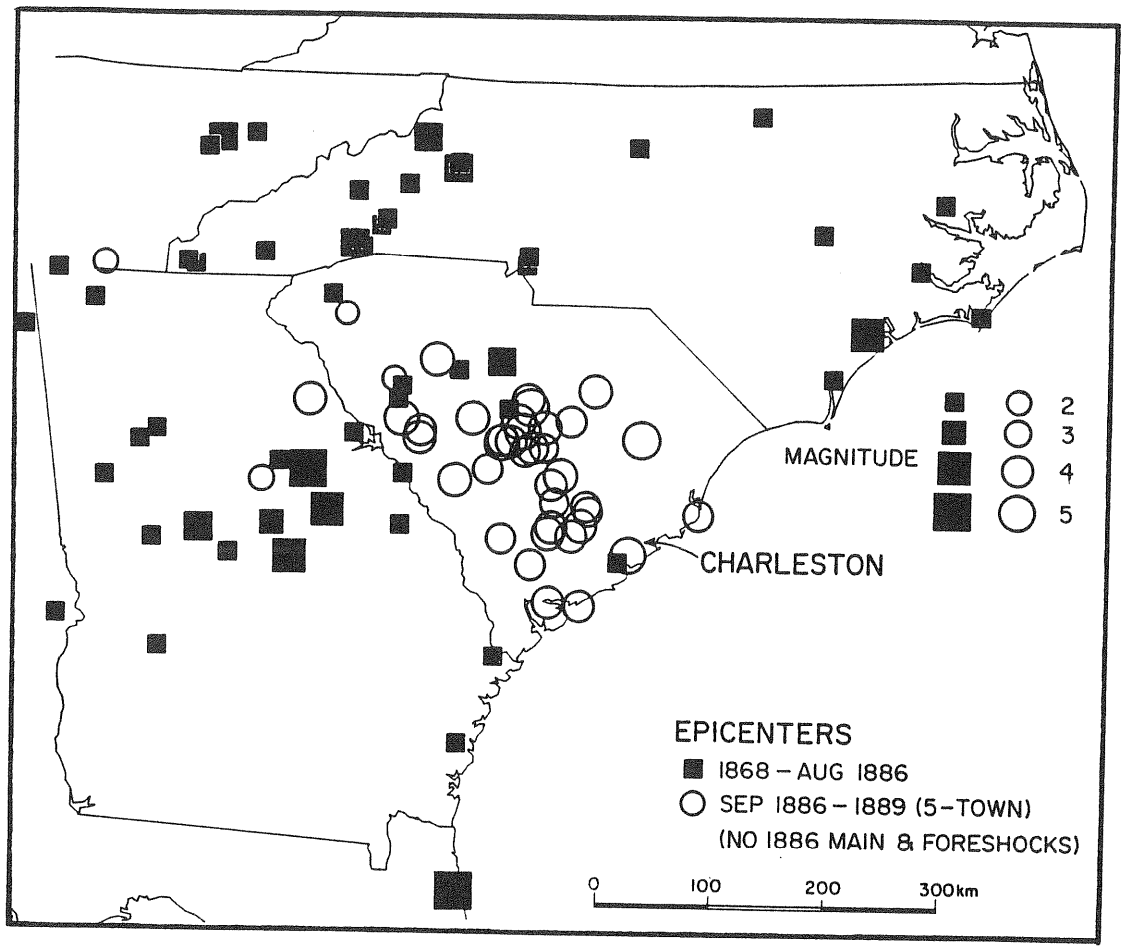

Figure 4. Seismicity before (filled squares) and after (open circles) the August 31, 1886 Charleston, S.C. earthquake. Epicenters and magnitudes of these pre instrumental earthquakes were obtained by an algorithm (MACRO) from felt reports in contemporary newspapers. The seismicity after the main shock is represented by the larger aftershocks (reported by at least 5 towns). They indicate a widespread aftershock zone measured in hundreds of kilometers. Except for immediate foreshocks, the level of seismicity prior to the main shock in the epicentral zone near Charleston was low and similar to other areas of the southeastern Coastal Plain.

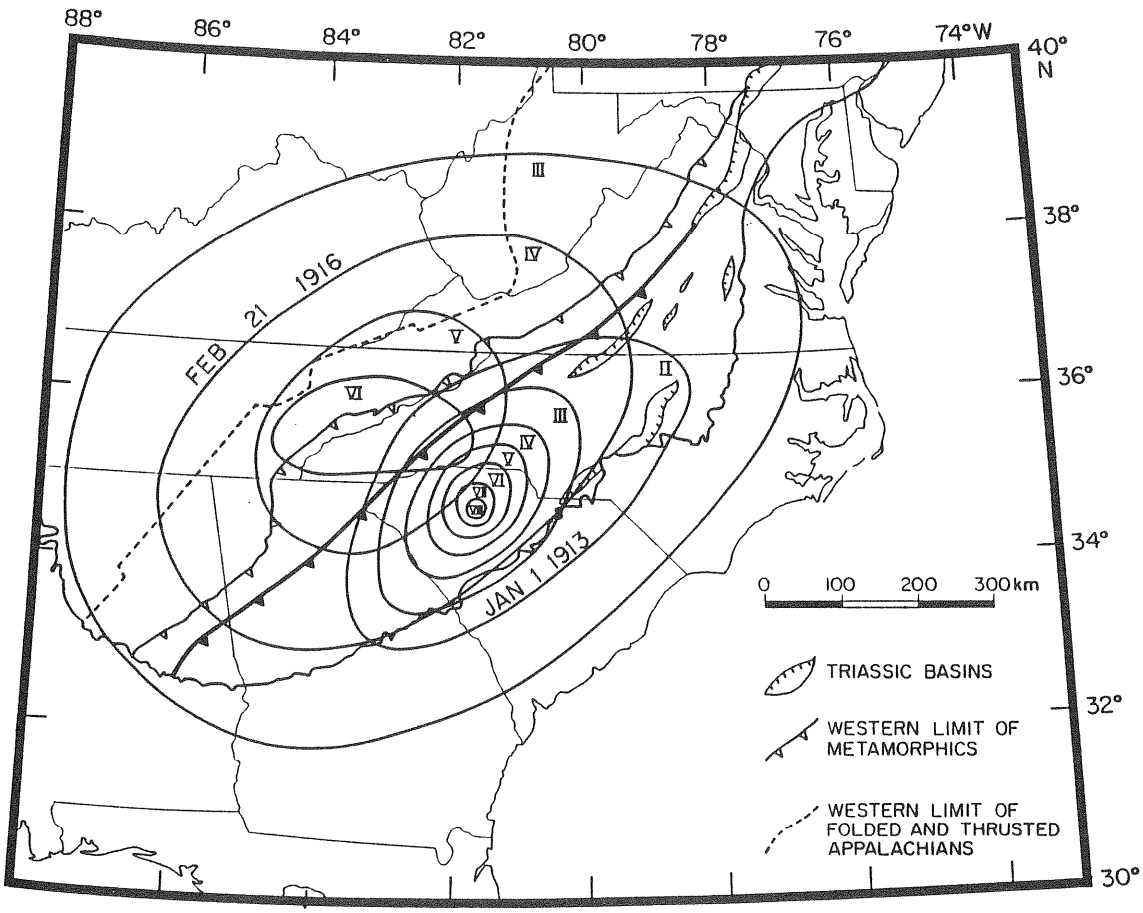

Figure 5. Example of two southern Appalachian earthquakes with drastically different rates of intensity fall-off: The 1913 Union Co. earthquake in the Piedmont of South Carolina has a maximum Rossi-Forel intensity VIII and a felt area of 43,000 sq. mi., while the 1916 earthquake straddling the Blue Ridge between North Carolina and Tennessee has a maximum RF intensity VI and a felt area of 200,000 sq. mi.

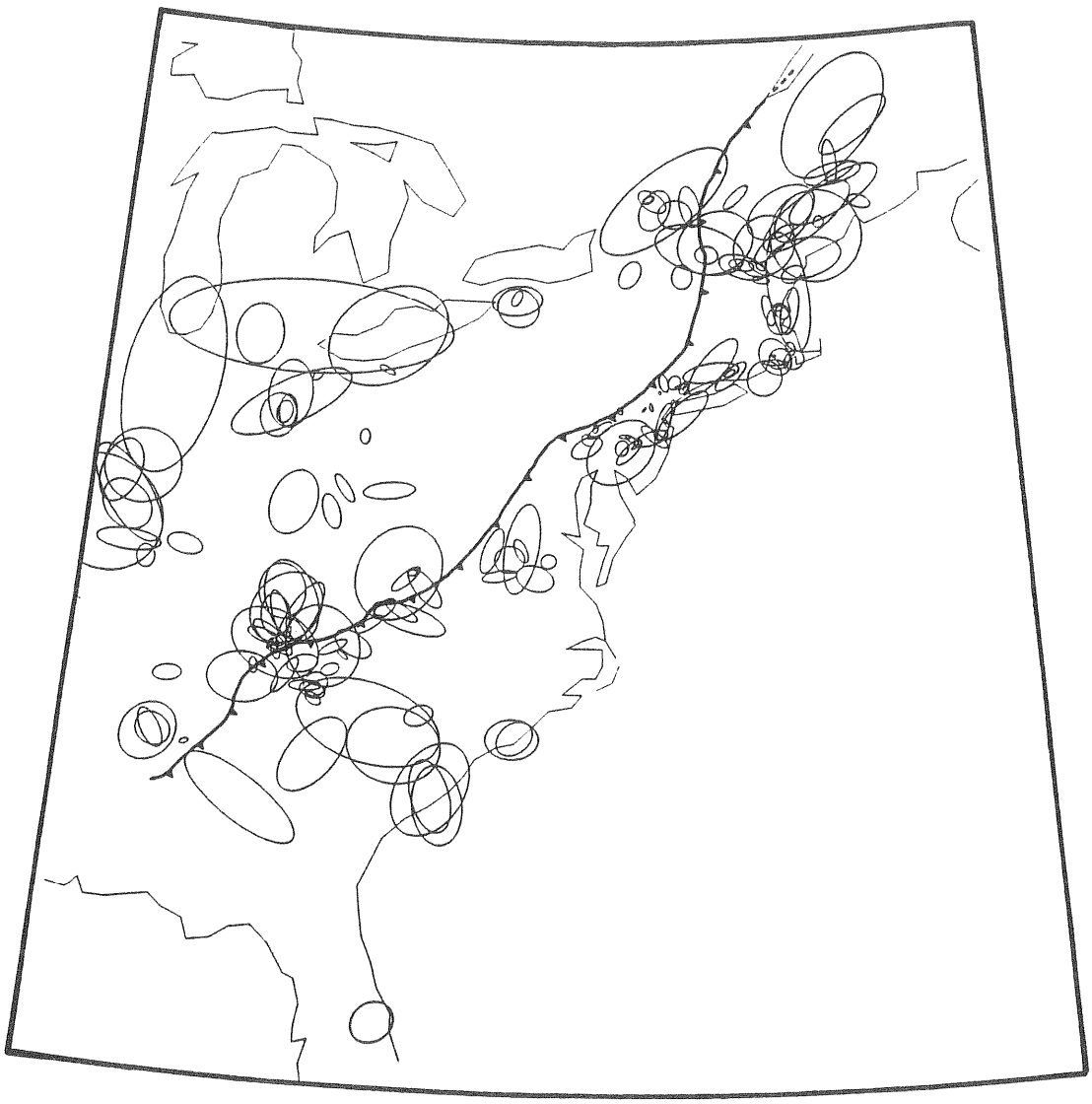

Figure 6. Seismicity (1928-1981) in the eastern U.S. from the NOAA Earthquake Effect File of intensity data (revised by the authors); only events with at least 10 intensity points are shown. The ellipses are isoseismal contours from MACRO solutions of these events where the model is an elliptical conoid (vertical axis = intensity; horizontal axes = space) with a linear slope. Each event is represented by the contour for the intensity level one unit below the conoid maximum intensity. The long axes of the isoseismals tend to be aligned with structural trends along the Appalachians, suggesting a structurally controlled attenuation anisotropy. The size of the ellipses is inversely proportional to the rate of intensity fall-off. This rate tends to scatter; nevertheless, regional patterns are detected.

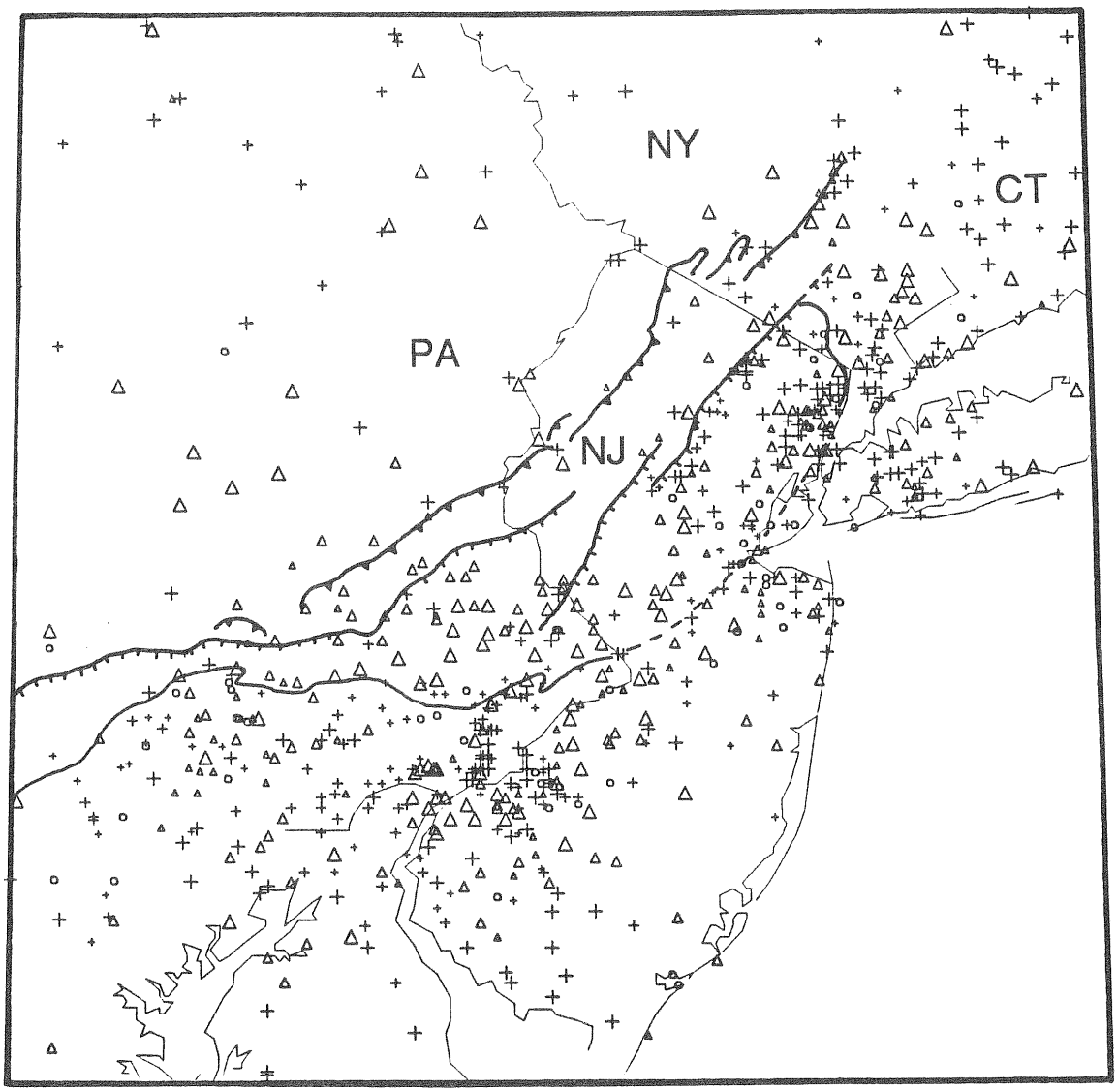

Figure 7. Average intensity residuals for the area surrounding the Newark Basin. Positive (higher then expected intensities) and negative residuals are represented by + and Δ, respectively. A null residual is indicated by a O. Sizes are proportional to the value of the residual. They are obtained by modeling with MACRO intensity data from the NOAA Earthquake Effect File (1928-1981; revised). Only events with at least 20 intensity points are considered. Systematic patterns can be recognized. These patterns can be the result of cultural and/or geologic factors. The "city effect" is the tendency for reported intensities to be higher where population is concentrated. Geologic factors are probably responsible for the tendency for positive residuals along the Ramapo fault, and for negative residuals in the Newark Basin.

elongations tend to be parallel to structural trends. Thus, attenuation of seismic waves is significantly lower along structural trends than across them. This attenuation anisothropy can apparently account for a factor as high as two between maximum and minimum slopes of the intensity fall off. These results concerning intensity fall off rates can be quantitatively interpreted in terms of attenuation after developing scaling relations comparing instrumental and intensity data.

Intensity Residuals and Seismic Zonation

When MACRO fits the data with an intensity distribution model, each data point is associated with a residual. These residuals reflect a high level of scatter in the data, but they may also reflect particularities in the seismic response of the site. Since intensity data is remarkably abundant (more than 20,000 intensity data points have been collected from the eastern U.S. during the last half century), the superposition of all available residuals may average out random noise and extract the component of the residuals that is characteristic of the site. Preliminary results (e.g., Figure 7) show patterns of residuals that can be related to geologic features. They also show patterns that can be associated with the cultural environment. Population centers, for example, tend to be associated with positive residuals (high intensities). The positive relation between population density and intensity level is the result of the tendency to assign to a location the highest intensity reported from there. This undesirable bias is not present in data files where the assigned intensity reflects the mode for a particular location, rather than the maximum at that location. Correction factors are being developed by comparing intensity residuals and population density.

Acknowledgements

We are grateful for helpful reviews by Klaus Jacob and David Simpson. This work was supported by NSF- EAR86-18658 and NCEER-87130

References

Armbruster, J.G., and L. Seeber, Seismicity 1886-89 in the Southeastern United States: The aftershock sequence of the Charleston, S.C. Earthquake, U.S. Nuclear Regulatory Commission, Washington, D.C., NUREG/CR-4851, 153 pp., 1987.

Barstow, N.L., K.G. Brill Jr., O.W. Nuttli, and P.W. Pomeroy, An approach to seismic zonation for siting nuclear electric power generating facilities in the eastern United States, U.S. Nuclear Regulatory Commission, Washington, D.C., 1981.

Boston Edison Company, Historical seismicity of New England, U.S. Nuclear Regulatory Commission, Docket No. 50-471, 641 pp., December 1976.

Coffman, J.L., and C. Angel, Summary of earthquakes intensity file, Key to Geophysical Records Documentation, No. 19, NOAA, Boulder, CO., 1983.

Coppersmith, K.J., A.C. Johnson, and W.J. Arabasz, Assessment of maximum earthquake magnitudes in the eastern United States, (abstract), Earthquake Notes, 57, p. 26, 1986.

Karnik, V.T., Seismicity of the European area, D. Reidel Publishing Co., Dordrecht, Holland, part 1,2, 1969.

Nuttli, O.W., The Mississippi Valley earthquakes of 1811 and 1812: Intensities ground motion and magnitudes, Bull. Seism. Soc. Amer., 63, 227-248, 1973.

Nuttli, O.W., Seismicity of the Central United States, Geol. Soc. Amer. Rev. Engin. Geol., 4, 67-93, 1979.

Seeber, L., and J.G. Armbruster, The 1886-1889 aftershocks of the Charleston, South Carolina, earthquake: A widespread burst of seismicity, Jour. Geophys. Res., 92, 2663-2696, 1987.

THE SEISMICITY OF THE NORTHEASTERN UNITED STATES

by John E. Ebel

Weston Observatory
Boston College Dept. of Geology & Geophysics
381 Concord Rd., Weston, MA 02193

ABSTRACT

The seismicity of the northeastern United States (NEUS) is reviewed. Earthquakes are spread generally, but not uniformly, throughout the region and those areas which were most active historically are experiencing a preponderance of the modern events. The events depths are almost all less than 20 km, and they tend to show E-W to NE-SW P axes and near vertical T axes. Mean return times for larger earthquakes in the region have been estimated from recurrence curves based on the instrumental record, and zones of common seismicity have been delineated.

1. INTRODUCTION

The northeastern United States (NEUS) is one of the most seismically active parts of the eastern U.S., and its seismicity is characterized by persistent small magnitude events as well as by occasional shocks of a size sufficient to cause damage to structures. As in the rest of the region east of the Rockies, earthquakes in the NEUS are felt over a very wide area compared with those in the western U.S. [Street and Turcotte, 1977], meaning that earthquakes of even moderate magnitude can have widespread consequences throughout the region. The largest event known to have been centered in the NEUS, the Cape Ann, Massachusetts earthquake of 1755, caused damage in Massachusetts, New Hampshire and Maine and was felt noticeably 450 km down the coast in Washington, D.C. Earthquakes exceeding or approaching a size capable of producing damage have occurred near the major metropolitan areas of New York, Philadelphia, Boston and Hartford, and many other cities within this densely populated region have experienced earthquake ground shaking of an alarming character. In addition to the threat from the seismicity from within the NEUS itself, areas of high seismic activity from nearby Canada in Ontario, Quebec, New Brunswick and Nova Scotia also pose a seismic hazard to the NEUS.

A several-hundred-year long record of earthquake activity in the region is known from written reports of felt earthquakes and from instrumental monitoring. Historical records yield accounts of earthquakes dating to the early 1600's and even earlier. Several investigators have compiled and edited listings of these historical earthquakes, most recently Chiburis [1981] and Nottis [1983]. By 1935 a sufficient number of seismic instruments had become operating in the region that the Northeastern Seismological Asociation (NESA) was formed to report instrumental readings of earthquakes. Widespread seismic monitoring with a relatively

dense network of stations in the region became a reality in the early and middle 1970's and continues to the present time. Since 1975 epicenters of all earthquakes in the NEUS and in nearby Canada have been reported by the Northeastern United States Seismic Network (NEUSSN) Bulletin, published quarterly by Weston Observatory of Boston College.

2. SPATIAL DISTRIBUTION OF THE EARTHQUAKE ACTIVITY

2.1 Epicentral Locations

As is evidenced on Figure 1, earthquake epicenters are widespread throughout the NEUS, although the distribution is far from uniform. The coastal areas as well as central Maine, central New Hampshire and northern New York have the large majority of the earthquakes, along with several areas in eastern Canada. By contrast, northern Maine, southcentral New York and

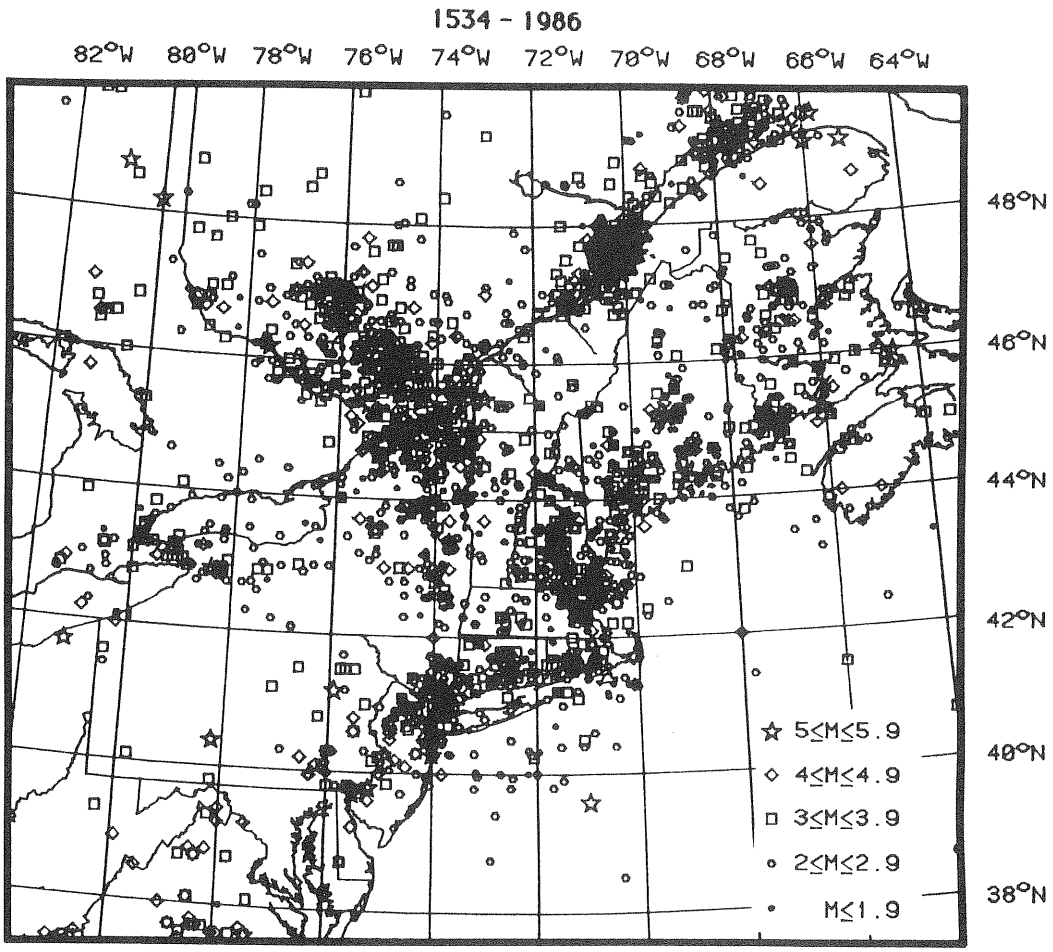

Figure 1. Map of all known earthquake activity for the NEUS and adjacent Canada, 1534-1986. Maxiumum epicentral intensities for historic events have been converted to magnitudes for plotting purposes.

western Pennsylvania are the most quiet areas seismically. The epicenters do not follow the major Paleozoic faults of the region, nor are they only confined to particular geologic structures or terranes. However, there are some structures which are associated with locally higher numbers of earthquakes: the Adirondack Mountains uplift of northern New York [Seeber et al., 1984], the region surrounding the Newark Basin in northern New Jersey [Kafka et al., 1985], and the subsiding Passamaquoddy Bay in eastern Maine [Anderson et al., 1984; Reilinger et al., 1986]. Even where detailed studies of individual earthquake sequences have been made, the relationship between the present earthquake activity and known geologic structures has usually proved elusive [Ebel and Kafka, 1987].

Modern monitoring of the small earthquakes in the region demonstrates that the areas that have been active in the historic past are generally the same areas which are active today (Figure 2). One major exception to this generalization is the Cape Ann

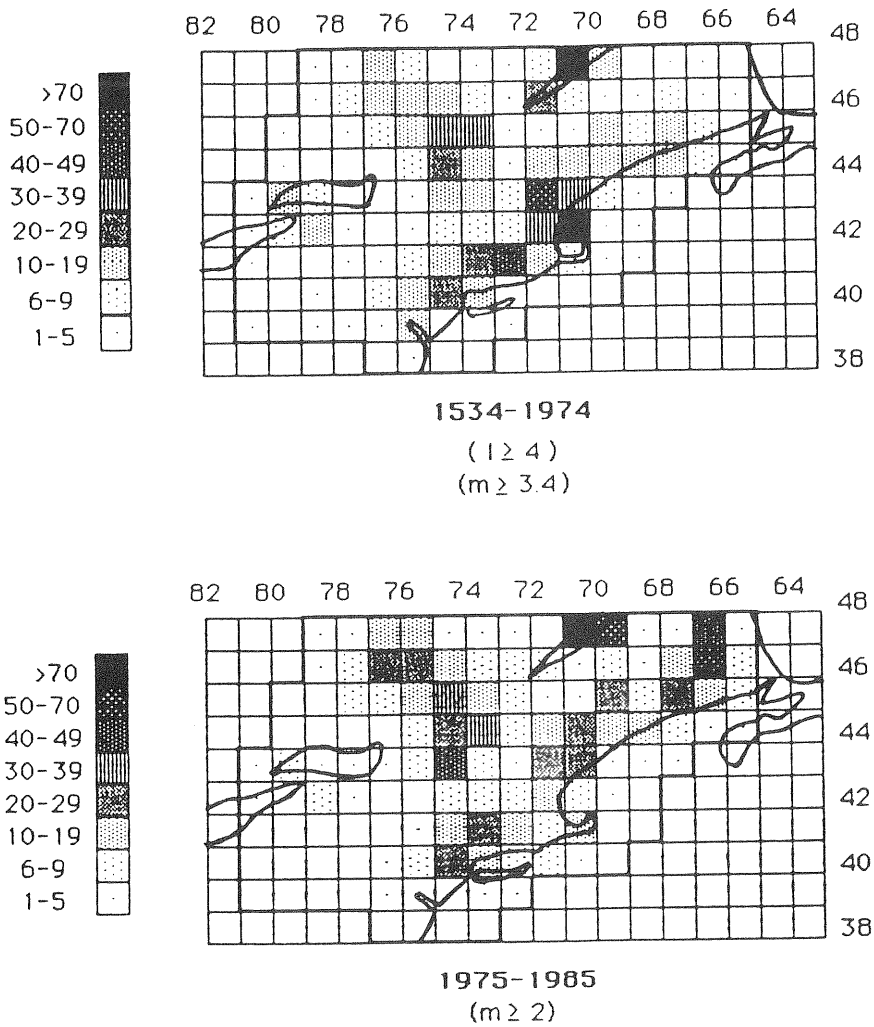

Figure 2. Number of earthquakes per 10,000 km^2 in each 1° X 1° cell for (a) the historical catalog and (b) the modern catalog (since 1975).

area of eastern Massachusetts which has been relatively quiet during the period of modern instrumentation as compared with its very active character during historic time, especially in the 1700's. Central New Brunswick is an exception in the opposite sense. It has been quite active since a magnitude 5.7 earthquake in 1982 whereas it shows little activity in historic time, although this observation may be biased due to the sparse population of that region which was available to report and record small, locally felt events. All of the moderate and large earthquakes known to have occurred in the NEUS have been centered in one or another of the more active parts of the region although not all active localities have been the sites of larger earthquakes. However, there is no evidence to argue that these sites cannot have moderate or large earthquakes at some point in the future.

There is no good method at present for determining what the largest possible earthquake in the region could be [Ebel and Kafka, 1987]. The Cape Ann earthquake of 1755 (m_b estimated to be about 6.0 [Street and Lacroix, 1979]) sets a minimum upper limit. Earthquakes in the Charlevoix - La Malbaie area of Quebec have reached at least $m_b = 6.6$ [Ebel et al., 1986], and the Charleston, South Carolina earthquake of 1886 was thought to be $m_b = 6.9$ [Nuttli et al., 1979]. At present, neither seismological nor geological arguments preclude the possibility that a Charlevoix-La Malbaie-sized or even a Charleston-sized earthquake can take place in the NEUS.

2.2 Earthquake Depths

Because the station spacing of the NEUSSN network averages about 60 km, the depths of most earthquakes in the region are not well resolved. For events with good constraint on all hypocentral parameters, depths are found to range from the surface to about 20 km, with the median depth being about 11 km (Figure 3). It is likely that this is an accurate representation of earthquake depths in the region since earthquakes with depths greater than 20 km are easier to resolve than shallower earthquakes, given the regional station spacing. Ebel et al. [1986] found the strongest earthquakes of this century from northeastern North America had hypocenters between 6 and 10 km deep, the same depth range where much of the smaller earthquake activity originates.

2.3 Regional Stress Field

The instrumental earthquake record contains a number of events for which focal mechanisms have been determined, although the average station spacing coupled with the small sizes of most recorded events makes focal mechanism determinations impossible in most cases. Ambiguities in some station polarities (for older events), in crustal models and in event depths also adversely affect the reliability of many focal mechanism solutions. Earthquakes with many first motion observations usually contain large numbers of readings from head wave first arrivals. Since head waves tend to have lower amplitudes and attenuate faster with

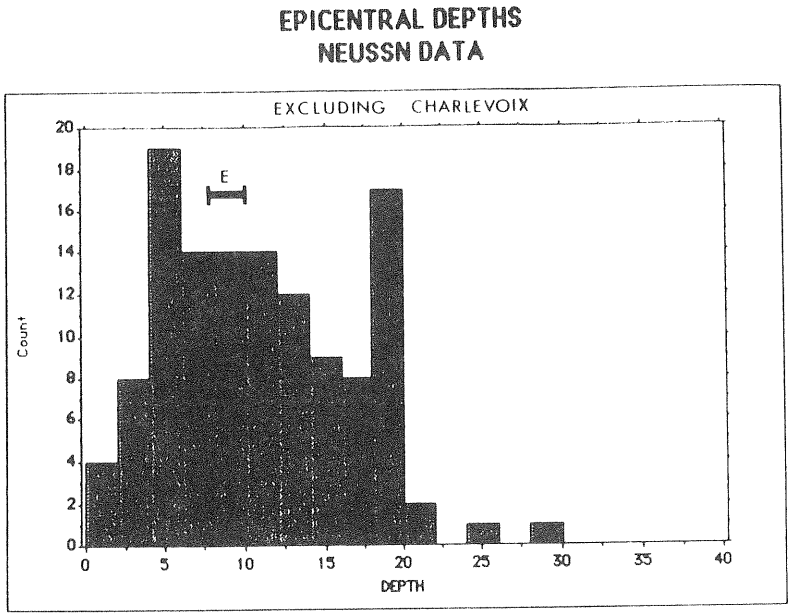

Figure 3. Histogram of depths of earthquakes in the NEUS and adjacent Canada since 1975. Bar labelled E indicates the range of depths for large events in northeastern North America, from Ebel et al. [1986].

distance than direct waves, they often suffer from signal-to-noise ratio problems when first motion directions are read. This leads to cases where even relatively good focal mechanism solutions have a number of inconsistent first motion readings.

A summary of the horizontal component of P axes from unblished focal mechanisms of 80 events is illustrated in Figure 4 [Ebel and Kafka, 1987]. There are a number of cases where the same earthquake was published in two or more papers with radically different focal mechanism solutions (most often with regard to the azimuth of the P axis). On Figure 4 all such determinations are shown. The average P axis for this data set has an azimuth of 87°±36° and a plunge of 3°±22°, while the average T axis is essentially vertical with a plunge of 88°±34°. These results are broadly consistent with the stress directions expected from modern plate tectonic forces [Richardson et al., 1979; Yang and Aggarwal, 1981].

Relatively little is known about earthquake stress drops in the NEUS. Using data from larger, instrumentally recorded events from northeastern North America, Ebel et al, [1986] and Somerville et al. [1987] have argued that there is a wide range in stress drops, ranging from 2 MPa to 50 MPa. There is no reliable information on the stress drops of earthquakes with magnitudes less than about 4.5.

2.4 Seismic Zones in the NEUS

The non-uniform nature of the spatial pattern of earthquake

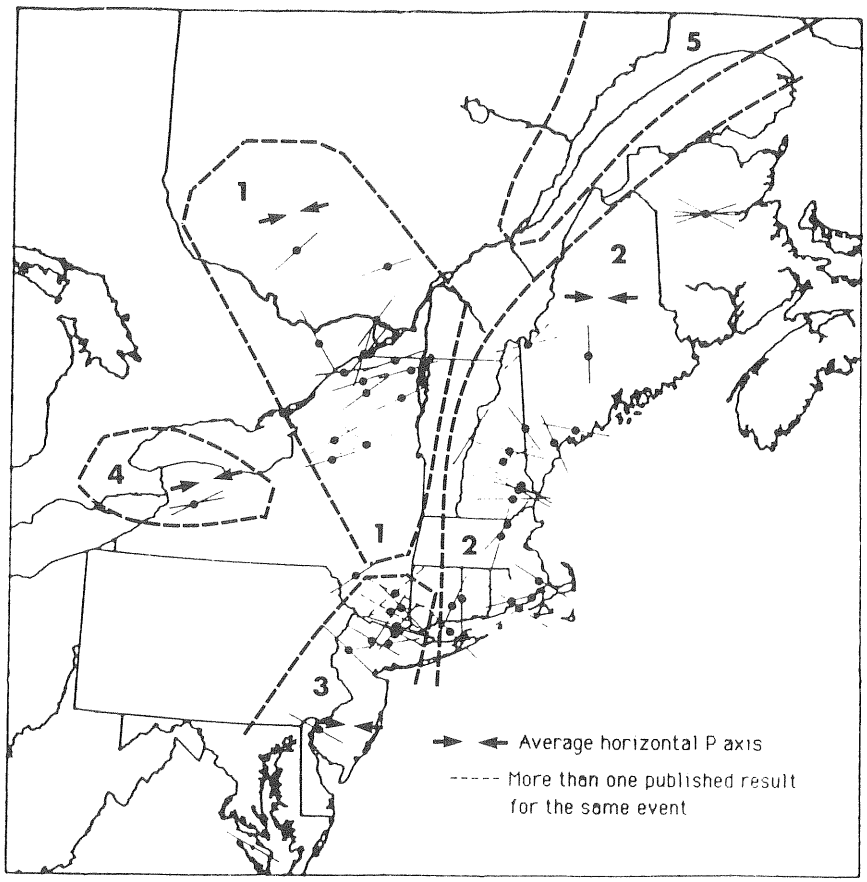

Figure 4. Map showing major seismic zones of the NEUS and adjacent Canada. The zones are: 1. Western Quebec-Adirondacks zone; 2. New England-New Brunswick Appalachian zone; 3. Southern New York-Eastern Pennsylvania-New Jersey zone; 4. Western New York State zone; 5. Charlevoix-Lower St. Lawrence zone. Azimuths of P axes from focal mechanisms in the NEUS and Canada are also shown.

epicenters as well as the variations in focal mechanisms throughout the NEUS suggest that it should be possible to divide the NEUS into seismotectonic zones. Unfortunately, the generally poor correlation of the seismicity with geologic structures makes it quite difficult to use geologic criteria to delineate seismic zones. Following Ebel and Kafka [1987], the criteria used to select seismic zones in this study are, in order of importance: The rate of seismicity in both the instrumental and the historic catalogues; the occurrence of moderate and/or large ($m_b \geq 5$) earthquakes; and distinctive geological or geophysical characteristics. With these criteria five broad seismic zones have been identified (Figure 4): a Western Quebec-Adirondack zone, two coastal-Appalachian zones, a western New York State zone and a Charlevoix-Lower St. Lawrence zone. The average P azimuths in these first four zones are 69°±32°, 94°±43°, 97°±32°, and 68°±8°, respectively. No average P axis was computed for the fifth zone.

Similar zones were chosen by Yang and Aggarwal [1981].

Within each of these broad zones there are areas or pockets of locally enhanced seismicity, and these areas have been further delineated in Figure 5. Many but not all of these areas have had one or more moderate or large earthquakes centered within them. Also indicated in Figure 5 are several areas with recent seismic activity which inferred to be possible active areas not recognized in the historic record. The correlation of moderate or large events with localities with a long record of seismic activity may

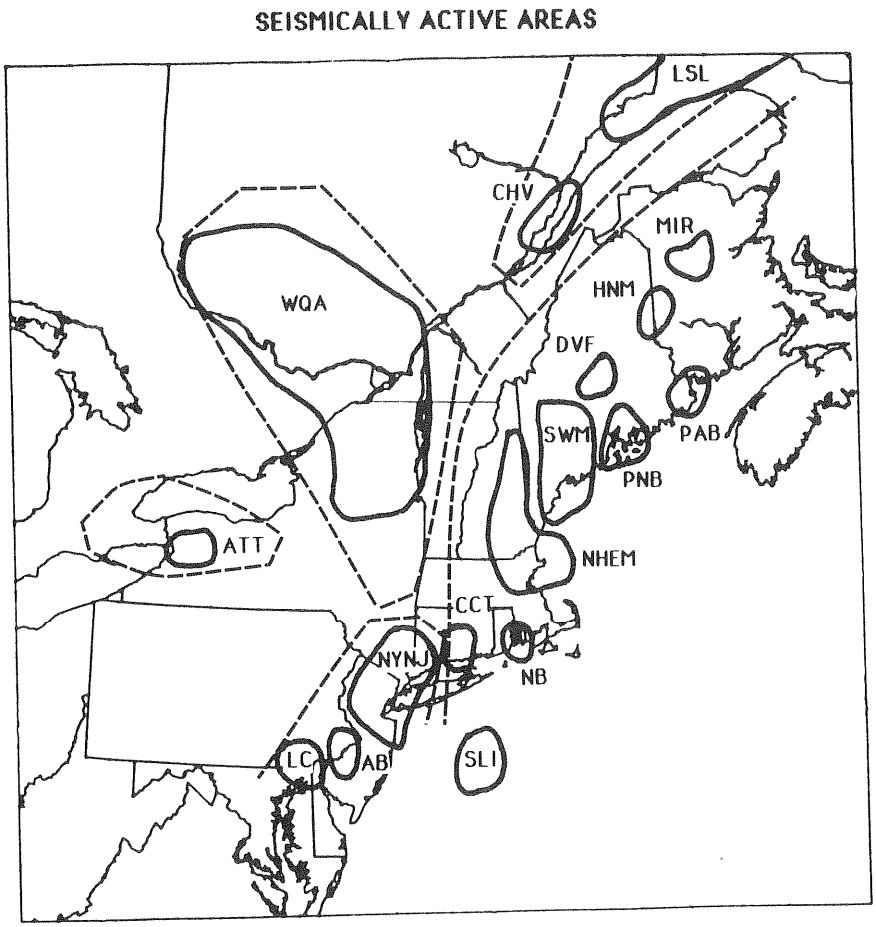

Figure 5. Map of areas of locally higher seismic activity in the NEUS. The dashed lines show the major seismic zones of Figure 4. Area initials are: LSL - northern St. Lawrence; CHV - Charlevoix; WQA - Ontario-Quebec-Adirondacks; ATT - Attica; MIR - Miramichi; HNM - Houlton; DVF - Dover-Foxcroft; PAB - Passamaquoddy Bay; PNB - Penobscot Bay; SWM - southwestern Maine; NHEM - New Hampshire-eastern Massachusetts; NB - Narragansett Bay; CCT - Central Connecticut; SLI - south of Long Island; NYNJ - northern New Jersey-southern New York; AB - Abington; LC - Lancaster County. The Canadian active areas follow Basham et al. [1985].

be an indication that these are the areas with a higher probability of having a large event in the future. However, there is no good reason to rule out the possibility that large earthquakes can occur outside these areas or even outside the four major zones themselves. Zonations based primarily upon the seismic record are inherently quite sensitive to the stability, or lack thereof, of the spatial pattern of earthquake occurrences with time.

3. TEMPORAL ASPECTS OF THE EARTHQUAKE ACTIVITY

3.1 Recurrence curves and Earthquake Return Times

The instrumental earthquake record provides a good, complete data base for the calculation of recurrence curves for the NEUS. Recurrence curves based upon NEUSSN data from 1975-1986 and upon all instrumentally recorded activity from 1938-1986 [Ebel and Zakimi, 1987] are listed in Table 1 along with mean return times for larger events calculated from these curves. The linear extrapolation of recurrence curves to large magnitudes and long time frames, as was done to calculate the return times of Table I, yields numbers of questionable accuracy. It assumes that the seismicity rate for the region is stable with time, an assumption which is explored in more detail below. It also assumes the proper shape of the curve continues to be a straight line at large magnitudes. Ebel [1984] and Ebel and Kafka [1987] have noted that there are fewer large shocks in the earthquake record since the early 1700's than expected based upon recurrence curves calculated from the instrumental data. This could be due to variable seismicity rates with time, to missing or misreported events in the catalogue, or to a roll-off of the recurrence curve at large magnitudes. The last possibility could be caused by the existence of a maximum possible earthquake in the region [Berrill and Davis, 1980; Main and Burton, 1984]. Leblanc and Burke [1985] have recently done a careful reevaluation of the seismicity of easternmost Maine around Passamaquoddy Bay and have shown that some events there had larger magnitudes than previously thought. Thus the historic catalogs may not accurately reflect magnitudes of all of the larger events which occurred in historic time.

The time since the last earthquakes of at least m_b of 5, 5.5 and 6.0 in the NEUS proper are 4 years, 43 years and 232 years respectively. If the return times in Table 1 are meaningful, the NEUS could be facing an enhanced chance of a damaging earthquake centered somewhere within the region. On the other hand, the uncertainties in the assumptions which are inherent in the numbers in Table 1 may mean that the times since the last earthquakes of magnitude 5.5 or greater are not unusual and do not portend a damaging earthquake sometime soon within the region. Also, earthquakes of m_b of at least 5.5 and 6.0 have occurred more recently (1982 and 1935, respectively) than those in the NEUS proper. Restricting this analysis to only the NEUS may not represent fairly the present chances of a large earthquake in this area.

3.2 Stability of the Earthquake Process with Time

The mean rate of earthquake occurrence in the NEUS appears to have been approximately stable with time [Chiburis, 1981; Shakal and Toksoz, 1977; Ebel, 1984], although some variations in the rate of occurrence of large events [Shakal and Toksoz, 1977] and of small events [Ebel, 1985] have been noted. The similarity of the a-values (Table I) for 1938-1986 and 1975-1986 supports the argument that the average seismicity rate has been relatively constant throughout the past 50 years. However, it has not been established that this is the correct long-term activity rate for the region. If variations in the seismic activity rate with time do occur, the mean return times in Table I are too large or too small depending upon whether the average long-term rate is more or less respectively than that since 1938. Ebel [1984] has argued that the seismicity in New England has a predominantly random temporal component and that there are only vague hints of spatial migrations of the seismicity with time in the modern instrumental record.

Table I
Northeastern United States
Mean Return Times (Years)

Magnitude					
5.0	5.5	6.0	6.5	7.0	Time Period of Recurrence Curves
14	42	122	356	1,039	1975 - 1986
9	25	64	167	436	1938 - 1986

1938 - 1986 $\log N \text{ (per year)} = 3.49(\pm.06) - .93(\pm.02)M$
1975 - 1986 $\log N \text{ (per year)} = 3.19(\pm.04) - .83(\pm.02)M$

4. SUMMARY AND CONCLUSIONS

A great deal about the seismicity of the NEUS has been learned from the existing earthquake data, particularly that accumulated through modern instrumental monitoring. However, many questions are unanswered and will remain so until more data have been collected. The spatial distribution of epicenters defined in the historic record appears to be confirmed by instrumental monitoring. Almost all of the earthquakes in the region occur in the upper crust, with the deepest being about 20 km. The P axes found from the earthquake data show a rather large scatter but are consistent with plate tectonic forces producing the average stress field. Estimates of activity rates and earthquake return times have been made from recurrence relations calculated from the instrumental record. Major issues which still must be addressed include defining the relationship between the earthquakes and

geologic structures, reducing the uncertainty in estimating the return times of large earthquakes in the region, determining the largest earthquake possible in the region, and finding the sources of stress causing the earthquakes both on a regional and on a local scale.

REFERENCES

Anderson, W.A., J.T. Kelly, W.B. Thompson, H.W. Borns, Jr., D. Sanger, D.C. Smith, D.A. Tyler, R.S. Anderson, A.E. Bridges, K.J. Crossen, J.W. Ladd, B.G. Anderson, and F.T. Lee, Crustal warping in coastal Maine, Geology, 12, 677-680, 1984.

Basham, P.W., D.H. Weichert, F.M. Anglin, and M.J. Berry, New Probabilistic strong seismic ground motion maps of Canada, Bull. Seism. Soc. Am., 75, 563-596, 1985.

Berrill, J.B., and R.O. Davis, Maximum entropy and the magnitude distribution, Bull. Seism. Soc. Am., 70, 1823-1831, 1980.

Chiburis, E.F., Seismicity, recurrence rates and regionalization of the northeastern United States and adjacent southeastern Canada, Prepared for the U.S. Nuclear Regulatory Commission, NUREG/CR-2309, 1981.

Ebel, J.E., Statistical aspects of New England seismicity from 1975 to 1983 and implications for past and future earthquakes, Bull. Seism. Soc. Am., 74, 1311-1330, 1984.

Ebel, J.E., A study of seismicity and tectonics in New England, U.S. Nuclear Regulatory Commission Final Report, NUREG/CR-4354, 1985.

Ebel, J.E., and A.L. Kafka, Earthquake Activity in the northeastern United States, Submitted to Decade of North American Geology, GSMV-1, Neotectonics of North America, 1987.

Ebel, J.E., P.G. Somerville, and J.D. McIver, A study of the source parameters of some large earthquakes of northeastern North America, J. Geophys. Res., 91, 8231-8247, 1986.

Ebel, J.E. and Z. Zakimi, Northeastern earthquake magnitudes from 1938 to 1975, Final Report on U.S.G.S. Contract No. 14-08-22049, 1987.

Kafka, A.L., E.A. Schlesinger-Miller, and N.L. Barstow, Earthquake activity in the greater New York City area: magnitudes, seismicity, and geologic structures, Bull. Seism. Soc. Am., 75, 1285-1300, 1985.

Leblanc, G., and K.B.S. Burke, Re-evaluation of the 1817, 1885, 1869 and 1904 Maine-New Brunswick area earthquakes, Earthquake Notes, 56, 107-124, 1985.

Main, I.G., and P.W. Burton, Information theory and the earthquake frequency-magnitude distribution, Bull. Seism. Soc. Am., 74, 1409-1426, 1984.

Nottis, G.N., ed., Epicenters of northeastern United States and southeastern Canada, onshore and offshore; time period 1534-1980, New York State Geological Survey, New York State Museum, Map and Chart Series Number 38, 1983.

Nuttli, O.W., G.A. Bollinger, and D.W. Griffiths, On the relation between modified Mercalli intensity and body-wave magnitude, Bull. Seism. Soc. Am., 69, 893-909, 1979.

Reilinger, R., S. Larsen, and P. Krumhansl, Reanalysis of contemporary crustal downwarping of coastal Maine, Earthquake Notes, 57, 113, 1986.

Richardson, R.M., S.C. Solomon, and N.H. Sleep, Tectonic stress in the plates, Rev. Geophys. & Space Phys., 17, 981-1019, 1979.

Seeber, L.E., E. Cranswick, J. Armbruster, and N. Barstow, The Oct., 1983 Goodnow aftershock sequence, regional seismicity and structural features in the Adirondacks, EOS, Trans. Am. Geophys. U., 65, 240, 1984.

Shakal, A.F., and M.N. Toksoz, Earthquake hazard in New England, Science, 195, 171-173, 1977.

Somerville, P.G., J.P. McLaren, L.V. Le Fevre, R.W. Burger, and D.V. Helmberger, Comparison of source scaling relations of eastern and western North American earthquakes, Bull. Seism. Soc. Am., 77, 322-346, 1987.

Street, R.L., and F.T. Turcotte, A study of northeastern North American spectral moments, magnitudes and intensities, Bull. Seism. Soc. Am., 67, 599-614, 1977.

Yang, J.P., and Y.P. Aggarwal, Seismotectonics of northeastern United States and adjacent Canada, J. Geophys. Res., 86, 4981-4998, 1981.

SEISMOTECTONICS OF THE CENTRAL UNITED STATES

Arch C. Johnston and Susan J. Nava
Center for Earthquake Research
Memphis State University
Memphis, Tennessee 38152

INTRODUCTION

The seismicity and tectonics of the Central United States have been the subjects of extensive previous investigations in the literature [e.g., Nuttli and Herrmann, 1978; Nuttli, 1979; Van Schmus et al., 1987; Bickford et al., 1986; Hatcher et al., 1987]. In the space of this brief note a detailed and comprehensive review is not possible. Rather, our objective will be to define the seismicity and large-scale tectonic features in a general sense in order to delineate the problem of seismic hazard assessment in the region. In our view the single most difficult problem is the estimation of the "seismic potential" of a zone or a crustal structure. This potential has two components: an estimate of the maximum possible earthquake and an estimate of the frequency of occurrence of moderate-to-large events (m>5). Both components are essential input parameters for hazard estimation, yet quantitative constraints are nearly entirely lacking. For a region such as the Central United States where the historical seismicity record is short, where the character of the seismogenic crystalline basement crust is obscure, and where the earthquake potential of most of the known crustal structures is not known, the process of assigning seismic potential is more intuitive than systematic. In what follows we will present an overview of the study region and its seismicity and then return to the question of seismic "intuition".

THE CRUST OF THE CENTRAL UNITED STATES

The Central U.S. as defined for this report is bounded on the north by Canada, to the south by Mexico/Gulf of Mexico, to the west by the Rocky Mountain Cordillera/Rio Grande Rift (105°W longitude), and to the east by the New York-Alabama aeromagnetic lineament as defined by King and Zietz [1979]. It includes the states of North and South Dakota, Nebraska, Kansas, Oklahoma, Minnesota, Iowa, Missouri, Arkansas, Louisiana, Mississippi, Michigan, Wisconsin, Illinois, Indiana, Kentucky, Ohio, and portions of West Virginia, Tennessee, Alabama, Texas, New Mexico, Colorado, Wyoming and Montana.

How is the crust of this region usefully characterized for assessing seismic potential? To begin, there is little doubt that the earthquake generation process occurs in the upper crust, above the brittle-ductile transition at 20-30 km depth, but beneath the veneer of Paleozoic sedimentary rock that blankets the crystalline basement throughout the study region. Virtually all large earthquakes, for which data are sufficient to place good constraints on hypocentral depth, occur within the igneous and metamorphic upper crust, although some aftershocks may extend into the Paleozoic section. Moreover, there is no documented instance of

surface fault rupture accompanying any Central U.S. earthquake. The Meers fault of southwest Oklahoma appears to represent a remarkable exception to this rule for a prehistoric earthquake and will be further discussed later in this review.

The crystalline crust of the Central United States is wholly of Precambrian age, with the possible exception of the Southern Coastal Block. The shield and platform areas together comprise a collage of at least five cratonic elements (Figure 1) which correlate with major Precambrian orogenic episodes, ranging in age from Superior craton nucleation in the Archean (3.8 to 2.5 b.y.) to the middle Proterozoic Grenville orogeny (1.1 b.y.). Most age determinations have been from drill hole samples; the principal basement outcrops [the Superior craton in Minnesota, the Ozark dome in Missouri, the Llano uplift and Van Horn/Franklin Mountains of Texas, and the Black Hills uplift of South Dakota] are few and isolated.

This representation of a Precambrian Central U.S. crust that grew to the south and east via lateral accretion during successively younger orogenies is derived from data only recently available. Perhaps the most important technique for applying these data to problems of mid-continent crustal evolution is U-Pb age dating on zircon concentrates from drill cuttings [Van Schmus et al., 1987]. Reliable dates are obtained from small samples for which – unlike Rb-Sr or K-Ar dating – a degree of weathering and/or alteration is tolerable. A comprehensive framework for our study region is rapidly being worked out.

TECTONICS OF THE CENTRAL UNITED STATES

North of the Paleozoic Ouachita system, Phanerozoic tectonics have little affected the Central U.S. The interior platform region had consolidated into a vast composite craton by about 1,300 m.y. This is not to say, however, that tectonic processes ceased to operate in the region. The most prominent example of this is the Midcontinent rift system [Chase and Gilmer, 1973; Van Schmus and Hinze, 1985] (see Figure 2). It is defined by the strongest gravity signature in the Central U.S., consisting of a sharply defined belt of linear positive Bouguer gravity anomalies extending from Michigan to Kansas, with central highs reaching +60 mgal flanked by -100 mgal lows. Its rocks are contemporaneous with those of the Grenville province to the east suggesting the two are genetically related. Although the origins of Grenville province remain poorly understood, one possible model is that of a continental collision zone with the Midcontinent rift system forming behind the collision (suture) in response to extensional forces. A present-day analog to this process would be the Baikal rift zone of Central Asia well north of the India-Asia collision zone.

Figure 2 depicts a number of other primary tectonic features and indicates whether they are expressed at the surface (geologically defined) or are subsurface (geophysically defined). We have preferentially emphasized rifts and sutures for this figure because a recent study by Coppersmith et al. [1987] has identified such structures as the most important in localizing seismicity in the stable interiors of continents.

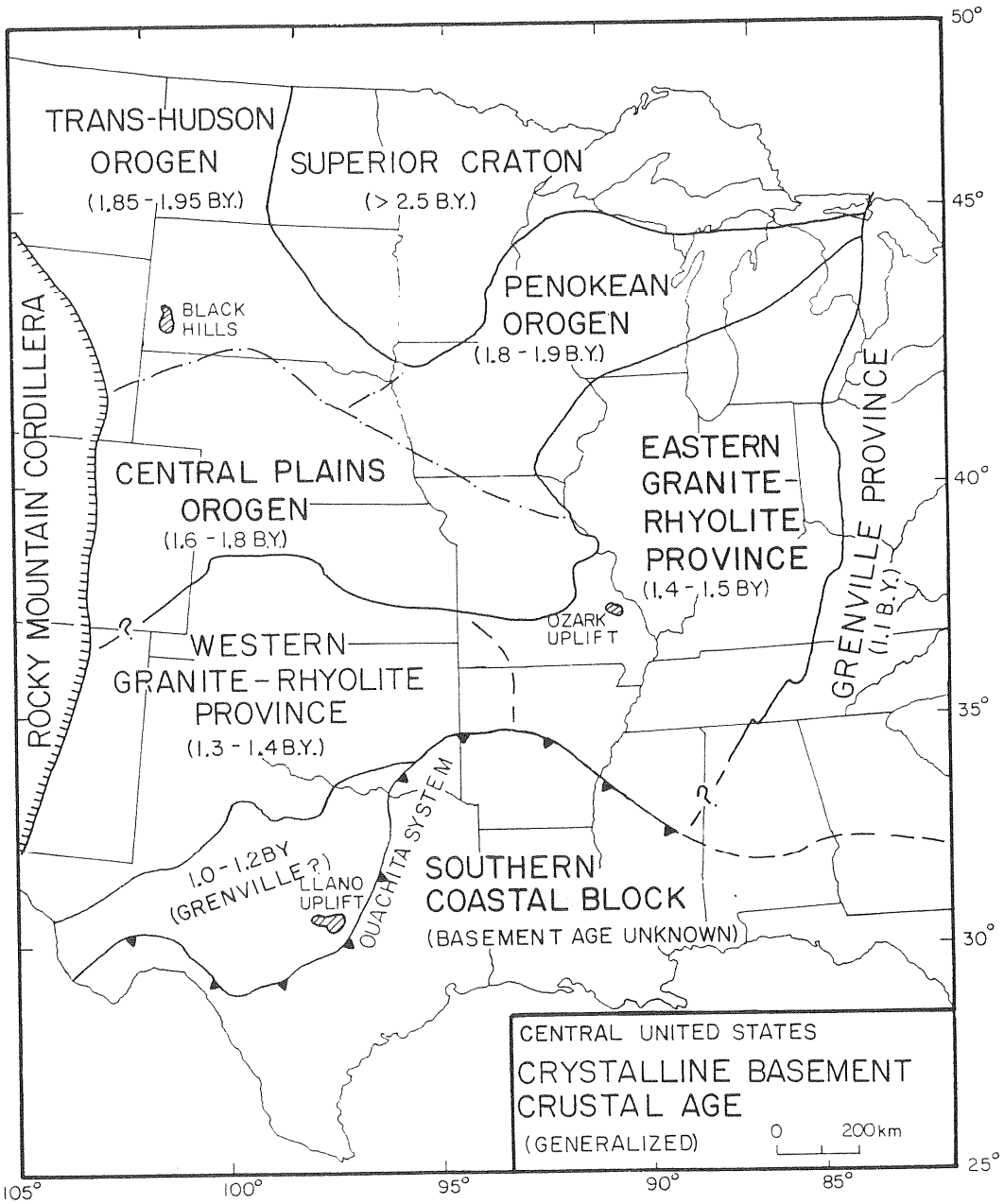

Figure 1. Age subdivisions of the crust of the Central United States.

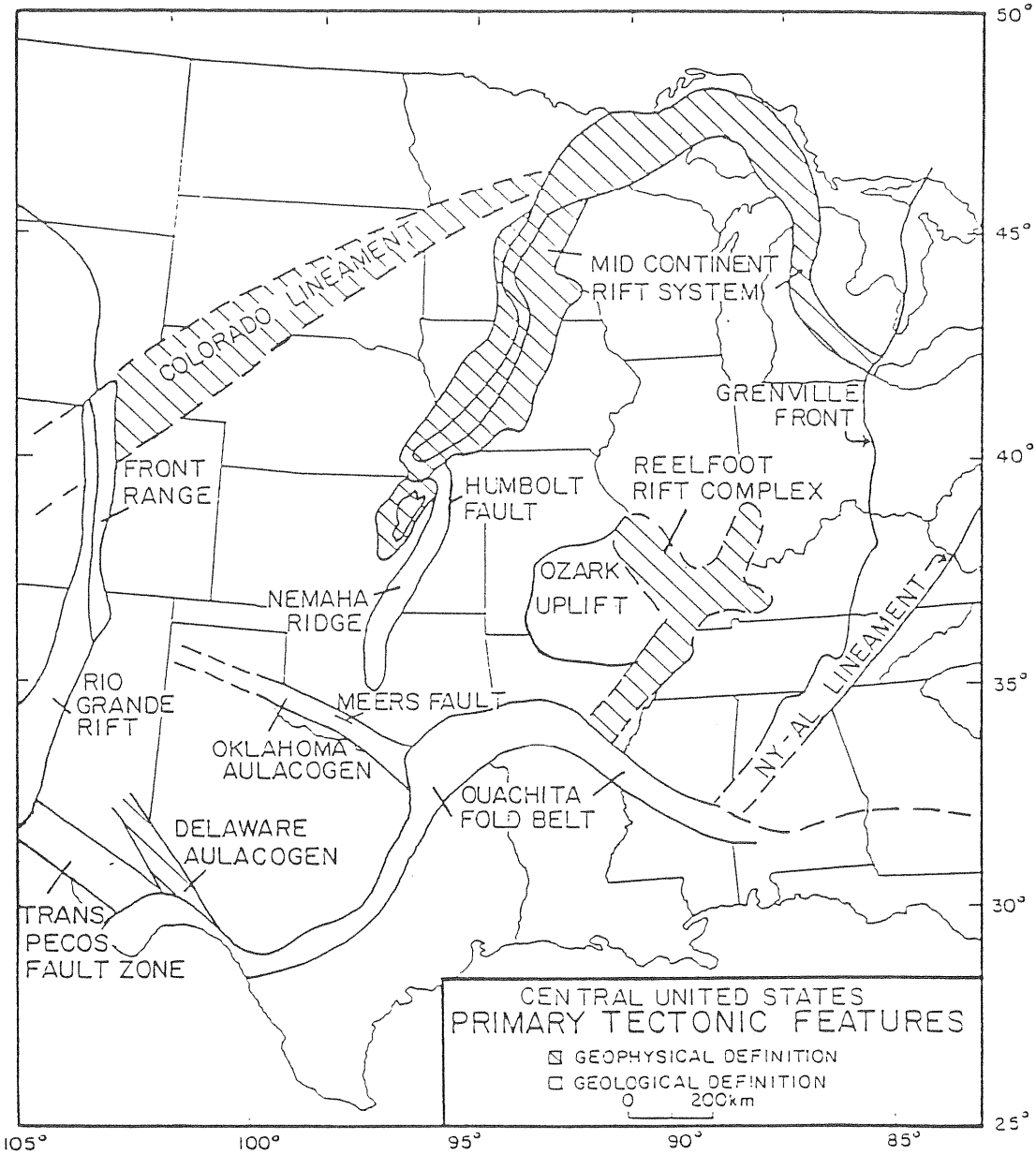

Figure 2. Principle tectonic elements of the crust of the Central United States.

The major suture transversing the study area is the Paleozoic Ouachita thrust and fold belt. It is generally interpreted as a continuation of the Appalachian system, connecting with it beneath the Gulf Coastal Plain sediments of Alabama. The Ouachita belt represents the southern boundary of Precambrian North America; it juxtaposes Proterozoic cratonic crust to the north with crust of unknown age and uncertain character (continental or transitional oceanic) to the south.

Another possible continental suture is the eastern boundary of the study area, the New York-Alabama lineament. The crustal structure giving rise to this aeromagnetically-defined feature lies in Grenville-age crust beneath the Appalachian decollement. It has been interpreted as a major strike-slip fault associated with continental collision [King and Zietz, 1978]; and alternate interpretation is that it demarks the suture between Grenville North America and an accreted terrane named the Clingman block by Johnston et al. [1985] or the Bristol block by Hatcher et al. [1987].

Three major failed continental rift complexes or aulacogens intersect the Ouachita belt at high angles: the Delaware aulacogen of west Texas, the Oklahoma aulacogen, and the Reelfoot rift complex. All are Eocambrian (575-700 m.y.) in age, but at least the Reelfoot rift and probably the others underwent additional extension and intrusion during Mesozoic-to-Cretaceous time [Braile et al., 1984]. The age of formation of these rifts suggests they formed as perhaps failed arms of triple junctions (the Reelfoot rift may represent more than one) during an episode of late Precambrian continental break-up that predated the Ouachita-Appalachian orogenies.

Many other crustal tectonic elements could be illustrated in Figure 2 as perhaps relevant to earthquake occurrence in stable continental settings. For example, basement uplifts and basins, gravity and magnetic highs and gradients, mafic and felsic plutons, shallow crustal grabens, and faults over a large range of dimensions have been discussed in the literature. A cause-and-effect relationship between such features and seismicity remains tenuous and is not promoted here. Local stress concentrations arising from these crustal inhomogeneities may produce some moderate earthquakes (up to magnitude 5.0-5.5), but we contend that larger events will require the major throughgoing crustal disruption of the primary structures of Figure 2. In fact, the absence of such events in the Central U.S. except in the New Madrid/Reelfoot rift region argues that special conditions beyond the presence of major crustal structures is required before large earthquakes are produced.

THE SEISMICITY AND STRESS REGIME OF THE CENTRAL UNITED STATES

The seismicity of the Central United States is depicted in Figures 3 and 4. In the interest of space, a map of the deviatoric horizontal stress regime is not shown: recent important compilations by Zoback

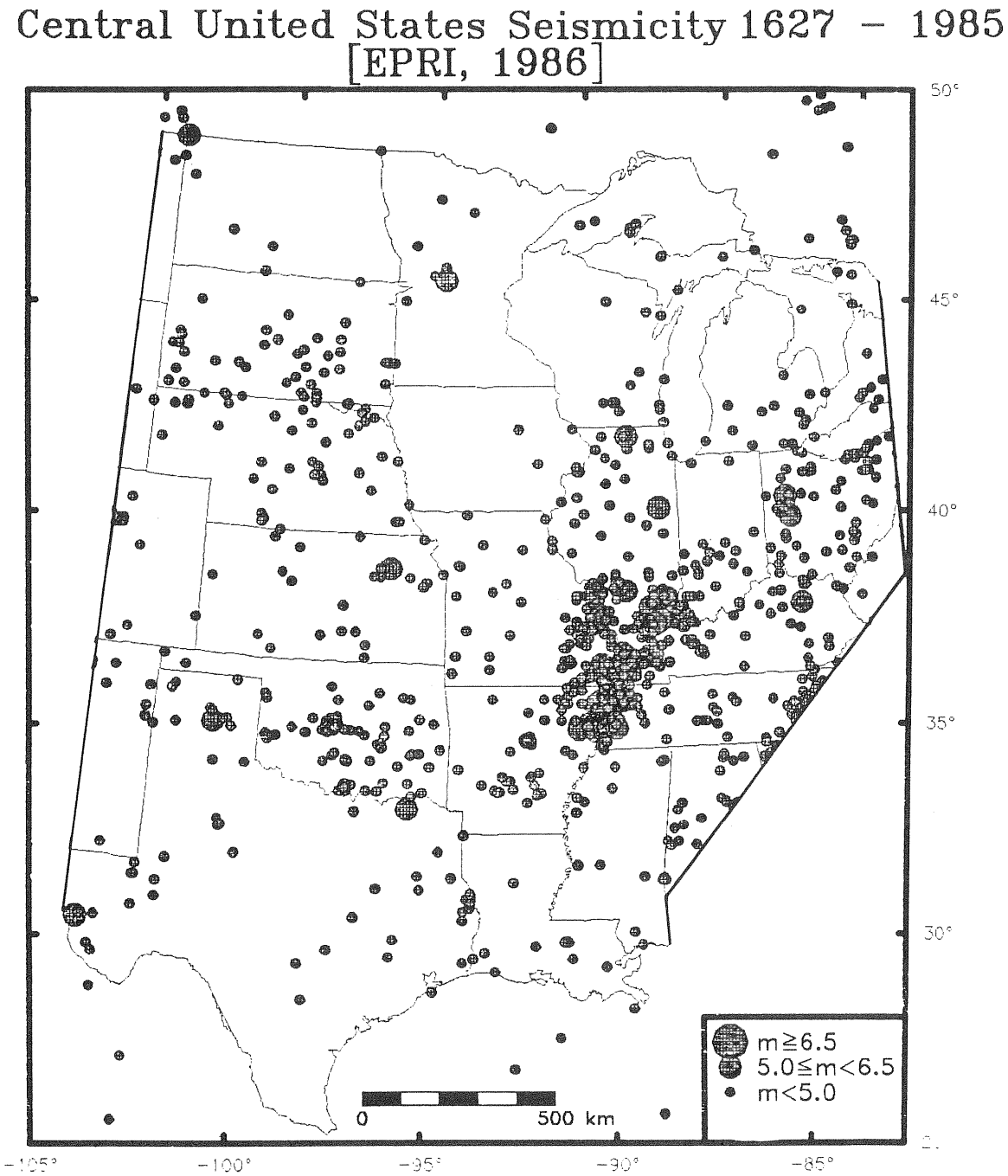

Figure 3. Seismicity of the Central United States. The source is the EPRI catalog [1986]. A plot from the other major catalog for the Central United States [Nuttli & Brill, 1981] would exhibit a similiar pattern, but would differ considerably in detail.

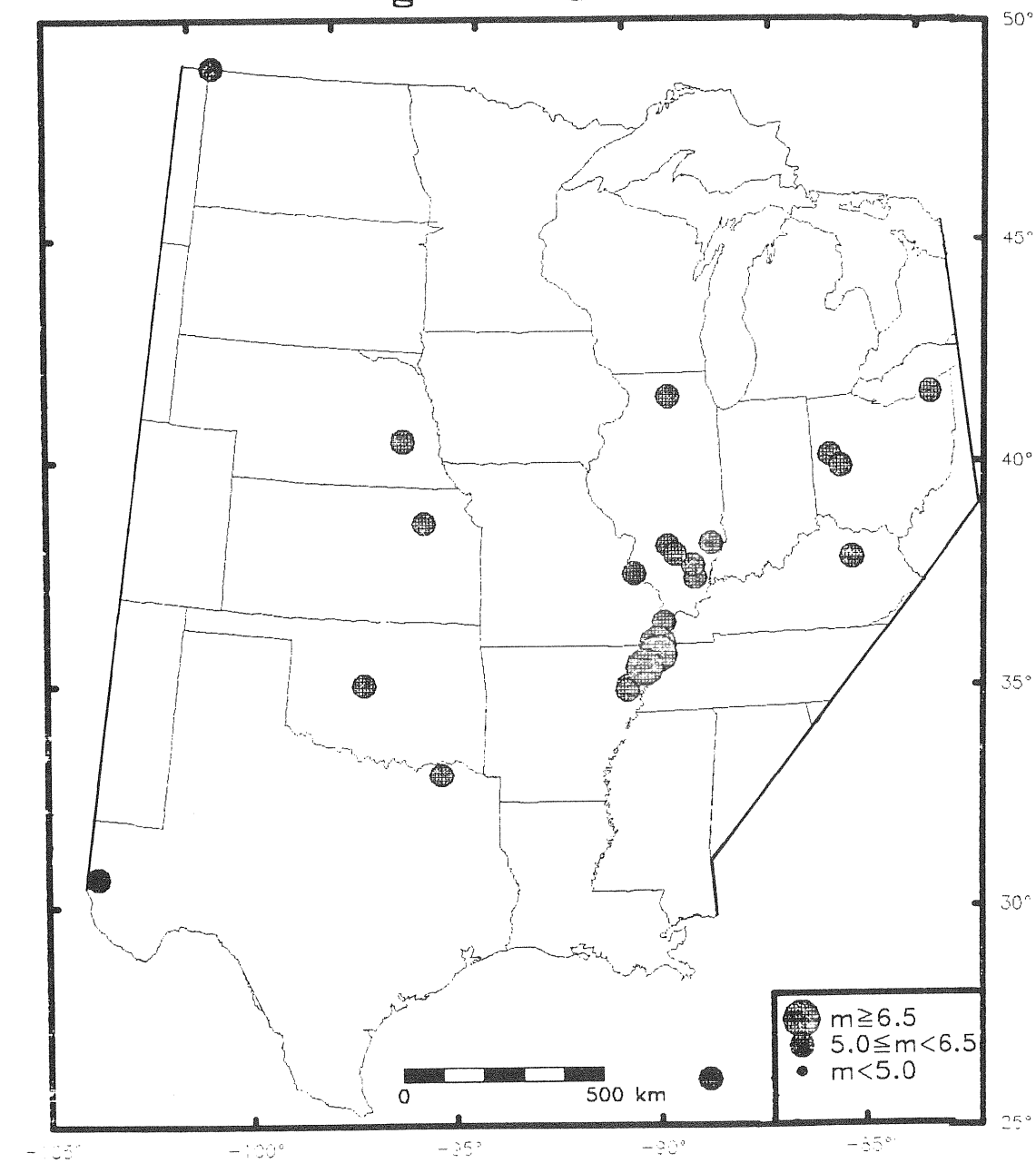

Figure 4. Known earthquakes of magnitude 5 and above of the Central United States, compiled from the sources listed in Table I. Another 13 events, not shown in this figure, would fall between magnitude 4.7 and 5.1, but were judged to probably be less than 5.0.

and Zoback [1980; 1986] indicate that its orientation is remarkably uniform throughout most of the study area, trending from northeast to east-northeast, and compressional in character, as the study area as traversed from northeast to southwest. An extensional province may exist in the extreme southwest in Texas and New Mexico. The magnitude of the horizontal stress deviation from gravitational lithostatic conditions is not known. Nor is the stress orientation known for the in basement of the Southern Coastal Block (Figure 1) beneath the thick coastal plain deposits.

Although stress regime orientation in the Central U.S. is very uniform, the distribution of earthquakes decidedly is not. Whether one looks at total known seismicity (m>3.5, Figure 3) or only the larger events (m>5.0, Figure 4), nonrandomness is apparent. Although it is likely that this two-to-three century 'snapshot' of seismicity is inadequate to identify the complete, detailed pattern, we would argue that it is sufficient to establish an inherent high degree of nonrandomness. Something must be causing the clustering of seismic energy release in the Central U.S.

By far the most pronounced cluster of activity of Figures 3 and 4 centers on the confluence of the Mississippi and Ohio Rivers at the head of the Mississippi embayment and is clearly spatially associated with the Reelfoot rift complex of Figure 2. A remarkable fact is that no earthquake exceeding magnitude 6 has occurred in the Central United States outside of this zone since settlement of the region by Europeans. [The 1931 West Texas event – arguably a magnitude 6 – occurred in a zone of active faulting associated with the Rio Grande rift and thus bears a closer affinity to the active tectonics of the western U.S. as opposed to the stable midcontinent.]

The great New Madrid earthquakes of the winter of 1811-1812, as well as the current seismicity of the zone, have been extensively examined in the literature; we will not repeat that examination here. Clearly from Figures 3 and 4 and Table I, the New Madrid zone, including its northward extensions, completely dominates Central United States seismicity. The same holds true when stable continental interiors are examined worldwide [Coppersmith et al., 1987]: no zone comparable to New Madrid exists on any other continent. How is this to be explained when these regions all contain numerous primary tectonic structures and are thought to be subject to fairly uniform regional stress regimes?

Seismic 'Intuition'

We conclude this short review by trying to answer the preceeding question. One possible answer is that if a much longer time span were available for examination, many of the other crustal structures of the Central U.S. would be the loci of large earthquakes, i.e., the assumption of a temporally stochastic pattern of earthquake occurrence is invalid. While we cannot exclude this possibility, we do not favor it and cite the highly stochastic and much longer seismicity record of China [e.g., McGuire, 1979].

TABLE I

CENTRAL UNITED STATES EARTHQUAKES $m \geq 5.0$

DATE	LOCATION/LOCALE	MAGNITUDE	MMIo	REFERENCE
	TWENTIETH CENTURY (1901-1987)			
1987 06 10	38.713/87.954 [SE Illinois]	5.1 m_{blg}	VII	PDE
1986 01 31	41.642/81.109 [NE Ohio]	5.0 m_b	VI	Nicholson et al., 1987
1980 07 27	38.18 /83.94 [NE Kentucky]	5.2 m_b	VII	Herrmann et al., 1982
1978 07 24	26.729/88.743 [Gulf of Mexico]	5.0 m_b	--	Frohlich, 1982
1976 03 25	35.59 /90.48 [NE Arkansas]	5.0 m_b	VI	Nuttli & Brill, 1981
1968 11 09	37.96 /88.46 [SE Illinois]	5.5 m_{blg}	VII	Gordon et al., 1970
1952 04 09	35.525/97.850 [Central OK]	5.1 m_b	VII	Gordon, 1986
1937 03 09	40.470/84.280 [W. Ohio]	5.0 m_b	VII	Nuttli & Brill, 1981
1931 08 16	30.69/104.57 [SW Texas]	5.9 m_b	VIII	Dumas et al., 1980
1917 04 09	38.10/90.20 [E. Missouri]	5.0 m_b	VI	Nuttli & Brill, 1981
1909 05 16	49.0 /104.0 [U.S. Can. Border]	5.5 m_b	VI	Horner & Hasegawa, 1978
1909 05 26	42.0 /89.0 [N. Illinois]	5.0 m_b	VII	Nuttli & Brill, 1981
	NINETEENTH CENTURY (1801-1900)			
1895 10 31	37.0 /89.4 [SE Missouri]	6.2 m_b	IX	Nuttli & Brill, 1981
1891 09 27	38.25/88.50 [SE Illinois]	5.5 m_b	VII	Street, 1980
1882 10 22	33.6 /95.6 [NE Texas]	5.5 m_b	VIII	Nuttli & Brill, 1981
1877 11 15	41.0 /97.0 [E. Nebraska]	5.0 m_b	VII	Nuttli & Brill, 1981
1875 01 18	40.2 /84.0 [W. Ohio]	5.3 m_b	VII	EPRI Catalog, 1986
1867 04 24	39.2 /96.3 [S-Central Illinois]	5.1 m_b	VII	Nuttli & Brill, 1981
1867 04 24	39.17/96.30 [NE Kansas]	5.1 m_b	VIII	Dubois & Wilson, 1978
1865 08 17	36.5 /89.5 [SE Missouri]	5.3 m_b	VII	Nuttli & Brill, 1981
1857 10 08	38.7 /89.2 [SW Illinois]	5.1 m_b	VII	EPRI Catalog, 1986
1843 01 05	35.5 /90.5 [NE Arkansas]	6.0 m_b	VIII	Nuttli & Brill, 1981
1838 06 09	38.5 /89.0 [S. Central Illinois]	5.0 m_{blg}	VI	EPRI Catalog, 1986
1812 02 07	36.5 /89.6 [SE Missouri]	7.4 m_b/8.8M_s	XII	Nuttli, 1983
1812 01 23	36.3 /89.6 [SE Missouri]	7.1 m_b/8.4M_s	X-XI	Nuttli, 1983
1811 12 16	36.0 /90.0 [NE Arkansas]	7.0 m_b/8.3M_s	--	Street & Nuttli, 1984
1811 12 16	36.0 /90.0 [NE Arkansas]	7.2 m_b/8.5M_s	XI	Nuttli, 1983

There are four factors that we propose as making the Reelfoot rift complex especially, perhaps uniquely, susceptible to a high seismicity rate and the generation of major earthquakes. First, as previously mentioned, it is a major, throughgoing crustal structure. This may be essential to the localization of a high strain rate.

Second, it is ideally oriented with respect to the regional stress regime for the ratio of shear-to-normal stress to be maximized on preexisting fault systems. [Note that its active west-northwest segment is a good left lateral strike-slip representation of the auxiliary nodal plane for the right lateral strike-slip mechanism of the southwest axial zone.] Other major structures of Figure 2 tend to strike perpendicular or parallel to the regional stress, yielding a less-than-optimum ratio of shear-to-normal stress.

Third, the Reelfoot rift (or more precisely its Mesozoic-Cenozoic reactivation) is tectonically young and its crustal disruption has not had time to heal. This appears to be the factor that explains the aseismicity of the middle Proterozoic Midcontinent rift system.

Fourth, and most speculative, is the observation that the Reelfoot rift complex is saturated with water from the largest of the North American drainage systems.It is a "wet" seismogenic structure and evidence is accumulating that this is an important contributing parameter for intraplate earthquake generation [Nava and Johnston, 1984; Costain et al., 1987].

Epilogue: The Meers Fault

The Meers fault, located in the Oklahoma aulacogen (Figure 2) represents a probable exception to the domination of Central U.S. seismicity by the New Madrid zone. Evidence is now sufficiently strong to require a magnitude 7+ earthquake there within the past 1,100 to 1,400 years [Luza et al., 1987; Ramelli et al., 1987]. If the fault's dip is subvertical at hypocentral depth, its orientation is favorable for left lateral strike-slip movement which is the observed dominant slip component. It has been virtually aseismic throughout the historical past (Figure 3).

Thus the Meers fault, with its prominent surface scarp, appears to represent a western-style, active fault within the Central U.S. stable interior. It is already forcing a reexamination of seismic zonation practices, which in the past have relied heavily on historical seismicity patterns, because it represents a clear violation of the assumption of stationarity of seismicity on which much seismic hazard analysis is based. It constitutes an important reminder that we must continually question our assumptions and strive to improve our understanding of the tectonics underlying the seismogenic process in the Central United States.

REFERENCES

Bickford, M.E., W.R. Van Schmus, and I. Zietz, Proterozoic history of the midcontinent region of North America, *Geology*, **14**, 492-496, 1986.

Braile, L., W. Hinze, J. Sexton, G.R. Keller, and E. Lidiak, Tectonic development of the New Madrid seismic zone, in *Proceedings of the Symposium on "The New Madrid Seismic Zone"*, Hays, W.W. and P.L. Gori, eds., *U.S. Geol. Surv. Open File Report*, **84-770**, 204-233, 1984.

Chase, C.G. and T.H. Gilmer, Precambrian plate tectonics: The midcontinent gravity high, *Earth Planet. Sci. Ltrs.*, **21**, 70-78, 1973.

Coppersmith, K.J., A.C. Johnston, A.G. Metzger, and W.J. Arabasz, Methods for assessing maximum earthquakes in the central and eastern United States, Working Report, *Electric Power Research Institute, RP2556-12*, Palo Alto, CA, 109 pp., 1987.

Costain, J.K., G.A. Bollinger, and J.A. Speer, Hydroseismicity: A Hypothesis for the role of water in the generation of intraplate seismicity, *Seism. Res. Ltrs.*, **58**, 41-64, 1987.

DuBois, S.M. and F.W. Wilson, A revised and augmented list of earthquake intensities for Kansas, 1867-1977, *U.S. Nuc. Reg. Comm., NUREG/CR-0294*, Washington, D.C., 56 pp., 1978.

Dumas, D.B. H.J. Dorman, and G.V. Latham, A reevaluation of the August 16, 1931 Texas earthquake, *Seism. Soc. Amer. Bull.*, **70**, 1171-1180, 1980.

Electric Power Research Institute (EPRI), *Catalog of central and eastern North America earthquakes to 1985*, EPRI Seismic Hazards Research Program, Palo Alto, CA.

Frohlich, C., Seismicity of the central Gulf of Mexico, *Geology*, **10**, 103-106, 1982.

Gordon, D., Revised instrumental hypocenters and correlation of earthquake locations in the central U.S., submitted to *Central Technical Reports, U.S. Geol. Surv.* as a Professional Paper; awaiting Director's approval, 184 manuscript pages, 1986.

Gordon, D.W., T.J. Bennett, R.B. Herrmann, and A.M. Rogers, The south-central Illinois earthquake of November 9, 1968: macroseismic studies, *Seism. Soc. Amer. Bull.*, **60**, 953-971, 1970.

Hatcher, R.D., Jr., I. Zietz, and J.J. Litehiser, Crustal subdivisions of the eastern and central United States and a seismic boundary hypothesis for eastern seismicity, *Geology*, **15**, 528-532, 1987.

Herrmann, R.B., C.A. Langston, and J.E. Zollweg, The Sharpsburg, Kentucky earthquake of 27 July 1980, *Seism. Soc. Amer. Bull.*, **72**, 1219-1239, 1982.

Horner, R.B. and H.S. Hasegawa, The seismotectonics of southern Saskatchewan, *Can. J. Earth Sci.*, **15**, 1341-1355, 1978.

Johnston, A.C., D.J. Reinbold, and S.I. Brewer, Seismotectonics of the southern Appalachians, *Seis. Soc. Amer. Bull.*, **75**, 291-312, 1985.

King, E.R. and I. Zietz, The New York-Alabama lineament: Geophysical evidence for a major crustal break in the basement beneath the Appalachian basin, *Geology*, **6**, 312-318, 1978.

Luza, K.V., R.F. Madole, and A.J. Crone, Investigation of the Meers fault in southwestern Oklahoma, *U.S. Nuc. Reg. Comm., NUREG/CR - 4937*, Washington, D.C., 55 pp., 1987.

McGuire, R.K., Effects of uncertainty in seismicity on estimates hazard for the east coast of the United States, *Seism. Soc. Amer. Bull.*, **67**, 827-848, 1977.

Nava, S.J. and A.C. Johnston, Rivers and earthquakes: A correlation for New Madrid and the Mississippi River, (abs.), *Earthquake Notes*, **55**, 15, 1983.

Nicholson, C., E. Roeloffs, and R.L. Wesson, The northeastern Ohio earthquake of January 31, 1986: Was it induced?, *Seism. Soc. Amer. Bull.*, in press, 1987.

Nuttli, O.W., Seismicity of the central United States, in *Geology in the Siting of Nuclear Power Plants, Reviews in Engineering Geology*, Vol. **IV**, Hatheway, A.W. and C.R. McClure, Jr., eds., *Geol. Soc. Am.*, 67-93, 1979.

Nuttli, O.W., Average seismic source-parameter relations for midplate earthquakes, *Seism. Soc. Amer. Bull.*, **73**, 519-535, 1983.

Nuttli, O.W. and K.G. Brill, Jr., Earthquake source zones in the central United States determined from historical seismicity [and Appendix B2, Earthquake Catalog], in *An Approach to Seismic Zonation for Siting Nuclear Electric Power Generating Facilities in the Eastern United States*, prepared by Barstow, N.L., K.G. Brill, Jr., O.W. Nuttli, and P.W. Pomeroy, *U.S. Nuc. Reg. Comm., NUREG/CR-1577*, Washington, D.C., 97-143, B2-1 to B2-31, 1981.

Nuttli, O.W. and R.B. Herrmann, Credible earthquakes for the central United States, in *State-of-Art for Assessing Earthquake Hazards in the United States, Miscellaneous Paper S-73-1, Report 12*, U.S. Army Corps of Engineers, Geotechnical Lab., Vicksburg, Mississippi, 99 pp., 1978.

Ramelli, A.R., D.B. Slemmons, and S.J. Brocoum, The Meers fault: Tectonic activity in southwestern Oklahoma, *U.S. Nuc. Reg. Comm., NUREG/CR-4852*, Washington, D.C., 25 pp., 1987.

Sims, P.K. and Z.E. Peterman, Early Proterozoic Central Plains orogen: A major buried structure in the north-central United States, *Geology*, **14**, 488-491, 1986.

Street, R.L., The southern Illinois earthquake of September 27, 1891, *Seism. Soc. Amer. Bull.*, **70**, 915-920, 1980.

Street, R. and O.W. Nuttli, The central Mississippi Valley earthquakes of 1811-1812, in *Proceedings of the Symposium on "The New Madrid Seismic Zone"*, Hays, W.W. and P.L. Gori, eds., *U.S. Geol. Surv. Open File Report* **84-770**, 33-63, 1984.

Van Schmus, W.R., M.E. Bickford, and I. Zietz, Early and middle Proterozoic provinces in the central United States, in *Proterozoic Lithospheric Evolution*, Geodynamics Series, Vol. **17**, Kroner, A., ed., *Amer. Geophys. Union*, 43-68, 1987.

Van Schmus, W.R. and W.J. Hinze, The midcontinent rift system, *Ann. Rev. Earth Planet. Sci.*, **13**, 345-383, 1985.

Zoback, M.L. and M.D. Zoback, State of stress in the conterminous United States, *J. Geophys. Res.*, **85**, 6113-6156, 1980.

Zoback, M.L. and M.D. Zoback, Tectonic stress field of the continental U.S., submitted for publication in *Geophysical Framework of the Continental United States*, Pakiser, L. and W. Mooney, eds., *Geol. Soc. Amer. Memoir*, 36 manuscript pages, 1986.

SEISMOTECTONICS OF THE VIRGINIA AND EASTERN TENNESSEE SEISMIC ZONES

G. A. Bollinger
Seismological Observatory, Virginia Polytechnic Institute and State University,
Blacksburg, Virginia 24061

ABSTRACT

The Appalachian seismic zones in eastern Tennessee and southwestern (Giles County) Virginia exhibit markedly different characteristics from those of the central Virginia zone in the Piedmont province. The Appalachian zones are northeasterly in trend, occur primarily below a décollement (90% of the focal depths ≤ 20 km) on fault planes that strike generally northerly or easterly and dip steeply (≈65°). Focal mechanism P axes are sub-horizontal and trend northeasterly. The central Virginia seismic zone is roughly circular in map view (≈100 km diameter) and occurs mostly above a décollement; 90% of the focal depths are ≤ 13 km. Focal mechanism nodal planes are northerly or easterly and steep (≈ 60°) with sub-horizontal P axes exhibiting a bimodal trend distribution: northeasterly for shallow (3-7 km depths) shocks and northwesterly for the deeper earthquakes (8-13 km depths). The cause of this variation in trend is not known.

Magnitude recurrence relations for the zones indicate that eastern Tennessee has the highest rate of activity with the highest proportion of small shocks while central Virginia has the lowest activity rate with the lowest proportion of smaller earthquakes. The Giles County, Virginia, seismic activity is intermediate between those two. Historically, the Giles County zone has experienced a $m_b = 5.8$ shock [1897] while the other two zones have had maximum earthquakes of $m_b = 5$.

INTRODUCTION

There are three seismic zones in Virginia and eastern Tennessee: two in the Appalachian Highlands (eastern Tennessee and southwestern (Giles County) Virginia) and one in the Piedmont of central Virginia. The seismotectonics of the Appalachian zones are similar but are, in turn, different from that found in the Piedmont zone. Ten years of seismic network monitoring results (Fig. 1) have revealed something of the distribution of focal depths and focal mechanisms for these zones of historically persistent, but generally low level, strain energy release. The largest historical earthquake was a $m_b = 5.8$, MMI = VIII, shock in Giles County, Virginia in 1897 with the other two zones experiencing $m_b = 5$, MMI = VII shocks [Bollinger and others, 1987].

The following topics will be discussed: first, the Appalachian zones and then, the central Virginia (Piedmont) zone. In each case, the following topics will be dealt with in order: Epicentral Patterns, Focal Depth Distribution, Focal Mechanism Solutions, Reflection Seismic Results and Magnitude Recurrence Relations. The paper concludes with a summary discussion of results.

THE GILES COUNTY, VIRGINIA, SEISMIC ZONE

Epicentral Pattern.

The distribution of epicenters defines a lineated, northeasterly trending zone some 40 km in length, centered on the inferred epicenter of the $m_b = 5.8$, 1897 shock, and surrounded on the north and the south by a scattering of mostly small (not felt) events (Fig. 2). This zone was the earliest documentation that the trend of a seismic zone (NE) in the eastern U.S. could be different from the trend of the host geologic province's structural fabric [ENE; Bollinger and Wheeler, 1982, 1983]. The apparent de-coupling between subsurface seismicity and bedrock geologic structures offered an

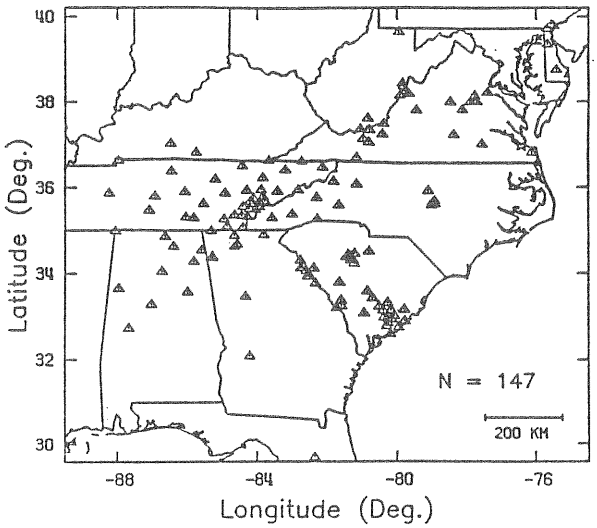

Figure 1. Southeastern U. S. Seismic Network - configuration as of 1986. Triangles represent one or more seismographs.

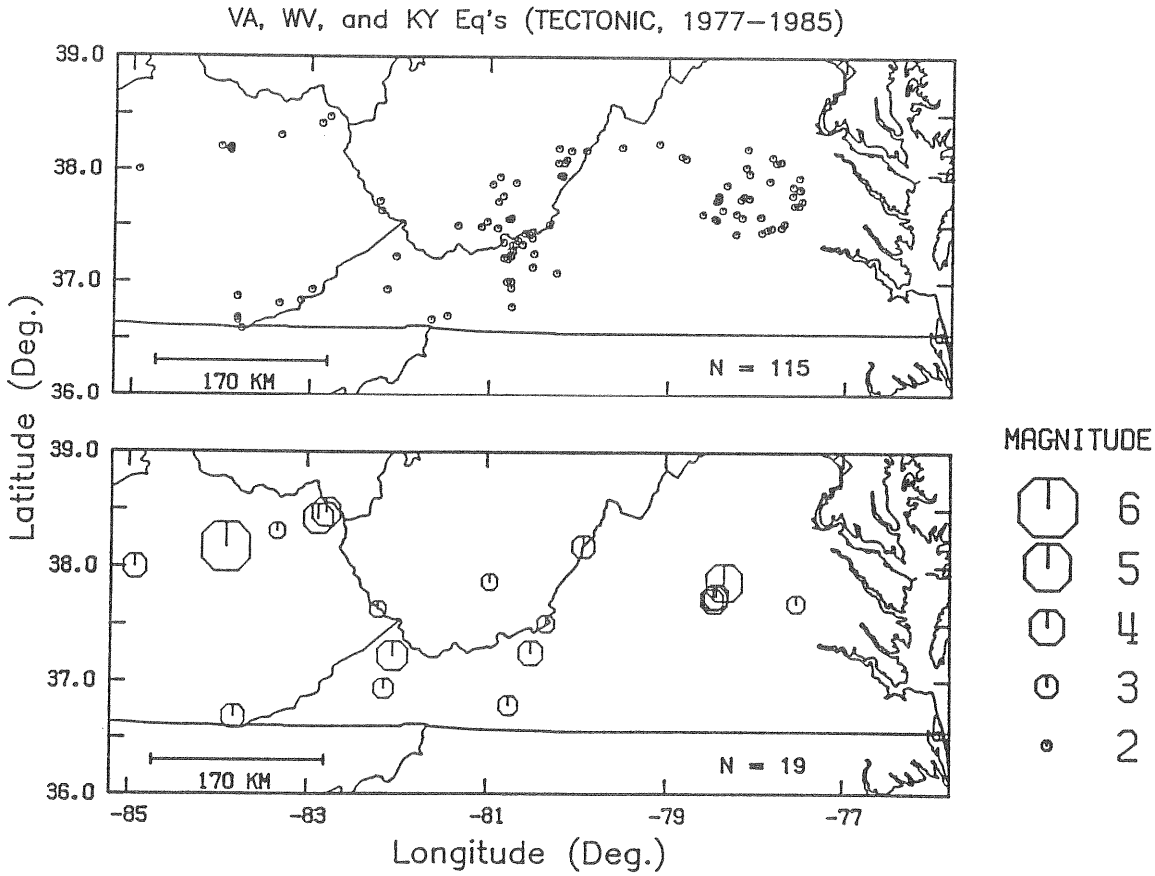

Figure 2. Epicenter Map for Virginia, West Virginia and eastern Kentucky for the period 1977 - 1985. Shown are Giles county and central Virginia seismic zones ; Giles county zone is the lineation of epicenters in southwestern Virginia near the West Virginia state line. **Upper :** All earthquakes (circles) with magnitude ≥ 0. **Lower :** Only earthquakes with magnitude ≥ 2. N = number of epicenters plotted.

explanation for the puzzling lack of correlation between those elements that was well known to workers in the region. The relationship of the diffuse activity about the main zone to that of the northeasterly trending structure is not known.

Focal Depth Distribution.

Earthquake foci in the Giles County zone, whose depth error estimates are ± 5 km or less, range from about 5 km to 25 km, with a mean depth of 11 km and with 90% of the depths at 16 km or less (Fig. 3 shows a regional summary; Bollinger and others, 1985, 1987). The minimum depths place the seismic activity in the crystalline basement below a regional décollement(s). The 90% depth implies a relatively thick seismogenic upper crust and thereby the potential for larger earthquakes.

Focal Mechanism Solutions.

Eight, single-event mechanisms for the Giles County zone were derived from both P-wave polarity and $(SV/P)_z$ amplitude ratios [Fig. 4; Munsey and Bollinger, 1985]. The mode of faulting is predominately strike-slip on north-northeasterly (right lateral; average strike = 16 ± 28°) and east-southeasterly (left lateral; average strike = 99 ± 24°), steeply dipping (average dip = 68 ± 22°) nodal planes, although there are some mostly dip-slip (reverse) solutions. The in-situ stress field, inferred from the focal mechanisms, exhibits uniform northeasterly trending, sub-horizontal P axes (maximum compressive stresses; average trend = 37 ± 28°; average plunge = 24 ± 15°).

Table 1 lists the parameters for all of the focal mechanism solutions considered herein, and Table 2 gives the amount of input data for determination of the solutions along with the levels of its agreement with the resulting mechanisms.

Reflection Seismic Results.

Approximately 37 km of predominately 24 fold P-wave Vibroseis and 16 km of 24 fold SH-wave Vibroseis data were acquired over the Giles County seismic zone [Gresko, 1985, Gresko and others, 1985]. Interpretation of those data suggests the presence of large, normal faults within the basement rocks beneath the overthrust surface rocks (Fig. 5). Distinct offsets of deep (5-10 km) reflections are evident at 1.8-2.5 sec two-way traveltime and those offsets were interpreted to be a series of down-to-the-east normal faults. These faults, which are located some 150 km west of the inferred early Paleozoic continental shelf, were probably formed during the opening of the proto-Atlantic (Iapetus) Ocean [Bollinger and Wheeler, 1982, 1983]. They are interpreted to offset basement reflectors (Precambrian) while the overlying Upper Cambrian and Ordovician sequences appear to be undisturbed, evidence that growth along the faults ended during the Cambrian. The recent seismicity suggests that these faults are now being reactivated by the current stress regime [Gresko, 1985, Gresko and others, 1985].

Magnitude Recurrence Relations.

Recently, Bollinger and Davison [1987] developed magnitude recurrence relations, according to the Gutenberg-Richter model: Log N = a -bm, for the southeastern U. S. and various subregions therein. For the Giles County zone they gave,

$$\text{Log } N_I = (0.76 \pm 0.20) - (0.56 \pm 0.078)\, m_{bLg} \ ,$$

where N_I is the incremental number of earthquakes / year in area of 7800 km^2 (radius of 50 km about the center of the zone). The rather large standard deviations of the intercept (activity parameter 'a') and slope (b - value) indicate that the maximum likelihood fit [ML; Weichert, 1980] is not well constrained. Indeed, 30 earthquakes served as input to the Stepps [1972] completeness

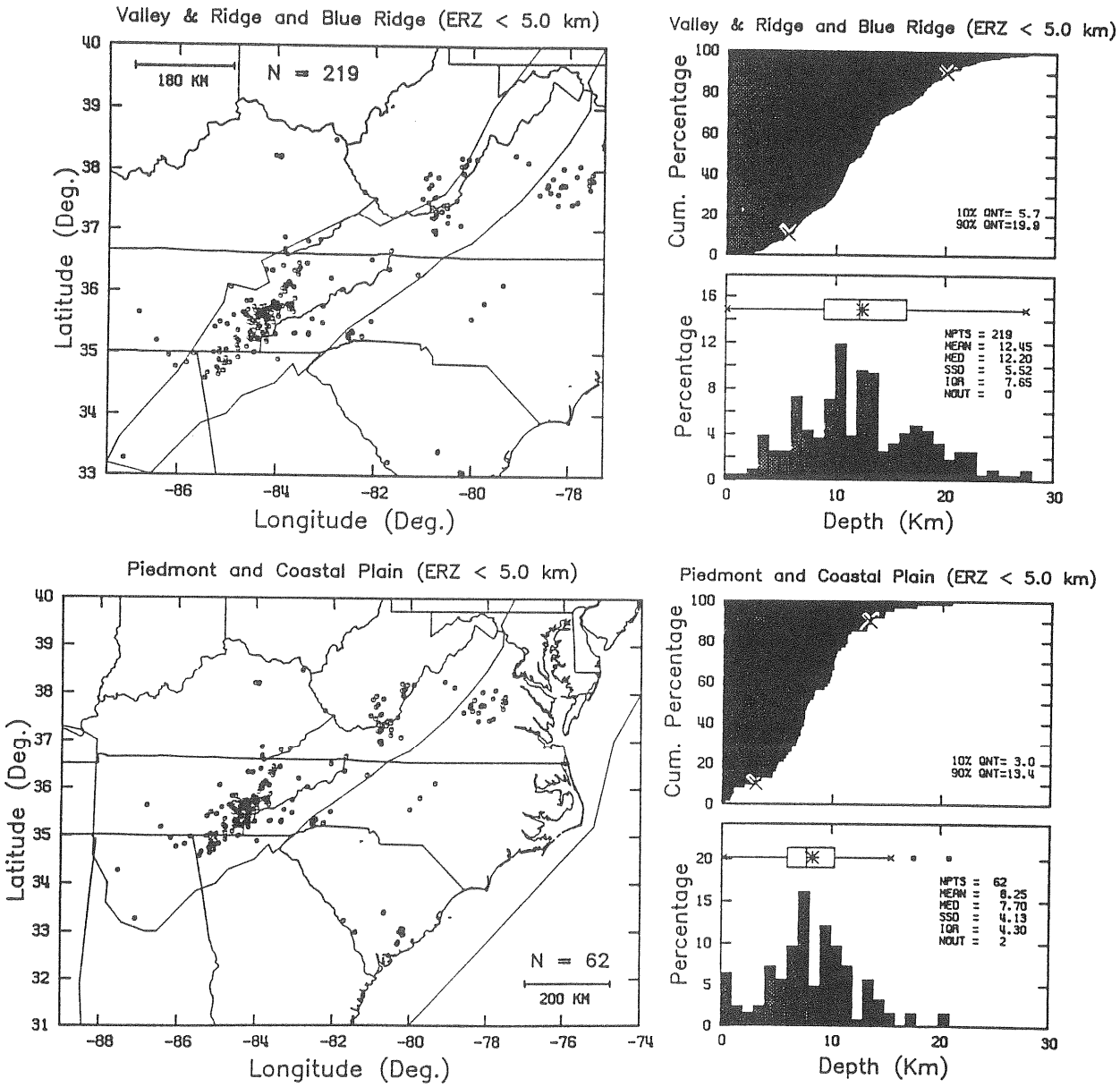

Figure 3. Focal Depth Distribution in the southeastern U. S. Provincial boundaries shown by segmented lines. Incremental and cumulative plots and box plots (shows central 50% of the data) shown on the right. QNT = Quantile ; NPTS = Number of points ; Mean (* in box) = Average focal depth ; MED (center bar in box) = Median focal depth ; SSD = Sample standard deviation ; IQR = Inner quartile range ; NOUT = number of outliers present in the data. (From : Bollinger and others, 1987).

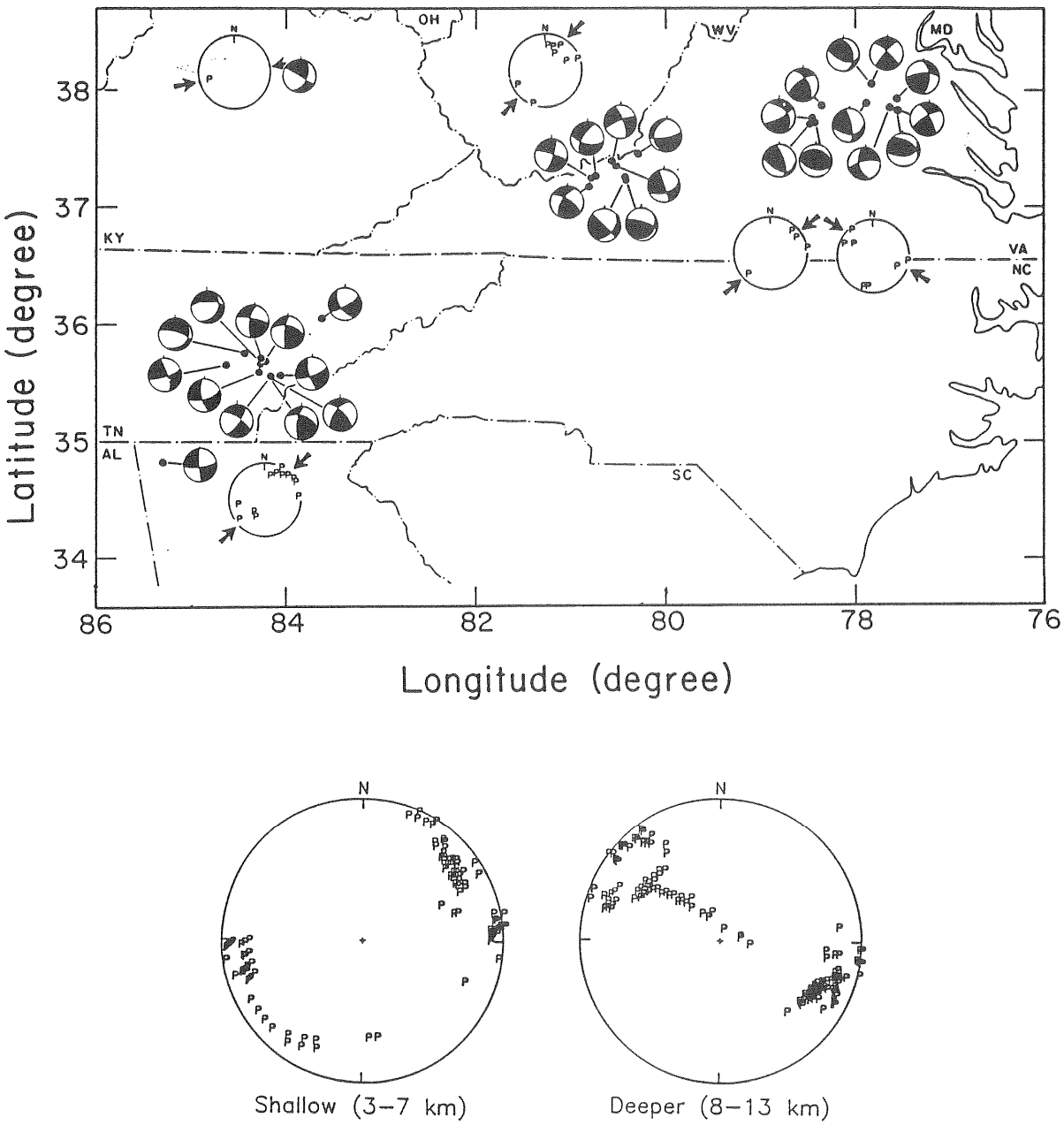

Figure 4. Upper : Focal mechanism solutions for Virginia and eastern Tennessee earthquakes. All plots are lower hemisphere, equal area ; compression quadrants shown black. P axes shown in separate plots with heavy arrows indicating average azimuth. (Modified from : Bollinger and others, 1987). **Lower :** Central Virginia P axes for all of the focal mechanism solutions that met minimum acceptance criteria between input data and theory according to the computer program FOCMEC (Snoke and others, 1985). All of the solutions shown above are the preferred solutions selected on the basis of minimum squared error criteria. Lower hemisphere, equal area projections for two different focal depth ranges for central Virginia shocks.

TABLE 1. PARAMETERS FOR FOCAL MECHANISM SOLUTIONS IN VIRGINIA AND EASTERN TENNESSEE.

EVENT (Date)	DIP	STRIKE	RAKE	P (TREND, PLUNGE)	T (TR, PL)	B (TR, PL)
			GILES COUNTY			
12/20/80	85	340	-178	205, 5	295, 2	45, 85
	88	250	-5			
1/25/83	90	340	145	31, 24	289, 24	160, 55
	55	70	0			
5/26/83	30	180	-171	21, 42	147, 34	260, 30
	86	82	-60			
7/10/83	82	20	-174	245, 10	335, 1	70, 80
	84	290	-8			
12/9/83	64	206	164	73, 7	167, 29	330, 60
	76	303	27			
7/2/84	66	207	-147	67, 40	334, 3	240, 50
	60	102	-28			
6/10/85	35	44	0	14, 35	254, 35	134, 35
	90	314	125			
3/26/86	21	54	44	360, 29	212, 57	98, 15
	76	282	105			
			CENTRAL VIRGINIA			
8/4/80	60	111	55	225, 9	329, 58	130, 30
	45	346	135			
9/26/80	82	220	174	85, 1	175, 10	350, 80
	84	310	8			
2/11/81	67	346	117	56, 18	294, 58	155, 25
	35	113	42			
2/11/81	35	278	81	194, 10	41, 79	285, 5
	55	108	96			
1/18/82	79	346	136	43, 21	296, 38	155, 45
	47	86	15			
5/6/82	61	158	-8	119, 26	22, 14	265, 60
	83	252	-151			
6/25/82	42	316	129	199, 9	308, 63	105, 25
	59	89	60			
9/20/82	79	327	17	99, 3	191, 20	0, 70
	74	233	168			
8/10/83	45	333	-5	300, 33	191, 27	70, 45
	86	66	135			
8/17/84	59	335	16	288, 11	191, 33	35, 55
	76	236	148			
10/17/84	63	3	14	318, 10	222, 28	65, 60
	78	267	152			
12/10/86	30	151	80	69, 15	268, 74	160, 5
	60	343	96			
4/11/87	25	340	35	291, 28	152, 54	32, 20
	76	217	111			

EASTERN TENNESSEE

11/25/81	78	76	9	30, 3	300, 15	130, 75
	81	344	168			
9/24/82	64	284	16	237, 7	143, 29	340, 60
	76	187	153			
9/24/82	86	280	9	55, 3	145, 9	305, 80
	81	190	176			
1/18/83	74	78	-12	36, 20	304, 3	205, 70
	79	172	-163			
1/27/83	84	63	-35	14, 28	115, 19	235, 55
	56	157	-173			
4/5/83	78	318	28	88, 10	183, 28	340, 60
	63	222	166			
5/16/83	87	69	-20	23, 16	117, 11	240, 70
	70	161	-176			
5/25/83	85	287	-70	217, 46	359, 37	105, 20
	21	29	-167			
5/26/83	74	277	-53	226, 48	340, 20	85, 35
	40	27	-154			
7/8/83	63	293	31	60, 0	150, 40	330, 50
	63	187	149			
7/15/83	71	304	-7	261, 18	169, 8	55, 70
	83	36	-161			

NOTE: All entries (except date) in degrees.

Sign conventions for angles, according to Aki and Richards (1980, *Quantitative Seismology: Theory and Methods*, p. 106). The strike is the azimuth of the fault with the convention that if one faces down dip, the strike direction is to the left. The dip is measured down from the horizontal and is bounded by 0° and 90°. The rake angle (Θ) is measured within the fault plane and is bounded by -180° and +180° measured from the strike direction. If $0° < \Theta < +180°$ the fault is a **reverse fault or thrust fault**, and if $-180° < \Theta < 0°$, the fault is a **normal fault**. If $\Theta = +90°$ or $\Theta = -90°$, the fault is **dip-slip**. A **right-lateral** fault is one for which an observer standing on one side of the fault sees the block on the other side move to the right. If $\Theta = 0°$, the fault is **left-lateral strike-slip**, and if $\Theta = +180°$, the fault is **right-lateral strike-slip**. Herrmann (*Earthquake Notes*, 1975, vol. 46, pp. 29 - 39) includes a complete discussion about relationships among these different parameterizations.

TABLE 2. FOCAL MECHANISM SOLUTIONS - SUMMARY FOR VIRGINIA AND TENNESSEE.

Number of Solutions: 32 (1980 - 1987; M ≤ 4.2)

Agreement of data and theory: 96% of P wave polarities (9 / 203)
75% of SV/P ratios (42 / 165)
within a factor of 1.4 to 1.8

Average number of data points / solution: P = 203 / 32 = 6
SV/P = 165 / 32 = 5

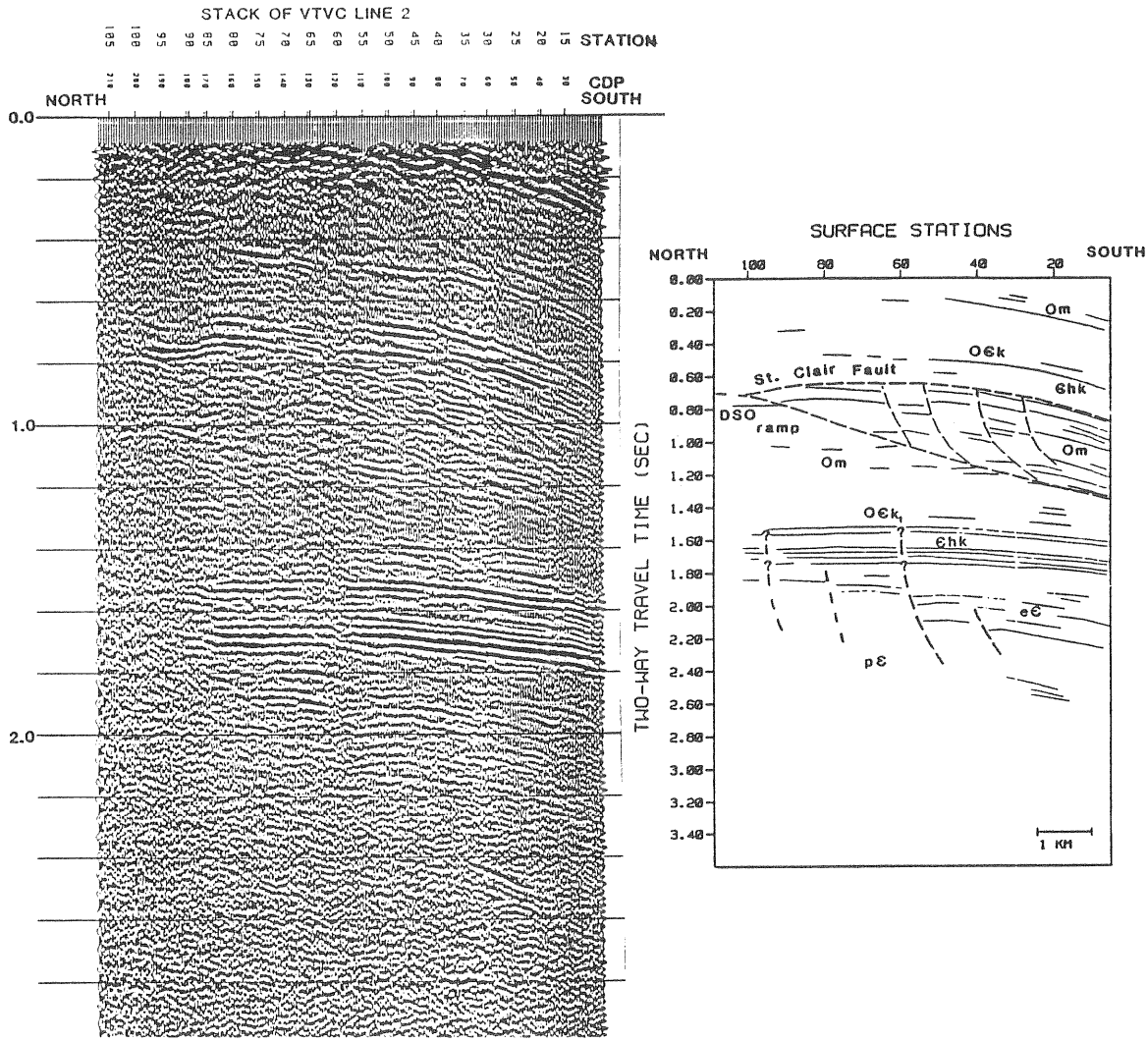

Figure 5. Reflection seismic (Vibroseis) section (left) and Line Drawing interpretation (right) for the structure in the Giles county, Virginia seismic zone according to Gresko (1985). Shows inferred basement (Precambrian) faulting at about 2 sec two-way travel time (approx. 6 km depth).

analysis and then 20 events for the ML calculations. For a cumulative plot (Log N_c vs m_{bLg}), which is the more useful form for seismic hazard considerations, the 'a' value changes from 0.76 to 0.94, which in turn implies an average recurrence interval of 200 years for the m_b 5.8 (or larger) 1897 shock. Normalizing for area (N_c per 10^4 km^2) to allow activity rate comparisons with other zones results in an a = 1.04.

THE EASTERN TENNESSEE SEISMIC ZONE

Epicentral Pattern.

Johnston and others [1985] have discussed the seismotectonics of this area in terms of results from seismic networks and potential field studies. As shown in Figure 6, the recent seismicity is in the form of a poorly defined, northeasterly trending distribution, some 200 km in length and 100 km in width. This zone has, for the past several years, been the most active in the southeastern U.S., both in terms of numbers and sizes of earthquake occurrences. For example, during the years 1985-1986, the southeastern U. S. experienced 157 earthquakes with $0.0 \leq m \leq 3.8$ and of those, 92 (59%) were in eastern Tennessee [see, e.g., Sibol and others, 1987]. Also, the largest event in the last two decades was the m_{bLg} = 4.6, Knoxville, Tennessee, shock in 1973. Johnston and others [1985] argue that the horizontal spatial control for the eastern Tennessee seismicity is provided by major, northeast trending, structural features in the basement that have been identified by potential field (aeromagnetic) analyses.

Focal Depth Distribution.

The vertical distribution of foci in eastern Tennessee is mostly sub-décollement and virtually identical with that in Giles County, Virginia. Johnston and others [1985] present a histogram for 58 well constrained focal depths that shows a range from 3 to 29 km, but with a concentration between 9 and 15 km; 90% of the foci are above 21 km.

Focal Mechanism Solutions.

Teague and Bollinger [1986] developed 11 single event focal mechanisms for the zone (Fig. 4). The earthquake faulting is predominately strike slip on northerly (right lateral; average strike = $1 \pm 25°$) and easterly (left lateral; average strike = $88 \pm 25°$) nodal planes; average dip = $71 \pm 16°$. The P axes are northeasterly and sub-horizontal: average trend = $41 \pm 21°$, average plunge = $18 \pm 17°$. A focal mechanism solution by Williams and others [1986] across the state line in North Carolina suggests the possibility of low angle reverse faulting; again with the P axis northeast and sub-horizontal. Recently, a precision aftershock study of a m_{bLg} 4.2 shock 50 km SSW of Knoxville (36^oN-84^oW) by Munsey and others [1987] defined a source zone with azimuth $N3^oE$ and with dimensions: 2.7 km long, 0.5 km wide and 3.2 km high, centered at a depth of 16.5 km. The 3X3 km area is larger than required by scaling relationships for a magnitude 4.2 shock in the region [Nuttli, written comm., 1987]. It is important to note here that the nodal plane and aftershock trends are northerly (and easterly) while the overall trend of the eastern Tennessee seismic zone is northeast. In Giles County, some 250 km along strike to the northeast, both the zone and the nodal planes trend north-northeasterly to northeasterly.

Reflection Seismic Results.

The regional Vibroseis profiling for the Appalachian ultra-deep core hole site study approaches to within 50 km of this zone on the southeast (in North Carolina). Those profiles image Eocambrian-Cambrian (?) rift basins in the Grenville basement [Coruh and others, 1987b] similar to those found by Gresko [1985] in Giles County, Virginia.

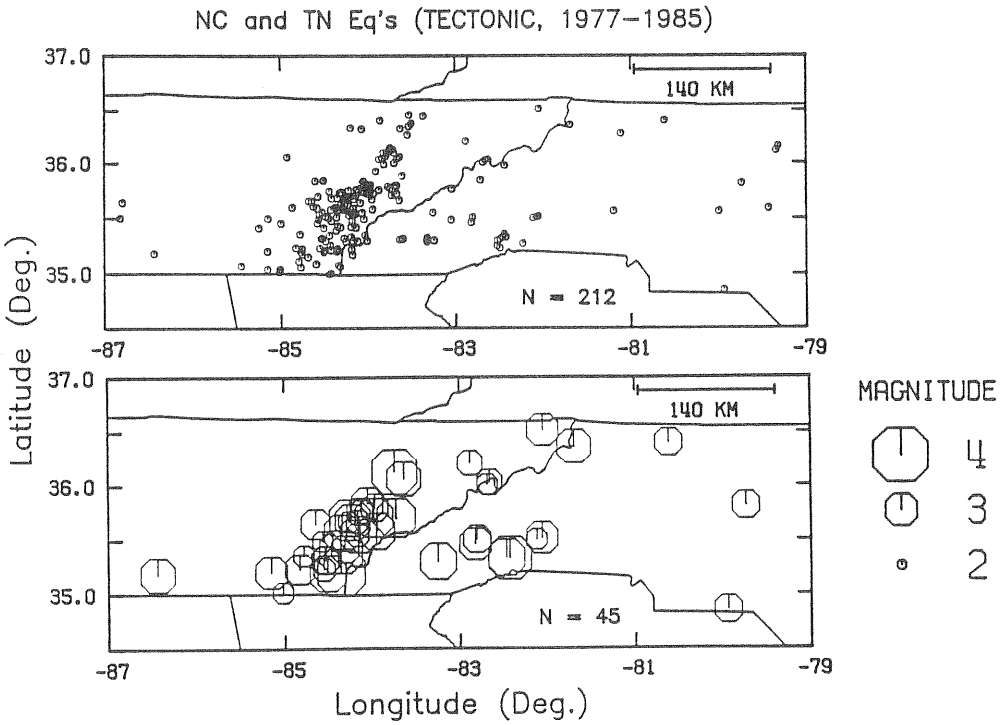

Figure 6. Epicenter Map for eastern Tennessee and western North Carolina. **Upper :** All earthquake (circles) with magnitude ≥ 0 ; **Lower :** All earthquakes (octagons) with magnitude ≥ 2. N = number of epicenters plotted.

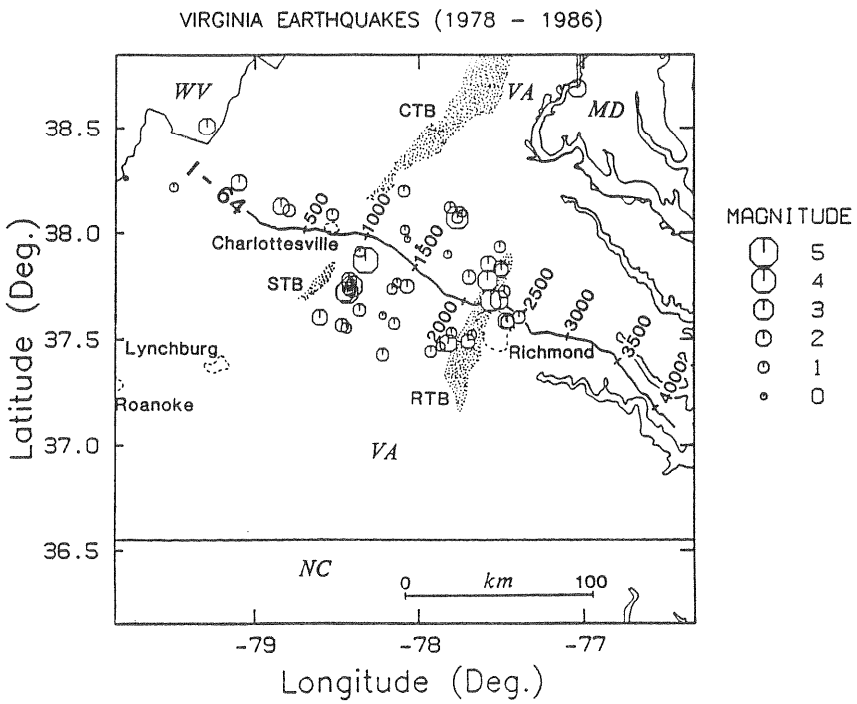

Figure 7. Central Virginia seismic zone. Epicenters (octagons) for the period 1978 - 1986. The I-64 seismic reflection profile (heavy line), profile station numbers (1 - 4000+) and locations of the Richmond (RTB), Scottsville (STB) and Culpeper (CTB) Triassic basins are shown. City outlines shown as dashed lines. (From : Coruh and others, 1987).

Magnitude Recurrence Relations.

The Bollinger and Davison [1987] equation for eastern Tennessee is,

$$\text{Log } N_I = (2.69 \pm 0.16) - (0.88 \pm 0.049)\ m_{bLg}\ ,$$

where the modest standard deviations result from 273 earthquakes used as input to the Stepps [1972] analysis and 102 earthquakes input to the ML analysis. Activity parameter 'a' values are 2.67 for N_c and 2.01 for N_c / 10^4 km^2 (45,200 km^2 ; 120 km radius about the center of the zone). Recurrence time for a $m_{bLg} \geq 5.8$ is 272 years, slightly longer than the 203 years for Giles County, Virginia.

THE CENTRAL VIRGINIA SEISMIC ZONE

Epicentral Pattern.

Bollinger and Sibol [1985] presented a detailed review of the seismicity of this unique seismic zone - unique in the fact that it is a spatially isolated, diffuse distribution of epicenters with a roughly circular (diameter $\cong$ 100 km) map view (Fig. 2). The width of the zone is about equal to, and coincident with, the width of the exposed Mesozoic rift basins and many of the focal mechanism nodal planes (see below) are generally consistent in strike and dip with the Mesozoic dikes in the area [Munsey and Bollinger, 1985]. The historical, pre-instrumental seismicity [Bollinger, 1973, Hadley and Devine, 1974] had revealed the existence and persistent nature of this seismic energy release in the Piedmont of central Virginia. However, it took the instrumental results from a modern network of seismographs to confirm its diffuse nature and then to define its roughly circular configuration. That symmetrical epicenter pattern may be fortuitous.

Focal Depth Distribution.

In contrast with the Appalachian zones, the central Virginia earthquake foci occur mostly **above** a detachment surface (Figs. 3 and 8). The focal depth range is from about 4 km to 16 km. The mean depth (foci with standard errors $\leq$ 5 km) is 8 km and 90% of the depths are at 13 km or less. It is important to note here that the surface rocks of the Piedmont are crystalline 'basement', i.e., they are mostly Cambrian and Precambrian igneous and metamorphic rocks.

Focal Mechanism Solutions.

Thirteen single-event mechanisms (of which 11 are shown in Fig. 4) exhibit both strike-slip and dip-slip modes of faulting on a range of nodal plane orientations. Those orientations are - average strikes: north-northwesterly (334 $\pm$ 20°) and east-northeasterly (81 $\pm$ 32°); average dip: 61 $\pm$ 18°. The P axes exhibit a bimodal distribution based on focal depth. For depths of 3 to 7 km , the average trend is northeasterly, 47 $\pm$ 26° with an average plunge of 12 $\pm$ 7°, while for depths of 8 to 13 km, those figures are northwesterly, 296 $\pm$ 13° and 18 $\pm$ 12°, respectively. That apparent division, at an 8 km depth, is in the vicinity of a décollement in the area which Pratt and others [1987] and Coruh and others [1987a] place at about 12 km on the west (near Scottsville, Virginia, see Fig. 7) shallowing to 4-5 km on the east (near Richmond, Virginia; see Fig. 7). That structural feature may be acting in some sort of a de-coupling role.

Reflection Seismic Studies.

Pratt [1986] studied a reflection seismic profile along Interstate 64 in Virginia that essentially bisects the central Virginia seismic zone (Fig. 7). Those data provided an exceptional opportunity to correlate earthquake foci with seismic reflection data. Using Pratt's reprocessed data, subsequent studies by Coruh and others [1987a] have provided an eastern U. S. example of the relationship between reflection seismic images and earthquake foci (Fig. 8). The distribution of

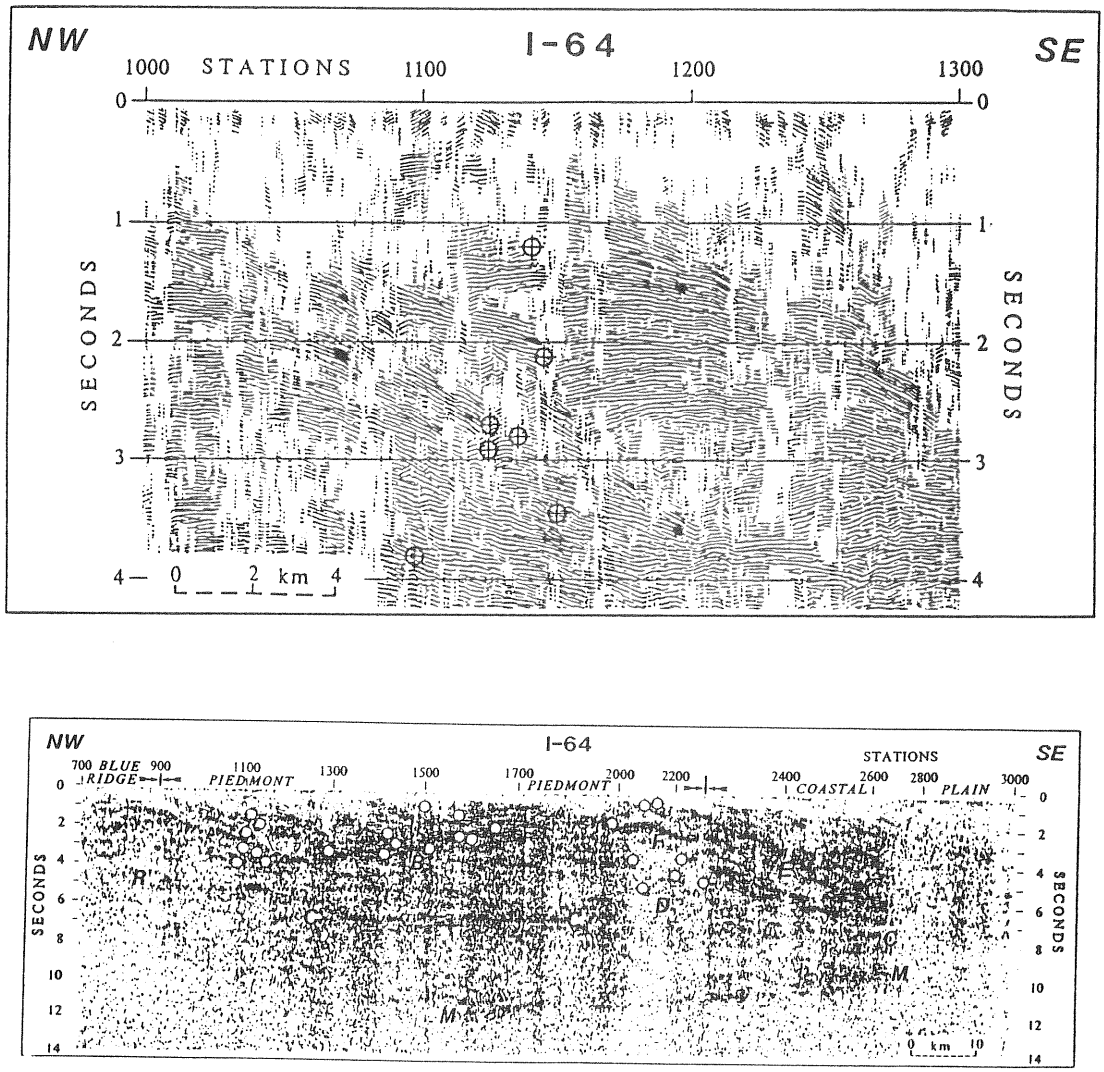

Figure 8. Automatic Line Drawing (ALD) analyses of the I-64 seismic reflection data from the central Virginia seismic zone (Coruh and others, 1987). **Upper :** Expanded version, between stations 1000 and 1300 (cf. Fig 7), from the western portion of the zone where the hypocenters exhibit a vertical alignment. The westward and eastward dipping reflection groups between 1.0 and 3.0 sec (two-way travel time) are interpreted as indicating a steeply dipping fault or faults. Waveform correlations (not visible at the scale of this figure) suggest reverse faulting - as was observed in the focal mechanism solutions (cf. Fig. 4). **Lower :** ALD analyses for the I-64 reflection profile over the Blue Ridge, Piedmont, and Coastal Plain (stations 700 - 3000 ; cf. Fig. 7). Hypocenters shown as white dots ; note their correlation with an undulating group of reflections between 1 and 4 sec on the west and with a vertical, low reflectivity zone (stations 2000+ - 2250) on the east. The undulating group of reflections is interpreted to be the southern Appalachian decollement and the low reflectivity zone a vertical dike swarm. From : Coruh and others, 1987).

hypocenters in the western portion of the seismic zone is mostly above the roof of an antiformal / synformal structure that is bounded by mid-crustal reflections on the bottom and by major thrusts (décollements) on the top. The hypocenters in the eastern portion of the seismic zone near Richmond are the deepest and are interpreted to be related to an extensive vertical dike swarm there marked by a vertical band of relative absence of reflections. This model suggests that the seismicity in the central Virginia seismic zone is due to reactivation of steeply dipping faults (to give the dips required by the focal mechanisms (Fig 4) and imaged by the seismic reflections (Fig. 8)) above the main thrust feature on the west and steeply dipping fractures / density discontinuities associated with a vertical dike swarm on the east.

Magnitude Recurrence Relations.

For central Virginia, Bollinger and Davison [1987] give,

$$\text{Log } N_I = (0.88 \pm 0.12) - (0.55 \pm 0.070)\, m_{bLg} \cdot$$

Input to the Stepp's [1972] completeness analysis was 100 earthquakes and to the ML analysis, 65 earthquakes. Activity parameter 'a' values are 1.07 for N_c and 0.57 for N_c / 10^4 km^2 (31,400 km^2; 100 km radius about the center of the zone). The recurrence time for a repeat of the $m_b = 5$ (or larger) shock of 1875 is given as 48 years and for a $m_b = 5.8$ (or larger) Giles County size earthquake, 132 years. It is now 112 years since the 1875 earthquake; the Poisson probability for that duration including a repeat event is 90%. The average recurrence time for the $m_b = 5.8$ event is roughly half (49% and 65%) of what it is for the Appalachian zones (that have such an event in their seismic history) but require extrapolation for the central Virginia zone.

SUMMARY

Three-Dimensional Geometry of the Zones.

The two Appalachian zones tend to be somewhat concentrated in a northeasterly direction and surrounded by a diffuse cloud of low energy level 'satellite' activity. The seismogenic crust, as defined by the 90% seismic activity depth, is 20 km thick. The central Virginia zone shows no tendency to develop any lineations, but rather takes the form of an isolated, coin-shaped volume some 100 km in diameter. Release of seismic energy is primarily above principal décollements in a seismogenic crust some 13 km in thickness. The mean focal depths for all three zones (Giles County = 11 km; eastern Tennessee = 14 km; central Virginia = 8 km) are statistically different by the Wilcoxon Rank Sum Test at a p-value < 0.05.

Mechanics of the Zones.

Thirty-two single event focal mechanism solutions indicate a remarkably uniform maximum compressive stress (P axes) throughout the area that is oriented northeasterly (average trends = 37-47°) and sub-horizontal (average plunges = 18-26°). The single exception is for deeper (8-13 km) shocks in central Virginia where the average trend is 296° and the average plunge is 18°. The reason for the bimodal P axis distribution is unknown. It occurs in the vicinity of major décollements and may be related to those structural discontinuities. Bollinger and others [1985] point out that differences in strain rate and / or composition are also involved in this problem.

The seismic response to the regional stress field is slippage on planes with a tendency to be steep (average dips = 61-68°) and northerly (average strikes = 334-16°) or easterly (average strikes = 81-99°) in orientation. Such orientations are expectable given the northeasterly compressive stress found in the area.

The basic geologic model that emerges is one of reactivation of ancestral rift structures; Eocambrian - Cambrian (?) in age in the Appalachian zones and of Mesozoic age in central

Virginia.

Temporal Characteristics of the Zones.

Recurrence relations indicate that the average return times for larger shocks, $m_b \geq 5$ is shortest for the central Virginia zone and longest for the eastern Tennessee zone. This is somewhat surprising in that the earthquake history for the region has the larger shocks occurring in the Appalachian zones. Both the activity parameter 'a' and the slope 'b', in Log N = a - bm, normalized for area, are largest for eastern Tennessee and smallest for central Virginia. That combination suggests that eastern Tennessee has the highest level of seismicity with proportionally more small earthquakes, while central Virginia has the lowest activity but with a lower proportion of smaller to larger shocks. The activity in the Giles County zone is between those two levels. It is important to emphasize here that these are **average** characteristics within the context of the model employed, i.e., Log N = a - bm is applicable with 'a' and 'b' being constant, positive parameters. Finally, while the standard deviations associated with the 'a' and 'b' parameters are modest, they are founded on a combination of both historical and modern network data bases.

ACKNOWLEDGMENTS

Thanks are extended to J. A. Snoke, J. K. Costain and C. Coruh for their critical reading of this manuscript. This research was supported in part by the Nuclear Regulatory Commission under NRC-04-85-121.

REFERENCES

Bollinger, G. A., Seismicity of the southeastern United States, Bull. Seismol. Soc. Am., vol. 63, 1785-1808 (see also Errata, vol. 64, 733-734), 1973,

Bollinger, G. A., and R. L. Wheeler, The Giles County, Virginia, seismogenic zone - Seismological results and geological interpretations, U. S. Geol. Surv. Open File Rep 82-585, 95 pp., 1982.

Bollinger, G. A., and R. L. Wheeler, The Giles County, Virginia, seismic zone, Science, vol. 219, 1063-1065, 1983.

Bollinger, G. A., and M. S. Sibol, Seismicity, seismic reflection studies, gravity and geology of the central Virginia seismic zone: Part 1. Seismicity, Geol. Soc. Am. Bull., vol. 96, 49-57, 1985.

Bollinger, G. A., M. C. Chapman, M. S. Sibol, and J. K. Costain, An analysis of earthquake focal depths in the southeastern U. S., Geophys. Res. Lett., vol. 12, 785-788, 1985.

Bollinger, G. A., and Frederick C. Davison, Magnitude recurrence relations for the southeastern U. S. - Preliminary results, Seismol. Res. Lett.,vol. 58, in press (Abstract - presented at 59th ann. mtg., St. Louis, Mo., Oct. 7-9, 1987), 1987.

Bollinger, G. A., Arch C. Johnston, Pradeep Talwani, Leland T. Long, Kaye M. Shedlock, M.S. Sibol, and M. C. Chapman, Seismicity of the southeastern United States - 1698 to 1986, Geol. Soc. Am. DNAG Series, in review, 1987.

Coruh, Cahit, G. A. Bollinger, and J. K. Costain, Seismogenic structures in the central Virginia seismic zone, Geology, in review, 1987a.

Coruh, Cahit, J. K. Costain, R. D. Hatcher, Jr., T. L. Pratt, R. T. Williams, and R. A. Phinney, Results from regional Vibroseis profiling: Appalachian ultra-deep core hole site study, Geophys. J. R. Astron. Soc., vol. 89, 147-156, 1987b.

Gresko, Mark J., Analysis and interpretation of compressional (P wave) and shear (SH wave) reflection seismic and geologic data over the Bane dome, Giles County, Virginia, PhD Dissertn., 74 p., Va. Poly. Inst. & St. Univ., 1985.

Gresko, M. J., J. W. Munsey, and G.A. Bollinger, Structure of the Giles County, Virginia seismogenic zone interpreted from seismic reflection data, EOS, vol. 66, p. 974, 1985

Hadley, J. B., and J. F. Devine, Seismotectonic Map of the Eastern United States, U.S.Geol. Surv. MF-620, 1974.

Johnston, Arch C., D. J. Reinbold, and S. I. Brewer, Seismotectonics of the southern Appalachians, Bull. Seismol. Soc. Am., vol .75, 291-312, 1985.

Munsey, J. W., and G. A. Bollinger, Focal mechanism analyses for Virginia earthquakes (1978 - 1984), Bull. Seismol. Soc. Am., vol. 75, 1613-1636, 1985.

Munsey, J. W., S. J. Nava, and A. C. Johnston, The m_{bLg} 4.2 Vonore, Tennessee earthquake of 27 March 1987 aftershock sequence: a 3 X 3 km source area, Seismol. Res. Lett., vol. 58, in press. (Abstr. presented at 59th ann. mtg., St. Louis, Mo., Oct. 7-9,1987).

Pratt, Thomas L., A geophysical study of the earth's crust in central Virginia with implications for lower crustal reflections and Appalachian crustal structure, PhD Dissertn, Va. Poly. Inst. & St. Univ., 62 p., 1986.

Pratt, Thomas L., C. Coruh, J. K Costain, and L. Glover III, A geophysical study of the earth's crust in central Virgina: Implications for Appalachian crustal structure, J. Geophys. Res., in press, 1987.

Sibol, M. S., G. A. Bollinger, and E. C. Mathena, Seismicity of the southestern U. S., July 1, 1986 - December 31, 1986, Southeastern U. S. Seism. Network Bull. No. 19, 64 p, 1987.

Snoke, J. A., J. W. Munsey, A. G. Teague, and G. A. Bollinger, A program for focal mechanism determination by combined use of polarity and SV-P amplitude ratio data, Earthquake Notes, vol. 55, 15, 1985 (Abstr.)

Stepp, J. C., Analysis of the completeness of the earthquake hazard sample in the Puget Sound area and its effect on statistical estimates of earthquake hazard, Proc. Intl. Conf. Microztn. for Safer Construct. Res. Appl., vol. 2, Seattle, WA, 897-909, 1972.

Teague, Alan G., G. A. Bollinger, and Arch C. Johnston, Focal mechanism analyses for eastern Tennessee earthquakes (1981 - 1983), Bull. Seismol. Soc. Am., vol. 76, 95-105, 1986.

Weichert, D. H., Estimations of the earthquake recurrence parameters for unequal observation periods for different magnitudes, Bull. Seismol. Soc. Am., vol. 70, 1337-1346, 1980.

Williams, R. L., Pradeep Talwani, and A. C. Johnston, Seismicity and focal mechanisms in the Great Smoky Mountains, Earthquake Notes, vol.. 57, 106, 1986. (Abstr.)

ESTIMATING MAXIMUM EARTHQUAKES IN THE CENTRAL AND EASTERN UNITED STATES:

A PROGRESS REPORT

K.J. Coppersmith
Geomatrix Consultants
One Market Plaza
San Francisco, California 94105

A.C. Johnston
Center for Earthquake Research
Memphis State University
Memphis, Tennessee 38152

W.J. Arabasz
Department of Geology and Geophysics
Salt Lake City, Utah 84112

INTRODUCTION

This paper summarizes the results of an ongoing study [Coppersmith, et al., 1987] sponsored by the Electric Power Research Institute to develop scientifically-supportable methods for assessing maximum earthquakes in the central and eastern United States (CEUS). The study will be completed in mid-1988.

Maximum earthquake estimates are made typically for seismic hazard assessments, which lead to a characterization of expected seismic shaking at a site or region of interest. Because of the need for *site-specific* hazard predictions, we attempt to establish the expected largest event that may be generated by a particular seismic source. The kinds of seismic sources that are identified typi-cally in the central and eastern United States for hazards assessments include tectonic provinces, seismicity zones, and tectonic features. Unlike the western United States or other interplate regions, rarely are the causative geologic structures known active faults. Therefore, approaches that assume a knowledge of the seismogenic fault or details of its behavior will not be generally applicable in the East. For example, maximum earthquakes associated with active faults in the western United States are estimated typically on the basis of evaluations of the total length, rupture length, rupture area, coseismic displacement per event, etc. These parameters have been empirically correlated with earthquake magnitude so that an estimate of the parameter value provides the expected magnitude associated with it. The data that provide the basis for these relationships are almost entirely plate boundary-related earthquakes, thus their applicability to the CEUS is limited. Indeed, unless a CEUS seismic source can be defined as a fault, the relationships are essentially useless. As a consequence, appropriate methods for the CEUS must be based on the types

of data that are generally available such as historical seismicity, regional tectonics, etc.

Maximum earthquakes have been estimated in the CEUS primarily from the seismicity record because seismicity data are commonly available for identified source zones – not because of a general acknowledgement that seismicity-based methods are scientifically supportable. All such methods suffer from the possibility that the observational record is not sufficiently long to have captured the max-imum event or to provide an adequate basis for extrapolating to the maximum event. It is generally acknowledged that recurrence intervals for large events are much longer within intraplate regions than elsewhere. This is supported by recent comparisons of seismic moment release rates in the eastern and western United States [Anderson, 1986]. However, recurrence rates developed locally for the more active seismicity zones (such as New Madrid, La Malbaie, and Charleston), are very similar to those within interplate sources (i.e., hundreds to few thousand years). Therefore, for these sources at least, there is a higher likelihood that the historical record places meaningful constraints on the maximum earthquake.

The importance of maximum earthquake estimates varies considerably as a function of the type of seismic hazard assessment being made as well as details of the seismic source being considered. Deterministic hazard approaches that consider only the occurrence of the maximum-size earthquake are, of course, very sensitive to the choice of maximum earthquake. Probabilistic hazard estimates, which consider the frequency of occurrence of all earthquakes up to the maximum on perhaps several sources, vary in their sensitivity to the maximum event as a function of the source-to-site distance and the ground motion period of interest [Youngs and Coppersmith, 1985]. At large source-to-site distances or longer period ground motions, the hazard values are more sensitive to the choice of maximum earthquake. At small distances and shorter periods, the smaller magnitude earthquakes tend to contribute most to the hazard and the results become relatively insensitive to the choice of maximum magnitude.

Because estimation of maximum earthquakes is a prediction of the unknown future behavior of a seismic source, it is uncertain. Uncertainties lie in both the choice of methods to arrive at maximum earthquake estimates and the parameters required to use the methods. It is important, then, to capture this uncertainty when arriving at estimates to be used in a seismic hazard analysis. One approach is to define a range or distribution of values that reflects the confidence given to any particular value within the range. Simple subjective probability structures, such as logic trees [e.g., Coppersmith and Youngs, 1986] can provide a framework for specifying the maximum earthquake distribution. In any case, the uncertainty in the estimate should be clearly represented and propagated through the hazard analysis.

The following discussion summarizes the methods that are currently used to estimate maximum earthquakes and those methods

that are under development. First, seismologically-based methods are considered, followed by approaches related to the global earthquake data base. The latter are under development for the present study. The various methods considered are summarized in Table 1 by the data required to implement them and the limitations associated with each.

METHODS BASED ON SEISMOLOGICAL/ANALYTICAL APPROACHES

Approaches to using seismological information for estimating a maximum magnitude for a seismic source involve: 1) addition of an increment to the size of the maximum historical event, 2) extrapolation of a magnitude-recurrence curve to some specified long period of time, 3) statistical treatment of the earthquake record to assess the likelihood of a maximum event, 4) estimation of maximum seismic moment (or equivalent magnitude) from strain rate or from the long-term rate of moment release in a region, and 5) use of well-resolved seismicity information to constrain rupture dimensions on a specific structure.

Historical Seismicity Record

Estimating maximum earthquakes by the addition of an increment to the size of the largest historical event in a seismic source has become commonplace in the central and eastern United States. The associated logic is straightforward. In a domain characterized by long inter-event times for large earthquakes, the largest historical event in most source zones will generally represent the minimum size for the maximum earthquake [McGuire, 1977; Chinnery, 1979]. The addition of some increment to the maximum historical size can be viewed as an extension of the sample period. Accordingly, say for b = -0.9, an increment of 0.5 units of magnitude is equivalent to multiplying the sample time by 3.2 and for an increment of 1.0, multiplying the sample time by 7.9. One then needs to justify the reasonable length of time during which the maximum event might be expected.

Linear extrapolation of recurrence curves based on instrumental and/or historical seismicity raises the issue of appropriate recurrence modeling of the largest earthquakes in a seismic region. Nonlinearity between recurrence of background seismicity and large "characteristic" earthquakes in some domains is now well documented [Wesnousky, and others, 1983; Schwartz and Coppersmith, 1984; Youngs and Coppersmith, 1985; Davison and Scholz, 1985].

Intuitively, inspection of characteristic earthquake recurrence relationships suggests that some rationale might be developed for estimating the maximum event in terms of some incremental relation to observed seismicity. The magnitude increment, however, must be measured on some horizontal baseline corresponding to a specified level either of cumulative number or frequency of occurrence. *A priori* specification of that level is clearly difficult. If the approximate recurrence interval of maximum-size events were known--say, from some reasonable approximation of the recurrence interval for significant faulting (with or without surface rupture)--one might argue that the maximum event appears to be about

TABLE 1

SCI MAXIMUM EARTHQUAKE ESTIMATION METHODS*

Method	Data Required	Limitations
1. Addition of increment to largest historical magnitude (usually 1/4 to 1/2 magnitude units).	- Historical seismicity data - Assessment of the association of seismicity with seismic source	- Usually short historical record - Uncertainties in recurrence models
2. Extrapolation of frequency - magnitude curves.	- Earthquake recurrence data from historical/instrumental data - Area of seismic source being evaluated	- Reliant on recurrence data and associated data base - Calibrated only to Charleston and New Madrid regions
3. Statistical (extreme-value) treatment of seismicity data	- Seismicity catalog - Assumed model of earthquake occurrence (e.g., Poisson, exponential magnitude distribution)	- Historical record provides very poor statistical constraints on largest earthquakes.
4. Strain rate/moment rate	- Strain rate over region or seismic source - Recurrence (frequency - magnitude) relationships	- Strain rates poorly constrained in SCI - Recurrence relationships subject to short period of record
5. Maximum seismic source dimensions	- Inferred dimensions from seismicity data - Other evidence for source dimensions (geologic, strain volumes, etc.)	- SCI seismicity data usually define seismic sources poorly - SCI scaling relations between dimensions and magnitude are subject of current debate.
6. Analogy to other SCI areas in global data base	- Global data base of large SCI earthquakes - Correlation of SCI earthquake sizes with seismic source characteristics	- Must characterize seismic source for use of data base

*Included are various methods for assessing the maximum earthquake for a seismic source that lies within a stable continental interior (SCI) region.

one magnitude unit to the right of the extrapolated recurrence curve. That is, for data at least from the Wasatch and San Andreas faults [Schwartz and Coppersmith, 1984] and from the Aleutians [Davison and Scholz, 1985], the size of the characteristic event might be reasonably approximated given the recurrence curve for background seismicity. Again, however, one needs to know the approximate recurrence interval for the maximum-size event.

Extrapolation of Frequency-Magnitude Curves

Nuttli (1981) has developed the logic and basis for extrapolation of frequency-magnitude curves to estimate the maximum size event for a seismically active region. He hypothesized that the maximum-magnitude earthquake in a region may be estimated by extrapolating the frequency-magnitude curve to an annual probability of occurrence of 0.001 (1,000-yr recurrence) for normalized areas of 30,000 km^2 or 100,000 km^2. The size of the 1,000-yr event for both the New Madrid and Charleston areas approximately equals that of the largest historical event in the respective seismic zones. The areas of normalization forming part of Nuttli's [1981] working hypothesis are based on the approximate sizes of the Charleston and New Madrid source zones.

Statistical Approaches

Chinnery [1979] reviewed earlier attempts in the international literature to use statistical approaches for estimating maximum earthquakes from earthquake catalogs. Beyond the varied use of frequency-magnitude curves, another general approach involves the use of extreme-value theory [e.g., Yegulalp and Kuo, 1974; Kijko, 1984] in which it is assumed that the occurrence of a maximum earthquake within a certain time interval is a random independent event and that maximum earthquakes in the future will behave similarly to the past observational period.

Fundamental problems with extreme-value theory as applied to earthquake occurrence seem to be that the quality of the data set is critical, assumptions are critical, and application of the theory to simulated data sets gives unacceptably large probable errors [e.g., Knopoff and Kagan, 1977]. Given critical dependence on the largest values in the data set in defined time intervals, the reliability of those largest values is also critical, and magnitude uncertainties have a recognized effect on the entire statistical analysis [Tinti and Mulargia, 1985]. For the general problem of estimating maximum earthquake magnitude based on a set of observed magnitudes, there seems to be evolving consensus that large data sets are needed for estimating the maximum size with any confidence. For sparse data sets, as those typical for subset regions (i.e., seismic sources) of the central and eastern United States, statistical confidence in estimating a maximum event is low.

The estimation of the maximum event size for seismic sources on the basis of a maximum-likelihood analysis of the earthquake record has been discussed by McGuire [1977]. He concludes that the earthquake record for the eastern United States is not adequate to

define with any confidence the maximum possible event size for a given seismic source.

Use of Strain Rate or Rate of Moment Release

Because seismic moment is fundamentally related to the average dislocation or average slip on a fault surface, seismologists have recognized that rates of fault slip, moment release, and strain accumulation can be related analytically for individual faults as well as deformational volumes [e.g., Brune, 1968; Kostrov, 1974; Molnar, 1983]. A. McGarr et al. [1987] have outlined an approach that is potentially applicable to the central and eastern United States for estimating the maximum moment for a seismic volume.

A similar analytical approach for estimating the maximum moment for a region has been outlined by Joyner and Fumal [1985]. In the latter case, implications of using conventional magnitude-frequency relations are compared to use of an independent model for estimating ground-motion values that will be exceeded at a specified annual rate. The obvious problems associated with these approaches stem from the uncertainties associated with estimating strain rates in the East. It is expected that this type of data will become more available in the future [e.g., Anderson, 1986].

Dimensional Arguments from Seismicity

A persistent thesis in this study has been that approaches based on a knowledge of specific seismogenic faults (e.g., fault length, rupture area, coseismic displacement) are not generally applicable for estimating maximum earthquake size in the central and eastern United States. Nevertheless, well-resolved seismicity might in some cases be applicable for assessing the maximum length or area of a fault source, which might then be empirically related to expectable earthquake size. Here also concepts related to fault-zone segmentation and possible constraints on total rupture area could be applied, as they are for faults in the western U.S.

METHODS BASED ON GLOBAL DATA BASE

The most common methods for estimating maximum earthquakes in the central and eastern United States are based on seismicity data, as discussed above. The chief weakness of these approaches is the generally short time period of historical observation. One way to overcome this problem is to substitute space for time to make the historical record more meaningful. To do this, one can expand the region of data collection beyond the central and eastern United States to other parts of the world that are analogous in terms of geologic and tectonic characteristics important to the earthquake process.

The present study for EPRI builds on this space for time substitution to allow utilization of a global earthquake data base. The first phase of the study had the following objectives:

- Development of a working definition of "stable continental crust" subject to the restriction that the defined regions must be geologically and tectonically similar to

North America east of the Cordilleran thrust and fold belt.

- Preparation of maps of the regions of the world that are analogous to stable North America. Within these zones the upper crust is classified so far as possible in terms of age, stress regime and principal tectonic features.

- From all available sources, compilation of a listing of large or significant earthquakes that have occurred within the global analogue regions.

- Characterization of each earthquake for which information is available with regard to source dimension, type of faulting, focal depth, stress drop, and correlation with crustal parameters such as age, stress regime, background seismicity and tectonic features.

- Development of a bibliography of the most current and authoritative sources for both the geologic/tectonic setting and the seismicity compilation.

Our focus is on the identification of factors that control or limit the maximum size of stable continental interior (SCI) earthquakes. (The definition of SCI seismicity is more restrictive than "intraplate"--see below). Our approach is first to delimit explicitly the study regions and then systematically examine the larger earthquakes that have occurred within them.

Criteria for Eastern North America Analogue Regions

Because terms such as "intraplate" are loosely defined, a more restrictive definition was necessary. The guiding principle adopted was that a candidate area had to be tectonically and geologically similar or analogous to the North American continent east of the eastern margin of the Rocky Mountain Cordillera. While restrictive, this guideline still admits a wide range of tectonic environments including Archean and Proterozoic shields, continental platforms, Paleozoic orogenic belts (in places overprinting or overthrusting more ancient crust), Paleozoic or older accreted terranes, passive continental margins, continental shelves and slopes, and attenuated continental crust. Intracontinental rifting and zones of intrusive/extrusive igneous activity (anorogenic processes) present in the study area are no younger than Eocene. The Gulf Coastal Plain, part of the study area, may not even be continental but rather consists of transitional or oceanic crust.

With application of the above guidelines, the term "intraplate" was suitably replaced by "stable continental crust" for the purposes of this study.

Definition. A region is to be considered a stable continental analogue to eastern North America (ENA) if:

- It is continental crust (including shelves, slopes and attenuated continental crust)

- It exhibits no deformation associated with early Mesozoic to Cenozoic orogenic belts

- Zones of rifting or volcanism younger than early Cenozoic are excluded.

The above criteria for ENA analogue areas are based mainly but not entirely on age of crystalline basement. The ENA study area encompasses no orogenic belts younger than Paleozoic/early Mesozoic (we exclude the Innuitian orogeny of the Canadian Arctic) but does contain:

- Magmatism of Mesozoic to early Cenozoic age, e.g., the Monteregian Hills of New England [Fairbairn et al., 1963; King, 1977], the Eocene intrusives of West Virginia [Dennison and Johnson, 1971], the Cretaceous-to-Eocene plutons flanking Reelfoot Rift [Ervin and McGinnis, 1975] or the ~ Eocene extrusives of the western Greenland coast [King, 1969].

- Zones of Neogene-to-present epeirogenic uplift or subsidence.

- Crust that is possibly transitional between continental and oceanic (the Gulf Coastal Plain).

- A late-Paleozoic to mid-Mesozoic passive margin, with younger intrusives (the Atlantic Coastal Plain).

Thus ENA is "stable" since the Paleozoic only in the sense that large portions of the region have not been subjected to major Mesozoic/Cenozoic tectonic activity. Therefore, minor-scale magmatic activity or epeirogenic movement do not automatically disqualify a global region from being analogous to stable ENA.

Seismicity Data Compilation and Analysis

Once a definition of SCI regions had been developed, a seismicity data base was constructed containing information on the larger earthquakes ($M \geq 5$, $MMI_o \geq$ VIII) that have occurred in these regions. A full discussion of this data base is given in Coppersmith et al. [1987] and is only briefly summarized here.

The total data consists of over 400 events and each of these events has been evaluated according to a number of characteristics. There are two categories: a) those parameters that provide information on the earthquake's source processes and b) those that provide information on its geologic and tectonic setting.

- (a) Source Dimension estimated from:
  - S — spectra, geodetic, or waveform modeling
  - F — observed surface faulting
  - A — aftershocks

- (a) Focal Depth estimated from:
  - L — local network data or waveform modeling
  - R — regional network data
  - H — teleseismically determined hypocenter (depth not restricted)
  - A — depth of aftershocks

- (a) Type of Faulting estimated from:
  - M — published focal mechanism
  - F — observed surface faulting
  - O — other, e.g., inferred from other events on same feature

- (a) Source parameters, i.e., stress drop or seismic moment, estimated from:
  - S — spectra, waveform modeling
  - O — other, e.g., field observations

- (a) Elevated Prior Seismicity:
  - H — historical
  - I — instrumental
  - O — other (inferred from measured elevated background subsequent to the event, e.g., New Madrid, Charlevoix, San Juan, Argentina)

- (b) Crustal Age of last major tectonic activity in the region:
  - B — estimated from base maps
  - L — published literature value

- (b) Stress Regime estimated from:
  - M — focal mechanism
  - L — published literature for that location
  - O — other (inferred from other data)

- (b) Association with tectonic feature estimated from:
  - B — base map
  - L — reported in literature

  Primary features considered are:
  - — Continental rifts (Cenozoic, Mesozoic, Paleozoic, Precambrian)
  - — Continental margins (coast out to slope/continental rise)
  - — Suture zones/pre-Mesozoic orogenic belts
  - — Faults/Block boundaries/lineaments
  - — Plateau basalts/extrusives
  - — Plutons/intrusives
  - — Intersecting features
  - — Foreland basins of orogenic belts
  - — Grabens/Basins (Passive margins)
  - — Folding/Uplift (Mesozoic/Cenozoic)
  - — Other

In each case, a judgement was made whether (a) data were available, (b) if the data were available, the value of each parameter, and (c) a level of confidence in the value assigned.

The problems that arose in the compilation effort included: wide variations in the availability and quality of catalogs, uncertainties in the completeness of earthquake reporting spatially and as a function of time, and, most importantly, serious deficiencies in the level of documentation for many events. For example, nearly all of the data for pre-1800 historical events have not been subject to authoritative documentation and are included in the compilation merely as catalog listings. Fortunately, we are concerned most with the largest events, and there is a better chance that these events will be documented than smaller magnitude seismicity. Experience with the data base suggests that it is unlikely that a great SCI earthquake has gone undocumented in the period since 1800 on a global basis, and for several centuries longer than that in some areas such has China and Europe.

The size of the largest observed magnitudes and the number of large events do not appear to be equal continent to continent. As summarized in Table 2, only five events qualify as great earthquakes ($M \geq 8$) and fewer than twenty events have been larger than M_s 7. Most of these events have occurred in eastern North America. Some large stable continental regions have not experienced earthquakes as large as 7: South America (M 6.8), Antarctica (m_b 5.1), Asia (M_L 5.8), and Europe (M_s 6.6). Given the large regions and long cumulative history represented in the data base, these results suggest strongly that the maximum earthquake within stable continental regions varies considerably from place to place. Further, the large earthquakes in eastern North America are exceptional rather than typical for worldwide SCI regions.

If the size and frequency of large earthquakes varies with location on a worldwide basis, what are the tectonic characteristics that these events are associated with? To answer this question, an attempt was made to correlate each of the earthquakes in the compilation with characteristics that can be used in a predictive way to estimate earthquake size. For example, if the earthquakes are each associated with a crustal age province and a correlation exists between the crustal age and the occurrence or size of earthquakes, then a knowledge of crustal age may be used to predict the expected maximum earthquake. Characteristics were selected that appear to be both important to the earthquake process and were found to be available for a significant portion of the total data set. Unfortunately, many events, particularly the older historical events, are not well-documented in the literature. For many earthquakes, the local geologic conditions are not specified, coseismic geologic and seismologic parameters are not reported (e.g., surface deformation, aftershocks, prior seismicity), and source parameters are often not carefully specified (magnitude scale, etc.). As a result, the level of confidence is low in characterizing many events. It is felt that an attempt at this characterization is warranted, however, even if only a subset of the of the earthquakes in the total data base can be defined with high confidence.

TABLE 2

SCI EARTHQUAKES ($M \geq 7.0$)
(events clearly in ENA or analogue ENA regions)

NOTE: This list does not include a number of pre-1800 events for which authoritative documentation is unavailable.

		Date	Location	m_b	M_s	Other[1]	MMI_o	Correlation
CLASS I [All events considered magnitude 8 or greater]								
1.	NORTH AMERICA	07 Feb 1812	New Madrid, MO	7.3	8.7	---	X-XI	Mesozoic Rift
2.	NORTH AMERICA	16 Dec 1811	New Madrid, MO	7.2	8.6	---	XI	Mesozoic Rift
3.	NORTH AMERICA	23 Jan 1812	New Madrid, MO	7.1	8.4	---	X-XI	Mesozoic Rift
4.	INDIA	16 Jun 1819	Kutch (NW India)	---	>8.0	---	X-XI	Coast; M/C folding, uplift
5.	CHINA	29 Dec 1604	Southeast coast	7.3	---	$>8.0M_I$	XI	Coast/Continental margin
CLASS II [All other events, considered magnitude 7 or greater]								
1.	AUSTRALIA	19 Nov 1906	West. Cont. Margin	---	---	$7.8M_R$	---	Continental Margin
2.	NORTH AMERICA	31 Aug 1886	Charleston, SC	6.6	7.3-7.5	---	X	Coast/Continental Margin
3.	CHINA	13 Feb 1918	southeast coast	6.9	7.3-7.5	---	X?	Coast/Continental Margin
4.	NORTH AMERICA	20 Nov 1933	Baffin Bay, Canada	---	7.3	---	---	Continental Margin
5.	NORTH AMERICA	18 Nov 1929	Grand Banks, NS	---	7.2	---	---	Continental Margin
6.	AUSTRALIA	24 Apr 1941	Meeberrie, W. Aus.	(7.3)[2]	6.8	$7.2M_L$	VIII	Archean Craton
7.	AFRICA	19 Apr 1935	Libya, G. of Sidra	6.0	6.9	7.1	VII	Coast/Mesozoic. rift
8.	INDIA	21 Jul 1956	Anjar, S. of Kutch	---	6.5	$7.0\text{-}7.2M_L$	IX	Coast; M/C folding, uplift
9.	AFRICA	-- --- 1862	Accra, Ghana	---	---	$7.0M_I$	IX	Continental Margin
10.	CHINA	13 Jul 1605	SE Coast, Hainam Is.	---	---	$7.5M_I$	X	Coast/Suture
11.	CHINA	29 Sep 1600	Southeast coast	---	---	$7.0M_I$	IX	Coast/Continental Margin
12.	NORTH AMERICA	05 Feb 1663	Charlevoix Zone, CA	6.5	---	$7.4M_I$ $7.0M_L$	IX-X	Mesozoic rift

[1] M_I = magnitude inferred from intensity data, usually MMI_o
M_R = Richter magnitude, roughly equaling M_s [Gutenberg and Richter, 1958]

[2] Doubtful magnitude assignment

The results of the global data compilation and the tectonic correlations that have direct implications for maximum earthquake assessments are briefly summarized below.

1. Europe and North America are clearly the most active continents in terms of the numbers of large events; Antarctica and Asia are the least active. North America has experienced the most events larger than magnitude 7 (7 of 17), whereas Europe has not historically experienced any events of this size.

2. The rate of occurrence of large earthquakes within stable continental crust is very low relative to plate boundary (interplate) regions, although the area of stable crust is about three times larger. Fewer than twenty earthquakes have occurred having magnitude equal to or greater than 7 and only five events of magnitude 8 or greater. About 45 years have passed since the last $M \geq 7$ event occurred in stable continental regions worldwide and over a century and a half since the last $M \geq 8$ event.

3. Surface rupture appears to be very rare in stable continental regions. Only seven cases have been documented, four of these in Australia.

4. Most (68%) locations of large events appear to have been the location of prior seismicity. Far fewer cases of no prior seismicity (18%) are known and for many cases (14%) no data are available. This suggests that the occurrence of large events away from recognized seismicity is uncommon.

5. Paleozoic crust is by far the most active crustal age province when compared to Precambrian crustal age categories in terms of the number of observed large events.

6. Most (71%) of the large events are associated with embedded continental rifts or passive continental margins (one-sided rifts). Further, Mesozoic and younger rifts tend to dominate over older rifts. The association of these tectonic features is especially strong with $M \geq 7$ events (15 of 17 events).

7. It appears that earthquakes as large as magnitude $6\frac{1}{2}$ to 7 occur in a variety of tectonic environments, but $M \geq 7$ earthquakes are restricted primarily to areas of Mesozoic rifting.

8. The state of the horizontal deviatoric stress appears to be compressive in the vast majority of cases (86%) where the stress regime could be assessed from focal mechanisms or geologic evidence. This state of stress and its uniformity is in agreement with far-field plate tectonic mechanisms rather than local stress generating mechanisms.

Several tectonic characteristics appear to be important to the occurrence of large events: the age of the crust, the tectonic feature, timing of deformation, the continent, and the presence of prior seismicity. In addition, these characteristics have, to some extent, been correlated with the size of the earthquake (e.g., whether they correlate with earthquakes of magnitude less than 7, larger than 7, or larger than 8). This information provides a powerful tool for estimating the expected occurrence of large earthquakes. If the tectonic characteristics of a region or seismic source are known, then, roughly, the magnitude of the maximum earthquake can be estimated. At present, this estimate is qualitative, but can provide insights that greatly assist the maximum earthquake decision-making process.

For example, suppose that a seismic source in the north-central United States has the following characteristics: 1) it lies within Precambrian crystalline crust, 2) is roughly correlated with a lineament but no other major crustal feature, 3) the most recent deformation in the region occurred in the late Paleozoic, and 4) no prior seismicity has been correlated with the source above background levels. Based on the findings of this study, the expected largest earthquake associated with this source would be about 6 to 6½ and certainly less than 7. The uncertainties in both the characteristics of the seismic source and the expected magnitude given the characteristics would demand that a range of maximum earthquake estimates, or a distribution, be specified to properly display the uncertainty.

FUTURE STUDY

As discussed above, the methods that are currently being used to assess maximum earthquakes in the central and eastern United States are based largely on interpretations of the historical seismicity records tempered by subjective judgement. Because of the inadequacy of the historical period of observation in the East, methods are needed that draw on the larger global data base of SCI seismicity. The first phase of the EPRI Maximum Earthquake study has centered around the development of this global data base and drawing first-order conclusions regarding characteristics of SCI earthquakes. The ongoing second phase of the study focuses on several activities that utilize the data base to arrive at specific methods for arriving at maximum earthquakes for seismic hazards assessments in the East. The second phase activities are summarized briefly below.

- Refine and update the definition of global regions that are analogous to eastern North America. SCI regions will be further identified and justified and portrayed in full color continental maps depicting the tectonic characteristics of analogue re-gions and the associated seismicity. These maps will be updates of those accompanying the first phase report [Coppersmith et al., 1987].

- Continue the seismicity data compilation for all stable continental earthquakes greater than or equal to magnitude

5. An attempt will be made to develop a common base magnitude scale for the data set. Historical events down to MMI_o VII will be included (the original compilation stopped at MMI_o VIII). "Transitional" events and tectonic feature correlations will be reassessed.

- Carry out a systematic inventory of continental rift zones, sutures, and passive continental margins. Because most of the large SCI earthquakes appear to be associated with these features, a detailed examination of their characteristics (age, geometry, reactivation, etc.) and association with seismicity will be carried out.

- Create a computerized key word data base for the seismicity compilation, the inventory of rifts, tectonic feature associations, and the bibliography (about 1000 entries). The data base system will have a multiple key word format so that listing's by parameter or tectonic feature association will be possible.

- Develop models and carry out statistical analyses of the data base to arrive at methods that can be used in a predictive sense to estimate likely maximum earthquake size for seismic sources having particular tectonic characteristics. These studies will quantify correlations between large earthquake occurrence and particular tectonic characteristics. Also, we will examine the validity of using the global data base to substitute a larger spatial area for the relatively short time period of historical seismicity observation. Our goal is to arrive at scientifically-supportable methods for maximum earthquake estimation that will be appropriate for routine use in the central and eastern United States.

ACKNOWLEDGEMENTS

This work is part of a larger seismic hazard research effort being conducted by the Electric Power Research Institute under the direction of J. Carl Stepp.

REFERENCES

Anderson, J.G., 1986, Seismic strain rates in the central and eastern United States: **Seismological Society of America Bulletin**, v. 76, p. 273-290.

Brune, J.N., 1968, Seismic moment, seismicity, and rate of slip along major fault zones: **Journal of Geophysical Research**, v. 73, p. 777-784.

Chinnery, M.A., 1979, Investigations of the seismological input to the safety design of nuclear power reactors in New England: **NUREG/CR-0563**, U.S. Nuclear Regulatory Commission, Washington, D.C., 67 pp.

Coppersmith, K.J., Johnston, A.C., Metzer, A.G., and Arabasz, W.J., 1987, Methods for assessing earthquakes in the central and eastern United States: **Working Report EPRI Research Project 2556-12**, Electric Power Research Institute, Palo Alto, California.

Coppersmith, K.J., and Youngs, R.R., 1986, Capturing uncertainty in probabilistic seismic hazard assessments within intraplate tectonic environments: **Proceedings Third U.S. National Conference on Earthquake Engineering**, v. 1, p. 301-312.

Davison, F.C., Jr., and Scholz, C.H., 1985, Frequency-moment distribution of earthquakes in the Aleutian arc: A test of the characteristic earthquake model: **Seismological Society of America Bulletin**, v. 75, p. 1349-1361.

Dennison, J.J., and Johnson, R.W., Jr., 1971, Tertiary intrusions and associated phenomena near the thirty-eight parallel fracture zone in Virginia and West Virginia: **Geological Society of America Bulletin**, v. 82, p. 501-507.

Ervin, C.P., and McGinnis, L.D., 1975, Reelfoot rift - Reactivated precursor to the Mississippi Embayment: **Geological Society of America Bulletin**, v. 70, no. 4, p. 1171-1180.

Fairbairn, H.W., Faure, G., Pinson, W.H., Hurley, P.M., and Power, J.L., 1963, Initial ratio of strontium 87 to strontium 86, whole-rock age, and discordant biotite in the Monteregian igneous province, Quebec: **Journal of Geophysical Research**, v. 68, p. 6515-6522.

Joyner, W.B., and Fumal, T.E., 1985, Predictive mapping of earthquake ground motion: **U.S. Geological Survey Professional Paper 1360**, p. 203-220.

Kijko, A., 1984, Is it necessary to construct empirical distributions of maximum earthquake magnitudes? **Seismological Society of America Bulletin**, v. 74, p. 339-347.

King, P.B., 1969, Tectonic Map of North America, U.S. Geological Survey, scale 1:5,000,000.

King, P.B., 1977, The evolution of North America, revised edition: Princeton University Press, Princeton, New Jersey, 197 p.

Knopoff, L., and Kagan, Y., 1977, Analysis of the theory of extremes as applied to earthquake problems: **Journal of Geophysical Research**, v. 82, p. 5647-5657.

Kostrov., B.V., 1974, Seismic moment and energy of earthquakes and seismic flow of rock: **Physics of the Solid Earth, Izvestia Academy of Science USSR**, v. 1, p. 23-44.

McGarr, A., Mueller, C., Fletcher, J.B., and Andrews, M., 1987, Ground motion and source parameters at the 1983 Coalinga, California earthquake sequence: **U.S. Geological Survey Professional Paper**, in press.

McGuire, R.K., 1977, Effects of uncertainty in seismicity on estimates of seismic hazard for the eastern United States: **Seismological Society of America Bulletin**, v. 67, p. 827-848.

Molnar, P., 1983, Average regional strain due to slip on numerous faults of different orientations: **Journal of Geophysical Research**, v. 88, p. 6430-6432.

Nuttli, O.W., 1981, On the problem of the maximum magnitude of earthquakes: in **Proceedings of Conference XIII, Evaluation of Regional Seismic Hazards and Risk, U.S. Geological Survey Open-File Report 81-437**, p. 876-885.

Schwartz, D.P., and Coppersmith, K.J., 1984, Fault behavior and characteristic earthquakes: examples from the Wasatch and San Andreas fault zones: **Journal of Geophysical Research**, v. 89, p. 5681-5698.

Tinti, S., and Mulargia, F., 1985, Effects of magnitude uncertainties on estimating the parameters in the Gutenberg-Richter frequency-magnitude law: **Seismological Society of America Bulletin**, v. 75, p. 1681-1697.

Wesnousky, S., Scholz, C.H., Shimazaki, K., and Matsuda, T., 1983, Earthquake frequency distribution and the mechanics of faulting: **Journal of Geophysical Research**, v. 88, p. 9331-9340.

Yegulalp, T.M., and Kuo, J.T., 1974, Statistical prediction of the occurrence of maximum magnitude earthquakes: **Seismological Society of America Bulletin**, v. 64, p. 393-414.

Youngs, R.R., and Coppersmith, K.J., 1985, Implications of fault slip rates and earthquake recurrence models to probabilistic seismic hazard estimates: **Seismological Society of America Bulletin**, v. 75, p. 939-964.

LOCAL MODELS OF SEISMICITY AND THEIR ESTIMATION

Daniele Veneziano and Luc Chouinard

Department of Civil Engineering
Massachusetts Institute of Technology
Cambridge, Massachusetts 02139

INTRODUCTION

For the purpose of seismic hazard analysis, it is generally assumed that main events occur according to a Poisson process, which is stationary in time and homogeneous in space within so-called seismogenic provinces. It is also frequently assumed that main events in each province have exponentially distributed size (macroseismic intensity I or magnitude m), hence that the rate of main events with size in the interval $(I-\underline{\Delta}I/2, I+\underline{\Delta}I/2)$ in a unit area of Province i is

$$\lambda_i(I) = \exp\{a_i - b_i(I-I^*)\} \qquad (1)$$

where a_i and b_i are parameters and I^* is a given value of I, so that $a_i = \ell n\{\lambda_i(I^*)\}$.

This simple model is frequently contradicted by the observation that, over periods of a few decades or a few centuries, the seismicity of extended provinces is spatially non-homogeneous, or non-Poisson, or both. In the present study, we describe seismicity through a non-homogeneous Poisson process, with parameters a and b that vary as functions of the geographical location vector $\underline{x}$. Stationarity is assumed, at least during the time periods of the data and of the needed earthquake predictions. These assumptions correspond to the model of Veneziano and Van Dyck (1986) and Van Dyck (1985).

Our objective here is to discuss methods to estimate the spatially varying parameters $a(\underline{x})$ and $b(\underline{x})$ using historical earthquake data. We consider alternative estimators of $a(\underline{x})$ and $b(\underline{x})$, obtained by smoothing the data in different ways, and compare two types of optimality criteria: we either impose that certain observed statistics equal their mean or median values under the model or maximize cross-validated measures of goodness-of-fit, such as the likelihood or a negative squared error.

The cross-validated likelihood and squared error are defined so that they measure how accurately the model predicts future events. Therefore, these are attractive statistics for selecting seismicity models to be used in earthquake hazard studies. The estimation procedures are applied to the Northeastern U.S. using the earthquake catalog compiled by Chiburis (1981). The original catalog extends from 1534 to 1981, but only main earthquakes with MM intensity greater than 3 that have occurred between 1627 and 1981 are used in the analysis, due to the high degree of incompleteness of the historical record for early and very small events. Main earthquakes have been identified through the declustering procedure of Veneziano and Van Dyck (1985) and are plotted in Fig. 1.

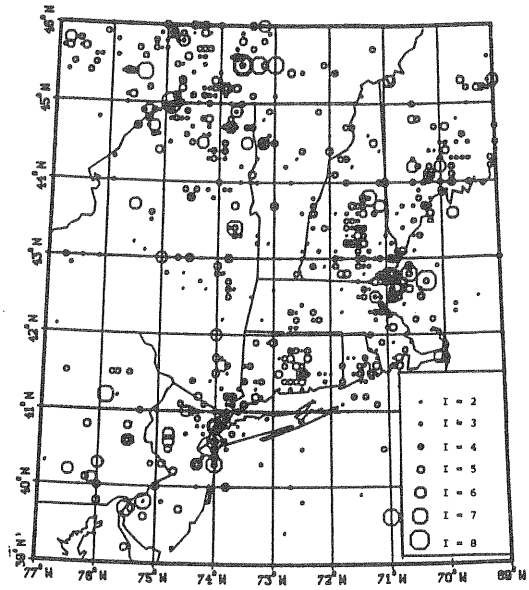

Fig. 1. Main events in the Chiburis catalog for the period 1627-1981.

For the Northeastern U.S., we find that half-degree cells give an appropriate geographical discretization. The optimal degree of smoothing for $b(\underline{x})$ is high, reflecting the low accuracy with which this parameter is estimated from small samples. By contrast, the optimal estimator of $a(\underline{x})$ is highly variable and closely follows the pattern of historical seismicity.

The estimators $\hat{a}(\underline{x})$ and $\hat{b}(\underline{x})$ proposed by Veneziano and Van Dyck (1986) and Van Dyck (1985) are among those considered here. These estimators smooth the data by penalizing the deviation of $a(\underline{x})$ and $b(\underline{x})$ from moving averages $\tilde{a}(\underline{x})$ and $\tilde{b}(\underline{x})$. Because the two-dimensional averaging windows have fixed shape and size, the estimators are appropriate for geographical regions where the parameters a and b do not vary abruptly (discontinuities in space of a and b are not recognized and are blurred). This is why, in all applications, the above estimators have been used inside externally specified quasi-homogeneous regions; see for example EPRI (1985) and Veneziano and Van Dyck (1986). A new form of roughness penalty is proposed here, which automatically identifies spatial discontinuities of the seismicity parameters and in the limit can generate, when supported by the historical data, earthquake recurrence models of the seismic-source type. In the absence of strong physical evidence on the location of major discontinuities, this is the estimator we recommend.

We consider also estimators of $a(\underline{x})$ and $b(\underline{x})$ based only on the more recent historical data and find that the resulting models may differ considerably from long-term representations of seismicity. This raises the issue of possible lack-of-fit of the model. Problems of lack-of-fit are not examined here, but will be the subject of a separate paper.

ESTIMATION PROCEDURES FOR $a(\underline{x})$ AND $b(\underline{x})$

Estimation of $a(\underline{x})$ and $b(\underline{x})$ from historical seismicity is, in essence, a data-smoothing operation. Many procedures could be used for this purpose, including kernel, Bayes, and penalized likelihood methods; see for example Titterington and Bowman (1985), Silverman (1986), and Hand (1982). The present analysis is limited to the penalized likelihood procedures proposed by Veneziano and Van Dyck (1986) and Van Dyck (1985), with modifications to improve the goodness of fit. These procedures maximize the likelihood function, multipled by penalty factors that reduce the spatial variability of $a(\underline{x})$ and $b(\underline{x})$.

As in the last two quoted references, the region of interest is partitioned into small geographical units of approximately equal size, called cells. Nonstationarity is attributed to incomplete reporting and the detection/non-detection of different earthquakes are treated as independent events. Therefore, reported events conform to a Poisson process with intensity function ν given by

$$\nu(\underline{x},I,t) = P_D(\underline{x},I,t) \cdot \lambda(\underline{x},I) \tag{2}$$

where $\lambda(\underline{x},I)$ is the recurrence rate of the complete process and $P_D(\underline{x},I,t)$ is the probability that an earthquake of size I that occurs at location $\underline{x}$ and time t is reported. In terms of discrete intensity I, discrete space $\underline{x}$, and discrete time t, the log-likelihood function is (Van Dyck, 1985, p. 147),

$$L = \sum_{\underline{x}} \{a(\underline{x})N(\underline{x}) - b(\underline{x})I'(\underline{x}) - \sum_{I} T(\underline{x},I) \exp[a(\underline{x}) - b(\underline{x})(I-I^*)] + \sum_{t} \sum_{I} n(\underline{x},I,t) \ln P_D(\underline{x},I,t)\} \tag{3}$$

where $N(\underline{x}) = \sum_{I} \sum_{t} n(\underline{x},I,t)$

$I'(\underline{x}) = \sum_{I} \sum_{t} n(\underline{x},I,t) \cdot (I-I^*)$

$T(\underline{x},I) = \sum_{t} T_t \cdot P_D(\underline{x},I,t)$

In the previous expressions, I^* is a fixed reference intensity as in Eq. 1 and $n(\underline{x},I,t)$ is the number of events of intensity I reported at location $\underline{x}$ during the t^{th} time period, which has duration T_t.

Smoothness is introduced in the solution through penalties on the functions $a(\underline{x})$ and $b(\underline{x})$ and, if desired, through an independent prior on $b(\underline{x})$ at each location $\underline{x}$. The prior on $b(\underline{x})$ and the penalties on $a(\underline{x})$ and $b(\underline{x})$ appear in the penalized log-likelihood function as additive terms $Q(\underline{x})$, one for each location $\underline{x}$. These terms are given by

$$Q(\underline{x}) = -P_a[a(\underline{x}) - \tilde{a}(\underline{x})]^2 - P_b[b(\underline{x}) - \tilde{b}(\underline{x})]^2 - \frac{1}{\sigma_b^{2'}}[b(\underline{x}) - m_b^{'}]^2 \tag{4}$$

where the constants P_a and P_b control the degree of smoothness of $a(\underline{x})$ and $b(\underline{x})$. The quantities $\tilde{a}(\underline{x})$ and $\tilde{b}(\underline{x})$ are interpolated values using estimates from neighboring cells (cell $\underline{x}$ is excluded), and m'_b and σ'^2_b are the mean and variance of the prior distribution of $b(\underline{x})$, assumed to be normal.

Interesting variants of the above estimation method are obtained by changing the form of the interpolators $\tilde{a}(\underline{x})$ and $\tilde{b}(\underline{x})$. One that is especially attractive in geographical regions with highly variable and possibly discontinuous seismicity consists of using for interpolation a "local neighborhood" that includes only cells where the parameters a and b are similar to $a(\underline{x})$ and $b(\underline{x})$. Preferential data smoothing procedures of this type are described in the literature under the names of oriented or variable kernels and penalty functions (Hand, 1982; Hall, 1981, 1983). The use of local neighborhoods allows one to smooth more in regions where the earthquake data is sparser or more homogeneous and to stay closer to the empirical rates where the earthquake density is higher or more variable in space. Importantly, such neighborhoods avoid the blurring of discontinuities, which therefore do not need to be externally specified.

Local neighborhoods are found here by performing repeated pairwise statistical tests of equality of the recurrence rate in different cells (Lehmann, 1957, p. 140). More specifically, cell $\underline{y}$ is considered to be part of the neighborhood of cell $\underline{x}$ if two conditions are satisfied: 1. the test of equal Poisson rates in the cells passes at the chosen significance level α and 2. cells $\underline{x}$ and $\underline{y}$ are connected in the local neighborhoods of both $\underline{x}$ and $\underline{y}$. The neighborhoods may have large spatial extent if one performs the test beyond the set of eight closest cells. However, in all cases, the neighborhoods remain small in regions of non-uniform seismicity, for example near "peaks" and "valleys" of the functions $a(\underline{x})$ and $b(\underline{x})$.

It is interesting that, if earthquakes are generated by homogeneous sources with high seismicity contrasts, the above local procedure automatically identifies the source boundaries and reproduces the classical seismicity solution, with the only approximation of the chosen spatial discretization.

Local neighborhoods are used here only for the estimation of $a(\underline{x})$. Similar neighborhoods could be defined for $b(\underline{x})$, but such neighborhoods would be large and less useful, due to the high statistical uncertainty on b given the data in single cells. Therefore, for $b(\underline{x})$, we always use moving-average windows of fixed shape and size.

CHOICE OF ESTIMATOR AND SMOOTHING PARAMETERS

One should distinguish between the maximum-penalized-likelihood method by which $a(\underline{x})$ and $b(\underline{x})$ are estimated under a given set of conditions (spatial discretization, interpolators $\tilde{a}(\underline{x})$ and $\tilde{b}(\underline{x})$, penalty coefficients P_a and P_b, etc.) and the procedure to optimally select such conditions. For the latter operation, which is the one discussed in the remainder of the paper, we have compared two methods: one is analogous to the method of moments and consists of reproducing certain observed statistics, the other maximizes a cross-validated measure of goodness-of-fit, for example the likelihood or the negative squared error. Bayesian procedures are discarded because they are

either computationally too demanding (if they require calculation of the posterior distributions of $a(\underline{x})$ and $b(\underline{x})$) or inferior to cross-validation alternatives (if one wants only the a-posteriori most likely values of $a(\underline{x})$ and $b(\underline{x})$). We shall describe in brief the "target statistics" method and then turn to a more detailed analysis of cross-validation procedures, which are conceptually more appealing, especially for application to earthquake risk.

Target-Statistics Method

Let $\underline{\theta}=[\theta_1,\theta_2,\ldots,\theta_n]$ be the vector of parameters on which the seismicity estimates $\hat{a}(\underline{x})$ and $\hat{b}(\underline{x})$ depend ($\underline{\theta}$ includes the cell size, the penalty coefficients P_a and P_b, etc.). A way to select $\underline{\theta}$ is to choose a set of statistics $S_1,\ldots,S_n$ that measure in different ways the degree to which the model fits the data and then solve for $\underline{\theta}$ the equations

$$S_i^*(\underline{\theta}) = s_i(\underline{\theta}), \quad i = 1,\ldots,n \tag{5}$$

where the $s_i(\underline{\theta})$ are the empirically observed statistics and $S_i^*(\underline{\theta})$ are target values for the case when $a(\underline{x}) = (\hat{a}(\underline{x})|\underline{\theta})$ and $b(\underline{x}) = (\hat{b}(\underline{x})|\underline{\theta})$. For example, one might choose S_i^* to be the mean or the median of $[S_i(\hat{a}(\underline{x})|\underline{\theta}), (\hat{b}(\underline{x})|\underline{\theta})]$, as proposed respectively by Titterington and Bowman (1985) and Good and Gaskins (1981). Skilling et al. (1979) use the 95% fractile of the same distribution. The idea behind the method is that the statistics $a_i(\underline{\theta})$ should be neither excessively good (an indication of overfitting) nor excessively bad (an indication of underfitting). In our case, goodness-of-fit statistics such as the Chi-square (χ^2), the Kolmogorov-Smirnov statistic, and the likelihood are possible choices. For the calculation of χ^2, neighboring low-density cells should be aggregated into regions such that the number of expected events in each region is at least 5, whereas for the Kolmogorov-Smirnov test the cells should be ordered, for example row after row, and a univariate distribution function constructed by cumulating counts as one moves from cell to cell (Skilling et al., 1979). The likelihood ℓ may be written in different ways, depending on whether and how earthquakes are classified according to size and time of occurrence. For example, if the events are classified only according to geographical location $\underline{x}$, then

$$\ell = \prod_{\underline{x}} \nu(\underline{x})^{N(\underline{x})} e^{-\nu(\underline{x})} \tag{6}$$

where $\nu(\underline{x})$ and $N(\underline{x})$ denote expected and actual counts, respectively. Notice that $\nu(\underline{x})$ depends on the parameters $a(\underline{x})$ and $b(\underline{x})$ and on the incompleteness of the catalog for cell $\underline{x}$.

The target-statistics method is illustrated here for the selection of the parameter P_a which controls the smoothness of the estimator $\hat{a}(\underline{x})$. The analogous parameter for $\hat{b}(\underline{x})$ is fixed to 1000, a value which produces high smoothing. In this and in following applications, a prior mean of 1.3 is assigned to b, which is the value obtained under complete smoothing of the b

parameter. A prior variance of 10 is specified on the basis of work by Van Dyck (1985) . This is a mild prior, which however stabilizes the estimate of $b(\underline{x})$ in areas of sparse data. The interpolators $\tilde{a}(\underline{x})$ and $\tilde{b}(\underline{x})$ are the averages of a and b over the eight cells that are closest to $\underline{x}$.

Figure 2a shows the variation with P_a of the Chi-square and the Kolmogorov-Smirnov statistics, computed for half-degree cells. The dashed line corresponds to a diagnostic quantity proposed by Good and Gaskins (1981), which combines the previous statistics and whose minimum identifies the optimal penalty. If one selects medians as the target values S^*, one finds optimal penalties P_a between 20 and 35 and rather smooth associated estimates of $a(\underline{x})$. Contour plots of $\hat{a}(\underline{x})$ for selected penalties (Fig. 3) indicate that it is quite important to choose the proper value of P_a. In these and in later plots, I^* is set to 4, ΔI is 1.0, and the unit geographical area is set to one equatorial degree ($111.1^2 Km^2$). Therefore, a is the log-rate of events of MM intensity 4, per year and over such a unit area. For example, a value a = -1.0 indicates that earthquakes of intensity I=4 occur in a half-degree cell at latitude 42°N at the rate of exp(-1)·cos(42°)/4 = 0.068 events/year.

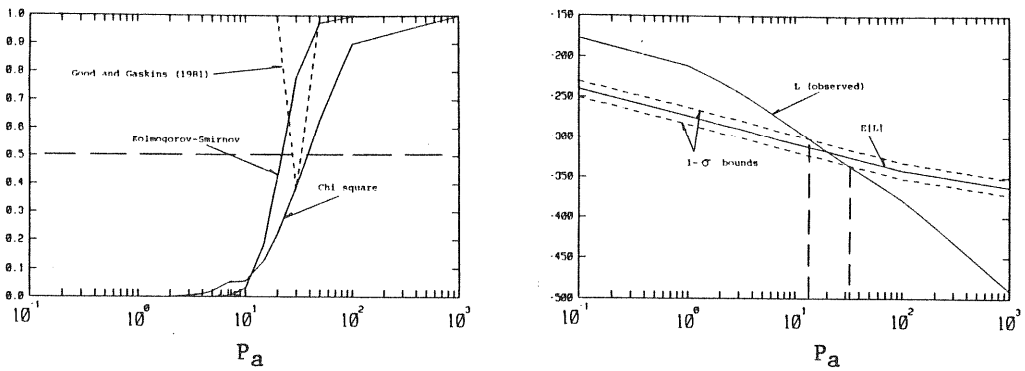

Fig. 2. Selection of the penalty parameter P_a using the target-statistics method.

The log-likelihood based on the total rate in each cell, L = ln ℓ with ℓ in Eq. 5, is plotted in Fig. 2b as a function of P_a. Also shown in that figure are the expected value and the one-standard-deviation bounds on L, under the assumption that the estimated model is correct. The log-likelihood equals its expected value for a penalty P_a of about 20 and the one standard deviation bounds on L correspond to a range of P_a between about 12 and 30.

The target-statistics method has the advantage of being intuitive and easy to implement. However, the method lacks predictive interpretation and cannot be used to rank alternative estimators. On the latter scores, cross-validation procedures should be preferred.

Cross-Validation Method

Cross-validation aims at maximizing the predictive ability of a model: Suppose that, besides the original earthquake catalog (estimation data set E), additional observations (validation data set V) are available from the earthquake generation process. Also let S be a statistic that compares the validation data with predictions when the model is fitted to the estimation data. It would then be natural to rank alternative estimators of $a(\underline{x})$ and $b(\underline{x})$ based on the values of S.

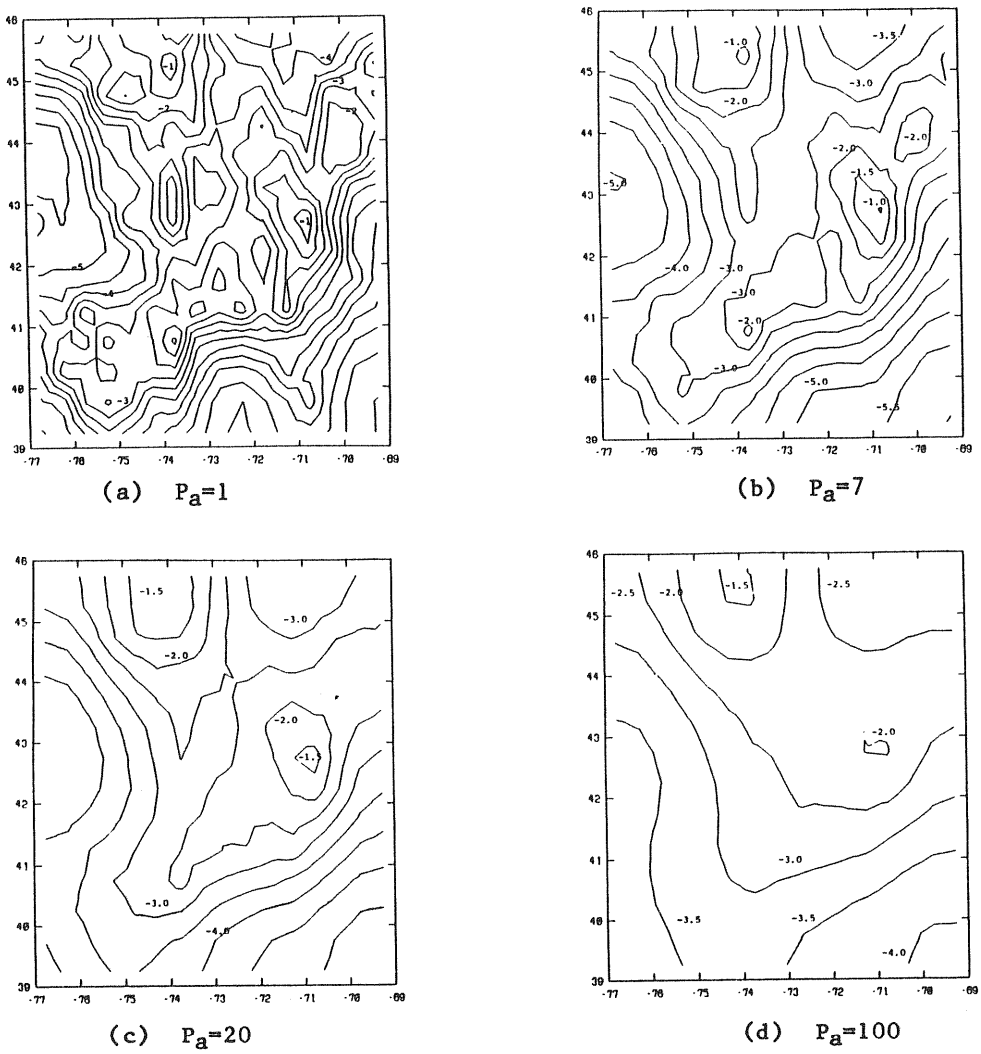

(a) P_a=1 (b) P_a=7

(c) P_a=20 (d) P_a=100

Fig. 3. Fixed neighborhoods of eight closest cells. Estimates $\hat{a}(\underline{x})$ for selected values of the penalty P_a.

In practice, validation data are not available and the method is applied by partitioning the actual sample in various ways i into an estimation subset E_i and a validation subset V_i. The cross-validated estimator is the one which optimizes the total score, say $\sum S_i$ or $\prod S_i$ (Silverman, 1986; Titterington and Bowman, 1985; Hand, 1982).

The estimation and validation subsets should be defined so as to replicate as closely as possible the features of the actual data and of the events to be predicted. In our analysis of Northeastern U.S. seismicity, we have divided the Chiburis catalog into ten intervals with nearly equal number of recorded main events and we have used the last five intervals as validation subsets $V_i (i=1,\ldots,5)$. For the more recent time intervals, this corresponds to validation periods of approximately 15 years. The associated estimation subsets E_i contain data prior to V_i. The reason why data following V_i have not been included in E_i is that, if the assumptions of stationarity and Poisson independence do not hold exactly, the use for estimation of events on both sides of the validation subset artificially increases the prediction ability of the fitted model.

The cross-validated log-likelihood is given by

$$L_{CV} = \sum_t \sum_I \sum_{\underline{x}} L[n(\underline{x},I,t) \,|\, (\hat{a}(\underline{x}),\hat{b}(\underline{x}))_t] \qquad (7)$$

where $(\hat{a}(\underline{x}),\hat{b}(\underline{x}))_t$ are estimators from observations prior to the t^{th} time interval. For the purpose of computing the cross-validated likelihood, the probability of detection has been evaluated using the entire catalog and has been kept constant for all the cross-validation intervals. Starting with a fixed neighborhood, a given value of P_a (P_a = 7, which turns out to be the optimum value), and a discretization into half-degree cells, optimization was first performed with respect to P_b (Fig. 4). The large optimal penalty (P_b=1000) is a consequence of the inaccurate estimation of b using data

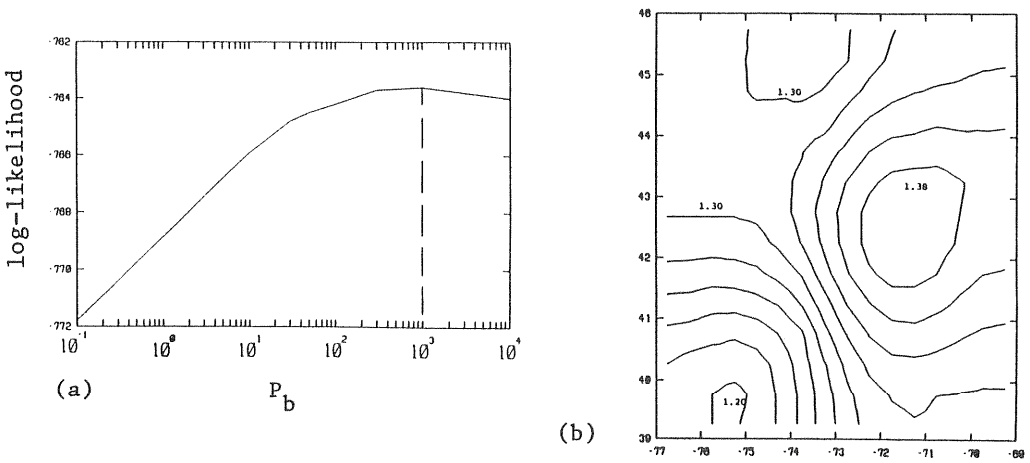

Fig. 4: (a) Optimal penalty P_b and (b) associated estimate of $b(\underline{x})$. The penalty P_a is fixed to 7.

from only one cell or from very few cells: Fig. 4 indicates that it is best to use a high penalty P_b and introduce bias into $\hat{b}(\underline{x})$, in order to reduce the large estimation variance.

With P_b fixed to 1000, the optimal penalty for $a(\underline{x})$ has been determined and found to be low (P_a=7), meaning that this parameter is best estimated locally; see Fig. 5a.

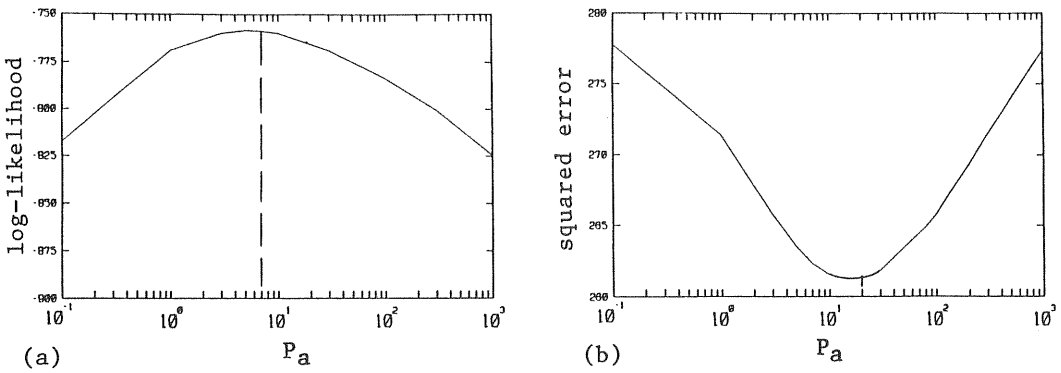

Fig. 5. Optimal penalty P_a according to the cross-validated likelihood and cross-validated squared error criteria.

A higher optimal penalty, around 15, is found when using a cross-validated squared-error criterion; see Fig. 5b. In this case, one penalizes quadratically the deviations of the actual counts $n(\underline{x},I,t)$ from the (incomplete) expected counts according to the model, $\nu(\underline{x},I,t)$. Notice that the log-likelihood penalizes the same deviations, but in a way that depends on $\nu(\underline{x},I,t)$ (higher penalty for lower expected counts). The reason for the increased optimal penalty for the squared error is that this quantity is more sensitive than the log-likelihood to large deviations of the actual counts from the expected counts. These deviations are reduced by using higher smoothing. The only combinations to which the log-likelihood is very sensitive (nearly zero expected counts and large actual counts) do not occur in the data.

Cross-validation can be used also to select the best discretization of the region into cells. We have found that, for the region under study, there is a significant gain in prediction accuracy when going from one-degree to half-degree cells, but that no additional gain results from using quarter-degree cells. This may be a consequence of the fact that many events in the catalog are located with an accuracy not higher than one quarter degree.

All previous results are for interpolation neighborhoods of fixed geometry and size. An undesirable feature of the solutions is that the boundaries

between highly active and less active areas, which should appear as sharp discontinuities of $\hat{a}(\underline{x})$, are blurred. A procedure to preserve these boundaries is to use local interpolation neighborhoods, as explained in a previous section. The contrast in $\hat{a}(\underline{x})$ between more and less active areas increases as the significance level α used in the definition of the local neighborhoods increases. Various plots of $\hat{a}(\underline{x})$ are presented in Fig. 6 to show the effect of changing α, the number m of rings of cells around $\underline{x}$ to which the local

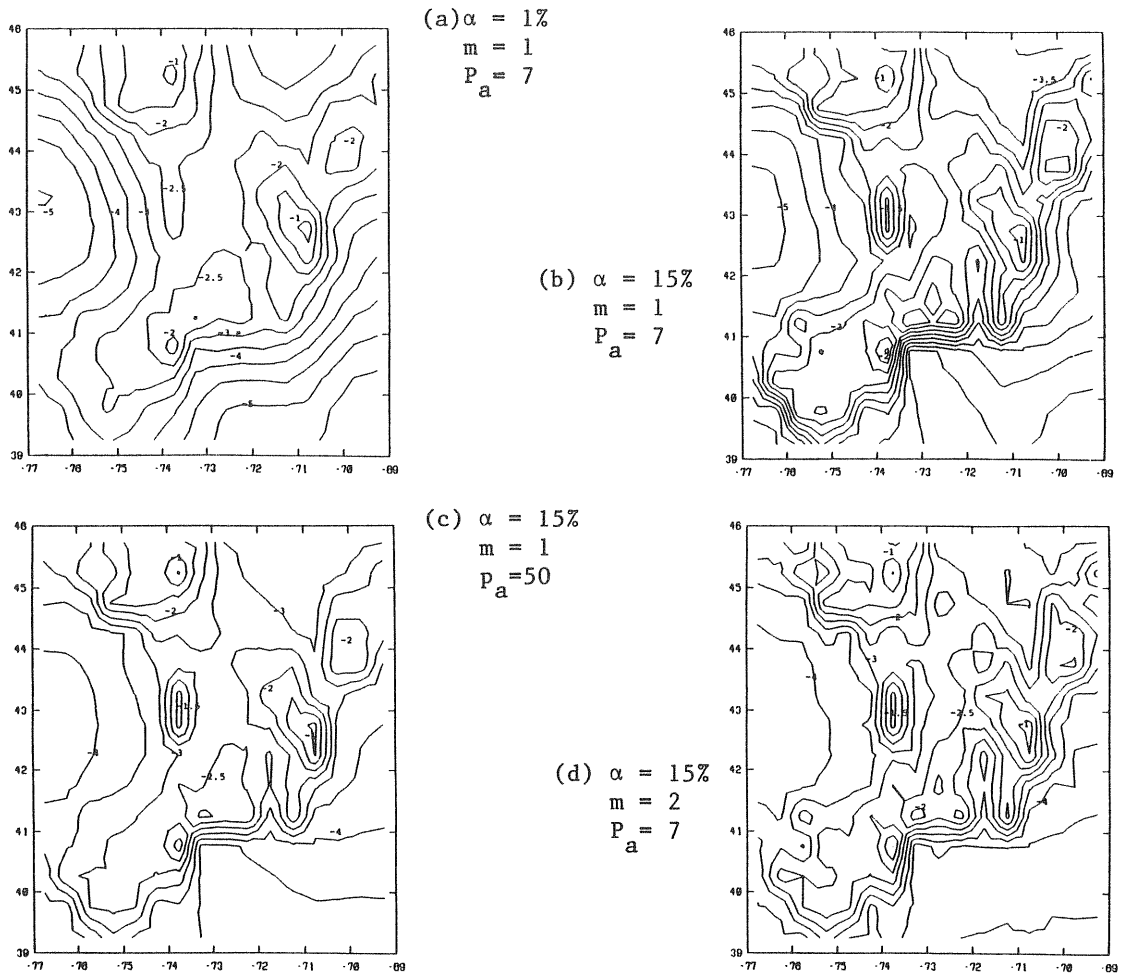

Fig. 6. Local-neighborhood estimates $\hat{a}(\underline{x})$ using different penalties P_a and different values of α and m. α is the level of significance used to define the neighborhoods and m is the number of rings of cells around $\underline{x}$ to which the neighborhoods are confined.

neighborhood is confined, and the penalty P_a. For α=0.01, only few of the neighborhoods have an irregular shape and the estimate $\hat{a}(\underline{x})$ is similar to that for fixed neighborhoods (compare Figs. 3b and 6a). For α=0.15, the function $\hat{a}(\underline{x})$ displays plateaus of nearly constant activity, in some cases separated by sharp discontinuities, in other cases connected by gradual "ramps". The solution is insensitive to m and P_a. In fact, it is interesting to notice how, also for a high penalty P_a, the estimate $\hat{a}(\underline{x})$ preserves a high level of contrast. This is not the case when fixed neighborhoods are used (compare with Fig. 3).

In order to compare fixed-neighborhood with local-neighborhood estimators on the basis of L_{CV} in Eq. 7, one should cross-validate the local neighborhoods. One can do so in two different ways: For each i, one can estimate the local neighborhoods 1. using only the data set E_i, or 2. using all the data with V_i removed. If P_a is kept to 7, the cross-validated likelihoods for the two options are respectively -774 and -745. The value L_{CV} for the case with fixed neighborhoods is -760, as shown in Fig. 5. These results indicate that accurate estimation of the local neighborhoods requires large amounts of data, hence that Option 1 may not be representative of the accuracy achievable at the present time. Option 2 gives a more realistic evaluation and shows improvement over the analysis with fixed neighborhoods.

As one would expect, a decomposition of the cross-validated likelihood in space indicates that, in regions of pronounced seismicity gradients, the likelihood increases with increasing α. The opposite is true in areas where the long-term seismicity appears homogeneous, although the earthquake pattern has changed, sometimes significantly, over shorter intervals of time. One way to further improve the local-neighborhood solution is to allow α to vary as a function of location. We have made analyses of this type, limiting the choice of $\alpha(\underline{x})$ to just two values: the value 0, which corresponds to a neighborhood of fixed geometry, and the value 0.15, which may produce an irregular neighborhood. The cross-validated likelihood of each cell was calculated for both α=0 and α=0.15 and the value of $\alpha(\underline{x})$ was fixed to 0 or to 0.15 if the local likelihood in one solution was larger than the same likelihood in the other solution by more than a given factor; see unshaded and heavily shaded cells in Fig. 7a. For the other cells, two cases have been considered, one favoring the fixed neighborhoods (α=0), the other favoring the local neighborhoods (α=0.15).

The estimates $\hat{a}(\underline{x})$ that result from the two analyses are displayed in Fig. 7b. Except in the Southwestern corner (New Jersey, Eastern Pennsylvania, and Northeastern Maryland), the contour lines of $\hat{a}$ are almost the same in the two cases. The reason is that, for most of the cells that are indifferent to setting α equal to 0 or 0.15, the local and fixed neighborhoods coincide or are very similar. Because keeping α fixed is a special case of letting α vary with $\underline{x}$, one cannot compare the estimators of Fig. 7 with those of Fig. 6 in terms of their cross-validated likelihood. It is however clear that the estimates $\hat{a}(\underline{x})$ are not much different in the two cases and hence that, for the region under study, there is little incentive to use the more complicated estimator with variable α.

(a)

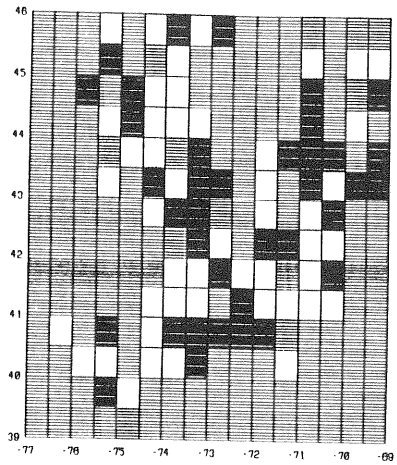

(b) Local neighborhoods favored

Fixed neighborhoods favored

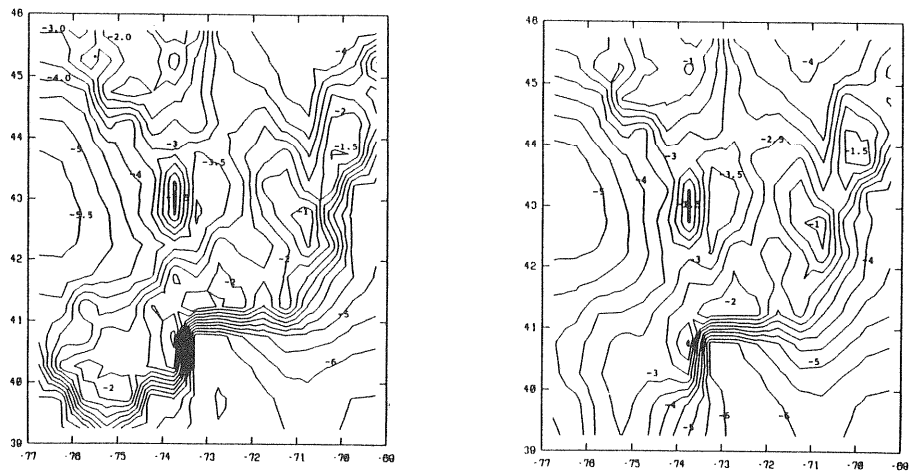

Fig. 7. Two solutions with α that varies from cell to cell. Fig. a shows the cells that are insensitive to α and those for which the optimal values of α are 0% and 15%.

Another modification of the estimators in Fig. 6 that we have considered consists of finding $\hat{a}(\underline{x})$ and $\hat{b}(\underline{x})$ from only the more recent part of the catalog. Doing so should produce better predictions if the earthquake process has memory or is nonstationary, so that seismicity in the near future should resemble more the recent past than the average seismicity during long periods of time. We have implemented this idea by including in the estimation subsets E_i only the two time intervals that precede V_i. The estimate of $\hat{a}(\underline{x})=\ell n\lambda(4)$

from the last two time periods (1957-1981) is shown in Fig. 8a and is quite different from estimates that use the entire catalog, e.g. the estimate of Fig. 6b, which is reproduced as Fig. 8b.

The optimum penalty P_a when using only the more recent data is around 10, and this is the value used in Fig. 8a. The penalty P_b and the prior on $b(\underline{x})$ are the same as for Fig. 8b. Because of the reduced amount of data, the estimates of $a(\underline{x})$ and $b(\underline{x})$ based only on recent seismicity are smoother (b is almost flat over the entire region, with values between 1.23 and 1.29). Other differences between the estimates of $a(\underline{x})$ in Figs. 8a and 8b are that, in the former, earthquake activity is higher in New Jersey and lower in Eastern Massachusetts and Southern New Hampshire.

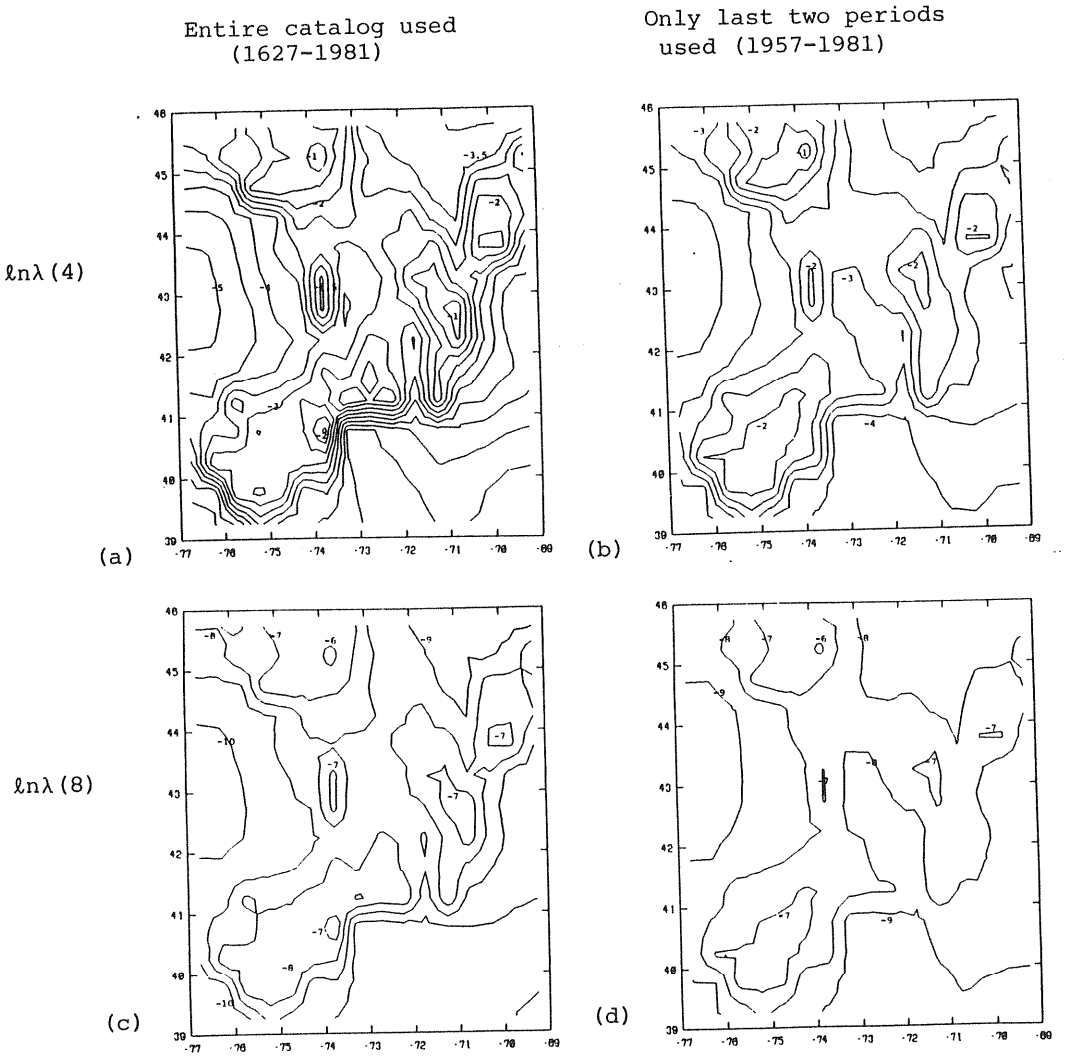

Fig. 8. Comparison of the log-rates using the entire catalog and the last 2 time intervals.

The cross-validated likelihood is nearly the same for the two analyses. This is probably the net effect, in the case when only recent data are used, of an increase in prediction accuracy due to the higher similarity of seismicity and a decrease in prediction accuracy from the smaller estimation samples. In order to evaluate how the differences in $\hat{a}(\underline{x})$ and $\hat{b}(\underline{x})$ affect the recurrence of large events, Figs. 8c and 8d show contour plots of $\ell n\lambda(8) = \hat{a} - 4\hat{b}$. It is interesting, but perhaps fortuitous, that the differences in a and b in the two analyses have compensating effects, so that the estimate of $\ell n\lambda(8)$ are more similar than the estimates of $\ell n\lambda(4)$. The main differences for earthquakes of MM intensity 8 are that, when only the recent data are used, the estimated rate is smoother over the entire region and is higher (by a factor of about 2) in the New Jersey area. Because $\hat{a}(\underline{x})$ is sensitive to the portion of the catalog used for estimation and the compensation of $\hat{a}$ and $\hat{b}$ for high for high intensities is of suspect generality, it is our conclusion that one should consider seismicity estimators that are local in time, especially when their cross-validated likelihood is high.

CONCLUSIONS

The optimization of cross-validated statistics is the method we recommend to estimate seismicity parameters from historical earthquake data. The method is appealing for seismic hazard applications because it emphasizes the predictive ability of the model. The method is also well suited for local seismicity representations, i.e. for models that do not postulate the existence of homogeneous earthquake sources.

Existing estimators of local models require that major discontinuities of seismicity be identified externally, as boundaries of quasi-homogeneous geographical regions. The estimators are then applied inside each region, to allow for further local variations in the earthquake rate or in the magnitude distribution. New estimators are proposed, which, by smoothing the data inside "local neighborhoods" of irregular shape, are able to automatically identify major discontinuities. Results from application of the local estimators to the Northeastern U.S. are quite satifactory.

We have found no advantage from allowing the parameter α that controls the homogeneity of the local neighborhoods to vary on the geographical plane. We do however recommend that alternative estimators be considered, which use different portions of the historical record. Doing so is especially important in regions where nonstationarities of the earthquake process have been observed or are suspected to exist. The possible presence of nonstationarity and of other "anomalies" leads to questioning the validity of common modeling assumptions, in particular that main events conform to a stationary Poisson process and have exponentially distributed magnitude. Methods to investigate the goodness-of-fit of seismicity models have been developed by the authors and will be reported in a sequel to this paper.

ACKNOWLEDGEMENT

This study was sponsored by the National Science Foundation through the National Center for Earthquake Engineering Research, under Grant No.NCEER86-1023.

REFERENCES

Chiburis, E.F. (1981) "Seismicity, recurrence rates and regionalization of the Northeastern U.S. and adjacent Southeastern Canada," NUREG/CR-2309, Washington, D.C.

EPRI (1985) "Seismic hazard methodology for nuclear facilities in the Eastern United States," Research project P101-29, Electric Power Research Institute, Palo Alto, California.

Good, J.J. and R.S. Gaskins (1980) "Density estimation and bump-hunting by the penalized likelihood method exemplified by scattering and meteorite data," J. Amer. Statistical Assoc., Vol. 75, No. 369, pp. 42-72.

Hall, P. (1983) "On near neighbour estimates of a multivariate density," J. of Multivariate Analysis, Vol. 13, pp. 24-39.

Hall, P. (1981) "Optimal near neighbour estimator for use in discriminant analysis," Biometrika, Vol. 68, pp. 572-5.

Hand, D.J. (1982) Kernel discriminat analysis, Research Studies Press, John Wiley & Sons, New York.

Lehmann, E.L. (1959) Testing statistical hypotheses, John Wiley & Sons, New York.

Silverman, B.W. (1986) Density estimation for statistics and data analysis, Chapman and Hall, New York.

Skilling, J., A.W. Strong, and K. Bennett (1979) "Maximum entropy image processing in gamma-ray astronomy," Mon. Nat. R. Astr. Soc., Vol. 187, pp. 145-152.

Titterington, D.M. and A. W. Bowman (1985) "A comparative study of smoothing procedures for ordered categorical data," J. Statist. Comput. Simul., Vol. 21, pp. 291-312.

Van Dyck, J. (1985) "Statistical analysis of earthquake catalogs," Ph.D. thesis, Department of Civil Engineering, MIT, Cambridge, Massachusetts.

Veneziano, D. and J. Van Dyck (1986) "Statistical analysis of earthquake catalogs for seismic hazard," Proceedings, Int. Symp. on Engrg. Geology Problems in Seismic Areas, Bari, Italy.

Veneziano, D. and J. Van Dyck (1985), "Statistical discrimination of 'after-shocks' and their contribution to seismic hazard," Appendix A-4 of EPRI (1985).

TOPIC 3

Seismic Sources, Attenuation, and Ground-Motion Estimates

D. M. Boore: *Quantitative Ground Motion Estimates*

J. G. Anderson: *How Important is Attenuation for Characterization of Ground Motions?*

F. T. Wu: *Analysis of Accelerograms from Small to Moderate Earthquakes in Northeastern U.S. and Southeastern Canada*

A. Papageorgiou: *Estimation of Earthquake Strong Ground-Motion in Eastern North America: Preliminary Estimates Vis-a-Vis Existing Data*

J. Nabelek and G. Suarez: *The 1983 Goodnow Earthquake in the Central Adirondacks, NY: A Broadband Teleseismic Analysis*

D. H. Weichert and R. B. Horner: *The Nahanni Earthquakes*

P. Somerville: *Source Scaling Relations of Large Eastern North American Earthquakes and Implications for Strong Ground Motion*

J. S. Barker, P. Somerville and J. P. McLaren: *Modeling Ground-Motion Attenuation in Eastern North America*

R. B. Herrmann and O. W. Nuttli: *Strong Motion Studies in the Central U.S.*

R. K. McGuire and G. R. Toro: *Issues in Strong Ground Motion Estimation in Eastern North America*

G. M. Atkinson: *Implications of Eastern Ground Motion Characteristics for Seismic Hazard Assessment in Eastern North America*

QUANTITATIVE GROUND MOTION ESTIMATES

by

David M. Boore

U. S. Geological Survey, Menlo Park, CA 94025

ABSTRACT

Several papers have been published recently using the stochastic model for the prediction of ground motions in eastern North America (ENA). This model, based on the work of Hanks and McGuire, constructs the ground motion from filtered random Gaussian noise, for which the filter parameters are determined by a seismological model of both the source and the wave propagation. The model has the potential advantage over most other methods for predicting ground motion in ENA that it does not require data from western North America; many of the parameters in the model can be determined from independent seismological investigations in ENA or in other regions with similar tectonic characteristics. In recent papers by Boore and Atkinson and by Toro and McGuire predicting ENA ground motions, simple ω^2 source spectra with a constant stress parameter of 100 bars and a simple inverse power law geometrical spreading were found to give reasonable agreement with the sparse observed data at rock sites, most of which come from earthquakes near moment magnitude 4.5. Since those papers have been published, Boatwright and Choy and Nuttli et al have proposed alternate scaling laws. Both laws lead to motions similar to those from the 100 bar stress model for magnitude 4.5 earthquakes, and therefore the existing ENA accelerograph data cannot distinguish between the recently proposed scaling laws. The various models, however, lead to different motions for larger earthquakes: the Nuttli et al and the Boatwright and Choy scaling leading to motions a factor of more than 3 higher and a factor of 2 lower, respectively, than the motions estimated from the 100 bar model for a M 7.5 earthquake. Comparisons with data from 3 stations close to the M 6.8 Nahanni, Northwest Territories, Canada earthquake suggests that response spectral predictions of Boore and Atkinson are in reasonable agreement with data from 2 out of the 3 stations; the estimates are up to a factor of 5 too high at station 3. In contrast, the Boatwright and Choy scaling leads to estimated ground motions in close agreement with the data from station 3. The interpretation of this comparison is complicated, however, by the point source assumption used in the theoretical predictions. This is clearly an invalid assumption for the Nahanni near-source recordings.

INTRODUCTION

The stochastic model for estimating ground motions is best described with reference to Figure 1; more complete descriptions can be found in Boore (1987), Boore and Atkinson (1987), and Toro and McGuire (1987), and the references therein. The spectra of the radiated motion is specified by a seismological model (in this case, the ω^2 spectrum with constant stress parameter), and the motion is assumed to be spread out in a stochastic manner over a specified duration (in this case, the inverse of the corner frequency). The peak motions can be determined either by a suite of time-domain simulations or, more conveniently, by random process theory. Boore and Atkinson (1987; hereafter referred to as BA87) used this model with a 100 bar stress parameter to predict pseudo-relative velocity spectra (PSV) as well as peak acceleration for hard rock sites in eastern North America

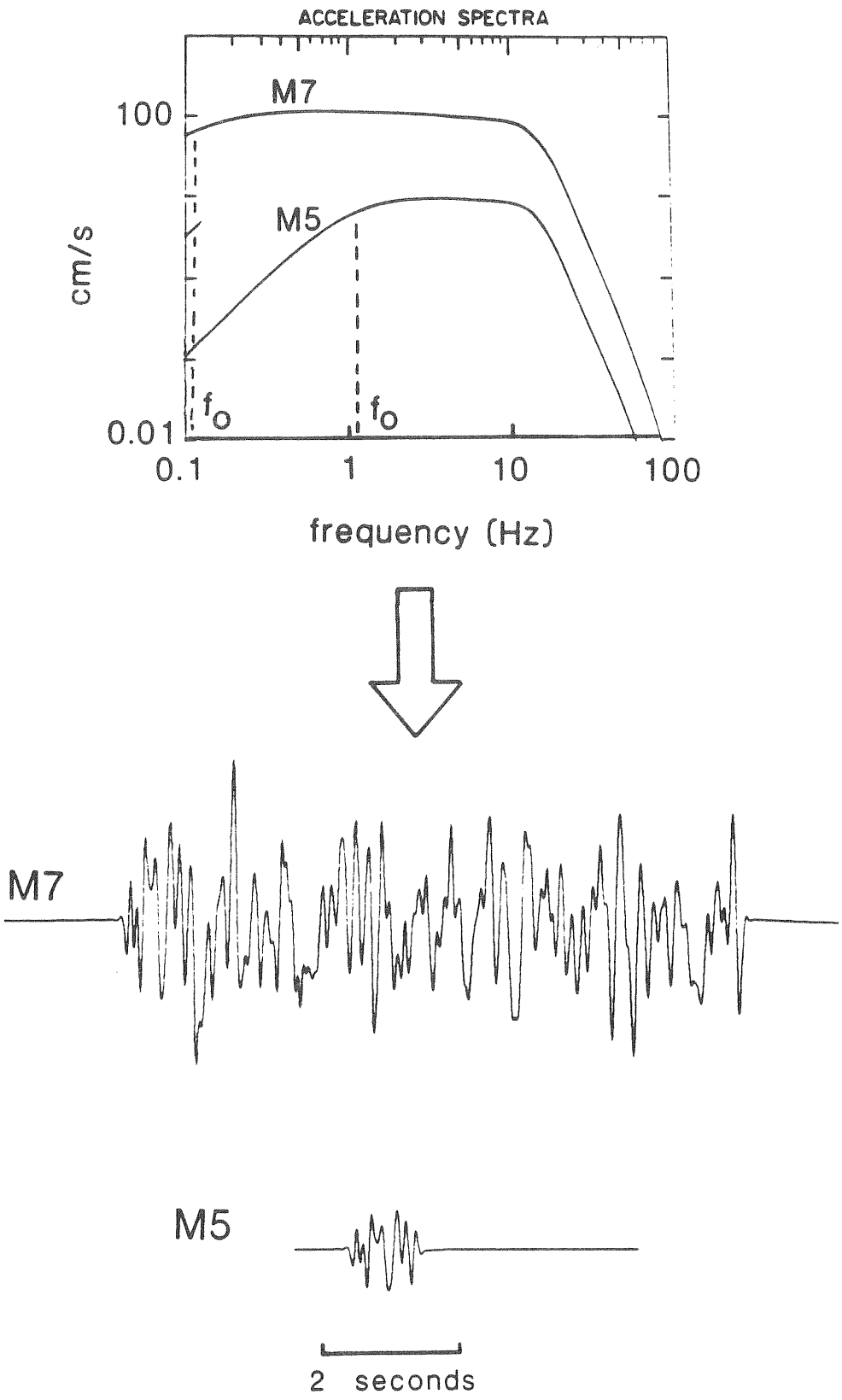

Fig. 1. Basis of stochastic model. Radiated energy described by spectra in upper part of figure are assumed to be distributed randomly over a duration equal to the inverse of the lower frequency corner (f_0). Time series are one realization of a random process.

(ENA). Note that the spectra and time series shown in Figure 1 have not been sketched by hand; they were computed for the magnitudes shown.

SOURCE SCALING

Crucial to the ground motion predictions is the specification of the source spectrum. This usually is comprised of two parts: the shape of the spectrum, and the way in which the spectral corners depend on seismic moment (this dependence is usually referred to as the 'scaling law'). At the time BA87 was written, the only scaling law offered for ENA earthquakes was that of Nuttli (1983; referred to hereafter as N83). BA87 considered this scaling law, but found it to lead to ground motions significantly lower than the few available recordings (mainly for earthquakes around M4.5). BA87 found that scaling with a constant stress parameter of 100 bars gave reasonable predictions of the available data. Since publication of BA87, Nuttli et al (1987, referred to hereafter as N87) and Boatwright and Choy (1987; referred to hereafter as B&C) have published scaling laws for ENA and intraplate earthquakes. Figure 2 compares the magnitude scaling of the high frequency level of $(2\pi f)^2$ times the moment rate spectrum (in effect, this is the acceleration spectrum normalized such that the long period level of the corresponding displacement spectrum is equal to the seismic moment) for the various scaling laws.

Boatwright and Choy (1987) used teleseismic P-waves to derive their source spectra. In order to apply their results to the radiation of S-waves, I have assumed that the shape of the source spectra is the same for both P- and S-waves, with a specified ratio between the P- and S-wave corner frequencies. A frequency-independent multiplicative factor accounted for the radiation pattern and seismic velocity differences. The high-frequency spectral level of the S-wave depends on this multiplicative factor and on the ratio of corner frequencies. In most of the computations presented here, the corner frequency ratio has been taken to be unity. This produces a result that is consistent with Choy and Boatwright's derivation of high-frequency S-wave spectral amplitudes from their P-wave scaling (Choy and Boatwright, 1988). For comparative purposes, Figure 2 also contains results for a corner frequency ratio of 1.5.

From Figure 2 alone, we can see that all other things being equal, the N83 scaling will lead to much lower ground motions than the 100 bar scaling, and that the revised scaling given by N87 will lead to motions similar to those given by the 100 bar relation used by BA87. The B&C relation with a corner frequency ration of 1.5 leads to low motions, as will their relation with a ratio of 1.0 (except for events near M4.5).

The spectral shapes assumed for the constant stress (100 bar) and B&C scalings, for earthquakes of magnitudes 5.5 and 7.5, are shown in Figure 3. The left and right frames are for corner frequency ratios of 1.0 and 1.5, respectively. The B&C spectra are characterized by two corner frequencies. The higher of the two corners is determined by a least square line fit to B&C observations of corner frequency vrs moment magnitude; the lower corner is found by intersection of the low frequency part of the spectrum, determined by moment, and a line of unit slope between the observationally determined high-frequency corner and spectral level.

COMPARISON WITH ENA GROUND MOTIONS

Figure 4, patterned after Figure 7 in BA87, shows the predicted PSV as a function of distance for the various scaling laws. The symbols are available data from rock sites in ENA. Coincidentally, the N87 and B&C (with corner frequency ratio of unity) laws give virtually identical motions (see the previous figure also). It would be difficult to choose between the 100 bar, N87, and B&C laws based on a comparison of the predictions to the observations.

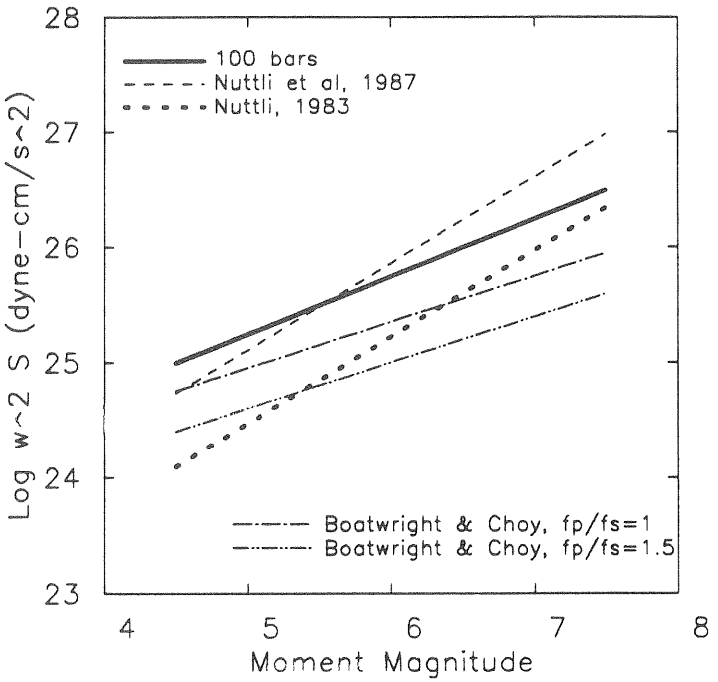

Fig. 2. High-frequency acceleration spectral levels predicted by various scaling laws.

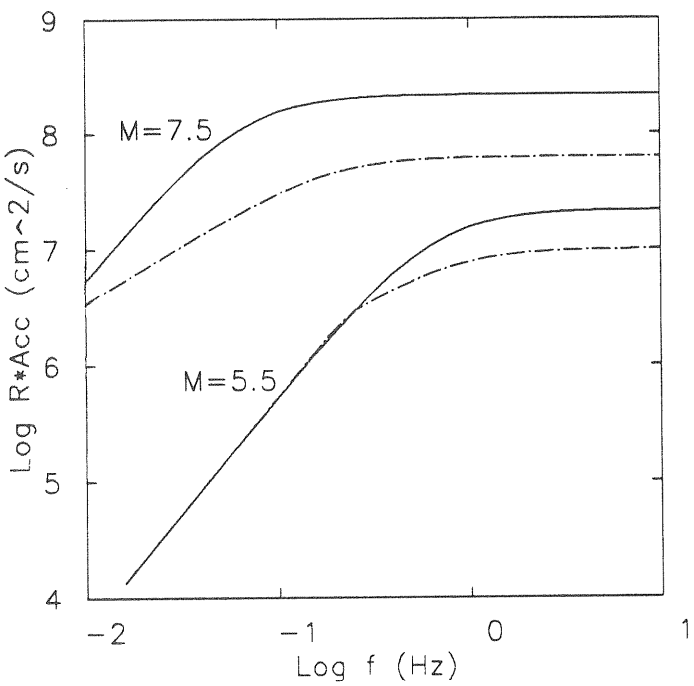

Fig. 3. Distance-corrected acceleration spectra for 100 bar (solid line) and Boatwright and Choy (dot-dash line) scalings. The ratio of P-wave to S-wave corner frequencies was 1.0.

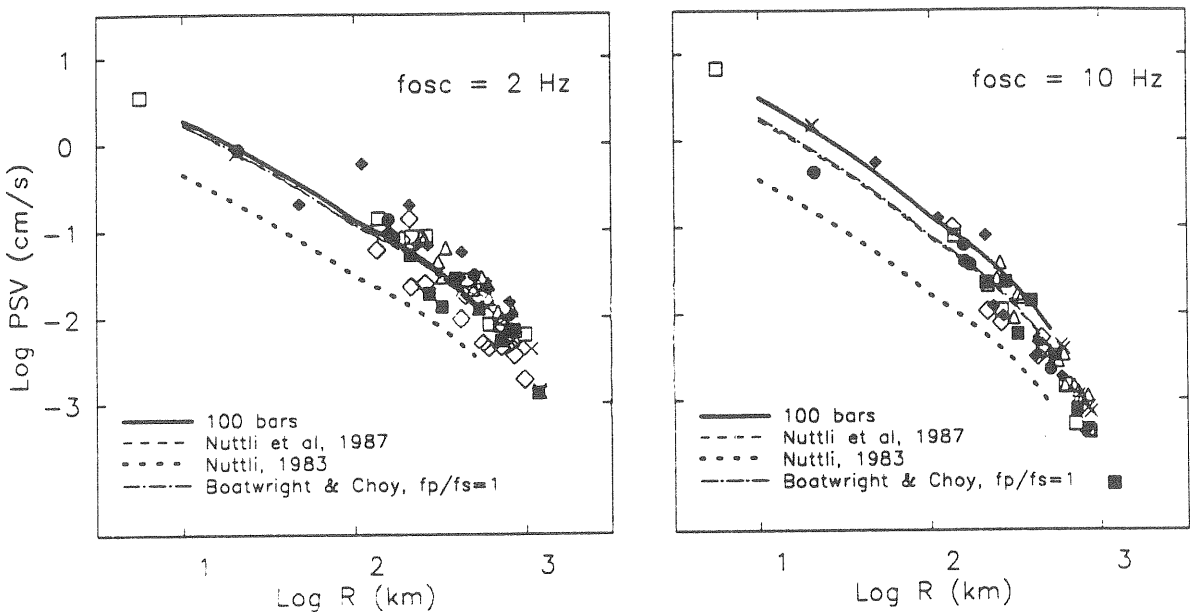

Fig. 4. Comparison of observed (symbols) and predicted (lines) 5 percent damped pseudo-velocity response spectra (PSV) for 2- and 10-Hz oscillators. Data have been normalized to M 4.5, using scaling obtained from the theoretical predictions using 100 bar scaling. See Fig. 7 in Boore and Atkinson (1987) for key to symbols.

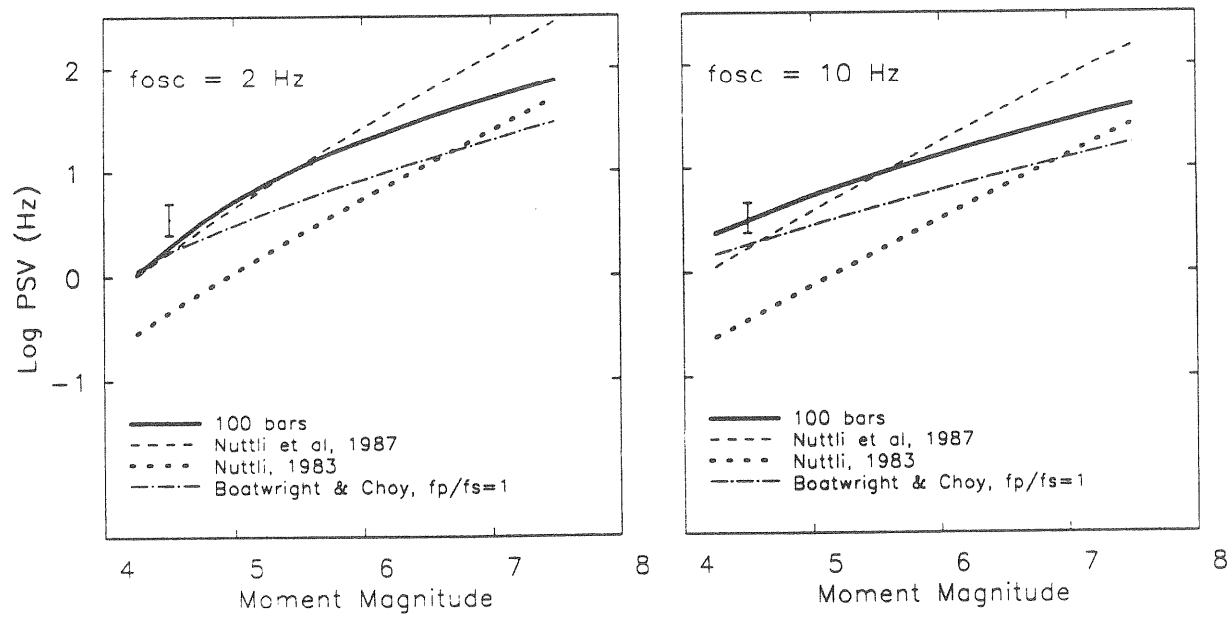

Fig. 5. Scaling of PSV with moment magnitude (M) at 10 km distance for 2- and 10-Hz oscillators. The skant data suggest PSV values indicated by the bar at M4.5.

The scaling with magnitude of PSV for the various scaling laws, at a fixed distance of 10 km, is shown in Figure 5. It is clear that although the 100 bar, N87, and B&C laws lead to similar motions at M4.5 (see previous figure also), the predictions diverge for the large earthquakes of most importance for engineering design. Data from these large events are needed to distinguish between the models. B&C based their study on teleseismic recordings of earthquakes greater than M5, and so preference should perhaps be given to their law. On the other hand, the 100 bar relation gave a reasonable prediction of m_{Lg} values for larger ENA earthquakes (BA87 and Atkinson and Boore, 1987), and Somerville et al (1987) found an average stress drop of 100 bars in their analysis of teleseismic recordings of large earthquakes in eastern North America.

COMPARISON WITH NAHANNI EARTHQUAKE DATA

The December 23, 1985, Nahanni, Northwest Territories earthquake was recorded on three nearby SMA stations. These records offer an important data set for the discrimination between models. The aftershock locations and instrument locations are shown in Figure 6, which was taken from Weichert et al (1986).

Observed and predicted pseudo-relative velocity spectra (PSV) at the three stations are shown in Figure 7. The PSV at station 1 was computed using the first 7 seconds of record, thereby eliminating the large burst of energy late in the record. The open circles are predictions using equations in BA87, with two distance measures– closest distance, and distance to the center of aftershocks; the x's are predictions from Joyner and Boore's analysis of records from western North America (Joyner and Boore, 1982). The agreement between observed and predicted values is reasonable, especially in view of the large scatter of individual observation that exists in any attempt to predict mean values of ground motion.

The comparison in Figure 7 was between PSV derived from observations and previously published predictions of the PSV. The relation between the data and theoretical predictions using Boatwright and Choy's scaling, as well as the 100 bar stress parameter model, are shown in Figures 8 and 9. The comparison is in terms of Fourier amplitude spectra (FAS) rather than PSV (the relative agreement of observations and predictions should be similar for both quantities, however). The observations are given by heavy lines (where, as with PSV, only the first 7 seconds were used in computing the FAS for station 1). In Figure 8, the predictions used the distances and radiation pattern terms used by Boatwright and Choy in an unpublished manuscript. The predictions in Figure 9 use my estimates of distances (closest distance and distance to center of aftershocks) and the radiation pattern term used in BA87. B&C give a better fit to the observations when using their parameters, and as expected from the comparison in Figure 7, the 100 bar prediction is reasonable for stations 1 and 2 when using the BA87 parameters. B&C, however, consistently have a better fit to the station 3 acceleration spectrum than given by the 100 bar model. Some cautions are necessary before drawing any firm conclusions from these comparisons. First, the BA87 predictions are for the mean value of motion, and the motions from any one earthquake could be systematically higher or lower than the mean value. Second, radiation pattern and geometrical spreading terms, as well as directivity and partition of energy into various components, affect the overall amplitude level but are somewhat uncertain, especially close to large faults. For this reason, a firm conclusion that one scaling model is better than another should not be reached solely on the basis of the Nahanni data.

ACKNOWLEDGMENTS

I thank Jack Boatwright, Tom Hanks, and Bill Joyner for comments on this paper. The research reported here was funded by the U. S. Nuclear Regulatory Commission.

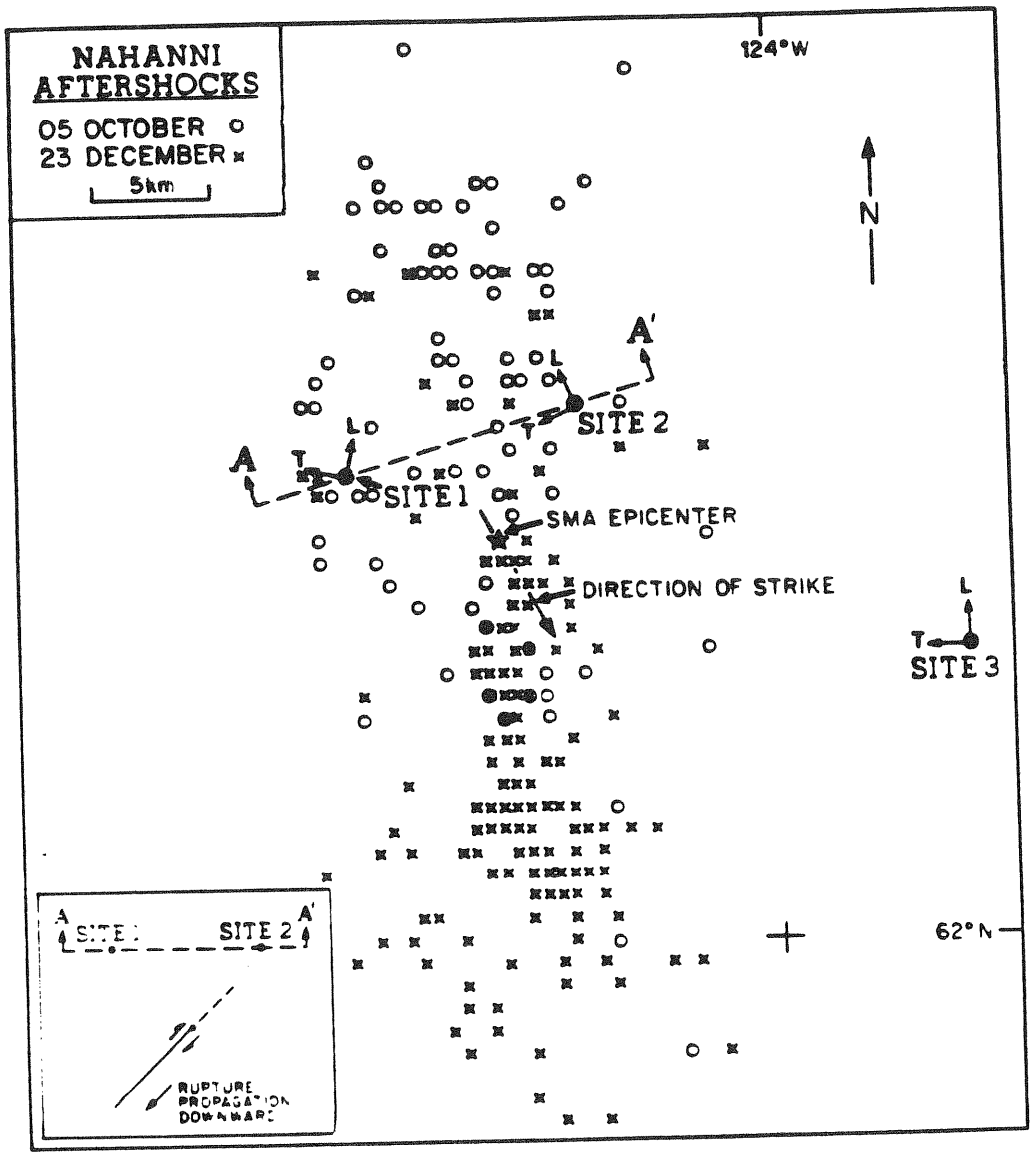

Fig. 6. Station locations of SMA instruments (filled circles) and aftershocks of Nahanni earthquakes (taken from Weichert et al, 1986)

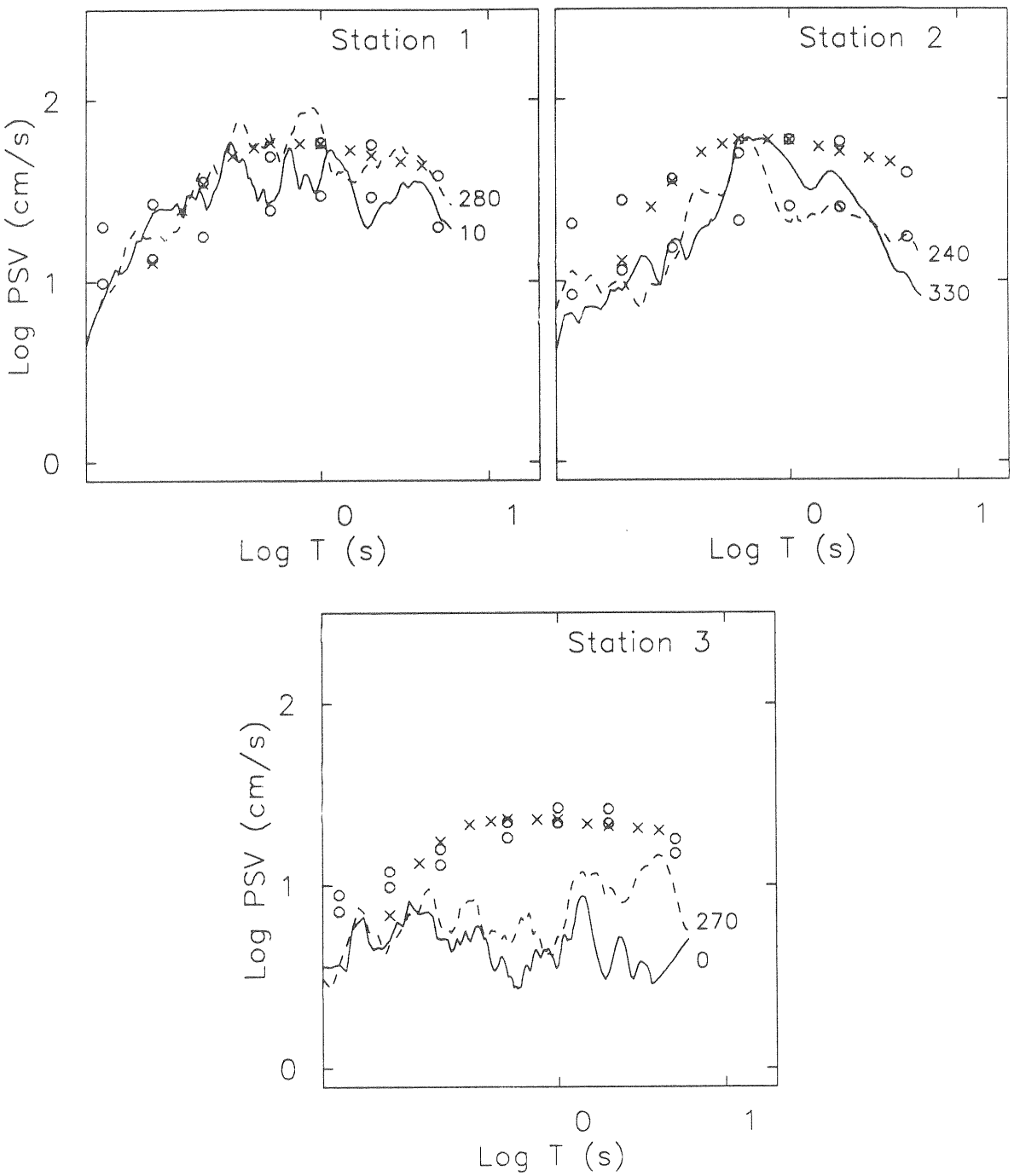

Fig. 7. (*lines*) 5-percent damped response spectra calculated from first 7 seconds of horizontal components at sites 1, 2, and 3 recorded during December 23, 1985, Nahanni, Northwest Territories earthquake; (*circles*) theoretical predictions from stochastic model, using equations in Boore and Atkinson (1987) and two estimates of distance to rupture surface; (*x's*) estimates from regression analysis of western North America recordings prior to 1981, from equations in Joyner and Boore (1982).

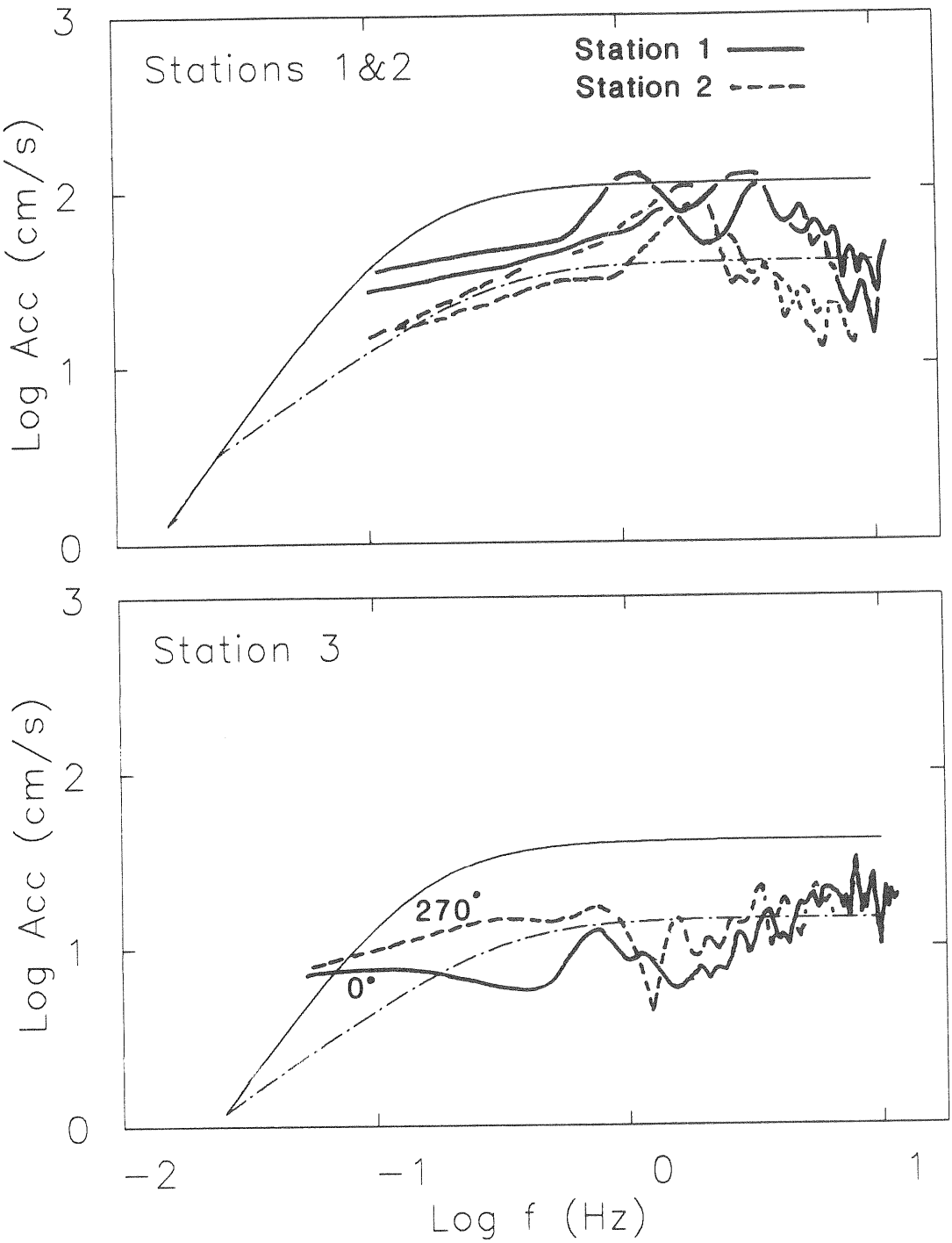

Fig. 8. (*heavy lines*) Acceleration spectra from first 7.5 seconds of horizontal components at sites 1, 2, and 3 recorded during the 23 December 1985 Nahanni earthquake; (*light lines*) estimated spectra, using 100 bar model (solid line) and Boatwright and Choy model (dash-dot: P- to S-wave corner frequency ratio=1.0). Distances and radiation patterns from Choy and Boatwright (1988).

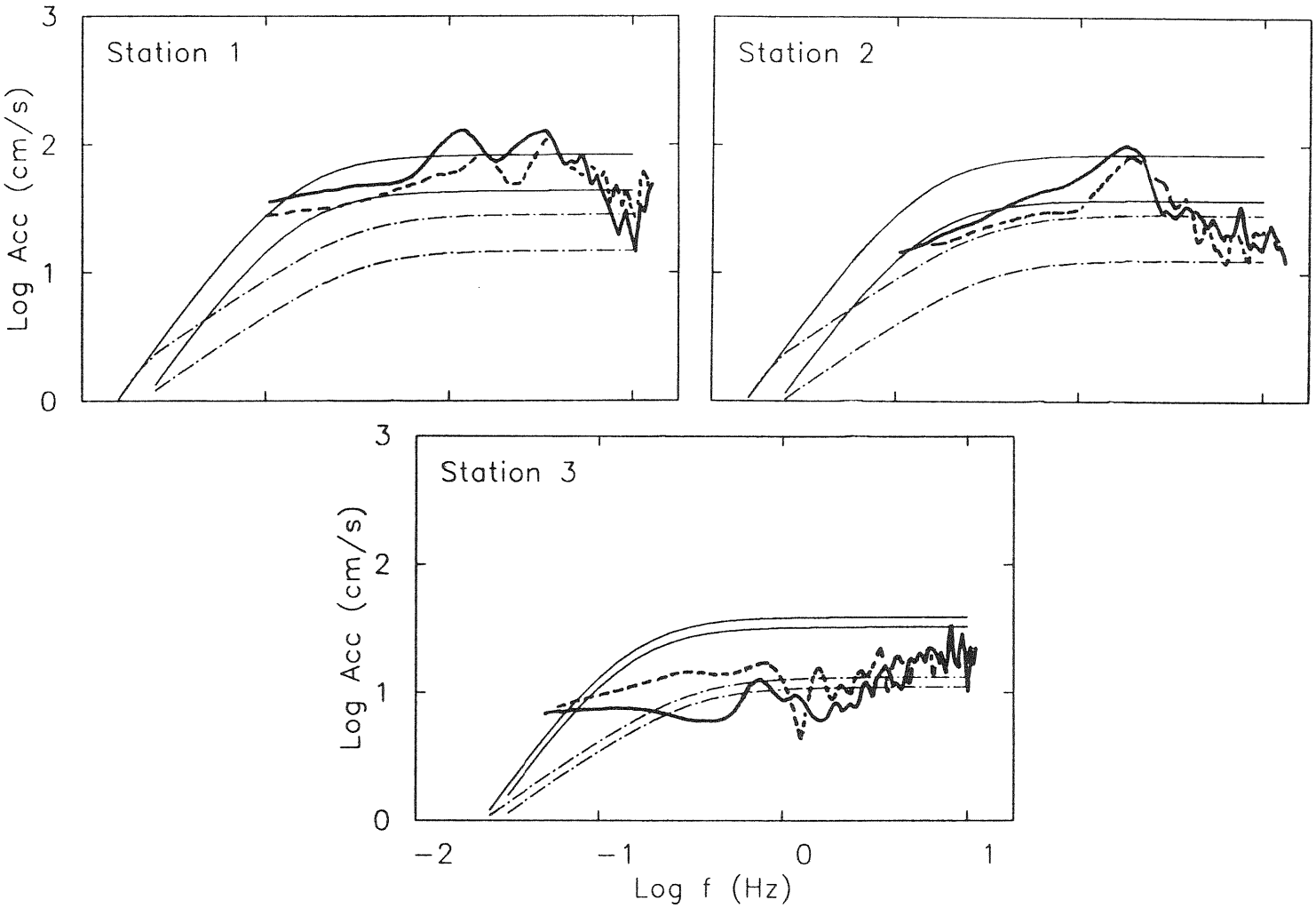

Fig. 9. Observed and predicted acceleration spectra from 23 December 1985 Nahanni earthquake. Predictions used my estimates of distances and the radiation pattern correction of Boore and Atkinson (1987). The upper and lower curve of each pair used the closest distance to the rupture surface and distance to the center of the rupture surface, respectively. The solid curves used the 100 bar model and the dot-dashed curves used the Boatwright and Choy scaling.

REFERENCES

Atkinson, G. M. and D. M. Boore, On the m_N, M relation for eastern North American earthquakes, *Bull. Seismol. Soc. Am.* ,*58*, (in press), 1987.

Boatwright, J. and G. L. Choy, Acceleration source spectra for large earthquakes in North Eastern North America, in *Proc. of Workshop on Earthquake Ground-Motion Estimation in Eastern North America*, Electric Power Research Institute, Palo Alto, Calif. (in press), 1987.

Boore, D. M., The prediction of strong ground motion, in *Strong Ground Motion Seismology*, M. Ö. Erdik and M. N. Toksöz, eds., D. Reidel Publishing Co., Dordrecht, pp. 109–141.

Boore, D. M. and G. M. Atkinson, Stochastic prediction of ground motion and spectral response parameters at hard-rock sites in eastern North America, *Bull. Seismol. Soc. Am.* , *77*, 440–467, 1987.

Choy, G. L. and J. Boatwright, Teleseismic analysis of the Nahanni earthquakes in the Northwest Territories, Canada, *Bull. Seismol. Soc. Am.* (submitted), 1988.

Joyner, W. B. and D. M. Boore, Prediction of earthquake response spectra, *U. S. Geol. Surv. Open-File Rep. 82-977*, 16 pp., 1982.

Nuttli, O. W., Average seismic source-parameter relations for mid-plate earthquakes, *Bull. Seismol. Soc. Am.* , *73*, 519–535.

Nuttli, O. W., D. S. Bowling, J. E. Lawson, Jr., and R. Wheeler, Some aspects of seismic scaling and the strong ground motion of the eastern Missouri earthquake of January 12, 1984, *Bull. Seismol. Soc. Am.* , *58*, 53–58.

Somerville, P. G., J. P. McLaren, L. V. LeFevre, R. W. Burger, and D. V. Helmberger, Comparison of source scaling relations of eastern and western North American earthquakes, *Bull. Seismol. Soc. Am.* , *77*, 347–365, 1987.

Toro, G. R. and R. K. McGuire, An investigation into earthquake ground motion characteristics in eastern North America, *Bull. Seismol. Soc. Am.* , *77*, 468–489.

Weichert, D. H., R. J. Wetmiller, and P. Munro, Vertical earthquake acceleration exceeding 2 *g*? The case of the missing peak, *Bull. Seismol. Soc. Am.* , *76*, 1473–1478.

HOW IMPORTANT IS ATTENUATION FOR CHARACTERIZATION OF GROUND MOTIONS?

J. G. Anderson

Institute of Geophysics & Planetary Physics, UC San Diego, La Jolla, CA 92093

ABSTRACT AND SUMMARY

This paper summarizes the results of several studies of the spectrum of ground motion at high frequencies. We describe the Fourier spectral amplitude of seismic ground acceleration by an overall shape, with fine structure superimposed. In normal cases, the shape of the Fourier spectrum, $A(f)$, falls off exponentially with frequency, f, at high frequencies, i.e. $A(f) \propto e^{\pi \kappa f}$. The size of κ ranges from 0.01 sec or less for hard rock sites and earthquakes recorded at close distances, to 0.1 sec or a little more for earthquakes recorded on sediments at distances of 150 to 200 km. An understanding of this phenomenon will lead to insight into geophysical processes in the Earth and improved capabilities to generate synthetic seismograms. This report studies several aspects of this observation, taking as an underlying viewpoint that the exponential decay is caused by attenuation someplace along the propagation path of the seismic waves. The attenuation mechanism is completely consistent with the observations; the alternative that the exponential decay is caused by a source effect is less consistent.

Both whole path and site effects contribute to determine the value of κ estimated from seismograms, and these two contributions can be separated. For southern California, a descriptive model gives the average increase in κ with distance, and can be used to estimate the site contribution to κ from a few seismograms recorded at arbitrary distances.

The observational parameter, κ, is modeled as the result of attenuation at all depths in the earth. On high quality data from the digital network at Anza, California, observations of the spectral decay are consistent with observations of Q obtained by the usual technique of considering the decrease in the amplitude of seismic waves as a function of distance. It is essential to recognize that Q can be regarded as a sum of effects from many phenomenon, some of which contributions are independent of frequency (Q_i), and others of which are frequency dependent (Q_d). The spectral decay parameter is modeled as a consequence of the frequency-independent process. The size of κ as a function of distance has been inverted under this model to find an estimate of Q_i as a function of depth in the Earth. In the vicinity of Anza, in southern California, Q_i is moderate near the surface, very large at seismogenic depths, and decreases somewhat below these depths. The total Q also contains a contribution Q_d which depends on frequency, and modeled by $Q_d \propto qf$. At seismogenic depths, Q_d contributes more to the total attenuation for frequencies less than about 20 Hz, and Q_i contributes more above 20 Hz. These results are important for an eventual understanding of the physical processes which control Q, and how they may vary from one region to another.

If exponential decay is a path-dependent phenomenon, independent of the amplitude of the seismic waves, then the phenomenon would modify the spectra of small earthquakes as well as large, and would potentially contaminate estimates of the corner frequency and stress drop [Anderson, 1986]. Therefore, it is essential to be sure that it is not a factor in source mechanism studies.

Keeping this in mind, in a study of aftershocks of the Coalinga, California, earthquake Anderson & Reichle [1988] developed a method to separate the spectral decay from the falloff associated with the corner frequency in data of limited bandwidth. To do this, a Brune spectral shape modified by the exponential decay is fit to the entire spectrum. This three-parameter model seems to be consistently successful in fitting the spectra for small to moderate sized events from both California and eastern North America. The technique naturally tells when it is possible to separate the effect of exponential fall-off from spectral fall-off caused by the corner frequency, and for small events it seems to indicate that stress drop is independent of earthquake moment to the highest corner frequencies (i.e., smallest events) for which these two effects are separable. For events of magnitude 3.3 to 6.7, there was apparently no systematic variation of the decay parameter with the size of the earthquake, but the quality of data in that study was not high enough

to definitively rule it out.

In the application to data from eastern North America, a limited selection of accelerograms show spectral shapes which fit the same model as found for the California data. Decay parameters take on similar values, correlated with the shallow geology of the site. Stress drop parameters are similar to estimates obtained from California data, and are also consistent with estimates obtained from larger events in the eastern North America region. Thus for small source- to- station distances, the source geometry and the site conditions (including attenuation and amplification due to material in the weathered zone) are more important determinants of the nature of ground motion than are regional differences in attenuation.

Finally, we initiate a consideration of the effect of modifying the spectral decay parameter for an accelerogram, holding everything else the same. This technique might be useful in the future to help extend the strong motion data set to regions with a paucity of data.

OBSERVATIONS

This research begins with the observation that at high frequencies, the trend of the spectrum of seismic ground accelerations, $A(f)$, can be fit by an exponentially decaying curve, as in the example in Figure 1. A spectral decay parameter, κ, is defined through the equation

$$A(f) \propto A_0 e^{-\pi \kappa f} \quad \text{(high frequency asymptote)} \tag{1}$$

The second fundamental observation is that the decay parameter is a function of the conditions near the site, and also a function of distance fron the earthquake to the site. Figure 2 shows several measurements of κ taken at two sites, one at El Centro in the Imperial Valley and the other at Pinyon Flat, both in California. This figure shows κ increasing at a similar rate with distance at both stations, but with differing values at the origin.

This paper will summarize several papers, which, taken together, provide a model for this phenomenon. Two models for the origin of the high frequency rolloff of the spectrum have been proposed. The first is that it is due to attenuation, and the second is that it is caused by a source effect. Indeed, from any one seismogram, it is impossible to definitively separate source and attenuation effects.

The two sites in Figure 2 are separated by about 120 km. The Pinyon Flat site is on weathered granite within the southern California batholith, in the Peninsular Range. Although at the surface the granite has decomposed to soil, drill holes nearby demonstrate that it becomes very hard within a few meters of the surface. The seismometers are on a pier below the loose soil layer. Thus we expect high Q at this site. The El Centro site is underlain by perhaps 4 to 5 km of Colorado River sediments, and thus the shallow layers are expected to have a much lower Q than at Pinyon Flat. If κ is an attenuation parameter, then the behavior seen in Figure 2 is easy to explain: the intercept can be attributed to attenuation in the shallow geological structure below the station, and the increase in κ with distance can be attributed to the regional Q structure, which would affect both of the stations more or less in the same way.

To explain the observations in Figure 2 as a source effect would require that the sources of the earthquakes have systematically larger rolloffs as the distances from the stations increase, even though the station locations are random relative to the earthquake locations. Unfortunately, there are no common earthquakes, recorded at both of the stations in Figure 2. However, one segment of the San Jacinto fault has produced earthquakes which were recorded at the El Centro station (between 45 and 70 km) and at the Pinyon Flat station (between 50 to 70 km). As seen in Figure 2, these events from a common region do not introduce any anomalies in the curves of κ as a function of distance.

DESCRIPTIVE MODEL OF THE DATA

The above considerations suggest a model for κ as follows:

$$\kappa(R,S) = \tilde{\kappa}(R) + \kappa_0(S) \tag{2}$$

In equation 2, R is the epicentral distance, and S identifies the recording site; $\tilde{\kappa}(0) = 0$. Anderson [1987] applied (2) to the data obtained by Anderson & Hough [1984] and Hough et al. [1988].

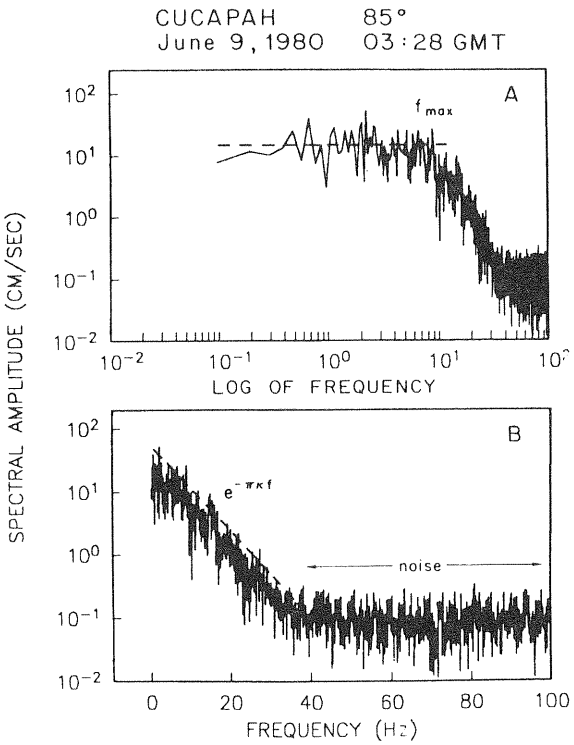

Figure 1. Fourier amplitude spectrum of the N85°E component of strong ground acceleration recorded at Cucapah during the Mexicali Valley earthquake of 9 June 1980 (M_L 6.2). Accelerograph was a digital recorder which samples at a rate of 200/sec. (A) Log-log axies. (B) Linear-log axes.

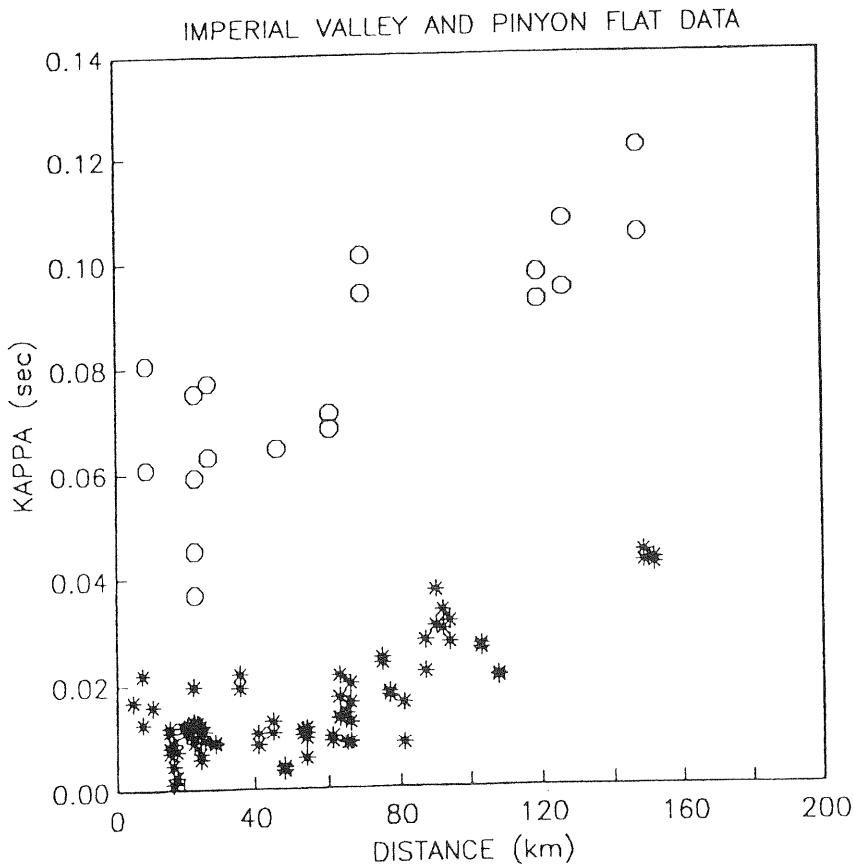

Figure 2. Spectral decay parameter, κ, from earthquakes at El Centro (circles) and PFO (asterisks). El Centro data from Anderson and Hough [1984]. Data previously published by Anderson [1986].

Hough et al. estimated κ from seismograms of 68 separate earthquakes recorded on the 10-station Anza network. Together with the El Centro data shown in Figure 2, this gives a total of 11 stations. The resulting model is given in Table I and shown in Figure 3 for S-waves. The individual station terms are listed in Table II. Figure 3 shows that equation (2) is justified as a fit to summarize all of the κ observations included in the regression.

Table II also gives a brief description of the geological conditions for several of the stations where we have estimated $\kappa_0(S)$. We suggest that there is a qualitative relationship between the site condition and κ_0, with harder rock leading to lower values of κ_0; $\kappa_0(S)$ can be considered a quantitative measure of site quality.

In Table I and Figure 4 the value of $\tilde{\kappa}(R)$ for P and for S waves, determined from the Anza and Imperial Valley data sets, are given. These results are discussed more thoroughly by Anderson [1987].

IMPLICATIONS FOR Q STRUCTURE

The papers by Hough et al. [1988] and Hough & Anderson [1988a,b] study the spectral decay parameter estimated from moderate sized events recorded on the digital network at Anza, California. These high quality data show that the observations of the spectral decay are consistent with observations of Q obtained by the usual technique of considering the decrease in the amplitude of seismic waves as a function of distance. It is essential to recognize that Q can be regarded as a sum of effects from many phenomenon, some of which cause Q to be independent of frequency (Q_i), and others which cause Q to be frequency dependent (Q_d). The spectral decay parameter can then be modeled as a consequence of the frequency-independent processes. These considerations suggest two lines of investigation, the first to estimate the size of Q_d, and the second to estimate Q_i. We consider Q_i first.

Observations of κ *(R,S)* have been inverted by Hough & Anderson [1988a] to find an estimate of Q_i as a function of depth in the Earth. The preferred result for a Peninsular Range site (PFO, KNW) is shown in Figure 5 for S waves. This model is based on a first-arrival ray tracing for the estimation of the effect of Q within each layer. This approximation is tested in Figure 6, from Hough & Anderson [1988b] through the use of synthetic seismograms. The synthetics were computed using the velocity model for Anza and the Q_i model obtained in the inversion. Then the S-waves of the synthetics were Fourier transformed using windows similar to those used in the actual data analysis, thus including multiple reflections rather than only first arrivals. The values of κ at various distances based on these synthetics are shown as large circles in Figure 6. The original data are shown based on small circles. The solid line in Figure 6 is the prediction for κ as a function of distance based on the value of Q_i encountered by the first ray arrival. Based on this, and other comparisons, Hough & Anderson [1988b] conclude that the Q_i model shown in Figure 5 has the correct main features.

Figure 5 shows a high-Q_i layer coincident with the depths of earthquakes near Anza, and also coincident with the depths of maximum strength in the crust based on pressure and temperature considerations. Hough & Anderson [1988a] therefore suggested that Q_i might be controlled by a physical process which is also controlled by pressure and temperature, although that conclusion is not unique. In any case, it will be of great geophysical interest to study Q_i in this manner for other parts of the North American continent to see how the results differ.

As indicated above, the second line of investigation is to estimate the size of Q_d. Hough et al. [1988] investigated this by two approaches, both of which made use of the absolute high frequency amplitudes of a suite of events with magnitudes between 4.0 and 4.5 recorded at distances from 20 to 160 km. Assuming that all of these events had similar spectral amplitudes at the source, the first approach looked at the spectral amplitudes as a function of distance, and estimated total Q, Q_t, at selected frequencies assuming geometrical spreading is proportional to $1/r$. The second approach was to make use of the coefficient A_0 (equation 1), which gives spectral amplitudes which have been adjusted for the exponential decay term. The amplitude of A_0 decreases more rapidly than $1/r$, and this additional falloff was attributed to Q_d proportional to frequency. In Figure 7, we have shown the amplitudes of Q_i, Q_d, $(1/Q_i + 1/Q_d)$, and Q_t, where Q_i is appropriate for depth of lateral wave propagation. Within errors, we find that Q_t and $(1/Q_i +$

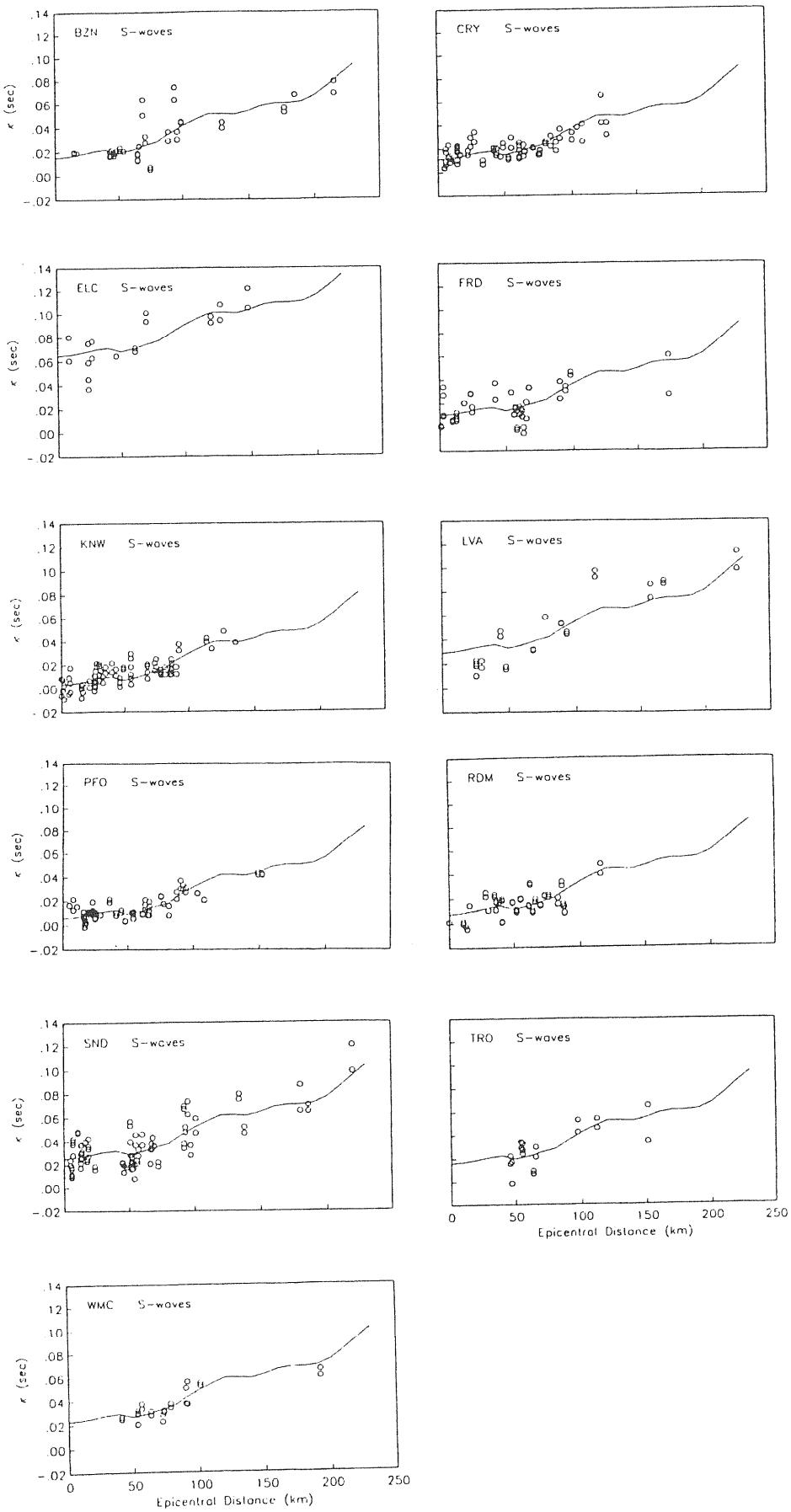

Figure 3. Fit of equation (2) to observations of κ for S-waves at eleven stations in southern California, from Anderson [1987].

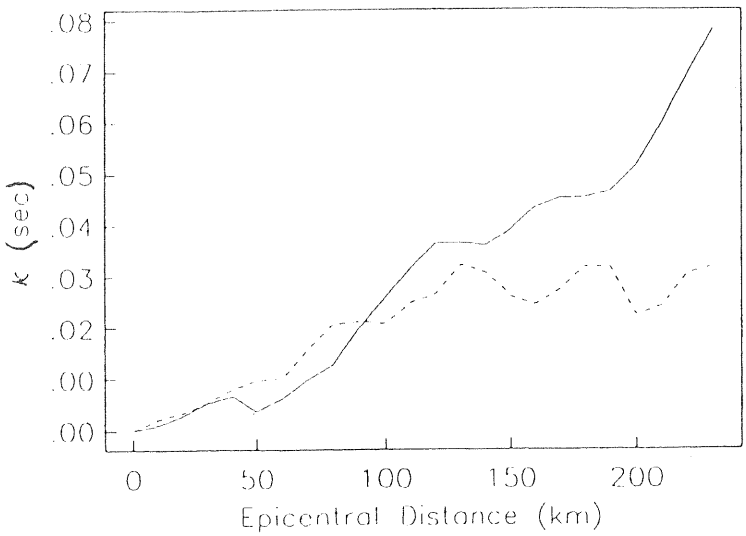

Figure 4. Distance function $\tilde{\kappa}(R)$ (eqn. 2) for southern California for P-waves (dashed) and S-waves (solid), from Anderson [1987].

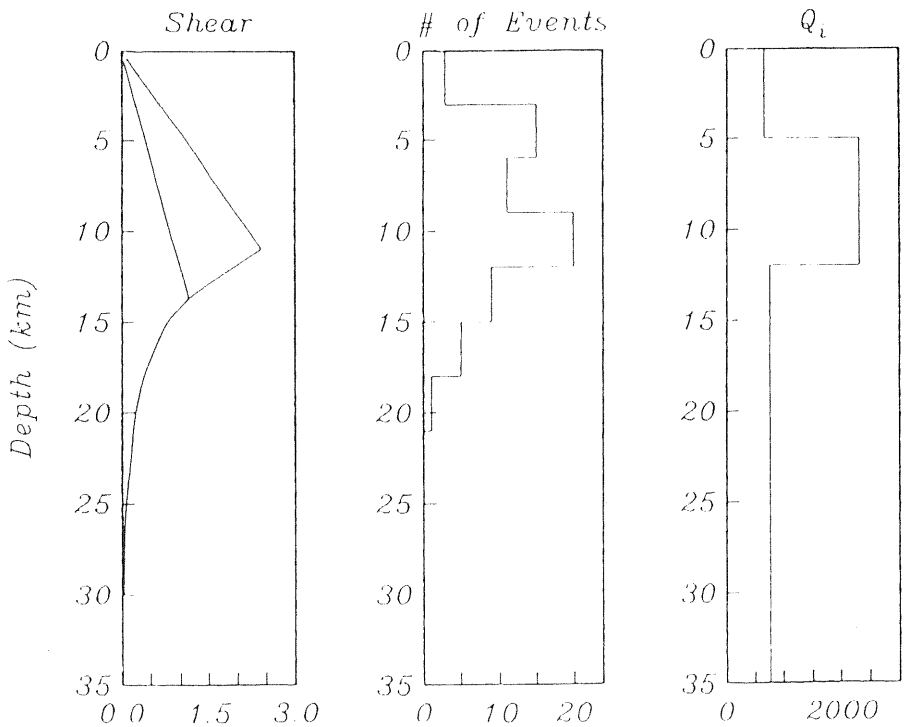

Figure 5. Theoretical maximum shear resistance [after Sibson, 1984] depth of earthquakes near Anza [after Doser and Kanamori, 1986], and Q_i as a function of depth. Shear resistance is in kbars. The Q_i model is an idealized 3-layer model for S waves. [from Hough & Anderson, (1988a)

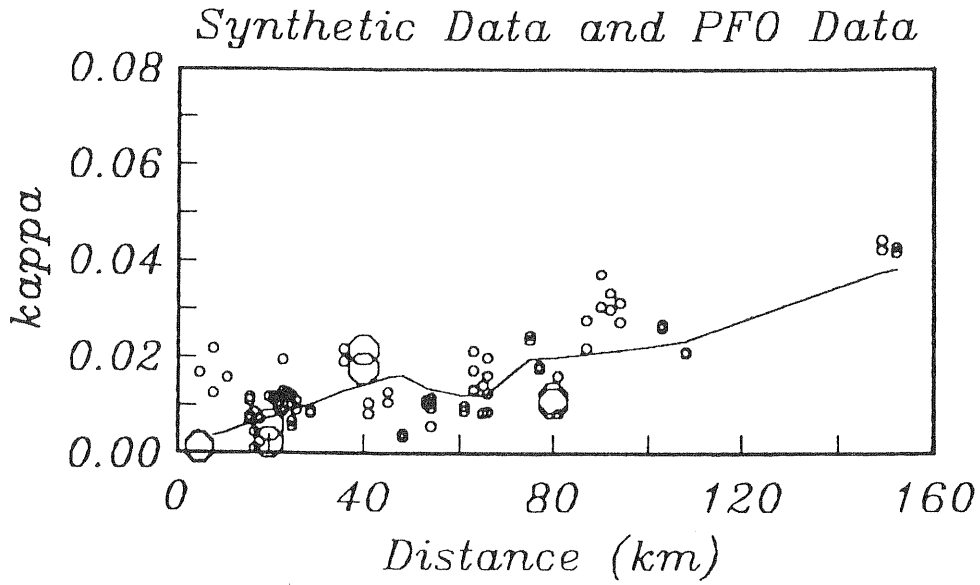

Figure 6. Calculated decay parameters from the Q_i model shown in Figure 5 (large circles). Observations of spectral decay parameters at station PFO (small circles). Also shown is predicted $\kappa(r)$ curve obtained by Hough & Anderson [1988] based on attenuation along the first arriving ray for Q_i model for PFO. (from Hough & Anderson [1988b[

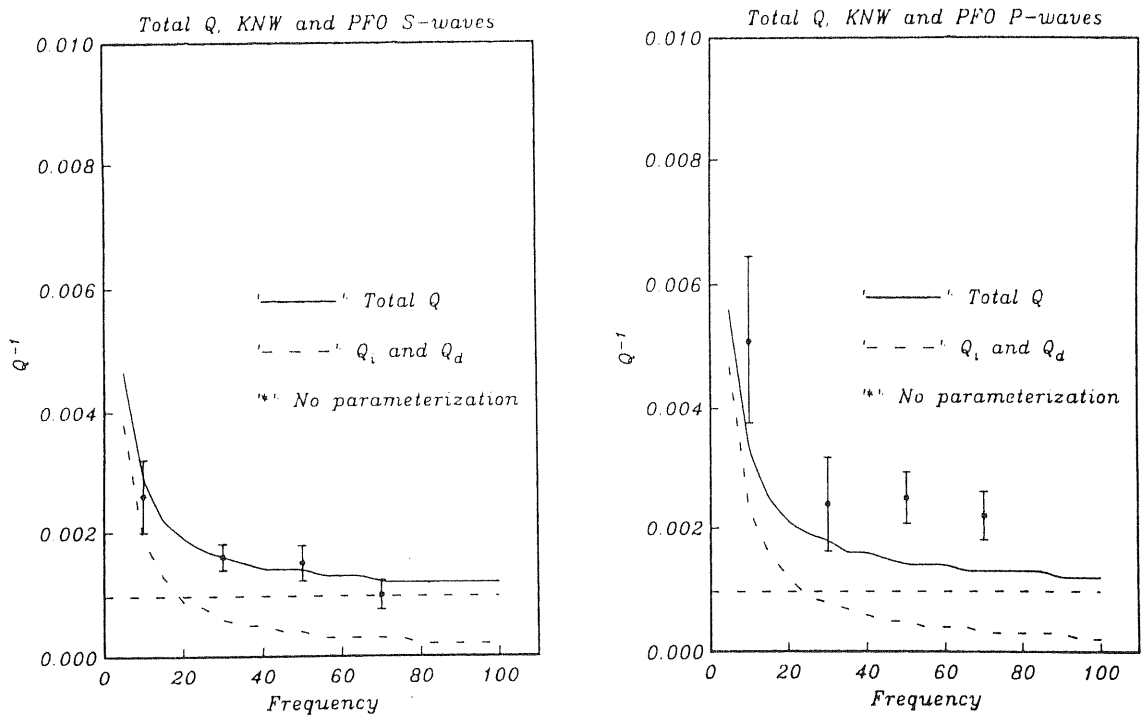

Figure 7. Comparison of Q estimates for S-waves and P-waves observed at Anza stations for KNW and PFO. Dashed lines show Q_i and Q_d estimated separately by Hough et al. [1988], and solid line shows the total Q obtained as a sum of these two contributions. The individual data points with error bars were obtained directly by Hough et al. from spectral amplitudes averaged over 20 Hz frequency band. [from Hough et al., 1988]

Table I
Preliminary numerical values for $\tilde{\kappa}(R)$ in southern California

R	S-waves	# data	P-waves	# data
0	0.0	13	0.0	5
10	1.0	57	2.2	27
20	2.8	62	3.4	32
30	5.3	51	5.5	27
40	6.7	40	8.1	18
50	3.7	80	9.7	29
60	6.2	70	10.1	23
70	9.8	58	15.6	26
80	12.8	36	20.8	12
90	19.9	52	21.3	26
100	26.2	22	20.9	6
110	31.7	8	25.0	7
120	36.5	10	26.6	6
130	36.6	9	32.4	3
140	36.1	3	30.8	3
150	39.1	8	26.2	3
160	43.4	2	24.6	2
170	45.2	4	27.4	2
180	45.3	4	31.9	1
190	46.5	6	32.0	3
200	51.6	0	22.6	1
210	59.9	0	24.4	5
220	69.5	4	30.7	3
230	78.4	2	32.1	3

Table II
Preliminary estimates of $\kappa_0(S)$ for the stations used in this study

Station	Geology	S-waves $\kappa_0(S)$ (msec)	S-waves # data	P-waves $\kappa_0(S)$ (msec)	P-waves # data	Ratios* R_a	Ratios* R_b
ELC	deep alluvium	64.6	20		0		
BZN		15.1	43	5.1	22	3.0	1.8
CRY		11.2	86	13.8	31	0.8	0.5
FRD		10.2	47	-0.6	27	?	
KNW	polished granite	3.4	96	-2.1	44	?	
LVA		29.2	26	16.1	13	1.8	1.1
PFO	granite weathered to 10 m	5.8	88	2.0	40	2.9	1.7
RDM		7.2	55	2.1	31	3.4	2.0
SND	in San Jacinto fault zone	25.5	94	13.2	50	1.9	1.1
TRO		16.1	20	10.4	2	1.5	0.9
WMC		22.9	26	8.4	14	2.7	1.6

*R_a is $\left[\dfrac{\kappa_0(S) \text{ for S waves}}{\kappa_0(S) \text{ for P waves}}\right]$

Ratio $R_b = \dfrac{R_a}{1.7}$, and thus for a Poisson's ratio of 0.25, $R_b = \dfrac{Q_{Pi}}{Q_{Si}}$ where Q_{Pi} is the frequency independent contribution to attenuation of P waves, and Q_{Si} is the frequency independent contribution to attenuation of S waves.

$1/Q_d$) are indistinguishable for S waves. At frequencies below about 20 Hz in Anza, frequency dependent Q seems to be more important than the frequency-independent contribution.

Rebollar et al. [1985] have estimated coda Q from small earthquakes recorded in the Peninsular range south of Anza. They have expressed their model in the familiar form for coda-Q, $Q=Q_0 f^a$. For $0<a<1$, results in this form can also be expressed in the form of $(1/Q_i + 1/Q_d)$ over a limited frequency band. Thus for example, the results of Rebollar et al., $Q=70f^{0.74}$, can be rewritten:

$$\frac{1}{70f^{0.7}} \approx \frac{1}{1340} + \frac{1}{57f} \qquad 3 < f < 24 \text{ Hz}$$

This model is similar to the total Q model shown on Figure 7, $\frac{1}{Q_{\text{total}}} = \frac{1}{1025} + \frac{1}{53f}$, and it is thus evidently consistent with the models derived from the data at Anza.

IMPLICATIONS FOR PREDICTION OF STRONG GROUND MOTION

As shown by Hanks [1979], the root mean square, and peak accelerations are determined by the bandwidth of the signal in the frequency domain. The decay parameter is one measure of this bandwidth. The amplitude of a signal which is reduced by the exponential factor $e^{-\pi\kappa f}$ has been reduced by a factor of $1/e$ at frequency $f' = \frac{1}{\pi\kappa}$. In Figure 8, we show the effect of different values of κ on an accelerogram. Two of the accelerograms in the figure have been obtained from the third by transforming the record to the frequency domain, modifying the spectrum by multiplication by a real number which corrects to a different value of κ, and then transforming back to the time domain. The original accelerogram has κ=0.04 sec; the two new traces have κ=0.07 sec and 0.01 sec. These values of κ correspond to frequencies f'=8 Hz for the original, and 4.5 Hz and 32 Hz, respectively, for traces modified to have a high and low κ. (The bandwidth for the accelerogram with κ=0.01 sec has not really been expanded all the way to 32 Hz, because the original seismogram was filtered with a cutoff of about 18 Hz.). The traces with smaller values of κ are characterized by increased amplitudes and conspicuous high frequencies. The peak accelerations are 286, 392, and 940 cm/sec^2 for κ of 0.07, 0.04, and 0.01 sec. Figure 9 illustrates the effect of these changes on the pseudo-relative velocity response. At long periods, the response spectra are nearly identical, but as the periods shorten, the level is increasingly affected, and some characteristics of the shape of the response spectrum, such as v_{max}/a_{max}, d_{max}/a_{max}, and $(a_{max}d_{max})/v^2_{max}$ are affected by κ.

There are many factors which affect the ground motion at high frequencies in addition to the value of κ_0 which is apparently introduced by attenuation directly below the site. These include resonances due to layers and broad band amplification due to decreased velocities and shear modulus. Thus κ, by itself, may not be a successful parameter for use in regression studies with the aim of reducing the scatter in predicted peak accelerations. On the other hand, while keeping the limitations in mind, it might be useful under some circumstances to modify the values of κ from some of the existing accelerograms to values appropriate for target sites as a help in extending the strong motion data set.

Acknowledgments. This research was supported by NSF grant EAR 8518647 and Electric Power Research Institute project RP 2556-2.

REFERENCES

Anderson, J. G., Implication of attenuation for studies of the earthquake source, in **Earthquake Source Mechanics**, Geophys. Monog. **37**, American Geophys. Union, Washington, D.C. 311–318, 1986.

Anderson, J. G, A preliminary descriptive model for the distance dependence of the spectral decay parameter in southern California, (in preparation), 1987.

Anderson, J.G. and S. E. Hough, A model for the shape of the Fourier amplitude spectrum of acceleration at high frequencies, **Bull. Seism. Soc. Am. 74**, 1969–1994, 1984.

Anderson, J. G. and M. S. Reichle, Study of spectra and site effects from Coalinga aftershocks

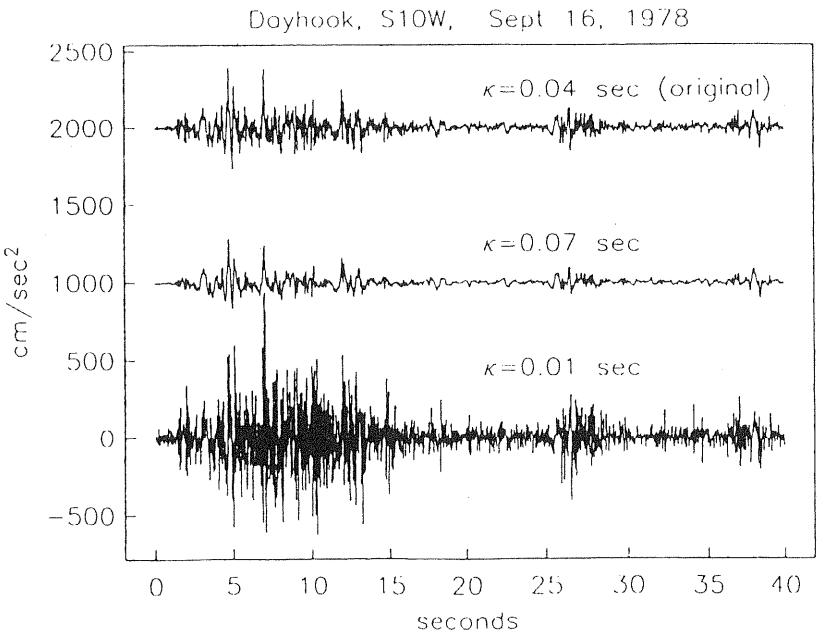

Figure 8. Accelerograms from station Dayhook for the Tabas, Iran 1978 earthquake (*M* 7.8) from Shoja-Taheri & Anderson [1988], and two modifications of this accelerogram generated by changing the spectral decay parameter of the original record.

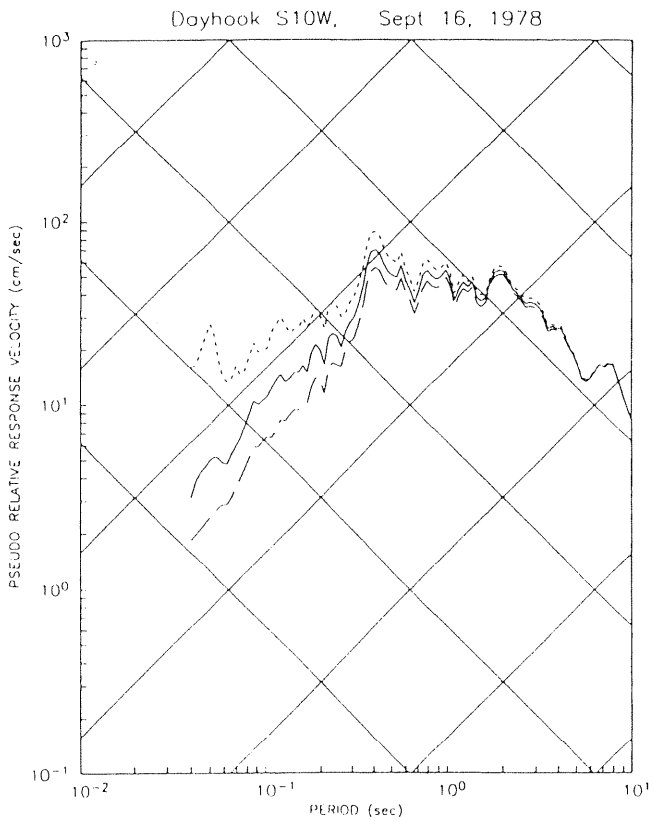

Figure 9. Response spectra from the accelerograms in Figure 8.

recorded near Parkfield, California, submitted to **Bull. Seism. Soc. Am. 74**, 1988.

Doser, D. and H. Kanamori, Depth of seismicity in Imperial Valley Region (1977-1983) and its relationship to heat flow, crustal structure, and the October 15, 1979 earthquake, **J. Geophys. Res. 91**, 675–688, 1986.

Hough, S. E., J. G. Anderson, J. N. Brune, F. L. Vernon III, J. Berger, J. Fletcher, L. Haar, T. Hanks, and L. Baker, Attenuation near Anza, California, in press **Bull. Seism. Soc. Amer.**, 1988.

Hough, S. E. and J. G. Anderson, High frequency seismic acceleration spectra observed at Anza, California: Implications of Q structure, in press
Bull. Seism. Soc. Amer., 1988.

Hough, S. E. and J. G. Anderson, An investigation of the effects of attenuation and geometrical spreading on the spectra of synthetic seismograms, submitted to **Geophys. J. R. Astr. Soc.**, 1988.

Rebollar, C.J., C. Traslosheros, and R. Alvarez, Estimates of seismic wave attenuation in Northern Baja California,
Bull. Seism. Soc. Amer. 75, 1371–1382, 1985.

Shoja-Taheri, J. and J. Anderson, Strong motion records of September 16, 1978 Tabas, Iran earthquake (M_S=7.4–7.8), in press
Bull. Seism. Soc. Am., 1988.

Sibson, R.H., Roughness at the base of the seismogenic zone: Contributing factors,
J. Geophys. Res. 89 5791–5799, 1984.

ANALYSIS OF ACCELEROGRAMS FROM SMALL TO MODERATE EARTHQUAKES IN NORTHEASTERN U.S. AND SOUTHEASTERN CANADA

Francis T. Wu
Department of Geological Sciences and
Center for Study of Natural Hazards
State University of New York
Binghamton, New York 13901

ABSTRACT

Analyses of single station digital accelerograms of seven earthquakes in southern Canada, northeastern New York and eastern Ohio have shown that magnitude 2.4 to 3.3 events have corner frequencies ranging from 15 to 6.5 and for magnitude 5.0 and 5.1 events 3 to 4 Hz. The frequency-independent Q for Cornwall-Massena area is estimated to be about 500.

A. MONITORING OF GROUND MOTION IN NEW YORK STATE SINCE 1980

Five accelerograph stations have been deployed in New York State since 1980 to monitor ground motions. During this period several small to moderate earthquakes occurred. Acceleration records were obtained at two sites in northeastern and western New York state, Long Sault dam and Bennington, respectively). Magnitude 2.4 to 3.3 events (near Cornwall, Canada) were recorded at a distance of 23 km (at Long Sault) and magnitude 5 (Painesville, Ohio) and 5.1 (Goodnow, New York) events were recorded at distances of 250 and 350 km respectively (at Bennington).

This report summarizes the results obtained to date and our experience in recording accelerations with triggered digital instruments.

1. Instrumentation

Instrument specifications are listed in Table 1. Experience shows that the sensor-recorder combination is capable of recording, in triggered mode, events with peak accelerations as low as 0.2 gal (.02% g) and as high as 1g (the total range can be shifted up or down). The least significant bit of the 12-bit digital system represents 0.005 gal.

Table 1
INSTRUMENT SPECIFICATION

Recorder		Sensor	
Word length	12 bits	Type	Force-balanced accelerometer
Trigger	Short term Av./ Long term Av.	Suspension	Torsion
Gain	1x,5x,25x,100x Manual or auto. down-ranging	Output	+/- 5 Volts
		Range	1 g (variable)
Filter	Butterworth 5 poles	Power	12 Volts
Buffer	1.7 seconds		
Tape Capacity	15 minutes		
Power	+/-12 Volts, 1 amp.		

2. Stations

The two stations that were deployed the longest and produced the only usable data (Fig. 1) are quiet sites suitable for operating instruments in triggered mode with limited recording capacity (15 minutes) and infrequent service (about 2 months). The power and temperature (>15^{O}C) requirements mandate interior placements. The two stations are the Long Sault and the Bennington stations (LS and BN in Fig. 1).

The Long Sault site is located at the bottom of a holding dam; no water flows over or through the dam. The recording instrument is bolted to the bottom level floor on the north side of the dam. The dam is coupled solidly to the rock. For the Cornwall, Canada events the station back azimuth is 238^{O} (clockwise from the North); with the horizontal components oriented in S26^{O}E and N64^{O}E; the S26^{O}E component is nearly in the transverse direction and the other nearly in the radial direction.

The Bennington station is located in the basement corner of an underground American Telephone and Telegraph building, solidly built on an excavated site on massive sandstone strata, about 50 ft underground. Here the horizontal components are placed in the N-S and E-W direction.

The other sites that have been used as test sites include basement of school buildings, private homes or transformer stations. The intermittent high noise level at these locations rendered long term operations impossible.

3. Data

The events recorded at the two stations and their source parameters are listed in Table 2. In this table, D is the epicentral distance; M_n, the Nuttli magnitude (Nuttli, 1973) determined by Lamont-Doherty Geological Observatory; a_{max} the combined maximum horizontal acceleration in cm/sec^2; f_c, the single station corner frequency in Hz.

Table 2
EVENT PARAMETERS

#	Date	Time	D (km)	M_n	a_{max}	f_c
1	03/18/81	125849.90	23.00	2.4	0.72	15
2	03/18/81	130324.61	23.00	2.6	1.36	15
3	07/04/81	231633.05	23.35	3.3	3.20	7
4	07/04/81	231917.50	23.73	2.8	2.97	12
5	07/05/81	214723.87	23.28	3.3	4.89	6.5
6	10/07/83	101846.10	350.70	5.1	3.1	3.2
7	01/31/86	164643.30	250.00	5.0	3.1	4.5

Figures 2, 3 and 4 show the accelerograms for events 1, 3, 4 and 5, all recorded at a distance of 23 km. The shift in frequency content to the lower end of the spectrum for the larger event is clear. Event 3 is a double event with subevents separated by 6 seconds. Figure 4 also shows displacement seismograms for events 4 and 5 obtained by integrating the accelerograms. Although events 3 and 5 have the same magnitude, the combined peak

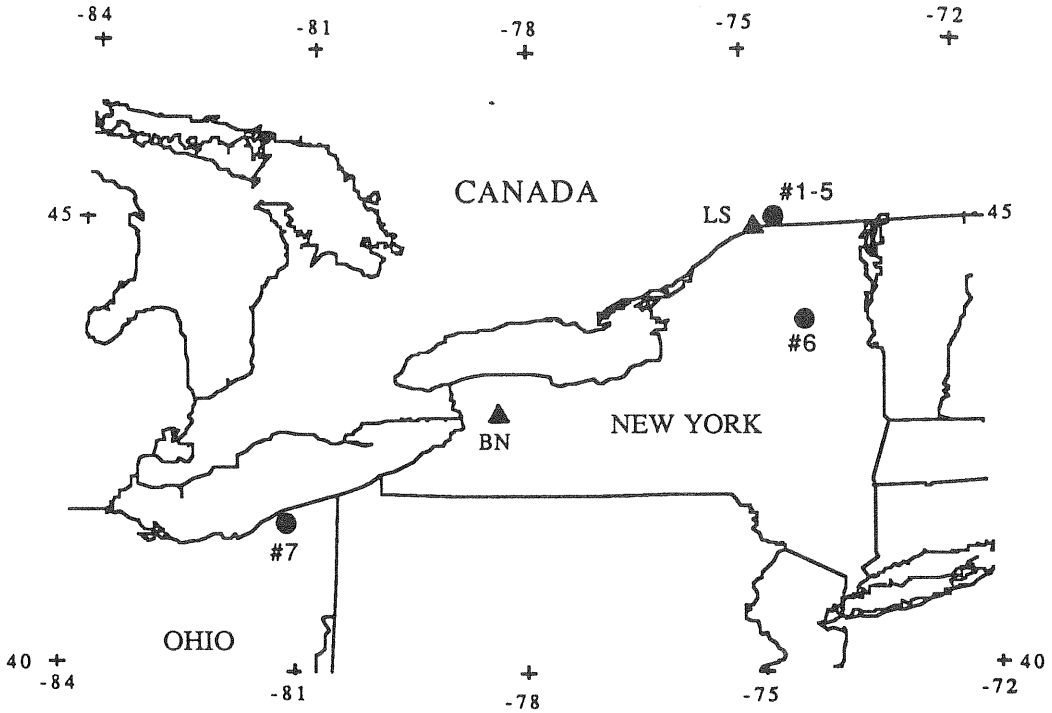

Figure 1. Location of stations in New York state and events recorded. Triangles mark the locations of Long Sault (LS) and Bennington (BN) stations. Circles mark the locations of events 1 through 7.

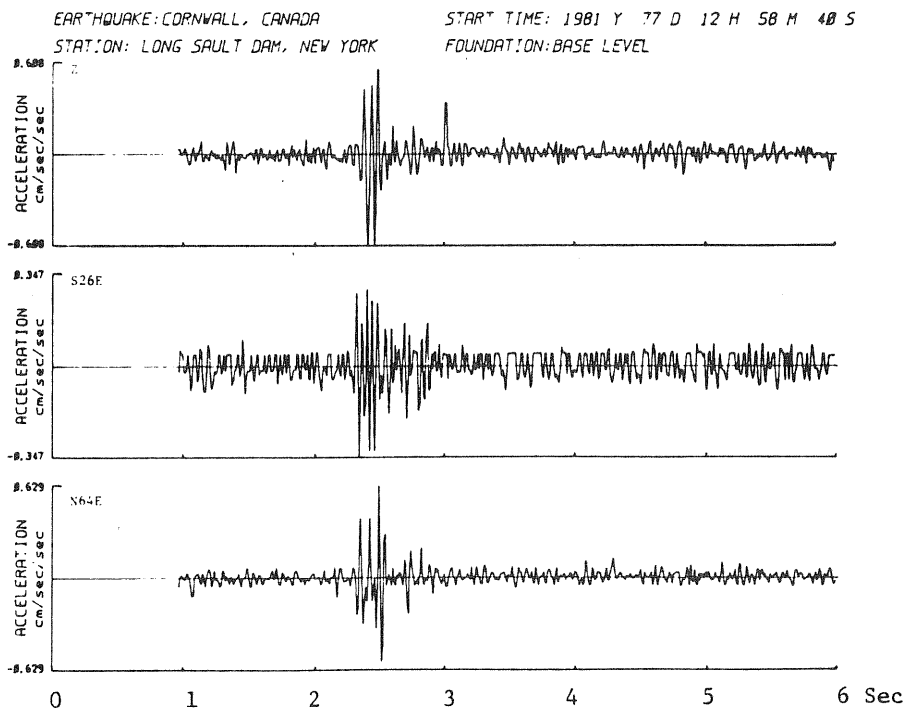

Figure 2. Accelerograms from event 1 recorded at Long Sault station (see Table 2).

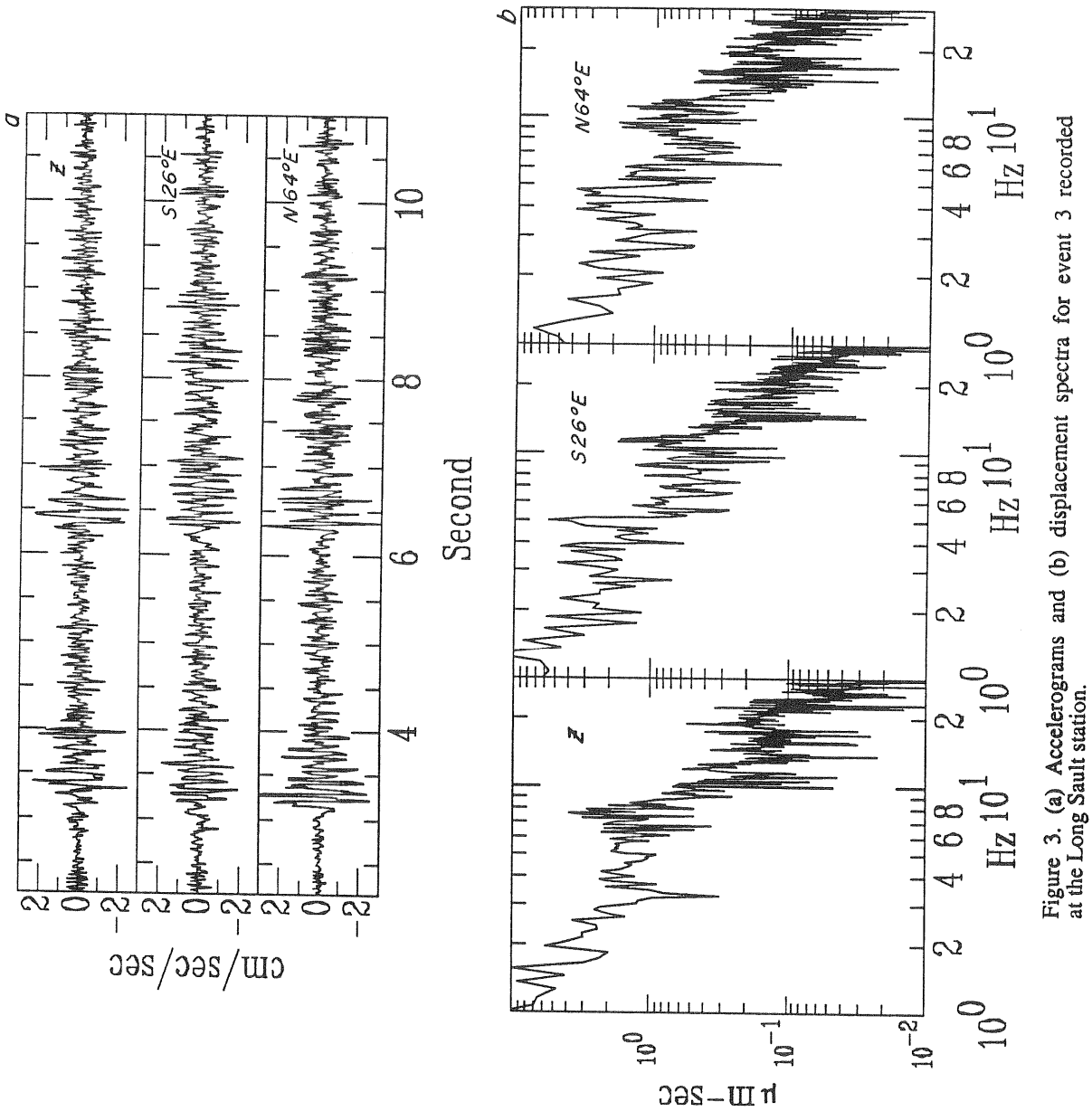

Figure 3. (a) Accelerograms and (b) displacement spectra for event 3 recorded at the Long Sault station.

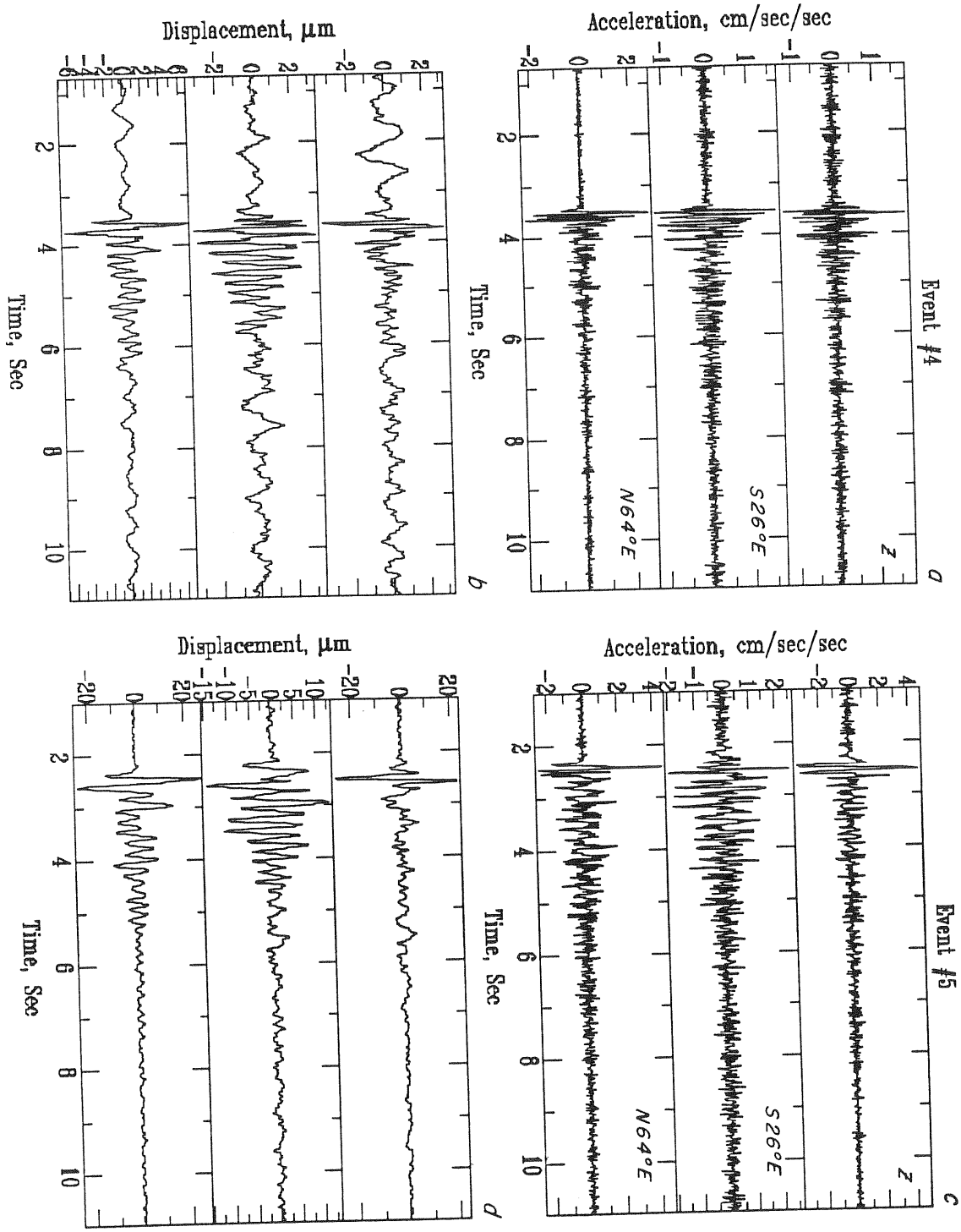

Figure 4. (a) Acceleration and (b) displacement seismograms for event 4 recorded at the Long Sault station. (c) Acceleration and (d) displacement seismograms for event 5 recorded at the Long Sault station.

horizontal acceleration and displacement for event 3 are smaller than those of event 5. These difference are consistent with the somewhat different mechanisms of these two earthquakes (Schlesinger-Miller et al., 1984). The S wave radiation pattern has a value of 0.9 for event 5 and 0.75 for event 3.

Figures 5a-d show the acceleration and displacement seismograms from the 1983 Goodnow, New York and 1986 Painesville, Ohio earthquakes. The clear phase in the beginning of the displacement seismograms for the Goodnow event is P_g. For the Painesville record, triggering occurred amidst later P phases. In both record sets the maximum accelerations are evidently associated with the L_g phases.

B. SOURCE SPECTRAL CHARACTERISTICS

1. Cornwall-Massena earthquakes

Five earthquakes on Table 2 are located within 1 km of each other (events 1 through 5). The S26^{o}E component spectra for events 4 and 5 are plotted both in linear-log and log-log scales in Figure 6a and 6b. Clear peaks exist for both sets of spectra at 4.8 and 11 Hz. The structures of the peaks are quite similar for the two events. Relative to the amplitudes of the 4.8 Hz peaks, the 11 Hz peak for event 4 is larger than that for event 5.

The presence of spectral peaks make the estimation of corner frequencies difficult. To avoid this, we divided the two spectra to obtain a ratio. As is shown by Aki (1967) and Bakun and Bufe (1975), the ratio for events of different magnitudes with different corner frequencies should ideally contain three line segments. At the low frequency end, the level indicates the ratio of the moment; at the mid-frequency band, a sloping line indicates the fall-off of the source spectra for the larger of the two events; and the third segment at the high frequency end shows the ratio of the high frequency content. The two intersections occur at the corner frequencies of the two events. Using this technique corner frequencies at about 12 and 6.5 Hz for events 4 and 5 respectively are obtained. The observation above concerning the relative sizes of the 11 Hz peak for events 4 and 5 small is consistent with the result that for event 5 it is beyond the corner of the source spectrum while for event 4 it is near the corner. From this ratio the high frequency fall-off of the source spectrum of the larger event (event 5) is estimated to be close to w^{-2}.

Since the peaks in the spectra occur at exactly the same frequencies as shown in Figure 6b, they are therefore most likely to be site effect. We shall discuss their significance later.

2. Goodnow and Painesville earthquakes

Figures 7a and 7b show the three component displacement spectra of the Goodnow and the Painesville earthquakes. For the Goodnow event, the corner frequency is located at about 3 Hz and for the Painesville event, a 4 to 5 Hz corner frequency can readily be discerned. Formula proposed by Street (1975) is used for computing the moment since the dominant waves in these records are Lg waves. The corner frequencies are shown in Table 2 and the derived source parameters are shown in Table 3.

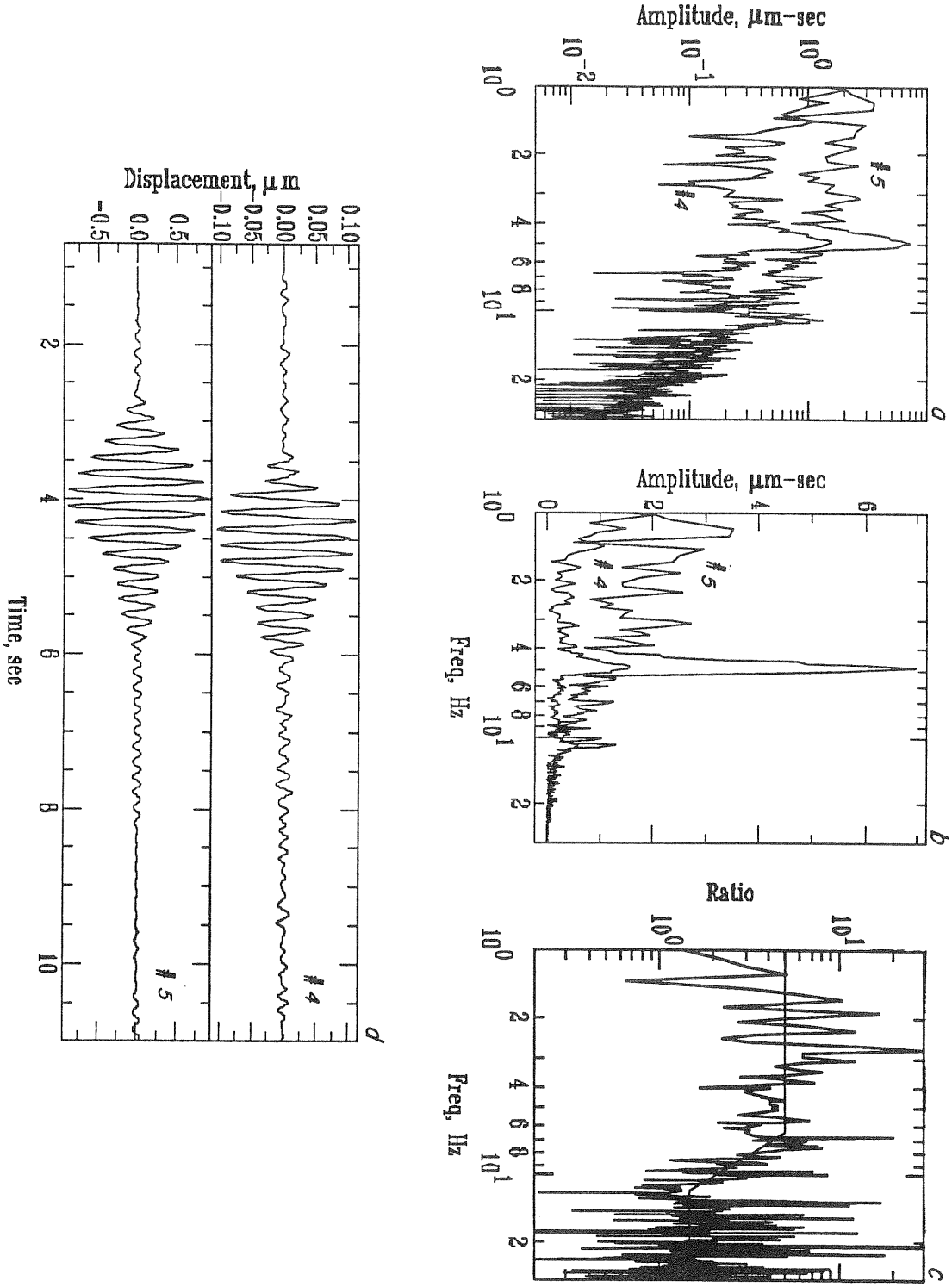

Figure 5. (a) Log-log spectra of the S26°E component of event 4 and 5. (b) Linear-log spectra of the S26°E component of event 4 and 5. (c) Spectral ratio of event 5 over 4. (d) Narrow-band passed (center frequency 4.8 Hz) displacement seismograms of event 4 and 5.

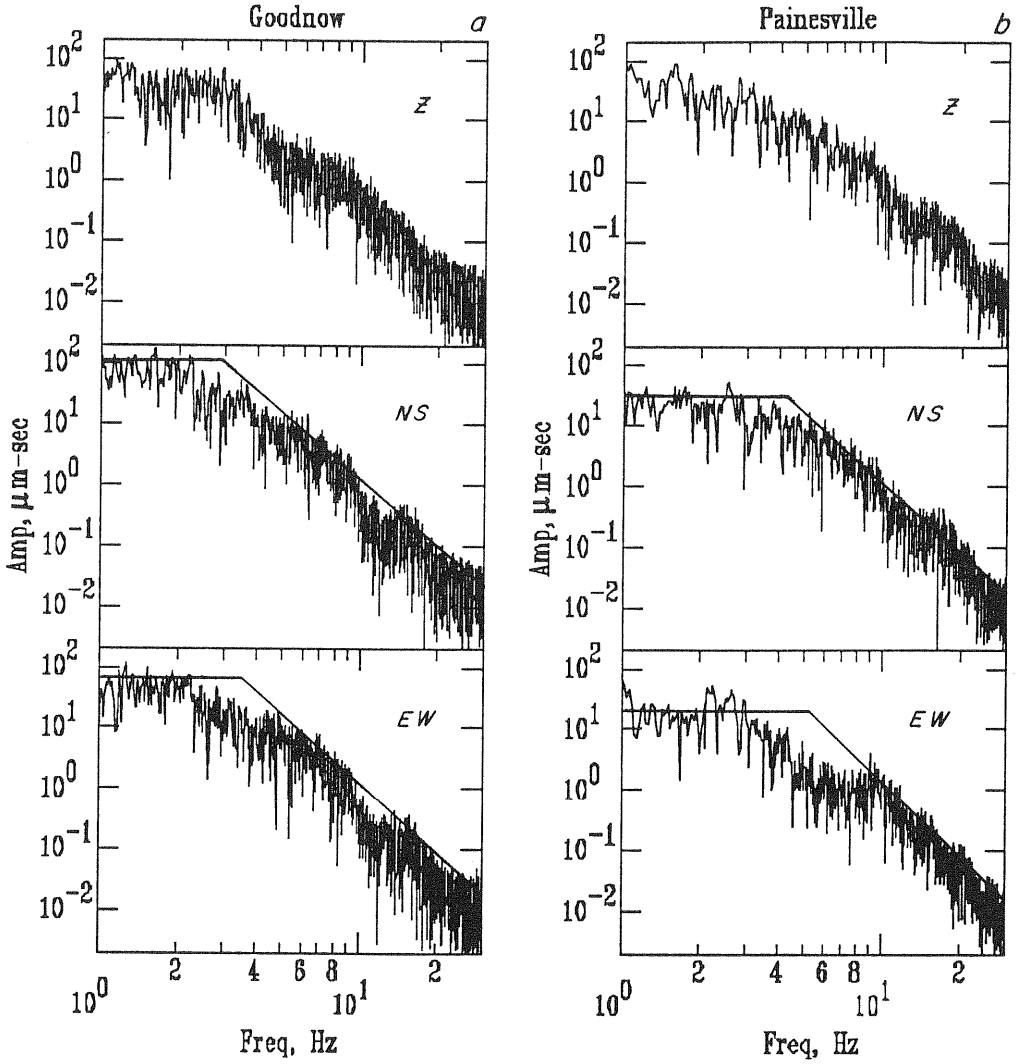

Figure 6. (a) Acceleration and (b) displacement seismograms for the 1983 Goodnow, New York event recorded at the Bennington station. (c) Acceleration and (d) displacement seismograms for the 1986 Painesville, Ohio earthquake recorded at the Bennington station.

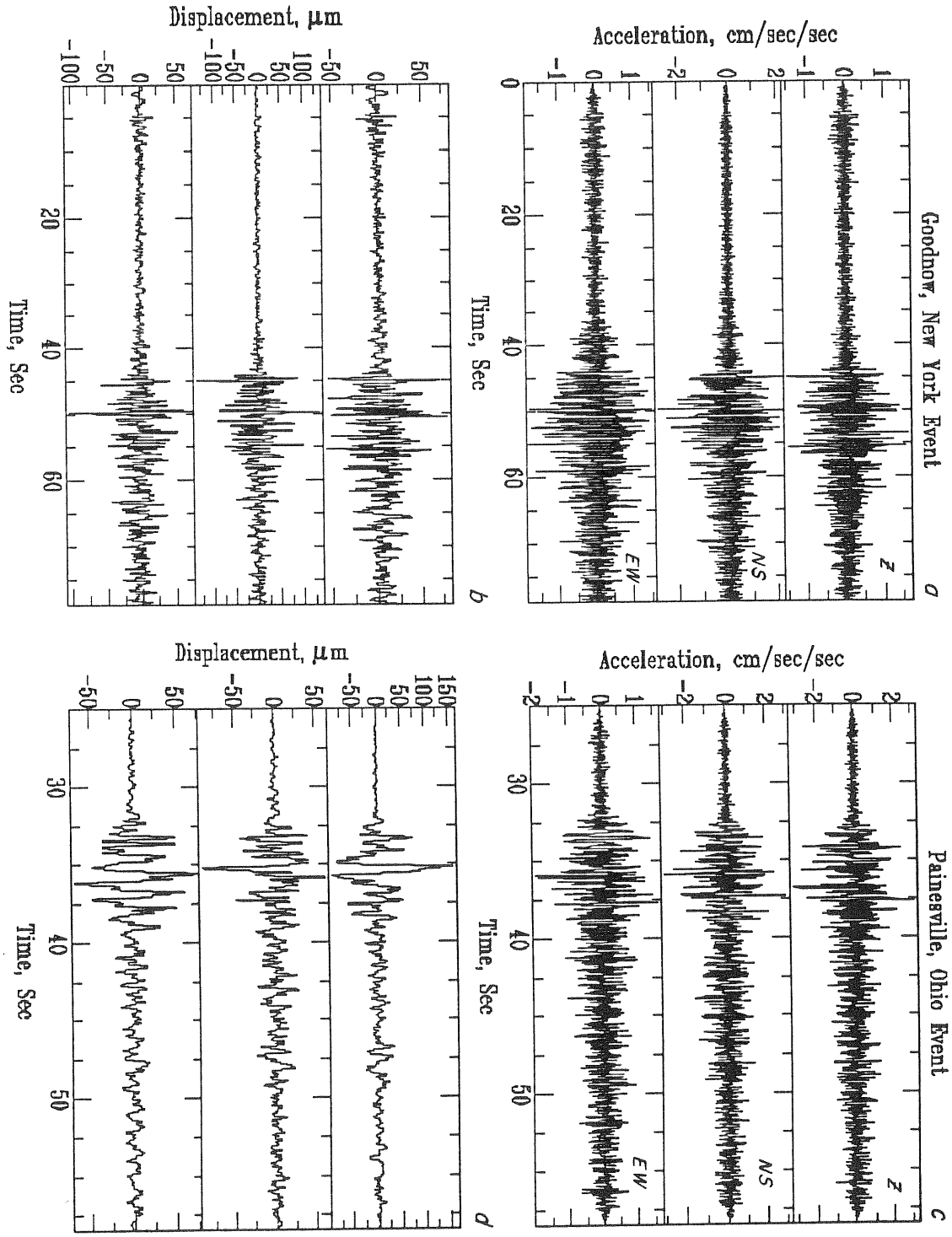

Figure 7. (a) Displacement spectra for the 1983 Goodnow, New York event. (b) Displacement spectra for the 1986 Painesville, Ohio event. The asympototes of the N-S and E-W spectra are shown.

C. ATTENUATION STUDY

Figure 5c shows the source spectral slope of event 5. By assuming that Q is frequency independent, we can compensate the spectrum (Fig. 5a) until the high-frequency fall-off attains the same slope as that shown in Figure 5c. The Q values that restore the slope (to w^{-2}) is the Q for the path in question. The value is found to be about 500.

D. DISCUSSION AND CONCLUSIONS

Although the amount of data is still very small, some interesting observations can be made. First, the moments obtained from the spectra for events 3, 4 and 5 (Table 3) fall well on the M_L-M_o curve of Johnson and McEvilly (1974) for Central California and the scaling law proposed by Street (1976) and Nuttli (1983) (note that M_n is used for the Cornwall events which is either determined from Lg or 1 second P wave). Secondly, the corner frequency we have determined is generally higher than those estimated for earthquakes of corresponding magnitudes in mid-plate regions (Nuttli, 1983) or even in eastern Canada (Hasegawa, 1983). Finally, the stress drops calculated from the the spectra are significantly higher than those found in Central California or estimated for eastern North America (Nuttli, 1983), a result of relatively high corner frequencies (Table 3). In Table 3, source dimension, r_o, and stress drop (S.D.) are calculated according to Brune's formulae (1970, 1971) and for event 6 and 7 they are also calculated using formulae contained in Nuttli (1983) for comparison. It is to be noted that M_o in Table 3 is not corrected for radiation pattern, but free surface effect is removed.

Table 3
PARAMETERS DERIVED FROM SPECTRAL VALUES

#	$M_o x 10^{22}$	r_o[1]	S.D.[1]	r_o[2]	S.D.[2]
1	0.015	87	100		
2	0.024	87	160		
3	0.12	190	76		
4	0.053	110	174		
5	0.15	200	82		
6	40.	410	253	1290	450
7	12.	290	215	900	400

[1] Brune (1970, 1971)

[2] Nuttli (1983)

The frequency-independent Q estimated for the upper crustal path between Cornwall and Long-Sault is about 500, three to four times higher than corresponding values in central California. This value cannot be directly linked to the coda Q determined in other studies (e.g., Hasagawa, 1985 and Shin and Herrmann, 1987).

In our spectral studies of the Long Sault dam station data, we have detected two well resolved peaks at 4.8 Hz and 11 Hz. They are evidently a site effect that is related to the modal response of the dam. Fig. 4d shows the S26°E component displacement seismograms of events 4 and 5 after

narrow band-pass filtering at 4.8 Hz. They show the build-up and the decay of the resonance. Such data can be used for monitoring the characteristics of the dam with future seismic data at this site.

This report shows that large dynamic-range accelerograph systems are useful in data acquisition for source and path studies of earthquakes in the northeastern United States. Earthquakes occur infrequently here and installation of high-quality digital stations is recommended to quickly broaden our database.

It should also be pointed out that the instruments used in this study are first generation portable digital equipment. The digital recorder design is only marginally adequate. With recent advances in micro-processors and magnetic storage technology, a more suitable system can be specified. First, for long-term recording, a system from which data can be retrieved remotely and whose functions can be monitored remotely will be highly desirable. Secondly, to avoid losing data through the use of incorrect trigger criteria, larger buffer storage (perhaps on Winchester disk) is needed. Thirdly, from our experience in New York state as well as from extensive data collecting activities elsewhere, the 12-bit recording system is still inadequate in many respects. Gain-ranging solves a part of the problem by allowing us to record the ground noise level so that true zero can be estimated even when the top limit is set at 1g. Gain-ranging, however, adds an uncertain noise level to the record. A 16-bit system with high- and low-gain settings (20 to 40 dbs apart) will serve our purposes much better.

ACKNOWLEDGMENTS

This work was initiated under NSF grant 76-23897. The Organized Research Program through the Center for Study of Natural Hazards at the State University of New York at Binghamton and NSF grant CEE8213972 supported a portion of the research effort.

REFERENCES

Aki, K.,Scaling law of seismic spectrum, J. Geophys. Res., vol 72, 1217-1231, 1967.

Bakun, W.H., and C. G. Bufe,Shear-wave attenuation along the San Andreas fault zone in central California, Bull. Seism. Soc. Am., vol 65, 439-459, 1975.

Bakun, W. H., C. G. Bufe, and R. M. Stewart, Body-wave spectra of California earthquakes, Bull. Seism. Soc. of Am., vol. 66, 363-384, 1976.

Brune, J.N., Tectonic stress and the spectra of seismic shear waves from earthquakes, J. Geophys. Res., vol. 75, 4997-5005, 1970.

Brune, J.N., Correction to tectonic stress and the spectra of seismic shear waves from earthquakes, J. Geophys. Res., vol. 76, 5002, 1971.

Hasegawa, H.S., Attenuation of Lg waves in the Canadian Shield, Bull. Seism. Soc. Am., vol 75, 1569-1582, 1985.

Johnson, L.R. and T. McEvilly, Near-field observation and source parameters

of Central California earthquakes, Bull. Seism. Soc. Am., vol. 64, 1855-1886, 1974.

Nuttli, O., Seismic wave attenuation, J. Geophys. Res., vol. 78, 876-885, 1973.

Nuttli, O., Average seismic source-parameter relations for mid-plate earthquakes, Bull. Seism. Soc. of Am., vol. 73, 519-535, 1983.

Schlesinger-Miller, E., N.L. Barstow, and A.L. Kafka, The July 1981 earthquake sequence near Cornwall, Ontario and Massena, New York, Earthquake Notes, vol. 54, Number 4, pp 11-26, 1984.

Street, R.L., Scaling northeastern United States/southeastern Canadian earthquakes by their L_g waves, Bull. Seism. Soc. of Am., vol 66, pp1525-1537, 1976.

ESTIMATION OF EARTHQUAKE STRONG GROUND-MOTION IN EASTERN NORTH AMERICA: PRELIMINARY ESTIMATES VIS-A-VIS EXISTING DATA

by

Apostolos Papageorgiou
Department of Civil Engineering
Rensselaer Polytechnic Institute

Paper presented
at the NCEER Symposium
"Seismic Hazards, Ground Motions, Soil Liquefaction
and Engineering Practice in Eastern North America".
Sterling Forest, N.Y., October 20-22, 1987

and at the NCEER Conference
"Earthquake Hazards and the Design of
Constructed Facilities in The Eastern U.S."
New York, City, February 26-28, 1988

ABSTRACT

We present observed Pseudo-Velocity Spectra of strong motion accelerograms recorded during moderate and large intraplate earthquakes. For reference, we also show predictions based on a self-similar ω-square model with a scaling parameter $\Delta\sigma$ equal to 100 bars. Direct comparison of the theoretical specta with the observed ones is not possible because the former are far-field spectra of a point-source while the latter are near-field spectra of extended sources. We demonstrate that a self-similar (constant stress drop) ω-square model is a phenomenological model with a stress parameter that has no physical meaning and which can be interpreted only as a scaling factor. Consequently, it cannot be used as an input parameter in numerical syntheses of strong ground motion.

INTRODUCTION

Evaluation of seismic hazards in Eastern North America (ENA) - i.e. the part of the conterminous United States east of the Rocky Mountains - is a difficult task involving considerable uncertainties for two primary reasons: (i) Damaging earthquakes are infrequent events and thus the rarity of large earthquake events compounded with the scarcity of ground motion recording instruments explains the lack of data in ENA. (ii) Geologic structures are not easily identifiable because they do not exhibit as clear surface expressions as in the western United States [Hanks, 1985]. Nevertheless, recent investigations have unveiled such geologic features and, based on growing evidence, it is almost established that ancient zones of weakness, when favorably oriented with respect to modern stress regimes, contribute to contemporary seismicity and have the potential to generate large destructive earthquakes [Zoback and Zoback, 1981]. For instance, the New Madrid earthquakes of 1811-12 were generated by an ancient rift buried beneath geologically younger strata [Zoback et al., 1980; Sykes, 1978].

The complete lack of strong motion data from large earthquake sources in ENA (with the only exception the records of the recent Nahanni earthquakes) leaves no alternative but to look for data recorded during earthquakes which occurred in other "stable continental interiors" (i.e. tectonic environments similar to that of ENA) with the implicit assumption that intraplate earthquakes have quantitatively similar source properties. Earthquake events of this kind, for which both strong motion data as well as teleseismic data have been recorded, are the following: Gazli, 1976; Tangshan, 1976 (aftershocks); Nahanni, 1985; Tabas, 1978. The purpose of this paper is to discuss some of the above data that are available to us at the present time, and compare their spectral characteristics with estimates proposed recently by Boore and Atkinson [1987] and Boatwright and Choy [1987].

COMPARISON OF ESTIMATES OF STRONG-GROUND MOTION WITH DATA

Recently Boore and Atkinson [1987] proposed a theoretical technique for predicting ground motion and spectral response

parameters in Eastern North America (ENA). According to their model, the high-frequency strong ground motion is treated as filtered random Gaussian noise, for which the filter parameters are determined by a seismological model of the source. The above authors constrained the essential parameters of their model using existing data from small to moderate ($M_o < 10^{24}$) ENA earthquakes.

In a parallel effort, Boatwright and Choy [1987] have presented a set of acceleration source spectra for large earthquakes in ENA based on broadband teleseismic data of moderate and large earthquakes ($10^{24} < M_o < 10^{27}$) which occurred in "stable continental interiors" or "transition zones" around the world.

In what follows we compare near field data ($\leq$ 20 km) recorded on rock or rock-like/stiff alluvium sites during three intraplate earthquakes: (1) Tabas, 1978, (2) Gazli, 1976 and (3) Nahanni (12/23), 1985. Consideration of near field data only has for our purpose both positive and negative aspects. By studying only records with small source to station distance we avoid the problem of correction for attenuation. On the other hand the comparisons that follow are not strictly valid because the theoretical spectral estimates are based on point source models while the real earthquake sources have a finite size. Consequently, as the distance to the source becomes small compared to the dimensions of the source, only portions of the source contribute effectively in the observed ground motion [e.g. Papageorgiou and Aki, 1985; Archuleta and Hartzell, 1981]. It is not clear what is the reduction factor that one must apply to the theoretical far field spectra in order to be able to compare them with near field observations. Boore and Atkinson [1987] estimate that for magnitude 7 events, this reduction factor is roughly equal to 2 at a distance of 10 km, increaing for smaller distances, and diminishing gradually to one near 50 km. It is not clear though how the above authors obtain these estimates. According to the specific bearrier model of Papageorgiou and Aki [1983] (to be discussed further below) the high frequency spectral level of the far-field Fourier amplitude spectra of acceleration $|\tilde{\ddot{u}}_{hf}(f)|$ scale proportionally to the square root of the total number N of subevents that compose the earthquake event, times the intensity of the high frequency spectral amplitudes $|\tilde{\ddot{u}}_{hfe}(f)|$ of a typical subevent, [Papageorgiou, 1988], i.e.,

$$|\tilde{\ddot{u}}_{hf}(f)| \sim \sqrt{N}\ |\tilde{\ddot{u}}_{hfe}(f)| \qquad (1)$$

In the near-field, the intensity of ground motion is influenced primarily by the near-field radiation of the closest of these typical subevents. Consequently, the reduction factor that has to be applied to the point source estimates may be considerably different than 2. With the above coveats in mind, we present near-field data together with point-source far-field estimates as a reference.

We start by comparing in Figure (1) the two scaling laws we mentioned above. The pseudo-velocity (PSV) spectral amplitudes obtained from Boatwright and Choy's scaling law are clearly lower

than those of Boore and Atkinson. The discrepancies as expected, are small in the long and intermediate period range (<0.5 Hz) but increase with increasing frequency. The Boatwright and Choy source spectra were inferred from teleseismic broadband seismograms. Correction of such data for propagation path effects entails considerable uncertainty, especially in the high frequency (> 0.5 Hz) range [Papageorgiou, 1987, 1988]. Because spectral estimates of the Boore and Atkinson model are in reasonable agreement with observed data of at least small and moderate earthquake events we do not consider any further the Boatwright and Choy spectra.

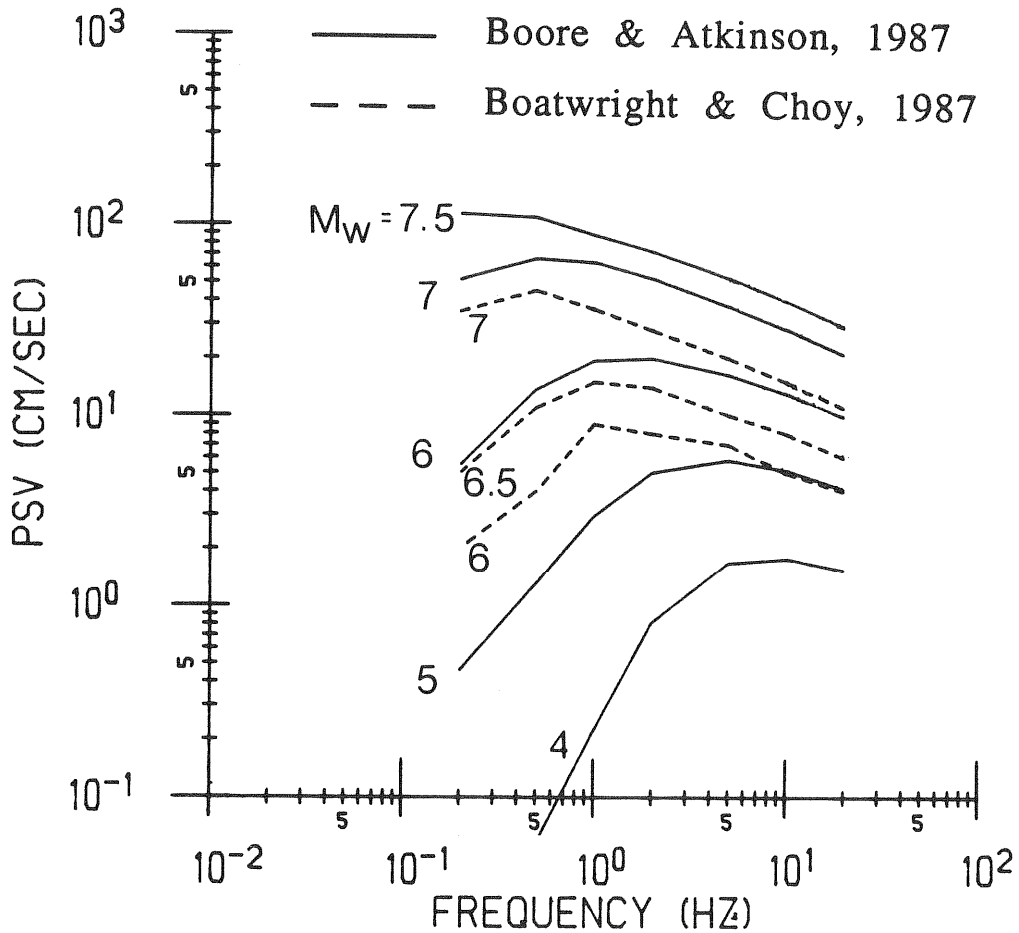

Fig. 1. Predictions of the 5 per cent damped pseudo-velocity response spectra (PSV) at 10 km based on the source scaling models of Boore and Atkinson [1987] and Boatwright and Choy [1987].

The September 16, 1987 Tabas, Iran earthquake: Figure 2 shows the recorded acceleration time histories of the three components of the Tabas record of the September 16, 1978 Tabas, Iran, earthquake (M_S = 7.4 to 7.7 (NEIS), M_L = 7.0 ± 0.4 [Shoja-Taheri and Anderson, 1987], M_o = 0.82 to 1.5 x 10^{27} dyn-cm [Niazi and Kanamori, 1981]).

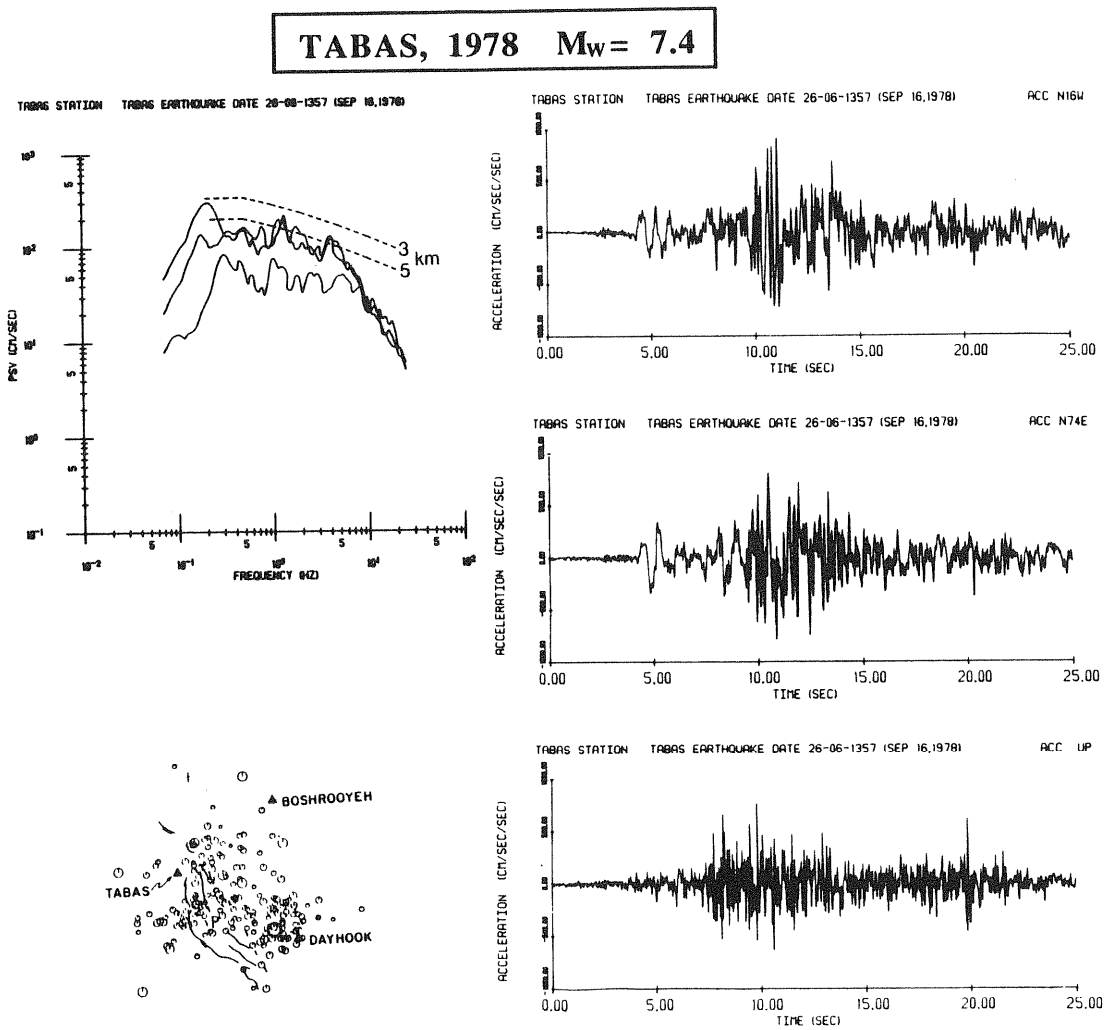

Fig. 2. The three components of ground acceleration recorded at Tabas station during the September 16, 1978 Tabas, Iran earthquake, and the corresponding 5 per cent PSV spectra. Predicted spectral amplitudes based on the Boore and Atkinson [1987] scaling model are shown for reference. The position of the Tabas station is indicated relative to the fault outcrop [from Shoja-Taheri and Anderson, 1987].

The Tabas recording station is located ~ 3 km southwest from the nearest fault outcrop. The subsurface condition at the site of this station, although not very well known, have been reported to have rocklike or stiff alluvium characteristics. The rupture initiated near the site of Dayhook at a depth less than 10 km, and propagated toward Tabas. The fault break shown in Figure 2 had an overall north-northwest strike and a dip to the northeast of about 30° [Berberian et al., 1979]. The Tabas, 1978 earthquake is a complex event [Niazi, 1986] with at least four subevents identified on the strong motion records [Shoja-Taheri and Anderson, 1987]. The first subevent, which originated approximately 20 km to the southwest of the Dayhook station at a hypocentral distance of 60 km from the Tabas station, is clearly seen on the horizontal components of acceleration as a distinct pulse at around 5 seconds after triggering of the instrument. The intense part of the ground motion, observed on the records around 10 sec, is the signature of the passage of the rupture front by the Tabas station. Clearly, for such a small distance of the recording station from such a large source, the comparison of the point source far-field estimates to the observed near source spectral amplitudes is not possible. Finally, it should be pointed out that the spectral amplitudes of the vertical component are smaller than those of the two horizontals but relatively richer in high frequencies giving a vertical peak acceleration almost as high as that of the two horizontal components (Vertical a_{max} = 0.732 g, Horizontal a_{max} = 0.867 g and 0.911 g).

The May 17, 1976 Gazli, USSR-earthquake: This event (M_S = 7.0, M_L = 6.4, M_o = 1.6 x 10^{26} dyn-cm) had a predominantly thrust fault mechanism initiating at a depth of 15 km with a massive rupture (local stress drop ~ 1 kbar) and propagated upwards towards the surface in a manner very similar to that of the San Fernando, 1971 earthquake [Hartzell, 1980] (Figure 3). The Karakyr point accelerograph station that provided the only strong motion record for this event, was located ~ 5 km south of the nearest fault break, and about 20 km from the hypocenter. The station is located on top of a 1420-meter thick sedimentary layer consisting of clays and sandstones underlain by highly resistant metamorphic schist [Hartzell, 1980]. Visual comparison of the Gazli records with those of Tabas reveals that the strong ground motion is characterized by unusually high-amplitude, high-frequency (~ 10 Hz) accelerations. These features are particularly dramatic on the vertical component, and may be due in part to the focusing effect of the propagating rupture. Hartzell [1980] points out that high-frequency resonances, caused by the faulting of the surface sediments, may also play an important role. We refrain from passing judgement about the quality of agreement of predictions with observations because this would require proper quantification of two effects: (i) the small station-to-fault plane distance which we pointed out above and (ii) the interaction of the sediment layer and the rupture front. Bouchon [1979], in simulating the recorded displacement at station No. 2 during the 1966 Parkfield earthquake, found that penetration of the surface sediment layer of lower rigidity by the rupture front may have a pronounced effect on the ground motion recorded at the surface [see also discussion by Aki, 1983].

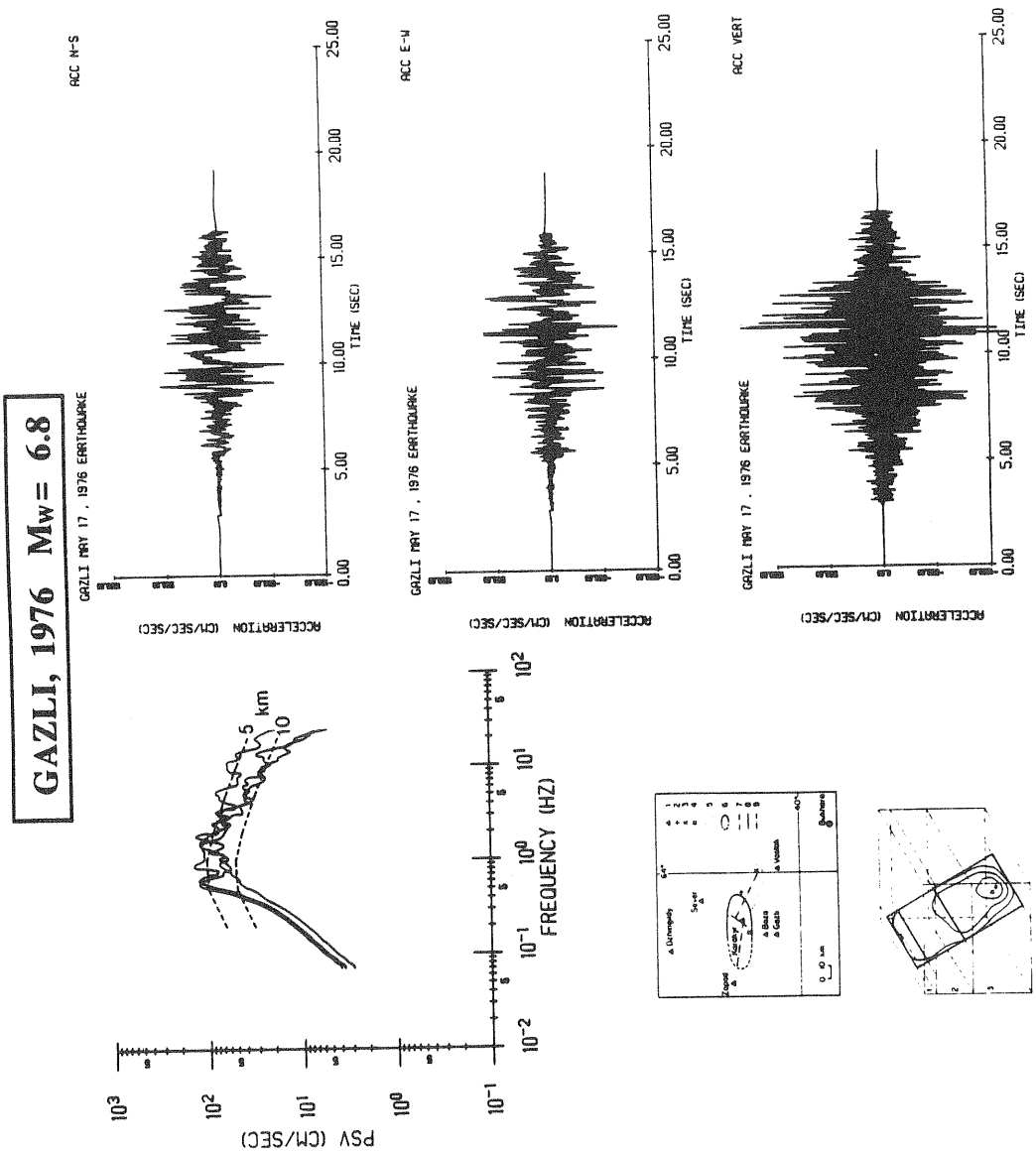

Fig. 3. Ground acceleration recorded at the Karakyr point station during the May 17, 1976 Gazli earthquake. Also, shown is a model of the slip distribution on the fault plane as inferred from teleseismic data [Hartzell, 1980].

The Nahanni, 1985 earthquake-sequence: This earthquake sequence, which occurred close to the western border of the Canadian shield, is characterized by a pair of strong earthquake events - the October 5, 1985 (M_S = 6.6) event and the December 22, 1985 (M_S = 6.9) event. The second event was recorded by three strong motion instruments that were installed in the epicentral area during aftershock surveys of the October event [Weichert et al., 1986]. Contrary to the Gazli earthquake which initiated with a massive rupture at a depth of 15 km and propagated upwards, the Nahanni December 23, 1985 event initiated at a shallow depth ($\leq$ 6 km) and propagated downwards and to the South on a shallow dipping ($\delta \simeq 20°$) fault plane [David Wald, personal communication, Horner et al., 1987]. This suggests high stress concentrations at shallow depths of the crust. Cracks with very high local stress drops near the surface of the ground may explain the very intense ground accelerations recorded at station 1 (Figure 4). Such high stresses at shallow depths explain why faulting in the intraplate shield area of Australia is a near surface phenomenon [Langston, 1987]. Analysis of events such as the Meckering, 1968 (M_S = 6.8) and Cadoux (M = 6.1) revealed thrusting at hypocentral depth of only 2 km.

Visual inspection of the accelerograms shown in Figure 4a reveals that the earthquake was composed by at least 3 to 4 subevents. The records at site 3 (not shown in Figure 4) recorded ground motions of considerably lower intensity as compared to the motions at the other two stations. Site 3 appears to be located close to a node of the radition pattern of the energy release and recorded the rather homogeneous field of scattered high-frequency waves. The transducer of the vertical component at site 2 malfunctioned and is not shown in Figure 4. All three accelerographs were bolted directly on hard rock [Weichert et al., 1986].

Direct comparison of the observed spectra with the analytical predictions is not possible. As we already discussed above, this is due to the fact that the stations are very close to an extend source. Consequently the seismic radiation arriving at any one of the stations from the various subevents traveled different distances, depending on the position of the subevents on the fault plane. Nevertheless, on Figure 4 we show the observed spectra together with the analytical ones for reference. It should be pointed out that the rupture propagation away from sites 1 and 2 and consequently the focusing effect observed in the Karakyr point accelerogram is absent.

Finally on Figure (5), the same kind of comparisons have been made for three smaller events (M 4.2 to 5.3) of the Nahanni sequence. Events in this size range were used by Boore and Atkinson to calibrate their model. Clearly the theoretical estimates are in good agreement with the observed ones except for event 9/11/85 which may have originated closer to site 2 than indicated in Figure (4b) and which propagated towards the station as can be judged from the compressed and intense signal.

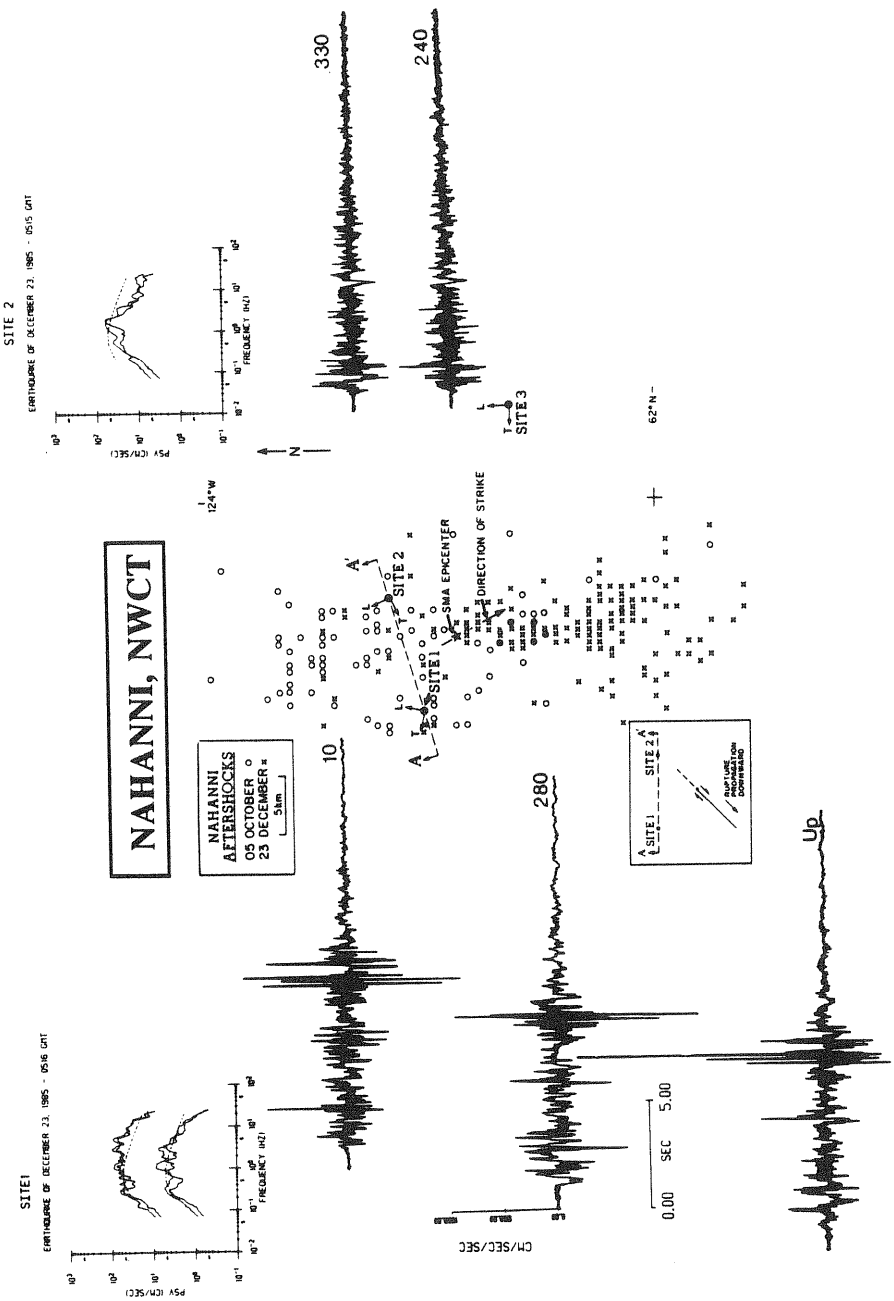

Fig. 4. Accelerograms recorded at sites 1 and 2 during the December 23, 1985 Nananni earthquake. For site 1 we computed spectra considering the entire time history (upper spectra) and only the first 7 seconds (lower spectra, shifted downwards by a logarithmic unit).

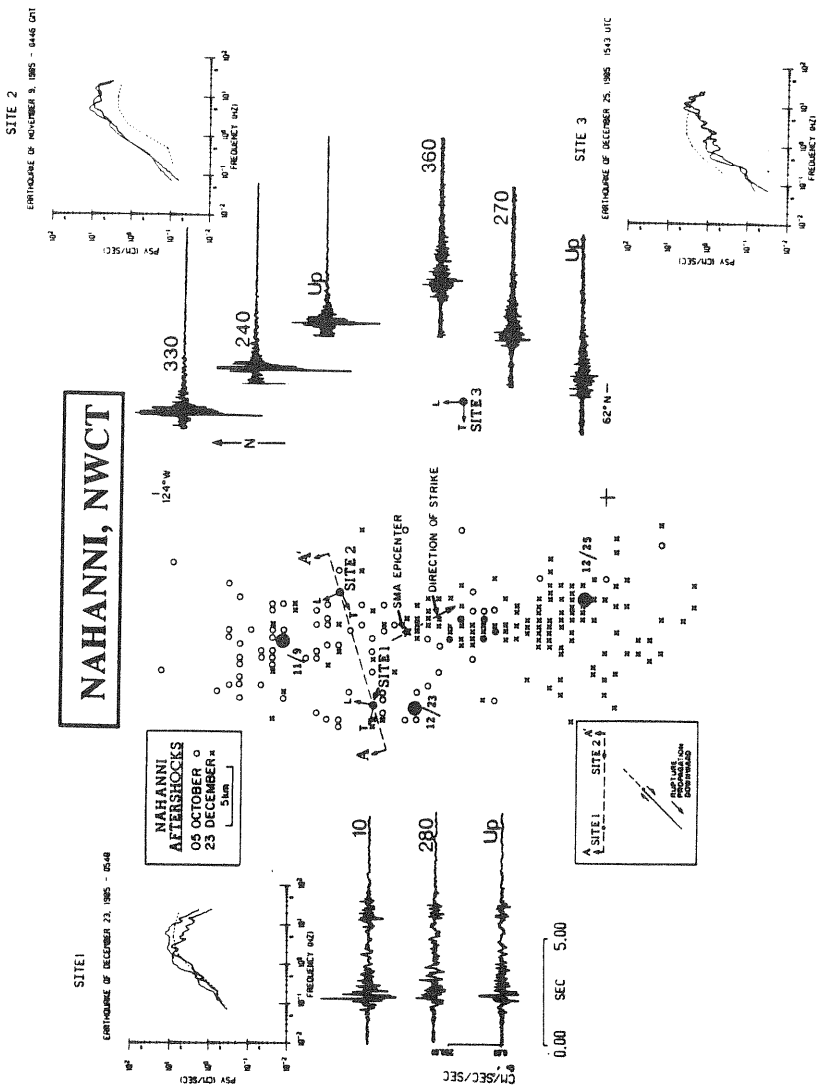

Fig. 5. Ground accelerations recorded at sites 1, 2 and 3 during the 12/23/85, 11/9/85 and 12/25/85 earthquake events respectively. The size of these events ranged from M 4.2 to M 5.3.

DISCUSSION

We have presented observed PSV spectral amplitudes of strong motion accelerograms recorded during moderate and large intraplate earthquakes. For reference we have also shown predictions based on a self-similar ω-square model with a scaling parameter $\Delta\sigma$ equal to 100 bars. We have pointed out that a direct comparison of the theoretical spectra with the observed spectra is not possible for reasons already discussed. Therefore, based on these data alone and on the analysis presented so far, it is not clear how successful are the predictions of the above analytical model. The question remains whether the spectral amplitudes of Figure 1 are representative of strong ground motion at rock sties in ENA. An even more fundamental problem is the validity of the source model based on which the spectral amplitudes were obtained. In the following let us address these questions very briefly. More extensive discussions can be found in Papageorgiou [1987, 1988].

Boore and Atkinson [1987] based their predictions on a self-similar ω-square model with a constant stress drop. According to this model the high frequency spectral amplitudes of acceleration scale as

$$|\ddot{\tilde{u}}_{hf}(f)| \sim f_1^2 M_o \qquad (2)$$

where f_1 is the corner frequency of the ω-square spectrum and M_o is the seismic moment. Boore and Atkinson [1987] adopted Brune's [1970] formula for the scaling of f_1 with earthquake size (as measured by the seismic moment M_o),

$$f_1 = 4.9 \times 10^6 \beta (\Delta\sigma/M_o)^{1/3} \qquad (3)$$

where M_o is in dyn-cm, $\Delta\sigma$ is in bars, f_1 is in Hz and β (= shear wave velocity) is in km/sec. Equation 3 was derived based on the assumption that the entire earthquake source can be represented by a circular crack with a uniform stress drop $\Delta\sigma$. The radius of the crack is inversely proportional to the corner frequency f_1.

Combining equations (2) and (3) we obtain,

$$|\ddot{\tilde{u}}_{hf}(f)| \sim \Delta\sigma^{1/3} M_o^{1/3} \qquad (4)$$

From equation 4 it becomes apparent that if the stress drop parameter is constant (i.e. independent of earthquake size) then the high-frequency spectral amplitudes scale proportionally to $M_o{}^{1/3}$.

Let us now compare the scaling of the source spectrum discussed above with the scaling of high frequency amplitudes according to the specific barrier model of Papageorgiou and Aki [1983 a,b]. The specific barrier model was successfully used to interpret strong motion data of California earthquakes. This model

consists of circular cracks of equal diameter filling up a rectangular plane. As the rupture front sweeps the fault plane, the individual cracks rupture statistically independently. The high-frequency spectral amplitudes of acceleration are expressed as [Papageorgiou and Aki 1985; Papageorgiou, 1987],

$$|\ddot{\tilde{u}}_{hf}(f)| \sim \Delta\sigma_{\ell}^{1/3} M_o^{1/3} \qquad (5)$$

where $\Delta\sigma_{\ell}$ is the local stress drop that occurs inside each individual crack. Papageorgiou and Aki [1983b] found that the local stress drop appears to be very stable, increasing only slightly with earthquake size. Therefore, from equation (5) we concluse that for the specific barrier model the high frquency spectral amplitudes scale proportionally to $M_o^{1/3}$, which agrees with the scaling of the ω-square model.

Then what is the difference between the two models discussed above in predicting the level of the high frequency plateau of acceleration spectra? The answer to this question is related to the stress drop parameter that appears in both models. In the ω-square model, and more specifically in the derivation of equation (3), $\Delta\sigma$ was originally interpreted as the "global stress drop" i.e. as the stress drop which is inferred by assuming it to be uniform over a smooth fault plane without barriers or asperities [Papageorgiou and Aki, 1983a]. But, as it is now widely accepted on the basis of overwhelming observational evidence, earthquake rupture in general is not a smooth process, causing fault slip, and consequently stress drop, to be nonuniform over the fault plane. The generation of the high frequency waves is controlled by the localized stress drops [e.g. Papageorgiou and Aki, 1982]. Furthermore, it has been observed that while the global stress drop varies greatly (1 bar to 100 bars) - and if used in connection with equation 3 usually underestimates the level of high frequency spectral amplitudes - the value of the stress parameter necessary to interpret high-frequency strong motion data is stable [Hanks and McGuire, 1981; Papageorgiou and Aki, 1983a]. Thus the stress parameter which appears in equations 3 and 4 lost its original physical meaning and now can be interpreted only as a scaling factor with the dimensions of stress, depleted of any physical meaning.

On the contrary, the local stress drop $\Delta\sigma_{\ell}$ of the specific barrier model has a clear physical meaning; it is the stress drop inside the cracks/subevents and is related to the radius/size of the cracks/subevents by

$$\frac{\Delta u_{max}}{\rho_o} = \left(\frac{24}{7\pi}\right)\left(\frac{\Delta\sigma}{\mu}\right) \qquad (6)$$

The diameter $2\rho_o$ of the cracks is the barrier interval (= distance between strong patches of the fault plane which lock the fault and arrest the rupture of the cracks/subevents) which may be inferred from geological/paleoseismological studies of identified fault

zones that rupture the surface [Aki, 1980]. This kind of information may be used to predict strong ground motion in tectonic regions for which there exist no strong motion data but for which such geologic studies have been made.

Finally, it should be pointed out that near-field velocities and accelerations are controlled by the size and stress drop of the localized cracks [Artchuleta and Hartzell, 1981; Campillo and Bouchon, 1983]. Consequently the barrier interval $2\rho_0$ and the local stress drop $\Delta\sigma_\ell$ are very important parameters for synthesizing strong ground motion using either analytical or empirical Green functions [Irikura and Aki, 1985]. Particularly relevant are the observations made by Irikura in connection with his attempts to synthesize strong motion seismograms of two Japanese main events from their aftershocks [Irikura, 1983; 1985]. he observed that he could improve considerably the agreement of the synthesized seismograms with the observed ones by using as Green functions for the synthesis, aftershcoks with diameters equal to the barrier interval of the mainshocks.

In Figure 6 we compare the source spectra of a California event with the source spectra of the two models discussed above. Clearly, the source spectra of the specific barrier model describe much better the overall shape of the observed spectra. Thus, synthesizing all the evidence presented above we conclude that the ω-square model (with a constant stress drop parameter) is a phenomenological model with no physical basis.

Having addressed the validity of the source model that Boore and Atkinson [1987] used in predicting the PSV spectra shown in Figure 1, let us now address the question of whether the level of the high-frequency spectral amplitudes are representative of the ground motion at rock sites in ENA, irrespective of the validity of the model used to obtain them. The paucity of strong motion data from large midplate earthquakes does not permit a definite answer to this question. Nevertheless, there are indications that the predictions may underestimate observations by a factor of 2 or more:

(1) The global stress drop of the Gazli, 1976 event was estimated by Hartzell [1980] to be $\sim$ 200 bars which in effect would require spectral amplitudes higher than those in Figure 1 at least by a factor of 2.

(2) Stress drop estimates from corner frequencies of displacement spectra (i.e. Brune stress drops) of the Friuli, 1976, earthquake sequence (which may be characterized as "transition zone" events) were found to be equal to 200 to 300 bars [De Natale et al., 1987]. This again means that predicted amplitudes shown in Figure 1 may underpredict high-frequency spectral amplitudes of large events by a factor of 2 to 3.

A possible physical explanation of these observations is that large events ($M > 6$) may be associated with deeper and/or stronger regions of the Earth's crust than smaller events ($M \leq 5$). The

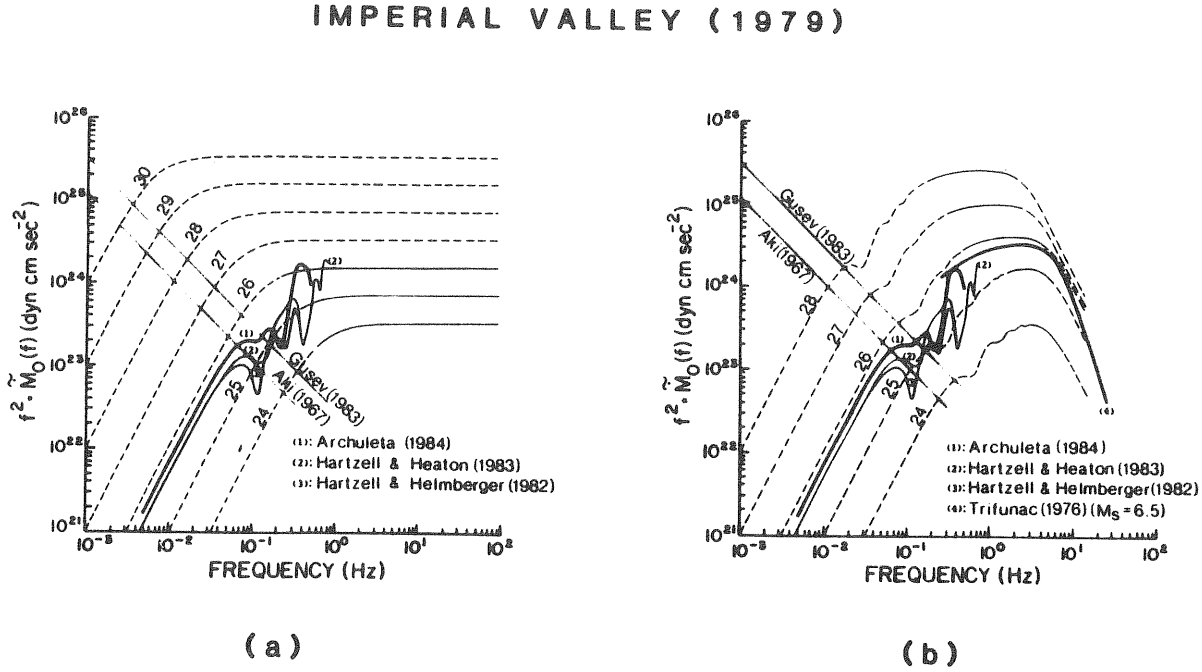

Fig. 6. The slip functions obtained by three inversion studies [Archuleta, 1984; Hartzell and Heaton, 1983; Hartzell and Helmberger, 1982] of the 1979 Imperial Valley earthquake (M_W = 6.5, M_O = 6.3 x 10^{25} dyn-cm) are used to compute the acceleration source spectra shown in (a) and (b). These spectra are compared with: (a) the spectra of an ω-square model with $\Delta\sigma$ = 50 bars [Boore, 1986] and (b) the spectra of the specific barrier model discussed in the test. Triffinac's [1976] empirical spectrum for a magnitude of 6.5 is shown as a reference for high frequency spectral amplitudes. Also shown are the relations of the corner frequency f_1 vs $f_1 . M_O$ proposed by Aki [1967] and Gusev [1983].

reader should be reminded that Boore and Atkinson [1987] calibrated their scaling law using strong motion data of events with magnitudes around 4.5 and then extrapolated to large events using equation 4.

CONCLUSION

Synthesis of high-frequency strong ground-motion using empirical or analytic Green functions necessitates the use of parameters such as the barrier interval and local stress drop. We demonstrated that a self-similar ω-square model with constant stress drop is a phenomenological model if used for the description of high frequency waves and consequently its stress drop parameter, being only a scaling factor with no physical meaning, cannot be used as an estimate of the local stress drop. Because there exist only a few strong motion recordings from large intraplate earthquakes, estimates of the above parameters for midplate tectonic environment may be obtained only from careful waveform modelling of the available near-field records. The number of subevents that compose these large events and an estimate of the value of the local stress drop will enable us to estimate the level of the high frequency spectral amplitudes.

ACKNOWLEDGEMENTS

The author would like to thank Dr. Monsour Niazi for providing a copy of the Tabas acceleration record, and Dr. Stephen Hartzell for providing the strong motion data of the Gazli earthquake. Support for this research has been proided through the National Center for Earthquake Engineering (Grant No. NCEER86-1021).

REFERENCES

Aki, K., Reevaluation of stress drop and seismic energy using a new model of earthquake faulting, in "Mechanisme et Prevision Seismes," Hommage au Professeur Jean Coulomb, Publie sous la direction de Claude J. Allegre, Edition du Centre National de la Recherche Scientifique, 1980.

Aki, K., Strong motion seismology, in earthquakes: Observation, Theory and Interpretation, Proc. Enrico Fermi School of Physics Edited by H. Kanamori and E. Boschi, pp. 223-250, 1983.

Archuleta, R.J., A faulting model for the 1979 Imperial Valley earthquake, J. Geophys. Res., 89, 4559-4585, 1984.

Archuleta, R. and S. Hartzell, Effects of fault finiteness on near source ground motion, Bull. Seism. Soc. Am., 71, 939-957, 1981.

Berberian, M., I. Asudeh, R.G. Bilham, C.H. Scholz, and C. Soufleris, Mechanism of the main shock and the aftershock study of the Tabas-e-Golsham (Iran) earthquake of September 16, 1978: a preliminary report, Bull. Seism. Soc. Am., 69, 1851-1859, 1979.

Boatwright, J. and G.L. Choy, Acceleration source spectra for large earthquakes in North Eastern North America, EPRI Workshop on Earthquake Ground-Motion Estimation in Eastern North America, March 31 to April 2, 1987, Palo Alto, CA, 1987.

Boore, D.M., Short-period P-and S-Wave radiation from large earthquakes: implications for spectral scaling relations, Bull. Seism. Soc. Am., 76, 43-64, 1986.

Boore, D.M. and G.M. Atkinson, Prediction of ground motion and spectral response parameters at hard-rock sites in eastern North America, Bull. Seism. Soc. Am., 77, 440-467, 1987.

Bouchon, M., Predictability of ground displacement and velocity near an earthquake fault. An example: the Parkfield earthquake of 1966, J. Geophys. Res., 84, 6149-6156. 1979.

Brune, J.N. Tectonic stress and the spectra of seismic shear waves from earthquakes, J. Geophys. Res., 75, 4997-5009, 1970.

Campillo, M. and M. Bouchon, A theoretical study of the radiation from small strike-slip earthquakes at close distances, Bull. Seism. Soc. Am., 73, 83-96, 1983.

De Natale, G., R. Madariaga, R. Scarpa, and A. Zollo, Source parameter analysis from strong motion records of the Friuli, Italy, earthquake sequence (1976-1977), Bull. Seism. Soc. Am., 77, 1127-1146, 1987.

Hanks, T.C., The National Earthquake Hazards Reduction Program-Scientific Status, U.S. Geological Survey Bulletin, 1659, 1985.

Hanks, T.C. and R.K. McGuire, The character of high frequency strong ground motion, Bull. Seism. Soc. Am., 71, 2071-2995, 1981.

Hartzell, S.H., Faulting process of the May 17, 1976 Gazli, USSR earthquake, Bull. Seism. Soc. Am., 70, 1715-1736, 1980.

Hartzell, S. and D.V. Helmberger, Strong-motion modeling of the Imperial Valley earthquake of 1979, Bull. Seism. Soc. Am., 72, 571-596, 1982.

Hartzell, S.H. and T. Heaton, Inversion of strong ground motion and teleseismic waveform data for the fault rupture history of the 1979 Imperial Valley, California, earthquake, Bull. Seism. Soc. Am. 73, pp. 1553-1583, 1983.

Horner, R.B., D. Weichert, R.J. Wetmiller, M. Lamontagne, and M. Plouffee, A fault model for the Nahanni, NWT, Canada, earthquake from aftershock studies, EOS 68, (44), 1244, 1987.

Irikura, K., Semi-empirical estimation of strong ground motions during large earthquakes, Bull. Disaster Prev. Res. Inst., 33, Kyoto Univ., 1983.

Irikura, K., The synthesis of the strong ground motions for large earthquakes using the records of small earthquakes as empirical Green's functions, Abstract, Earthquake Notes, 55, (1), 6, 1985.

Irikura, K. and K. Aki, Scaling law of seismic source spectra and empirical Green Function for predicting strong ground motions, Abstract, AGU Fall Meeting (Dec. 1985), 1985.

Langston, C.A., Depth of faulting during the 1968 Meckering, Australia, earthquake sequence determined from waveform analysis of local seismograms, J. Geophys. Res., 92, 11561-11574, 1987.

Niazi, M., Accelerograms of the 1978 Tabas, Iran, earthquake, Earthquake Spectra, 2, 635-651, 1986.

Niazi, M. and H. Kanamori, Source parameters of 1978 Tabas and 1979 Qainat, Iran, earthquakes from long-period surface waves, Bull. Seism. Soc. Am.. 71, 1201-1213, 1981.

Papageorgiou, A.S., Earthquake source spectra - a comparison between western and eastern U.S. earthquakes, EPRI Workshop on Earthquake Ground-Motion Estimation in Eastern North America, March 31 to April 2, 1987, Palo Alto, CA, 1987.

Papageorgiou, A.S., On two characteristic frequencies of acceleration spectra; patch corner frequency and f_{max}, Bull. Seism. Soc. Am. (to appear), 1988.

Papageorgiou, A.S. and K. Aki, Aspects of the mechanics of earthquake rupture related to the generation of high frequency waves and the prediction of strong ground motion, Soil Dynamics and Earthquake Engineering, 1 (2), 67-74, 1982.

Papageorgiou, A.S. and K. Aki, A specific barrier model for the quantitiative description of inhomogeneous faulting and the prediction of strong ground motion. I. Description of the model, Bull. Seism. Soc. Am. 73, 693-722, 1983a.

Papageorgiou, A.S. and K. Aki, A specific barrier model for the quantitative description of inhomogeneous faulting and the prediction of strong ground motion. II. Application of the model, Bull. Seism. Soc. Am. 73, 953-978, 1983b.

Papageorgiou, A.S. and K. Aki, Scaling law of far-field spectra based on observed parameters of the specific barrier model, PAGEOPH, 123, 353-374, 1985.

Shoja-Taheri, J. and J.G. Anderson, The 1978 Tabas, Iran earthquake: an interpretation of the strong motion records, Bull. Seism. Soc. Am. (submitted).

Sykes, L.R., Intraplate seismicity, reactivation of preexisting zones of weakness, alkaline magnatism, and other tectonism postdating continental fragmantation, Geophysics and Space Physics Review, 16, 621-688, 1978.

Weichert, D.H., R.J. Wetmiller and P. Munro, Vertical earthquake acceleration exceeding 2 g? The case of the missing peak, Bull. Seism. Soc. Am. 76, 1473-1478, 1986.

Zoback, M.D., R.M. Hamilton, A.J. Crone, D.P. Russ, F.A. McKeown, and S.R. Brockman, Recurrent intraplate tectonism in the New Madrid seismic zone, Science, 209, 971-976, 1980.

Zoback, M.D. and M.L. Zoback, State of stress and intraplate earthquakes in the United States, Science, 213, 96-104, 1981.

The 1983 Goodnow Earthquake in the Central Adirondacks, NY: A Broadband Teleseismic Analysis

JOHN NABELEK
College of Oceanography, Oregon State University, Corvallis, OR 97331

GERARDO SUAREZ
Insituto de Geofisica, Universidad National Autonoma de Mexico, Mexico DF 04510

ABSTRACT

On October 7, 1983 a magnitude 5.1 (m_b) earthquake occurred in the central Adirondack Mountains, near the town of Goodnow, N.Y. The earthquake was clearly recorded both by local stations and by a large number of digital and analog seismographs in North and South America, and Europe. This teleseismic information is complemented by accurate locations of aftershocks recorded by a portable network from about 17 hours after the mainshock, providing an unusually large dataset to study the source process of an intraplate earthquake. The results of a broadband analysis involving the formal inversion of the vertical component Rayleigh waves and of short-period P waves show that the earthquake was due to reverse faulting with a centroidal depth of 7.5 km, striking almost north-south and dipping at 60° to the west. The scalar seismic moment is 1.9×10^{23} dyn cm. Plausible values of t^* (attenuation) range from 0.4 to 0.7 s, and for these values the estimates of source duration range from 0.75 to 0.35 s. Assuming a circular crack rupture model with a rupture velocity of 3.0 km/s, the bounds on source duration give upper and lower bounds for the fault radius of 0.9 and 0.5 km, and for the stress drop of 670 and 115 bar. The preferred value of $t^* = 0.6$ s yields a source duration of 0.45 s, a radius of 0.7 km, and a stress drop of 265 bar. The inferred stress drop for the Goodnow earthquake suggests that shallow intraplate events in eastern North America have higher stress drops than average interplate events, a fact which may partially explain the large felt areas of these intracontinental earthquakes.

INTRODUCTION

On October 7, 1983 a moderate-sized earthquake ($m_b = 5.1$) occurred in the central Adirondack Mountains of New York state. This earthquake is particularly interesting because it is the largest event to have occurred in the eastern United States since the 1944 Massena earthquake in northern New York [*Basham et al.*, 1979; *Smith*, 1962, 1966].

The earthquake was well recorded by several stations of the Global Digital Seismic Network (GDSN) in North America, Europe and South America, as well as by a variety of local stations installed in the northeastern United States and southeastern Canada to monitor intraplate microseismicity. This information was complemented by a network of portable instruments deployed in the epicentral zone of the Goodnow earthquake by Lamont-Doherty Geological Observatory (L-DGO) from 17 hours to 22 days after the mainshock,

and by the United States Geological Survey (USGS), which installed digital GEOS instruments from 3 to 12 days after the main event [*Seeber and Ambruster,* 1986].

This combination of high-quality, digital teleseismic information and aftershock data is unusual for small intraplate events in general, and particularly for earthquakes in northeastern North America. Thus the Goodnow event represents an unusual opportunity to study such an earthquake in detail, making possible a comparison of results obtained from a teleseismic analysis with characteristics of the source inferred from the aftershock distribution.

In this paper we present results of a broadband teleseismic analysis using seismic waves with periods ranging from 66 to 0.5 s. Long-period surface waves at teleseismic distances are used to constrain the source mechanism and to obtain an accurate estimate of the scalar seismic moment. The results of the surface wave analysis are then used to bootstrap a formal inversion of short-period P waves recorded at various North and South American stations. The inversion results allow us to determine precisely the duration of the source rupture, from which the upper and lower bounds of the source area and stress drop are derived.

LOCATION OF THE EARTHQUAKE AND THE FOCAL MECHANISM

Seismicity in the Central Adirondacks

The epicenter of the Goodnow earthquake is located in the central Adirondack Mountains in upstate New York. In this region, the seismicity data collected by the New York State Network shows an arcuate lineation oriented almost east to west (Figure 1). It is along this seismicity trend that in 1971 and 1973 swarms of seismic activity occurred at Blue Mountain Lake, approximately 20 km west of the epicenter of the Goodnow earthquake. More recently, on November 3, 1975, a magnitude 3.9 earthquake occurred near Raquette Lake, also close to the Blue Mountain Lake seismicity area [*Yang and Aggarwal,* 1981].

This east-west trending seismicity in the central Adirondacks appears to be related to structural and lithologic features of Greenville age [*Seeber et al.,* 1983; *Seeber and Ambruster,* 1986]. *Seeber and Coles* [1984] suggested that it is controlled by a belt of calcitic marble that outcrops to the north of the epicenter of the 1983 Goodnow event. Nevertheless, there is no clear structural evidence controlling the seismicity in this area.

Focal Mechanism of the Main Event and the Aftershocks

The focal mechanism of the mainshock was obtained by combining first motion data from the local seismic networks operating in the area, from the World Wide Standarized Seismographic Network (WWSSN), the Canadian Seismic Network (CSN) and GDSN recordings. Although there are some inconsistent first motion readings, probably due to errors in the polarity of some of the local stations and to inaccuracies in the earth model used to calculate the take-off angles, the focal mechanism indicates a reverse faulting earthquake with nodal planes oriented north to south and dipping at a steep angle (60° and

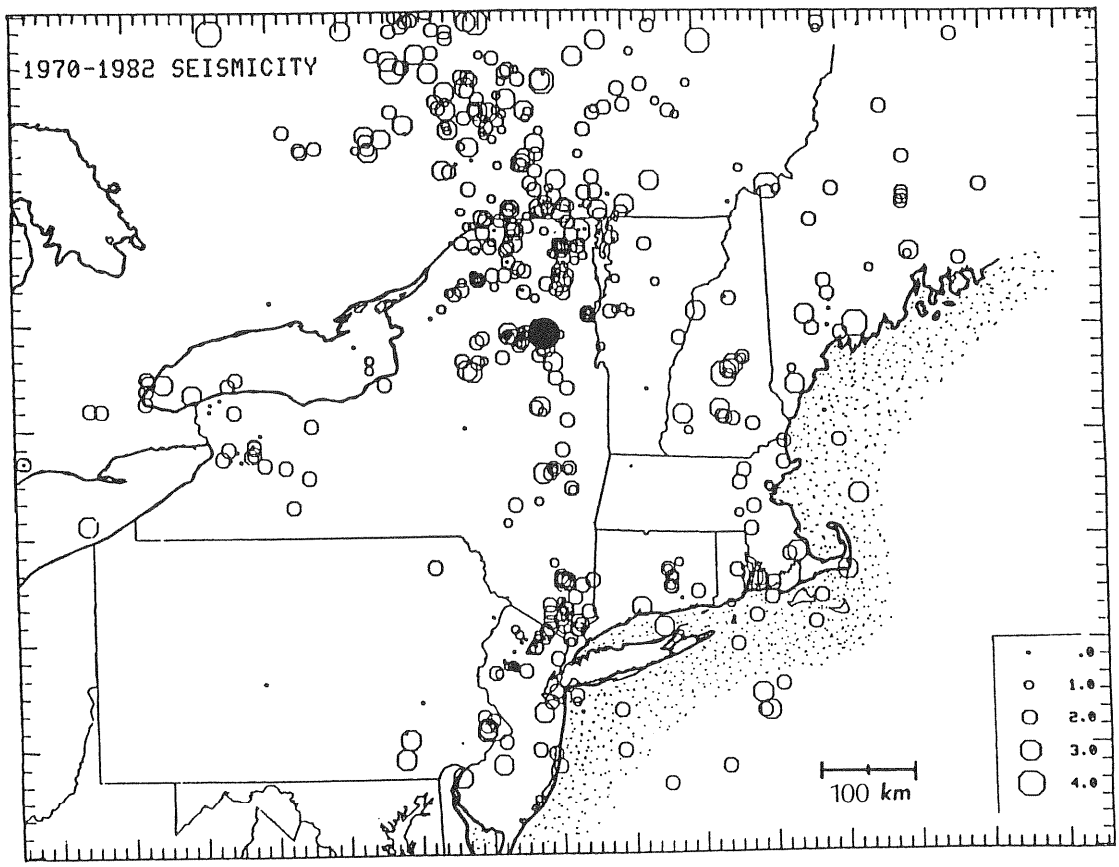

Figure 1. Seismicity of the northeastern United States and southeastern Canada from 1970 to 1982. Note the east-west trend of seismicity in the central Adirondacks, New York. The Goodnow earthquake of 1983 is shown as a solid circle.

TABLE 1. Epicentral Parameters of the 1983 Goodnow Earthquake[1]

Date	Origin Time, h:m:s	Latitude, deg N	Longitude, deg W	Centroid Depth[2], km	m_b,	Seismic Moment[3], dyn cm
Oct. 7, 1983	10:18:46	43.938	74.258	7.5	5.1	1.9×10^{23}

[1]National Earthquake Information Service
[2]Short-period body wave inversion
[3]Surface-wave, moment tensor inversion

TABLE 2. Results of Rayleigh Wave Inversion of the 1983 Goodnow Earthquake

Moment Tensor at 9 km Depth

M_{zz}, 10^{23} dyn cm	$M_{yy} - M_{xx}$, 10^{23} dyn cm	M_{xy}, 10^{23} dyn cm	M_{xz}*, 10^{23} dyn cm	M_{yz}*, 10^{23} dyn cm
2.19	2.22	1.05	0.0	0.0

Principal Axes

	Eigen Value, 10^{23} dyn cm	Azimuth, deg	Plunge, deg
P	2.18	112	0
T	1.70	210	90
B	0.47	22	0

*constrained

30°; Figure 2). The P axis is horizontal and is oriented east-west. A composite fault plane solution of the aftershocks occurring from within 22 days of the mainshock shows a very similar mechanism solution, clearly indicating a reverse faulting mechanism [*Seeber and Ambruster,* 1986] (Figure 2). Source parameters of other earthquakes in northeastern Canada and northern New England, obtained using first motion data recorded at local and regional stations, show a similar orientation of the regional stress field [*Horner et al.,* 1978, 1979; *Sbar and Sykes,* 1973, 1977; *Sykes,* 1978; *Zoback and Zoback,* 1980; *Yang and Aggarwal, 1981; Nabelek,* 1984; *Ebel et al.,* 1986].

In plan view, the distribution of the aftershocks of the Goodnow earthquake shows a tight cluster (Figure 3). The epicentral locations of the aftershocks suggest a north-south trending fault, approximately 2 km long. Projecting the hypocenters along a cross section A-B (Figure 3), the aftershocks indicate clearly that the earthquake occurred on a fault plane dipping west at an angle of about 60° (Figure 4), in close agreement with the fault plane solutions of the main event and the aftershocks. In this cross sectional view, the down-dip width of the fault is also approximately 2 km, suggesting the source area has essentially a circular shape.

SURFACE WAVE ANALYSIS

Surface Wave Data

The Goodnow earthquake produced excellent recordings of surface waves at various stations in North and South America. These stations provide good azimuthal coverage, and wave propagation is generally over relatively simple continental paths. Thus the surface waves represent an excellent dataset to constrain the focal mechanism and the scalar seismic moment of the Goodnow earthquake. Before proceeding with a formal inversion of the dataset, a simple analysis is presented to assess its quality and resolution in constraining the focal mechanism.

The vertical component of the Rayleigh waves was selected for various stations surrounding the epicenter. Each of the waveforms was equalized to a common distance of 4000 km, eliminating the effects of geometrical spreading, anelastic attenuation and phase velocity dispersion along the path of propagation [*Aki,* 1960]. In order to eliminate the effect of different recording seismographs, the instrument response was deconvolved and all waveforms were then convolved with a common GDSN instrument response. Thus the resulting wavetrains are equivalent to those which would theoretically be recorded on a flat, laterally homogeneous earth, at a common distance of 4,000 km from the epicenter, and using the same recording instrument (Figure 5).

The results of this experiment clearly show two nodes in the radiation pattern for stations to the north and south of the epicenter (RSNT, MBC, ZOBO, and BOCO; Figure 5). A clear lobe is evident for stations lying to the west of the epicenter. The resulting shape of the radiation pattern confirms a dip-slip mechanism oriented in a north-south direction. The only exception is station STJ which shows an anomalously low signal amplitude; this can perhaps be due to a calibration problem at the station.

Moment Tensor Inversion

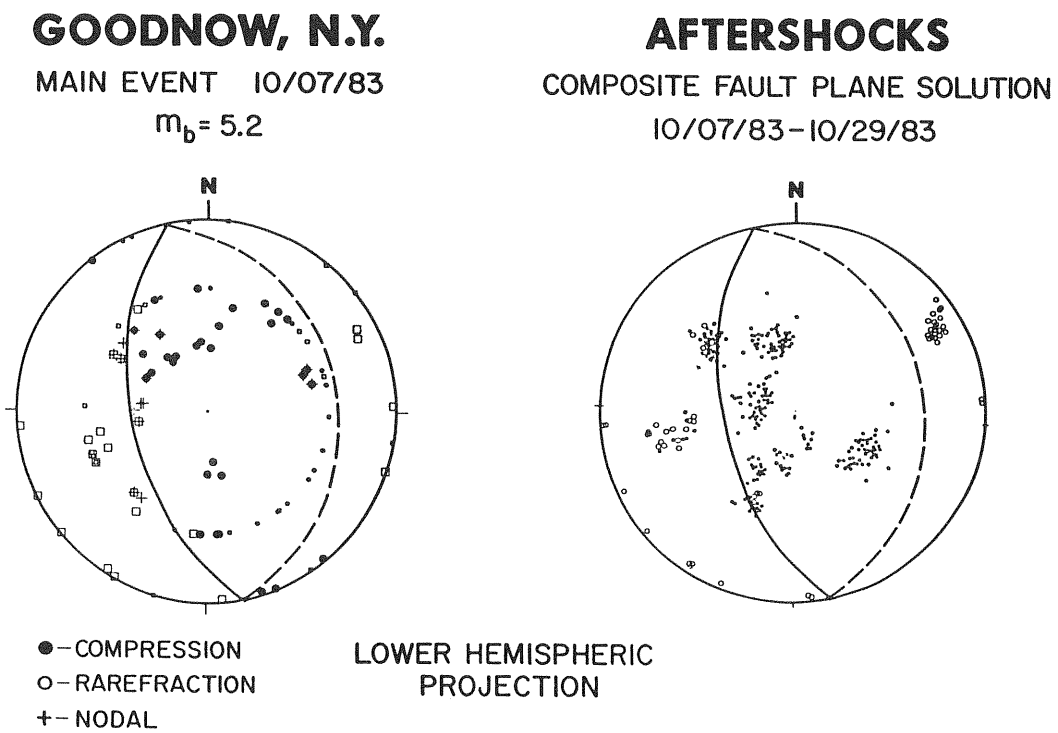

Figure 2. A fault plane solution of the Goodnow earthquake and a composite solution of the aftershocks occurring within 22 days after the main shock. Solid circles are compressional and open circles are dilatational first motions; crosses indicate nodal readings. Data are plotted using a lower hemisphere, equal-area projection.

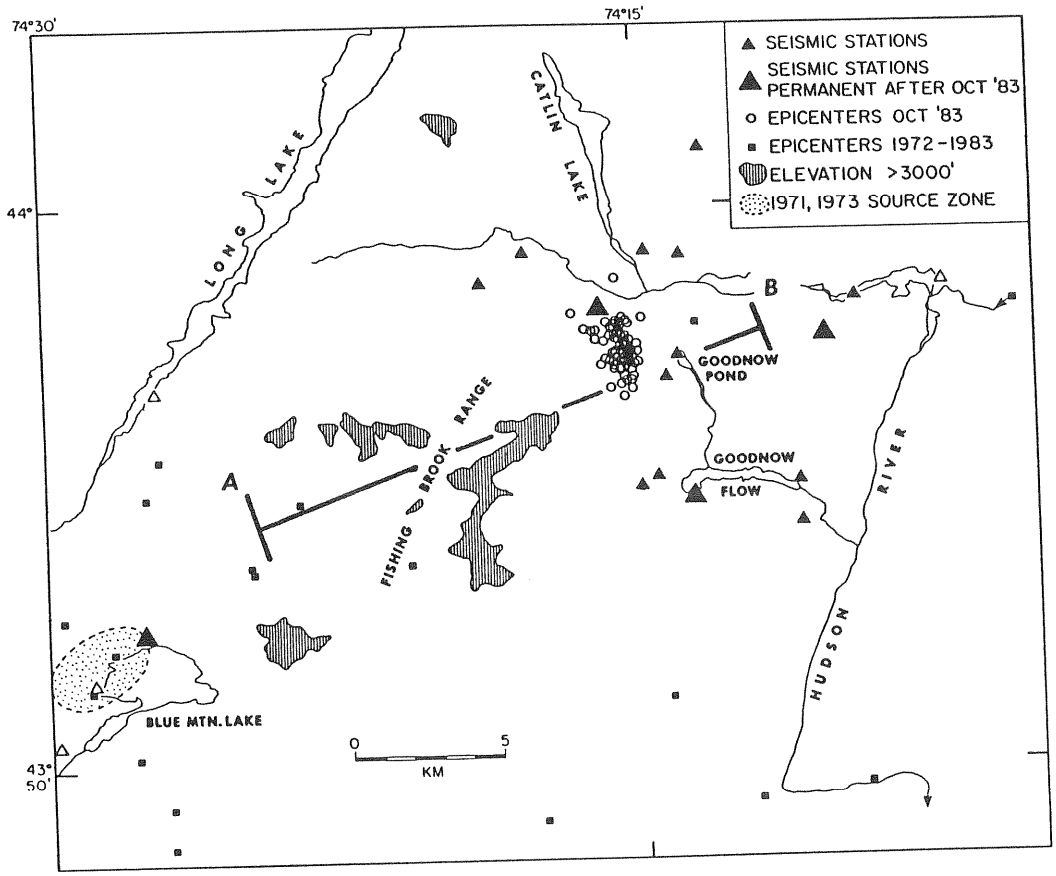

Figure 3. Map of the aftershock epicenters (open circles). Note the north-south trend of the aftershocks and the location of the temporary network of seismographs (small triangles).

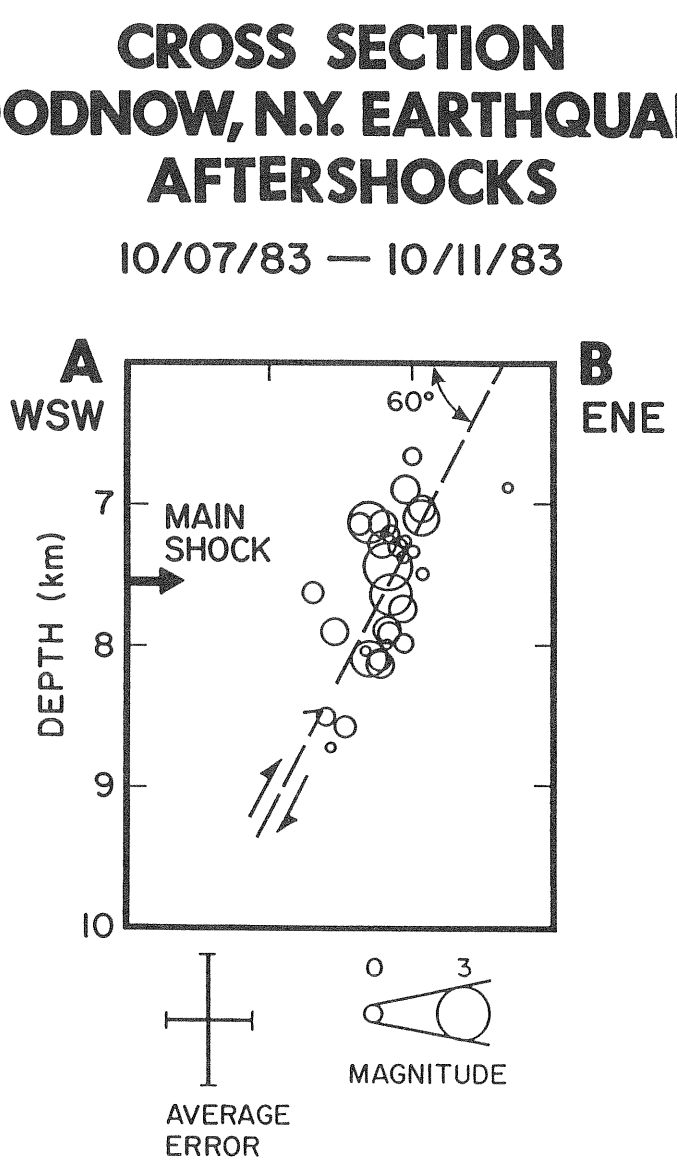

Figure 4. Vertical cross section (along line A-B in Figure 3) of the aftershock hypocenters located from October 7 to October 11, 1983. The dip of approximately 60° of the aftershock distribution agrees well with the fault dip estimated from the body wave inversion (Table 3 and Figure 8). Arrow at 7.5 km indicates the centroid depth inferred from the body wave inversion.

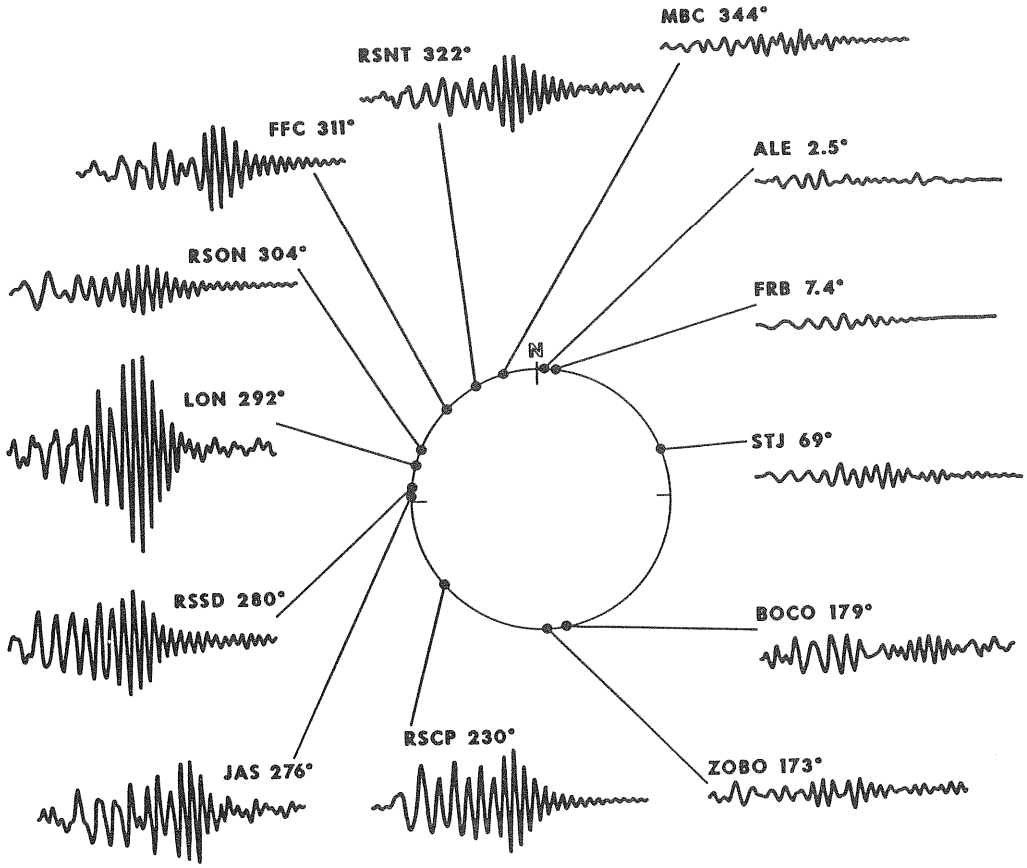

Figure 5. Vertical-component Rayleigh waves of the 1983 Goodnow earthquake equalized to a distance of 4000 km from the epicenter and to a GDSN instrument. The numbers besides the station names are the azimuths from the epicenter to the stations measured from the north.

The above analysis shows that the Rayleigh wave data are of good quality and have the resolution necessary to determine the source mechanism of the Goodnow earthquake by a formal inversion. The method used is that of *Romanowicz and Suarez* [1983], in which the amplitude spectra of vertical component Rayleigh waves are inverted in a least-squares sense for the moment tensor and the centroidal depth of the source. The centroidal depth is determined by applying the inversion scheme at several trial depths and finding the one with the smallest variance. The orientation of the moment tensor components is defined as in *Patton* [1980].

A correction is applied to the Rayleigh waves to account for geometrical spreading and anelastic attenuation [*Tsai and Aki,* 1969]. The spectra for the inversion were sampled at eight different periods ranging from 66 to 28 s; in this period range the maximum signal-to-noise ratio was observed. The inversion was performed at twelve trial focal depths ranging from 1 to 35 km. In order to accentuate the variance reduction at the true focal depth, the moment tensor was constrained with $M_{xz} = M_{yz} = 0$. This constraint forces the solution to be a pure strike slip fault on a vertical plane, or a pure dip slip fault dipping at 45°. The mechanism obtained from first motion data (Figure 2) indicate that the Goodnow earthquake occurred on an essentially pure, dip slip reverse fault. Thus the constraint imposed in the inversion is reasonable and will help to make the inversion more robust by eliminating components that are very close to zero.

The results show a sharp reduction in variance for the trial depths between 7 and 11 km (Figure 6), indicating a centroidal depth of moment release of about 9 km. This depth range is in good agreement with the occurrence of aftershocks (Figure 4). The resulting moment tensor is shown in Table 2; the implied source mechanism agrees with a north-south striking reverse fault. Besides confirming the fault orientation and the depth of the faulting, the surface wave inversion served to obtain an accurate estimate of the scalar seismic moment of 1.9×10^{23} dyn cm. In the next section, this estimate of seismic moment from the surface waves will help to determine the duration of the rupture of the Goodnow earthquake.

SHORT-PERIOD BODY WAVE INVERSION

Data Analysis and Inversion Procedure

Short-period P waves with good signal-to-noise ratio were recorded at several GDSN and CSN instruments. The GDSN were recorded digitally at a rate of 20 samples per second, while the CSN data were hand digitized on a table-top digitizer at the same sampling rate. For the GDSN data, the instrument response was deconvolved to provide broader bandwidth seismograms. All seismograms were filtered with a high-pass filter with a cutoff frequency of 0.4 Hz (2.5 s) to eliminate long-period noise.

The parameters of the best fitting double-couple point source were determined using the inversion scheme of *Nabelek* [1984], which matches the short-period body wave shapes in a least squares sense and solves for the source orientation, centroidal depth, scalar seismic moment and the shape and duration of the source time function.

The synthetic seismograms were computed for a crustal model with a compressional velocity of 6.0 km/s, Poisson's ratio of 0.25, and density of 2.8 g/cm^3. When inverting or constructing synthetic waveforms of short-period P waves, a crucial

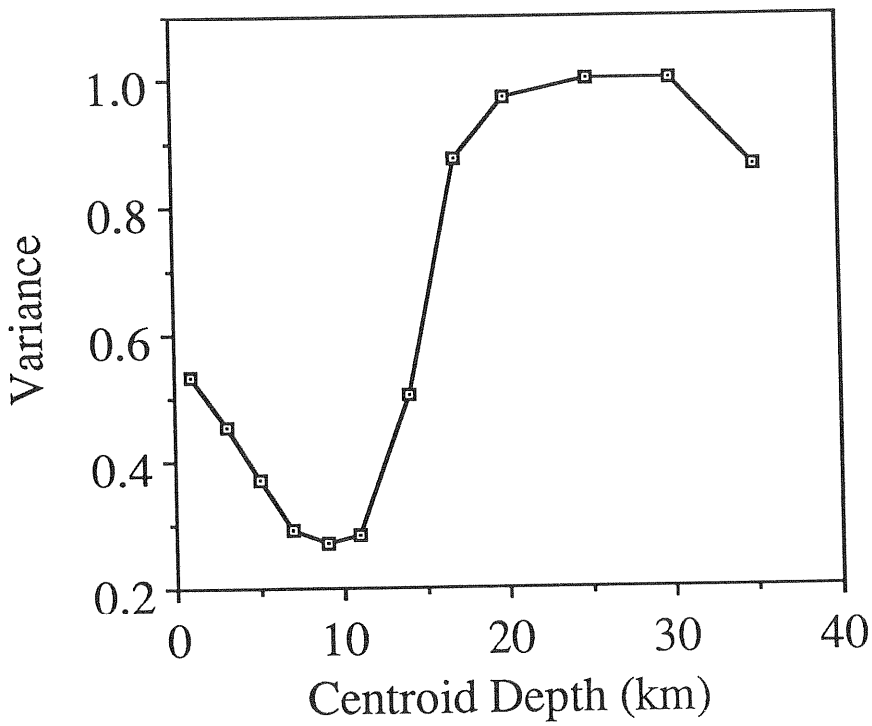

Figure 6. Variance reduction as a function of depth for several trial depths of the source in the inversion of Rayleigh waves. The centroidal depth of the Goodnow earthquake appears to be between 7 and 11 km.

parameter is the assumed anelastic attenuation along the path between source and recording station. The attenuation is parameterized by the value of t^* (travel time / average Q). The selected value of t^* will not only affect the duration of the source time function obtained but also affect the inferred scalar seismic moment, because of the peaked nature of the spectra of the observed and synthesized waveforms [*Nabelek,* 1984]. As we discussed above, one of the main objectives of this paper is to constrain the dimensions of the source of the Goodnow earthquake in order to compare it with the aftershock locations, and to use the derived source dimensions to estimate the stress drop. The proper selection of the attenuation parameter is therefore crucial.

Inversion Results

Inversions were performed for a range of values of t^* (0.4 - 1.0 s). The estimates of seismic moment determined from the inversion for these various t^* show that a value 1.0 s yields a seismic moment that is almost twice as large as that obtained from the surface waves, whereas the value of 0.4 s results in a seismic moment which is too small (Figure 7). From these results, an average value of t^* near 1.0 s can be ruled out, and it is inferred that the actual value of this parameter is between 0.4 and 0.7 s. Our preferred value is 0.6 s, which reproduces the value of scalar seismic moment obtained from the Rayleigh waves.

The various assumed values of t^* do not affect the the source orientation or the centroidal depth obtained from the inversion. The inferred mechanism (Table 3) indicates a reverse faulting striking almost north-south, which agrees well with the first motion data. The centroidal depth is 7.5 km, agreeing well with the result of the moment tensor inversion of the Rayleigh waves and the distribution of aftershocks. For our preferred value of $t^* = 0.6$ s, the duration of the source time function is 0.45 s. The model provides an excellent match of the observed waveforms for about 6 to 8 s, the duration of the main bodywave train (Figure 8).

DISCUSSION AND CONCLUSIONS

The acceptable values of t^* (between 0.4 and 0.7 s) obtained above give upper and lower bounds for the duration of the source time function of the Goodnow earthquake of 0.75 and 0.35 s. Assuming a rupture velocity of 3.0 km/s on a circular crack, these estimates of source duration indicate the radius of the ruptured fault between 0.9 and 0.5 km. Our preferred estimate of $t^* = 0.6$ s gives a source radius of 0.7 km.

These estimates of the source dimension based on the teleseismic data can be compared with the fault area determined from the distribution of aftershocks [*Seeber and Ambruster,* 1986]. Figure 9 shows the aftershock distribution projected onto the fault plane derived from the short period inversion (Table 3). We observe a crescent-shaped distribution of the larger aftershocks.

When the circular source inferred from the teleseismic analysis is centered on this aftershock distribution (Figure 9), we notice that the larger aftershocks tend to fall on the perimeter of the fault area. This distribution of earthquakes is suggestive of a circular fault where the aftershocks occur preferentially on the perimeter of the rupture, where a stress concentration occurs. Only a few smaller aftershocks occur in the center of the rupture

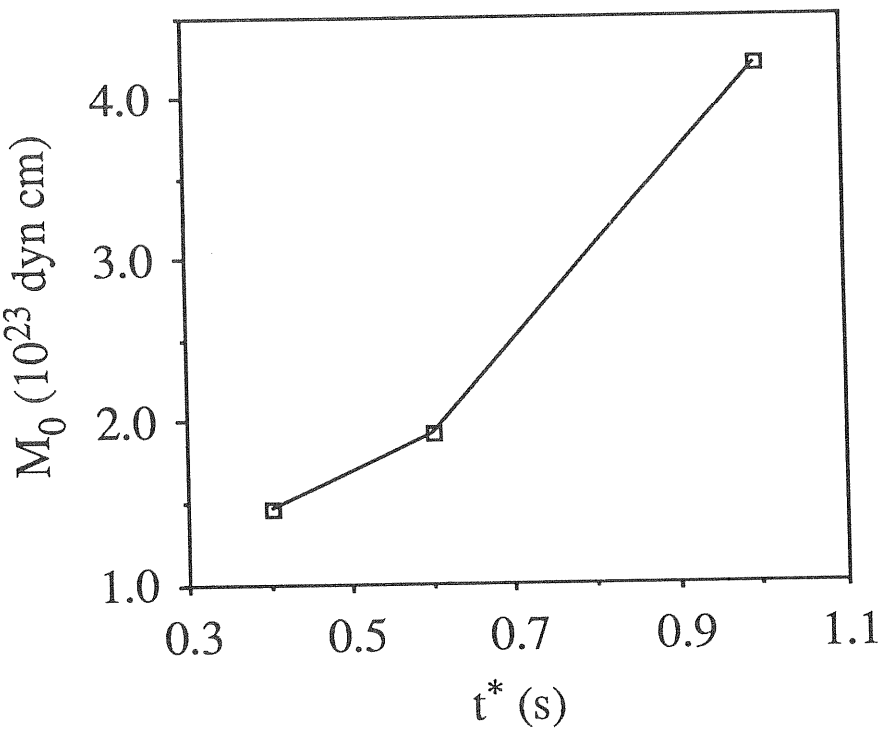

Figure 7. Variation of the estimated seismic moment for different values of t^* used in the inversion of short-period P waves.

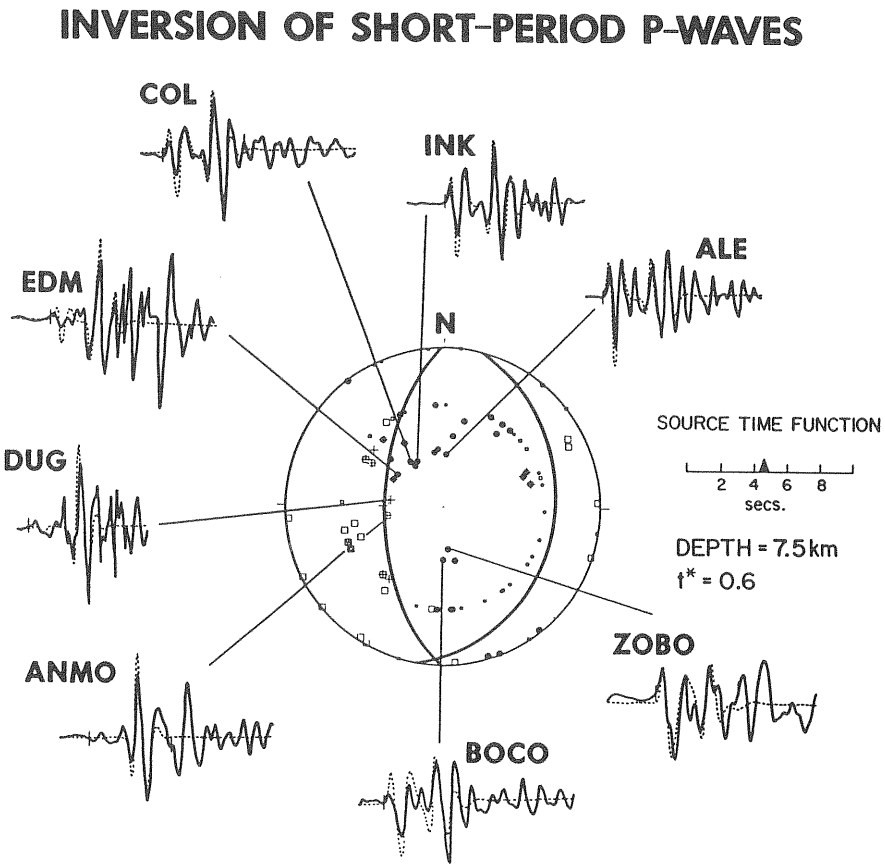

Figure 8. The match between the observed (solid lines) and theoretical (dashed lines) short-period seismograms for the preferred parameters (Table 3) of the Goodnow earthquake. Vertical bars on observed waveforms mark the data windows used in the inversion. The inferred fault plane solution is also shown.

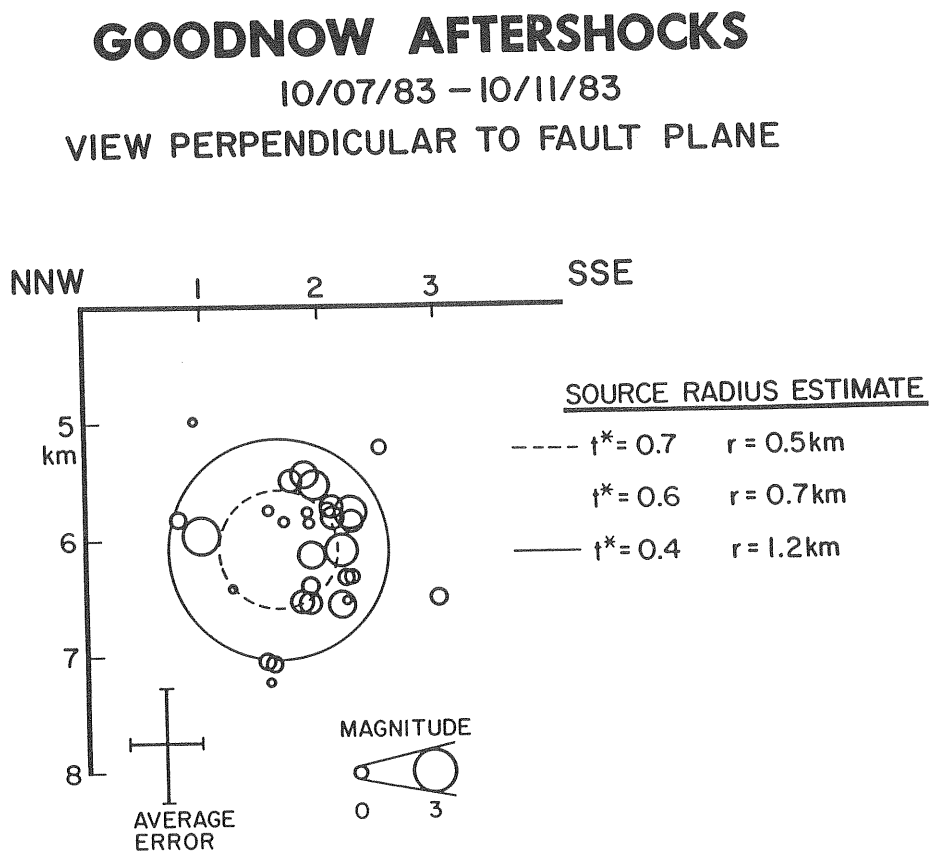

Figure 9. Aftershock distribution of the Goodnow earthquake projected onto the fault plane. The aftershock distribution shows a quasi circular geometry. The inferred radius of the fault agrees well with that obtained from the short-period weveforms assuming a value of $t^* = 0.6$ s. Note that the larger aftershocks fall on the perimeter of the inferred rupture, suggesting that the earthquake was caused by a nearly circular crack.

TABLE 3. Results of Short-period Body Wave Inversion of the 1983 Goodnow Earthquake

Strike, deg	Dip, deg	Slip, deg	Depth, km	Source Duration, s	Seismic Moment, 10^{23} dyn cm
180	61	81	7.5	0.45	1.9

zone, implying that the slip during the main event released the accumulated stress. The aftershock distribution and the simplicity of the short-period bodywave forms therefore suggest that the Goodnow earthquake was produced by a simple, smooth faulting with an approximate radius of 0.7 km.

The plausible estimates of t^* give stress drops between 670 and 115 bar. Our preferred estimate of the stress drop for a $t^* = 0.6$ s is 265 bar. The determination of stress drop for other recent earthquakes of similar size in eastern North America range from a few bars for the 1980 Sharpsburg, Kentucky earthquake [*Herrmann et al.*, 1982], to hundreds of bars for the 1982 Miramichi earthquake in New Brunswick [*Nabelek*, 1984]. A common problem in these estimates of the stress drop is the uncertainty in measuring the size of the rupture area, resulting in considerable scatter in the estimated stress drop values [*Somerville et al.*, 1987]. The availability of high-quality aftershock locations for the Goodnow earthquake reduce the uncertainty of this estimate and produce evidence that suggests that the stress drop for at least some intraplate events in the eastern part of North America is higher than that usually observed for interplate or near interplate events in the western part of the continent [e.g., *Kanamori*, 1986; *Ebel*, 1986; *Ebel et al.*, 1986; *Somerville et al.*, 1987]. This observation of high stress drop may account partly for the very large felt areas produced by relatively small earthquakes in the eastern United States.

ACKNOWLEDGMENTS

We would like to thank J. Ambruster and L. Seeber for comments throughout this work and for allowing us the use of their aftershock data. This work was performed under the contract NRC-04-81-179 of the Nuclear Regulatory Commission, the National Science Foundation grant 86-18453, and the National Center for Earthquake Engineering Research project 86-1013.

REFERENCES

Aki, K. (1960). Study of earthquake mechanism by a method of phase equalization applied to Rayleigh and Love waves, *J. Geophys. Res., 65,* 729-740.

Basham, P.W., D.H. Weichert, and M.J. Berry (1979). Regional assessment of seismic risk in eastern Canada, *Bull. Seismol. Soc. Am., 69,* 1569-1602.

Ebel, J. (1986). Comparison of eastern and western North American earthquake source parameters (Abs.), *Earthquake Notes, 57,* 12.

Ebel, J.E., P.G. Somerville, and J.D. McIver (1986). A study of the source parameters of some large earthquakes in northeastern North America, *J. Geophys. Res., 91,* 8231-8247.

Herrmann, R.B., C.A. Langston, and J.E. Zollweg (1982). The Sharpsburg, Kentucky earthquake of 27 July 1980, *Bull. Seism. Soc. Am., 72,* 1219-1239.

Horner, R.B., A.E. Stevens, H.S. Hasegawa, and G. Leblanc (1978). Focal parameters of the July 12, 1975 Maniwaki, Quebec earthquake - An example of intraplate seismicity in eastern Canada, *Bull. Seismol. Soc. Am., 68,* 619-640.

Horner, R.B., R.J. Wetmiller, and H.S. Hasegawa (1979). The St. Donat, Quebec earthquake sequence of February 18-23, 1978, *Can. J. Earth Sci., 16,* 1892-1898.

Kanamori, H. (1986). Spectral differences between intraplate and interplate earthquakes, (Abs.), *Earthquake Notes, 57,* 11.

Nabelek, J.L. (1984). Determination of eartquake source parameters from body waves, *Ph. D. Thesis,* M.I.T., 361 pp.

Patton, H. (1980). Reference point equalization method for determining the source and path effects of surface waves, *J. Geophys. Res., 85,* 821-848.

Romanowicz, B., and G. Suarez (1983). On an improved method to obtain the moment tensor and depth of earthquakes from the amplitude spectrum of Rayleigh waves, *Bull. Seismol. Soc. Am., 73,* 1513-1526.

Sbar, M.L., and L.R. Sykes (1973). Contemporary compressive stress and seismicity in eastern North America: an example of intraplate tectonics, *Bull. Geol. Soc. Am., 84,* 1861-1882.

Sbar, M.L., and L.R. Sykes (1977). Seismicity and lithospheric stress in New York and adjacent areas, *J. Geophys. Res., 82,* 5771-5786.

Seeber, L., and J.G. Ambruster (1986). A study of earthquake hazards in New York State and adjaecent areas, Final Report Covering the period 1982-1985, *Report to the Nuclear Regulatoy Commission,* NUREG/CR-4750, Washington D.C., 98 pp.

Seeber, L., and K.S. Coles (1984). Seismicity in the central Adirondacks wiht emphasis on the Goodnow, October 7, 1983, epicentral zone and its geology, in D.B. Potter, ed., *N.Y. State Geological Association Field Trip Guidebook,* 56 Annual Meeting, Sept. 20-23, 1984, 334-352.

Seeber, L., A. Kafka, J.G. Ambruster, and S. Nishenko (1983). A comparison of the seismotectonics of the northern and southern Appalachians, *Geol. Soc. Am.,* Abst. with Programs, 15, 137 pp.

Smith, W.E.T. (1962). Earthquakes of eastern Canada and adjacent areas, 1534-1927, *Publ. 26,* Dominion Observ., Ottawa, Ont.

Smith, W.E.T. (1966). Earthquakes of eastern Canada and adjacent areas, 1928-1959, *Publ. 22,* 87-121, Dominion Observ., Ottawa, Ont.

Somerville, P.G., J.P. McLaren, L.V. LeFevre, R.W. Burger, and D.V. Helmberger (1987). Comparison of source scaling relations of eastern and western North American earthquakes, *Bull. Seismol. Soc. Am., 77,* 322-346.

Sykes, L.R. (1978). Intraplate seismicity, reactivation of preexisting zones of weakness, alkaline magmatism, and other tectonism postdating continental fragmentation, Rev. Geophys. Space Phys., 16, 621-688.

Tsai, Y.B., and K. Aki (1969). Simultaneous determination of the seismic moment and attenuation of seismic surface waves, *Bull. Seismol. Soc. Am., 59,* 275-287.

Yang, J.P., and Y.P. Aggarwal (1981). Seismotectonics of northeastern United States and adjacent Canada, *J. Geophys. Res., 86,* 4981-4998.

Zoback, M.L., and M. Zoback (1980). State of stress in the conterminous United States, *J. Geophys. Res., 85,* 6113-6156.

THE NAHANNI EARTHQUAKES

D.H. Weichert and R.B. Horner, Geological Survey of Canada, Dept. of Energy, Mines and Resources, Pacific Geoscience Centre, Box 6000, Sidney, B.C. Canada.

ABSTRACT

In October 1985, an earthquake of magnitude M_S6.6 initiated a series of earthquakes in a hitherto only moderately seismic intra-continental region close to the western border of the Canadian shield. In December 85, another earthquake with M_S6.9, with almost identical epicentre initiated a new aftershock series. Accelerographs installed during an aftershock survey in October recorded ground motion within 8 to 12 km of the energy release centre. The records included several seconds of strong vertical ground motion exceeding 2 g, nine seconds after the beginning of the first shear motion, with little or no corresponding subevents recorded on other instruments. Recent field investigations revealed no site anomaly, so that these large records must be accepted as real, probably coming from asperities of a few hundred metres in size within 4 to 6 km of the site.

The mechanism of the two main shocks and most aftershocks was thrusting due to NE-SW horizontal compressive stress, with inferred ruptures lying mainly in the 9 km thick cover of Proterozoic and Paleozoic sediments, but penetrating to depths of 12 km, into the underlying Canadian shield.

This seismotectonic environment is similar to that in the Charlevoix seismic zone of eastern Canada near the eastern margin of the Canadian shield, where large earthquakes are known to have occurred since at least 1663, but where relevant strong motion records have not yet been captured. The Nahanni strong motion records therefore constitute valid samples for design of structures near suspected seismic sources in eastern Canada with little or no magnitude extrapolation.

INTRODUCTION

A pair of unprecedented large earthquakes occurred in the North Nahanni River area, NWT, in October and December, 1985. The earthquakes had moment magnitudes 6.6 and 6.8, surface-wave magnitudes 6.6 and 6.9, and body-wave magnitudes of 6.5 and 6.4, respectively. Although the latter magnitude is most representative of the strong motion energy in the frequency range of engineering interest, the surface-wave magnitude is more suitable for comparison with historical earthquakes that are relevant for earthquake hazard in eastern Canada.

The Geological Survey of Canada (GSC) installed three strong motion accelerographs in the epicentral region immediately following the occurrence of the first large earthquake in October. These instruments produced 82 earthquake records to mid-June 1987. The most important records were those from the 23 December earthquake which produced peak horizontal accelerations of 1.25 g and peak vertical accelerations that were off the recording film, but must have exceeded 2 g.

The Nahanni earthquakes occurred in an area of relatively low seismicity, the so-called "Mackenzie" earthquake source zone of the source zone model developed by Basham et al. [1982]. Based on the short historical record available, the Mackenzie source zone was

assigned an upper-bound magnitude of 6.0, which was significantly exceeded by the 1985 earthquakes.

The seismicity in the Mackenzie and the smaller "Richardson Mountains" source zone, enclosed within the Mackenzie, essentially parallels the western margin of the Canadian shield with a diffuse pattern of earthquakes. The transition region, where the Cordilleran geologic terrains overlie the Precambrian Shield, has similarities with seismic source regions near the eastern margin of the Shield, where large earthquakes have been known to occur in the Charlevoix seismic source zone over the last three centuries.

This paper presents a short review of the geologic and tectonic setting and the faulting mechanisms of the Nahanni earthquakes. A comparison of the intensity patterns with that of the 1925 Charlevoix earthquake is presented as circumstantial evidence for the relevance of the Nahanni observations to the eastern seismicity. The strong ground motions recorded from the December event are reviewed and evidence is presented that they should not be interpreted as site effects.

TECTONIC SETTING AND HISTORICAL SEISMICITY

Figure 1 shows the location and relative level of seismicity of the Mackenzie region in the context of the total Canadian seismicity. While the activity along the Pacific plate boundary is high and well defined, the earthquakes within the continent and surrounding the Canadian shield occur in diffuse low-activity clusters. Periods of complete reporting for the northern Cordillera are short, with magnitude 6. or larger only complete since 1920, and magnitude 5 since about 1950 [Leblanc & Wetmiller 1974].

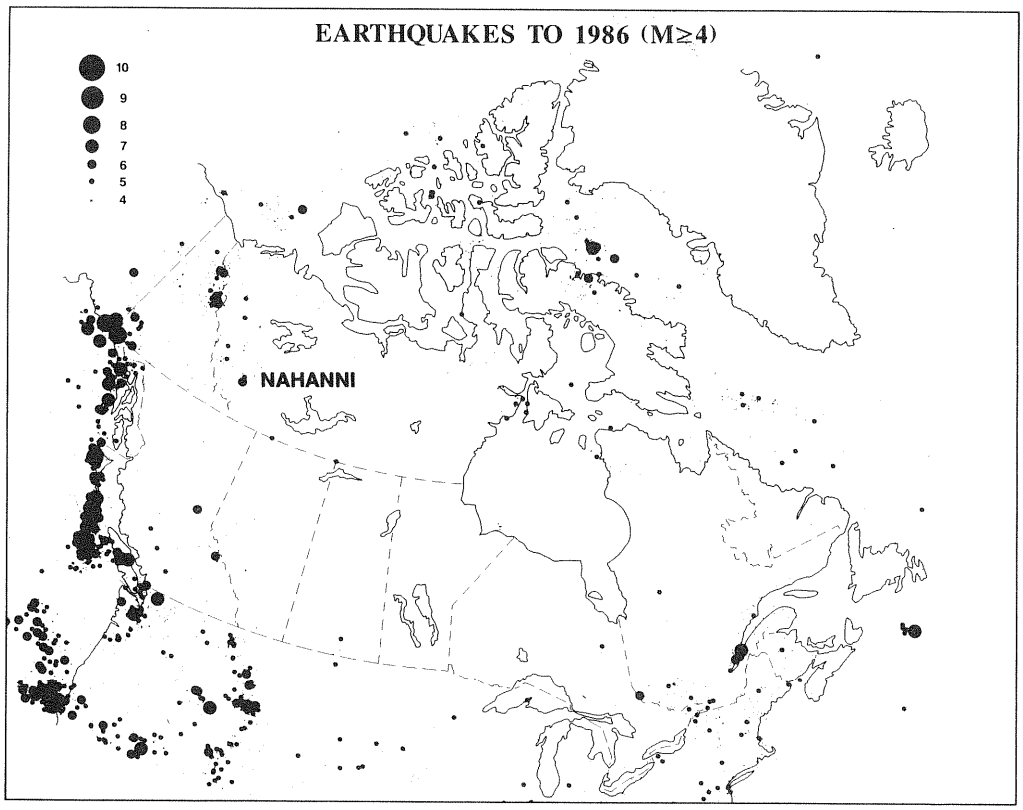

Fig. 1 Canadian Earthquakes above M4

Magnitude 6 and 6.5 earthquakes have occurred in the Beaufort Sea and in the Richardson Mountains, about 500 km northwest of the current activity in the Mackenzie Mountains, but within the diffuse cluster that includes the Nahanni events, the largest previous historical earthquakes have only been near magnitude 5. If, however, the Nahanni aftershock series continues, it may eventually resemble the clustered activity in the Richardson Mountains near the 1940 and 1955 M6.5 and M6.6 earthquakes.

The Nahanni earthquakes occurred in the Mackenzie Plain, part of the Mackenzie Fold Belt of the northeastern Cordillera. This fold belt underwent various degrees of deformation during the late Cretaceaous to early Tertiary Laramide Orogeny, which was the main deformational episode in the region.

The Mackenzie Plain has a total thickness of about 9 km of sedimentary rocks above the crystalline Precambrian basement. The Plain is bounded on the west by the Iverson Thrust and the Mackenzie Mountains, and on the east by the Battlement Thrust of the Franklin Mountains.

Contemporary stress indicators [Adams, 1985] suggest that the crustal rocks in this region are subjected to high horizontal compressive stress in NE-SW direction, similar to that found in most of northeastern North America.

EARTHQUAKE FAULT MECHANISMS

The mechanism of the two large Nahanni earthquakes have been determined from P-wave first motions, analysis of surface-wave spectra, teleseismic p-waves and interpretation of aftershock distributions [Wetmiller et al. 1987]. Both rupture surfaces strike 175° with uncertainties of about 30°; rake angles are 90° with uncertainies of about 20°. The October fault rupture dips toward the west at about 34°, while the December rupture dips at a shallower 25° to the west. The mechanisms for some of the smaller shocks that have been determined tend to agree with those of the main shocks, with the exception of one subarea just south of the main shocks, where strike-slip was observed [Horner et al. 1988].

The aftershock zone defining the active area was determined from data obtained during field experiments and data from the Canadian seismograph network [Horner et al. 1988]. Aftershocks occurred over an area about 15 by 50 km, but could not be associated with any of the mapped surface faults, nor with their inferred extension at depth. Aftershock depths located from field data ranged from 3 km to 12 km. The fault ruptures appear to have started in the sedimentary rocks and propagated downward, taking the rupture into the crystalline rocks of the Precambrian craton.

MERCALLI INTENSITIES

Approximately 2000 intensity questionnaires were mailed following the main shocks, to locations up to 1400 km from the epicentres; about 70 percent were returned. The isoseismal contours of the larger (December) event is shown in Figure 2 [Wetmiller et al. 1987]. To the north and east the data are quite sparse due to lack of habitation.

Neither earthquake caused any significant damage, as the immediate epicentral area is uninhabitated. Several cases of cracked plaster were reported in single-storey, wood-frame buildings in the

closest communities of Wrigley (120 km) and Fort Simpson (160 km). The felt area of the October event was estimated as about 1.5 million km², judged from the macroseismic data from the south and east. The December felt area may have been 50 per cent greater based on relative areas inside the intensity IV contour.

The distribution of intensities shows a strong elongation in NW-SE direction, parallel to the strike of the Cordillera; intensity IV was reported to at least 1000 km to the southeast of the epicentres, but to only about 500 km to the west. This effect has been noted previously by Rogers et al. [1980] and is thought to be due to more efficient propagation of L_g parallel to the structural trends in the Cordillera, implying ground motion attenuation conditions in this direction similar to those observed in the Shield areas of eastern Canada. The effect was again clearly observed for the 1983 Idaho [Drysdale & Horner 1986] and the 1986 Prince George earthquakes [Wetmiller et al. 1988].

Because the epicentral area was devoid of human habitation and engineered structures, it is not possible to establish accurate epicentral intensities. One occupied cabin at a distance of 60 km experienced intensity V. Extrapolating inward from the extent of the intensity V contours using either Richter's relation, or Topozada [1975], we feel that maximum epicentral intensity could have been about IX.

There were many small slope failures and one major rock avalanche in the epicentral region. Landslides are formally rated as intensity X on the modified Mercalli intensity scale, but significant mountain rock-slope failures have been observed at intensities as low as VI [Keefer 1984, Mathews 1979]. Slope failures may therefore not be very useful for establishing intensity.

Figure 2 also shows the St. Lawrence 1925 isoseismals [Smith 1963] on the same scale as the Nahanni isoseismals. When superimposed appropriately, the similarity in size and ratio of axes is striking, e.g. along the IV contours. Along the major axis, the Nahanni event was felt towards the SE about 1800 km into the US, the same distance as the 1925 event. The higher attenuation at right angles to the trend of the St. Lawrence River should also be noted.

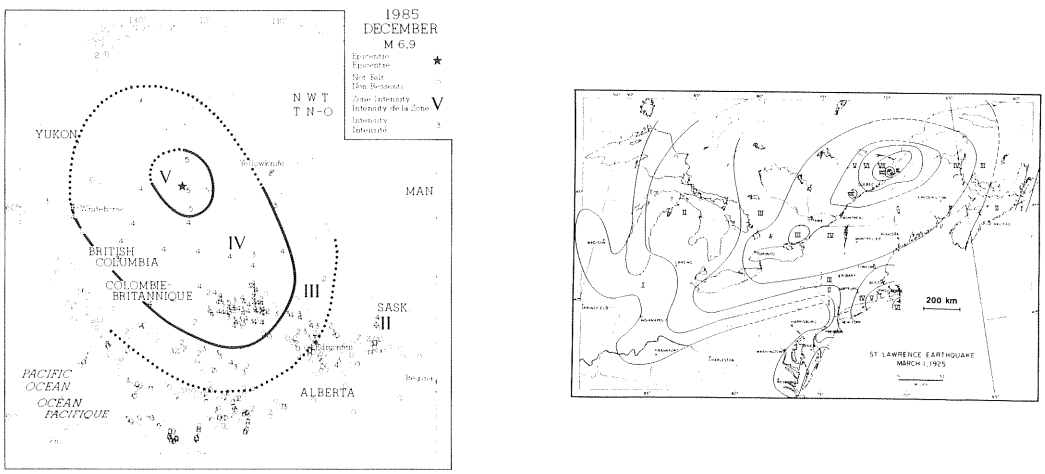

Fig. 2 Isoseismal contours at equal scales, of the 23 Dec. 1985 Nahanni (left) and the 1925 St. Lawrence earthquakes.

STRONG MOTION

Large Peak Acceleration at Site 1.

Figure 3 shows the location of the three, 3-component SMA-1 accelerographs that recorded the December event. Sites 1 and 2 are about 11 km apart, and 10 km from the 23 December epicentre; site 3 lies about 20 km to the east. The record at site 3 showed no unusual features; the strong shaking lasted about 10 seconds with peaks reaching about 0.18 g with dominant frequencies of 10 to 20 Hz. At site 2, the vertical accelerometer lost its damping for unknown reasons; this component is not useable because of the uncertainty in making instrument corrections for the small remaining damping. The horizontal components at site 2 show peak accelerations of 0.4 and 0.5 g occurring early in the record at frequencies between 1 and 3 Hz. The film records obtained at site 1 and 2 are shown in Figure 4 [Weichert et al. 1986 a,b].

Accelerations at site 1 behave quite differently from those at site 2. After starting with similar amplitudes, accelerations quickly increase, and show distinct subevents near 3, 6, 8 and 9 seconds. The film traces near 9 seconds overlap so severely that

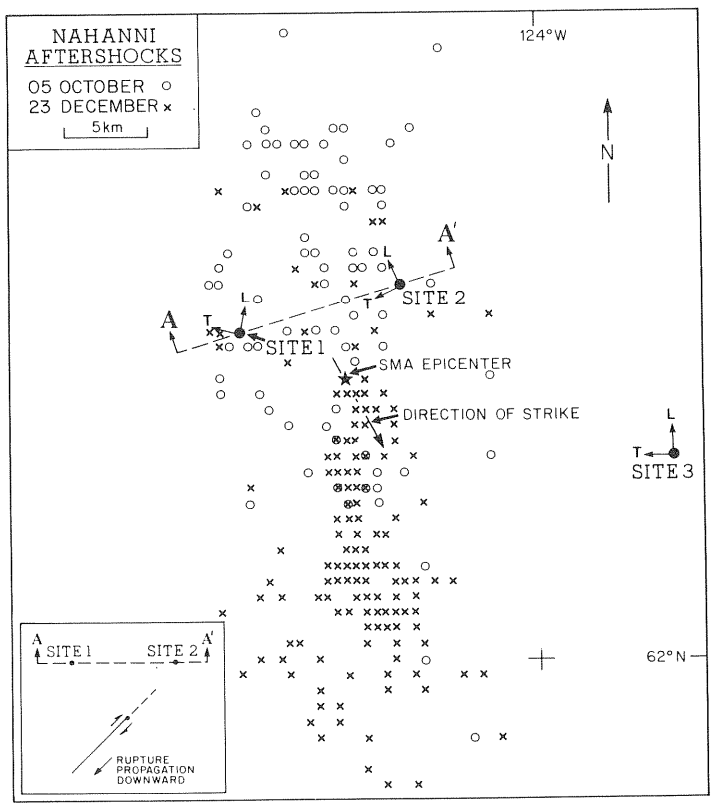

Fig. 3 Locations of accelerographs and aftershocks for October & Janunary field surveys. 'Direction of strike' reflects the regional trend. L and T are the orientation of the accelerograph axes.[from Weichert et al.,1986]

digitization is difficult. However, all peaks, except one, have been unambiguously identified on all three components. The one exception corresponds to an upward acceleration pulse (0.06 seconds half-period) the peak of which is not visible. Conservative estimates place this peak at about 2 to 2.3 g; this estimate is based on the trace thickness over the observed part of the peak, which reflects the light spot velocity, and on a hand-interpolation between the upgoing stems of the missing peak.

The time of this implied strong vertical acceleration closely coincides with a large eastward kick on the transverse component, which must have caused the ramp-like offset of both time bases. The baseline offset is small (0.1 mm) and may be within the lateral tolerance of the film position; its direction corresponds to a throw of the film towards the east, in agreement with the known source mechanism and the integrated displacement. During the digital processing of the records, no special allowance was made for the step offset, except for the usual baseline interpolation and subtraction from all components.

Since a number of peaks exceed the 1 g specification of the instrument, a recalibration out to the recording limits will still have to be done. A quasi-static simulation of the large upward acceleration by inverting the instrument manually shows no suspicious behaviour up to about 1.8 g, at which point the trace reaches the outer edge of the sprocket holes and disappears.

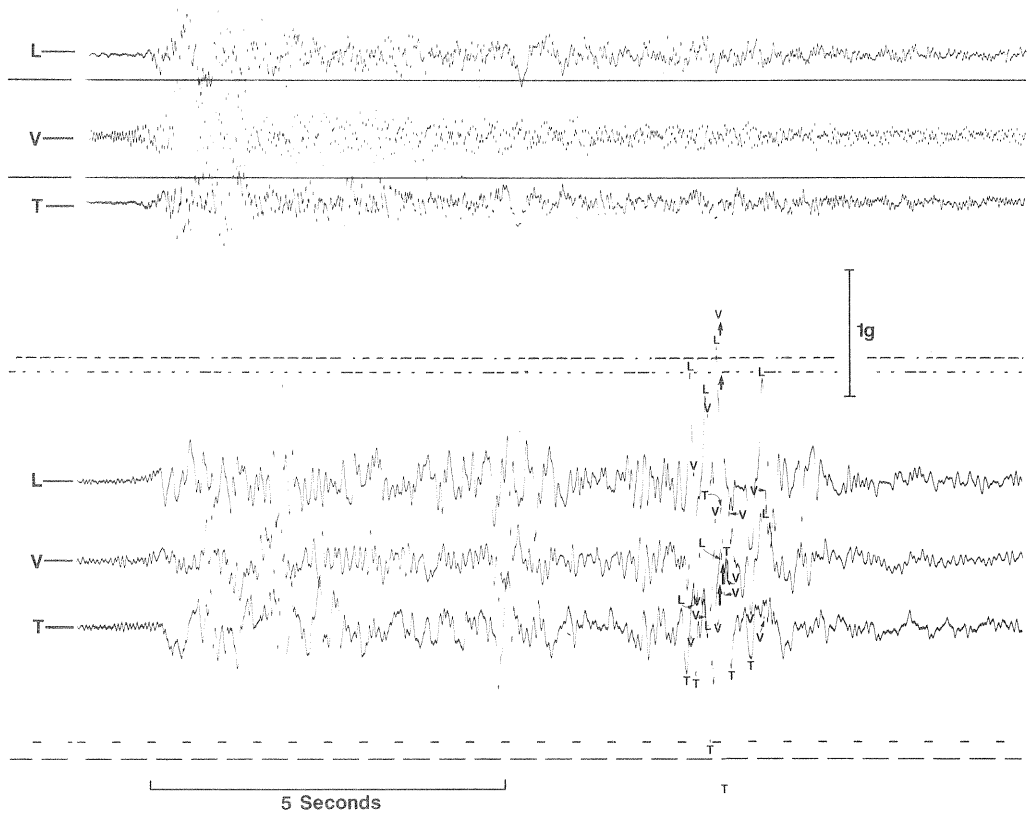

Fig. 4 Film records from site 1 and 2

Site Investigations.

The credibility of the strong ground motion at site 1 has obvious implications for building codes and engineering design, since all components of this particular record exceed the design spectrum for the highest seismic zone (6) in the National Building Code of Canada [1985], for periods shorter than 0.3 to 0.4 seconds [Weichert et al. 1986a]. The possibility of some site effect has been considered, especially since the the record at site 2 shows no hint of increased amplitudes corresponding to the site 1 energy around 9 seconds.

During an instrument service visit to the area in June 1987, a careful visual inspection of all sites was made. Figure 5 shows the general location of site 1. Partial excavation with pick and shovel

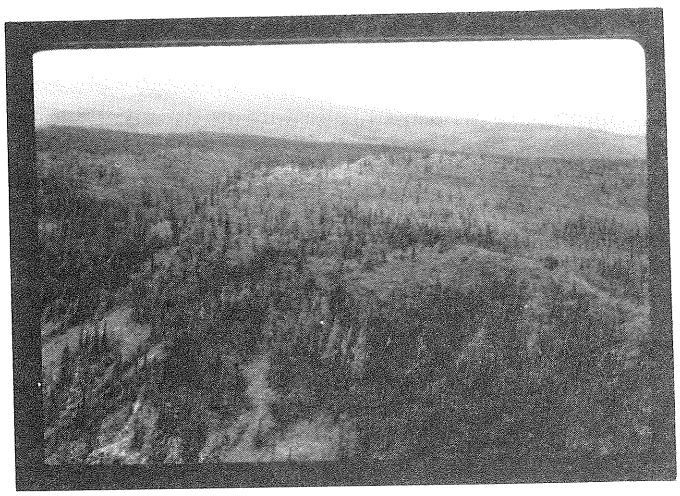

Fig. 5 Site 1, general view, looking SW. Foreground is Iverson Thrust, MacKenzie Mountains in background. Dot marks approximate site location.

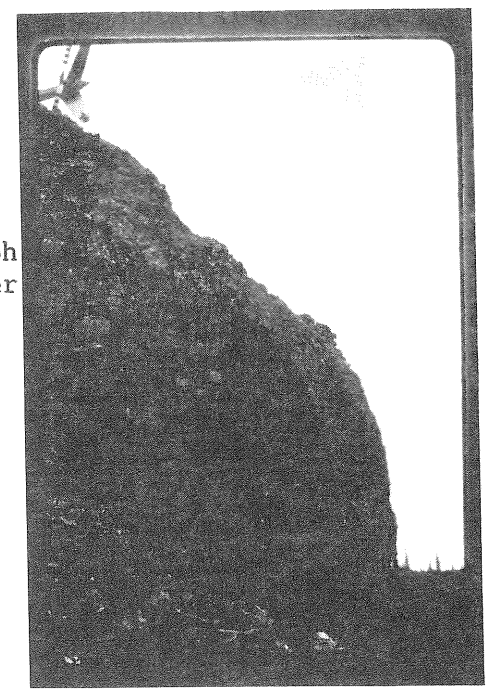

Fig. 6 Site 2, the accelerograph is in front of the helicopter

convinced the senior author that instrument 1 was firmly bolted to solid bedrock outcrop. The site was on top of the gently undulating plateau, west and on top of the escarpment shown in Figure 5, at a distance of about 30 to 50 m from the 100 to 150 m dropoff, that here marks the Iverson Thrust. Apart from possible topographic amplification due to the nearby 50 to 75 percent slope, site 1 looked sound, with no nearby loose rock or debris.

Site 2 appears much less solid: it is located within a few metres of a steep dropoff near the nose of the helicopter, whose tail is visible in Figure 6; behind the photographer, the slope continues down at a more moderate 75% for about 200 m elevation drop. The rather fractured look of the rock rampart in Figure 6 qualitatively suggests the possibility of some high-frequency amplification. This may be the explanation of the 20 Hz content seen in the record of site 2. [Also see Fourier spectra, in Weichert et al. 1986b].

More evidence against unusual site amplification at site 1 comes from a comparison of peak acceleration amplitudes from 66 earthquakes recorded both at site 1 and 2 shows that on the average site 2 recorded almost 30 percent higher accelerations, after correction for epicentral distance. This is decribed in more detail in the next section, and shown in Figure 7.

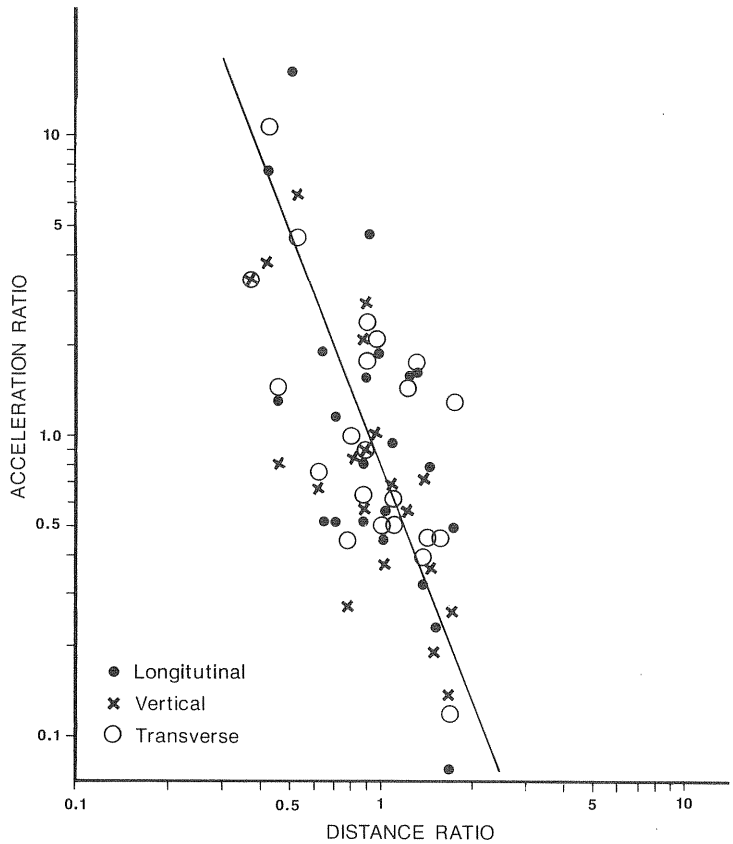

Fig. 7 Plot of peak acceleration ratios versus epicentral distance ratios for 66 earthquake records common to sites 1 and 2. The shown line indicates an $X^{-2.53}$ attenuation.

Near Source Attenuation.

Peak accelerations within a few kilometres of the source depend strongly on site geometry with respect to radiation pattern of subevents responsible for the peaks. However, a statistical estimate of near source attenuation can be obtained from an analysis of the earthquakes that produced common triggers at more than one station. Figure 7 shows the result for 66 events common to site 1 and 2. Plotted are peak acceleration ratios versus epicentral distance ratios (double logarithmic), using the epicenters given by Weichert et al. [1988]. The correlation coefficient is 0.68, so that only about one half of the data scatter is accounted by the distance correlation, but this is sufficient to recognize a negative bias for site 1 of almost 30%. The distance attenuation is $X^{-2.53}$, calculated as the geometric mean of the two least squares regression slopes (1.7 & 3.7). This strong attenuation obviously only applies to the higher frequencies that are usually associated with peak acceleration and generated by rupture of small-scale asperities that are randomly located on the rupture surface. Epicentral distances are only a crude parameterization, but hypocentral distances do not appear any better.

A similarly strong attenuation with exponent 2 to 2.5 is obtained at 10 to 20 Hz from analysis of the response spectra of the 23 December event for site 2 and 3. About 13 more records are now being digitized and may result in statistically improved results; these results and scaled parameters for all 82 earthquake-triggered strong motion records will appear shortly [Weichert et al. 1987]

Origin of Strong Motion.

Special site effects appear to be excluded as causes of the extreme acceleration peaks in the later part of the site 1 record; instead, they must originate from either very shallow asperities, or somehat deeper ones with a radiation pattern that favours site 1 strongly.

The three instruments were triggered by the longitudinal wave (P); the arrival of the transverse shear wave was recorded at all 3 sites and allows triangulation of the point of rupture initiation, i.e. the hypocentre. It appears to lie several km south of the site 1-2 axis at a depth of about 6 km, perhaps slightly closer to site 2. This is consistent with the hypocentre determination from other network data.

The shallow focus and the aftershock distribution indicate that the rupture of this thrust fault propagated down to the west. Thus the rupture would move closer to site 1, although at slightly increasing depths. We already know that the 23 December event ruptured on a shallower fault plane than the 5 October event; it is therefore not unreasonable, that some of the 23 December subevents ruptured even shallower splay faults, thus coming much closer to site 1, as suggested in Figure 8. The 3 or 4 subevents exhibit slightly decreasing S-P intervals, with the last and shortest perhaps 0.5 s, corresponding to about 4 km travel path. The period of the strongest acceleration spike is about 120 ms, which implies an asperity size of about 500 m.

An alternative to the shallow splay fault model would be an orthogonal thrust event, up to the west. This is not consistent with the displacement calculated from the site 1 record, which moved east and north [Weichert et al. 1986a b].

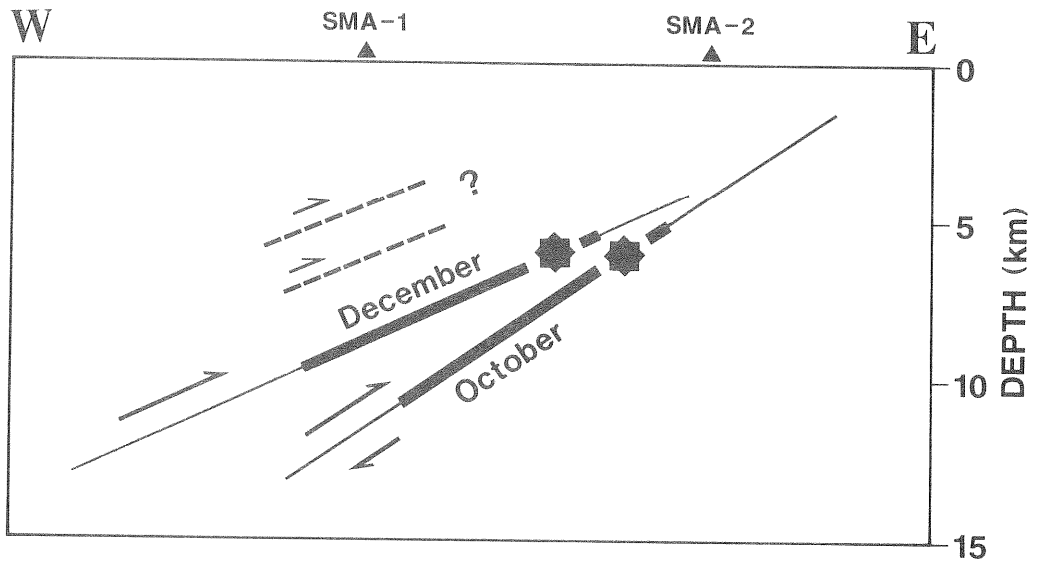

Fig. 8 Schematic relation of the 5 October and 23 December fault planes. Dashed curves with question mark suggest position of short splay fault ruptures that may have been responsible for large accelerations at site 1.

CONCLUSIONS

The Nahanni earthquakes occurred in geological structures and in a contemporary stress field that occurs throughout most of the eastern Cordillera. For conservative seismic hazard evaluation in western Alberta and eastern B.C. similar earthquakes, larger than hitherto observed may have to be considered. Moreover, as these earthquakes occurred in a region where the Cordilleran geologic terrains overlie the Precambrian Shield, they should be considered typical, not only of earthquakes that might occur further south, but of earthquakes that are expected to occur in the active zones of eastern Canada. In particular, estimated epicentral intensities and macroseismic intensity patterns suggest that the large Nahanni earthquakes may have been very similar to the 1925 St. Lawrence earthquake. Such earthquakes must now be expected to produce extreme, short-duration accelerations within about 10 km of the epicentre, but the high-frequency ground motion will attenuate rapidly outside the epicentral zone.

ACKNOWLEDGMENTS

Thanks are due to colleagues in the Geophysics, Hazards and Terrain Sciences Division of the Geological Survey of Canada for reading strong motion films, and for discussions.

REFERENCES

Adams, J., Canadian crustal stress data: a compilation to 1985. Earth Phys. Br. Open-File Rept., 85-31, 81pp., 1985.

Basham, P.W., D.H. Weichert, F.M. Anglin, and M.J. Berry, New probabilistic strong seismic ground motion maps of Canada: a compilation of earthquake source zones, methods and results. Earth Phys. Br. Open-File Rpt., 82-33, 205 pp., 1982.

Drysdale, J.A. and R.B. Horner, Canadian earthquakes 1983. Seis. Series Earth Phys. Branch, Dept. Energy, Mines & Resources, no. 93, 56pp., 1986.

Horner, R.B., R.J. Wetmiller, M. Lamontagne and M. Plouffe, Aftershock studies of the Nahanni earthquakes. In preparation., 1988.

Keefer, D.K., Landslides caused by earthquakes. Geol. Soc. Am. Bull., 95, 406-421, 1984.

Leblanc, G. and R.J. Wetmiller, An evaluation of seismological data available for the Yukon Territory and Mackenzie Valley. Can. Journ. Earth Scienc., 11,1435-1454, 1974.

Rogers, G.C., Ellis, R.M., and Hasegawa, H.S., The McNaughton Lake earthquake of May 14, 1978. BSSA, 70,1771-1786, 1980.

Smith, W.E.T., Basic seismology and seismicity of eastern Canada. Seism. Series of the Dom Obs. 1966-2, Ottawa, 1967.

Topozada, T.R., Earthquake magnitude as a function of intensity data in California and Western Nevada. BSSA, 65,1223-1238, 1975.

Weichert, D.H., R.J. Wetmiller and P. Munro, Vertical earthquake acceleration exceeding 2g? The case of the missing peak. BSSA, 76:1473-1478, 1986a.

Weichert, D.H., R.J. Wetmiller, Horner, R.B., Munro, P.S., and Mork, P.N., Strong motion records from the 23 December 1985, M_s6.9 Nahanni, Nwt, and some associated earthquakes. Geol. Surv. Canada, Open-File Rep. 1330, 1986b.

Weichert, D.H., R.J. Wetmiller, R.B. Horner, P.S. Munro, R.G. Lamontagne, Collection of strong motion records from the Nahanni earthquake sequence. Geol. Surv. Canada, Open-File Rep., 1988.

Wetmiller, R.J., Drysdale, J.A., Horner, R.B. and Lamontagne, R. Canadian earthquakes 1985/1986. GSC publication, in preparation, 1988.

Wetmiller, R.J., Horner, R.B., Hasegawa, H.S., North, R.G. Lamontagne, M., Weichert, D.H. & S.G. Evans, in press. An analysis of the 1985 Nahanni earthquakes. BSSA,1987.

SOURCE SCALING RELATIONS OF LARGE EASTERN NORTH AMERICAN EARTHQUAKES AND IMPLICATIONS FOR STRONG GROUND MOTIONS

Paul Somerville
Woodward-Clyde Consultants
566 El Dorado Street
Pasadena, CA 91101

ABSTRACT

Two important issues concerning the source scaling of earthquakes in eastern North America have been investigated. First, the source characteristics of earthquakes in eastern North America and other continental interiors are found to be consistent with constant stress drop scaling, and inconsistent with non-constant scaling models such as that of Nuttli [1983]. Second, the stress drops of earthquakes in eastern North America and other continental interiors are not significantly different from those of earthquakes in western North America, and have median values of approximately one hundred bars. This suggests that those aspects of strong ground motion amplitudes that are attributable to the earthquake source may also not be significantly different between eastern and western North America. However, differences in ground motion amplitudes may arise from differences in crustal structure, scattering, anelasticity, and local site effects between eastern and western North America.

INTRODUCTION

The use of synthetic seismograms to simulate strong ground motions is becoming an increasingly important approach to the evaluation of ground motions for seismic design (Boore and Atkinson [1987], Burger and others [1987], Barker and others [1987]). This approach is especially pertinent in regions such as eastern North America where earthquakes are relatively infrequent and strong ground motion recordings are correspondingly sparse. The simulation methods entail the use of a source model to specify the level of high frequency radiation from the source in relation to its seismic moment. This may be done for a given seismic moment by specifying the source duration (or equivalently, the spectral corner period), which then determines the stress drop. At present there are two principal uncertainties in the description of source characteristics required for the use of these methods in eastern North America. These uncertainties relate to whether earthquakes in eastern North America follow a constant or non-constant stress drop scaling relation, and whether their average stress drops are similar to or higher than those of earthquakes in other regions such as western North America. Unresolved, these issues give rise to uncertainty in the estimation of strong ground motion characteristics using simulation methods. It is therefore important to construct a well-constrained source scaling relation for earthquakes in eastern North America, and compare it to the scaling relation for earthquakes in western North America.

SCALING RELATIONS

Scaling relations were constructed from the source parameters of earthquakes from eastern North America, other continental interiors, and western North America. The other continental interior events were used to provide constraints on source scaling for the larger magnitudes which are sparse in eastern North America. The seismic moments and source durations used in constructing the scaling relationships were estimated from the time-domain modeling of body waves (Somerville [1986], Ebel and others [1986], Somerville and others [1987]). The parameters of the eastern North American events are given in Table I.

The source scaling relation for each regional category is given by a linear relation between the logarithm of seismic moment and the logarithm of source duration. Plots of seismic moment against source duration for eastern North America and western North America are shown in Figs. 1 and 2 respectively. The error estimates for each measurement are shown in order to indicate the weights given to each point in the least-squares fit. Also shown are scaling relations showing the best fit line, lines of one standard deviation in slope, and lines of slope 3 (corresponding to constant stress drop) and 4 (corresponding to Nuttli's [1983] scaling relation). The scaling relations obtained using the least-squares fitting method of York [1966] are summarized in Table II. The uncertainty in slope is represented by its standard deviation about the mean.

Comparison of Slopes of Scaling Relations

The slopes of the scaling relations for the different regions are summarized in Table II and Figure 3. The slopes of the scaling relations for eastern North America, other continental interiors, and these two sets combined are consistent with a slope of 3 and inconsistent with a slope of 4. This indicates that the source characteristics of eastern North American earthquakes are consistent with constant stress drop scaling, and inconsistent with the non-constant stress drop scaling proposed by Nuttli [1983]. The slope of the scaling relation for western North America was found to be 2.6, which is somewhat inconsistent with the value of 3 but very inconsistent with the value of 4. This indicates that the source characteristics of western North American earthquakes are somewhat inconsistent with constant stress drop scaling.

Comparison of Stress Drop

The source characteristics of earthquakes in the three regions are most conveniently compared using stress drop as a means of describing the relation of seismic moment to source duration. Uncertainties in the estimation and interpretation of stress drop include limitations in the model used to calculate stress drop, uncertainties in the seismic moment and source duration values used in the calculation, and ambiguities in the definition of stress drop of events having complex ruptures. In order to facilitate the comparison of stress drops, it is simplest to assume constant stress drop so that each population can be represented by a single average stress drop value. As we have seen, the scaling relations for eastern North America, other continental

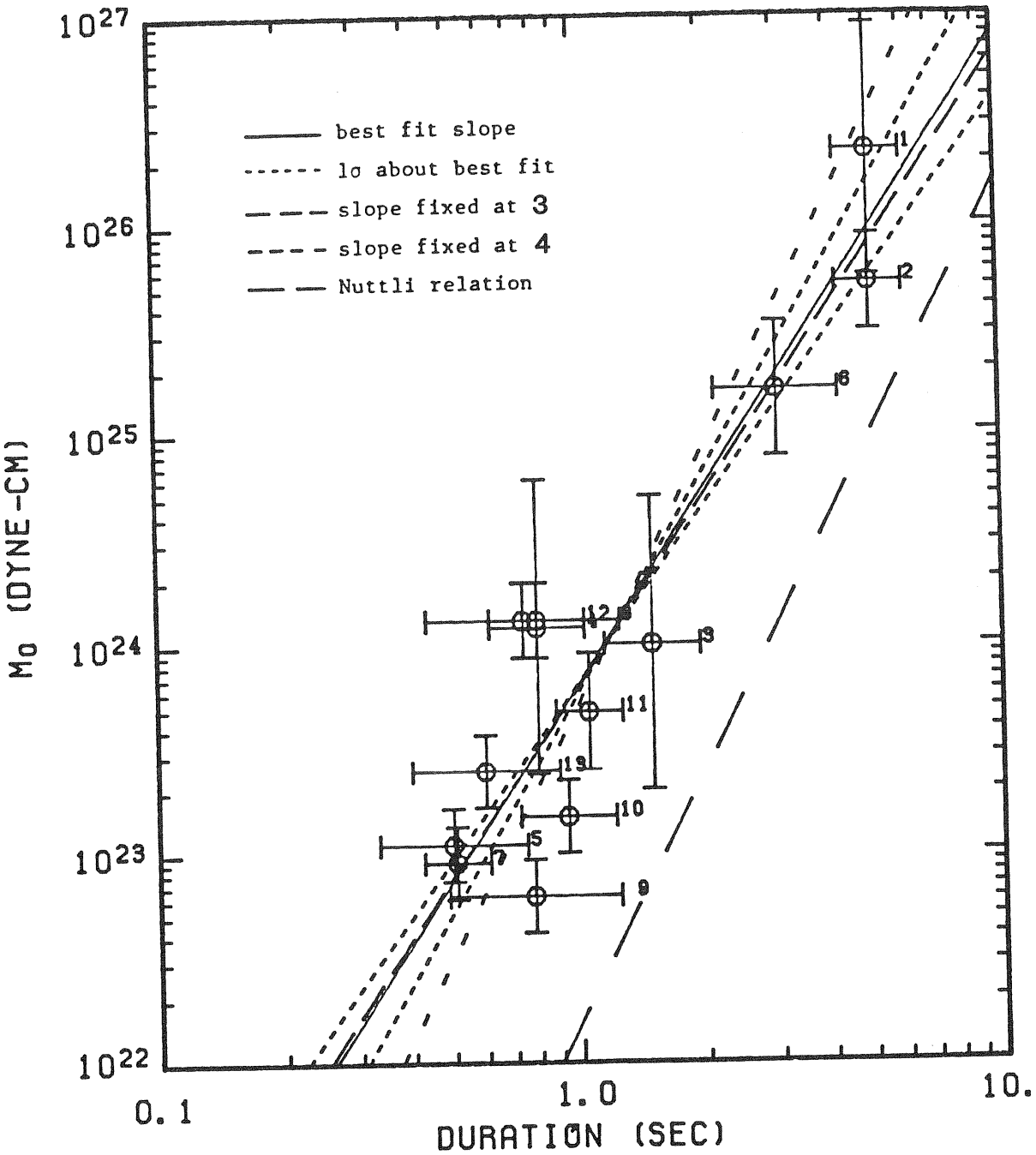

Figure 1. Source scaling relations for eastern North America. The median values and standard deviation factors of seismic moment and source duration are given in Table 1, and the scaling relations are given in Table 2.

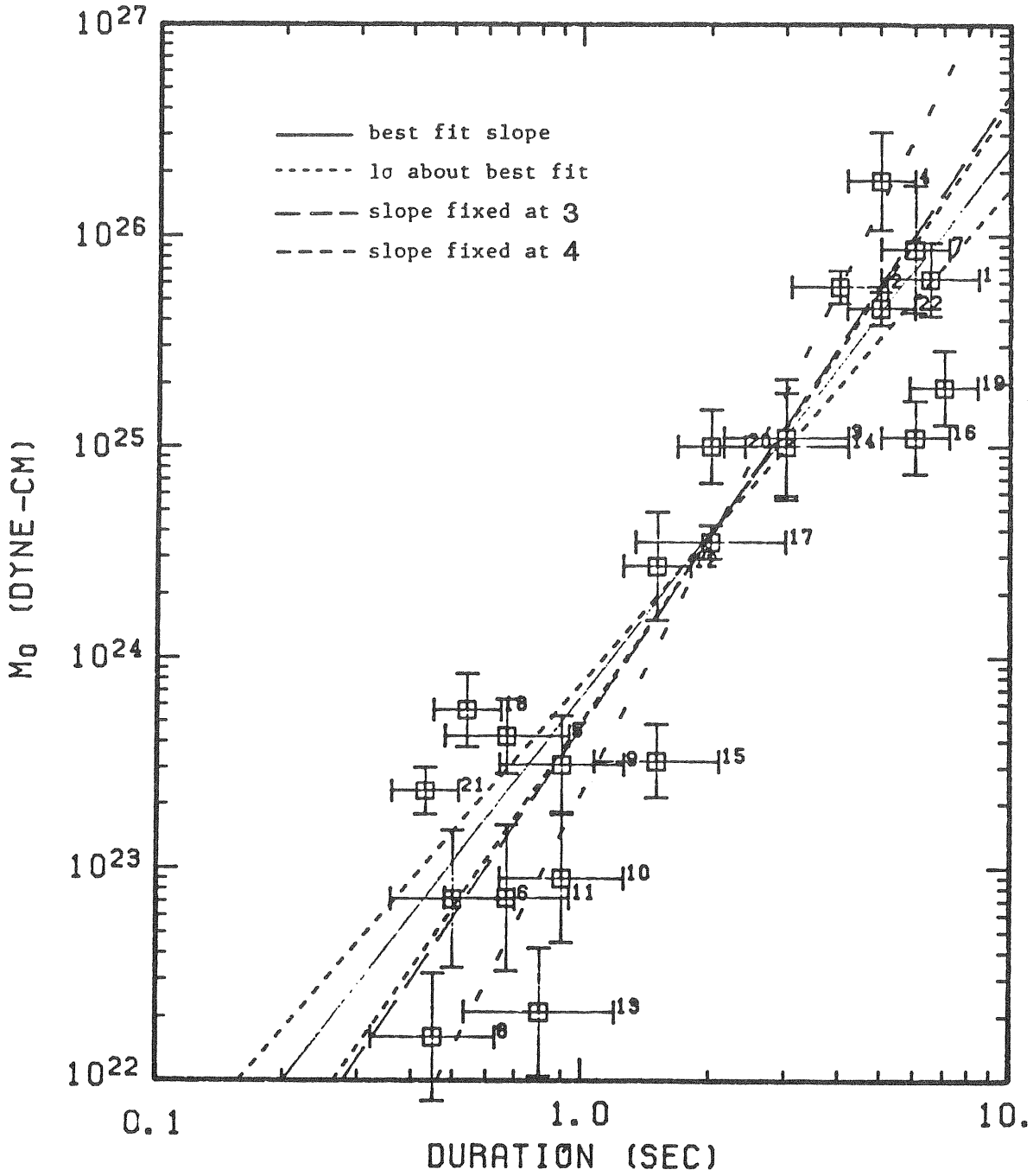

Figure 2. Source scaling relations for western North America. The scaling relations are given in Table 2.

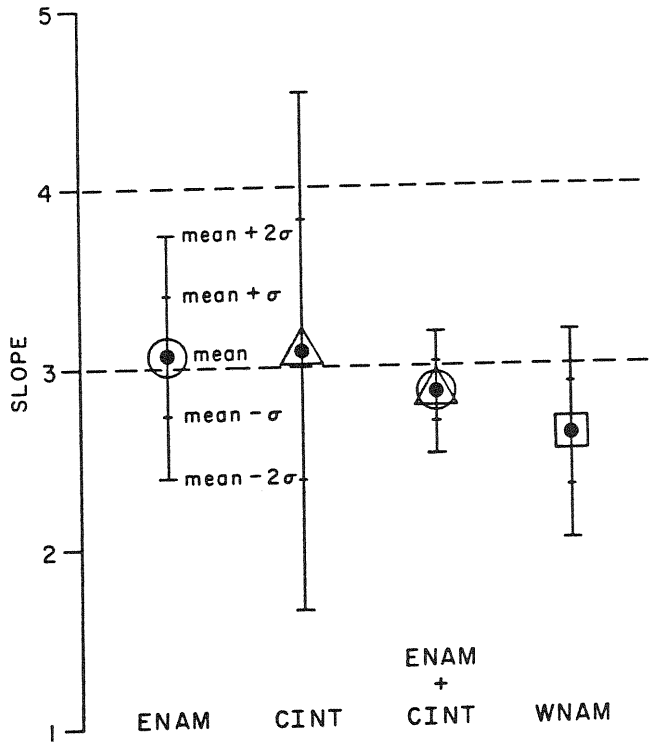

Figure 3. Means and standard deviations of slopes of the scaling relations

ENAM: eastern North America
CINT: other continental interiors
WNAM: western North America

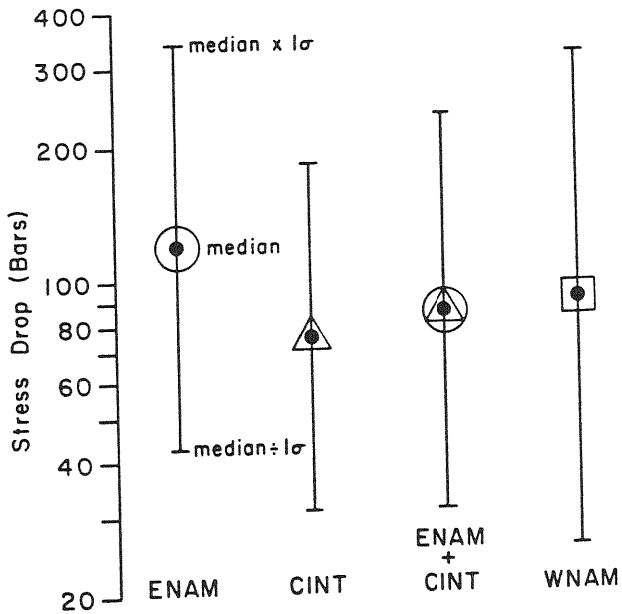

Figure 4. Median values and standard deviation factors of stress drops assuming constant stress drop scaling

ENAM: eastern North America
CINT: other continental interiors
WNAM: western North America

TABLE I

SEISMIC MOMENTS, SOURCE DURATIONS, DEPTHS, AND Lg MAGNITUDES
EASTERN NORTH AMERICAN EARTHQUAKES

No	Region	Date	Depth	m_{Lg}	Mo	U	DUR	U
1	Charlevoix	1925/ 3/ 1	10.0	7.0	0.22E+27	4.0	5.0	1.2
2	Timiskaming	1935/11/ 1	10.0	6.3	0.51E+26	1.7	5.0	1.2
3	Charlevoix	1939/10/19	8.0	5.6	0.10E+25	5.0	1.5	1.3
4	Ossippee	1940/12/20	10.0	5.7	0.12E+25	5.0	0.8	1.3
5	Missouri	1963/ 3/ 3	15.0	4.7	0.11E+24	1.5	0.5	1.5
6	Baffin Bay	1963/ 9/ 4	7.0	-	0.16E+26	2.1	3.0	1.4
7	Missouri	1965/10/21	4.0	4.8	0.90E+23	1.5	0.5	1.2
8	Illinois	1968/11/ 9	25.0	5.5	0.13E+25	1.5	0.7	1.7
9	Maine	1973/ 6/15	6.0	5.0	0.62E+23	1.5	0.8	1.6
10	Quebec	1979/ 8/19	6.5	5.0	0.15E+24	1.5	0.9	1.3
11	Kentucky	1980/ 7/27	13.5	5.2	0.48E+24	1.9	1.1	1.2
12	New Brunswick	1982/ 1/ 9	7.0	5.8	0.13E+25	1.5	0.8	1.3
13	New York	1983/10/ 7	7.0	5.2	0.25E+24	1.5	0.6	1.5

Mo: Seismic Moment in dyne.ent in
DUR: Source Duration in secoion in
U: Standard deviation factprecedinor of g value

TABLE II

SCALING RELATIONS

$$\text{Log}_{10}(\text{Moment}) = \text{Intercept} + \text{Slope} \times \text{Log}_{10}(\text{Duration})$$

Region	Intercept	Slope*	Slope St.Dev.	Degrees of Freedom	Sums**	Stress Drop
ENAM	23.81	3.09	0.34	11	8.7	
	23.80	3				120
CINT	23.53	3.09	0.72	9	16.2	
	23.61	3				75
ENAM & CINT	23.77	2.85	0.17	22	25.8	
	23.66	3				85
WNAM	23.80	2.60	0.29	20	48.8	
	23.67	3				90
ENAM, CINT (Nuttli, 1983)	22.20	4		11	109.4	

* upper values: slope unconstrained
lower values: slope constrained to 3 (constant stress drop)

** weighted sum of squares of residuals

ENAM: Eastern North America
CINT: Other Continental Interiors
WNAM: Western North America

interiors, and the combination of these two sets are consistent with constant stress drop, whereas the western North American events are somewhat inconsistent with this assumption.

The mean and standard deviations of the stress drops of the three populations are listed in Table II and illustrated in Figure 4. The eastern, western and other continental interior events have median stress drops of 120, 90 and 75 bars, respectively. The differences between these median values are not statistically significant, and all are consistent with a median stress drop of one hundred bars.

Comparison of Source Characteristics

The focal depths of large earthquakes in eastern North America, estimated within an accuracy of a few kilometers using depth phases, are confined to the upper crust as in western North America. The source functions of these events as observed teleseismically (Ebel and others [1986]) also show a range of complexity that is comparable to that of western North American earthquakes. However, subtle differences may exist in the variability of source parameters in each population. Comparing the number of degrees of freedom with the weighted sum of squares of residuals in Table II, it appears that individual events in western North America show significant departures from a single source scaling relation, while for eastern North America and other continental interiors, individual events are consistent with a single relation.

The uniformity in source properties of eastern events may be explained by the model of Kanamori and Allen [1986] which relates static stress drop to average repeat time. Although their data set does not contain any eastern North American earthquakes, they suggest that earthquakes in eastern North America have very long repeat times, and expect their stress drops to be high. According to this model, the relative uniformity in stress drops of eastern events may be due to their uniformity in repeat time.

Kanamori and Allen [1986] demonstrated that the static stress drops of western North American events span a wide range and that they show a tendency to increase with earthquake repeat time in accordance with their model. This wide variation in repeat times may be responsible for the wide range in stress drops of western events used in the present study. This variability indicates that it is inappropriate to group western events into a single category for the purpose of evaluating source characteristics.

These considerations notwithstanding, western events are commonly grouped together for the purpose of evaluating strong ground motion characteristics. This practice has been justified because the differences in ground motion between different kinds of events have not been clearly established, although they may exist. The combination of western events in this study rests on a similar justification. When this is done, the median stress drop of the western events is found to be not significantly different from that of the eastern events. While it may be true, as Kanamori and Allen [1986] state, that a factor of 5 difference in average stress drop is commonly seen between earthquakes with short and long repeat times, this difference is not observed between the median values for western and eastern North American earthquakes.

The principal differences in the source properties of eastern and western North American earthquakes are the greater variability of the source characteristics of the western events, and the tendency of their stress drops to decrease slightly with seismic moment. These differences may be interpreted by means of a model in which the largest stress drops in each region are controlled by the maximum shear strength of fault zones. The maximum strength is realized when the whole rupture surface is a large asperity, or contains a dense distribution of asperities. These conditions appear to be independent of earthquake size in eastern North America, giving rise to relatively uniform source characteristics and constant stress drop scaling. However, as earthquake size increases in western North America, the proportion of the rupture surface that consists of asperities decreases on some faults, causing a corresponding decrease in stress drop. This gives rise to a scaling relation in which stress drop decreases slightly with earthquake size, and to a great degree of variability in the source characteristics of earthquakes in western North America.

IMPLICATIONS FOR STRONG GROUND MOTION ESTIMATION

Detailed analysis of the uncertainties in the scaling relations has allowed two important issues concerning the source scaling of earthquakes in eastern North America to be addressed. First, the source characteristics of large earthquakes in eastern North America and other continental interiors are consistent with constant stress drop scaling, and are inconsistent with non-constant scaling models such as that of Nuttli [1983]. Second, the stress drops of large earthquakes in eastern North America and other continental interiors are not significantly different from those of earthquakes in western North America, and have median values of approximately one hundred bars. This result is constrained by seismograms whose frequency content does not extend very far above the corner frequency. Projection of this result to the higher frequencies of engineering interest using simple spectral models suggests that those aspects of strong ground motion amplitudes that are attributable to the earthquake source may also not be significantly different between eastern and western North America.

However, differences in ground motion amplitudes are expected to arise from differences in crustal structure, scattering, anelastic absorption, and characteristic site conditions between eastern and western North America. The influence of crustal structure, focal depth and other parameters on ground motion attenuation in eastern North America has been demonstrated by Barker and others [1987].

The seismic moment estimates of eastern North American earthquakes given in Table I can be used to construct an empirical relationship between seismic moment and Lg magnitude. The table contains twelve earthquakes whose seismic moments span the range from 6×10^{22} to 2×10^{26} dyne-cm and the m_{Lg} range from 4.7 to 7.0. Using the standard deviation factors of seismic moment given in Table I and a standard deviation of 0.3 for m_{Lg}, the least-squares procedure of York [1966] yields the relation:

$$m_{Lg} = 0.59 \log M_o - 8.6$$

This relation, shown in Figure 5, allows earthquake size in the eastern North American catalog to be quantified in terms of seismic moment, thereby facilitating the use of simulation methods for ground motion estimation in seismic hazard studies.

ACKNOWLEDGMENTS

Jim McLaren, Vicki LeFevre, Roy Burger and Don Helmberger participated in the determination of source parameters used in this study, and Ram Kulkarni provided guidance in the statistical analyses. This work is part of a program being conducted by the Electric Power Research Institute to develop seismic wave attenuation functions for the eastern United States, and was performed under the direction of Dr. J. Carl Stepp.

REFERENCES

Nuttli, O. W., "Average seismic source-parameter relations for mid-plate earthquakes," Bull. Seism. Soc. Am., 73, 519-535, 1983.

Boore, D. M. and G. M. Atkinson, "Stochastic prediction of ground motion and spectral response parameters at hard-rock sites in eastern North America," Bull. Seism. Soc. Am., 77, 440-467, 1987.

Burger, R. W., P. G. Somerville, J. S. Barker, R. B. Herrmann and D. V. Helmberger, "The effect of crustal structure on strong ground motion attenuation relations in eastern North America," Bull. Seism. Soc. Am., 77, 420-439, 1987.

Barker, J. S., P. G. Somerville and J. P. McLaren, "Wave propagation modeling of ground-motion attenuation in the northeastern United States and adjacent Canada", Report submitted to the Electric Power Research Institute, May 1987.

Somerville, P. G., "Source scaling relations of eastern North American earthquakes", Electric Power Research Institute, Palo Alto, California, 94303, NP-4789, September 1986.

Ebel, J. E., P. G. Somerville and J. D. McIver, "A study of the source parameters of some large earthquakes in eastern North America, J. Geophys. Res., 91, 8231-8247, 1986.

Somerville, P. G., J. P. McLaren, L. V. LeFevre, R. W. Burger, and D. V. Helmberger, "Comparison of source scaling relations of eastern and western North American earthquakes," Bull. Seism. Soc. Am., 77, 322-346, 1987.

York, D., "Least squares fitting of a straight line," Can. J. Phys., Vol. 44, 1079-1086, 1966.

Kanamori, H. and C. R. Allen, "Earthquake repeat time and average stress drop," in Earthquake Source Mechanics, Geophysical Monograph 37, (Maurice Ewing Series 6), American Geophysical Union, Washington, D. C., 227-235, 1986.

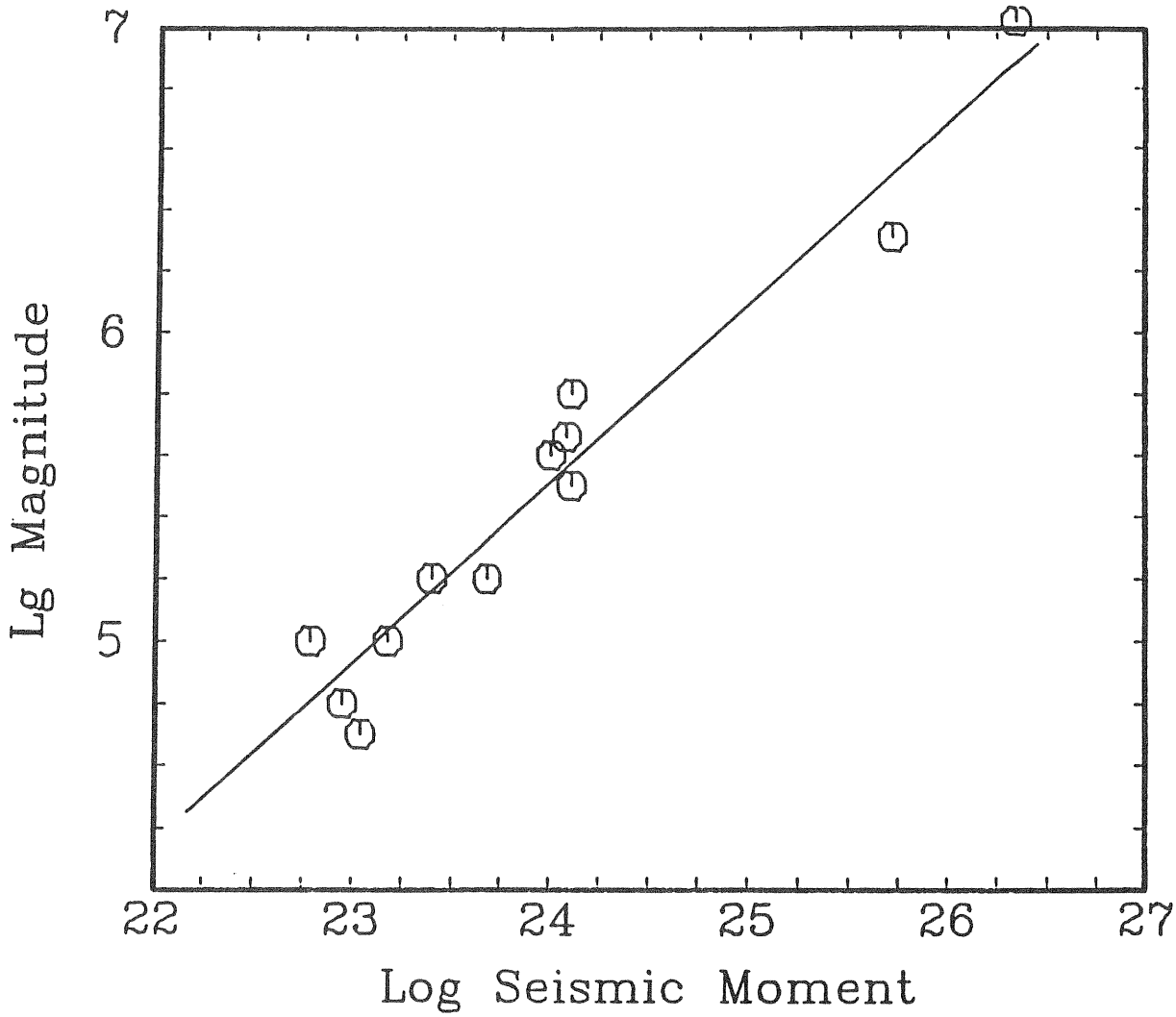

Figure 5. Independently determined values of seismic moment and m_{Lg} for twelve eastern North American earthquakes listed in Table 1. The least-squares linear fit to the data is given by the equation $m_{Lg} = 0.59 \log M_o - 8.6$.

MODELING GROUND-MOTION ATTENUATION IN EASTERN NORTH AMERICA

Jeffrey S. Barker
Department of Geological Sciences
State University of New York, Binghamton

Paul G. Somerville and James P. McLaren
Woodward-Clyde Consultants, Pasadena

A critical element in the estimation of seismic hazard in eastern North America is the accurate characterization of ground-motion attenuation. The empirical data set is extremely sparse in this region, particularly within 200 km of the source. Typical approaches to estimating ground-motion attenuation include scaling and combining these empirical data and solving for the best fitting one- or two-segment monotonically decreasing function of horizontal range. In this study, we utilize semi-empirical synthetic seismogram techniques in order to model the ground-motion attenuation for seven earthquakes in eastern North America. We find that along specific azimuths from a particular event, the ground motions result from the interference of upgoing, diving and post-critically reflected crustal S waves. The resulting attenuation curves contain far more detail than one or two simple, linear trends. Combining data from different azimuths, or from events at different depths or in different crustal structures, tends to obscure the details of attenuation.

The data modeled were digitally recorded on the Eastern Canada Telemetered Network (ECTN) from earthquakes in the northeastern United States and adjacent Canada (Figure 1). For this paper, we will concentrate on the 1983 Ottawa earthquake and one of the aftershocks of the 1982 New Brunswick earthquake. Information on other events modeled, as well as further details and illustrations may be found in Barker, et al. (1987).

GRENVILLE CRUSTAL VELOCITY STRUCTURE

As shown in Figure 2, the 1983 Ottawa earthquake was well recorded on the ECTN. This figure displays a profile of the observed vertical velocity waveforms within 1000 km recorded on the ECTN. For ranges greater than about 200 km, the peak ground motion is due to the dispersed L_g wavetrain defined by a group velocity window centered about 3.5 km/s. Ground motions within 200 km are due to the more impulsive crustal S-wave phases.

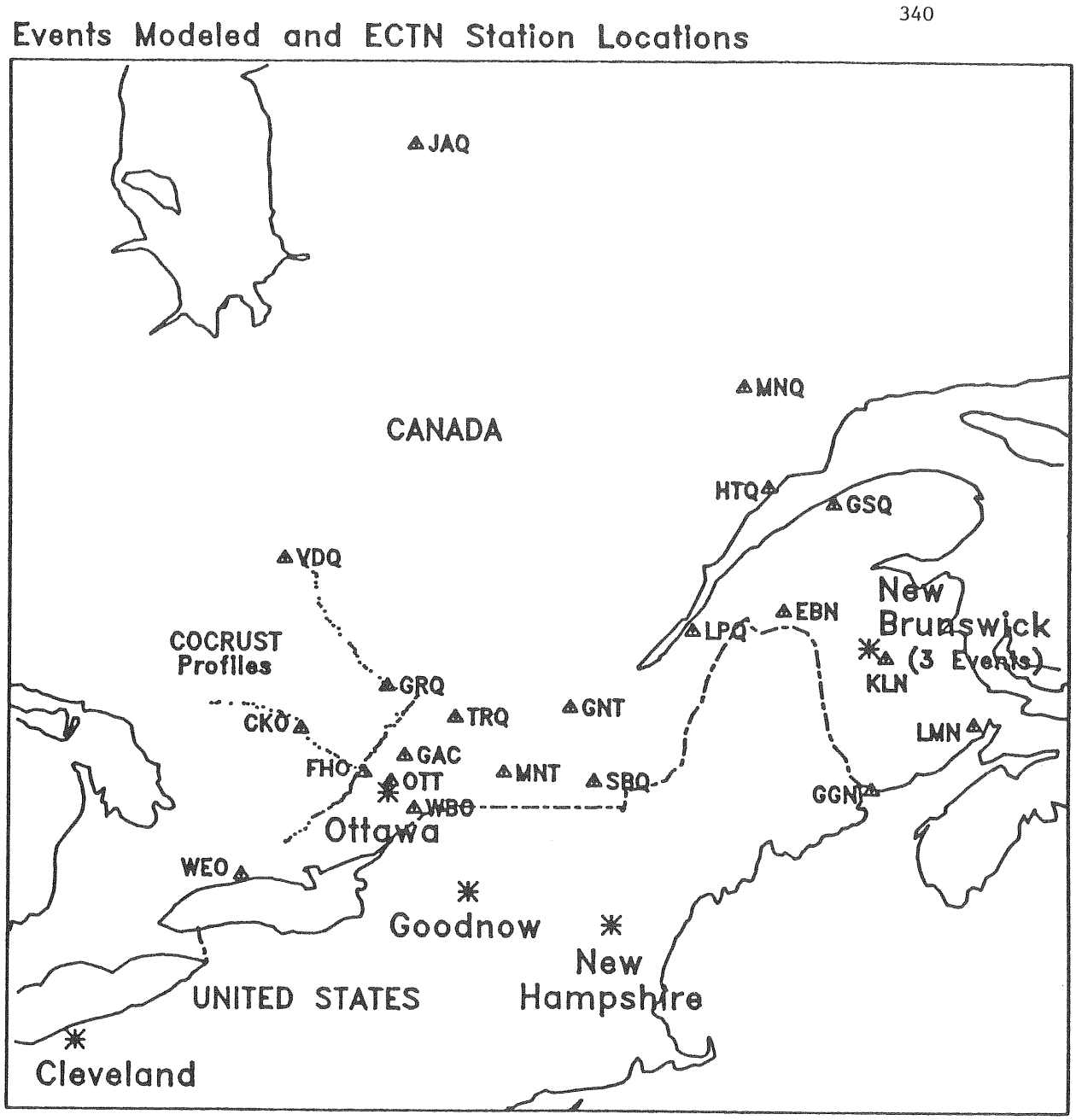

Figure 1. Map of the northeastern United States and adjacent Canada showing the seven earthquakes modeled in this study and the locations of the Eastern Canada Telemetered Network (ECTN) stations. Also shown as dotted lines northwest of Ottawa are the lines recorded during the COCRUST refraction survey.

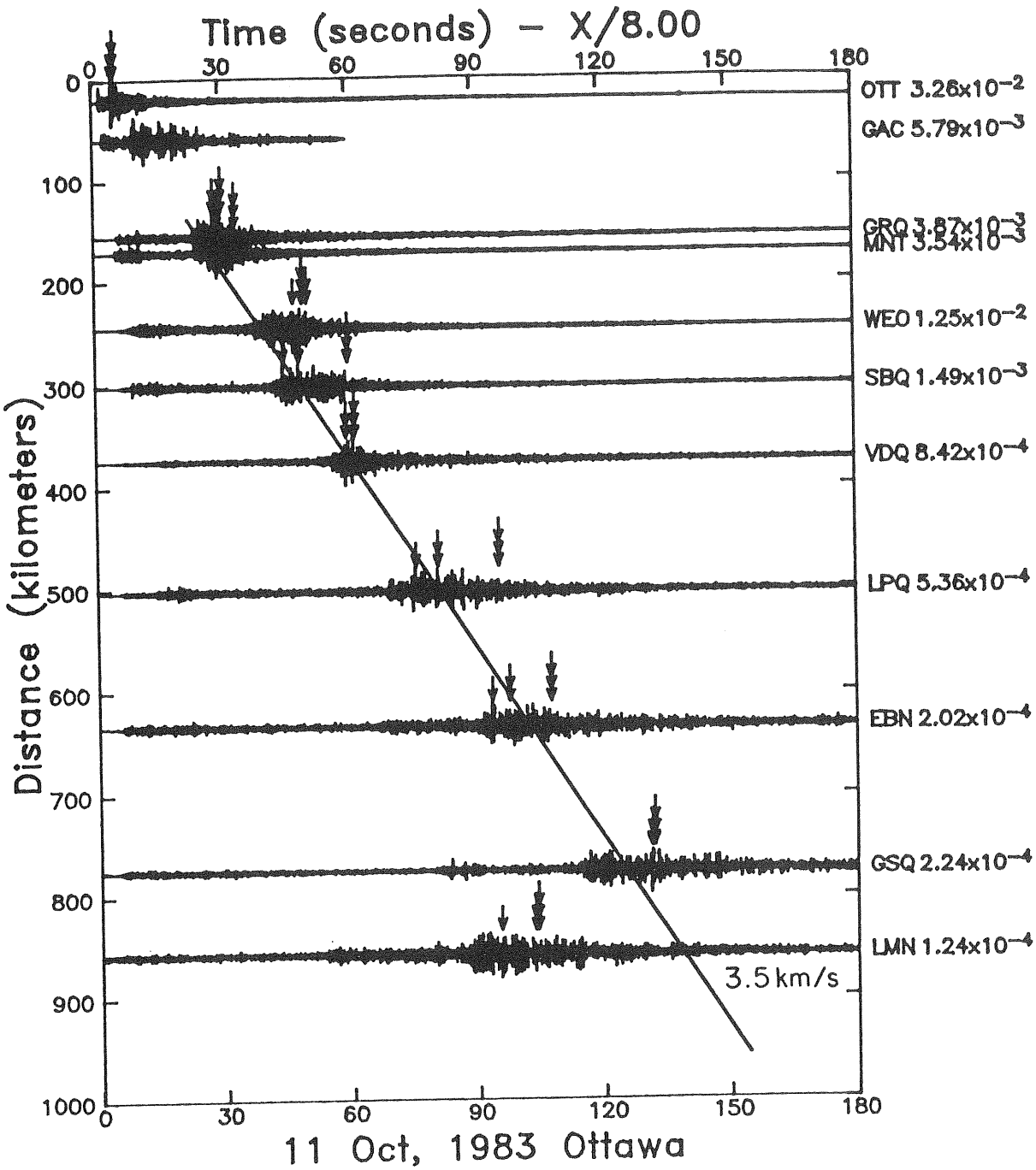

Figure 2. Observed vertical velocity records of the 1983 Ottawa earthquake recorded within 1000 km on the ECTN. The times of occurance of the peak velocity, acceleration and 5 Hz pseudo-relative velocity are shown as single-, double- and triple-headed arrows, respectively. Also shown is a line indicating the L_g group velocity of 3.5 km/s.

The detailed crustal velocity structure near Ottawa was obtained by modeling P and S waves from a nearby crustal refraction survey (Mereu, et al., 1986). The locations of the refraction lines are shown as dotted lines northwest of Ottawa in Figure 1. The resulting crustal velocity structure model appropriate for the Grenville province near Ottawa is shown in Figure 3. It consists of a smooth crustal gradient and a total crustal thickness of 39.4 km.

On the left side of Figure 4 is a profile of the vertical velocity records from ECTN stations within 200 km of the 1983 Ottawa earthquake plotted with an S-wave reduction velocity. Superimposed are the travel-times for a source at 15.5 km in the Grenville velocity structure model. The right side of Figure 4 includes a profile of semi-empirical synthetic seismograms computed using generalized ray theory including the upgoing, direct S ray and diving rays that turn at each of the layer interfaces beneath the source. The response was computed along a line N45°E from the source using the mechanism of Wahlstrom (1986). This was convolved with an empirical source function obtained by windowing and scaling the OTT record (at 20 km) to produce the seismograms shown. Comparing the two profiles, we see that although the observed data were recorded at a variety of azimuths, the arrival times and relative amplitudes of the S waves are well modeled. With the exception of unmodeled scattering and the development of L_g, which elongate the wavetrains recorded beyond 100 km, the character of the observed records is adequately described by the synthetic seismograms.

One of the benefits of waveform modeling with generalized ray theory is the ability to decompose the synthetic seismograms to obtain the responses for specific ray sets. Figure 5 includes such a decomposition, in which for a number of ranges, the top trace is due to the upgoing, direct S wave (S_{up}), the second trace is due to diving S waves that turn within the crustal gradient (S_{div}), the third trace includes the reflection from the Moho and rays that turn in the upper mantle (S_MS), and the bottom trace is the total synthetic seismogram. At 20 km, the response is due entirely to S_{up}. At 80 km, S_{div} constructively interferes with S_{up}, and S_MS is beginning to appear as a late arrival. By 100 km, S_{div} destructively interferes with S_{up}, S_MS has reached its critical angle and is of comparable amplitude to S_{up}. At 120 km, S_{up} is now smaller in amplitude than S_{div}, but the peak amplitude is now due to S_MS. From 160 km to 200 km, S_MS continues to account for the peak amplitude, but approaches S_{div} in time. The Moho head wave (S_n) may be seen as the first arrival at 200 km. Clearly with range, the predicted peak ground-motion amplitude results from the interaction and interference of different S-wave phases, each of which sample different features of the crustal velocity structure.

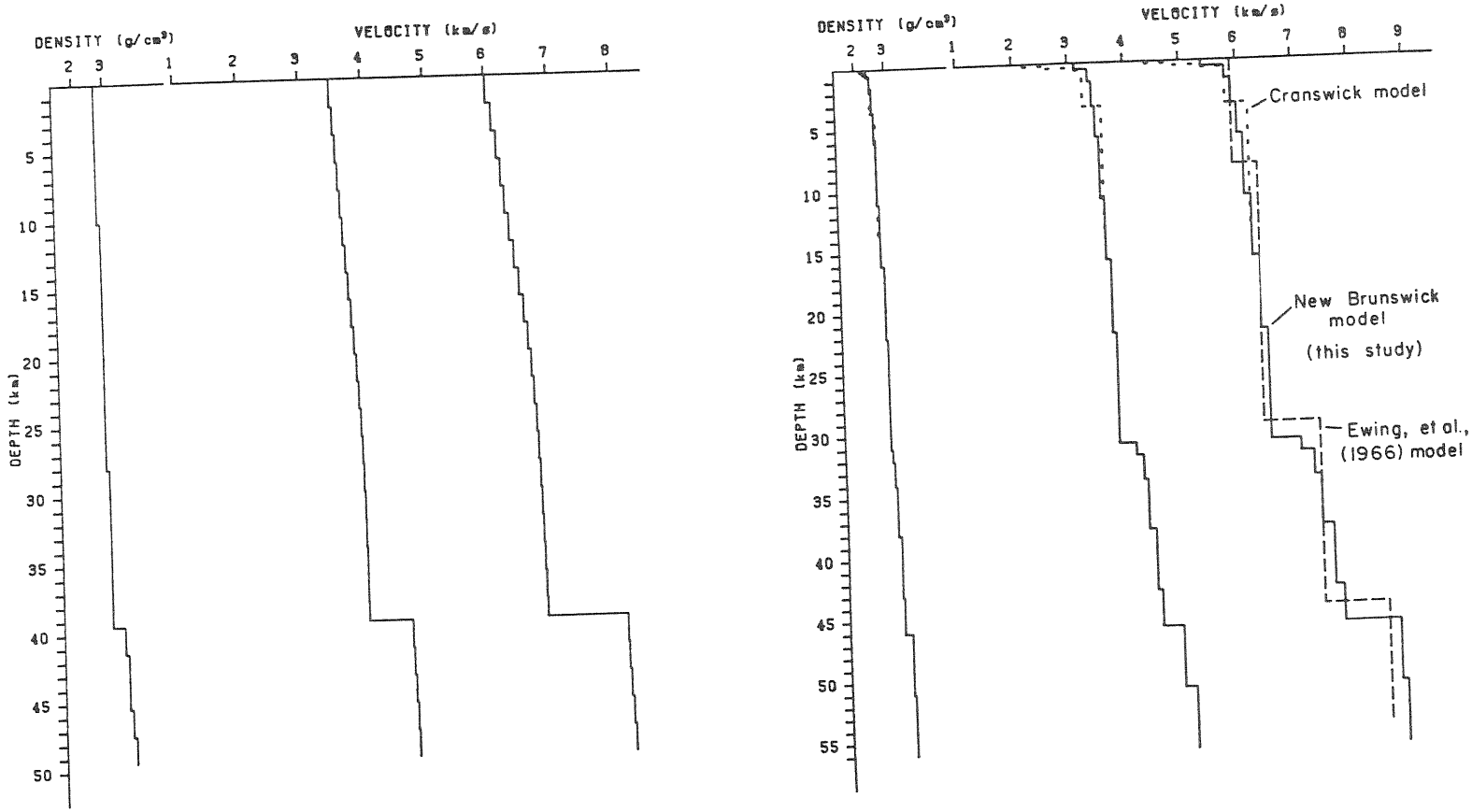

Figure 3. Crustal velocity structure models determined for the Grenville province near Ottawa (left) and for the Appalachian province near Miramichi, New Brunswick (right).

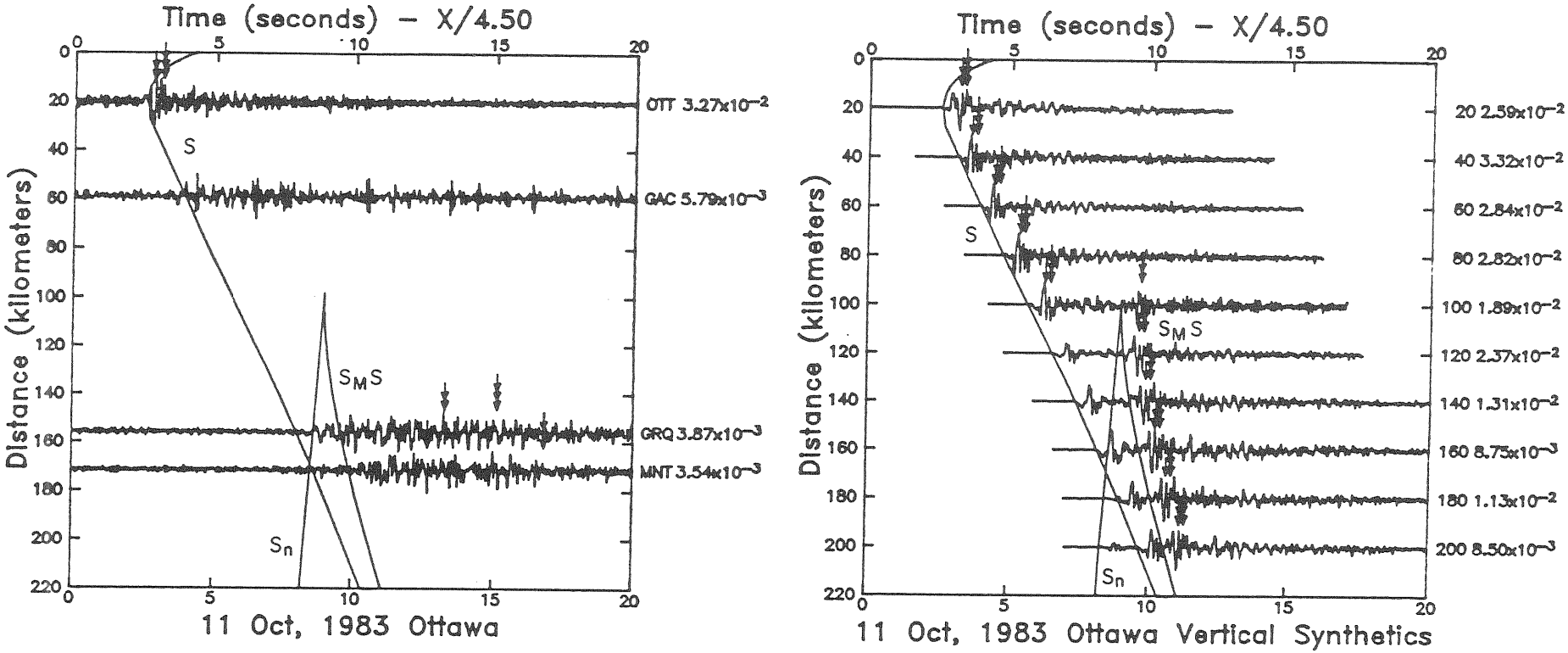

Figure 4 (left). Vertical velocity recordings from ECTN stations within 200 km of the 1983 Ottawa earthquake. Superimposed are the S-wave travel-time curves for a source at 15.5 km depth in the Grenville velocity structure model. (right) Semi-empirical, synthetic vertical velocity seismograms for a profile running N45°E from the Ottawa earthquake.

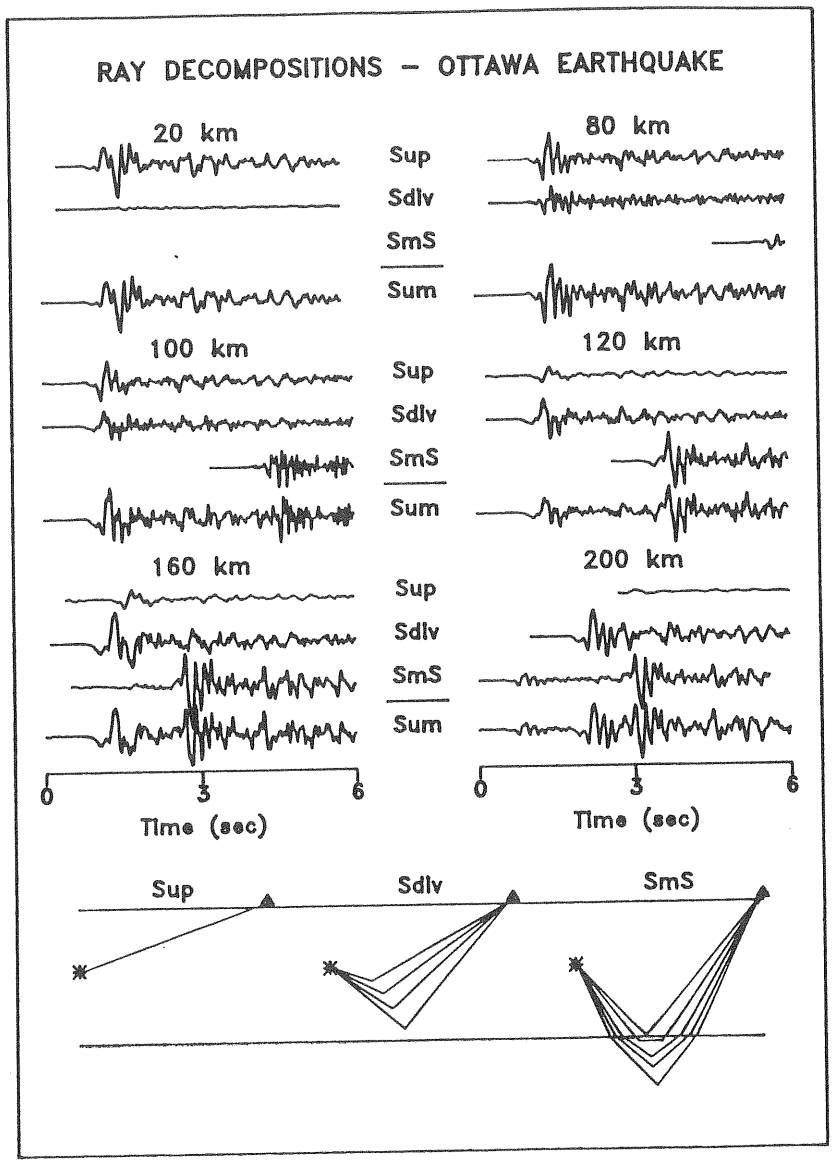

Figure 5. Ray decompositions of the semi-empirical synthetic seismograms for the Ottawa earthquake. For each range, the top trace includes only the upgoing, direct S wave (S_{up}), the second trace includes diving S waves that turn within the crustal gradient (S_{div}), the third trace includes the S wave that reflects from the Moho and rays that turn within the mantle (S_MS), and the bottom trace is the total synthetic seismogram.

The left side of Figure 6 shows a comparison of the observed and synthetic peak vertical velocity measured in the time domain as a function of epicentral range for the Ottawa earthquake. Observed ground motions are plotted as open symbols, while synthetic ground motions are plotted as closed symbols. Beyond about 200 km, the peak observed ground motions are due to L_g, while our synthetics include only crustal S waves. At a range of about 200 km, we expect crustal body waves and Lg waves in the observed data to have comparable amplitudes. Although computed along a single azimuth, the synthetic peak values appear to adequately interpolate the observed values between 20 and 200 km. Also indicated as dashed lines are the peak synthetic velocities obtained when only the upgoing S, diving S, or S_MS rays are included. The level of the upgoing S amplitude is almost constant due both to the source depth and to the rotation of the S-wave such that an increasing amount of the S energy appears on the vertical component as the incidence angle becomes more horizontal. The diving S wave becomes important beyond about 60 km, but arrives simultaneously with the upgoing S causing complicated interference phenomena. Between 100 and 120 km, the Moho-reflected S wave becomes post-critical and accounts for the largest ground motion to beyond 200 km.

APPALACHIAN CRUSTAL VELOCITY STRUCTURE

The structure model developed for the Appalachian province is also shown in Figure 3. It was obtained by fitting simultaneously the arrival times of P and S waves from three principal aftershocks of the 1982 Miramichi, New Brunswick earthquake recorded on the ECTN. The resulting model has a mid-crustal discontinuity and a total crustal thickness of 46 km. Semi-empirical synthetic seismograms were computed for the March 31, 1982 aftershock using generalized ray theory for the source mechanism of Nabelek (1985) at a depth of 3.5 km. An empirical source function was obtained by windowing the vertical S wave from a strong-motion recording 7.2 km from the source, integrating to velocity and correcting to the ECTN instrument response. The resulting synthetic profile along a N60°W azimuth is compared with ECTN recordings within 300 km in Figure 7. Once again, we see that the timing and relative amplitudes of the S-wave phases within 200 km are well modeled. Beyond 200 km, when arrivals can be interpreted from within the P coda, the arrival times are well matched, but the relative amplitudes suggest that the gradient beneath the mid-crustal discontinuity may be slightly too strong. Overall, with the understanding that scattering and the onset of L_g beyond 200 km are not modeled, the character of the observed waveforms has been adequately modeled by the semi-empirical synthetics.

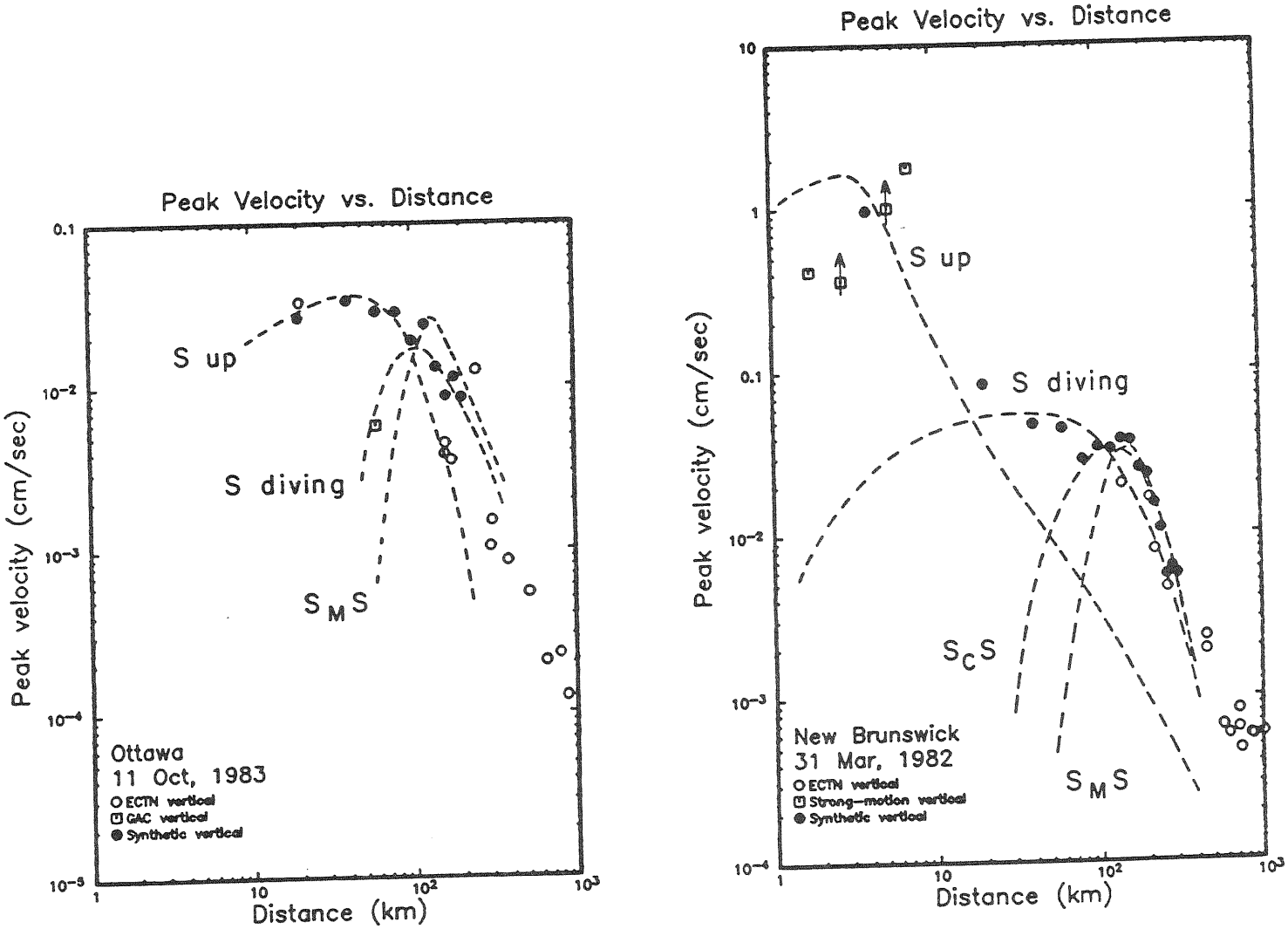

Figure 6 (left). Attenuation of observed (open symbols) and synthetic (solid symbols) peak vertical velocity for the Ottawa earthquake. The ground motion at station GAC has been corrected to resemble ECTN data. Also shown on the left is the attenuation of peak synthetic velocity when only specific sets of rays are included. (right). Attenuation of observed and synthetic peak vertical velocity for the March 31, 1982 New Brunswick aftershock. Strong-motion recordings from within 10 km (open boxes) have been corrected to resemble ECTN data. Also shown on the left is the attenuation of peak synthetic velocity when only specific sets of rays are included.

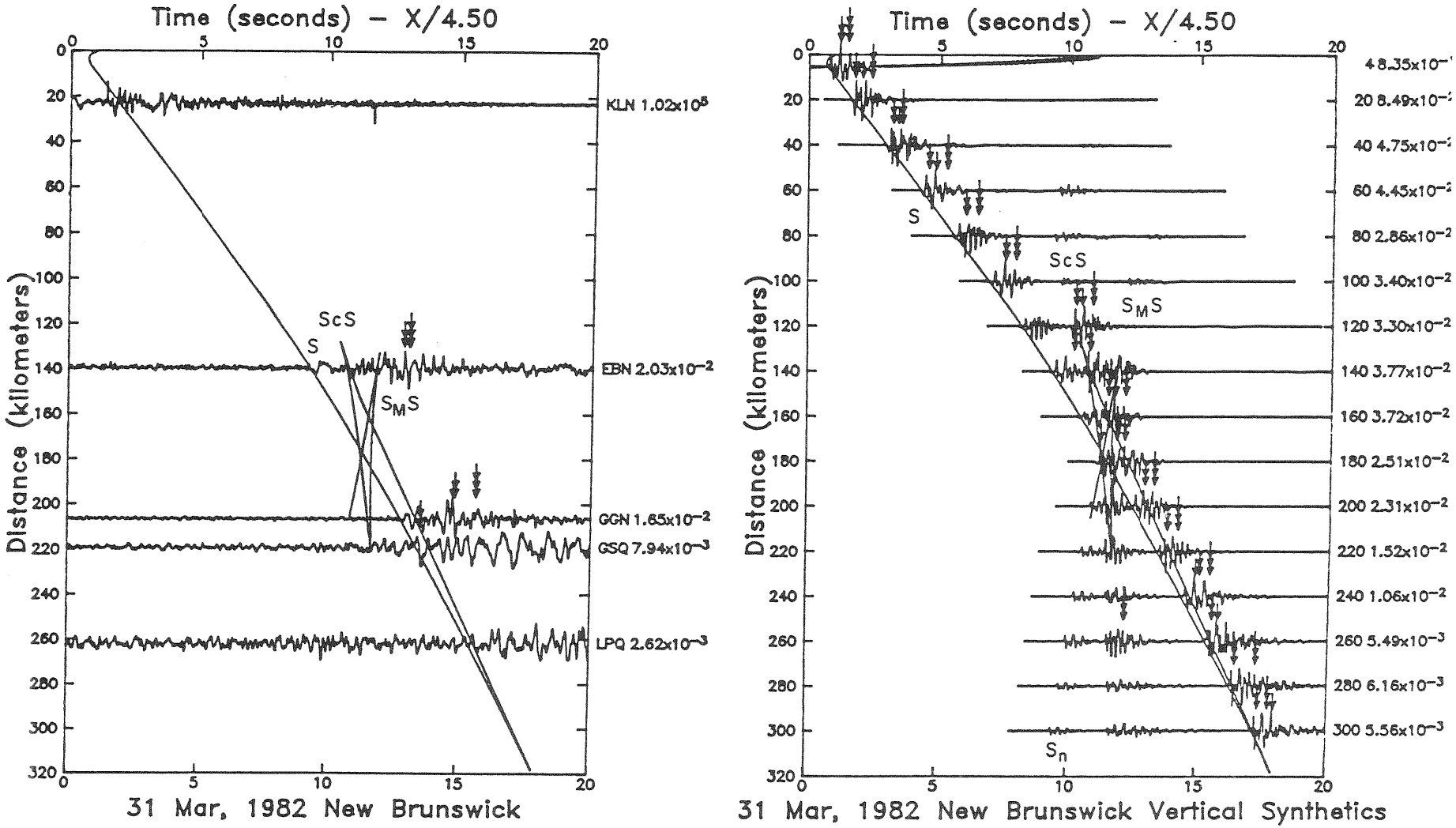

Figure 7 (left). Vertical velocity recordings from ECTN stations within 300 km of the March 31, 1982 principal aftershock of the New Brunswick earthquake. Superimposed are the S-wave travel-time curves for a source at 3.5 km depth in the Appalachian crustal velocity structure model. (right) Semi-empirical vertical velocity seismograms for a profile running N60°W from the March 31, 1982 New Brunswick aftershock.

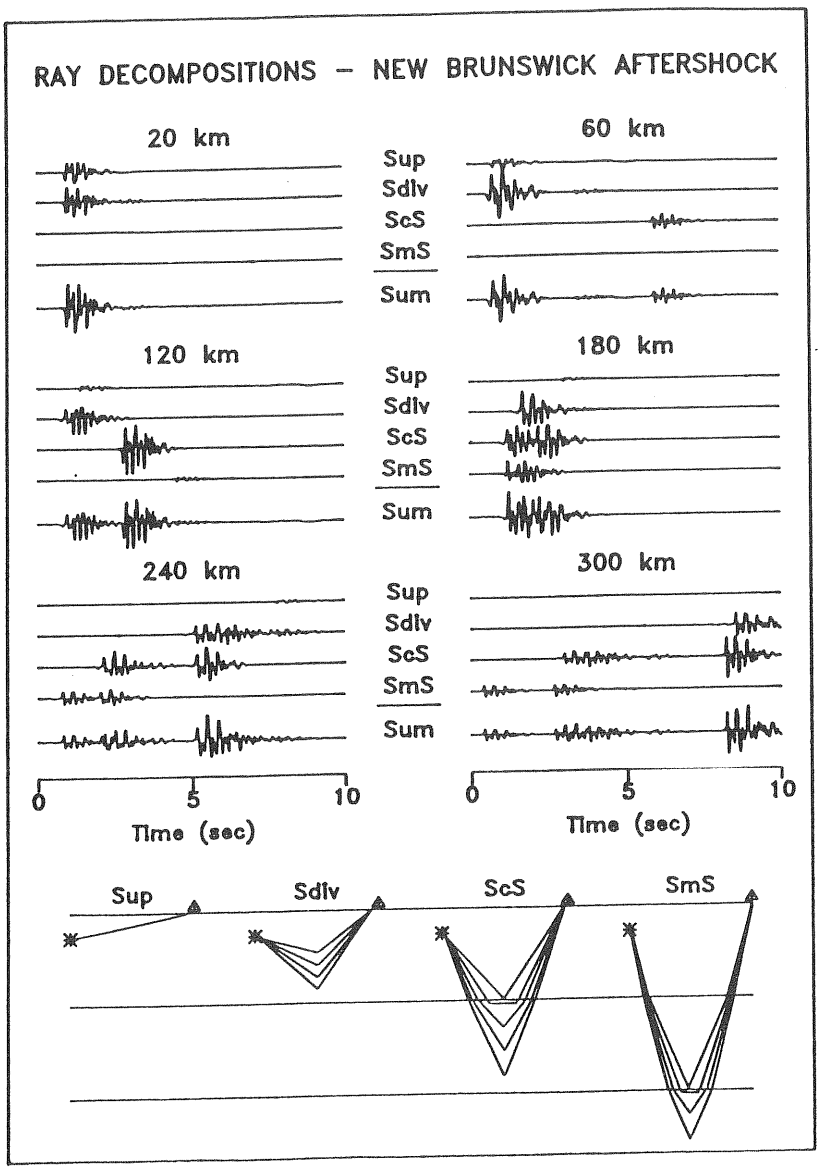

Figure 8. Ray decompositions of the semi-empirical synthetic seismograms for the New Brunswick aftershock. For each range, the top trace includes only the upgoing, direct S wave (S_{up}), the second trace includes diving S waves that turn within the crustal gradient (S_{div}), the third trace includes the S wave that reflects from the mid-crustal discontinuity and rays that turn between that depth and the Moho (S_cS), the fourth trace includes similar reflections from the Moho and rays that turn within the mantle (S_MS), and the bottom trace is the total synthetic seismogram.

We have developed crustal velocity models for the Grenville and Appalachian provinces, which differ primarily in crustal thickness and the existence or lack of a mid-crustal discontinuity. By comparing synthetic ground motions for events of similar depth and source mechanism but located within different velocity structures, we may isolate the effect of gross crustal structure on the shape of the attenuation curves. Of the events modeled by Barker, et al. (1987), the 1983 Goodnow, New York earthquake occurred in the Grenville structure while the January 11 aftershock of the New Brunswick earthquake occurred in the Appalachian structure. Otherwise, each was located at the same depth and had the same type of mechanism. The left side of Figure 9 includes a comparison of peak vertical acceleration for these events, in which we have scaled the peak ground motions of the Goodnow event to the moment of the New Brunswick aftershock. The Grenville ground motions (shown as solid circles) reflect large direct S at 20 km, low amplitudes at 40 - 80 km as direct and diving S interfere, and a slight increase in amplitude beyond the S_MS critical range at 100 km. The Appalachian ground motions (open circles) are much more variable in the 20 - 100 km range, reflecting the complex interaction of direct and diving S in the presence of the mid-crustal discontinuity. It is apparent from this comparison that ground-motion attenuation within 200 km of the source is highly sensitive to the gross features of the crustal velocity structure between the source and receivers.

On the right side of Figure 9, we illustrate the effect of source depth by comparing synthetic peak accelerations for the Ottawa earthquake (15.5 km, open circles) and for the Goodnow earthquake (7.0 km, solid circles). Both occurred in the Grenville structure and both had shallow reverse mechanisms. We have scaled the Goodnow ground motions to the moment of the Ottawa source. The Ottawa ground motions are controlled by the upgoing S wave out to about 80 km and the attenuation curve is quite broad. For the Goodnow event, upgoing S interferes with diving S between 40 and 100 km, causing peak ground motions to drop much more rapidly than those of a deeper source. This interaction of the direct, upgoing S wave and the diving S wave that turns within the crust appears to be the most important factor in determining ground-motion attenuation within 100 km from the source. Further, this interaction appears to be most sensitive to source depth.

These results indicate that ground-motion attenuation within a given region (crustal structure) may be described by a family of characteristic curves which depend primarily on the source depth within that structure. When strong-motion data from regions with contrasting crustal structures, or from events having different focal depths, are combined into a single data set, the detailed characteristics of regional attenuation relations are smeared out, leaving a data set having broad scatter that is most reasonably fit using a smooth attenuation curve. If the

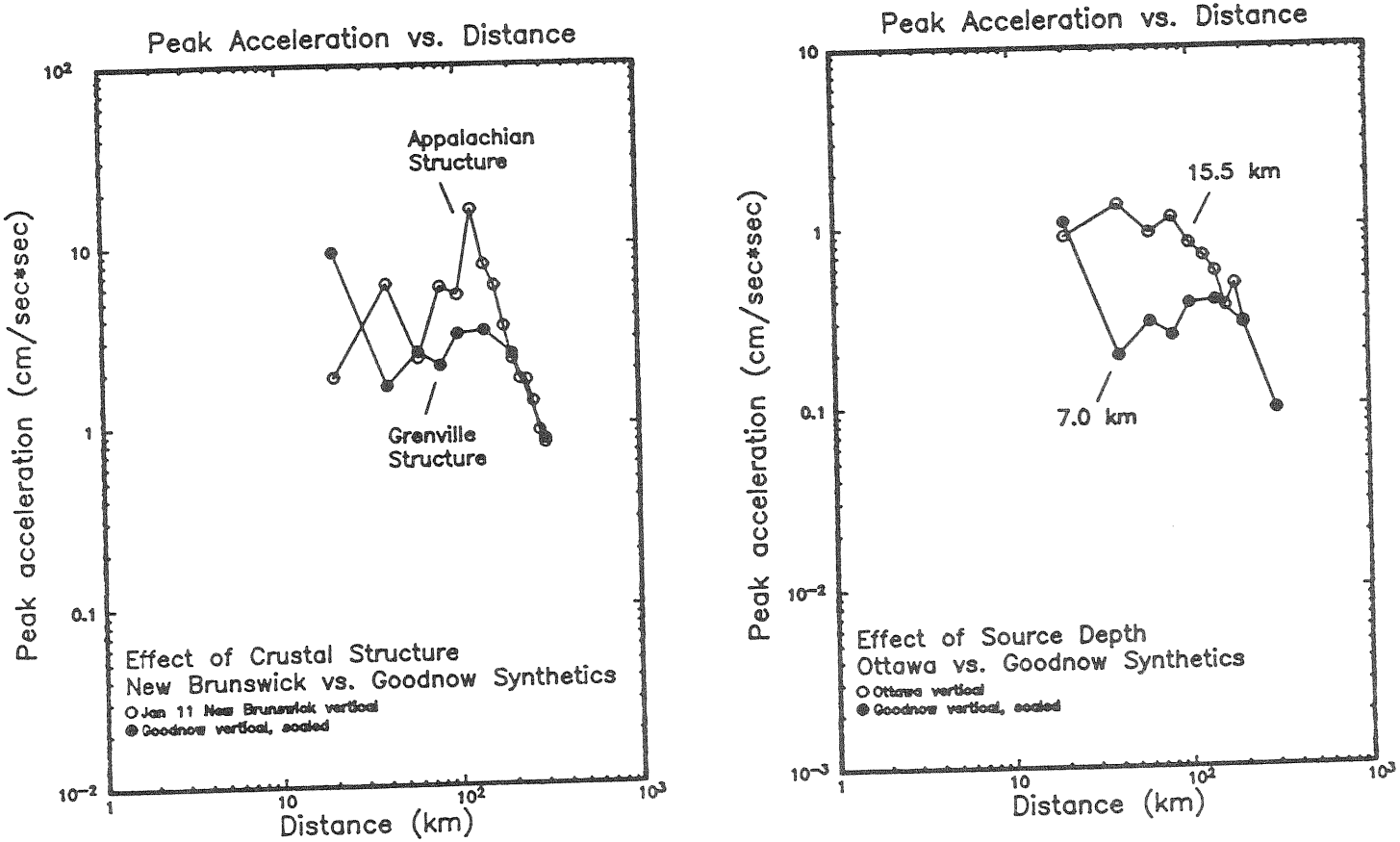

Figure 9 (left). A comparison of synthetic peak vertical acceleration for an event in the Appalachian crustal structure (January 11 New Brunswick aftershock, open circles) and an event in the Grenville crustal structure (Goodnow, solid circles). The Goodnow data have been scaled to the moment of the New Brunswick event. (right) A comparison of synthetic peak vertical acceleration for two events in the Grenville crustal structure at different depths. The Ottawa earthquake (open circles) was at 15.5 km depth, while the Goodnow earthquake (solid circles) was at 7.0 km depth. The Goodnow data have been scaled to the moment of the Ottawa event.

purpose of the attenuation curve is to predict ground motions over a very wide region such as eastern North America, the use of such a curve seems appropriate. However, if the purpose of the attenuation curve is to predict ground motions at a given site or within a given region, it seems more appropriate to use an attenuation curve that reflects the wave propagation characteristics of that region. This should produce a reduction in the uncertainty in ground-motion attenuation in the region. Our study has shown how empirical data and simulation methods that explicitly embody wave propagation effects can be used toward this end.

ACKNOWLEDGMENTS

Many of the results of this study were predicted by Don Helmberger, and we are grateful for his guidance. This research was carried out at Woodward-Clyde Consultants, Pasadena, and is part of a larger program to develop seismic wave attenuation relationships for the eastern United States being conducted by the Electric Power Research Institute under the direction of Dr. J. Carl Stepp.

REFERENCES

Barker, J. S., P. G. Somerville and J. P. McLaren (1987). Wave propagation modeling of ground motion attenuation in the northeast United States and adjacent Canada, report to the Electric Power Research Institute, Project RP2556-6, Woodward-Clyde Consultants, Pasadena.

Mereu, R. F., D. Wang, O. Kuhn, D. A. Forsyth, A. G. Green, D. Morel, G. G. R. Buchbinder, D. Crossley, E. Schwartz, R. duBerger, C. Brooks and R. Clowes (1986). The 1982 COCRUST seismic experiment across the Ottawa-Bonnechere graben and Grenville Front in Ottawa and Quebec, *Geophys. J.*, *84*, 491-514.

Nabelek, J. (1985). The January 9, 1982, New Brunswick, Canada earthquake, in A Study of New England Seismicity With Emphasis on Massachusetts and New Hampshire, Technical report covering 1982-1984, Earth Resources Laboratory, Massachusetts Institute of Technology, 104 pp.

Wahlstrom, R. (1986). The North Gower, Ontario, earthquake of 11 October, 1983: focal mechanism and aftershocks, *Earthquake Notes*, in press.

STRONG MOTION STUDIES IN THE CENTRAL U. S.

R. B. Herrmann and O. W. Nuttli
Department of Earth and Atmospheric Sciences
Saint Louis University
P. O. Box 8099
St. Louis, MO 65156-8099

INTRODUCTION

We have taken a holistic approach toward the earthquake problem in the central United States, being concerned about historical seismicity, modern instrumental seismicity, the seismic source, ground motion excitation and propagation, and, most importantly, interaction with the user community of engineers, public officials, and disaster response agencies.

Much has been accomplished during the last decade as a result of the National Earthquake Hazards Reduction Program. It is wise to review what has been accomplished, and what remains to be done.

SUCCESSES

The greatest success has been in the definition of seismicity patterns. Through the joint support of the U. S. Geological Survey, the U. S. Nuclear Regulatory Commission and individual states and universities, the central United States seismicity has been monitored well. An example of this is given in Figure 1, which shows the epicenters of 3208 earthquakes from a joint catalog of several regional networks. Distinct spatial patterns are apparent, but more importantly, it is seen that modern seismicity reflects the record of historically felt earthquakes (Figure 2). Results similar to this have been found in other regions in the United States where such comparisons are possible.

Focal mechanisms of earthquakes are routinely being determined for larger events, and distinct patterns are also seen. The intriguing observation is that, on the basis of somewhat limited numbers of events, earthquakes occurring at the same location, have similar focal mechanisms. Figure 3 presents the state of knowledge of focal mechanisms as of 1979 [Herrmann, 1979]. Subsequent studies in the Appalachians [Johnston et al, 1985], and in the Wabash River Valley [Taylor and Herrmann, 1987], show that earthquake mechanisms are uniform geographically. The focal mechanisms of the 31 January 1986 northern Ohio [Herrmann and Nguyen, 1986], 12 July 1986 western Ohio [Christensen and Pollack, 1986], the 12 June 1987 southeastern Illinois [Taylor and Herrmann, 1987] and the 27 July 1980 northern Kentucky earthquake [Herrmann et al., 1982] have very similar focal mechanisms in spite of the large region sampled. The depths of these events are in the range of 5 - 12 km.

By combining the limited strong motion data base with regional seismic network recordings, progress has been made in developing ground motion scaling relations for eastern North America. An intensive effort by the Electric Power Research Institute has led to state-of-the-art estimates for scaling peak acceleration and PSRV at selected frequencies. These results are reported in a special section in the April, 1987, issue of the Bulletin of the Seismological Society of America. We might say that the best possible scaling relations are now available.

Another area worth mentioning is the increase in awareness of the earthquake problem. Local disaster response agencies, FEMA, the Corps of Engineers, the Veterans Administration, cities, designers, and especially the public know about the existence of earthquakes on the New Madrid fault. A Central United States Earthquake Consortium has been formed to promote earthquake awareness.

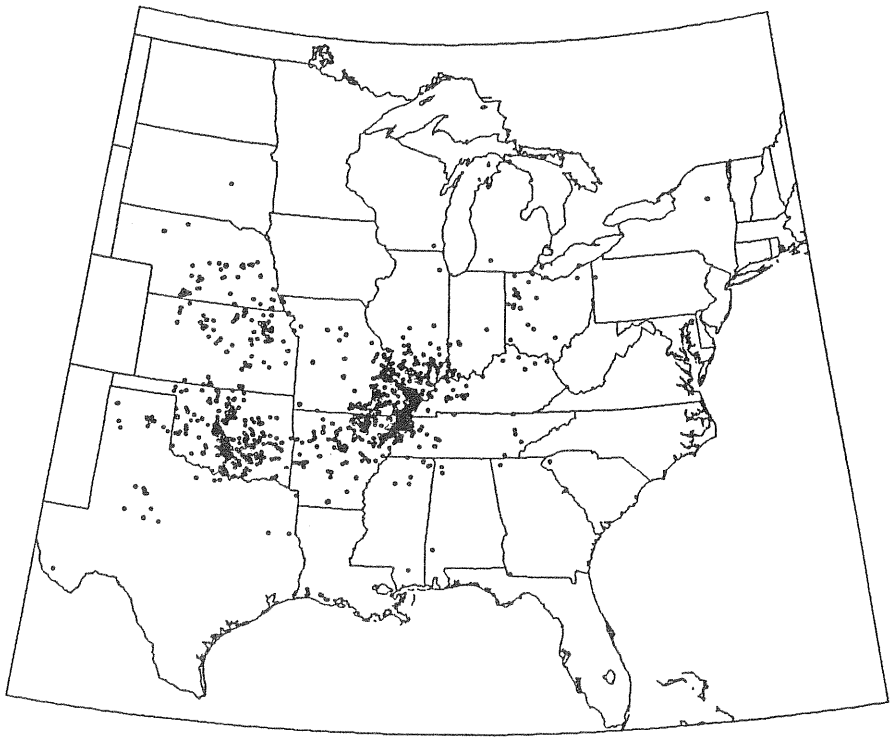

Fig. 1. Locations of 3208 earthquakes in the instrumental catalog for the period 1974 - 1986.

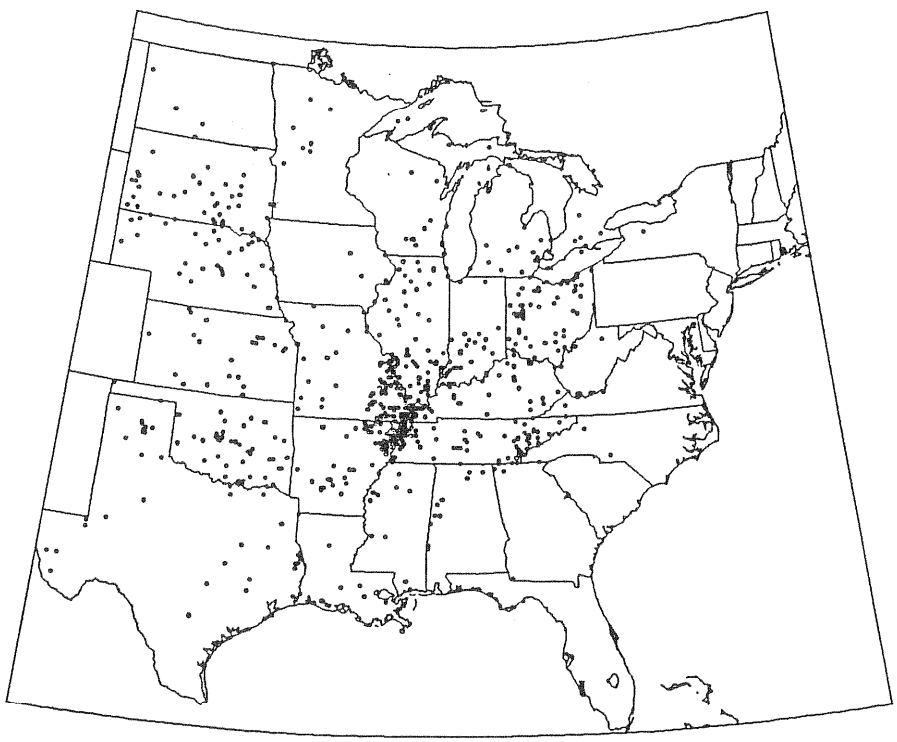

Fig. 2. Locations of 1200 historical, felt earthquakes in the central United States for the time period 1812 - 1985.

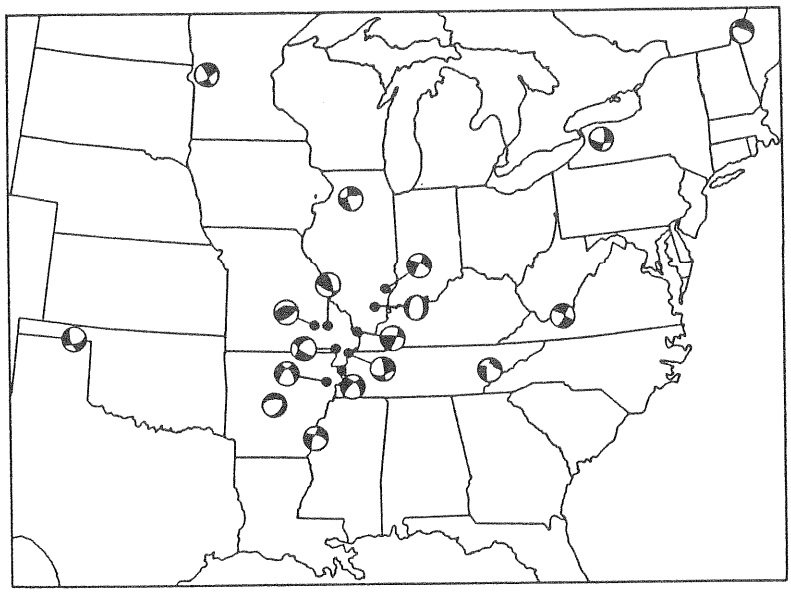

Fig. 4. Focal mechanism solutions. The black and white sectors indicate dilatational and compressional quadrants, respectively. For clarity, focal mechanisms for events 7, 19 and 22 were not plotted, since they were very similar to those of events 5, 1 and 21, respectively.

Fig. 3. Surface-wave focal mechanisms for eastern U. S. earthquakes [Herrmann, 1979].

In summary much has been accomplished.

PROBLEMS

Even though there are distinct seismicity patterns and these patterns are compatible with the historical record, the unanswered question is **why?** Other talks presented during this conference address stress patterns, recent tectonic processes, etc, but there is no self consistent model for the earthquake process as there is for plate margin earthquakes. Estimates of repeat times of large New Madrid earthquakes, for example, are not compatible with a continuity of the major earthquake process there for long periods of time. It is doubtful whether a viable model can be constructed. Certainly the problem will not be resolved in the next five years.

Ground motion scaling relations are crippled by the fact that there are no on-scale recordings in the region of large earthquakes at distances less than 20 km *and* distances greater than 20 km. The present modeling techniques are only a first step. Figure 4 shows an attempt by Toro and McGuire [1987] to calibrate their model by comparing an observed m_{Lg} vs M_o data set to model predicted values. At first glance the model does a good job, but a detailed examination shows systematic deviations on the order of 0.3-0.5 magnitude units, due either to the inability of the model to correctly account for source excitation or to systematic errors in magnitude. Can engineers accept a factor of 2-3 error? Figure 5, also from Toro and McGuire [1987] shows 1 and 5 Hz PSRV estimates for bedrock sites together with observed data. The *b* and *A* symbols represent data from instruments on the Mississippi Embayment alluvium. There seem to be site effects of at least a factor of 3-5 here. Do we have the earth structure parameters to model these?

At present magnitude 4.5+ events are not recorded on-scale by any high frequency instrument in the central U. S. Regional networks suffice to locate the event, but that is all. If we had on scale recordings, then we would be able to understand ground motion scaling with distance better, the relation between source estimates based on short distance data and distance at greater ranges.

Regional seismic networks have excelled at rapidly providing accurate epicenters, which is important for aftershock studies. The aftershock studies have been very successful in defining the spatial geometry of the aftershock sequence. Source studies have been made using digital data, but site effects can severely distort the analysis [Cranswick et al, 1985].

Increased public awareness is accompanied by a correlative request for solutions. The user community wants to know *what to do* to respond to the earthquake threat. Local communities have no one directly to assist them. They do not know whether to expect the worst or to just ignore the problem. The design community is somewhat better off in that they can be given ground motion values with which to work. The emergency response agencies are planning for the *big* earthquake and are unable to design responses for smaller events.

OPPORTUNITIES

Presuming that seismologists have a direct responsibility to the public for their support, what can realistically and should be accomplished during the next five years that will repay this debt?

The quality of data will improve substantially if the planned eastern portion of a U. S. national digital seismic network is implemented by the USGS with USNRC funding. A system of broadband digital, wide dynamic range instruments will be distributed throughout the eastern U. S. As proposed, we should no longer have the problem of not

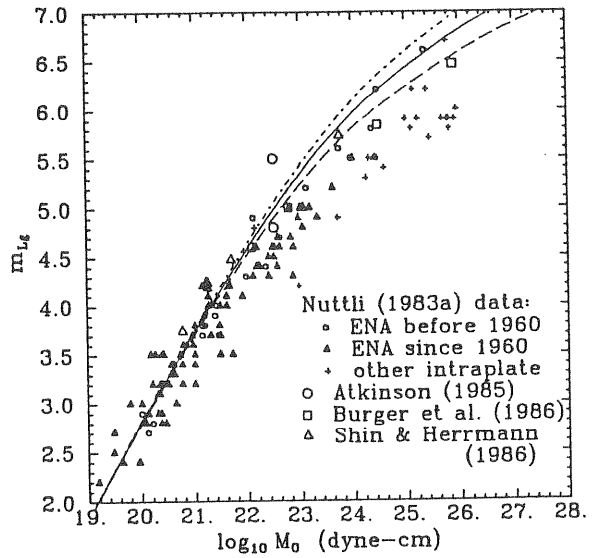

FIG. 5. Relationship between m_{Lg} and seismic moments. Curves shown correspond to stress drops of 50 (dashes), 100 (solid), and 200 (dot-dashes) bars.

Fig. 4. Plot of model predicted and observed m_{bLg} magnitudes [Toro and McGuire, 1987].

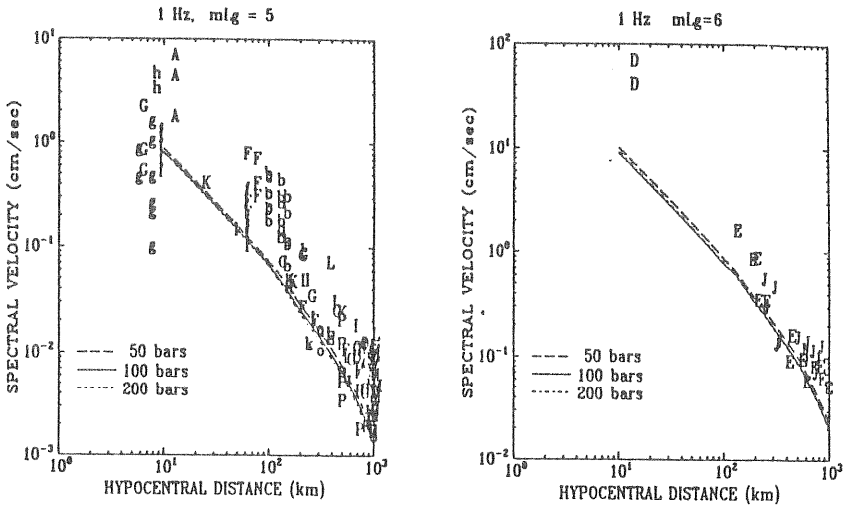

FIG. 6. Comparison of predicted and observed 1-Hz spectral velocity for m_{Lg} 5 and 6. See Table 5 for earthquake symbols; lowercase symbols indicate soil sites.

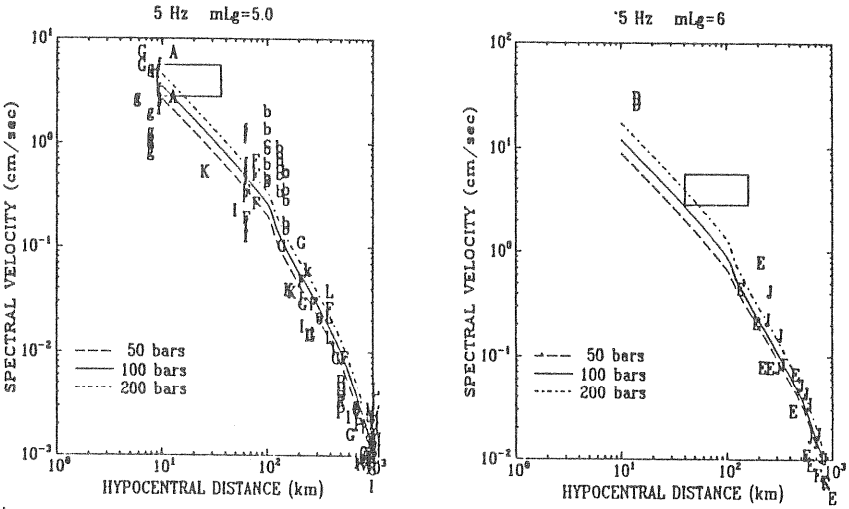

FIG. 7. Comparison of predicted and observed 5-Hz spectral velocity for m_{Lg} 5 and 6. See Table 5 for earthquake symbols; lowercase symbols indicate soil sites. Rectangles indicate ranges of ground motion and distance corresponding to MMI VI.

Fig. 5. Plot of 1 and 5 Hz PSRV for hard rock sites in eastern North America. Lower case sysbols as well as *A* represent soft sites [Toro and McGuire, 1987].

having magnitude 4.5+ earthquakes recorded on scale at distances less than 500 km. Detailed signal analysis will permit the recovery of source characteristics such as depth, focal mechanism, and especially rupture time history. Ground motion estimation models will be improved. The national network will also be able to provide locations of detected earthquakes within 15 to 30 minutes of their occurrence.

This capability should be of importance to the disaster response agencies. Imagine the following scenario: an earthquake occurs near New Madrid. Within minutes, the telephone lines to the state or federal emergency management agencies in Jefferson City and Kansas City, Missouri, respectively, become clogged. A clear picture of the disaster has not yet emerged, but a response is in order. Using private numbers, the disaster response agencies are notified by NEIS of the location and size of the earthquake. It is a magnitude 6.5, not a repeat of the big 1811-1812 earthquakes. The agency takes a number of transparent overlays keyed to this magnitude from a map drawer. By placing the center of the overlay at the earthquake location, and using the different overlays, the responsible official determines that strong shaking has occurred near a city with population of 30,000. The overlays indicate expected damage to buildings, utilities, and lifelines. On the basis of this preliminary assessment, the official initiates a response graduated according to the potential disaster.

This scenario illustrates the potential interplay of a national network together with basic earthquake disaster information, represented as a set of overlays. Developing the overlays would require only assembling small groups of experts to make ground motion, building damage, utility damage, etc, overlays. This would have the important effect of making the disaster response more realistic, e.g., rather than responding to the *big* earthquake and airlifting 10,000 military personnel from throughout the country to assist, an appropriate response is planned. The impediments to this are the poorly known site effects and, more especially, the poorly known relation between some combination of ground motion parameters and damage.

In the event of a large earthquake, magnitude 4.5+, digital instruments will usually be deployed to study aftershocks. They will typically be placed within 10 km of the epicenter. Larger aftershocks will be able to be detected by the national network and it will then be possible to test the consistency of ground motion estimation models by comparing the short and large distance observations. Site effects at the portable sites must also be estimated. If the portable instruments record the surface waves from local mining operations, these signals can be used to define the shallow shear wave velocity beneath the stations by inverting the surface-wave dispersion. In addition a simple refraction line can be run [Cranswick et al, 1985].

RESEARCH DIRECTIONS

The following problems should be performed:

1. What are site effects? What is hardrock motion? Should site effects be estimated relative to the thickness of the entire sedimentary rcok section, or restricted to superficial surface layering? How can these be best estimated?

2. What are the goals of the next phase of ground motion estimation models? Should ground motion scaling models by refined by incorporating site effects and by better knowledge of the relation between ground motion at large and short distances? Can apparent problems in observed and predicted magnitudesbe reconciled?

3. Can a U. S. national network be useful in disaster response?

4. How can a U. S. national network assist ground motion studies?

5. What is the relationship between ground motion and earthquake damage?

BIBLIOGRAPHY

Cranswick, E., R. Wetmiller, and J. Boatwright, High-frequency observations and source parameters of microearthquakes recorded at hard-rock sites, *Bull. Seismol. Soc. Amer., 75,* 1535-1567, 1985.

Christensen, D. H., and H. N. Pollack, Recent seismicity in the Anna, Ohio seismic zone: the July 12, 1986 St. Mary's earthquake (abs), *Earthquake Notes, 57,* 107, 1986.

Herrmann, R. B., Surface wave focal mechanisms for eastern North American earthquakes with tectonic implications, *J. Geophys. Res., 84,* 3543-3552, 1979.

Herrmann, R. B., C. A. Langston, and J. E. Zollweg, The Sharpsburg, Kentucky, earthquake of 27 July 1980, *Bull. Seismol. Soc. Amer., 72,* 1219-1239, 1982.

Herrmann, R. B., and B. Nguyen, Focal mechanism studies of the January 31, 1986 Perry Ohio earthquake, *Earthquake Notes, 57,* 107, 1986.

Johnston, A. C., D. J. Reinbold, and S. I. Brewer, Seismotectonics of the southern Appalachians, *Bull. Seismol. Soc. Amer., 75,* 291-312, 1985.

Toro, G. R., and R. K. McGuire, An investigation into earthquake ground motion characteristics in eastern North America, *J. Geophys. Res., 77,* 468-489, 1987.

ISSUES IN STRONG GROUND MOTION ESTIMATION IN EASTERN NORTH AMERICA

Robin K. McGuire and Gabriel R. Toro

Risk Engineering, Inc.
5255 Pine Ridge Road
Golden, Colorado, 80403

ABSTRACT

Proper characterization of uncertainties in ground motion estimation in eastern North America is important for any assessment of seismic hazard. The scientific issues surrounding these uncertainties are reviewed, as are the earthquake data available in ENA. A method of estimating ground motion that is based on a theoretical source spectrum attenuated to the site and modified by local soil conditions is preferred for estimating ground motion, as it can explicitly incorporate the scientific uncertainties that cause uncertainty in ground motion.

INTRODUCTION

The estimation of quantitative characteristics of strong earthquake ground motion in eastern North America (ENA) is difficult. No instrumental records are available from destructive shaking in the region, and there are perceived differences between shaking in ENA and in California, thereby invalidating the use of empirical equations from California (where data are abundant) in ENA. Quantitative estimation of ground motion is a critical step in the mitigation of risk for existing facilities and in the selection of design criteria for new facilities. Therefore in the absense of empirical observations of strong shaking we must evaluate and use relevant theories, low-amplitude seismographic observations, and data from other regions to deduce what might be the range of strong ground motion characteristics in ENA. Correct decisions (in the sense of optimal decisions under uncertainty) about seismic-risk mitigation will be made only if available alternatives are judged on their scientific merits and if current uncertainties on ground-motion characteristics are reported honestly. This paper summarizes the current scientific issues causing uncertainty in ground-motion estimation for ENA, and evaluates methods of ground-motion prediction on their ability to incorporate and represent current alternative viewpoints.

AVAILABLE DATA

While there are no instrumental records of strong shaking in ENA, there are abundant assessments of Modified Mercalli Intensity (MMI) values from earthquakes in the region. These data (and the descriptions on which they are based) document in a qualitative way that damaging earthquakes have occurred in ENA. MMI data are

of critical importance in establishing the locations and sizes of pre-instrumental shocks in the region, but are of very limited value in making estimates of strong ground motion (for reasons discussed below in "Ground Motion Estimates").

Instrumental records of ground motion in ENA are in fact quite abundant. Table 1 summarizes the available data for ENA and related areas (those for which the seismic source and attenuation characteristics might be similar to ENA). These are wide-bandwidth data that are generally available to the scientific community. Not included are analog seismograph records from instruments with peaked response, and data from aftershock and earthquake swarm studies that are not readily available (these are predominantly from $m_b \leq 3.5$ earthquakes). As Table 1 indicates, the data are primarily from small earthquakes at regional distances (100 to 1000 km). For this reason the accelerograph records from the Nahanni and Gazli events are important: if the crustal stress release causing these earthquakes was similar to what might be expected in ENA, the records give empirical evidence of the associated, near-source ground motions. This issue is important especially in the case of the Nahanni events, which were well-recorded from near-source to teleseismic distances.

Additionally the extent to which some records have been affected by underlying soil conditions is unclear, particularly for accelerograph data from Mississippi valley earthquakes and the Miramichi and New Hampshire shocks. To the extent that soil effects cannot be removed from a record, the usefulness of that record to predict ground motions for other geologic conditions (in particular, rock) is limited. The issue of soil effects in ENA is discussed more fully below.

THE SOURCE SPECTRUM

The most direct method to estimate earthquake ground motion is to start with a representation of energy released at the source. The energy can then be attenuated to the site, and any relevant soil effects can be added, to obtain an estimate of ground motion at a particular site for a specified earthquake. Both attenuation and soil effects are discussed in subsequent sections.

The Fourier spectrum of shear waves caused by slip displacement on a fault can generally be modeled by a shape proposed by Brune (1970, 1971). In this model, the Fourier spectrum of acceleration increases with frequency as f^2 up to some corner frequency f_o; above that spectral amplitudes are constant and proportional to $M_o (2\pi f_o^2)$, where M_o is the seismic moment of the earthquake. This simple representation of the source energy, coupled with relationships between the seismic moment, stress drop, source size, and corner frequency, provide a convenient means of estimating the energy released as shear waves during earthquakes.

Table 1

AVAILABLE GROUND MOTION RECORDS IN ENA AND RELATED AREAS

Description	Mag.	No. Records	Instr.	Distance	Soil Cond.	Comments
US earthquakes and expl., 1962-1967	mb 3.0 to 4.8	~250	LRSM	200 to 1000 km	Varied	3 component analog records
Blue Mtn. Lake, NY. July-Aug, 1973	ML 2.8	3	SMA-1	Near-source	Bedrock or buried boulder	Shallow events.
Miss. Valley earthquakes, 1975-1976	mb 4.2 to 5.0	9	SMA-1	10 to 100 km	Miss. embay.	Most records on earth dams
Monticello Reservoir, 1978	ML 2.8	3	SMA-1	Near-source	Alluvium	Shallow, induced events
Canada, eastern US events, 1980-1986	mb 4.1 to 5.6	60	ECTN	100 to 1000 km	Rock	Vertical component digital data
New Hampshire, January 19, 1982	mb 4.8	12	SMA-1	10 to 100 km	Alluvium	Most records from earth dams
New Brunswick, March and May 1982	mb 4.0 and 4.8	5	SMA-1	3 to 7 km	Shallow alluv. and rock	
US earthquakes 1983-1986	mb 3.2 to 5.1	~140	RSTN	200 to 1000 km	100 m boreholes in rock	3 component digital records
Painesville, Ohio 1986	mb 4.9	1	SMA-3	18 km	Shale	Recorded on massive foundation
Nahanni, NWT, Canada, Dec. 1985	Ms 5.0 to 6.9	~100	SMA-1	Near-source	Rock	Most records not yet widely available
Gazli, USSR, May 17, 1976	mb 6.2 Ms 7.0	1	Accel.	Near-source	Sandstone and clay	3 component optical record at Karakyr Point

More complicated representations of the source spectra have been synthesized for some California earthquakes (e.g. Papageorgiou, 1987). However, in spite of these more complicated spectral shapes, the simple Brune model of seismic shear wave spectra has been shown to provide adequate engineering estimates of strong ground motion in California, where there are sufficient data for evaluation (e.g. Hanks and McGuire, 1981; Boore, 1983; McGuire et al, 1984). This spectrum has also been used to estimate ground motion in ENA (e.g. Boore and Atkinson, 1987; Toro and McGuire, 1987; Toro, 1987), although most of the observations available for comparison with predictions are low amplitude ground motions. Thus the simple Brune model of the source spectrum can be considered adequate for engineering predictions of ground motions, recognizing that the spectrum from any particular earthquake might deviate from it to some degree.

In the Brune model, seismic moment M_o, stress drop $\Delta\sigma$, and corner frequency f_o are related by:

$$f_o = \left(\frac{\Delta\sigma \, \beta^3}{8.44 \, M_o} \right)^{1/3} \qquad (1)$$

The spectral amplitude above the corner frequency usually controls ground motions of engineering interest. This amplitude is proportional to $M_o^{1/3} \, \Delta\sigma^{2/3}$; the root-mean-square (rms) amplitude (assuming that duration is the reciprocal of corner frequency) is proportional to $M_o^{1/6} \, \Delta\sigma^{5/6}$. Thus, the stress drop that drives the high frequency is an important parameter for the prediction of ground motions of engineering interest.

The stress drop obtained by observing f_o from ground motion records, inverting equation 1, and calculating $\Delta\sigma$ as a function of f_o and M_o is a <u>static</u> stress drop, a measure of the average stress across the faulting surface before the earthquake, minus the average stress after the earthquake. Static stress drops for large earthquakes are typically in the range of 1 to 100 bars. The stress drop that drives the high frequencies of ground motion is not well-understood, but is more like an average dynamic stress drop across the faulting surface. This stress drop can be inferred from measurements of root-mean-square acceleration a_{rms} from accelerograph records, and is found to be 50 to 100 bars in California (Hanks and McGuire, 1981; Boore, 1983, 1986). This distinction is important, as the dynamic stress drops that drive high-frequency strong ground motion can be quite different from the static stress drop for the same event.

Several studies have examined the difference in stress drops between plate-margin and intraplate earthquakes. Liu and Kanamori (1980) have studied the relationship between M_s and m_b for various earthquakes and conclude that stress drops in intraplate regions are higher than for plate margins, by a factor of about 3. The stress drops driving these observations are more like dynamic stress drops. Using more indirect methods, Kanamori and Allen (1986) conclude that for a given magnitude, earthquakes with longer repeat times have shorter fault lengths (and thus higher stress drops) than events in more active regions. Scholz et al

(1986) come to a similar conclusion, deriving a factor of 6 difference in stress drops between plate-margin and intraplate events. These inferred differences are relevant to static rather than dynamic stress drops.

Nuttli (1983a, 1983b) compared relationships between m_b, M_S, and M_0 for intraplate earthquakes and concluded that stress drops increase as $M_0^{1/4}$ (or equivalently, corner frequency varies as $M_0^{-1/4}$). More recently, Nuttli (personal communication, 1987) has revised his earlier source scaling model based on M_0-f_0 data from ENA and Japan. In this new scaling relationship the stress drop still increases as $M_0^{1/4}$, but the seismic moment corresponding to a corner frequency of 1 Hz is 3×10^{23} (the corresponding moment in the 1983 model was roughly 10^{22}).

Somerville et al (1987) used time-domain modeling of teleseismic body waves to estimate the source parameters of thirteen ENA moderate and large earthquakes. They concluded that stress drops do not depend on source size, and have an average value of 100 bars.

The issue of stress drops of earthquakes in ENA cannot be unequivocally resolved with data because of scatter. Figure 1 illustrates one comparison of observations of m_{bLg} and M_0 and predictions using a constant stress drop of 100 bars and Nuttli's (1987) increasing stress drop. Either interpretation is allowed by the data, and the issue of whether and how stress drops in ENA are different from those in California likely will not be resolved until several moderate earthquakes are well-recorded in ENA.

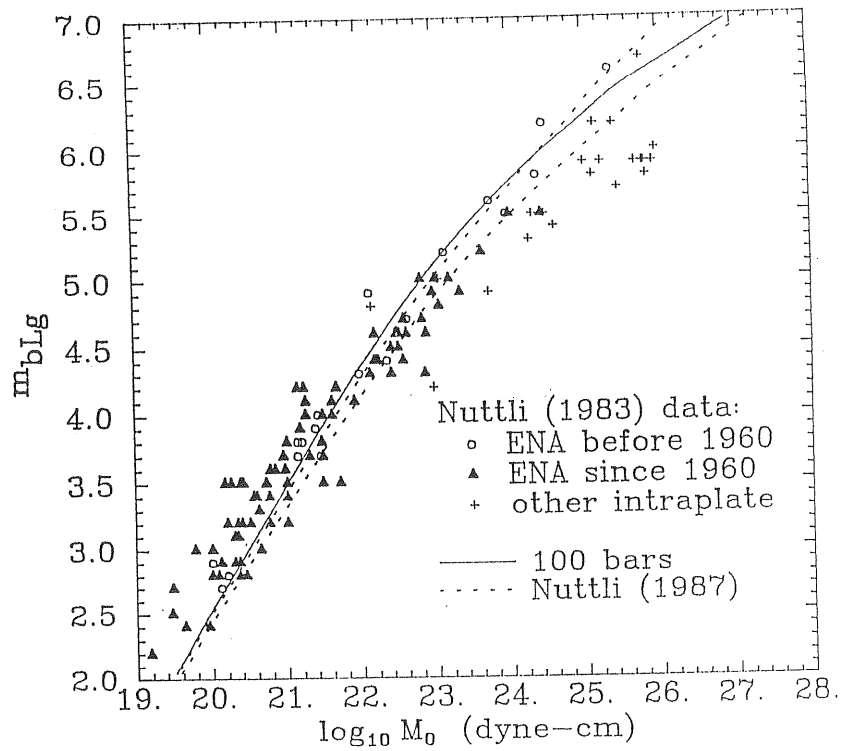

Figure 1: Theoretical relationships between M_{Lg} and M_o compared to data (after Toro, 1987).

In addition to issues of stress drop, ENA earthquakes are observed to generate higher amplitudes at high frequencies than California earthquakes. This may be an effect of higher frequency energy generated at the source, or of higher frequency being transmitted more efficiently through the earth's crust (including through near-surface rocks and soils). Whatever the cause, significant energy at frequencies up to 40 Hz is often observed at near-source distances in ENA. The energy at these frequencies has little effect on the response of ordinary engineering structures, but can result in records with high peak accelerations. For this reason the direct prediction of response spectrum amplitudes avoids issues of scaling spectral shapes to a high-frequency peak acceleration.

ATTENUATION OF GROUND MOTION

The manner in which ground motion attenuates with distance is important in two respects. At distances less than 100 km attenuation is critical to estimate amplitudes of strong shaking. At farther distances (100 to 1000 km) the attenuation of ground motion must be accurately modeled in order to predict seismograph responses and compare those predictions with observations, and to model magnitude measurements from specified source spectra.

At the closer distances (less than 100 km) empirical evidence in California indicates that 1/R geometric decay of body-wave amplitudes is accurate. This is also a reasonable assumption in ENA. Modeling of multiple wave arrivals for ENA earthquakes by Burger et al (1987) and Barker et al (1987) indicate that, while individual waves may attenuate faster or slower than 1/R, the composite representation of amplitude decay is adequately represented by 1/R (especially when considering the average over possible source depths and focal mechanisms).

At distances beyond 100 km Lg waves dominate high-frequency ground motions in ENA. The frequency-domain amplitudes of these surface waves decay as $R^{-1/2}$; their time-domain amplitudes decay as $R^{-5/6}$. Synthetic modeling has confirmed these attenuation rates (e.g. Shin and Herrmann, 1987).

The duration of shaking at near-source distances is usually taken to be equal to the source duration T_0. When surface waves dominate the motions, dispersion increases the duration of motion by 0.05 R, where R is distance in km. This effect has been confirmed by examining seismographic data (Toro and McGuire, 1987).

Anelastic attenuation in ENA is more problematic. This attenuation takes the form of a factor $\exp(-\gamma R)$, where $\gamma=\pi f/Z\beta$, f is frequency, and β is wave velocity. Depending on the investigator and the data set, various Q models have been reported in the literature for ENA; some of these are listed in Table 2.

There is some consistency among empirical results obtained in California for deep soils (thicker than, say, 30 m). Table 3 lists reported amplification factors (ratios of Fourier spectra or response spectra) as a function of frequency. The general trend is for a factor of unity (i.e. no amplification) at 10 Hz, and a factor of two at 1 Hz, with intermediate values between these two frequencies. (An exception is the study by Rogers et al, who used microseismic recordings of distant nuclear shots to derive amplification factors.)

Table 3

REPORTED AMPLIFICATION FACTORS (FOR RESPONSE OR FOURIER SPECTRA) OF DEEP SOIL/ROCK BASED ON ANALYSES OF EMPIRICAL DATA

Reference	10 Hz	5 Hz	3 Hz	2 Hz	1 Hz
Campbell (1981)	1.0	1.0	NR	2.0	2.0
Campbell (1983)[+]	1.0	1.0	NR	1.7-1.9	1.7-1.9
Bernreuter et al (1985)	0.8	1.1	1.3	1.5	1.7
Joyner and Fumal (1985)					
Generic Soil:	0.95	0.98	1.1	1.4	1.9
V_s=200 m/s	1.0	1.0	1.35	1.9	2.9
V_s=500 m/s	1.0	1.0	1.05	1.3	1.8
Rogers et al (1985)					
Mean:	NR	3.4	3.4	3.3	3.3
Range:	NR	2.8-5	2.8-5	1.6-5	1.6-5
Toro and McGuire (1987)	1.0	1.3	1.75[++]	1.8	2.1

NR = Not reported.
* = Value based on reported ratio for peak horizontal accel.
** = Value based on reported ratio for peak horizontal vel.
\+ = Values shown are maximum reported (soil depth > 6 km) for equations unaltered by special conditions in Utah.
++ = Average of values reported at 2 Hz and 4 Hz.

Shallow soils are more problematic. Both empirical and theoretical studies (e.g. Bernreuter et al, 1985) indicate that shallow soils can amplify high frequencies of ground motion, but it has not been demonstrated that this effect can be accurately be quantified with a few generic categories. This is a particular problem in assessing the strong motion data from Miramichi, which were obtained on shallow soils. The records may not be representative either of deep soil sites or rock sites. In a similar vein, the records from the New Hampshire earthquake were obtained mostly at earth dam sites (including crest, abutment, and downstream sites) that undoubtedly modified the ground motions from rock conditions. The estimation of ground motion effects for geologic conditions such as these is not easy in general, and it may be especially difficult in ENA for sites of unconsolidated glacial till overlying competent, high-velocity bedrock.

TABLE 2

ENA Q MODELS REPORTED IN LITERATURE

Model	Investigators
$Q = 1300\ f^{0.38}$	1. Dwyer et al (1983)
$Q = 900\ f^{0.20}$	2. Hasegawa (1985)
$Q = 982\ f^{0.376}$	3. Gupta and McLaughlin (1987)
$Q = 500\ f^{0.65}$	4. Shin and Herrmann (1987)
$Q = 1100\ f^{0.17}$	5. Atkinson (1987)

The effect of these different models is large (a factor of five in ground motion amplitude) at 10 Hz, as illustrated in Figure 2. The model by Shin and Herrmann (1987) gives results intermediate to the others.

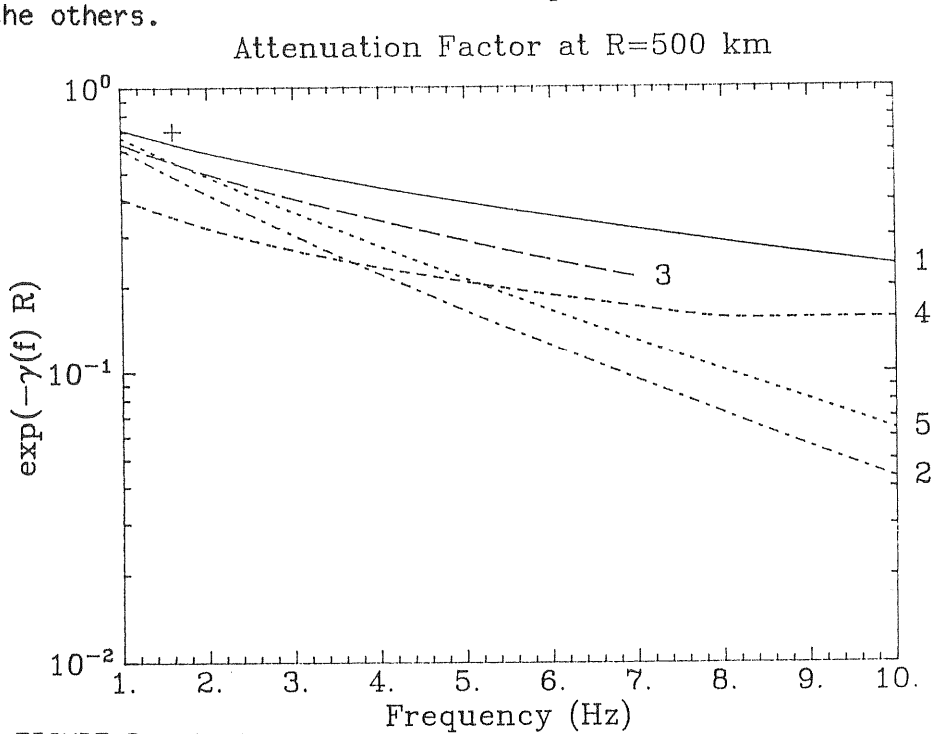

FIGURE 2: Anelastic factors at 500 km according to models in Table 2

SURFICIAL GEOLOGY

Estimating the effects of soils on ground motions is important both for the prediction of motion on soils during future earthquakes, and in understanding the effects that soils have had on the records currently available. To avoid a site-specific dynamic analysis at every site, requiring site-specific soil properties, it is common to designate several soil categories and to estimate the average effects of soils in each category.

ENGINEERING ESTIMATES OF GROUND MOTION

To estimate strong ground motion for engineering purposes, we classify available procedures into three groups. These are reviewed here.

"Calibrated theoretical methods" use a mathematical representation of the source spectrum and ground motion attenuation based on theory and seismological observations to derive the form of equations to estimate ground motion. The parameters in these equations are then chosen so that the absolute values of estimates match available observations. In this way low-amplitude instrumental data for small magnitude earthquakes and large distances can be used to calibrate the equations, and extrapolations to close distances, large magnitudes, and high ground-motion amplitudes can be made with some degree of confidence. Nuttli and Herrmann (1980) were the first to use methods of this type; they predicted peak acceleration and velocity. Other recent investigations (Atkinson, 1984; Boore and Atkinson, 1987; Toro and McGuire, 1987; Toro, 1987) have also used these methods to predict response spectrum amplitudes. These methods are the most preferred, because they can explicitly account for characteristics of ENA events (higher stress drops, higher amplitudes at high frequencies) as compared to California events. The effects of uncertainties in seismological interpretations (e.g. of stress drop versus magnitude) can be obtained by application of these models with different assumptions. Figure 3 illustrates the agreement between one application of a model of this type, and ENA data (see Toro, 1987, for definition of the symbols), including Nahanni data.

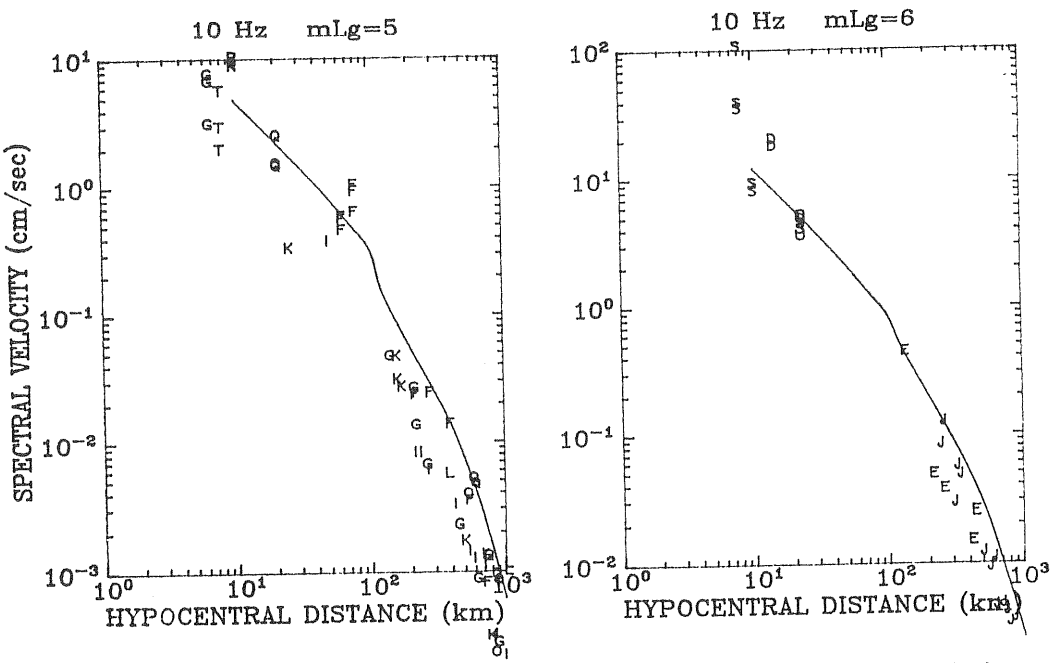

Figure 3: Estimates of 10 Hz response spectrum velocity and data from ENA; see Toro (1987) for definitions of symbols.

"Semi-theoretical methods" (also called "semi-empirical methods") make the assumption that, in the near-source region, ground motion

characteristics for ENA earthquakes will be identical to those for California earthquakes of the same magnitude. This would follow if the properties of the energy release during dynamic faulting were the same for earthquakes in the two regions. Estimates of ground motions near the source are based on empirical observations in California. At farther distances the near-source predictions are reduced using a geometric attenuation (which is region-independent) and an anelastic attenuation appropriate for ENA. In this manner the empirical, near-source estimates are modified by theory in ENA to account for the different attenuation in that region. Early work of this type was conducted by Nuttli (1979), Campbell (1981), and Algermissen et al (1976, 1982). More recently, ground motion records obtained in the near-source regions of ENA earthquakes indicate substantially more energy at high frequencies than do comparable records in California. This may reflect the generation of high-frequency energy by ENA faults (due perhaps to more small-scale heterogeneities) or may reflect greater ability of the Earth's crust and surficial rock to transmit these frequencies in ENA. In either case the assumption of similarity between California and ENA near-source ground motions likely is not valid; any difference in high-frequency content will affect response spectrum amplitudes at those high frequencies, and will have a particularly large effect on peak acceleration. For this reason, and because stress drops hypothesized to be different from California cannot be handled by these methods, they are not preferred.

Finally, "Intensity-based methods" use a qualitative intensity scale, typically the MMI scale, to estimate ground motion characteristics. In this method the dependence of MMI on earthquake size and source-to-site distance is quantified using equations calibrated with MMI observations from historical ENA earthquakes. From another region (typically California, where abundant instrumental records are available), correlations are developed between MMI and quantitative measures of ground motion (response spectrum amplitudes and peak acceleration and velocity). The two sets of equations are then combined, often by simple mathematical substitution, to obtain equations predicting ground motion as a function of earthquake size and distance in ENA. An exhaustive summary of studies that use these substitution methods is given in Bernreuter (1984). One major difficulty with these methods is that both the equation predicting MMI in ENA, and the equation converting MMI to ground motion amplitudes, are statistical correlations, not deterministic relationships. Mathematical substitution of one equation into the other leads to biased results (Cornell et al, 1979). A way to avoid these problems is to develop predictive statistical equations with the same independent variables for both steps (Veneziano, 1987), but this is difficult to accomplish and is almost never done in practice. Even if it were, it would still require the assumption that, for example, MMI = VIII is the same ground motion in ENA as in California, for the same earthquake magnitude, distance, and soil conditions. This is a strong assumption that is difficult to justify. Fundamental differences in ground motion amplitude, frequency content, contribution of different wave types, and duration of shaking could apply between ENA and California, and

still lead to the same MMI. Thus intensity-based methods should generally be given a low priority for the quantitative estimation of ground motion in ENA.

CONCLUSIONS

Estimates of strong earthquake ground motion in ENA are uncertain, because of the lack of instrumental data documenting this phenomenon and the perception that certain characteristics of earthquakes in ENA are different from those in California. The uncertainties can be characterized by the physical phenomena causing them, and can be modeled as alternative hypotheses that cannot be resolved given the scatter of available data. The important uncertainties are:

- The stresses released during ENA earthquakes. Are the dynamic stress drops different from California shocks, and if so, how are they different (in particular, do they increase with earthquake size)?

- The anelastic attenuation in ENA. Does it vary within the eastern part of the continent? What is the average anelastic attenuation for ENA?

- The effects of soils on earthquake ground motions. How have soils modified recorded ground motions, and how might they affect motion during future shocks? Particular uncertainty is attached to the response of shallow soils overlying competent bedrock, and whether geologic conditions of this type can be categorized sufficiently accurately to allow approximate amplification factors to be used without site-specific investigations.

Of available methods to estimate ground motion, the calibrated theoretical model is best able to represent these uncertainties in an explicit way, for engineering estimates of ground motion. Semi-theoretical methods based on California observations at near-source distances cannot reflect uncertainties in source characteristics, and intensity-based methods as usually applied are not theoretically sound.

It should be the goal of ground motion studies, and of seismic hazard and risk studies, to represent honestly the uncertainties in predicted ground motion amplitudes for earthquakes in ENA, and to determine the resulting uncertainty in hazard and risk. Only in this way will optimum solutions be found to mitigate earthquake risks.

ACKNOWLEDGMENTS

This research is part of a larger program being conduction by the Electric Power Research Institute under the direction of J. Carl Stepp to develop seismic wave attenuation curves for engineering use in the central and eastern United States. This source of support is gratefully acknowledged.

REFERENCES

Algermissen, S.T., and D.M. Perkins. "A probabilistic estimate of maximum acceleration in rock in the contiguous United States," U.S. Geol. Survey Open-File Rept. 76-416, 1976.

Algermissen, S.T. et al., "Probabilistic estimates of maximum acceleration and velocity in rock in the Contiguous U.S.," U.S. Geol. Survey Open-File Rept. 82-1033, 1982.

Atkinson, G.M. "Attenuation of strong ground motion in Canada from a random vibrations approach," Bull. Seis. Soc. Am., 74, 2629-2653, 1984.

Barker, J.S., P. G. Somerville, and J. P. MacLaren. "Wave propagation modeling of ground motion attenuation in the northeast United States and adjacent Canada," Proc., Workshop on Estimation of Ground Motion in the Eastern United States, EPRI Project RP2556-16 Rept., 1987.

Bernreuter, D.L., J.B. Savy, R.W. Mensing, and D.H. Chung. "Development of eastern United States ground motion models." Appendix C in "Seismic hazard characterization of the eastern United States: methodology and interim results for ten sites," U.S. Nuclear Reg. Comm. Rept. NUREG/CR-3756.

Boore, D.M. "Stochastic simulation of high-frequency ground motions based on seismological models of the radiated spectra," Bull. Seis. Soc. Am., 73, 1865-1984, 1983.

Boore, D.M., and G.M. Atkinson. "Prediction of ground motion and spectral response parameters in eastern North America," Bull. Seism. Soc. Am., 77, 440-467, 1987.

Brune, J.N. "Tectonic stress and the spectra of seismic shear waves from earthquakes" Jour. Geop. Res., 75, 4997-5002, 1971.

Brune, J.N. "Correction," Jour. Geop. Res., 76 5002, 1972.

Burger, R.W., P. G. Somerville, J. S. Barker, R. B. Herrmann, and D. V. Helmberger. "The Effect of crustal structure on strong ground motion attenuation relations in eastern North America," Bull. Seism. Soc. Am., 77, 1987.

Campbell, K.W. "A ground motion model for the central United States based on near-source acceleration data," Proc.,

Earthquakes and Earthq. Eng.: Eastern United States, Knoxville, 213-232, 1981.

Cornell, C.A., H. Banon, and A.F. Shakal, "Seismic motion and response prediction alternatives," Earthq. Eng. Struc. Dyn., 9, 9, 295-315. 1979.

Hanks, T.C. and R.K. McGuire. "Character of high-frequency strong ground motion" Bull. Seis. Soc. Am., 71, 2071-2095, 1981.

Kanamori, H. and C. R. Allen. "Earthquake repeat time and average stress drop," in Earthquake Source Mechanics, Maurice Ewing Symposium, 6, American Geophysical Union, 227, 1986.

Liu, H.L. and H. Kanamori. "Determination of source parameters of mid-plate earthquakes from the waveforms of body waves," Bull. Seism. Soc. Am., 70, 1989, 1980.

McGuire, R.K., A.M. Becker, and N.C. Donovan. "Spectral estimates of seismic shear waves," Bull. Seis. Soc. Am., 74, 1427-1440, 1984.

Nuttli, O.W. "The relation of sustained maximum ground acceleration and velocity to earthquake intensity and magnitude," Misc. Paper S-73-1, Report 16, U.S. Army Waterways Exp. Sta., Vicksburg, 74 p., 1979.

Nuttli, O.W. "Average seismic source parameter relations for mid-plate earthquakes," Bull. Seism. Soc. Am., 73, 519-535, 1983.

Nuttli, O.W. "Empirical magnitude and spectral scaling relations for mid-plate and plate-margin earthquakes," Tectonophysics, 93, 207, 1983.

Papageorgiou, A.S. "Earthquake source spectra--a comparison between western and eastern U.S. earthquakes," Proc., Workshop on Estimation of Ground Motion in the Eastern United States, EPRI Project RP2556-16 Rept., 1987.

Scholz, C., C. A. Aviles, and S. G. Wesnouski. "Scaling differences between large interplate and intraplate earthquakes," Bull. Seism. Soc. Am., 76, 65, 1986.

Shin, T.C., and R.B. Herrmann. "Lg attenuation and source studies using the 1982 Miramichi data," Bull. Seism. Soc. Am., 77, 1987.

Somerville, P.G., J.P. McLaren, L.V. LeFevre, R.W. Burger, and D.V. Helmberger. "Comparison of source scaling relations of eastern and western North American earthquakes," Bull. Seism. Soc. Am., 77, 322-346, 1987.

Toro, G.R. "Prediction of earthquake ground motions in eastern North America using simple models of source spectrum and wave

propagation," Proc., Workshop on Earthquake Ground-Motion Estimation in Eastern North America, EPRI Project RP2556-16 Rept., 1987.

Toro, G.R. and R.K. McGuire. "An investigation into earthquake ground motion characteristics in eastern North America." Bull. Seism. Soc. Am., 77, 468-489, 1987.

Veneziano, D. "The use of intensity data in ground motion estimation," Proc., Workshop on Earthquake Ground-Motion Estimation in Eastern North America, EPRI Project RP2556-16 Rept., 1987.

IMPLICATIONS OF EASTERN GROUND MOTION CHARACTERISTICS FOR SEISMIC HAZARD ASSESSMENT IN EASTERN NORTH AMERICA

Gail M. Atkinson
125 Dunbar Rd. S.
Waterloo, Ont. N2L 2E8

INTRODUCTION

There has been much recent work on the nature of ground motion in eastern North America (ENA) [Atkinson, 1984; Boore and Atkinson, 1987a; Toro and McGuire, 1987]. This has led to a new understanding of ENA ground motions, and in particular how they differ from better-observed western North American (WNA) ground motions [Boore and Atkinson, 1987b]. These differences in characteristics, combined with those in the occurrence rates of earthquakes, have important implications for seismic hazards in ENA.

The purpose of this paper is to review the salient features of ENA ground motions and their implications for seismic hazard, in simple engineering terms. Illustrative examples show typical expected response spectra for probability levels relevant to building codes and critical facilities. Conclusions are drawn as to how seismic hazard in ENA differs from that in the more active western regions.

CHARACTERISTICS OF ENA EARTHQUAKE OCCURRENCE

Ground Motion Characteristics

Understanding of the generation and propagation of seismic ground motion in ENA has advanced significantly in the past 5 years due to improvements in the empirical database, coupled with advances in theoretical modeling techniques. Until 5 years ago, the ground motion database for ENA consisted almost entirely of qualitative observations, such as maps of Modified Mercalli Intensity (MMI) from historical earthquakes. At present, the database contains about a hundred quantitative recordings, including peak ground accelerations, velocities, and response spectra. These records were gathered during recent moderate (magnitude > 4) earthquakes in New Brunswick, New Hampshire, New York, Ontario and Ohio. For some of these events there are strong motion recordings of the motions at distances close to the earthquake source [Weichert et al., 1982; Chang, 1983; Borcherdt, 1986], while other events were recorded by digital seismographic networks at distances of 100 to 1000 km [Atkinson, 1985].

Ground motion data show that ENA earthquakes have more energy at high frequencies than do western events. Western earthquakes exhibit a rapid decrease of ground motion amplitudes at frequencies above approximately 15 Hz [Hanks, 1982; Boore, 1983], whereas amplitudes for ENA events do not decline rapidly until frequencies of about 40 Hz or greater [Atkinson ,1984]. The high-frequency cutoff (often labelled fmax) may be a site effect [Hanks, 1982]; the relatively high fmax values in ENA could be attributed to the competent crustal conditions, which allow propagation of high-frequency energy. Alternatively fmax may be a source effect [Papageorgiou and Aki, 1981]. Because peak ground accelerations increase with increasing high-frequency content, higher values are observed in ENA than in WNA, for records at the same magnitude and distance [Atkinson, 1984]. This fact was not known prior to the recording of ENA earthquakes at near-source distances.

The quantitative database also shows that eastern ground motions decay more slowly with distance than do their western counterparts. This corroborates earlier MMI observations, which indicated that eastern earthquakes are felt at very large distances. The slower eastern attenuation is attributed to the relatively stable and unfractured crust.

The available ground motion data have been well-matched by a theoretical model (Atkinson, 1984; Boore and Atkinson, 1987a; Toro and McGuire, 1987]. The model, referred to as the stochastic model, has its origins in the work of Hanks and McGuire [1981], who showed that high-frequency ground motions can be treated as band-limited Gaussian white noise. The spectral amplitudes are determined by a seismological model of the source spectrum, filtered by regional attenuation properties. In the stochastic model, differences between eastern and western ground motions arise primarily from different fmax values, and from differences in anelastic attenuation. Different source properties and crustal constants are also factors. There is now reasonable confidence in ground motion relations derived using the model, although its validity for large magnitude earthquakes in ENA is still subject to ongoing debate concerning the underlying seismic source model [Boore and Atkinson, 1987a,b; Boore, 1988].

To illustrate the key differences between eastern and western ground motions, Figure 1 shows random horizontal acceleration time histories of simulated events of moment magnitude (M) 5 and 7, at hypocentral distances (R) of 10 and 100 km, for both regions. The simulations are based on the stochastic model, using the methodology of Boore [1983]. Note the much higher

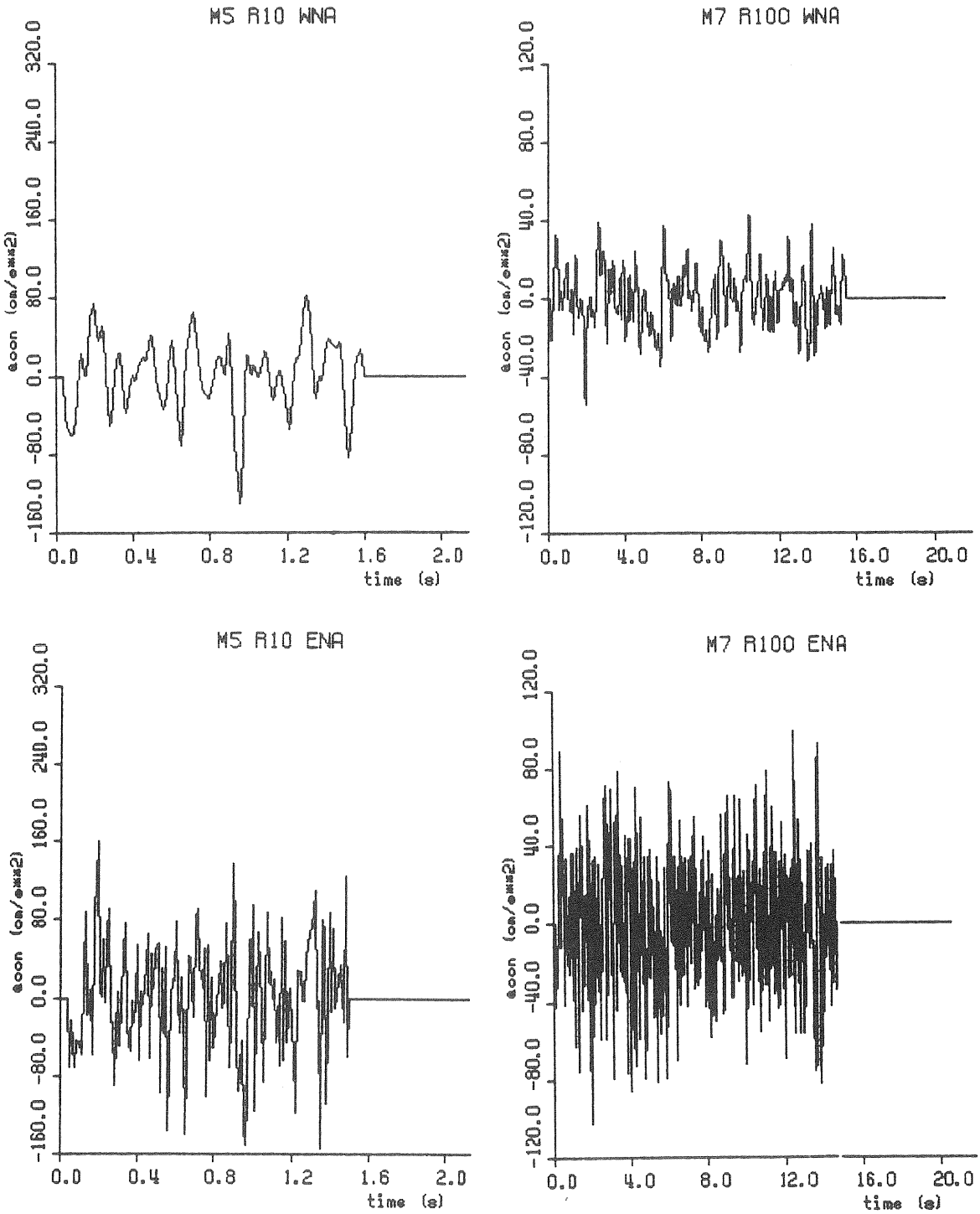

Figure 1. Simulated time histories for M 5 earthquake at R = 10 km, and M 7 at R = 100 km, for ENA and WNA.

frequency content of the eastern records, and the higher peak ground accelerations.

The higher peak ground acceleration (pga) values for eastern earthquakes do not necessarily imply a greater damage potential for most structures, because the eastern pga's are carried by frequencies higher than those to which most structures respond. Figure 2 illustrates the point by showing smoothed median response spectra (horizontal component) for events of M 5 and 7 at R = 10 and 100 km, for eastern and western events (from the relations of Boore and Atkinson [1987a], and Joyner and Boore [1982], respectively). The plots show the pseudo-acceleration (psa) values as a function of natural vibration frequency, for 5% of critical damping. The psa values are the maximum acceleration that a simple oscillator would experience during the ground motion. This method of depicting ground motions brings out their engineering significance, because many analysis methods for the response of structures use as their input the 'design' psa value for the natural frequency of the structure. (There may be more than one natural frequency if several modes of vibration are possible; the natural frequency of the structure is determined by analyzing its stiffness and geometry.) Because the psa values are directly related to structural response, higher psa values imply higher loads and thus greater damage potential.

The response spectral plots show that at distances close to the earthquake source, motions will be similar in the east and west for frequencies less than 10 Hz. This implies that the damage potential of the events would be similar for structures with vibration modes in this frequency range, such as most buildings, major dams and nuclear power plant reactor buildings. For frequencies above 10 Hz, psa values are higher in the east as a consequence of the higher fmax values. This may imply greater damage potential for high-frequency structures such as small concrete dams, and some nuclear power plant equipment; it also suggests that higher vibration modes may be important for many structures.

At large distances, the response spectra of eastern earthquakes are significantly higher than the equivalent western ones at all frequencies, due to the effects of differing attenuation rates. This implies that eastern earthquakes may cause damage (or at least be strongly felt) to greater distances than their western counterparts. Historical observations corroborate this prediction.

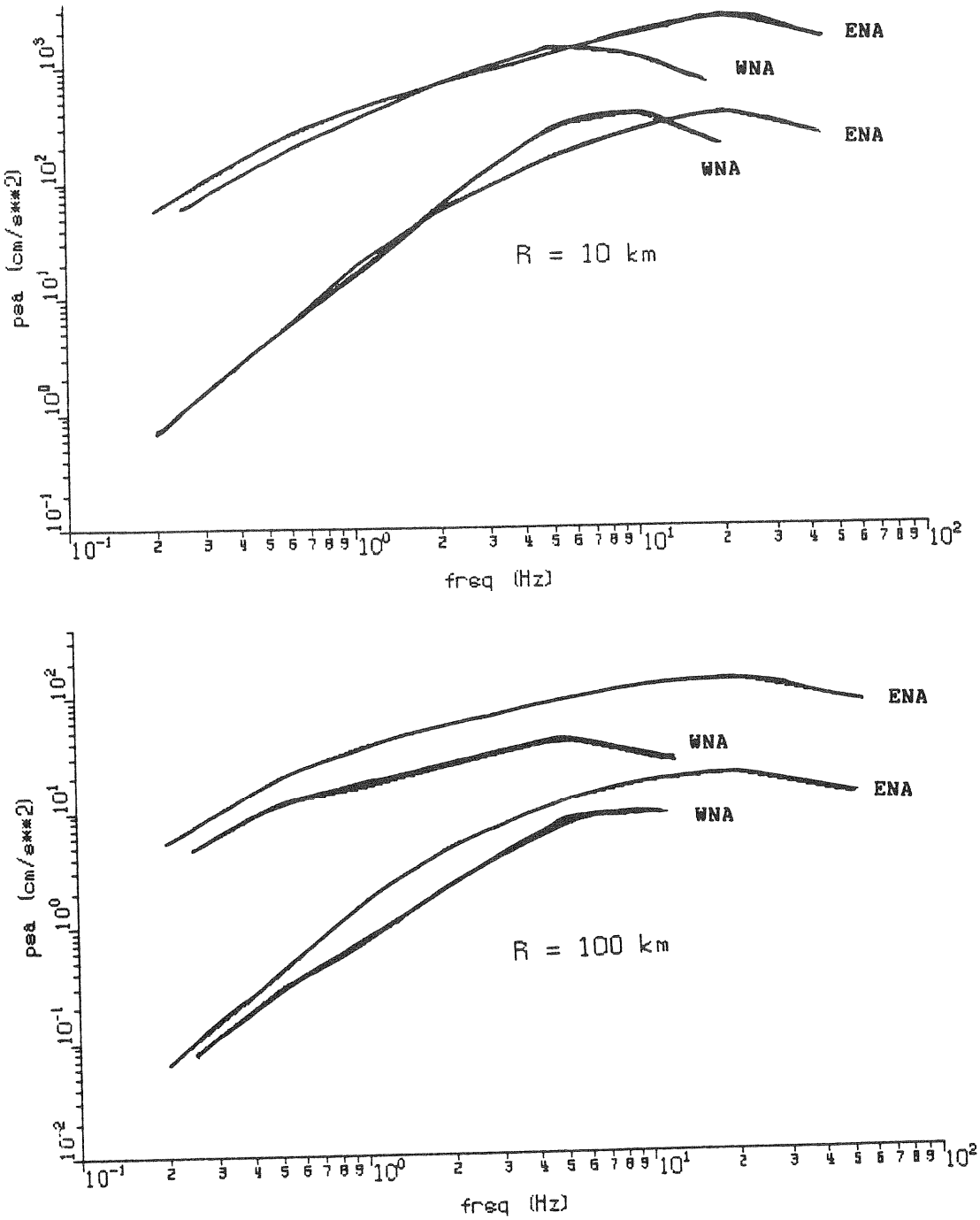

Figure 2. Median response spectra (5% damped) for M 5 and M 7 earthquakes at R = 10 and 100 km, for ENA and WNA.

Earthquake Occurrence Rates

Another important factor in comparing seismic hazards for different regions is differences in the occurrence rate of significant events. Figure 3 shows that although damaging earthquakes (say M > 5 to 6) are by no means restricted to WNA, they are certainly more frequent there, particularly in western California of course. In ENA, events tend to be more diffuse, correlate poorly with individual faults, and are relatively infrequent. There is considerable variability in seismicity patterns in ENA, with some areas (eg. Charlevoix, Quebec) being very active, some areas (eg. the Canadian prairies) nearly aseismic, and other areas (eg. the Appalachians; much of the St. Lawrence River valley) being moderately active.

As a broad generalization, one might say that earthquakes of any given magnitude are about 10 to 20 times more frequent in the active areas of California than in the moderately active regions that typify much of ENA. Of course, this implies greater hazard in the west than the east. As an interesting aside, however, note that this does not necessarily imply greater risk, since risk is also a function of consequence; it may be that the consequences of a large earthquake are more severe in many eastern areas due to the high population density. This paper does not attempt to treat this issue, and is restricted to comparing hazards only.

Another factor to consider when comparing eastern and western hazards is that maximum possible magnitudes (Mx) are likely higher in many active western regions than for most of ENA. Extended fault sources near the California coast would be capable of larger earthquakes than areas in the stable craton, for example. However, large events (M >7) have occurred in parts of ENA, often those underlain by ancient rift systems (eg. St. Lawrence River). This suggests that for many ENA situations Mx values may be similar to those for typical western fault systems, although the occurrence of such events may be less frequent.

SEISMIC HAZARD IMPLICATIONS

In this section, the combined effects of the differences in earthquake occurrence between ENA and WNA are considered. To illustrate the significance of the effects for seismic design of typical structures, a simple probabilistic hazard analysis is performed to obtain expected psa values for probability levels of 0.002 (500 year 'return period') and 0.0001 (10,000 year return period) per annum (p.a.). The 0.002 p.a. values are often used as the design basis in building codes for conventional structures, whereas the 0.0001

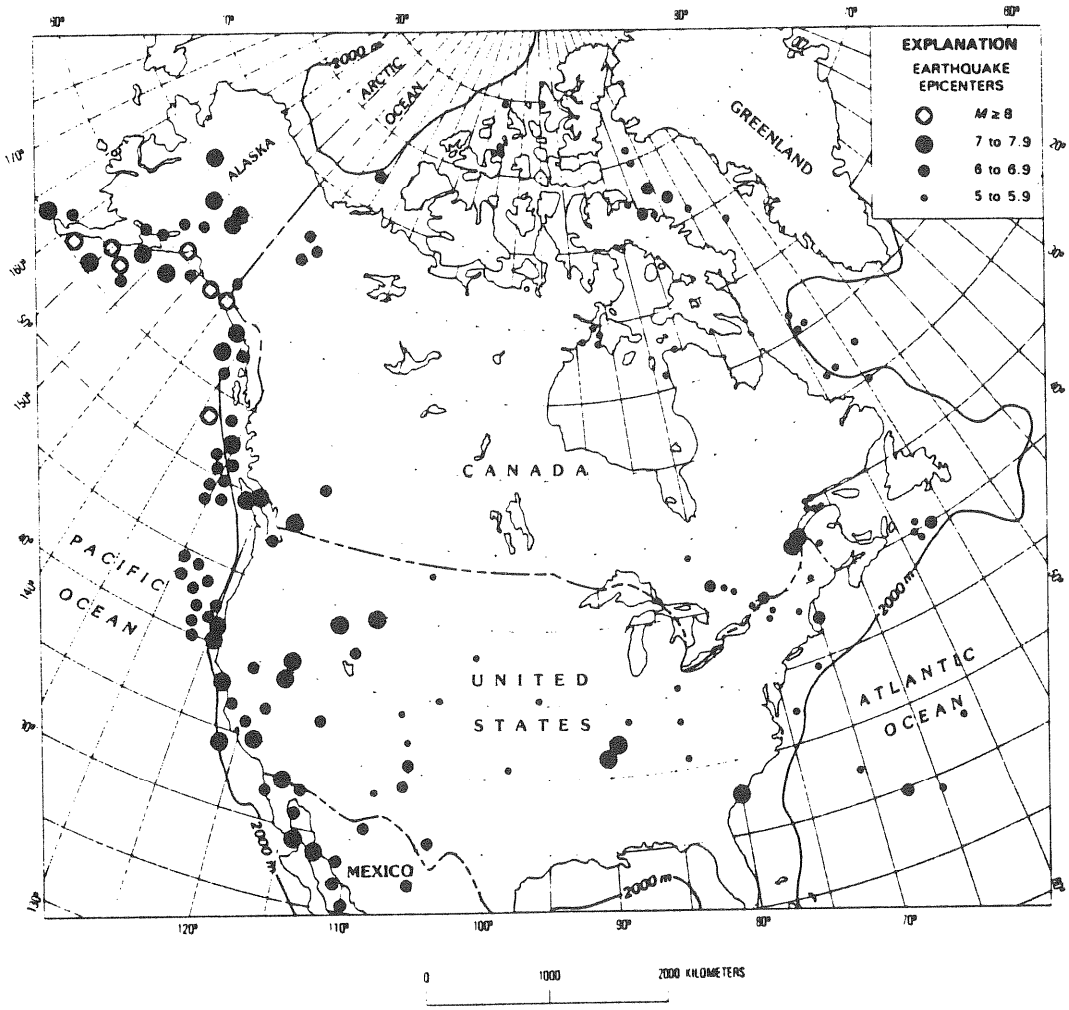

Figure 3. Epicenters of large (M > 6) historical earthquakes in North America. M > 5 events since 1930 also plotted for region east of 110 W. (after Page and Basham, 1985)

p.a. values are often used for critical facilities. The expected psa values for these probabilities are obtained by the Cornell-McGuire method [Cornell, 1968; McGuire, 1976, 1977]. The method integrates contributions to the exceedence probability of a specified psa value, at a given natural frequency, by summing over all possible magnitudes and distances. The input parameters to the calculations are the regional ground motion relations, and the earthquake occurrence rates and maximum magnitudes for all defined seismic source zones or faults.

For demonstration purposes, a large homogeneous source zone is assumed, about 200 km by 200 km, with the site located in the middle. Ground motion relations (for 5% damped horizontal psa) are assumed to be as given by Boore and Atkinson [1987a] for ENA, and by Joyner and Boore [1982] for WNA. (The effects of fault rupture length and different distance definitions are ignored for this illustration.) For the eastern example, earthquake occurrence rates within the zone are chosen so as to be fairly typical of moderately active areas. Accordingly, it is assumed that the rate for M 5 is N5 = 0.02, and the recurrence relation has slope b = 0.9 (also a typical value). For the western example, it is assumed that N5 = 0.4, and b = 0.9, typical of an active western area. These parameters mean that in the eastern zone a M 5 event would occur once in 50 years on average, a M 6 once in 400 years, and a M 7 once in 3200 years. In the western zone a M 5 would occur on average once in 2 years, a M 6 once in 20 years, and a M 7 once in 160 years. For both regions it is assumed that the maximum possible magnitude is 7.25.

Figure 4 shows the results of the hazard analysis, for probability levels 0.002 and 0.0001 p.a., for both the eastern and western cases. The important feature to note is the difference in the shape of the expected ENA spectra, relative to the WNA case. Expected psa values for the two cases are similar for frequencies of about 20 Hz, because the high-frequency content of eastern earthquakes is offset by the lower occurrence rates. For lower frequencies, the hazard is much greater in WNA. Note that the differences at low frequencies would be even more pronounced if a lower Mx value for the eastern region, relative to the western region, had been assumed.

The difference in shape of the expected spectra has important implications. First, any attempt to scale spectra to an index parameter such as pga would have to follow very different rules of thumb in the east than those devised for WNA, or the result would be gross overconservatism for low frequencies. Standard

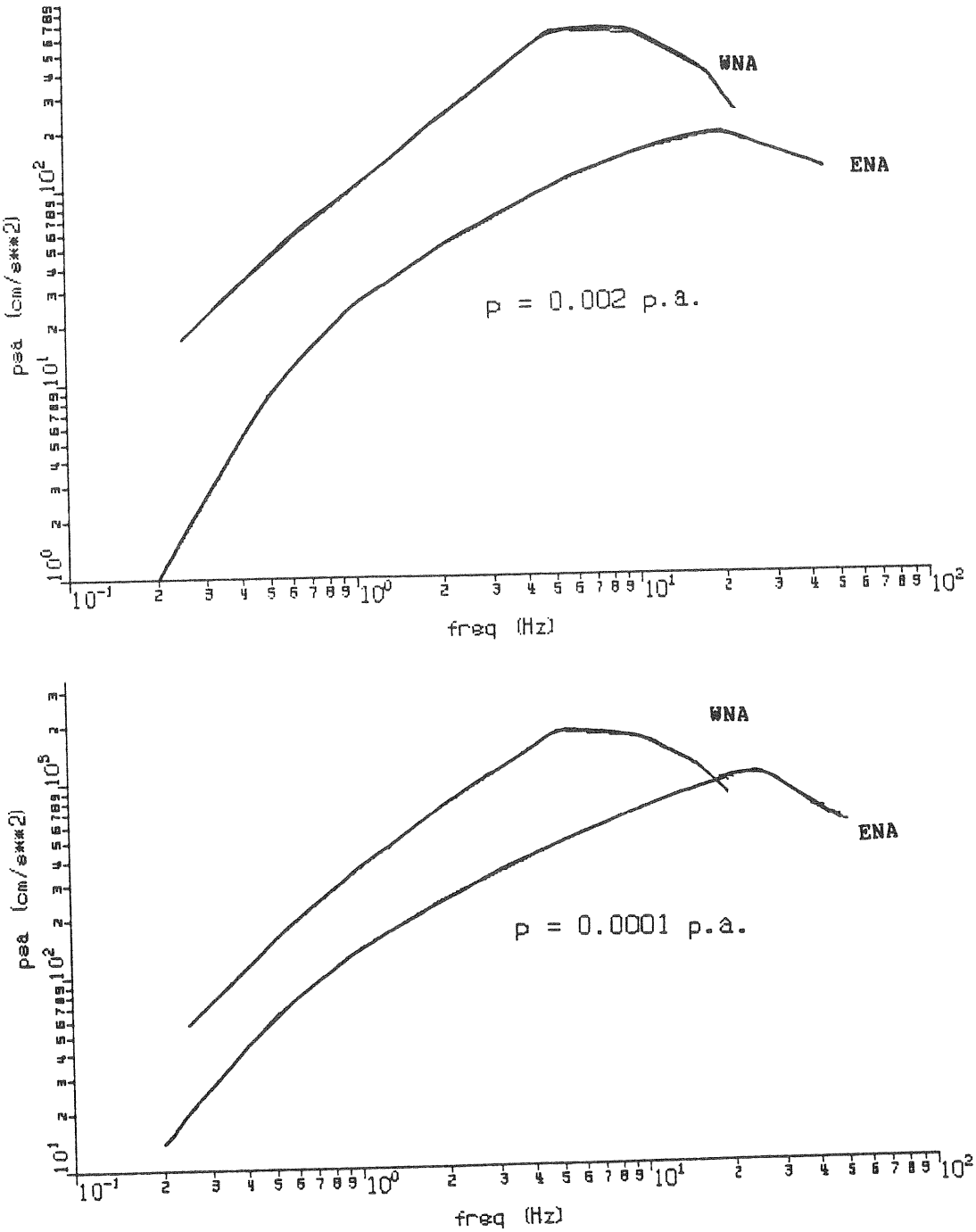

Figure 4. Expected response spectra (5% damped) for WNA (upper curves) and ENA (lower curves) examples, for probabilities of 0.002 and 0.0001 per annum.

spectra such as those developed by Newmark, Blume and Kapur for NRC Regulatory Guide 1.60 should not be used. In any event they are unnecessary since expected spectra can easily be calculated without resort to scaling by peak ground motion parameters.

Another consequence of the difference in shape is that it implies a fundamental difference in the nature of the hazard in ENA. For structures with significant high-frequency modes of vibration, the hazard may be just as great in much of ENA as for active areas of California. For structures with longer periods, the hazard will be much less in ENA. Thus generalizations about earthquake hazards derived from California experience cannot simply be 'transported' to the east on a scaled-down level. The types of structures at risk, and the types of damage to be expected, are potentially different.

CONCLUSIONS

The nature of seismic hazard in ENA differs from that in WNA due to the combined effects of differences in the character of ground motion, and in recurrence rates. Expected spectra for a constant probability level, which are a good indication of appropriate seismic design parameters and/or damage potential, have different shapes in the two regions. High-frequency structures in many parts of ENA face a hazard comparable to that in many active areas of California, whereas the hazard for low-frequency structures in ENA is relatively modest.

REFERENCES

Atkinson, G., Attenuation of strong ground motion in Canada from a random vibrations approach, Bull. Seism. Soc. Am., 74, 2629-2653, 1984.

Atkinson, G., Ground motions from moderate earthquakes recorded by the Eastern Canada Telemetered Network, Earth Phys. Branch Open-file Rpt. 85-5, 76pp, 1985.

Boore, D., Stochastic simulation of high-frequency ground motions based on seismological models of the radiated spectra, Bull. Seism. Soc. Am., 73, 1865-1894, 1983.

Boore, D., Quantitative ground motion estimates, Proc. NYAS Symposium on Earthquake Hazards and the Design of Constructed Facilities in the Eastern United States, New York City, 24 - 26 Feb., 1988.

Boore, D. and G. Atkinson, Stochastic prediction of ground motion and spectral response parameters at hard-rock sites in eastern North America, Bull. Seism. Soc. Am., 77, 440-467, 1987a.

Boore, D. and G. Atkinson, Notes on the prediction of ground motion and response spectra at hard-rock sites in Eastern North America, Proc. EPRI Workshop on Strong Ground Motion Predictions in ENA, Palo Alto, March 31 - Apr. 2, 1987b.

Borcherdt, R., Preliminary report on aftershock sequence for earthquake of January 31, 1986 near Painesville, Ohio, U.S. Geol. Surv. Open-file Rpt. 86-181, 1986.

Chang, F., Analysis of strong motion data from the New Hampshire earthquake of 18 Jan. 1982, U.S. Nuclear Reg. Commission, NUREG/CR-3327, 1983.

Cornell, C., Engineering seismic risk analysis, Bull Seism. Soc. Am., 58, 1583-1606, 1968.

Hanks, T., fmax, Bull. Seism. Soc. Am., 72, 1867-1879, 1982.

Hanks, T. and R. McGuire, The character of high-frequency strong ground motion, Bull. Seism. Soc. Am., 71, 2071-2095, 1981.

Joyner, W. and D. Boore, Prediction of earthquake response spectra, Proc. 51st Annual Conv. Struct. Eng. Assoc. Calif., 1982.

McGuire, R., FORTRAN computer program for seismic risk analysis, U.S. Geol. Surv. Open-file Rpt. 76-67, 1976.

McGuire, R., Seismic design spectra and mapping procedures using hazard analysis based directly on oscillator response, Intl. J. Earthq. Eng. Struct. Dyn., 5, 211-234, 1977.

Page, R. and P. Basham, Earthquake hazards in the offshore environment, U.S. Geol. Surv. Bulletin 1630, 1985.

Papageorgiou, A. and K. Aki, A specific barrier model for the quantitative description of inhomogeneous faulting and the prediction of strong ground motion, Proc. U.S. Geol. Surv. - Nuclear Reg. Commission Workshop on Strong Motion, Lake Tahoe, Oct., 1981.

Toro, G. and R. McGuire, An investigation into earthquake ground motion characteristics in eastern North America, Bull. Seism. Soc. Am., 77, 468-489, 1987.

Weichert, D., P. Pomeroy, P. Munro and P. Mork, Strong motion records from Miramichi, New Brunswick, 1982 aftershocks, Earth Phys. Branch Open-file Rpt. 82-34, Ottawa, 1982.

Topic 4

Geological Site Effects and Soil-Liquefaction

R. Dobry: *Some Basic Aspects of Soil Liquefaction During Earthquakes*

A. M. Rogers, J. C. Tinsley and R. D. Borcherdt: *Predicting Relative Ground Response*

C. Soydemir: *Liquefaction Criteria for New England: A Design Engineer's Overview*

C. J. Costantino and C. A. Miller: *Geotechnical Soil Properties in the Greater New York City Metropolitan Area and Their Impact on Transit Facilities*

M. Budhu, V. Vijayakumar, R. F. Giese and L. Baumgras: *Liquefaction Potential of Soils in Portions of Upper Manhattan and Buffalo*

M. P. Tuttle, L. Seeber and L. Bradley: *Liquefaction of Glaciomarine Sediments During the 1727 Earthquake in Newburyport, Massachusetts*

S. F. Obermeier, R. E. Weems and R. B. Jacobson: *Earthquake Induced Liquefaction Features in the Coastal South Carolina Region*

S. G. Wesnousky, E. S. Schweig, S. K. Pezzopane: *Observations of Soil Liquefaction in the New Madrid Seismic Zone*

SOME BASIC ASPECTS OF SOIL LIQUEFACTION DURING EARTHQUAKES

Ricardo Dobry
Dept. of Civil Engineering
Rensselaer Polytechnic Institute
Troy, New York 12180

INTRODUCTION

Seismic liquefaction of saturated sand deposits under level or almost level ground is an important cause of damage, both to the ground itself and to structures supported by (or buried in) the soil. Much research has been done on the subject which has clarified significant aspects, including: the basic character of cyclic shear strain amplitude in determining the rate of pore water pressure buildup, and the proven usefulness of empirical charts based on in situ Standard Penetration Tests (SPT), see Dobry et al. [1982], Seed et al. [1983] and NRC [1985].

However, some issues of great relevance to engineers are still not clear and are under discussion. They include the relative importance of partially drained versus purely undrained failure mechanisms, and the associated problem of the engineering significance of sand boil observations, NRC [1985], Castro [1987]. This paper explores those issues in the light of available field, laboratory and analytical evidence. Possible answers are proposed, and it is suggested that a main reason why the SPT charts work is because of the strong correlation between penetration measurements and the amount of water expelled by the liquefied sand.

PORE PRESSURE BUILDUP

Figure 1 sketches the typical situation in the field. A liquefiable saturated sand layer is located at a certain depth, overlain by a nonliquefiable stratum. This shallow layer includes all soils above the groundwater level, as well as submerged soils which are not susceptible to liquefaction because of their high density, cohesion, etc. (Ishihara [1985]). Excess pore pressures can develop in the liquefiable layer because of the cyclic shear straining induced by the earthquake shaking. As sketched in Fig. 1, the ground seismic accelerations a are associated with shear stresses τ, with τ being proportional to a. A more useful parameter is the associated shear strain, $\gamma = \tau/G$, where G is the shear modulus of the sand. Although G varies with γ because of the nonlinear stress-strain behavior of soil, G can be computed once its small-strain value, G_{max}, is known, and G_{max} is in turn readily obtained from in situ geophysical measurements of shear wave velocity (Dobry et al. [1981,1982], Sykora and Stokoe [1982], NRC [1985]).

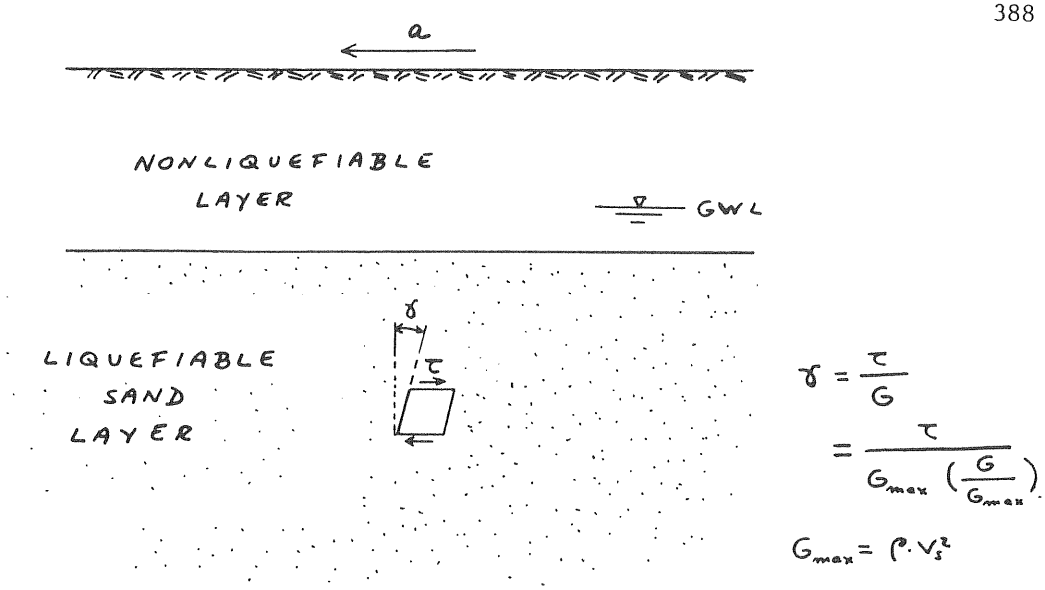

Figure 1. Typical soil and seismic loading conditions in liquefaction problem.

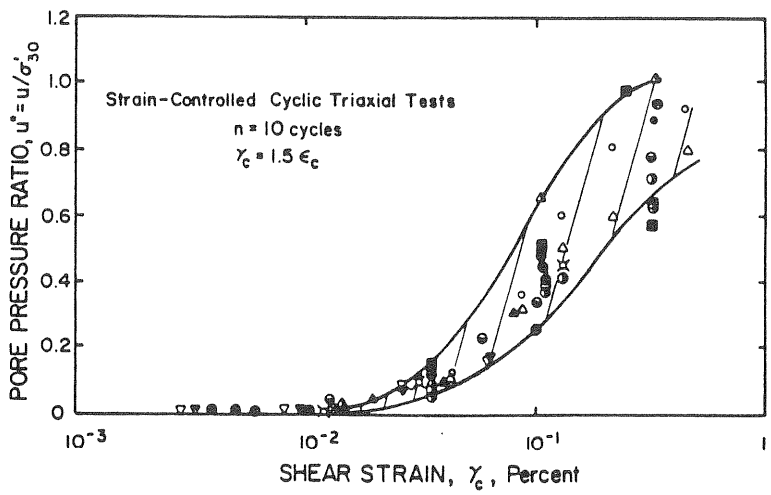

Figure 2. Pore pressure ratio in sands versus cyclic shear strain after ten cycles (correlation developed by the author and included in the NRC [1985] report).

Figure 2 presents the influence of cyclic strain amplitude, γ_c, on the pore pressure ratio after ten cycles; this correlation includes all available laboratory data and is valid for both loose and dense sands, as well as for clean and silty sands. The plot is very consistent, and it shows that any liquefiable sand deposit subjected to earthquake cyclic loading in one horizontal direction, having an equivalent duration of shaking of 10 cycles, will develop a pore pressure ratio, $u^* \approx 1$, if the induced γ_c is about 0.3 % or larger. For the usual calculations of seismic strain using a measured G_{max} and nondegraded G/G_{max}, a more relevant value to enter the plot is $u^* \approx 0.5$, as De Alba et al. [1975] have shown that once u* reaches 0.5, the soil weakens significantly, and the seismic strains and excess pore pressure increase rapidly during further earthquake loading. A new $\gamma_c \approx$ 0.1% is obtained for $u^* = 0.5$ and 10 cycles, which is further reduced to $\gamma_c \approx 0.06$ % once the influence of the second horizontal acceleration component is considered (Vucetic et al. [1987]). The corresponding value for a longer earthquake duration of 30-50 cycles is $\gamma_c \approx 0.04$ %.

SAND BOIL GENERATION

Liu and Qiao [1984] have reported shaking table experiments on stratified sand which clarify the mechanics of sand boil generation during earthquakes, both in the free field and around structures. One of these tests is reproduced in Fig. 3. Both in the free field and at great depths under the foundation, $u^* \approx 1$ was reached during the shaking. Significant amounts of water expelled from the pores of the soil accumulated under the more impervious layers, forming there "water interlayers". Sand boiling occurred when one of these water interlayers broke up to the ground surface.

In Liu and Qiao's tests, the liquefiable sand deposit extends to the ground surface. As pointed out by Ishihara [1985], a much more common situation which can also produce sand boils is that of Fig. 4, where a liquefiable sand stratum of thickness H_2 is located under a nonliquefiable layer of thickness H_1. If the sand stratum reaches a pore pressure ratio u* close to 1 due to the shaking, it will reconsolidate, and the water expelled will tend to flow upwards to the ground surface. This can induce significant vertical gradients in the upper layer, as sketched in the figure. These gradients, and the possibility that sand boils do appear, will be enhanced if the upper soil is thin (small H_1), relatively impervious and incompressible, and has vertical fissures or cracks. Features of the liquefiable layer which help the process are a large compressibility and thickness H_2 (which increase the total volume of water available for upward flow), and a large permeability (which makes the water available fast). (See Housner [1958], Ambraseys and Sarma [1969], Yoshimi and Kuwabara [1973], and Castro [1987].) In this latter publication, Castro suggests that the relative infrequent observed occurrence

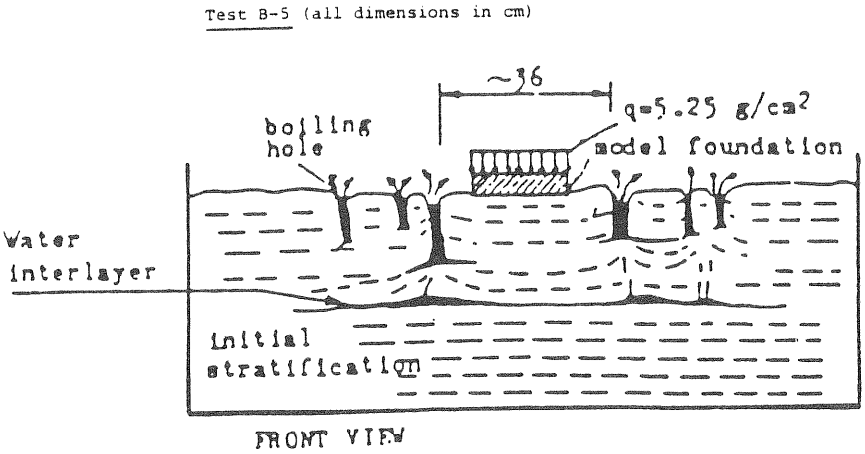

Figure 3. Shaking table test of stratified sand deposit (after Liu and Qiao [1984]).

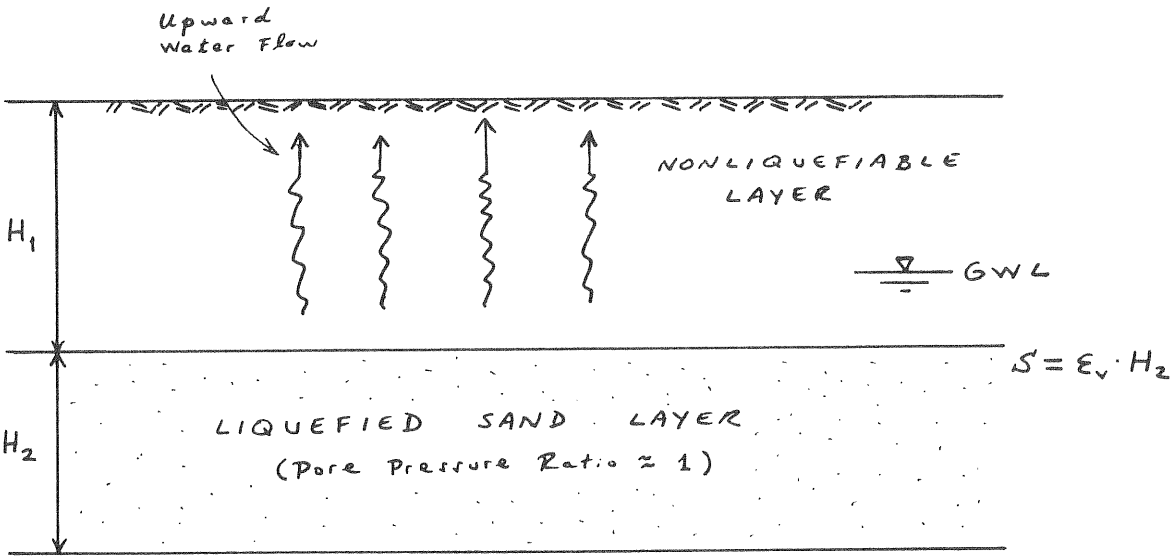

Figure 4. Upward water flow after liquefaction of lower layer.

of sand boils generated by the reconsolidation of silty sands is due to the low permeability of these soils.

Therefore, sand boils are mainly an indication of high upward gradients in the layer located between the ground surface and the stratum liquefied by the earthquake, caused by the water expelled by this lower liquefied stratum. In cases in which the upper layer is also made up of sand, high gradients have been oberved to produce a delayed liquefaction of this layer near the ground surface ("quicksand phenomenon"), often after the end of the shaking, as described in the next section. On the other hand, the fact that the lower stratum develops large values of u* ("it liquefies") does not automatically mean that high gradients and sand boils will appear in the upper layer; this may or may not occur depending on the other factors previously mentioned.

SAND BOILS AND ENGINEERING FAILURE

As noted by Castro [1987], sand boils by themselves are of very little engineering significance. They are potentially more important as indicators of the existence of water interlayers such as shown in Fig. 3, and of high gradients in the upper layer overlying the liquefied deposit. The NRC [1985] report defined several possible failure mechanisms which could produce a loss of stability of liquefying terrain, due to a decrease of the soil shear strength in the presence of driving (static) shear stresses. Two of those mechanisms are directly relevant to this discussion. In Mechanism B, a loose film of soil with a high water content and reduced shear strength develops at the top of the liquefied layer, similar to the "water interlayers" of Fig. 3, and the failure surface passes by this film (see also Seed [1986]). In Mechanism C, the high upward gradients near the ground surface decrease the effective stresses acting on the soil, with the corresponding decrease in shear strength of the shallow layer, which may cause heavy structures supported by it to sink or tilt, and buried light structures to float up. Therefore, mechanisms B and C are directly related to the same phenomena which generate the sand boils; and the engineering significance of sand boils as indicators will depend on how important are these two failure mechanisms in explaining observed engineering failures. The practical importance of the sand boil issue derives from the fact that the existence or nonexistence of sand boils after an earthquake is often taken as the same thing as stating that the site did (or did not) liquefy. Also, the SPT charts by Seed et al. [1983] are partially based on sand boil observations.

A cursory review of the literature reveals that, indeed, the appearance of sand boils and observations of upward water flow are well correlated with most types of engineering damage and ground failure caused by liquefaction. Photos taken for about half an hour starting immediately after the end of shaking, in an area which liquefied in Niigata, Japan in the 1964 earthquake,

reveal that strong water boiling started within 2-3 minutes after the end of shaking and lasted for about 20 minutes; the Annex building moved horizontally 2 meters after boiling had started (Soil and Foundation [1965]). In fact, most of the damage to structures in this earthquake was caused by the upward water flow near the ground surface. Summarizing a number of field observations for the same city and event, Ambraseys and Sarma [1969] state: "fountains of water continued to play for nearly 20 minutes after the earthquake...settlements and tilts (of buildings) occurred gradually during some minutes of time following the earthquake and considerable time, possibly many minutes, elapsed whilst structures continued not only to settle and tilt, but also to rise." A lateral spread ground failure occurred in part of the Heber Road site during the Imperial Valley, California earthquake of 1979, accompanied by many sand boils; another part of the site, located on denser sand, did not fail and did not exhibit sand boils (Youd and Bennett [1983]). A number of examples for other earthquakes are cited by Housner [1958], Ambraseys and Sarma [1969] and Tohno and Yasuda [1981].

VOLUME OF WATER EXPELLED BY LIQUEFIED LAYER

A key parameter in the development of water interlayers, high upward gradients near the ground surface and sand boils, as well as of engineering failures having mechanisms B or C, is the total volume of water expelled by the liquefied sand layer in Fig. 4. If this water volume is very small, it will not be able to sustain the process, and no liquefaction effect of any kind may be observed in the upper layer, even if $u^* \approx 1$ in the liquefied layer. This water volume is measured by the settlement S of the liquefied layer, and it is $S = \epsilon_v \cdot H_2$, where ϵ_v = permanent volumetric strain of the soil. Therefore, it should be expected that both H_2 and ϵ_v play a role in controlling the appearance of sand boils and engineering failure, after the earthquake generates large pore pressures in the liquefied layer.

Ishihara [1985] discussed in detail the thickness H_2 necessary for surface manifestations of liquefaction, and related it to the thickness H_1 of the nonliquefiable layer. For the 1964 Niigata earthquake, he concluded that surface manifestations took place only when $H_2 > 3$ m and $H_1 < 3$ m; this criterion is also consistent with observations from the 1977 Vrancea, Rumania earthquake and the 1979 Monte Negro, Yugoslavia earthquake. Figure 5 presents a similar correlation for the 1983 Nihonkai-Chubu, Japan event. Finally, Ishihara also reproduced a qualitatively similar correlation between H_1 and H_2 obtained by Chinese researchers after the 1976 Tangshan earthquake. In summary, there is overwhelming evidence that, for a given earthquake and type of soil profile, it is not enough that high pore pressures develop at depth for ground failure and other surface manifestations of liquefaction to happen; in addition, H_2 must be large enough and H_1 must be small enough. An illustrative example from Niigata is presented in Fig. 6, which includes

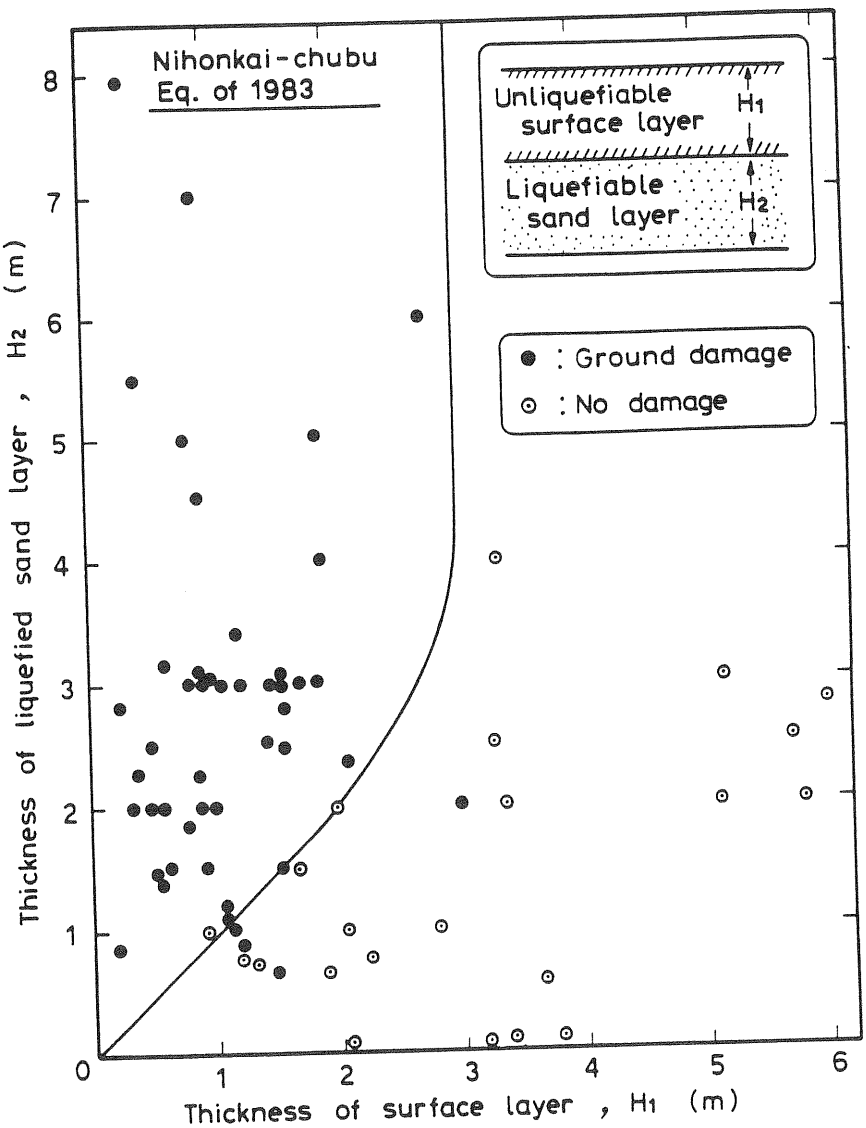

Figure 5. Liquefaction, ground damage and layer thicknesses in 1983 Nihonkai - chubu earthquake (after Ishihara [1985].

profiles from two sites: one which exhibited surface evidence of liquefaction (River Site), and another where this did not happen (South Bank Site). Both sites were subjected to essentially the same shaking, both have about 1 m of nonliquefiable surface soil, the groundwater level is at the same depth, and both contain very loose sandy soils below the surface layer. The difference is that the very loose layers, which must have developed $u^* \approx 1$ during the shaking, have a total thickness of more than 10 m at the River Site and only about 2 m at South Bank Site. Another factor which may have also contributed to this different performance is the fact that the very loose layer between 2 and 4 m in the South Bank site profile is predominantly silt, and thus has a low permeability

The second factor determining the value of S is the volumetric strain ϵ_v, which is mostly related to the degree of compaction or relative density of the sand. There are three main sources of information to estimate ϵ_v. The first are laboratory data on reconsolidation of sands after developing $u^* \approx 1$ by undrained cyclic loading (Yoshimi and Kuwabara [1973], Lee and Albaisa [1974], Bhatia [1980]). The second are laboratory data on drained compaction of sand by cyclic straining, such as provided by Silver and Seed [1971] and illustrated in Fig. 7; this would correspond to the assumption that the excess water is completely expelled from the sand in the field while the shaking is still taking place. The third source of information are measurements of surface settlement S and calculation of $\epsilon_v = S/H_2$, from the field after actual earthquakes (Lee and Albaisa [1974]) and from model centrifuge tests after simulated earthquakes (Whitman et al. [1981]). From all these measurements, a range of $\epsilon_v \approx 1.5$ to 5 % is obtained for loose sand, while a much smaller value, of the order of $\epsilon_v \approx 0.2$ % or less is estimated for very dense sand. The highest values of ϵ_v for loose sand (~ 3-5%), were obtained from the field observations and centrifuge tests, probably due to the much higher cyclic strains developed in the loose sand layer once $u^* \approx 0.5$ to 1; this phenomenon occurs to a much lesser extent in dense sand. Therefore, it is reasonable to estimate that, typically, ϵ_v is 0.2 % or less in a very dense sand and 3-5% in a loose sand. **That is, other things being equal, the amount of water expelled by a very loose sand can be as much as fifteen or twenty times larger than if the sand is dense !**

An example of the effect of this difference in ϵ_v values for loose and dense sand is provided by the liquefaction in the Heber Road Site, caused by the 1979 Imperial Valley, California earthquake. This case history, already mentioned, was reported by Youd and Bennett [1983] and is also discussed by Vucetic et al. [1987]. The profile of the site is reproduced in Fig. 8. The stratigraphy is essentially identical throughout the site: about one meter of artificial sand fill (nonliquefiable layer) above the water table, underlain by about 4 m of saturated silty sand (liquefiable layer) followed by clay. The site was within 2 Km of the fault rupture for this magnitude 6.6 event, and strong motions at comparable distances from the fault indicate thatthe

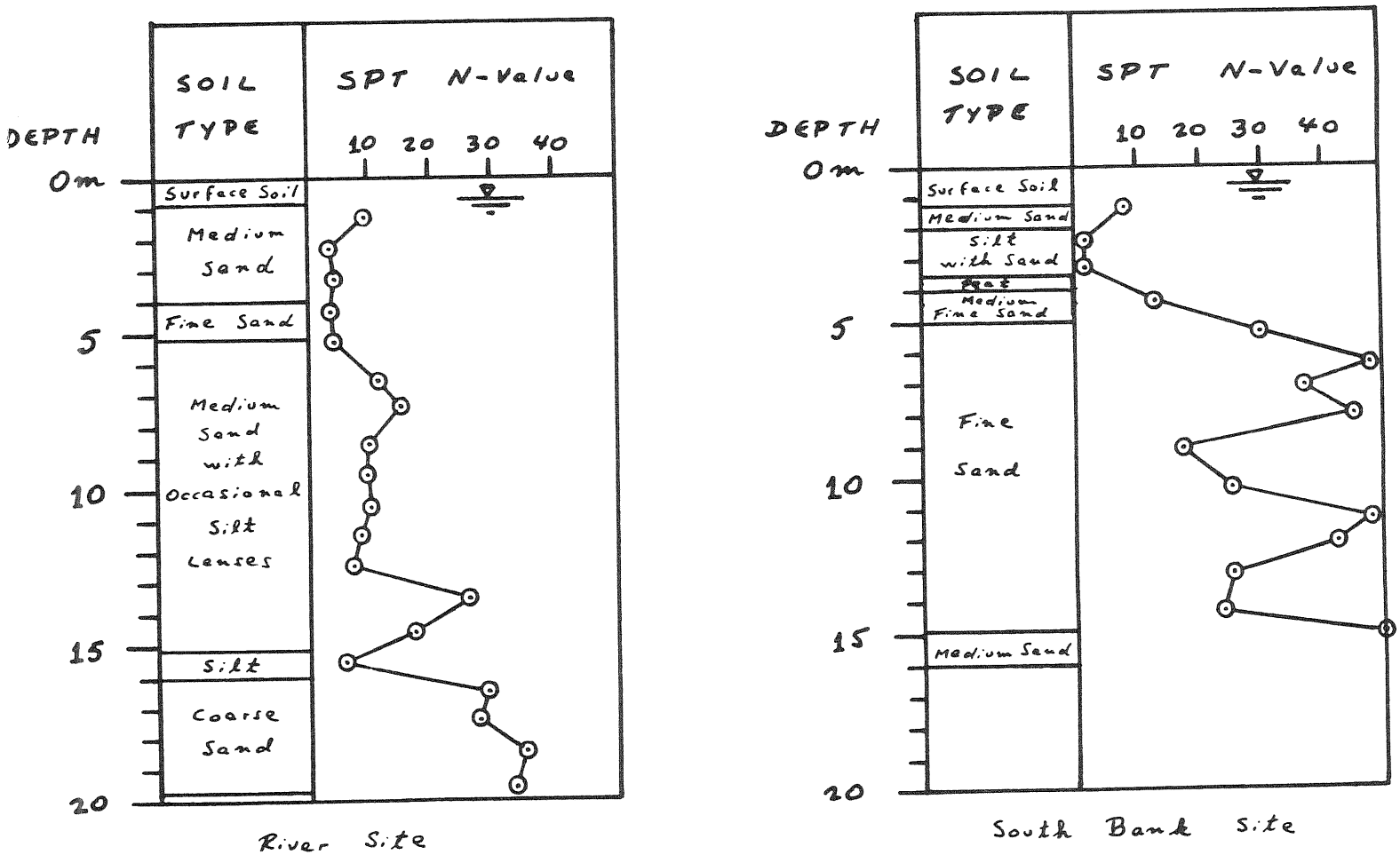

Figure 6. Soil profiles which exhibited surface evidence of liquefaction (River Site) and which did not (South Bank Site) during the 1964 Niigata earthquake (modified after Ishihara [1985]).

site was subjected to very large accelerations, of the order of 0.5 g or greater. Shear wave velocity measurements performed at the site by Sykora and Stokoe [1982] allowed Vucetic et al. [1987] to perform a detailed study of the seismic strains and pore pressures induced in the liquefied layer by the earthquake. In this last paper it is concluded that high values of $u^* \approx 1$ developed in the liquefiable layer throughout the whole site. However, although extensive sand boiling, cracking and lateral spreading did in fact occur at that part of the site labelled A_2 in Fig. 8, corresponding to very low SPT values between 1 and 7 blows/foot, none of these effects was observed in another part, labelled A_1, which had high SPT values between 29 and 36 blows/foot. After the previous discussion, the explanation for this dramatic difference in behavior was clearly the much larger value of ϵ_v in the loose sand A_2 compared with the dense sand A_1.

WHY DO THE SPT LIQUEFACTION CORRELATIONS WORK?

Until about ten years ago, the usual belief was that the SPT empirical correlations proposed by several authors to predict liquefaction were successful because the SPT, after correcting for the effect of overburden pressure, measures essentially the degree of compaction or relative density of the sand. The reasoning went like this: liquefaction in the field, including surface manifestations and engineering ground failure, occurs when a saturated sand layer at a certain depth reaches $u^* \approx 1$. For a given intensity of earthquake shaking (as measured by the cyclic stress ratio), undrained cyclic stress-controlled tests showed that the number of cycles of stress needed to reach the $u^* \approx 1$ condition was more or less uniquely related to the relative density of the sand. Therefore, the field SPT measures the key parameter (relative density) controlling rate of undrained pore pressure buildup and thus also liquefaction failure. Extensive laboratory investigations showed later that this picture was too simplistic, and that a number of factors jointly control the rate of pore pressure buildup in stress-controlled tests, with relative density being only one of them. These other factors include the method of sample preparation or fabric effect, preshaking of the soil, lateral earth pressure coefficient and overconsolidation, and increased time under pressure (aging effect), see Seed [1979]. In that paper, Seed suggested that the effect of all these factors on SPT is similar to their effect on pore pressure buildup, and this explains why the SPT charts work. The author (Dobry et al. [1982]) proposed an alternative explanation: that the main reason for the success of the SPT is that penetration values are correlated to shear wave velocity and G_{max}, which control pore pressure buildup through their effect on the amplitude of the seismic shear strain. Both of these explanations by Seed and Dobry share a main feature: they focus on the undrained pore pressure buildup, and the reaching of high values of u^* is assumed to be equivalent with liquefaction surface manifestations and associated ground failure.

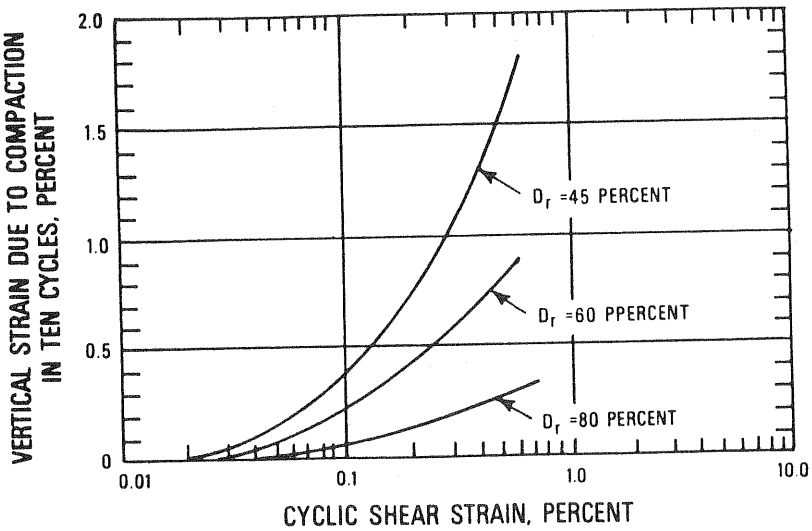

Figure 7. Volumetric strain ε_v due to compaction of sand after ten cycles, versus cyclic shear strain γ_c and relative density of soil (after Silver and Seed [1971]).

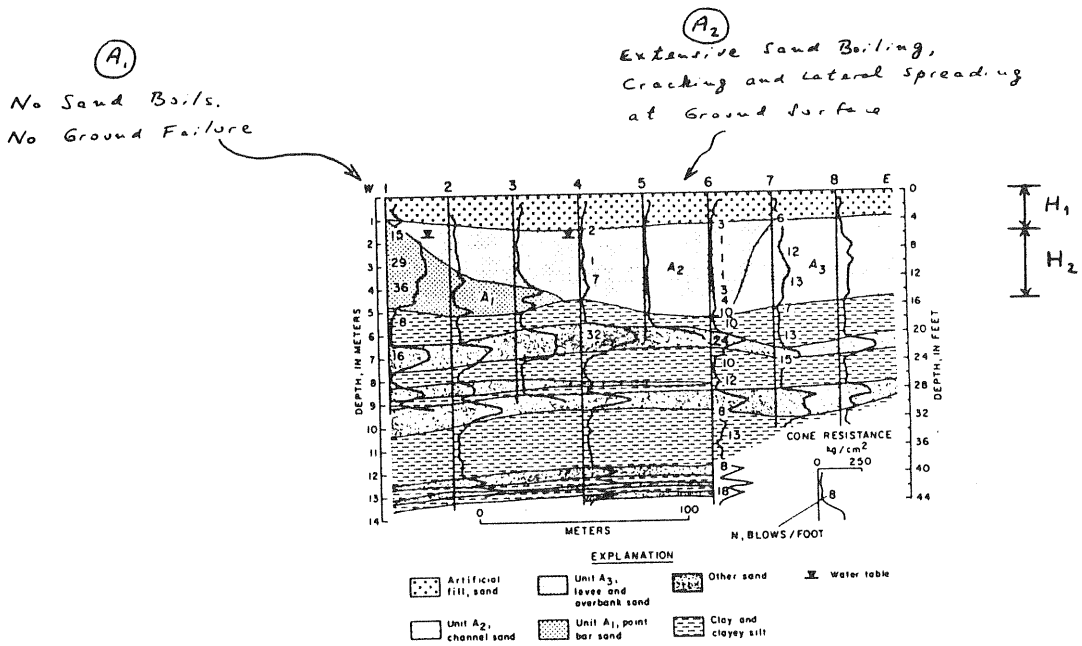

Figure 8. Soil conditions and surface manifestations of liquefaction, Heber Road Site, 1979 Imperial Valley earthquake (after Youd and Bennett [1983]).

However, the discussion above - including the evidence from the Heber Road Site case history - suggests that in addition to its relation with G_{max}, another key to the success of the SPT lies in its correlation to relative density and hence to ϵ_v. That is, both the penetration measurements and ϵ_v are very sensitive to changes in the density of the sand, and as a result the SPT correlates well with ϵ_v.

For example, Fig. 9 shows the analysis of the liquefaction at Heber Road Site performed by Youd and Bennett [1983] for the 1979 event, using Seed's SPT charts for earthquake magnitudes M = 6.6 and 7.5. The chart is successful in predicting the surface liquefaction effects and lateral spread failure on the loose sand A_2, as the corresponding points plot above Seed's curves; and it also successfully predicts the absence of any manifestation of liquefaction on the dense sand A_1, as the points plot below the curves. This complete success of the chart occurs despite the fact that the pore pressure ratio u* reached about 1 in both A_1 and A_2, as previously discussed.

Seed et al. [1983] have suggested that the curve of cyclic stress ratio versus N_1 for M = 7.5 in Fig. 9 corresponds to a constant cyclic shear strain, $\gamma_c \approx 0.03$ % for $N_1 < 30$ blows/foot. The author agrees with this value, which is of the same order of magnitude of $\gamma_c \approx 0.04$ to 0.06 %, estimated by the author at the beginning of this paper as the earthquake strain needed to reach u* ≈ 1 after 10-50 cycles. Therefore, up to $N_1 \approx 30$, the curves in Fig. 9 correspond to an approximately constant shear strain and to u* ≈ 1. The author suggests that the continuation of these curves of u* ≈ 1 beyond N_1 are either straight lines or downward curves, instead of the upward curves of the chart. One posible location for these u* ≈ 1 lines is indicated by the hatched band on the figure. This new band would have correctly predicted u* ≈ 1 for A_1 at Heber Road Site in 1979. The difference between this u* ≈ 1 band and Seed's curves, caused by the sharp turn upward of the latter for $N_1 > 30$, would correspond to dense sand layers which experience the u* ≈ 1 condition, but with this having no engineering consequence because of the low amount of water expelled by the soil during reconsolidation.

CONCLUSIONS

Some basic aspects of soil liquefaction at level sites during earthquakes which are still not clear, are discussed in the paper. These aspects, which are important both to an improved understanding of the phenomenon and to its engineering consequences, include: the mechanism of formation and the significance of sand boils, the relative importance of partially drained versus purely undrained failure mechanisms, and the relation between the widely used Standard Penetration charts and the behavior in situ. On the basis of available evidence, the author reached the following preliminary conclusions:

1) the amount of water expelled by the liquefied layer plays

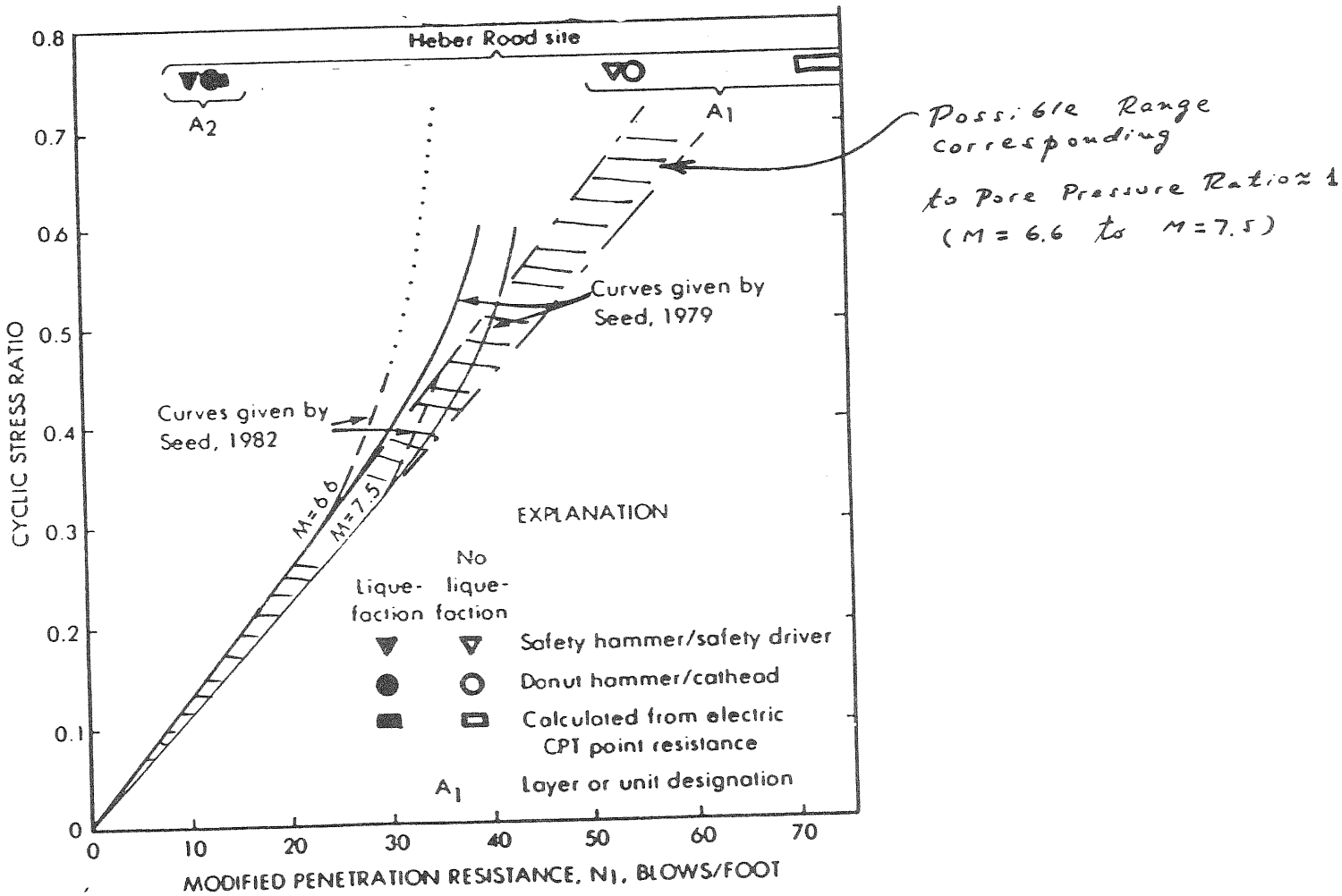

Figure 9. Application of liquefaction SPT chart to the Heber Road Site case history, and relation proposed by the author between chart and pore pressure buildup (modified after Youd and Bennett [1983]).

an important role both in the development of partially drained failure mechanisms, and in the appearance of sand boils;

2) the good correlation observed between liquefaction-induced failures and sand boiling strongly suggests that partially drained failure mechanisms are very significant;

3) the amount of water expelled by the liquefied layer depends on both the degree of compaction of the sand and the thickness of the layer, with this explaining the importance of both parameters in determining the effects of liquefaction; and

4) a main reason why the Standard Penetration charts work is the good correlation between penetration measurements and the amount of water expelled by the sand after liquefaction. Specifically, in a dense sand it is possible to generate a pore water pressure ratio close to unity without much water being expelled, and with insignificant settlement and no sand boils or engineering failure taking place. In this case the penetration charts correctly predict the absence of liquefaction manifestations rather than the level of pore pressure buildup in the soil, as is commonly believed.

ACKNOWLEDGEMENT

This paper was prepared as part of NCEER Research Project No. 86-2031 on "Investigation of Seismic Failure and Permanent Deformations of Soils During Earthquakes." This support is gratefully acknowledged by the author.

REFERENCES

Ambraseys, N. and S. Sarma. Liquefaction of soils induced by earthquakes. **BSSA, Vol. 59**, No. 2, pp. 651-664, April 1969.

Bhatia, S. K. The verification of relationships for effective stress method to evaluate liquefaction potential of saturated sands. **Ph.D. Thesis, Dept. of Civil Engineering, University of British Columbia**, 185 pages, November 1980.

Castro, G. On the behavior of soils during earthquakes - liquefaction. **Proc. 3d. Int. Conf. on Soil Dynamics and Earthquake Engineering, Soil Dynamics and Liquefaction (Vol. 42)**, pp. 169-204, Princeton U., June 1987.

De Alba, P., C. K. Chan, and H. B. Seed. Determination of soil liquefaction characteristics by large-scale laboratory tests. **Report No. EERC 75-14, College of Engineering, U. of California**, Berkeley, 153 pages, May 1975.

Dobry, R., K. H. Stokoe, II, R. S. Ladd, and T. L. Youd. Liquefaction susceptibility from S-wave velocity. **Insitu Testing to Evaluate Liquefaction Susceptibility, ASCE Nat. Convention**, St. Louis, Missouri, October 1981.

Dobry, R., R. S. Ladd, F. Y. Yokel, R. M. Chung, and D. Powell. Prediction of pore water pressure buildup and liquefaction of sands during earthquakes by the cyclic strain method. **NBS Building Science Series 138, National Bureau of Standards**, 150 pages, July 1982.

Housner, G. The mechanism of sandblows. **BSSA, Vol. 48**, pp. 155-161, April 1958.

Ishihara, K. Stability of natural deposits during earthquakes. **Proc. 11th. Int. Conf. Soil Mech. and Found. Engineering, Vol. 1**, pp. 321-376, San Fco., August 1985.

Lee, K. L. and A. Albaisa. Earthquake induced settlement in saturated sands. **Journal of the Soil Mechanics and Foundations Division, ASCE, 100**, pp. 387-406, April 1974.

Liu, H. and T. Qiao. Liquefaction potential of saturated sand deposits underlying foundation of structure. **Proc. 8th. World Conf. on Earthquake Engineering, Vol. III**, pp. 199-206, San Fco., July 1984.

NRC. Liquefaction of soils during earthquakes. Report by the **Committee on Earthquake Engineering, National Research Council**, Nat. Academy Press, 240 pages, 1985.

Seed, H. B. Soil liquefaction and cyclic mobility evaluation for level ground during earthquakes. **Journal of the Geotechnical Engineering Division, ASCE, 105**, pp. 201-255, February 1979.

Seed, H. B., I. M. Idriss, and I. Arango. Evaluation of liquefaction potential using field performance data. **Journal of Geotechnical Engineering, ASCE, 109**, pp. 458-482, March 1983.

Seed, H. B. Design problems in soil liquefaction. **Report No. UCB/EERC-86/02, College of Engineering, University of California, Berkeley**, 33 pages, February 1986.

Silver, M. L. and H. B. Seed. Volume changes in sands during cyclic load. **Journal of the Soil Mechanics and Foundations Division, ASCE, 97**, pp. 1171-1182, September 1971.

Soil and Foundation. Pictures taken at the moment of the Niigata earthquake. **Soil and Foundation, Vol. VI, No. 1**, pp. i-vi, January 1966.

Sykora, D. W. and K. H. Stokoe, II. Seismic investigation of three Heber Road sites after October 15, 1979 Imperial Valley earthquake. **Geotechnical Engineering Report GR82-24, Civil Eng. Dept., University of Texas at Austin**, 76 pages, February 1982.

Tohno, I. and S. Yasuda. Liquefaction of the ground during the 1978 Miyagiken-Oki earthquake. **Soils and Foundations, Vol. 21, No. 3**, pp. 18-34, September 1981.

Vucetic, M. et al. Analytical study of liquefaction observed at the Heber Road site during the October 15, 1979 Imperial Valley earthquake. (In preparation), 1987.

Whitman, R. V., P. C. Lambe, and B. L. Kutter. Initial results from a stacked ring apparatus for simulation of a soil profile. Proc. Int. Conf. on Recent Advances in Geotechnical Eng. and Soil Dynamics, Vol. III, pp. 1105-1110, St. Louis, Missouri, April-May 1981.

Yoshimi, Y. and F. Kuwabara. Effect of subsurface liquefaction on the strength of surface soil. Soils and Foundations, Vol. 13, No.2, pp. 67-81, June 1973.

Youd, T. L. and M. J. Bennett. Liquefaction sites, Imperial Valley, California. Journal of Geotechnical Engineering, 109, pp. 440-457, March 1983.

PREDICTING RELATIVE GROUND RESPONSE*

By A. M. Rogers, J. C. Tinsley, and R. D. Borcherdt

INTRODUCTION

The character of ground shaking at a point on the Earth's surface generated by an earthquake is influenced by distance from the causative fault, characteristics of the earthquake source, and geologic conditions within the Earth's mantle and crust. Geologic conditions at or near a site are known to exert an especially significant influence on the nature of ground shaking (Milne, 1898; Lawson and others, 1908; Kanai, 1952; Gutenberg, 1957; Medvedev, 1962; Borcherdt, 1970; Murphy and others, 1970; Rogers and others, 1979). In the Los Angeles region, Wood (1933) noted that the 1933 Long Beach earthquake caused more damage in Compton than it did in Long Beach and ascribed this difference to local geologic effects. For the same earthquake, Campbell (1976) showed that, for a given distance from the Newport-Inglewood zone, damage at sites underlain by unconsolidated soils was greater than that at sites underlain by consolidated soils. Certain frequencies of strong shaking may be amplified considerably by thin low-velocity surface layers, and the overall spectral level of ground motion may increase as the seismic velocity of near-surface materials decreases and (or) as the thickness of sediments increases (Murphy and Hewlett, 1975; Borcherdt and Gibbs, 1976; Rogers and others, 1979). Although the importance of local geologic conditions has long been recognized, the quantitative prediction of the influence of these conditions on ground shaking by either empirical or theoretical models is still in the developmental stage.

PREVIOUS STUDIES

Problems central to the theoretical or empirical prediction of site response are related to differences in wave types, angles of incidence, azimuth of approach, and Earth heterogeneity (Hudson and Douglas, 1975; Murphy and Hewlett, 1975; Esteva, 1977) and to the question of nonlinear soil behavior (Seed and Idriss, 1970; Hardin and Drnevich, 1972). Relative changes in the proportions of body- and surface-wave energy as a function of epicentral distance, for instance, might alter the ground response in a manner not predicted by either theory or empiricism. Nevertheless, site-specific velocity models have been used with linear or nonlinear models of shear-wave propagation in a layered geologic column to obtain theoretical estimates of local site-response effects (Kanai, 1952; Kanai and Yoshizawa, 1958; Murphy and others, 1971; Lastrico, 1970; Joyner and Chen, 1975). Comparisons of theory and observed data indicate that theoretical models can often be used to predict site response (Borcherdt and Gibbs, 1976; McEvilly and Johnson, 1980; Joyner and others, 1981). Simple one-dimensional models frequently are used because they provide first-order approximations of site response. These models also apply to either radial or transverse components of motion because the angle of incidence through near-surface low-velocity sediments is nearly vertical (Murphy and others, 1970). The disadvantage of these models is that essential subsurface data are not available everywhere; furthermore, the models are not applicable in all situations.

Empirical methods are not limited in the same manner that most theoretical solutions are. Because measurements of site response incorporate the effects of waves arriving from many directions (backscattering) and the effects of both body and surface waves, they provide a smoothed estimate to the solution of the more complex problem, reflecting the effects of true Earth geometry. Underground nuclear explosions were first used as distant seismic sources in empirical studies of site effects by Borcherdt (1970) and Murphy and others (1971). Low-strain measurements of small earthquakes or distant nuclear explosions obtained over a region on a variety of local site conditions can directly provide a map of potential geographic variations in site response (Murphy and Hewlett, 1975; Hays and Algermissen, 1982; Hays and King, 1982). Correlation of site response and known geologic data is also a useful technique for extrapolating relative shaking effects over a broad region or for making estimates at specific sites. Borcherdt and Gibbs (1976), for example, have established a relation between the age of surficial deposits and the mean spec-

*Reprinted from "Evaluating Earthquake Hazards in the Los Angeles Region - An Earth Science Prospective", J. I. Ziony ed., U.S. Geological Survey Professional Paper 1360, pp. 221-248 and 487-488, 1985.

tral amplification in the San Francisco Bay region that has enabled them to produce a regional map showing expected geographic variations in shaking intensity. These studies and those of Mueller and others (1982), King (1982), and Rogers and others (1984) suggest that, for many situations, effects of local site conditions may predominate over other effects such as changing source azimuth, wave type, and angle of incidence. These studies have shown that changes in mean spectral amplification from low-level ground motions are correlated with geologic structure, measured in-situ shear-wave velocities, and changing earthquake intensities and spectral levels; these correlations suggest that, in many cases, site effects can be predicted empirically as well as theoretically.

Using nuclear explosions to study or predict site amplification assumes that site effects produced by low-level ground motions from distant nuclear explosions are similar to those that would be observed during strong shaking. A significant question of engineering interest is, "To what extent can ground-response measurements determined from low levels of shaking (small strains less than 10^{-5}), such as those recorded from distant nuclear explosions, be extrapolated to predict ground response at higher levels of shaking induced by nearby damaging earthquakes?" Laboratory-based studies suggest that soils behave in a nonlinear fashion when strain levels exceed about 10^{-5} (Seed and Idriss, 1970) or 10^{-4} (Turner and Stokoe, 1982). That is, at strains of this level or greater, soils begin to lose strength (as reflected by a decrease in shear modulus, which causes increased wave amplitudes) and to increase wave attenuation or damping (as reflected by an increase in the damping coefficient, which causes decreased wave amplitudes). Theoretical modeling of soils suggests that, at certain frequencies, the ratio of surface to base-input motion for soils undergoing nonlinear high-strain behavior will be lower than the ratio for the same soils responding in a linear manner to lower base-input motions. This behavior is due to the fact that the effects of increased damping dominate the effects of reduction in shear modulus (Borcherdt and others, 1975; Joyner and Chen, 1975). The changes in soil properties produced by nonlinearity increase the fundamental resonant period of site shaking and lower the resonant peak level. For the most part, however, these effects of nonlinear soil behavior have not been observed in strong-ground-motion records.

On the contrary, field data suggest that high-amplitude soil response is similar to low-amplitude soil response, perhaps for strains up to 10^{-3}. Using recordings of nuclear events at two Nevada Test Site locations (Murphy and others, 1971), Rogers and Hays (1978) have shown that site response measured at strains of 10^{-3} and 10^{-4} are essentially equal. Joyner and others (1981) have demonstrated that linear theoretical models predict the site response at a recording site in the area of the Coyote Lake, Calif., earthquake for strains as large as 10^{-4}. Rogers and others (1984) have compared site response measured by using distant nuclear explosions (strains near 10^{-5}) with site response at the same locations measured by using data from the 1971 San Fernando earthquake (strains near 10^{-3}) and have found that the two data sets are equivalent within the expected variability of the statistics (fig. 103). Field observations of earthquake damage also suggest that high-amplitude soil response and low-amplitude soil response are similar.

A high correlation between mean spectral amplification was determined for sites near San Francisco from Nevada Test Site nuclear explosions and from observed 1906 earthquake intensities, up to San Francisco intensity level 4 (Borcherdt and others, 1975). Espinosa and Algermissen (1972) found a correlation between the thickness of alluvial sediments, mean spectral amplification derived from low-level ground motions generated by small earthquakes, and damage to highrise buildings in the 1967 Caracas, Venezuela, earthquake. These studies provide evidence supporting the assumption that soil responds to very high levels of damaging shaking without significant nonlinear behavior. These studies also support the argument that differences between wave types and other factors caused by ground motions resulting from distant low-level sources and those caused by nearby strong earthquakes have only second-order significance in comparison with the site-response phenomena. These results suggest that, for in situ soils, the changes produced in the shear modulus and in the damping factors by strong shaking are smaller than the changes suggested by the results of laboratory testing of samples.

Soils have been observed to sustain large damaging ground motions that include soil amplification effects. In addition to the examples cited in the introduction, table 37 shows that ground motions as large as 0.7 g and 108.8 cm/s have been recorded on soils. In the Italian earthquakes cited in table 37, accelerations (at some sites as large as 0.5 g) recorded on thin soils (less than 20 m) were higher by factors of as much as four in comparison with those recorded on thick soils or rock. These cases may or may not have exhibited nonlinear behavior but, nonetheless, demonstrate large damaging ground motions at sites underlain by soil. Even though nonlinear behavior can limit the magnitude of ground motions on soils, the upper limits of shaking on soils still appear to be high in some cases.

The effect of nonlinear soil response may also be restricted to a small area surrounding the causative

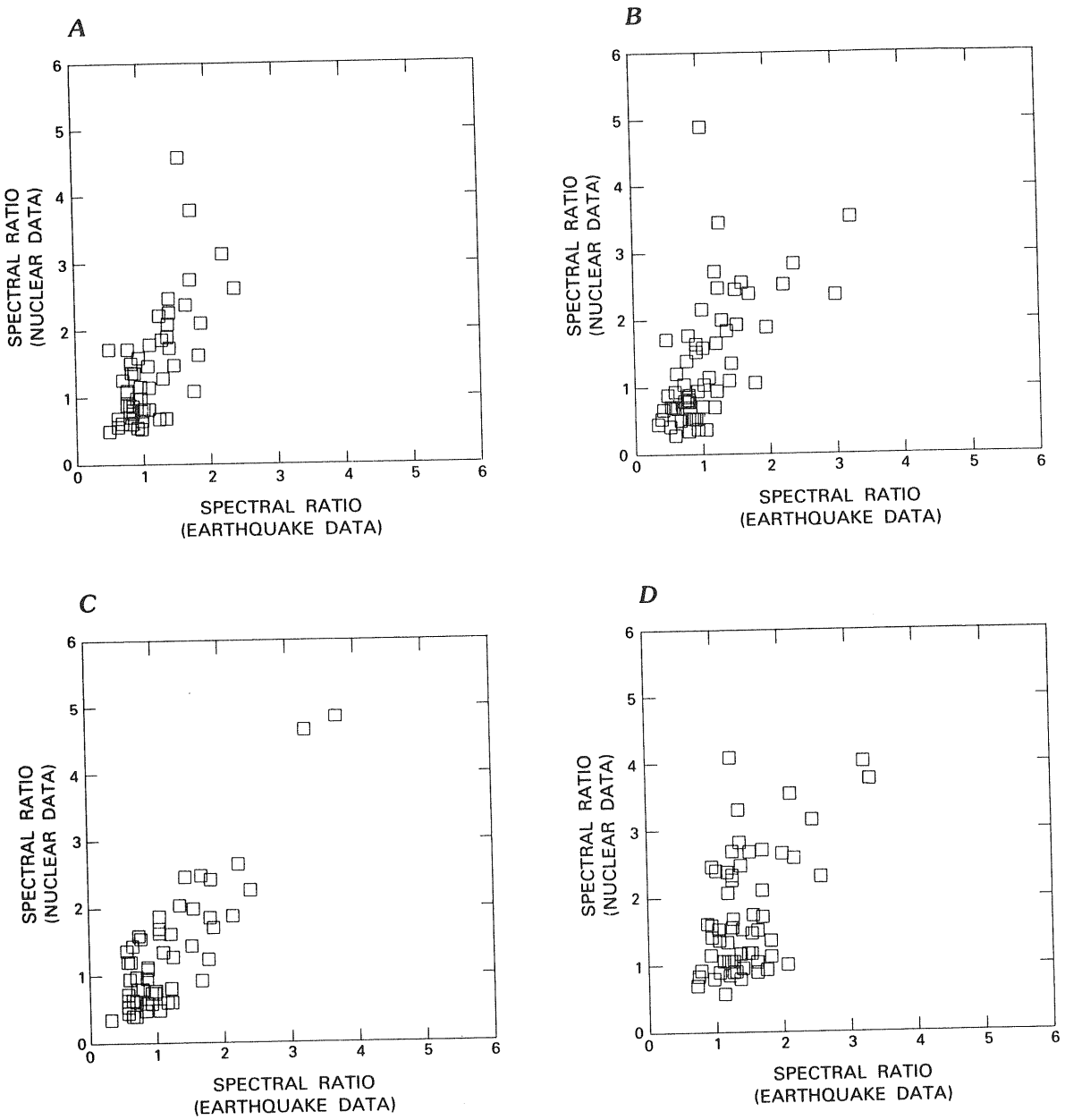

FIGURE 103.—Comparisons of the geometric mean spectral ratios in four period bands determined from ground-motion recordings of distant underground nuclear explosions and from the 1971 San Fernando earthquake (from Rogers and others, 1984). A, 0.2 to 10.0 s. B, 0.2 to 0.5 s. C, 0.5 to 1.0 s. D, 1.0 to 3.3. s. These data indicate that small ground motions obtained from distant sources can be used to estimate differences in ground response from nearby damaging earthquakes.

fault (Hays and Algermissen, 1982). A magnitude 7 to 7.5 earthquake, for instance, develops velocities on soil sites exceeding 100 cm/s at distances of less than 7 to 13 km from the fault (dependent on the magnitude) (Joyner and Boore, 1981). For soil sites having 200-m/s shear-wave velocities, strains of 5×10^{-3} will be developed

TABLE 37.—Peak ground motions and estimated strains recorded at selected sites underlain by unconsolidated sediments
[--, no data]

Earthquake	Station	Acceleration, in g	Velocity, in cm/s	Estimated strain	References
1966 Parkfield	2	0.48	78.1	5×10^{-3}	Earthquake Engineering Research Laboratory (1969–1975). Nuclear Regulatory Commission (1980)
1979 Imperial Valley	6	.72	108.8	5×10^{-3} to 10^{-4}	Porcella and Matthiesen (1979) Mueller and others (1982)
1972 Ancona, Italy, and 1976 Friuli, Italy	--	Up to 0.5	--	--	Chiaruttini and Siro (1981)

within this zone. Observations discussed in this section indicate that this strain level may still be below the level of significant nonlinear behavior. Because damaging motions on soils (Modified Mercalli intensities greater than or equal to VI) occur at distances of 60 to 100 km from the fault (Howell and Schultz, 1975), the region of damage within which nonlinear soil response is possible is about 2 to 9 percent of the total area of damage, if a 30-km rupture is assumed. Where the fault passes through developed regions, the zone of nonlinear behavior may be the area of greatest life loss, but a high percentage (as much as 90 percent) of the economic loss occurs outside this zone (Algermissen and others, 1972). Where the fault passes outside the developed zone or the earthquake is too small to induce nonlinear soil response, this behavior will not be a factor at all (for example, the 1967 Caracas, Venezuela, earthquake and the 1977 Romanian earthquake).

COMPARATIVE GROUND RESPONSE IN THE LOS ANGELES REGION

Comparative ground response to distant nuclear explosions was measured at 98 sites throughout the Los Angeles region. When these measurements are coupled with available geologic and geotechnical data, they provide an extensive data base to delineate potential geographic variations in strong ground shaking. Three-component recordings of Nevada Test Site nuclear explosions were made at each site. A total of 19 nuclear explosions were used; because some sites were reoccupied for several events, 159 three-component records were obtained. Sites for the study (fig. 104) were chosen to obtain as complete a sample of underlying geologic conditions and as broad a geographic coverage as possible. Because the seismic source lies between 400 and 450 km from the recording sites, the effects of azimuthal variations in the energy radiated by the source and the major portions of the crustal propagation paths are similar for all sites.

The response characteristics of each site over the period band 0.2 to 10 s were computed by using Fourier spectral ratios (Borcherdt and Gibbs, 1976). The Fourier spectral ratios (F) were computed from

$$F_{ij}(k/T) = [\, s_{ij}\,(k/T)\,] \;/\; [s_{0_j}\,(k/T)] \qquad \begin{matrix} k = 0,\ldots,n \\ i = 1,\ldots,m \\ j = v,\ t,\ r \end{matrix}$$

where $s_{ij}(k/T)$ corresponds to the smoothed Fourier amplitude spectra for a signal of length T at frequency k/T for the jth component at the ith station and $s_{0_j}\,(k/T)$ designates the corresponding smoothed amplitude spectra computed from a simultaneous recording at the reference station. The ratios were computed only at those frequencies for which a signal-to-noise ratio greater than a factor of two existed for both spectra. The noise level was determined by examining the spectra of a time segment before the arrival of the signal on each component of motion. These data, including processing techniques, copies of recorded time-histories, and spectral ratios, have been compiled and discussed by Rogers and others (1980).

A site located on crystalline rock (CIT) (fig. 104) was reoccupied for every recorded nuclear explosion. By using CIT spectra ($s_{0_j}\,(k/T)$) as the base rock site, it was possible to minimize the effects of source, transmission path, and instrument response in the spectral ratios (Rogers and others, 1979). Thus, the spectral ratios are assumed to reflect only frequency-dependent site amplification effects. The spectral ratio technique has been used by a number of investigators to obtain a first-

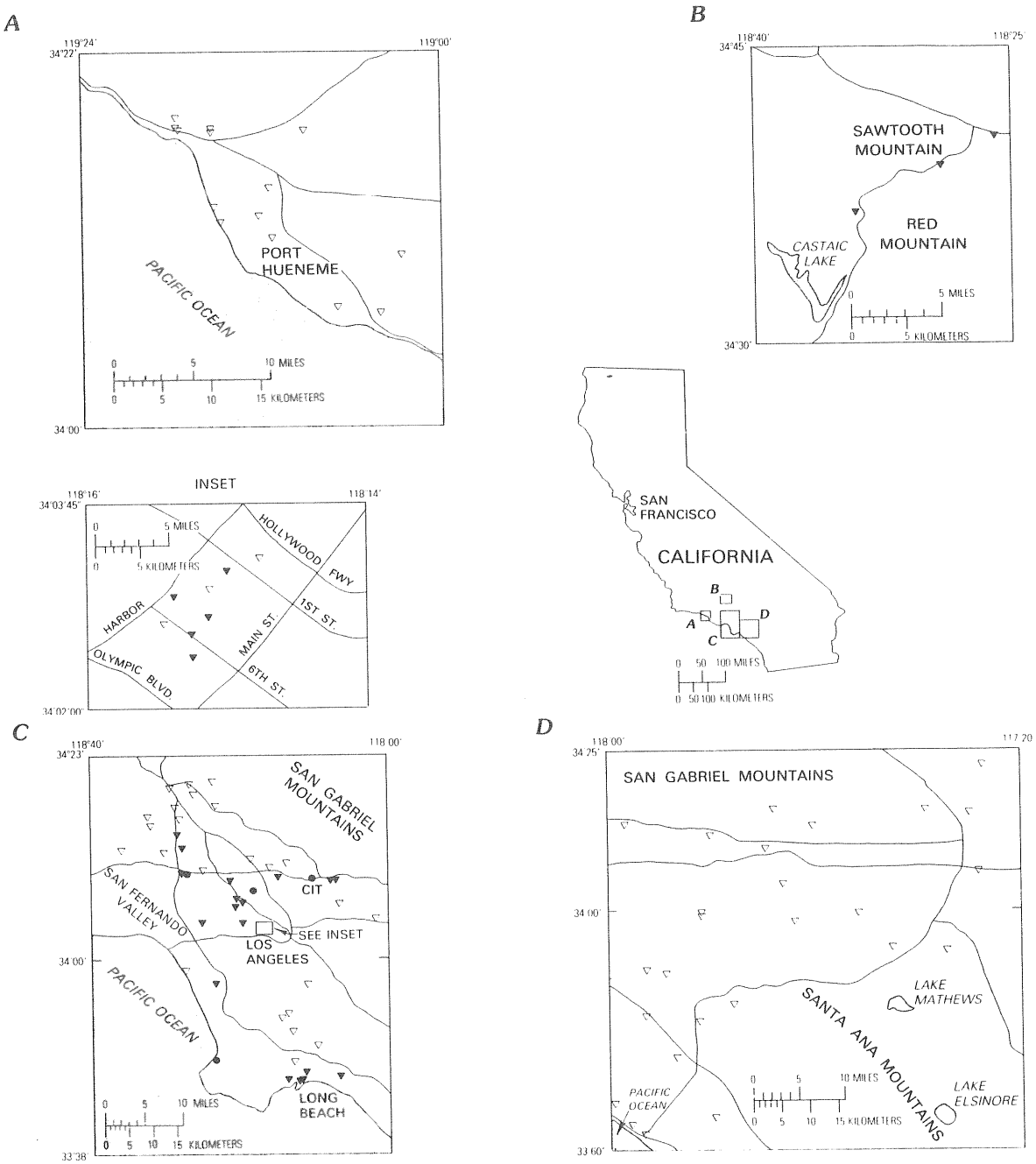

FIGURE 104.—Locations of sites (triangles) in the Los Angeles region at which ground-motion recordings of underground nuclear explosions at the Nevada Test Site were obtained. Strong-motion recordings of the 1971 San Fernando earthquake were also available at some of these locations, indicated by the solid triangles. Open triangles indicate that only nuclear test recordings are available at a site. Station names and locations are taken from Rogers and others (1980).

order approximation of the site amplification of local geologic deposits (Kanai and others, 1956; Gutenberg, 1957; Borcherdt, 1970; Rogers and others, 1979). The ease with which the extraneous effects are removed from nuclear-event recordings is one of the prime motivations for using such events; nearby earthquakes produce recordings in which site amplification, source, and propagation-path phenomena are intertwined and difficult to study individually (Hanks, 1975).

In the case of ground motions from distant nuclear explosions, the effects of site conditions dominate on the recorded time-histories. Figure 105, for example, shows time-histories from a single Nevada Test Site nuclear explosion recorded simultaneously at eight sites. The example illustrates several effects of local site conditions commonly observed on recorded time-histories from distant sources of shaking. Maximum amplitudes of motion recorded on the alluvial sites, for instance, are several times larger than those recorded on the sedimentary- or crystalline-rock sites. The duration of ground motion at the alluvial sites is generally longer than that at the rock sites. The degree of amplification occurring in the long-period peak amplitudes of these records is greatest at sites underlain by the thickest sediments. Comparison of all three components of ground motion recorded at each site (Rogers and others, 1980) shows that the amplification of horizontal ground motions is commonly larger than that of vertical motions. In the following discussion, only the horizontal components of ground motion are emphasized, because they are the most important in structural engineering.

The amplitude spectral ratios computed for the simultaneous recordings shown in figure 105 are presented in figure 106, where station CIT has been used as the reference station. The ratios show that the effects of site conditions relative to those at CIT are strongly frequency dependent and that amplification occurs for many of the sites over most of the frequency band for which a good signal-to-noise ratio exists. Horizontal amplification factors in the range 2 to 7 are apparent for the lower frequency ground motions (< 1 Hz) for those sites on thick sections of alluvium; lower amplifications are apparent at these periods for sites underlain by thin sections of alluvium. Considerable amplification at the intermediate frequencies (1–2 Hz) and at the higher frequencies (2–5 Hz) is readily apparent at several of the sites, the horizontal amplification at site FS4 being indicative of a predominant ground-resonant frequency. Note that resonance is not a factor for the thick alluvial sites, which display relatively flat spectra across the entire observed frequency range. The spectral ratios for the GOC and CIT sites show that the spectral levels of the two crystalline-rock sites are very similar for the lower frequencies, but the intermediate-frequency and higher frequency motions recorded at GOC are larger than those recorded at CIT. Site 3838, located on sedimentary rock, indicates a uniformly higher response in comparison with the response at CIT over most of the frequency band.

Amplification does not produce large peaks in the time-history for FS4 because the frequency of maximum incoming energy is not coincident with the resonance peak frequency. This result points out the pitfall of examining peak ground-motion parameters for site effects. A site may have a strong amplification effect that is not necessarily reflected by the peak accelerations, for instance.

The spectral ratios are similar for most of the nuclear explosions analyzed. An example of the spectral geometric means and their geometric standard deviations is shown in figure 107, together with data from the individual events used to compute the statistics. Additional examples have been computed by Rogers and others (1980), who have shown that the geometric standard deviation averages 1.38 independent of frequency (this result is seen more clearly in their log-log plots). By comparison, this dispersion is lower than that associated with the empirical prediction of root-mean-square acceleration on rock (Hanks and McGuire, 1981).

The spectral ratios computed from shaking induced by distant nuclear explosions suggest that the observed ground motions varied significantly from site to site, depending on the type of underlying geologic deposits. At many sites, amplification is strongly frequency dependent. The level of spectral response at alluvial sites commonly is higher than that at rock sites, and the amplitude and duration of shaking depend on the thickness of the underlying sediments. Sites having thin alluvium tend to amplify shaking over a narrow frequency range, whereas sites having thick alluvium amplify shaking over a broad frequency range. These general conclusions are consistent with similar data and a similar interpretation reported by Borcherdt and Gibbs (1976) for the San Francisco Bay region.

GEOLOGIC AND GEOTECHNICAL PARAMETERS AFFECTING GROUND RESPONSE

The diverse geologic framework of southern California offers a unique opportunity to study variations in earthquake-generated ground shaking as a function of geologic setting. Crystalline rocks, for example, are exposed in rugged mountains more than 3 km above sea level and, in the deepest parts of the Los Angeles basin, are buried beneath at least 10 km of sedimentary rock

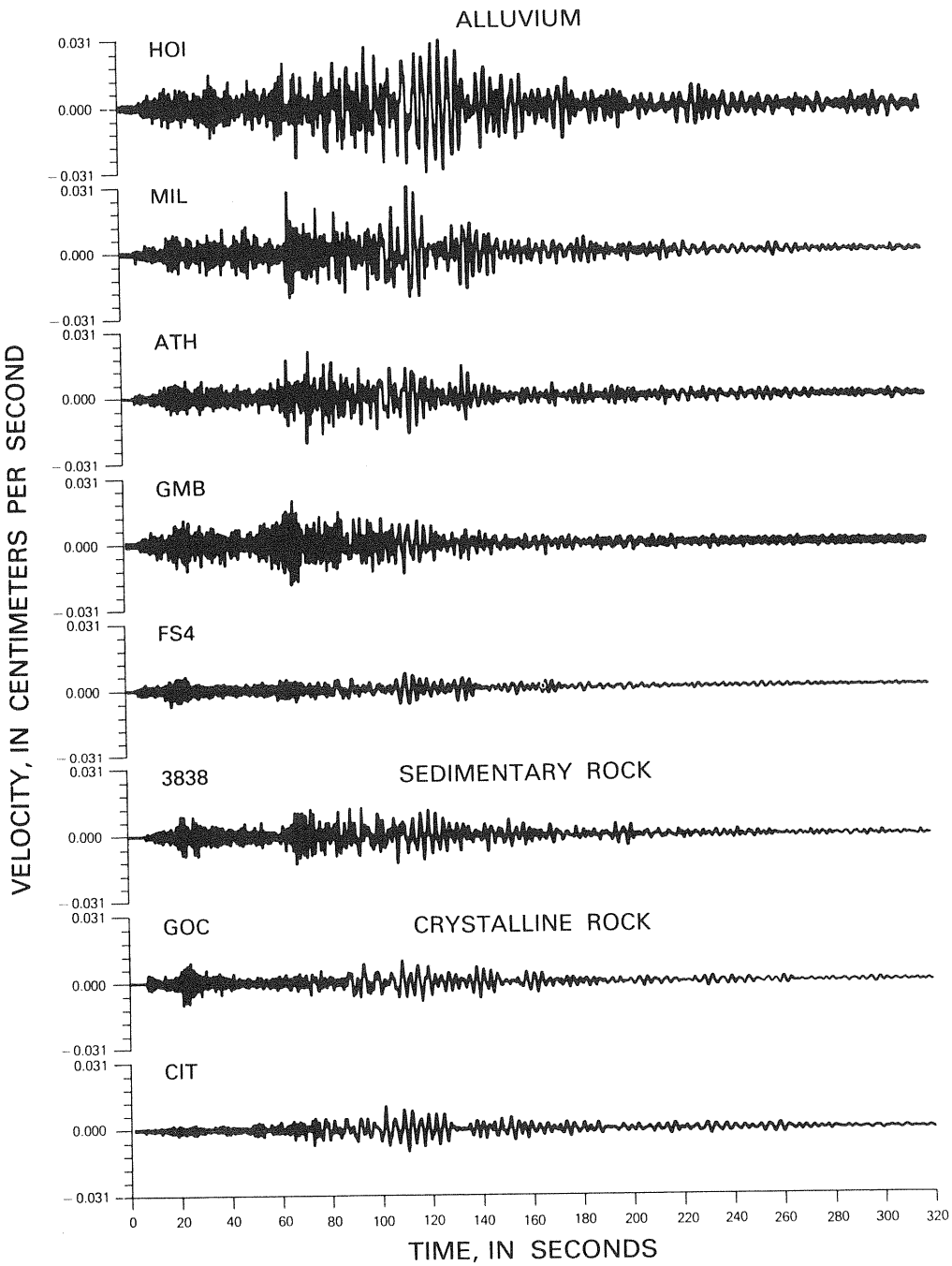

FIGURE 105.—Radial component time-histories of ground motion from a distant underground nuclear explosion in Nevada recorded simultaneously at eight sites in the Los Angeles region and grouped according to the type of geologic materials immediately beneath each recording station. The amplitude levels at locations underlain by alluvium clearly are greater than those at locations underlain by rock. The degree of amplification also appears to be related to the thickness of underlying alluvium: HOI, Holiday Inn, 300 m; MIL, Millikan Library, 372 m; ATH, Athenaeum, 372 m; GMB, Glendale Municipal Building, 120 m; FS4, Fire Station 4, 15 m. GOC, CIT, and 3838 are rock sites.

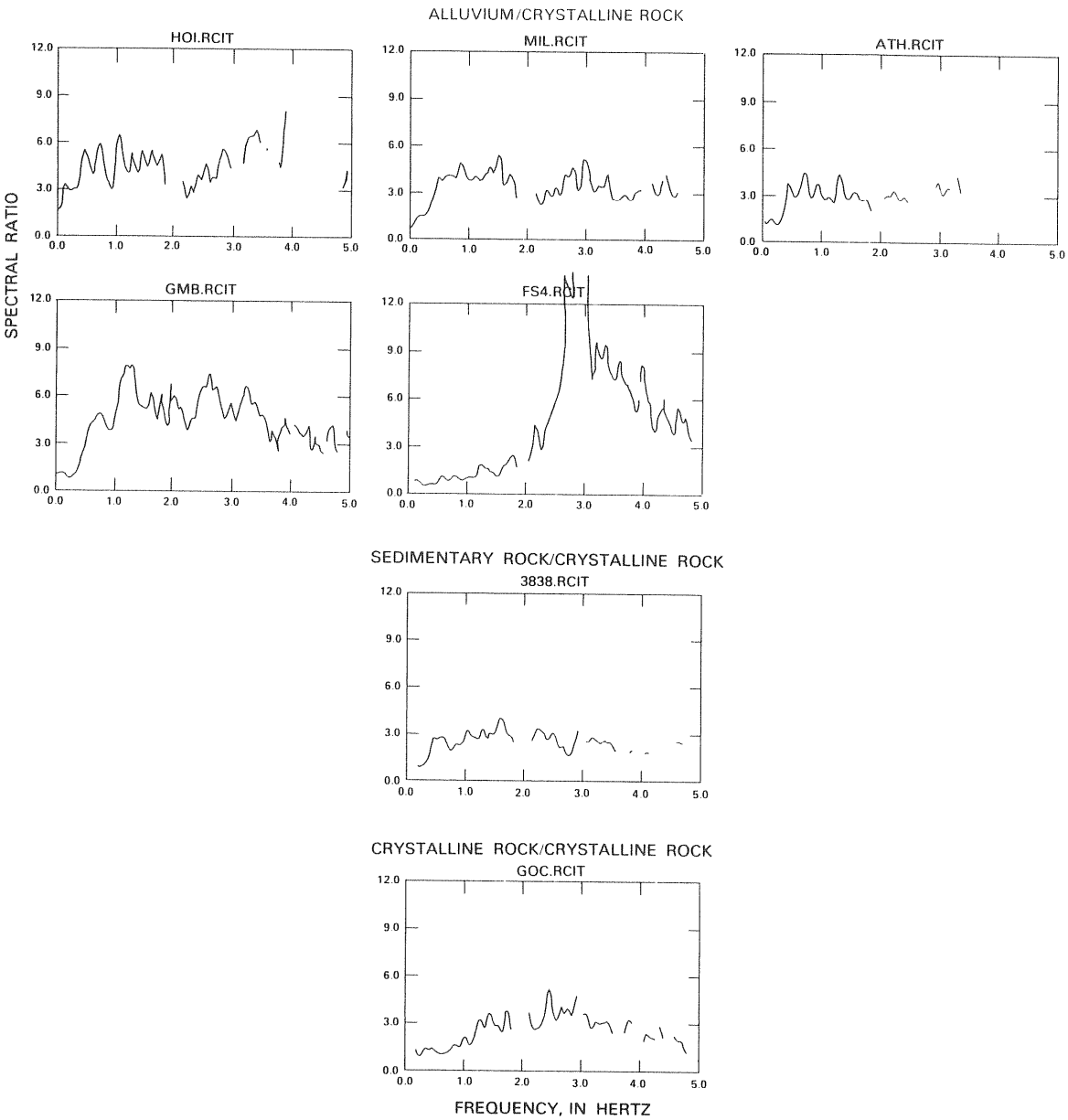

FIGURE 106.—Spectral ratios of the radial components of ground motion (see fig. 105) recorded on sites having geologic conditions different from the crystalline-rock site (CIT). These diagrams show that spectral site amplification ranges from about 1 to greater than 12; the highest ratios occur at sites underlain by alluvium. Site FS4 displays a resonant frequency between 2 and 3 Hz, whereas other sites have more uniform amplification, averaging as much as 6 in some frequency bands.

and alluvium (Yerkes and others, 1965). The youngest deposits in the basins of the Los Angeles region consist chiefly of unconsolidated to partly consolidated alluvial-fan and river flood-plain sediment. These deposits range in thickness from 0 to 10 m near basin margins to, perhaps, more than 50 m in coastal basins. Sand and mud occur in ancient and modern shore areas; wind-blown sands are present locally in inland basins. Basin

fill, mostly of Quaternary age and some of Pliocene age, ranges widely in texture; gravel, cobbles, and boulders occur chiefly near mountain fronts and in channels on alluvial fans emanating from the mouths of major canyons, and silt and some clay commonly are deposited on flood plains tens of kilometers from the mountains.

The 98 recording sites used in this study encompass a broad range of the variations in depth to basement rock and in the texture and physical properties of basin fill. Geologic and geotechnical information about the uppermost few tens of meters of basin fill at each ground-motion recording site was compiled from logs of soil-engineering boreholes, water wells, and limited field investigations (Gibbs and others, 1980; Fumal and others, 1981, 1982; J. C. Tinsley, written communication, 1982). The soil-engineering logs, chiefly of foundation studies, are from files maintained by city, county, State, and Federal agencies and from geotechnical consulting firms. These records describe the near-surface sediment in terms of its grain size, moisture content, and dry density. Many of these boreholes penetrate the uppermost 5 to 10 m of the alluvial deposits, although foundation studies for major structures may penetrate up to 30 m or more.

The general geologic character and the thickness of surficial sediments in the depth range from 15 to 300 m have been inferred from drillers' lithologic logs of water wells and from geophysical logs of oil and water wells filed with State and local agencies. Studies of the regional hydrology (Poland, 1959; Poland and others, 1956, 1959; Thomas and others, 1961; California Water Rights Board, 1961; Dutcher and Garrett, 1963; California Department of Water Resources, 1966) describing the geologic and hydrologic setting of the late Quaternary alluvial basins have been incorporated where pertinent.

For each recording site, several engineering and water-well logs were examined, and the most representative data—usually obtained from the borings closest to, if not beneath, the site—were used to characterize each site. We regard three thickness parameters as significant for characterizing the sites: (1) the total thickness of sedimentary deposits, expressed as the depth to the crystalline igneous and (or) metamorphic rocks underlying the basins; (2) the approximate thickness of semiconsolidated sediment, expressed as the approximate thickness of the Quaternary (less than 1.7 m.y. old) deposits; and (3) the approximate thickness of unconsolidated or poorly consolidated sediments, expressed as the approximate thickness of Holocene (less than 10,000 yr old) sediment. The lithologic and time-stratigraphic horizons bounding these rock units commonly correspond to physically significant interfaces in the subsurface across which the shear-wave velocities and relative densities of the sediment may change (Fumal, 1978; Gibbs and others, 1980; Fumal and others, 1981, 1982) and thus alter the response characteristics of the site.

A number of geotechnical factors (table 38) were chosen to characterize the recording sites either because they have some direct application in a theoretical model of site response and (or) because they have been reported to have some influence on ground shaking in past studies. Parameters such as mean percentage of silt and clay, void ratio, and depth to water table have been reported to influence site response (Barosh (1969) has summarized many of these studies), whereas shear-wave velocity, Holocene deposit thickness, Quaternary deposit thickness, depth to cementation, and depth to basement rocks are all parameters that might be used directly in a theoretical model of site effects. The alluvium-to-rock spectral ratios were reduced to a small set of numbers by computing the geometric mean spectral ratio over 10 period bands. Because a high degree of correlation was observed between the mean spectral values in some of these period bands, only three non-overlapping bands were used in further analysis. These bands are referred to as the short-period (0.2–0.5 s), intermediate-period (0.5–3.3 s), and long-period (3.3–10 s) bands. A discussion of the geotechnical parameters themselves follows.

Mean void ratio.—Void ratios (*e*) are computed from dry-density (*GD*) data obtained from the foundation-engineering data by using the relation $e = (GS/GD) - 1$, where *GS* is the density of the solids without voids. For most soils, *GS* varies from 2.65 to 2.70. By assuming the lower value for sand and the higher value for clay, mean *e* values were computed for each alluvial site, generally for the upper 8 m. At layered sites having several values of *e*, the depth-weighted mean was computed. Mean *e* rather than mean shear-wave velocity was used in this study to characterize the sites for several reasons. First, laboratory studies by Hardin and Drnevich (1972) have indicated that *e* and shear modulus are inversely related, and Rogers and others (1979) have determined that site response increases as *e* increases, a result that might be predicted from the relation between *e* and shear-wave velocity. Figure 108 uses data from Los Angeles and San Francisco to show this relation. The curve fit to these data can be used to estimate shear-wave velocity from *e*. Second, data on void ratios were readily available from engineering boreholes and were therefore a useful and inexpensive way to estimate near-surface shear-wave velocity. Data on void ratios were also available at nearly twice as many sites as data on shear-wave velocity; because of the effort and expense involved in collecting borehole measurements, the shear-wave velocities were not available for many sites until this study was almost complete. Third, void

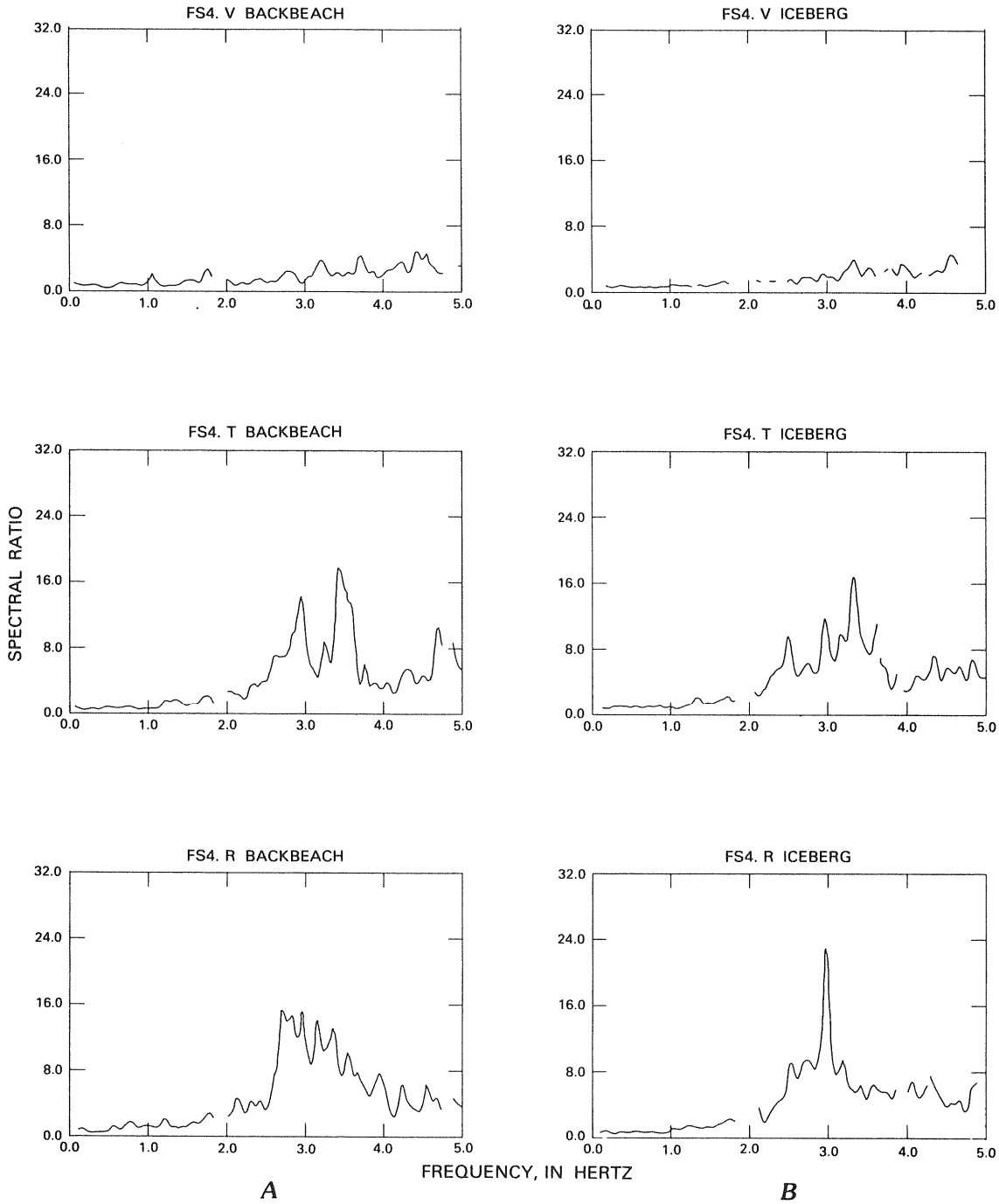

FIGURE 107.—Comparison of spectral ratios computed for stations FS4 (alluvium) and CIT (crystalline rock) for distant nuclear explosions. *A*, Backbeach. *B*, Iceberg. C, Fondutta. Components of shaking are vertical (V), transverse (T), and radial (R). The geometric mean spectral ratio (solid line) and one geometric standard deviation about the mean (dashed and dotted lines) are also shown (*D*). The geometric standard devia-

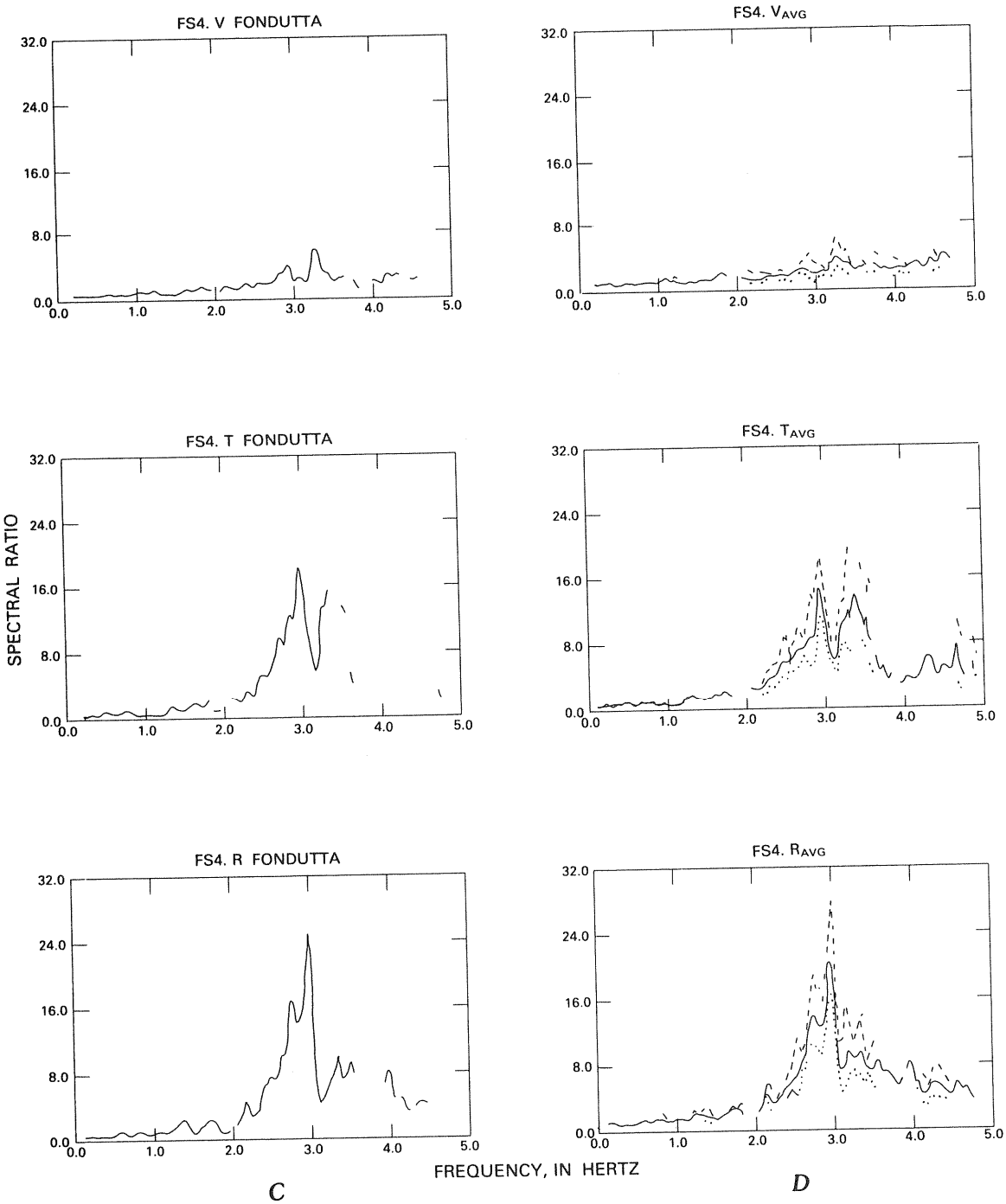

tion in this case averages to a factor of about 1.3 across the frequency band. Similar examples for other stations have been shown by Rogers and others (1984). These diagrams demonstrate the reproducibility of the spectral ratios between distant nuclear events.

TABLE 38.—Geotechnical parameters and the percentage of stations for which each parameter was available

Parameter	Stations for which parameter was available, in percent
Mean void ratio (0–8 m)	82
Mean percentage of silt and clay (four depth intervals).	37–95
Thickness of Quaternary	100
Age	100
Thickness of Holocene	99
Depth to water table	97
Textural type (very coarse to fine).	99
Depth to crystalline basement	100
Depth to cementation	91
Mean borehole shear-wave velocity (four depth intervals).	42

ratios were frequently measured at the building where the nuclear-event recordings were made, whereas shear-wave velocity measurements sometimes had to be taken tens to hundreds of meters away. Thus, in some cases, an e value computed for the recording site may be a more relevant measure of the shaking response at the recording site than a shear-wave velocity measurement made some distance away. Even though the void ratio is generally known only in the upper 8 m, which represents only a fraction of the near-surface wavelength in the short-period band, the high correlation observed in this period band between void ratio and shaking response indicates that the near-surface void ratio reflects information about the mean shear-wave velocity over a deeper sediment section. This supposition is supported by the highly significant correlation coefficient (−0.6) in our data between mean void ratio in the upper 8 m and mean shear-wave velocity in the upper 30 m.

Mean percentage of silt and clay.—The mean percentage of silt and clay was determined from the lithologic descriptions of boreholes for selected thicknesses of 8, 15, 30, and 122 m by summing the total incremental thicknesses of sediment logged as silt or clay within the interval, dividing that sum by the thickness of the interval, and then multiplying the quotient by 100.

Thickness of Quaternary.—The base of the Quaternary sedimentary deposits was selected arbitrarily at the base of the marine San Pedro Formation in the coastal basin areas and at the base of the nonmarine(?) sand and gravel that comprise the freshwater-bearing alluvium in the interior basins. Some of these basinal nonmarine(?) deposits are almost certainly pre-Quaternary in age, but correlations among these deposits are not reliable.

Age.—Recording sites were classed according to the geologic age of the underlying surficial deposits—for example, Holocene alluvium, Pleistocene alluvium, Tertiary sedimentary rock, Tertiary volcanic rock, or pre-Tertiary crystalline igneous and metamorphic rock (crystalline basement). Sites were classed as rock sites where a thin alluvial veneer had been excavated and had been removed during construction of the building that housed the recording instrument.

Thickness of Holocene.—Holocene deposits are commonly associated with historical flooding and are capped by soils having minimally developed profiles. In practical terms, in the field, the base of the Holocene section is placed generally at the top of the uppermost red or reddish-brown buried soil. Early Holocene deposits may have nonclayey (cambic) B horizons or nonreddened clay-enriched B horizons, except within historically active flood basins (McFadden and Tinsley, 1982).

Depth to water table.—The distance from the ground surface to free ground water, expressed here as "depth to ground water" (including perched water), was determined from logs of boreholes located near each instrument site and from selected maps and records maintained by the California Department of Water Resources, the Los Angeles County Flood Control District, and the City of Los Angeles Department of Water and Power.

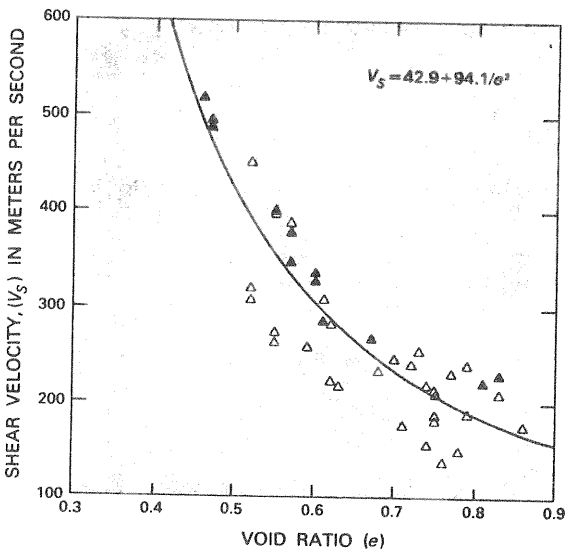

FIGURE 108.—Relation between mean shear-wave velocity in the upper 10 m and mean void ratio in the upper 8 m. Solid triangles are data from the San Francisco region (Fumal, 1978), and open triangles are data from the Los Angeles region. The curve , which is a least-squares fit to all of the data, can be used to estimate shear-wave velocity (V_S) for sediments in cases where only void-ratio (e) data are available.

Textural type.—The grain-size distribution of the surface sediment at the instrument site was classified as very coarse, coarse, medium, or fine, depending on the texture of the surface soil as mapped by the U.S. Department of Agriculture or the U.S. Bureau of Soils. Very coarse grained deposits contain boulders and cobbles, coarse-grained deposits contain gravel, medium-grained deposits contain chiefly sand, and fine-grained deposits contain chiefly silt and clay.

Depth to crystalline basement.—The depth to basement rock is the vertical distance from the land surface to crystalline igneous or metamorphic rock. Depths to basement, which may exceed 10 km in the Los Angeles basin (Yerkes and others, 1965, p. A4), have been estimated from electric logs, lithologic logs, and gravity models, such as McCulloh's (1957, 1960) model.

Depth to cementation.—Depth to cementation is defined as the distance from the land surface to sediments described in drilling logs as "cemented." The stratigraphic position at which this effect is noted apparently varied from driller to driller as well as from place to place.

Shear-wave velocity.—Borehole shear-wave velocity measurements were made to a depth of 30 m at 41 of the 98 nuclear recording sites (Gibbs and others, 1980; Fumal and others, 1981, 1982, 1984). Mean shear-wave velocity was computed for depth intervals of 0 to 2, 0 to 5, 0 to 15, and 0 to 30 m.

COMPARING GROUND RESPONSE WITH GEOLOGIC FACTORS

We will first explore the dependence between response data and geotechnical parameters to determine which factors have the strongest influence on site response in each period band. Having determined the most important factors, we will then present an empirical technique for predicting site response on the basis of these variables, whereby recording sites are grouped or clustered on the basis of similarity among the most important geologic site factors in a given period band. Grouping of the sites is accomplished by using the techniques of cluster analysis and discriminant analysis of cluster trials. To use these techniques, the mean site-response values and the geologic variables first must be assembled into a 98-station by 27-variable matrix, which permits us to easily extract relevant columns for analysis. After the clusters are formed, a geographic area is classified into one of the clusters on the basis of its geologically distinctive characteristics for a given period band, and the geometric mean cluster response is assigned as the response for that area. Although it is impractical to show all the details of the process leading to the final results of this study, we will examine the more important stages in the following discussions.

To examine the relation between site response and geologic parameters, the most straightforward approach is to group the sites according to variations in one of the geologic factors and to compute the mean response for each group, as table 39 does. These results indicate that, for the Los Angeles region, (1) levels of shaking at sites underlain by Holocene and Pleistocene sedimentary deposits are three to four times greater than those at sites underlain by crystalline rock for all period bands; (2) the void ratio has a strong influence on short-period response (void ratios in the 0.8 to 0.9 range indicate a mean response on soil that is six times greater than that on crystalline rock and three times greater than that on soils having low void ratios); and (3) amplitudes in the long-period band generally increase as the thickness of Quaternary deposits and (or) the depth to basement increases. The apparently anomalous finding (table 39) that the response of sites on Miocene rock is higher than that of sites on Pliocene rock may be attributed to causes other than age. Three of the Miocene rock sites are on ridges or areas of high topography and may be affected by topographic amplification (Boore, 1972; Rogers and others, 1974). The results given in brackets in table 39 are computed exclusive of these topographically high sites and show a closer correspondence between the two age groups at short and intermediate periods. In addition, the Pliocene rock sites that we have used are all located in downtown Los Angeles within an area of about 1 km² and thus do not represent an even geographic distribution of sites. The Pliocene rock sites in our sample may be characterized by anomalously low response, which reflects factors that we have not considered in our analysis. We have no means by which to analyze this possibility, however. The dependence of the response variables on each of the geologic factors was examined for each period band by grouping on one factor; table 39 shows some of the stronger interrelations between these variables, but a more elaborate analysis enabled us to study these interactions and others in more detail.

The smoothing techniques of exploratory data analysis (Mosteller and Tukey, 1977; Velleman and Hoaglin, 1981) can be applied to determine the influence of one factor on the response variable, given a body of data in which several factors are changing simultaneously. The chief problem is that, for a limited data set, it may not be possible to hold several factors constant while studying the influence of another; these smoothing techniques can be a helpful analysis tool for data satisfying certain assumptions. Figure 109, for instance, shows the smoothed short-period spectral ratio versus Holocene deposit thickness and void ratio. The broad

TABLE 39.—Comparision of mean ground response (relative to crystalline rock) from distant underground nuclear explosions recorded at sites within the Los Angeles region

[Geometric standard deviation in the response variable for these groups ranges from about 1.6 to 1.9. Short period, 0.2 to 0.5 s; intermediate period, 0.5 to 3.3 s; long period, 3.3 to 10.0 s]

Age of surficial materials	Short period	Intermediate period	Long period
Holocene	3.4	3.3	2.6
Pleistocene	3.2	3.1	2.6
Pliocene	1.4	1.6	2.0
Miocene	2.5 [1.9][1]	2.2 [1.8][1]	1.4 [1.3][1]
Mesozoic	1.7	1.1	0.8

Void ratio[2]	Short-period
0.2–0.4	2.3
0.4–0.6	3.1
0.6–0.7	3.0
0.7–0.8	4.2
0.8–0.9	6.2

Quaternary thickness, in meters	Intermediate period	Long period
0	1.6	1.3
0–75	2.3	1.4
75–200	3.6	2.9
200–500	3.6	3.1
500–1000	4.1	5.9
>1000	3.4	3.1

Depth to basement, in kilometers	Intermediate period	Long period
0	1.1	0.8
0–2	2.6	1.3
2–4	2.8	2.5
4–6	3.8	4.1
>6	3.8	3.9

[1]Bracketed value excludes topographically high sites.
[2]Average for uppermost 8 m.

peak in the Holocene thickness plot near 15 m is due to the shift through this period band of the fundamental resonance period of the Holocene layer. The general increase in the short-period response as void ratio increases is caused principally by the increase in shear-wave velocity between Holocene and Pleistocene deposits. For comparative purposes, theoretical spectral ratios were computed by using a horizontally layered SH-body-wave model and assuming viscous damping. The physical properties of the geologic column used in this modeling were generated by computer from the geologic data matrix; variable surface-layer velocities, fixed lower layer velocities, and depths to velocity contrasts were determined by Holocene and Quaternary deposit thicknesses and depth to basement, as figure 110 outlines. Surface-layer velocities were either measured borehole shear-wave velocities or computed from void ratios (fig. 108). The theoretical spectral ratios and the mean spectral values were processed in exactly the same fashion as the observed quantities. The concordance between observed data and theory supports our interpretation of the observed behavior and shows the utility of theoretical models for predicting mean site response. Although similar analysis of other factors indicates that variables such as depth to basement and Quaternary thickness have an effect on the short-period response, these variables and others are of secondary importance in comparison with Holocene deposit thickness and near-surface void ratio.

Identifying the chief geologic factors that control intermediate- and long-period response is more difficult than identifying those that control short-period response

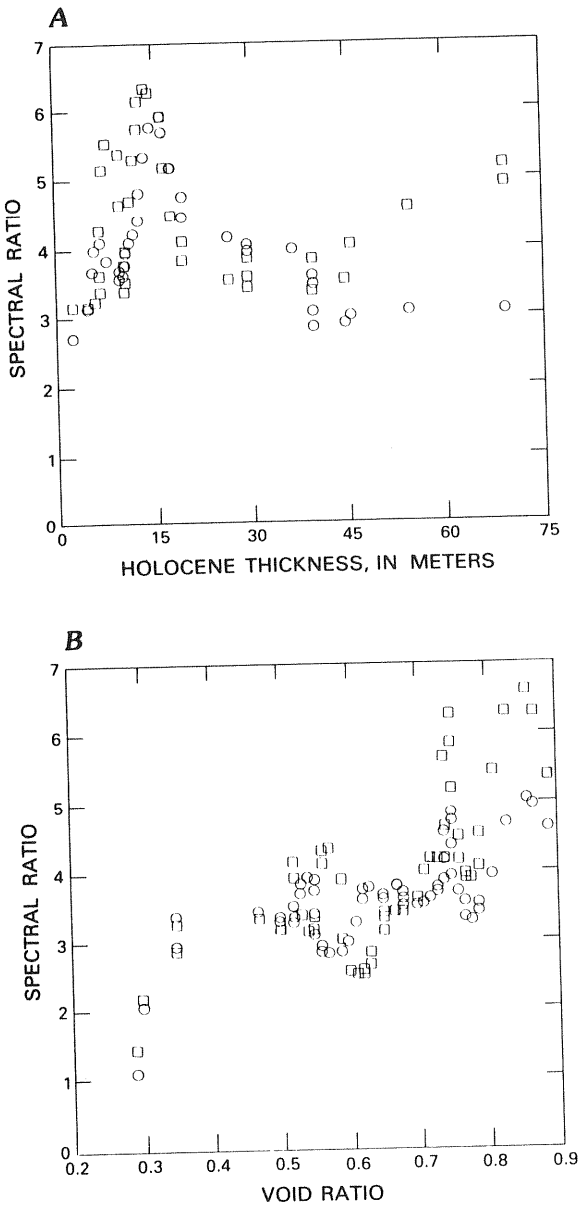

FIGURE 109.—Smoothed short-period spectral ratios at sites on Holocene deposits in comparison with Holocene thickness (*A*) and void ratio (*B*). To minimize the influence of void ratio in *A*, only sites having void ratios greater than 0.65 were included. A circle indicates theoretical values; a square indicates observed values.

because a larger number of variables may be involved. Some factors, such as Quaternary thickness and depth to basement rocks, are highly interdependent, because the deep parts of the Los Angeles basin have continued to subside during the Quaternary. Moreover, the deeper structural features and shear-wave velocities may not be as well determined as the geotechnical factors controlling the short-period response, and the amount of data (for the number of variables involved) may be too limited to fully explore the problem. Some consistent behavior in these two period bands is observed, nevertheless. For thin Quaternary soils and sedimentary-rock deposits, for instance, the response in these two bands is low, whereas, for thick deposits, high response is observed, as table 39 and figures 111 and 112 show. Although the SH-body-wave model partially predicts this behavior, the correspondence between observed and predicted values is poorer at longer periods, probably because the theory applied does not model the behavior of surface waves as they propagate through laterally inhomogeneous layers. Attempts to model surface waves in such media, however, have shown that surface-wave amplitudes increase as the waves propagate from thin layers to thicker ones (Drake and Mal, 1972; Murphy and Hewlett, 1975) and thus qualitatively support the results discussed above. Examination of factors other than Quaternary thickness and depth to basement indicates that the other factors have only secondary influence on the site response in these period bands.

After studying earthquake intensities in the Soviet Union, Medvedev (1962) reported that the presence of shallow ground water in alluvial sediments apparently increased the intensity of seismic shaking. On the basis of this conclusion, Evernden and Thomson (this volume) have increased predicted intensities by one unit where saturated alluvium occurs near the surface. We reevaluated Medvedev's (1962, figs. 2.1–2.7) data in light of the results of our study in the Los Angeles region. For the types of sites that Medvedev examined, as the depth to the water table decreased to less than 10 m, the thickness of the soil deposits increased to between 10 and 20 m. Thus, Medvedev's observation that the highest intensities occur at sites having shallow water tables (<10 m) can be attributed to resonant effects associated with soils between 10 and 20 m thick rather than to the effect of differences in depth to the water table. Our interpretation is supported by the lack of correlation between shear-wave velocities or site response and depth to water table in San Francisco (Borcherdt and Gibbs, 1976; Fumal, 1978). In Los Angeles, sites having a water table at less than 10 m have a distribution of void ratios whose mean is slightly higher than that of sites where the water table is deeper; furthermore, the number of Pleistocene sites in this group is proportionately larger than that in the group where the water table is shallow. Both of these occurrences may be due to some depositional or geomorphologic causes; in the data of this

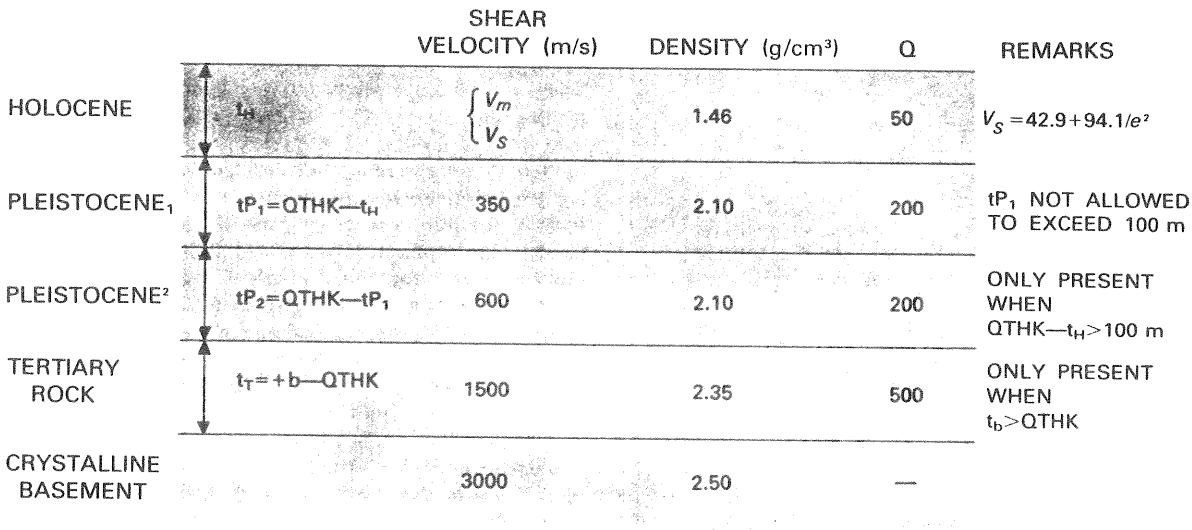

FIGURE 110.—Shear-wave-velocity model used to compute theoretical damped SH-wave response. The values for the symbols used in this figure either are calculated as shown or come from the geologic data matrix described in the text and table 38. t_h is the thickness of Holocene deposits; e, void ratio; V_S, shear-wave velocity calculated from the equation shown; V_m, borehole shear-wave velocity; t_p and t_{p2}, Pleistocene deposit thicknesses; t_Q, Quaternary deposit thickness; t_T, thickness of the Tertiary section; t_b, depth to crystalline rock. The quality factor, Q, is assumed in the model to include the effects of material attenuation.

study, however, these correlations are not strong enough to demonstrate a clear dependence between water table and site response. Thus, in the Los Angeles region, the lack of correlation between depth to the water table and mean short-period response or other factors controlling site response suggests that depth to water table apparently is not a reliable predictor of variation in shaking level, a view that conflicts with Evernden and Thomson's (this volume).

CLUSTERING SITES TO REFLECT GROUND-RESPONSE VARIABILITY

Sites having similar response characteristics can be clustered by computing some analytical measure of similarity between a list of items on the basis of their attributes. In our analysis, the items are recording sites, and the attributes are the geotechnical properties of each site (note that we do not use the response factor as an attribute, because we are attempting to predict response as a function of the geologic properties of a site). The clustering algorithm (Anderberg, 1973; Hartigan, 1975; IMSL, 1982) uses a computing rule to determine those items most nearly alike and the similarity level at which clusters of similar items are alike. The results can be plotted simply as an inverted hierarchical tree of similarity nodes (fig. 113). In this example, sites 5 and 6 are more nearly alike than any other pair, and 4 and 5 are more dissimilar than 1, 2, 3, and 4 or 5, 6, 7, and 8. The definition of clusters is determined by specifying the level of similarity below which clusters form. At similarity level one, 5 and 6 form a cluster; at level two, 1 and 2 and 5, 6, and 7 form two clusters; at level three, 1, 2, 3, and 4 and 5, 6, 7, and 8 form two clusters. The choice of a similarity level below which clusters form is subjective and, in practice, may change across the cluster diagram.

Once a set of clusters is formed by this procedure on a chosen set of factors, it is possible to analyze the degree to which these factors define unique groups by means of discriminant analysis (Morrison, 1969, 1974; Cooley and Lohnes, 1971; Nie and others, 1975), which determines the significance of each factor's discriminating power by using the statistics of factors within and between clusters. A set of discriminant functions is computed that permits calculation of the probability that a single member of a cluster belongs to that cluster or any other cluster; given a table of these probabilities, it is possible to calculate the percentage of sites that have been correctly classified.

Our application of this procedure was a trial-and-error process, during which some of the data analysis described above was done concurrent with the cluster and discriminant analysis. At the start, the site-response data were divided into rock and alluvial groups, and then clusters were examined in which many or all of the measured factors were part of the clustering model.

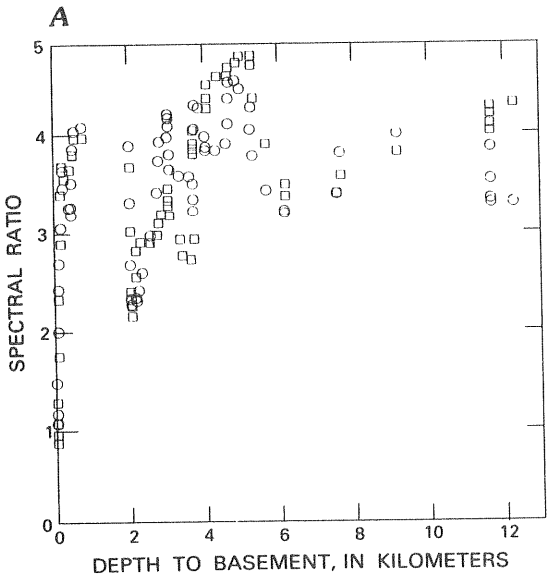

FIGURE 111.—Smoothed intermediate-period spectral ratio compared with depth to basement rock (*A*) and Quaternary thickness (*B*). A circle indicates theoretical values; a square indicates observed values.

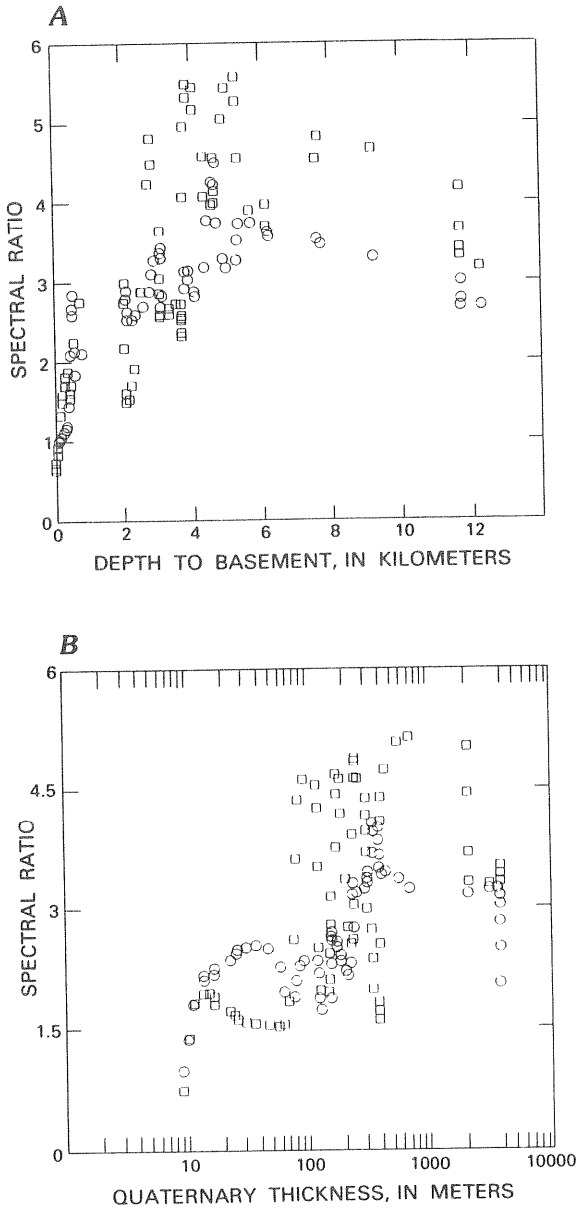

FIGURE 112.—Smoothed long-period spectral ratios compared with depth to basement rock (*A*) and Quaternary thickness (*B*). A circle indicates theoretical values; a square indicates observed values.

This approach, however, produced too many clusters, each of which had too few station members. The number of factors in the clustering process was reduced in a series of trials by gradually discarding factors that discriminated poorly between clusters on the basis of statistics produced by the discriminant analysis. Some continuous variables were categorized into discrete ranges to satisfy certain requirements of the analysis

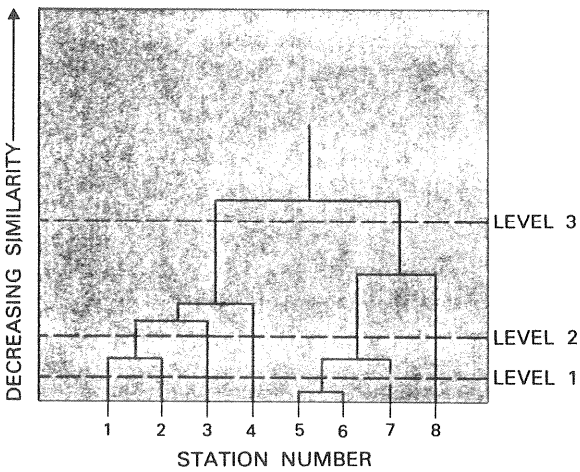

FIGURE 113.—A simple example of the clustering technique showing the cluster tree and the clusters that form at various levels of similarity.

techniques. In some cases, relevant ranges in this classifying scheme were apparent from the preliminary data analysis. For unconsolidated sediment thickness, for example, sites were classified into three ranges of thickness:

>0 m and <11 m
>11 m and <20 m
>20 m

These values are based on the behavior of the short-period response as a function of this variable. Comparison of the mean response values in the three period bands for each cluster set examined revealed that some cluster parameters reduced the response variance in each cluster better than others, in accord with the results of the preliminary data analysis (figs. 109, 111; table 39), which showed that the most important factors in each period band should be different. Ultimately, those cluster sets selected were chosen (1) because they had the lowest dispersion in the defining variables and because they used those factors having the strongest effect in a given period band, (2) because the probability of misclassification was low, and (3) because there was enough data in each cluster in the set to estimate the mean cluster properties. The final sets of clusters are a compromise between the many clusters that would be required to preserve all the complexity in the site response as a function of site geology and the requirement that each cluster contain enough cases to estimate its average response with acceptable variance.

Figure 114 shows the set of two rock clusters and eight alluvial clusters that was derived for the short-period band. This figure can be understood by using cluster 4A as an example. That cluster includes sites having a depth to basement rock of more than 0.5 km, an unconsolidated sediment thickness greater than 20 m, void ratios in the 0.6 to 0.7 range, and a geometric mean spectral ratio (hereafter shortened to spectral ratio) of about 3.6. The response predicted by using these clusters preserves the important features of site behavior noted above. For a given unconsolidated sediment thickness, for instance, the spectral ratio increases as the void ratio increases (for example, compare clusters 1A, 3A, and 6A). The spectral ratio also increases, for a constant void ratio, as the unconsolidated sediment (mostly Holocene sites) thickness increases to the critical range (for example, compare clusters 6A, 7A, and 8A). Note that the thin unconsolidated sediment clusters contain most of the Pleistocene sites; those unconsolidated Pleistocene sites in the thickness range 11 to 20 m, however, are grouped with the Holocene sites in this range. The spectral ratio of rock sites 1R and 2R is typically lower than that of the alluvial clusters, as one might predict on the basis of their shear-wave velocities. A comparison of clusters 1A and 2A shows that sites underlain by shallow alluvium over crystalline rock (2A) have a spectral ratio two times higher than that of the same type of site overlying a deep sedimentary basin; this difference further emphasizes the importance of high-impedance contrasts at shallow depths. Even though we were able to divide the sites into only 10 clusters, which result in a moderate range in the geologic and spectral ratio factors in each cluster, a useful result can be demonstrated by comparing average spectral level with shaking intensity. Borcherdt and others (1975) have shown that a factor of two in mean spectral level corresponds to a change in intensity units of 1 MM (Modified Mercalli); we infer, then, from the data in figure 114, that these clusters predict the true spectral ratio of a site more closely than one intensity-unit increment for 90 percent of the cases, because the geometric 90-percent confidence interval is less than a factor of two (1.45).

Figure 115 shows the clusters derived for the intermediate- and long-period bands. In principle, clustering for the intermediate-period band should be determined separately; it is known, for instance, that Holocene sites more than 30 m thick produce high spectral ratios in this period band. Because no clustering scheme was discovered for this band that was significantly better than that derived for the long-period band, however, these two bands are treated similarly. These cluster sets show that the spectral ratio increases as depth to basement rock increases up to 6 km; spectral ratios decrease slightly for greater sediment thicknesses. At the shorter periods in the intermediate-period

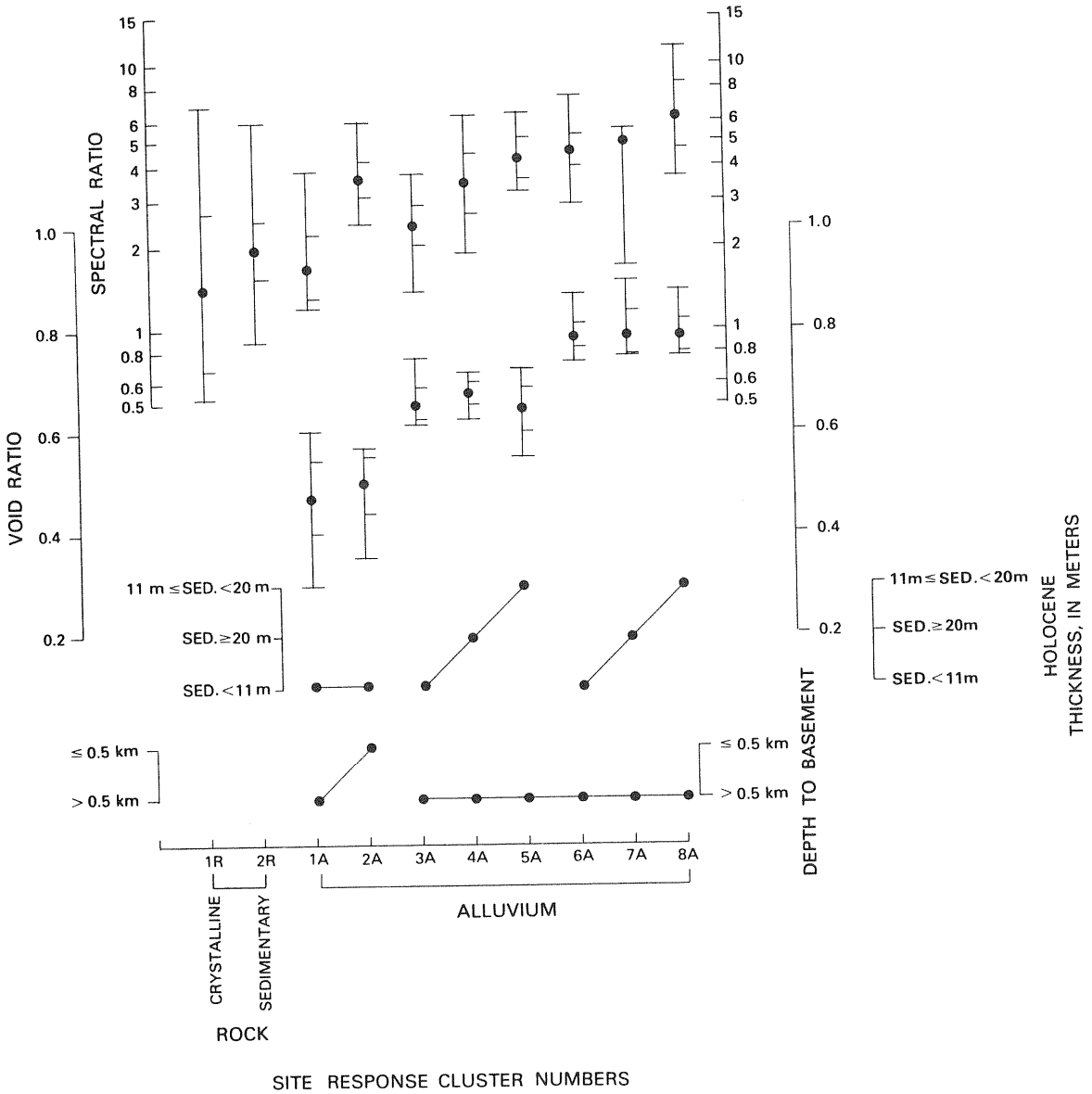

FIGURE 114.—Site clusters for short-period ground motions in the Los Angeles region. Solid circles indicate the geometric mean of the short-period spectral ratios, the mean void ratio, the unconsolidated sediment thickness, and the depth to basement rock for a given cluster. Vertical bars indicate the range in a variable, and side ticks indicate the 90-percent confidence intervals.

band, this decrease may be caused partially by wave attenuation in both the soil and the rock column. Although the cause of this behavior in the long-period band is not clear, it is also predicted by the SH-wave results shown in figures 111 and 112 and may be produced by the first minimum in the theoretical spectral ratio that occurs near 6 s owing to destructive wave interference. The geometric mean spectral ratios at rock sites range up to two, whereas those at soil sites can reach up to about five for clusters having a depth to basement rock in the

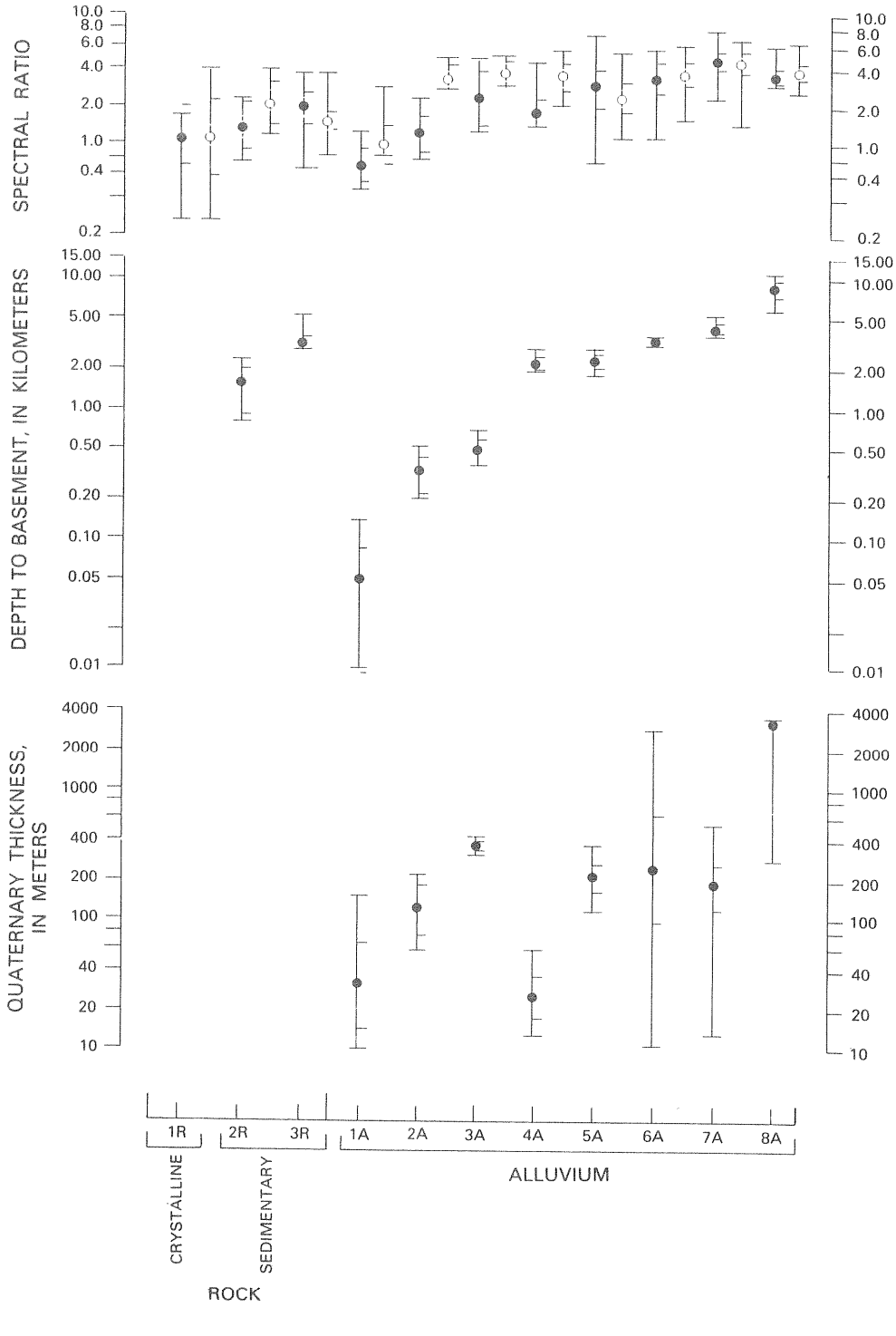

FIGURE 115.—Site clusters for intermediate- and long-period ground motions in the Los Angeles region. Top scale: Open circles and solid circles indicate the geometric mean of the intermediate- and long-period spectral ratio values, respectively. Bottom scales: Solid circles indicate the geometric mean depth to basement rock or Quaternary thickness. The range and the 90-percent confidence intervals for each factor are indicated by vertical bars and side ticks, respectively.

4- to 6-km range. The low spectral ratio (0.7) for sites underlain by very thin soils is not completely understood. Several of the sites that have the lowest amplification factors in this cluster lie within mountain ranges, however. Long-period surface waves may have unusually low amplitudes relative to CIT in such locations because surface-wave energy can be reflected by the boundaries of the ranges (Aki, 1969; Murphy and Hewlett, 1975; Johnson, 1979).

PREDICTING GEOGRAPHIC VARIATION IN GROUND RESPONSE

Cluster sets such as those described above can be used to map the relative ground response (in comparison with that at sites on crystalline bedrock) expected for a particular region from future earthquakes. As a demonstration of the methods and techniques, we have prepared a set of predictive ground-response maps for a small area approximately centered on the Los Angeles Civic Center (figs. 116*A*, 116*B*, 116*C*). In brief, our proposed procedure associates geographic areas having particular geologic attributes with a given site-response cluster. The spectral ratio for that cluster is then assigned to the geographic area.

We will discuss the procedures used to produce the relative ground-response map for the short-period band (fig. 116*C*) as an example of the general technique. Figure 117 schematically illustrates the method. The first two steps are (1) to prepare a cluster diagram for the study area that relates observed spectral ratios to geologic factors influencing levels of shaking and (2) to assemble a suite of maps that show rock and sediment types, depths to basement rocks, thicknesses of unconsolidated (Holocene and Pleistocene) sediments, and the distribution of void ratios characteristic of unconsolidated sediments. The third step combines the geologic maps assembled in step 2 into groups that reflect the geographic distribution of the important cluster factors for a given period band. The easiest method is to visually compare the geologic data maps (by using transparent overlays), noting where two or more sets of geologic attributes are coincident, and then draw zone boundaries. An area of high void ratio, for instance, may coincide with one or more of the three categories of unconsolidated sediment thickness. Where it coincides with an area in the thick category, cluster 7A is assigned to the area; where it coincides with an area in the thin catagory, cluster 6A is assigned, and so on. In the final step, each zone associated with a particular cluster is assigned a response value on the basis of spectral ratios from figure 114. This procedure was judged more reasonable than attempting to contour the response values, because it is known from damage studies that site response can vary rapidly over very short distances, particularly for low structures. Step changes in response can thus occur as a function of near-surface variations in geology, and this method of mapping predicted response reflects this behavior, at least for the short-period map. The long- and intermediate-period maps are prepared in the same manner, but, because ground response at these periods changes more gradually as a function of variable geologic factors, these maps are more nearly like contour maps on which transitions from low to high response occur over broad zones.

The map showing predicted relative ground response for long periods (fig. 116*A*) is of significance to structures more than 30 stories high. It predicts that low response will characterize areas underlain by rock and thin alluvial deposits; the highest levels of response will occur in areas where the depth to basement rock ranges from 4 to 6 km, and slightly lower levels are predicted in the deepest parts of the basin. The lowest response will be where crystalline basement is located at or near the surface in the Santa Monica Mountains and Verdugo Mountains areas. South of Burbank and west of Pasadena, the relatively thin alluvium in the intermontane basin areas and along the Los Angeles River valley near the eastern end of the Santa Monica Mountains and north of the Los Angeles Civic Center also will exhibit a low response. Response is expected to increase to the northwest (San Fernando Valley), to the east (San Gabriel Valley), and to the south (Los Angeles basin). The southwestern part of the map shows a relatively low response where crystalline basement rock is about 3 km deep along the Newport-Inglewood zone.

The map showing predicted relative ground response for intermediate periods (fig. 116*B*) is of significance to 5- to 30-story structures. This map is similar to the long-period map. The chief difference is that the response in this period band of areas covered locally by a thin veneer of alluvial deposits and overlying crystalline basement rock or Tertiary sedimentary rock (1A, 2A, and 4A of fig. 115) is expected to be higher than that in the long-period band.

The map showing predicted relative ground response for short periods (fig. 116*C*), which is most relevant to buildings in the two- to five-story class, has been prepared for only the central third of the area shown in the intermediate- and long-period maps. The lowest response is predicted for areas underlain by crystalline and sedimentary rock, and the highest response occurs in regions where thicknesses of near-surface alluvium (11–20 m) and high void ratios (≥ 0.7) produce significant resonant response in this period band. In some respects,

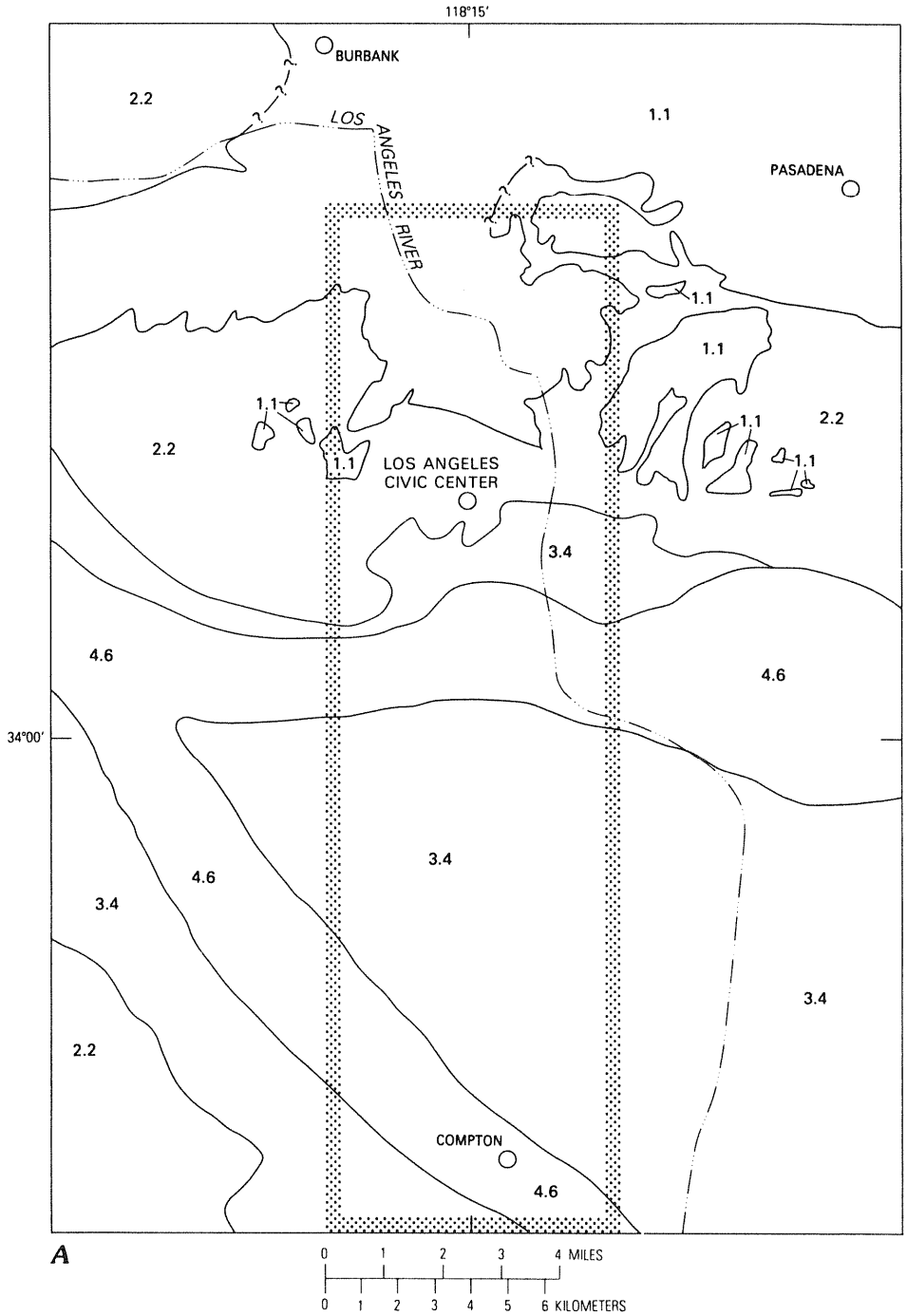

FIGURE 116.—Predicted relative ground response for part of the Los Angeles basin. Numbers are mean amplification factors compared with levels of shaking at sites on crystalline basement rock. *A*, Map for the long-period band (3.3–10 s) of significance to buildings 30 stories high or more. Stippling outlines area shown in *C*. *B*, Map for the

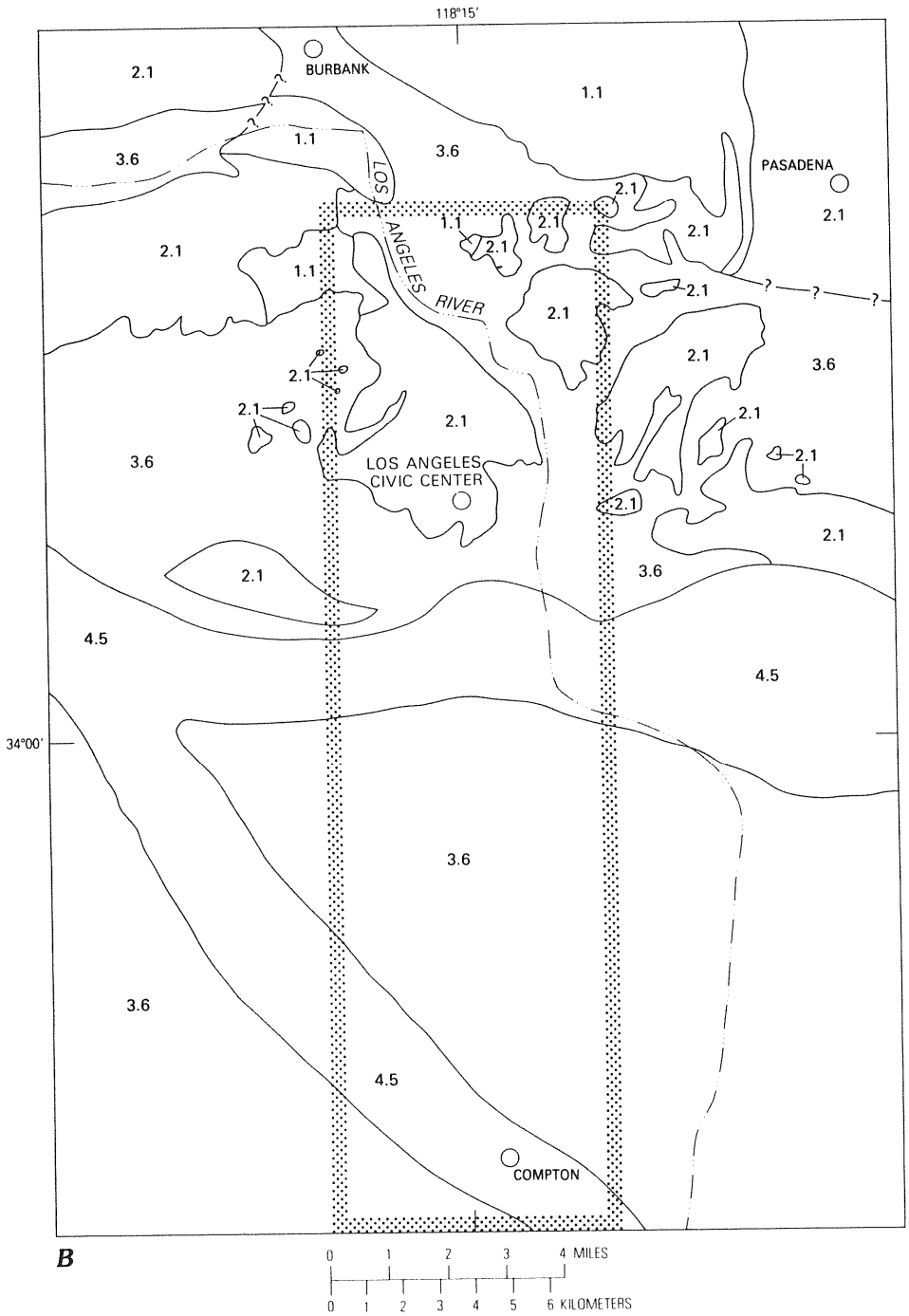

intermediate-period band (0.5–3.3 s) of significance to buildings 5 to 30 stories high. Stippling outlines area shown in C. C, Map for the short-period band (0.2–0.5 s) of significance to buildings two to five stories high.

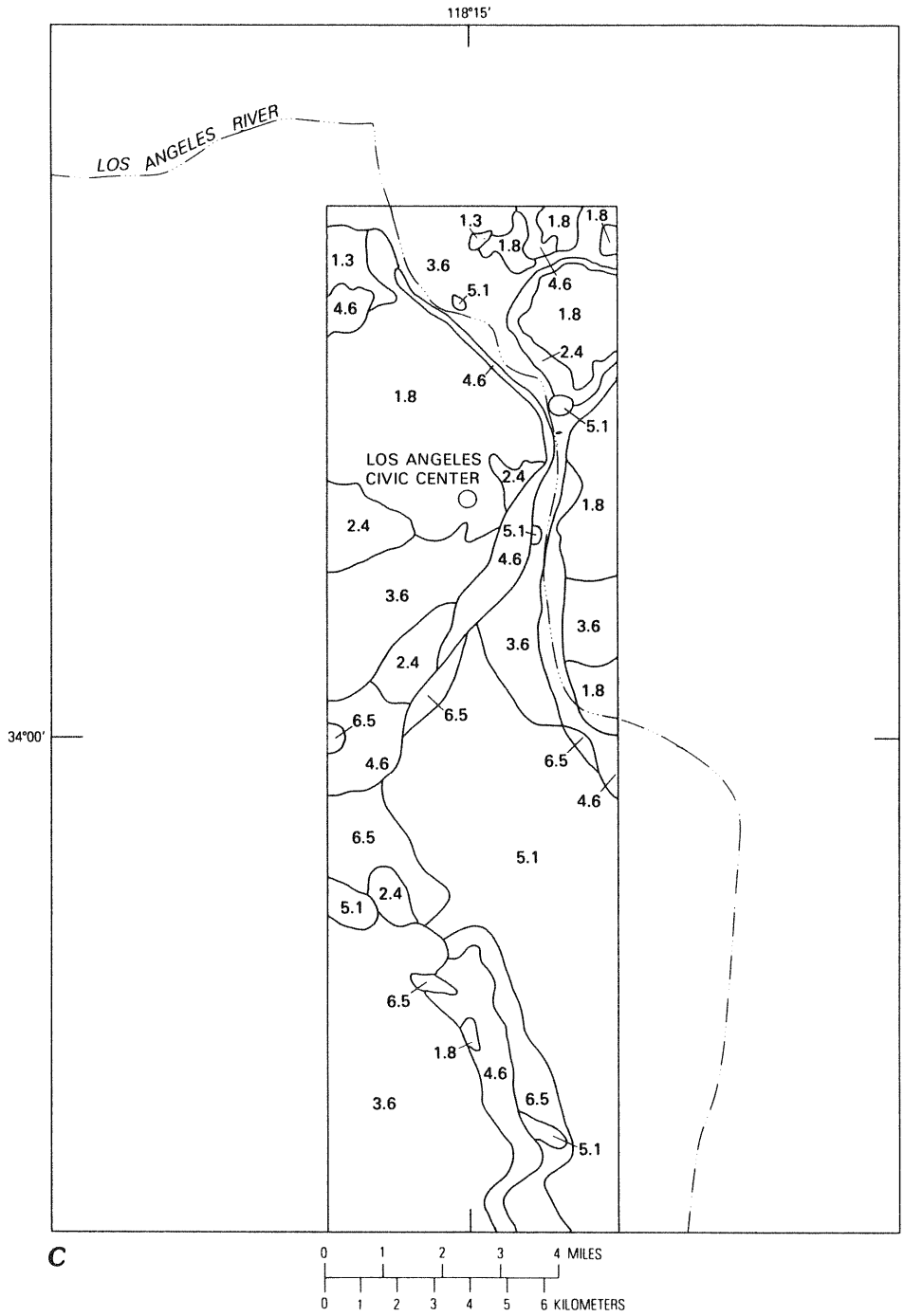

FIGURE 116.—Continued

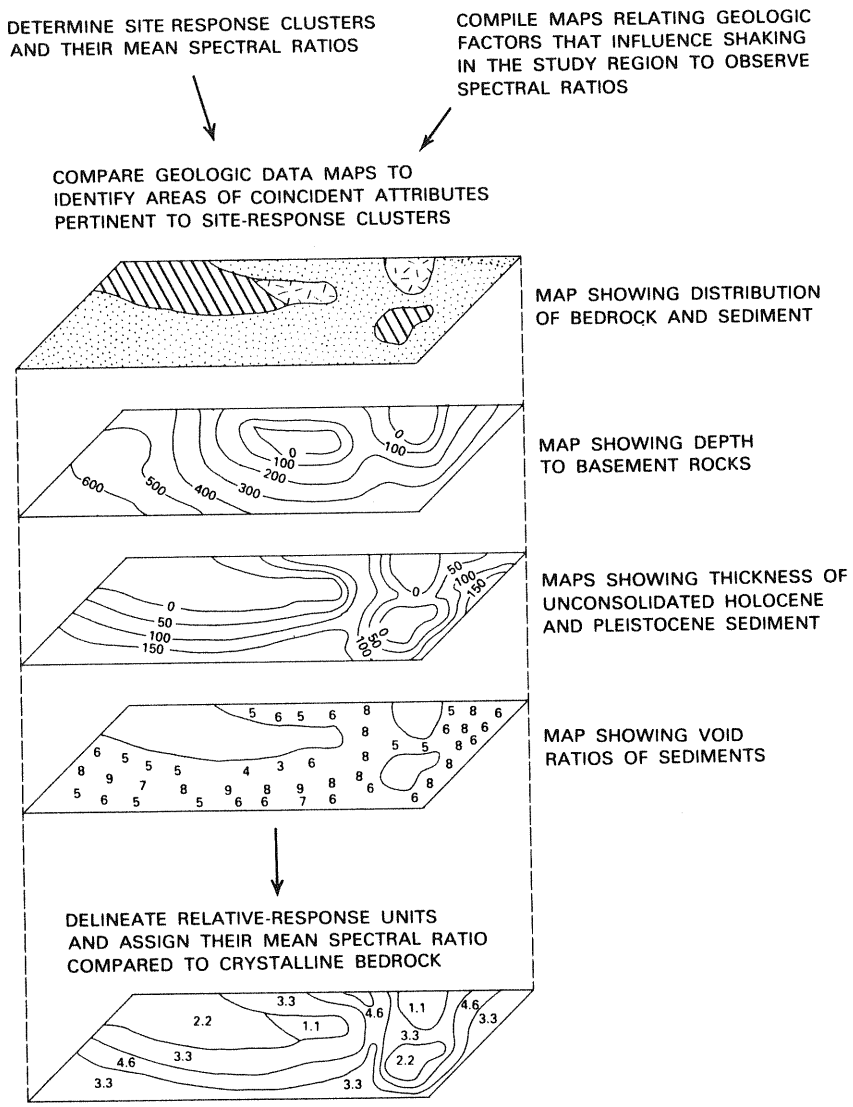

FIGURE 117.—Procedure used to construct the predicted relative ground-response maps shown in figure 116.

this map closely resembles a surficial geologic map; thus, sedimentologic details of the alluviated valleys, including those of the Los Angeles River valley, are expressed clearly by the mapped response units. The southwestern part of the map depicts an area where silt (characterized by high void ratios) deposited by the Los Angeles River thins to the west and wedges out along the eastern flank of the Newport-Inglewood zone, where deformed Pleistocene deposits characterized by low void ratios are exposed. It should be noted that high response at short periods may occur at sites underlain by rock if these sites are near the crest of a ridge or other pronounced topography, as the range of high response for clusters 1R and 2R (fig. 114) shows.

VALIDITY AND LIMITATIONS OF TECHNIQUE

In a qualitative way, data from several other studies support this study's conclusions about the importance of unconsolidated sediment thickness. As noted above, Chiaruttini and Siro (1981) have observed accelerations at sites underlain by thin soils (< 20 m) that were greater than those observed on rock or thicker soil sites by factors of four or five. The difference in the behaviors of thin and thick soil is not so great in the data of this study, but this discrepancy may be due to the fact that we have no data for periods shorter than 0.2 s, where peak acceleration energy commonly occurs and attenuation effects become strong. We infer from Chiaruttini and Siro's data that material attenuation may have an important effect at sites underlain by thick soils and for ground motions in the period range where peak acceleration energy occurs. This conclusion is also supported by the work of McEvilly and Johnson (1980), who have found that Q factors, which measure attenuation of seismic energy, must be between 6 and 40 for shear waves in order to explain the amplitude levels on their accelerograms.

The effect of near-surface sediment thickness can also be seen in the data of Minakami and Sakuma (1948) for the 1946 Nankai, Japan, earthquake. The highest levels of ground motion were observed in regions where the thickness of fine sand was in the 10- to 20-m range (figs. 103–109). Ooba (1957, fig. 10) has shown that, for the 1944 Tonankai, Japan, earthquake (M 8.0), the highest percentage of collapsed houses (> 50 percent) occurs where the thickness of clayey overburden is in the 15- to 35-m range, and the lowest (< 10 percent) occurs in regions underlain by thinner sediment or rock.

The clustering scheme proposed here to predict site response can be partially tested by applying it in other areas where strong ground motion has been recorded and sufficient data about site conditions are available. We classify the Richmond recording station (McEvilly and Johnson, 1980), for instance, into clusters 7A (short period) and 4A (intermediate period) and Coyote Lake earthquake recording station 2 (Joyner and others, 1981) into clusters 6A (short period) and 2A (intermediate period). At both sites, the predicted mean response for both period bands ranges between 3 and 5, and the observed response ranges between 3 and 4.

This clustering scheme, however, cannot be applied to all site conditions. If, for example, near-surface mean shear-wave velocity is considerably less (say, 100 m/s) or greater (say, 400 m/s) than the mean value for sites displaying resonant conditions in Los Angeles (about 200 m/s), then resonant conditions in the short-period band would occur at one-half or twice the thickness range, respectively, of this study, and the mean spectral values would also be modified by as much as twice or one-half the levels of this study. Thus, in regions where shear-wave velocities are exceptionally low, at least three additional high void-ratio clusters having different ranges of near-surface sediment thickness would be required. Applying these clusters to other regions requires critical evaluation of the important geotechnical factors to determine if sites in the region, in fact, fit the clusters of this study, which do not represent all geologic conditions.

SUMMARY

Local geologic conditions can significantly influence the relative levels of ground shaking caused by earthquakes. Based on the generally valid assumption that the relative responses of different sites are approximately equivalent for both low and high levels of motion, comparative studies of ground motion recorded within a region provide a reliable method for estimating the shaking effects likely to be caused by future earthquakes.

We have analyzed the geographic variation in relative ground response at 98 locations within the Los Angeles region by using a collection of ground-motion recordings from a series of underground nuclear test explosions at the Nevada Test Site. The mean spectral levels of the site responses from these distant events were evaluated in three period bands of engineering importance as a function of the underlying geotechnical conditions at each site. These properties were collected from a wide range of sources, including engineering borehole and water-well logs in city files, geologic and gravity maps, and a limited number of measured shear-wave velocities in near-surface sediments. In preliminary evaluations of the data, we determined, for instance, that the levels of shaking experienced by sites underlain by Holocene and Pleistocene sediments are three to four times greater than those experienced by sites underlain by crystalline rock for periods less than 0.5 s and that ground motions at periods greater than 0.5 s increase as Quaternary thickness and (or) depth to basement rock increases.

The geotechnical factors having the strongest influence on site response in each period band were identified by means of statistical clustering techniques. The results indicate that, at periods less than 0.5 s, the most significant factors controlling ground response are mean void ratio in the near-surface layers, unconsolidated sediment thickness (principally Holocene deposit thickness), and depth to basement rock, those sites having near-surface sediment thickness in the 10- to 20-m

range demonstrating site resonance effects. At periods greater than 0.5 s, depth to basement rock and the thickness of Quaternary sediments were found to be controlling factors.

These clusters were used in a procedure developed to produce maps of relative ground response for part of the Los Angeles basin. The clusters can also be used to make estimates of shaking effects at specific locations, if the necessary geotechnical information is available for the site. This technique has important implications for earthquake hazard reduction in Los Angeles and elsewhere, because it can be used to predict future relative ground response from geotechnical data that are ordinarily obtained in the course of urban development. The utility of the technique is further enhanced by provisions permitting ground-response estimates to be made for period bands pertinent to structures of different sizes. This mapping procedure may be useful for seismic zonation in other earthquake-prone urban areas, if clusters applicable to the specific geologic framework of the region being studied can be determined.

Aki, K., 1969, Analysis of the seismic coda of local earthquakes as scattered waves: Journal of Geophysical Research, v. 74, p. 615–631.

Algermissen, S. T., Rinehart, W. A., and Stepp, J. C., 1972, A technique for seismic zoning: Economic considerations, *in* International Conference on Microzonation for Safer Construction, 1st, Seattle, Wash., 1978, Proceedings: p. 943–956.

Anderberg, M. R., 1973, Cluster analysis for applications, *in* Probability and mathematical statistics, v. 19: New York, Academic, 359 p.

Barosh, P. J., 1969, Use of seismic intensity data to predict the effects of earthquakes and underground nuclear explosion in various geologic settings: U.S. Geological Survey Bulletin 1279, 93 p.

Boore, D. M., 1972, A note on the effect of simple topography on seismic SH waves: Bulletin of the Seismological Society of America, v. 62, p. 275–284.

Borcherdt, R. D., 1970, Effects of local geology on ground motion near San Francisco Bay: Bulletin of the Seismological Society of America, v. 60, p. 29–61.

Borcherdt, R. D., and Gibbs, J. F., 1976, Effects of local geologic conditions in the San Francisco Bay region on ground motions and the intensities of the 1906 earthquake: Bulletin of the Seismological Society of America, v. 66, p. 467–500.

Borcherdt, R. D., Joyner, W. B., Warrick, R. E., and Gibbs, J. F., 1975, Response of local geologic units to ground shaking, *in* Studies for seismic zonation of the San Francisco Bay region: U.S. Geological Survey Professional Paper 941–A, p. A52–A67.

California Department of Water Resources, 1966, San Gabriel Valley, Appendix A—Geohydrology: California Department of Water Resources Bulletin 104–2, 229 p.

California Water Rights Board, 1961, Report of referee, City of Los Angeles vs. the City of San Fernando, Superior Court of the State of California case no. 650048: Sacramento, Calif., 258 p., apps.

Campbell, K. W., 1976, A note on the distribution of earthquake damage in Long Beach, 1933: Bulletin of the Seismological Society of America, v. 66, p. 1001–1006.

Chiaruttini, C., and Siro, L., 1981, The correlation of peak ground horizontal acceleration with magnitude, distance, and seismic intensity for Friuli and Ancona, Italy, and the Alpide Belt: Bulletin of the Seismological Society of America, v. 71, p. 1993–2009.

Cooley, W. W., and Lohnes, P. R., 1971, Multivariate data analysis: New York, John Wiley, 364 p.

Drake, L. H., and Mal, A. K., 1972, Love and Rayleigh waves in the San Fernando Valley: Bulletin of the Seismological Society of America, v. 62, p. 1673–1690.

Dutcher, L. C., and Garrett, A. A., 1963, Geologic and hydrologic features of the San Bernardino area, California: U.S. Geological Survey Water-Supply Paper 1419, 114 p.

Earthquake Engineering Research Laboratory, 1969–1975, Strong-motion earthquake accelerograms, VI, pts. A–Y: Pasadena, Calif., California Institute of Technology, v. 2.

Espinosa, A. F., and Algermissen, S. T., 1972, A study of soil amplification factors in earthquake damage areas, Caracas, Venezuela: National Oceanic and Atmospheric Administration Technical Report ERL 280–ESL 31, 201 p.

Esteva, L., 1977, Microzoning: Models and reality, *in* World Conference on Earthquake Engineering, 6th, New Delhi, 1977, Proceedings: p. 27–43.

Fumal, T. E., 1978, Correlations between seismic wave velocities and physical properties of near-surface geologic materials in the southern San Francisco Bay region: Santa Cruz, Calif., University of California, unpublished M.Sci. thesis, 113 p.

Fumal, T. E., Gibbs, J. F., and Roth, E. F., 1981, In-situ measurements of seismic velocity at 19 locations in the Los Angeles, California, region: U.S. Geological Survey Open-File Report 81–399, 121 p.

———1982, In-situ measurements of seismic velocity at 22 locations in the Los Angeles, California, region: U.S. Geological Survey Open-File Report 82–833, 138 p.

———1984, In-situ measurements of seismic velocity at 16 locations in the Los Angeles, California, region: U.S. Geological Survey Open-File Report 84–681, 109 p.

Gibbs, J. F., Fumal, T. E., and Roth, E. F., 1980, In-situ measurements of seismic velocity at 27 locations in the Los Angeles, California, region: U.S. Geological Survey Open-File Report 80–378, 167 p.

Gutenberg, B., 1957, Effects of ground on earthquake motion: Bulletin of the Seismological Society of America, v. 47, p. 221–250.

Hanks, T. C., 1975, Strong ground motion of the San Fernando, Calif., earthquake: Ground displacement: Bulletin of the Seismological Society of America, v. 65, p. 193–225.

Hanks, T. C., and McGuire, R. K., 1981, The character of high-frequency strong ground motion: Bulletin of the Seismological Society of America, v. 21, p. 2071–2095.

Hardin, B. O., and Drnevich, V. P., 1972, Shear modulus and damping in soils: Measurement and parameter effects: Proceedings of the American Society of Civil Engineers, Journal of the Soil Mechanics and Foundations Division, v. 98, p. 603–624.

Hartigan, J. A., 1975, Clustering algorithms: New York, John Wiley, 351 p.

Hays, W. W., and Algermissen, S. T., 1982, Problems in the construction of a map to zone the earthquake ground shaking hazard, *in* International Earthquake Microzonation Conference, 3d, Seattle, Wash., 1982, Proceedings: p. 145–156.

Hays, W. W., and King, K. W., 1982, Zoning of the earthquake ground shaking hazard along the Wasatch Fault zone, Utah, *in* International Earthquake Microzonation Conference, 3d, Seattle, Wash., 1982, Proceedings: p. 1307–1318.

Howell, B. F., and Schultz, T. R., 1975, Attenuation of Modified Mercalli intensity with distance from the epicenter: Bulletin of the Seismological Society of America, v. 65, p. 651–666.

Hudson, J. A., and Douglas, A., 1975, Rayleigh wave spectra and group velocity minima, and the resonance of P waves in layered structures: Geophysical Journal of the Royal Astronomical Society, v. 42, p. 175–188.

IMSL, 1982, IMSL computer programs: Houston, Tex.

Johnson, C. E., 1979, I, Cedar—An approach to the computer automation of short-period local seismic networks; II, Seismotectonics of the Imperial Valley of southern California: Pasadena, Calif., California Institute of Technology, unpublished Ph.D. thesis, 332 p.

Joyner, W. B., and Boore, D. M., 1981, Peak horizontal accelerations and velocity from strong motion records including records from the 1979 Imperial Valley, California, earthquake: Bulletin of the Seismological Society of America, v. 71, p. 2011–2038.

Joyner, W. B., and Chen, A. T. F., 1975, Calculation of nonlinear ground response in earthquakes: Bulletin of the Seismological Society of America, v. 65, p. 1315–1336.

Joyner, W. B., Warrick, R. E., and Fumal, T. E., 1981, The effect of Quaternary alluvium on strong ground motion in the Coyote Lake, California, earthquake of 1979: Bulletin of the Seismological Society of America, v. 71, p. 1333–1349.

Kanai, K., 1952, Relation between the nature of surface layer and the amplitude of earthquake motion: Bulletin of the Earthquake Research Institute, University of Tokyo, v. 30, p. 31–37.

Kanai, K., and Yoshizawa, S., 1958, The amplitude and the period of earthquake motions: Bulletin of the Earthquake Research Institute, University of Tokyo, v. 36, p. 275–293.

Kanai, K., Takahasi, R., and Kawasumi, H., 1956, Seismic characteristics of ground, *in* World Conference on Earthquake Engineering, 1st, Berkeley, Calif., 1956, Proceedings: p. 31-1–31-16.

King, K. W., 1982, A study of surface and subsurface ground motions at Calico Hills, Nevada, Test Site: U.S. Geological Survey Open-File Report 82–1044, 19 p.

Lastrico, R., 1970, Effects of site and propagation path on recorded strong earthquake motions: Los Angeles, Calif., University of California, unpublished Ph.D thesis, 205 p.

Lawson, A. C., and others, 1908, The California earthquake of April 18, 1906, *in* Carnegie Institute of Washington Atlas: Washington, D.C., 2 v., 643 p.

McCulloh, T. H., 1957, Simple Bouguer gravity and generalized geologic map of the northwestern part of the Los Angeles basin, California: U.S. Geological Survey Geophysical Investigations Map GP–149, scale 1:48,000.

_____1960, Gravity variations and the geology of the Los Angeles basin of California, *in* Short papers in the geological sciences: U.S. Geological Survey Professional Paper 400–B, p. B320–B325.

McEvilly, T. V., and Johnson, L. R., 1980, The role of anelasticity in earthquake ground motion: U.S. Geological Survey Open-File Report 80–912, 36 p.

McFadden, L. D., and Tinsley, J. C., 1982, Soil profile development in xeric climates; a summary, *in* Tinsley, J. C., and others, eds., Guidebook; Late Quaternary pedogenesis and alluvial chronologies of the Los Angeles and San Gabriel Mountains, southern California, and Holocene faulting and alluvial stratigraphy within the Cucamonga fault zone: Boulder, Colo., Geological Society of America, p. 15–19.

Medvedev, J. V., 1962, Engineering seismology: Moscow, Academia Nauk. (Translated into English by Israel Program for Scientific Translations, Jerusalem, 1965, 260 p.)

Milne, J., 1898, Seismology, 1st ed.: London, Kegan Paul, Trench, Trüber, 320 p.

Minakami, T., and Sakuma, S., 1948, The earthquake-motions on various formations of the earth's surface, pt. I, Observations at Koti City: Bulletin of the Earthquake Research Institute, University of Tokyo, v. 26, p. 61–66.

Morrison, D. G., 1969, On the interpretation of discriminant analysis: Journal of Marketing Research, v. 6, p. 156–163.

_____1974, Discriminant analysis, *in* Ferber, R., ed., Handbook of marketing research: New York, McGraw-Hill, 1344 p.

Mosteller, F., and Tukey, J. W., 1977, Data analysis and regression: Reading, Mass., Addison-Wesley, 588 p.

Mueller, C. S., D. M. Boore, and R. L. Porcella, 1982, Detailed study of site amplification at El Centro strong-motion array station no. 6, *in* International Earthquake Microzonation Conference, 3d, Seattle, Wash., 1982, Proceedings, v. 1: p. 413–424.

Murphy, J. R., and Hewlett, R. A., 1975, Analysis of seismic response in the city of Las Vegas, Nevada: A preliminary microzonation: Bulletin of the Seismological Society of America, v. 65, p. 1575–1597.

Murphy, J. R., Weaver, N. L., and Lamers, G. B., 1970, Effects of local geology on the amplitudes of seismic waves, *in* U.S. Atomic Energy Commission Report NVO–1163–205: Springfield, Va., National Technical Information Service, 3 v.

Murphy, J. R., Weaver, N. L., and Davis, A. H., 1971, Amplification of seismic body waves by low-velocity surface layers: Bulletin of the Seismological Society of America, v. 61, p. 109–145.

Nie, N. H., Hull, C. H., Jenkins, J. G., Steinbrenner, K., and Bent, D. H., 1975, SPSS statistical package for the social sciences: New York, McGraw-Hill, 675 p.

Nuclear Regulatory Commission, 1980, Geotechnical data from accelerograph stations investigated during the period 1975–1979, *in* U.S. Nuclear Regulatory Commission Report NUREG/CR–1643 R6, RA: Springfield, Va., National Technical Information Service, 150 p.

Ooba, S., 1957, Study of the relation between subsoil conditions and the distribution of the damage percentage of wooden dwelling houses in the province of Totomi in the case of the Tonankai earthquake of December 7, 1944: Bulletin of the Earthquake Research Institute, University of Tokyo, v. 36, p. 201–295.

Poland, J. F., 1959, Hydrology of the Long Beach–Santa Ana area, California: U.S. Geological Survey Water-Supply Paper 1471, 257 p.

Poland, J. F., Garrett, A. A., and Sinnot, A., 1959, Geology, hydrology, and chemical character of ground water in the Torrance–Santa Monica area, California: U.S. Geological Survey Water-Supply Paper 1461, 425 p.

Poland, J. F., Piper, A. M., and others, 1956, Ground-water geology of the coastal zone, Long Beach–Santa Ana area, California: U.S. Geological Survey Water-Supply Paper 1109, 162 p.

Porcella, R. L., and Matthiesen, R. B., 1979, Preliminary summary of the U.S. Geological Survey strong-motion records from the Oct. 15, 1979, Imperial Valley earthquake: U.S. Geological Survey Open-File Report 79–1654, 41 p.

Rogers, A. M., and Hays, W. W., 1978, Preliminary evaluation of site transfer functions developed from earthquake and nuclear explosions, *in* International Conference on Microzonation, 2d, San Francisco, Calif., 1978, Proceedings, v. 2: p. 753–764.

Rogers, A. M., Katz, L. J., and Bennett, T. J., 1974, Topographic effects on ground motion for incident P waves: A model study: Bulletin of the Seismological Society of America, v. 64, p. 437–456.

Rogers, A. M., Tinsley, J. C., Hays, W. W., and King, K. W., 1979, Evaluation of the relation between near-surface geological units and ground response in the vicinity of Long Beach, California: Bulletin of the Seismological Society of America, v. 61, p. 1603–1622.

Rogers, A. M., Covington, P. A., Park, R. B., Borcherdt, R. D., and Perkins, D. M., 1980, Nuclear event time histories and computed site transfer functions for locations in the Los Angeles region: U.S. Geological Survey Open-File Report 80–1173, 207 p.

Rogers, A. M., Borcherdt, R. D., Covington, P. A., and Perkins, D. M., 1984, A comparative ground response study near Los Angeles using recordings from Nevada nuclear tests and the 1971 San Fernando earthquake: Bulletin of the Seismological Society of America, v. 74, p. 1925–1949.

Seed, H. B., and Idriss, I. M., 1970, Soil moduli and damping factors for dynamic response analysis: Berkeley, Calif., Report EERC 70–10, Earthquake Engineering Research Center, University of California, 15 p.

Thomas, R. G., Landry, J. J., and Turney, R. J., 1961, Planned utilization of the groundwater basins of the coastal plain of Los Angeles County, California, Appendix A—Groundwater geology: California Department of Water Resources Bulletin 104, 181 p.

Turner, E., and Stokoe, K. H., 1982, Static and dynamic properties of clayey soils subjected to 1979 Imperial Valley earthquake: Austin, Tex., Engineering Report GR 82–26, Geotechnical Engineering Center, University of Texas, 208 p.

Velleman, P., and Hoaglin, D., 1981, ABC's of EDA: Belmont, Calif., Duxbury Press, 354 p.

Wood, H. D., 1933, Preliminary report on the Long Beach earthquake: Bulletin of the Seismological Society of America, v. 23, p. 42–56.

Yerkes, R. F., McCulloh, T. H., Schoellhamer, J. E., and Vedder, J. G., 1965, Geology of the Los Angeles basin, California—An introduction: U.S. Geological Survey Professional Paper 420–A, 57 p.

LIQUEFACTION CRITERIA FOR NEW ENGLAND: A DESIGN ENGINEER'S OVERVIEW

Cetin Soydemir
Haley & Aldrich, Inc.
Cambridge, Massachusetts

INTRODUCTION

State-of-the-art criteria on regional seismicity generally consider New England States as of "moderate" seismicity. November 1957 Cape Ann, Mass. (MMVIII) earthquake has been the most strongly felt, historically known seismic activity in the region. More recent, instrumentally recorded earthquakes include 9 and 11 January 1982 New Brunswick (M = 5.7 and 5.4, respectively), 18 January 1982 Gaza, New Hampshire (M = 4.8), 10 April 1962 Middlebury, Vermont (M = 5.0), and 20 and 24 December 1940 Ossipee, New Hampshire (both M = 5.4) events.

Geological make-up and man-made land reclamation activity in the region have been the source of a significant number of areas underlain by saturated and relatively loose cohesionless deposits/fills. With due consideration in 1975 a set of criteria were included in the Massachusetts State Building Code (1980) to conduct an assessment of the liquefaction susceptibility of such deposits and fills with level ground.

The study is an attempt to update the 1975 criteria in the light of a better understanding of the regional seismicity, successive contributions to potential liquefaction assessment by the researchers at the University of California-Berkeley under Prof. H. B. Seed and detailed studies conducted by Schmertmann and his colleagues on the energy transfer mechanism of the standard penetration test (SPT).

DESIGN EARTHQUAKE FOR NEW ENGLAND

Historically, the National Building Code, NBC, of the American Insurance Association, has been used most extensively in the northeast United States. NBC's 1976 seismic zone map shows most of New England in Zone 2. The 1981 edition of the Basic Building Code, BOCA, which is adopted in Connecticut, follows the NBC's recommendations.

Nationally, more widely adopted Applied Technology Council's, Tentative Provisions for the Development of Seismic Regulations for Buildings, ATC 3-06 (1978), defines local seismicity by a seismicity index and two coefficients, A_a and A_v. These coefficients characterize the short and long period components of the ground motion, respectively. All New England States are categorized with the same seismicity index and coefficients.

In the Structural Engineers Association of California, SEACO's (1986) recently proposed revised seismic zone map, all New England States are included in Zone 2, except northerly portion of Maine and most northerly segments of New Hampshire and Vermont being in Zone 1.

Following ATC's recommendations, within the scope of this study it may be argued that all New England States may be assigned with the same design earthquake.

The Massachusetts State Building Code (1980) is the first building code in the United States which contains specific soil and foundation design provisions for earthquake resistant design. Recommendations by the Massachusetts Seismic Advisory Committee, MSAC, including guidelines to assess susceptibility of saturated, clean sands to potential liquefaction were incorporated in the Code in January 1975. In its deliberations for the Code provisions, MSAC selected a nominal design earthquake for the State characterized by a peak ground acceleration of 0.12 g on firm soil, and an epicentral intensity between MMVII and MMVIII (Luft & Simpson 1979). In its more recent discussion of a set of proposed revisions in the Code, including the 1975 liquefaction criteria, MSAC chose to consider a design earthquake with a maximum ground acceleration of 0.12 g on firm soil and M = 6.5. Within the framework of this study MSAC's design earthquake for Massachusetts has been adopted to apply to the New England region in general.

FACTORS AFFECTING THE SPT RESULTS

Assessment of susceptibility of saturated, loose sand deposits to potential liquefaction relative to SPT resistance (blow counts) has been widely accepted in the current practice of geotechnical earthquake engineering (National Research Council 1985). In parallel it has become even more relevant to have a better understanding of the factors which affect the SPT results.

Based on systematic theoretical and experimental studies Schmertmann and his co-workers (1978, 1979) at the University of Florida concluded that the measured blow counts (N values) in the SPT vary inversely with that portion of the theoretical free-fall hammer energy which reaches the spoon sampler through the drill rods. Further, they have documented that depending on various factors the energy which reaches the sampler in the form of a compression wave could vary from 30 to 85 percent of the free-fall energy (i.e., 140-lb. hammer falling freely 30 in.).

Kovacs et al (1981) presented a comprehensive summary of factors affecting the SPT N-values. Considering only those factors which cannot be controlled by the driller or typically overlooked, these factors are the length of drill rods (or the depth at which SPT is performed), use of no liner in the standard (ASTM D 1586-84) spoon, integrity of rope and, perhaps most important, the type of hammer (i.e., safety hammer or donut hammer).

In liquefaction investigations, Seed et al (1985) suggested the use of SPT data relative to safety hammer as "standard" for the United States since it is currently (1987) the prevelant method in conducting SPT in the country. They proposed an average efficiency (as a ratio of the free-fall hammer energy) of 60 and 45 percent for the safety hammer and donut hammer, respectively. Accordingly, Seed et al (1985) recommended to use a "correction" factor (multiplier) of 0.75 for N-values measured by using a donut hammer to obtain equivalent N-values for the "standard" safety hammer.

SPT PRACTICE IN NEW ENGLAND

The present (1987) SPT practice in New England almost exclusively utilizes a donut hammer and two turns of old to new rope around a rotating cathead. The split-barrel (spoon) sampler is used without a liner since it provides better sample recovery. In accordance with the New England SPT practice, the following "correction factors" have been adopted in the study for New England N-values to make direct use of the liquefaction envelopes (curves) proposed by Seed et al (1985):

1. For the use of donut hammer multiply by 0.75.

2. For the use of old to new rope multiply by 0.95.

3. For the use of split-barrel sampler without a liner multiply by 1.08 for the depth range of 5 to

15 ft., 1.10 for 15 to 30 ft., 1.15 for 30 to 40 ft., and 1.20 for 40 to 60 ft.

4. For the use of short drill rods multiply by 0.75 for the depth range of zero to 10 ft., 0.90 for 10 to 15 ft.

PROPOSED LIQUEFACTION CRITERIA FOR NEW ENGLAND

Liquefaction criteria for New England proposed herein, Figures 1 and 2, were developed basically following the methodology and making use of the liquefaction envelopes proposed by Seed et al (1983, 1984, 1985). Elements discussed in the previous sections relative to the regional seismicity and SPT practice were incorporated in the criteria. Step by step procedure to develop Figures 1 and 2 was outlined in an earlier paper (Soydemir 1987). The same procedure can be used to develop liquefaction criteria for other regions of the world with different seismicity and/or different SPT practice.

Figures 1 and 2 also incorporate the liquefaction envelopes from Massachusetts State Building Code, which are currently in use. The envelopes in the Code are specified for saturated, "clean" sands. A comparison of the Code's liquefaction envelopes with the proposed curves for saturated sands with less than 5 percent by weight passing No. 200 sieve (designated as Curve A) suggests overconservatism in the Code, especially within the depth range below 15 ft. As indicated the Code's liquefaction envelopes were developed in 1975 and are currently under consideration for revision.

Figures 1 and 2 also include Curves B and C which are liquefaction envelopes for saturated sands containing about 15 and 35 percent silt content, respectively. These envelopes are especially helpful in cases where a site may be classified as liquefaction susceptible even though sand deposits underlying the site may have appreciable silt contents. This in turn may lead to unnecessary expense to densify the particular silty sand deposits in order to meet the Code requirement.

It is expected that the manifestation of liquefaction at the New England sites underlain by loose, saturated, relatively clean medium to fine sands may be in the form of settlements and/or lateral spreading of structures supported by shallow foundations. An approximate, simplified approach to estimate such seismically induced settlements in the region was formulated by Soydemir (1986) in a form readily usable by geotechnical design engineers.

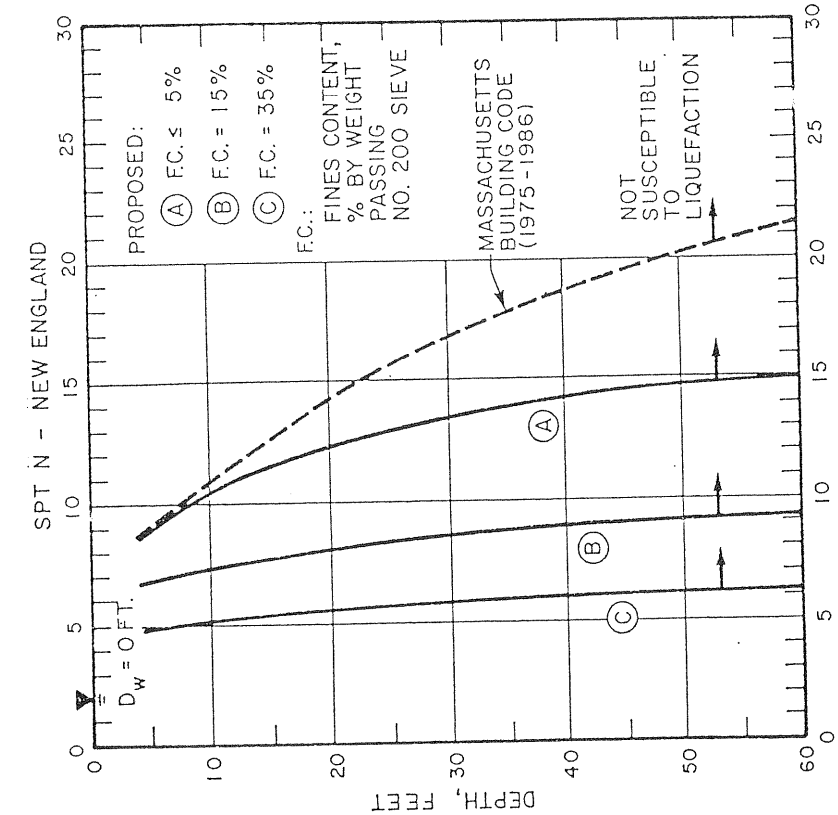

Figure 1. Proposed liquefaction criteria for New England for level ground and groundwater level at ground surface.

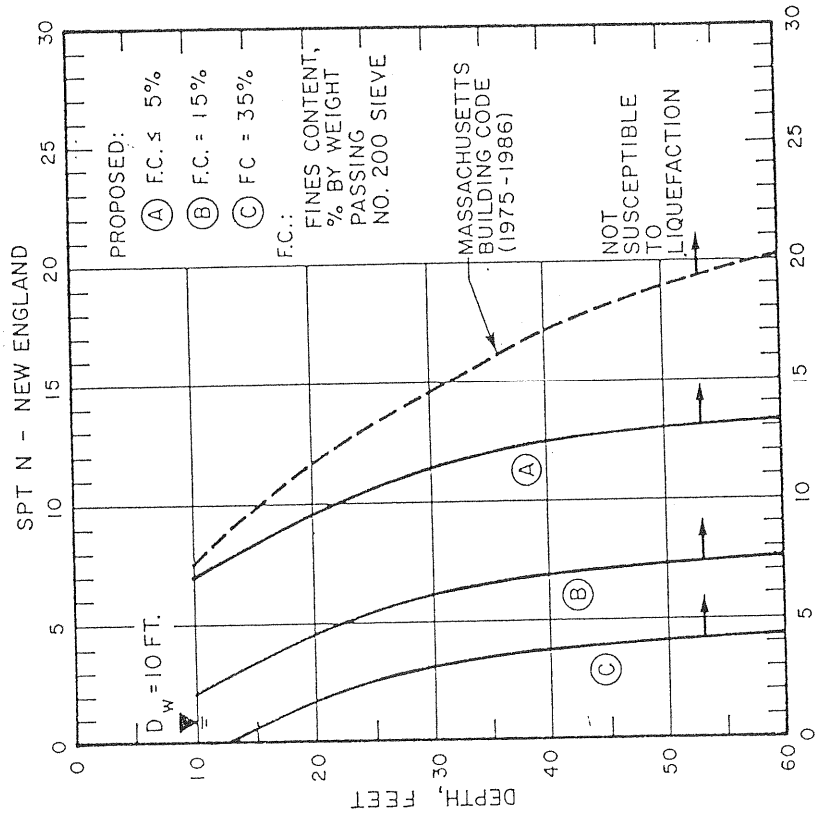

Figure 2. Proposed liquefaction criteria for New England for level ground and groundwater level at 10 ft. below ground surface.

REFERENCES

Applied Technology Council, Tentative provisions for the development of seismic regulations for buildings, ATC 3-06, National Bureau of Standards, 1978.

Kovacs, W. D., L. A. Salomone, and F. Y. Yokel, Energy measurement in the SPT, National Bureau of Standards, Building Science Series 135, 1981.

Luft, R. W., and H. Simpson, Massachusetts earthquake design requirements, J. Boston Soc. of Civil Eng./ASCE, Vol. 66, 2, 67-85, 1979.

Massachusetts Seismic Advisory Committee, Proposed changes to earthquake design sections, J. Boston Soc. of Civil Eng./ASCE, Vol. 69, 2, 209-234, 1983.

National Research Council - Committee on Earthquake Engineering, Liquefaction of soils during earthquakes, National Academy Press, 1985.

Schmertmann, J. H., Use the SPT to measure dynamic soil properties? Yes, but!, ASTM STP 654, 341-355, 1978.

Schmertmann, J. H., and A. Palacios, Energy dynamics of SPT, J. Geotech. Eng. Div., ASCE, Vol. 105, GT8, 909-926, 1979.

Seed, H. B., and I. M. Idriss, Ground motions and soil liquefaction during earthquakes, Earthquake Engineering Research Institute, 1982.

Seed, H. B., I. M. Idriss, and I. Arango, Evaluation of liquefaction potential using field performance data, J. Geotech. Eng. Div., ASCE, Vol. 109, GT3, 458-482, 1983.

Seed, H. B., K. Tokimatsu, L. F. Harder, and R. M. Chung, Influence of SPT procedures in soil liquefaction resistance evaluations, J. Geotech. Eng. Div., ASCE, Vol. 111, GT12, 1425-1445, 1985.

Soydemir, C., Seismically induced settlements: Two models for New England, Proceed. 3rd. U.S. Nat. Conf. on Earthquake Eng., Vol. 1, 565-576, 1986.

Soydemir, C., Liquefaction criteria for New England considering local SPT practice and fines content, Proceed. 5th Canadian Conf. on Earthquake Eng., 519-526, 1987.

GEOTECHNICAL SOIL PROPERTIES IN THE GREATER NEW YORK CITY METROPOLITAN AREA AND THEIR IMPACT ON TRANSIT FACILITIES

by

Carl J. Costantino and Charles A. Miller
Department of Civil Engineering
City College of New York

ABSTRACT

The NYC Metropolitan area presents foundation engineers with a wide variety of soil profiles with which to contend, varying from very soft, thick silt/clay deposits to very dense, heterogeneous sand/gravel glacial outwash deposits. Typically, ground water levels are found close to the ground surface. Local bedrock conditions are similarly extremely variable, with rock depths varying from relatively deep (several hundreds of feet) in the southern reaches of the area to very shallow in the northern sections. At construction sites, it is not unusual to encounter extreme ranges of depth to bedrock over plan distances of several hundred feet. Rock in the NYC area is typically hard schist or gneiss formations, although it is usually highly fractured, particularly in the upper zones near the ground surface.

From a seismic point of view, the thickness and quality of the soil overburden plays a significant role in controlling the primary frequency content and acceleration levels which may develop at or near the ground surface for a postulated seismic event. The seismic response of surface structures will then be directly influenced by the properties of the soil overburden. A summary of the extremes of the soil conditions encountered in this region is presented in this paper. Using standard convolution methods, the variation in potential seismic motions felt at the ground surface is investigated, given a specified broad-banded bedrock motion input with a peak acceleration level of 0.05 g's. This input motion corresponds to a low level seismic event of magnitude 4 or 5 which is generally considered to be a reasonable design input for this region. Finally, calculations are then presented of the impact of such a seismic environment on the structural response of a typical elevated line of the NYC Transit Authority subway system. They indicate that such structures, when subjected to these low level dynamic loading inputs, can become significantly overstressed, particularly when trains are stored on the structures.

INTRODUCTION

During the past several years, the New York City Transit Authority (NYCTA) has begun to investigate the impact of a potential seismic event upon their transportation system. This interest developed with the relatively recent discussions of East Coast seismicity that have appeared in the literature, as well as from reports of the several small events that have occurred in the Westchester County area just north of the City. These developments serve to indicate that New York City is located not in an area of benign seismicity, but rather in one of rather low seismic hazard, which should be suitably accounted for when considering the adequacy of the design of various systems of importance to the life of the area. Unfortunately, such consideration has not been included in system designs in this region to any significant degree in the past. This report presents a summary of the beginnings of such an effort to evaluate the response of the NYCTA system to a seismic event.

The objective of the study, being conducted jointly by the NYCTA and the City University of New York through the National Center for Earthquake Engineering Research, has two primary aspects, namely:

- to establish a broad assessment of the impact of the seismic hazard on the major components of the transportation system, and
- to establish the analytical framework within which detailed evaluations can be pursued after this initial assessment is completed.

It is clear that a major aspect of the study is concerned with the definition of the major components of the system under consideration as well as components of other systems nearby whose damage may impact on the timely operation of the transportation system. For example, even if small seismic events may not damage the rail system directly, they can make the transportation system virtually unusable if damage would occur to, say, a natural gas line or primary electrical component passing nearby.

HAZARD DEFINITION

The definition of the seismic hazard which should be included in any system evaluation for the eastern U.S (and in particular for New York City) has not as yet been completed since major questions still remain about the specific seismogenic processes involved. Recent work in this area (Refs. 1 - 4) indicates, however, that this hazard is significant and if anything is being revised upward. A summary of the seismic history in this area, presented in Ref. 3, indicates that several earthquakes in the range of magnitude 4 to 5 were centered in the NYC area or its immediate vicinity, with the latest being recorded in 1884. This event was centered near the mouth of New York harbor and caused minor structural damage throughout a region 200 km wide, from western Connecticut to eastern Pennsylvania. Seismicity studies associated with the Indian Point Nuclear Power Plant (Ref. 1) indicate return periods of from 50 to 100 years for earthquakes of this magnitude, based on a historical record of up to 250 years. Thus, an event of magnitude 5 is certainly a reasonable one for consideration as a lower bound estimate of the hazard in this area, although the record is not as yet sufficient to establish a reasonable upper bound estimate of the hazard for design purposes. Such a lower bound hazard definition will correspond to the following ground motion parameters of interest to structural systems:

- maximum relative displacement of 1.5 to 2.0 inches,
- peak acceleration of about 0.09 g's.

FOUNDATION CONDITIONS IN THE NYC AREA

As mentioned above, the foundation conditions encountered in the NYC area are extremely variable. Several areas of significant interest to foundation engineers, and which require specific consideration when evaluating foundation response to load, are shown on the map of Figure 1. At the west end of Brooklyn, the upper soils typically consist of very loose sands with SPT blow counts consistently less than 10. Much of this area has been reclaimed from the Bay by dumping and filling with little effort made to compact the soils. These loose sands, in conjunction with the high water table, are extremely susceptible to vibratory loadings. Experiences with vibratory pile driving in the area indicate that these soils are very susceptible to large settlements and loss of capacity from even low levels of shaking. Such behavior indicates that structures founded on these soils, as are the two to four story residences typical in the area, would be susceptible to major damage for even mild

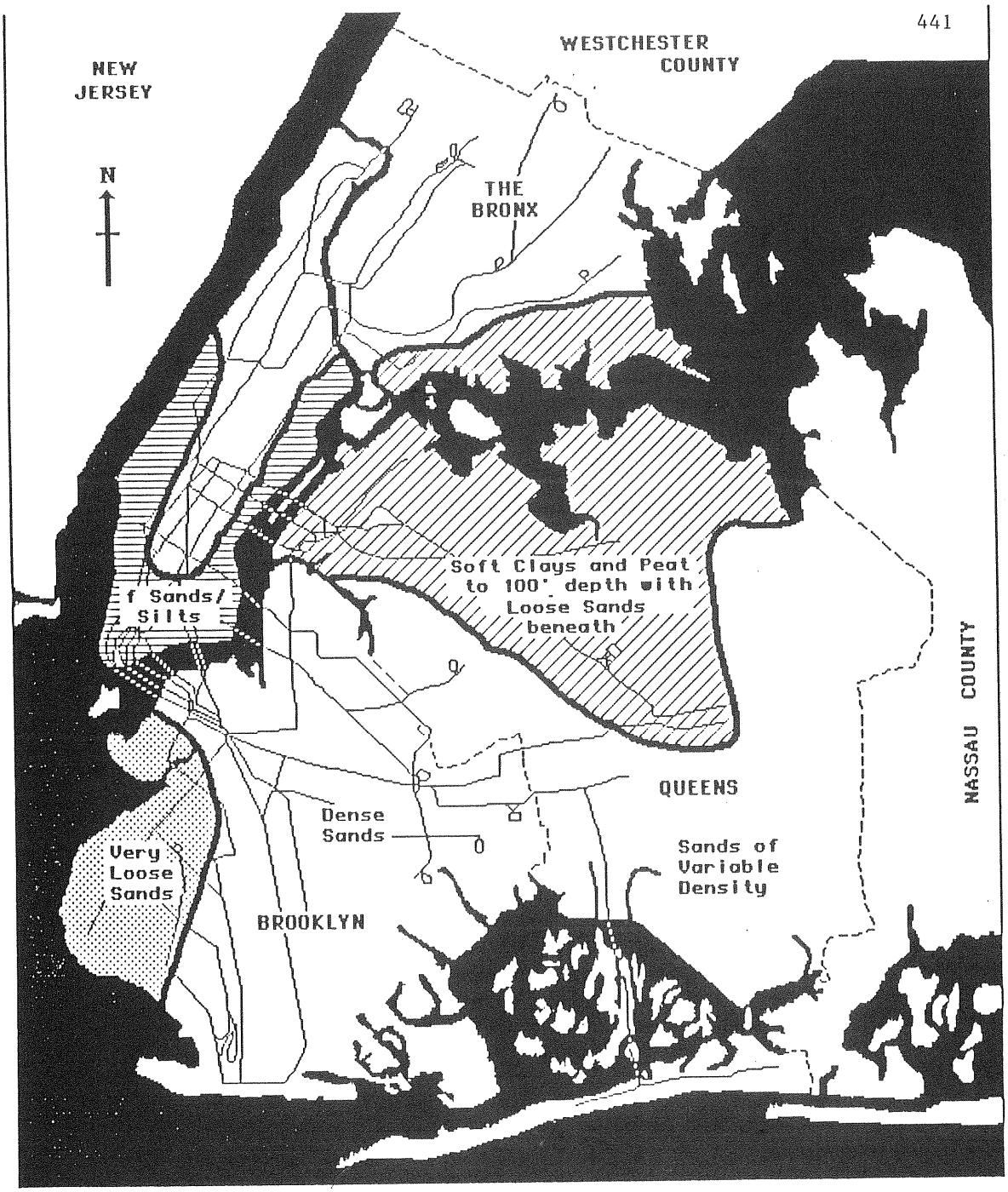

FIGURE 1 SOIL ZONATION IN THE NYC AREA

seismic events from both consolidation and liquefaction effects. Away from this region, the soils in the Brooklyn area are for the most part dense sands and gravels with high SPT blow counts. At the southern end of the borough, these sands extend to a depth of several hundred feet.

In both Queens and the Bronx, alongside the Long Island Sound, the upper soils are extremely soft silts, clays and peats (in some cases underconsolidated) which can extend to great depths, with the ground water table again being found near the ground surface. The depth of these soft soils can extend to as much as 200 feet. In addition, below these soft fine-grained soils exist fine sands which are of extremely variable density, with SPT blow counts, even at these great depths, varying from zero to about 30 bpf. Thus, these lower sandy soils may behave peculiarly during a low level seismic event. Since major structures in the area are often supported on friction piles driven to these sands for support, these structures may be affected by low level events. As will be discussed in a later section, the soft clays play a major role in modifying the ground motions which would be felt at the ground surface, given a particular motion at the lower bedrock. This in turn will influence the response of surface supported structures. In the Bronx, the soft silt/clays are typically not as thick as in Queens and are underlain by highly fractured bedrock.

In the remainder of both the Bronx and Manhattan, the vast majority of the area indicates bedrock at or near the ground surface, with the exception of relatively narrow zones along both river banks. In these zones, the soils are again highly variable, with silty soils of variable density being prevalent.

CONVOLUTION ANALYSES

To assess the impact of these variable soil conditions on response of structures founded at the ground surface, a series of convolution analyses were performed for three primarily different postulated soil conditions. These three site conditions were postulated to be representative of the variable conditions found in the NYC area, and cover a wide range of soil frequencies of interest to the structural problem. The first postulated condition consists of a 30 foot thick layer of medium dense sand (shear wave velocity of 1000 fps) overlaying the bedrock. This soil overburden possesses a primary frequency of about 8.3 hz. The second soil condition again considers a 30 foot thick soil layer atop the bedrock, but in this case the soil is assumed to be a soft silt with a shear wave velocity of 300 fps, leading to a primary soil frequency of 2.5 hz. The third soil condition postulated is a 100' thick soft soil layer, with a layer frequency of only 0.75 hz. The amplification function for these three postulated soil conditions are shown in Figure 2. The amplification functions indicate that the soil overburden will significantly modify any seismic motions input at the bedrock. Basically, at the primary soil layer frequency, the input motion will be significantly amplified, while the higher frequencies will be reduced. At frequencies much less than the soil layer frequency, the surface motions will be essentially unaffected.

For this study, a relatively broad-banded seismic input was used at the level of the bedrock with a peak acceleration of 0.05 g's. The acceleration-time history associated with this pulse possesses a wide range of frequencies, from about 0.5 to 20 hz, covering the range of interest for most structures. The assumed motion envelopes the design response spectrum used by the Nuclear Energy Commission to define input to seismic analyses for nuclear power plants (Ref. 5). The time duration of this pulse is longer than would normally be associated with a magnitude 5 event, since it contains lower frequency content included for safety in the structural analysis. Such long duration pulses in fact may develop, even for low magnitude events, for the case of deep soft soil sites. The pulse duration plays a role in assessing nonlinear response or amount of damage that will occur to the surface structures of interest to this study. As the study progresses, more effort will be required to properly

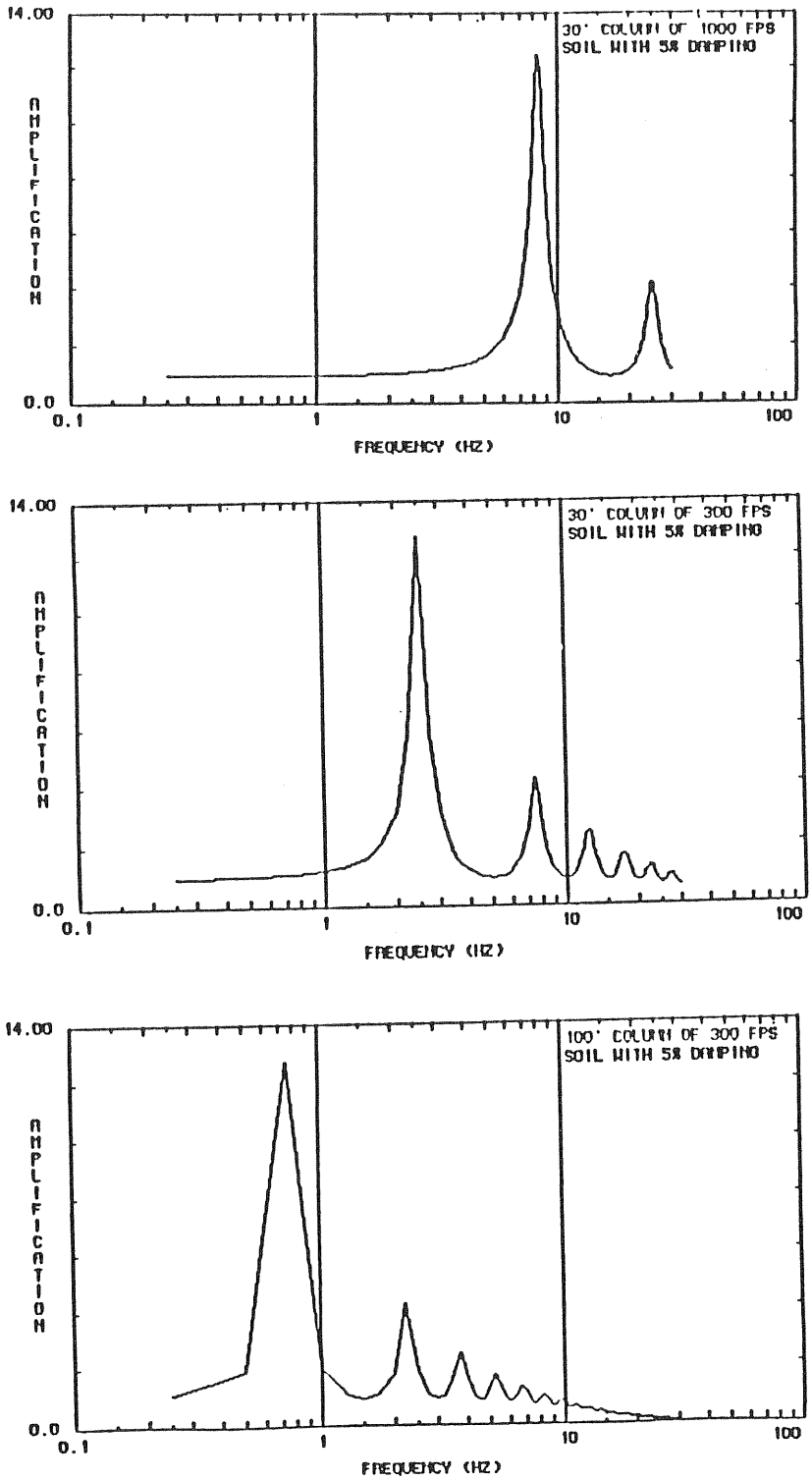

FIGURE 2 AMPLIFICATION FUNCTIONS FOR SOIL MODELS

define the properties of the seismic input.

For each of the three soil columns postulated, the criteria bedrock motion is convolved upward, assuming upward propagating horizontal shear waves, to yield the corresponding surface ground motion. These motions, in turn, are then used as input to structures founded at the ground surface. The impact of the properties and thickness of the soil column on the surface ground motions can be seen in Figure 3 for the three soil layers considered. The soil overburden in each case serves to filter out the higher frequencies and changes the magnitude of the peak acceleration sustained at the ground surface. Table 1 lists the peak acceleration sustained at the ground surface for each of the postulated soil conditions. As can be noted, the effect of the soil overburden is to increase the peak acceleration of the surface motion well above that of the input acceleration applied at the bedrock. For the case of the second soil column, which corresponds to a thirty foot layer of soft soil above the bedrock, the peak acceleration is over four times higher than the input acceleration corresponding to a magnitude 5 event. If a structure is placed at the ground surface which, in turn, has a primary frequency stiffer than that of the soil column, it will "feel" this increased seismic motion, and thus respond more severely. On the other hand, if the structure is significantly softer than the soil column, it will not "feel" such input magnitude, but would tend to ride out the peak inputs. Such behavior clearly indicates the importance of including the properties of the soil overburden within the seismic analysis for the structure. It should be noted that the pulse duration shown in Figure 3 is significantly longer than that used in the structural response calculations described below. Calculations were performed use the first 10 seconds of the pulses shown.

NYCTA SYSTEM COMPONENTS

The NYCTA system is an extensive one consisting of about 450 route miles, most of which are below ground in various tunnel sections, or on the surface in open sections, but with about 75 miles on elevated structures. The tunnel sections have been constructed in both hard rock and soil using various drilling, blasting and cut-and-cover methods of construction. River crossings are made via major bridge connections or through river tunnel sections. These tunnel sections have been typically placed along the river bottoms, which have been cleared of the soft silts and muds of the river. Connection to the land tunnels are made through portal sections which form the transition between the different tunnel sections used on land and under the rivers. To support this complex system, a variety of structures are required to house the various equipment and personnel required to operate and maintain this system.

In discussing the vulnerability of TA facilities to seismic loadings, several different categories of damage potential can be defined which are useful in a first cut evaluation of the system. First considering structural behavior only, these damage categories are

- catastrophic structural damage that poses an immediate danger to personnel within;
- structural damage that causes the structure to be classified as potentially unsafe;
- noncatastrophic damage to primary structures but significant damage to important subsystems within;
- noncatastrophic damage to the primary structure but serious damage to subsystems within or nearby.

With these categories of damage potential, we can then proceed to assess the impact of the earthquake on the various primary facilities of the system. We have defined nine different structural types which possess fundamentally different response characteristics due either to their structural properties or to method of construction. They will therefore tend to respond to seismic inputs in specific ways. These

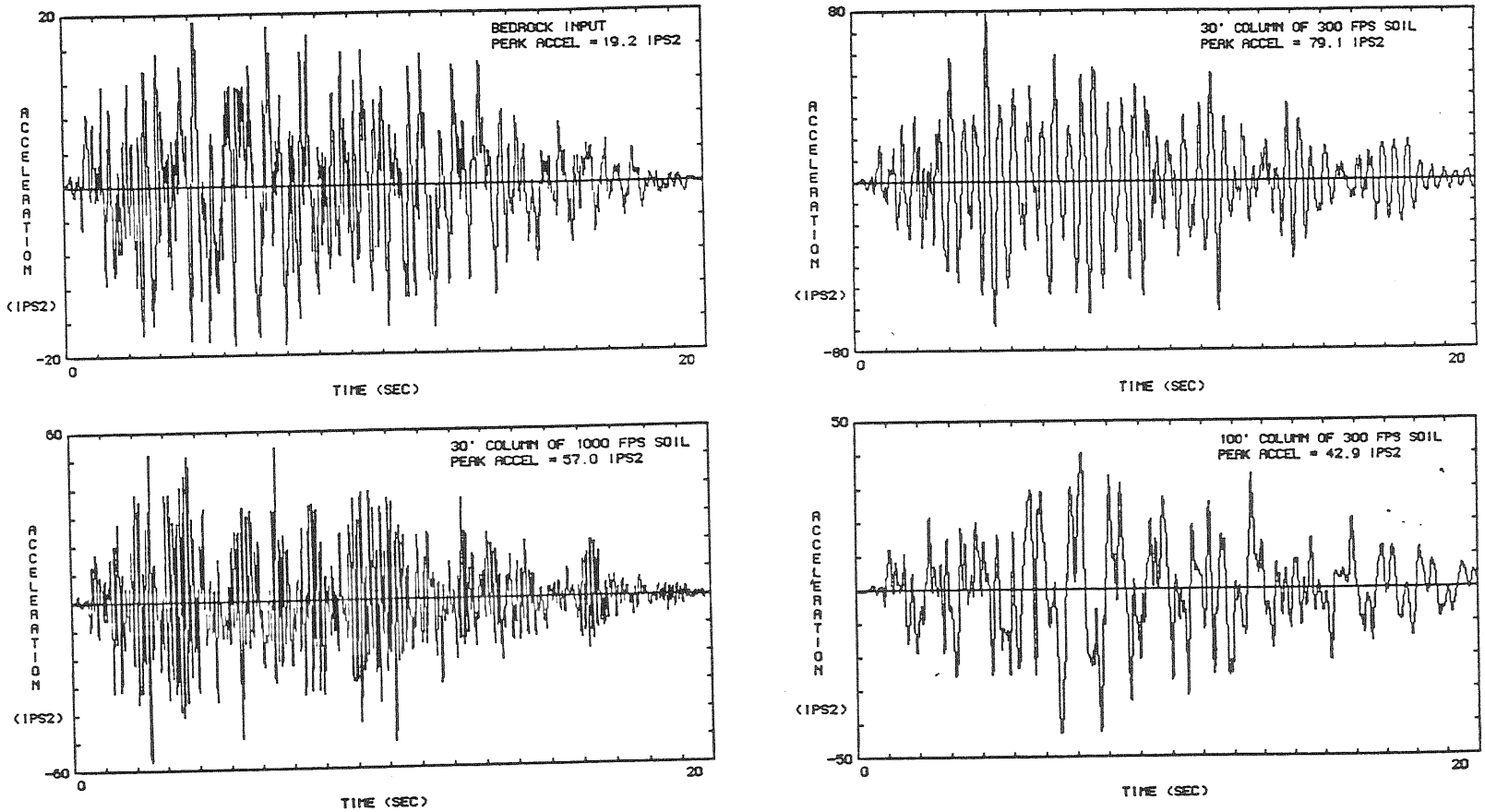

FIGURE 3 ACCELEROGRAMS OF SURFACE GROUND MOTIONS

TABLE 1 PEAK GROUND ACCELERATION AT TOP OF SOIL COLUMN FOR 0.05 G'S INPUT AT BEDROCK

Soil Column No.	Column Frequency (hz)	Peak Acceleration (g's)
1	8.33	.148
2	2.50	.205
3	0.75	.111

TABLE 2 PRELIMINARY STRUCTURAL VULNERABILITY ASSESSMENT

Catastrophic Structural Category	Serious Damage Damage to Primary Structure	Subsystem to Primary Structure That Impacts Safety	Subsystem Damage That Leads To Threat To People	Damage That Leads To Safety Concern
Cored Tunnel in Rock	No	No	No	Yes (Controls, water proofing)
Cut and Cover Box Tunnel	No	No	No	Yes (Controls, water proofing)
River Section	No	No	Yes (Water proofing)	Yes (Controls)
Large Span Bridge	No	No	No	Yes (Controls)
Small Span Bridge	No	No	No	Yes (Supports)
Buried Box Structure	No	No	No	Yes (Electrical Equipment)
Steel Framed Structures	No	No	Yes (Overhead Cranes)	No
Concrete Structures	No	Yes (Flat Slab Structures)	Yes (Overhead Cranes)	No
Overhead El Structure	No	Yes (Joint Yielding)	Yes (Derailing)	Yes (Controls)

generic structural types can be listed as:

- Cored tunnels in rock
- Cut and cover tunnel sections
- River sections laid by trench methods
- Track across large suspension bridges
- Track across small span rigid bridges
- Small buried structures
- Surface framed steel structures
- Surface concrete structures
- Overhead elevated structures

A 'broad brush' assessment of these structural types to a low level earthquake input of magnitude 5 has been made and is summarized in Table 2 below. As indicated therein, it is not anticipated that such a low level seismic event will cause catastrophic damage to occur to any of the structural systems considered to date.This assessment is based on relatively crude evaluations, and assumes, of course, that the structure under consideration is performing as originally intended. Clearly, if significant deterioration of the system element has occurred over the years, even such a small earthquake as a magnitude 5 event may cause significant damage, particularly for those structures which do not have a significant lateral load capability included in their original design.

For the overhead elevated structure, however, such low level events can cause serious damage to the primary structure. These elevated lines are designed as two dimensional rigid frame structures in the transverse direction, connected in the longitudinal direction by individual girders supporting the train tracks. The frames are supported on simple pedestal foundation elements at the ground surface, resting either directly on the ground or on pile clusters. Most often, the elevated line supports one trackway level with three separate lines, although some two level structures exist. The analyses performed herein are concerned only with the single level trackway.

RESPONSE OF ELEVATED STRUCTURE

In assessing the response of the elevated lines in the system, a typical transverse bent of the structure was considered. The stiffness, mass and strength properties of the structural model were determined from as-built drawings provided by the NYCTA. It was then subjected to the surface ground motions generated from the convolution analyses. As indicated in Figure 4 for the case of a soil layer lying above the bedrock, the criteria horizontal motion was input to the bedrock, the response of the ground surface calculated from the convolution analysis, and the peak structural response determined. For the case of the structure resting directly on the bedrock (no soil overburden), the criteria motion was input directly to the structure. It should be noted that in each response calculation, soil-structure interaction effects were included, but, as can be anticipated for this structure, were found to be small. Thus, dynamic evaluations were made for the case of the elevated structure placed directly on bedrock, on a thin stiff soil layer, on a thin soft soil layer, and on a thick soft soil layer.

For each problem considered, the peak lateral deflection of the upper girder was calculated by a step-by-step time integration procedure, assuming the structure to behave in an elastic-perfectly plastic manner. That is, the structure was considered to behave linearly until the yield moment at the upper column joint is reached, as shown in Figure 4. For displacements greater than this yield displacement, the structure is assumed to maintain its capacity with no strain-hardening effects. The results of these calculations are presented in Table 3 for a variety of parameter variations.

Table 3 presents the number of yield deflections sustained by the structure after responding to the seismic input for each support condition (soil type and thickness). If this number exceeds a value of unity, then the stresses developed at the upper column joint to the girder exceeds the yield stress of the steel, with permanent strains remaining in the steel. Such behavior indicates overstressing of the

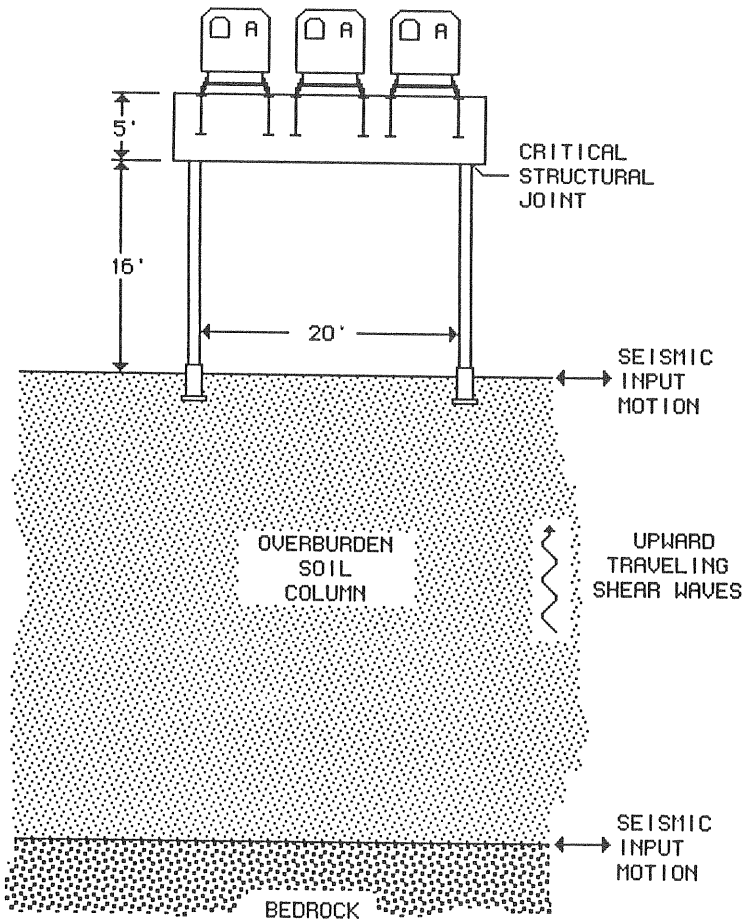

FIGURE 4 CONFIGURATION FOR ANALYZING ELEVATED STRUCTURES

TABLE 3 NO. OF YIELD DISPLACEMENTS INDUCED BY MAGNITUDE 5 SEISMIC INPUT

Joint Capacity	Support Condition	No. of Trains on Structure 0	1	2	3
100%	Bedrock	1.15	1.47	1.42	1.09
100%	Soil Layer 1	1.16	1.36	1.44	1.09
100%	Soil Layer 2	1.30	1.44	1.59	1.15
100%	Soil Layer 3	2.00	1.89	2.51	1.53
80%	Soil Layer 3	2.35	2.09	3.60	2.38

joint occurring from the dynamic effects. The results of Table 3 indicate that the postulated magnitude 5 earthquake time history causes yielding of the steel to occur for each case investigated. For the case of stiffer support (bedrock or soil layer 1), the yield deflections are the smallest. For the deep soft soil deposit of soil layer 3, the yielding is the largest. This results from the fact that the soil frequency is lowered enough to amplify the ground motions at the frequency close to that of the structure. In Table 3, some results are also included for the case of deterioration of the joint capacity to 80% of its design value. Due to the age of the actual elevated structures, some deterioration has been found to have taken place in some actual systems. As can be expected, the amount of yielding of the joint increases significantly.

CONCLUSIONS

We have presented herein the initial results of a study being undertaken to evaluate the impact of seismic effects on the transportation system of the NYCTA. The results obtained to date indicate that some primary structural damage can occur in a particular structure of the system, namely, the elevated structure, and that the magnitude of the damage developed will be a function of the location of the structure within the City, as defined by the local soil conditions. Other structures may sustain damage to ancillary systems housed within when subjected to a low level earthquake, but most likely will not be damaged seriously itself. It should be pointed out that the calculations completed to date do not take into account the effects of other loads acting simultaneously with the seismic load, such as normal dead and live loads. Such load combinations can be expected to make the effects of the seismic load more pronounced. Now that seismic loadings have been found to be serious for the elevated structure, more completed response analyses can be completed which account for these effects.

ACKNOWLEDGEMENT

This effort was supported in part by the National Center for Earthquake Engineering Research, SUNY Buffalo, under contract with the Research Foundation of the City University of New York.

REFERENCES

1. Y.P. Aggarwal and L. R. Sykes, "Earthquakes, Faults and Nuclear Power Plants in Southern New York and Northern New Jersey", Reprint Series, American Assoc. for the Advancement of Science, vol. 200, pp. 425-429, April, 1978
2. N.L. Barstow, K.G. Brill, O.W. Nuttli, P.W. Pomeroy, "An Approach to Seismic Zonation for Siting Nuclear Electric Power Generating Facilities in the Eastern United States", NUREG/CR-1577, Rondout Associates, May, 1981
3. L. Seeber, "Earthquakes and Related Phenomena That Constitute a Hazard in New York City", Lamont Doherty Geological Observatory, 1987, in preparation.
4. L. Seeber, "Eastern Mysteries of Intraplate Earthquakes: United States and China",1983-86 Lamont Doherty Geological Observatory Yearbook, LDGO Publications, Palisades, NY 1986
5. U.S. Nuclear Regulatory Commission Regulatory Guide 1.60

LIQUEFACTION POTENTIAL OF SOILS IN PORTIONS OF UPPER MANHATTAN AND BUFFALO*

by

M. Budhu[1], V. Vijayakumar[2],
R. F. Giese[3], and L. Baumgras[4]

1. Assistant Professor, Department of Civil Engineering, State University of New York at Buffalo
2. Graduate Research Assistant, Department of Civil Engineering, State University of New York at Buffalo
3. Professor, Department of Geology, State University of New York at Buffalo
4. Graduate Research Assistant, Department of Geology, State University of New York at Buffalo

---

*This contribution has been abstracted by the authors from a report prepared for the

NATIONAL CENTER FOR EARTHQUAKE ENGINEERING RESEARCH
State University of New York at Buffalo

1 INTRODUCTION

1.1 General

The integrity of a structure, a transportation system, or a lifeline utility located in an area affected by an earthquake is challenged by two factors: the ability of the structure itself to withstand the seismic waves and the resistance of the environment about the structure to ground failure. It is possible that structures which are adequately designed to survive earthquakes can readily be damaged or destroyed if they rest on or within soils that liquefy. Thus, in designing earthquake resistant structures, it is also necessary to consider the geological and geotechnical characteristics of the site upon or in which the structure is to be situated. Little effort has been expended in identifying regions of the Eastern United States which are susceptible to this type of earthquake damage.

Clearly, there is more interest in earthquakes in those states lying to the west of the Rocky Mountains; there are many more earthquakes there than in the states lying to the east. But this difference, while true, tends to give the eastern United States a false sense of security. The two regions of the United States are underlain by very different geological provinces. The eastern continental United States is underlain by a cooler and relatively denser plate than is found in the west. This difference allows seismic waves from earthquakes to travel greater distances for a given attenuation in the east than in the west. Hence, a moderate to large earthquake in the east affects a much larger area than an equivalent earthquake in California. As the area which is shaken by an earthquake increases, the possibility of ground failure also increases.

The regions which have the potential for ground failure can be identified by evaluating the liquefaction potential for the area. Once identified, it should be possible to design structural codes so that the damage due to the next large earthquake can be minimized.

1.2 Scope of Study

Three tasks were identified for the first year of this project. These were-

---

1. Collect subsurface geotechnical data from previous field investigations of two restricted sites. These were chosen to represent two types of environment in New York State - a large and a medium sized urban region. The sites which were investigated were in upper Manhattan (approximately 6 sq. mi.), New York City and the central part of Buffalo (approximately 11 sq. mi.).

2. Design and implement a database system capable of storing the large quantities of geotechnical and geological data generated by Task 1. This database will ultimately provide the information necessary to accomplish Task 2.

3. Develop liquefaction potential maps for these two regions, identifying those areas which have a high, moderate, or low probability of liquefaction for an assumed acceleration. The evaluation of the liquefaction potential for this initial study is based on data selected from the information assembled during Task 1.

---

2 LIQUEFACTION EVALUATION

2.1 Liquefaction

Liquefaction is a phenomenon by which saturated soils - essentially cohesionless soils - are temporarily transformed into a liquefied state. In the process, the soil undergoes transient loss of strength which commonly allows ground displacement or ground failure to occur. Liquefaction in the context of this report implies liquefaction induced ground failure. The assessment of liquefaction in this project is based on data of actual liquefaction ground failures recorded elsewhere.

Three basic types of ground failure are associated with liquefaction.

1. flow failures - soil materials flowing rapidly downslope in a liquefied state.

2. lateral spreading - limited displacement of surface soil layers down mild slopes.

3. loss of bearing strength - bearing capacity failure of foundations because of weakening of underlying or adjacent soil material.

Liquefaction can also cause transient horizontal oscillations as the ground surface layers are decoupled from more rigid material underlying the liquefied layer. Such decoupled vibrations can cause severe damage to buildings, pipelines, and other structures.

Of specific interest to this proposal is the liquefaction of soils under stress conditions induced by an earthquake, either close by or at some distance. Past experience has shown that seven factors are important in determining the potential for a particular soil to liquefy. These are 1) age of the soil, 2) depth to groundwater, 3) the grain sizes present in the soil and their relative proportions, 4) density, 5) origin of the soil, 6) thickness of the soil, and 7) the acceleration experienced by the soil.

2.2 Evaluation of Liquefaction Potential

Over the past decade or two, efforts have been made to establish a scientific basis for the prediction of liquefaction under earthquake conditions. From this work, two different approaches have developed: one based on essentially geological characteristics of the soils, and the other relies on geotechnical measurements of the soil.

2.2.1 geological criteria

Youd and Perkins [1978] developed a method for the construction of liquefaction potential maps. In essence, this is done by combining information from two different types of maps for the same region: a map showing the liquefaction opportunity, and a map showing the liquefaction susceptibility. The former is derived from the seismicity of the area; the latter is determined from the geologic age and the depth to ground water. In theory, the greater the seismic activity, the younger the soil, and the closer the ground water is to the surface, the greater will be the liquefaction potential.

As a general rule, young sediments are weaker than older equivalent sediments. Typically, sediments which are most susceptible to liquefaction are late Holocene (1000 yrs or less), with early Holocene having moderately liquefiable, and late Pleistocene having a low probability of liquefaction. With the variety of processes which can take place in geological materials, it is to be expected that exceptions will be found.

Similarly, because water saturation is necessary for liquefaction, depth to the water table is important. A second factor enters here; the increase in the strength of a soil as it is buried deeper. For these reasons, the most easily liquefiable soils will be those which have the ground water lying within 10 ft. of the surface. As the depth to the water table increases, the likelihood of liquefaction decreases.

These criteria have the advantage that they are easily applied to a variety of geological terrains, and they require data which is normally at hand from routine geotechnical borings. A weakness is that they are all strictly qualitative. To date, several regions, mostly in California, have been investigated and liquefaction potential maps for them have been published. These are listed in the reference section.

2.2.2 criteria based on standard penetration test (SPT) data

The standard penetration test, though widely used, is acknowledged to be an extremely crude procedure. There are many features which are not standardized so that the way the test is performed varies from operator to operator. This requires converting the results from one set of conditions to another and this introduces uncertainty.

In the United States, there has been an attempt to codify the conditions under which the test is performed, and these are described by ASTM D1587-67. The existence of an ASTM standard has not prevented the continued use of a proliferation of different tests in the field. According to the standards, the test consists of driving an 18 inches split tube (2 inches outside diameter with a wall thickness of 5/8 inches) into a soil by repeated blows from a 140 lb hammer falling onto an anvil attached to the top drill rod, from a distance of 30 inches. The number of hammer blows for each 6 inches of penetration by the tube is recorded. The standard penetration number, N, is the number of blows required to penetrate the last 12 inches (of the total of 18 inches). This N-value is sensitive to a number of factors which can vary from site to site and even within the same site: the overburden pressure, lateral soil pressure, and the density of the soil. It is now a common practice to correct the N-value for these variables to yield a presumably unbiased number, N_{60}, which is considered to be equivalent to the use of hammer of 60% efficiency in the test (Seed *et al.*, 1984).

Many variations of the SPT test have been used, particularly in the past. Variations occur principally in the size of the split tube, the drill rods, the driving technique, the weight and type of hammer, and the height of the drop. Studies were conducted (for example, Lowe and Zaccheo, 1975) to correct the N-values for these non-standard test to the ASTM D1587-67. We will refer to this standard in this report. Lowe and Zaccheo [1975] proposed a relationship which accounts for variations in hammer weight, drop height, and the diameters of the split tube. Based on an extended series of field tests, they showed that there is a linear relationship between hammer ratio, Rs, and the N-value. The hammer ratio is defined as:

$$R_s = \frac{D_0^3 - D_i^3}{144 W H} \tag{1}$$

where D_o and D_i are the external and internal diameters (in inches)
W is the weight of the hammer (in lbs)
H is the drop height (in inches)

This equation does not consider the dynamics of the hammer. It appears from the data reported by Lowe and Zaccheo [1975] that for cohesionless soils at relative densities below 50% (which is appropriate for liquefaction studies) the following conversion is sufficiently accurate for practical purposes.

$$N_e = 4050 N R_s^{5/7} \tag{2}$$

where N and N_e are the actual and corrected standard values respectively.

2.2.3 liquefaction potential

Seed *et al.* [1984] proposed a method of evaluating the liquefaction potential of soils on the basis of field observations. They showed that for sites in Pan America, Japan, and China where soils were observed to liquefy during earthquakes, the liquefaction potential of clean sands and non-plastic silt is related to the $(N)_{60}$ value.

Their procedure for evaluating the liquefaction potential is:

1. Establish the soil conditions and choose a design earthquake.
2. Compute the average shear stress ratio τ_{av}/σ_o (where τ_{av} is the average shear stress and σ_o is the effective overburden stress) for the maximum acceleration (a_{max}) of the design earthquake from the relationship-
$$\tau_{av}/\sigma_o = 0.65(a_{max}/g)\cdot(\sigma_o^t/\sigma_o) r_d \tag{3}$$
where g is the acceleration due to gravity, σ_o^t is the total overburden stress, and r_d is a stress reduction coefficient which varies from a value of 1.0 at the surface to about 0.9 at approximately 35 ft. depth.
3. Correct the N_e value to N_{60} using the equation-
$$N_{60} = C_n N_e \tag{4}$$
where C_n is a correction factor equal to $\sigma_o^{-1/2}$ (Liao and Whitman, 1986).

4. The presence of fine particles in a sandy soil strongly influences the liquefaction potential. The possibility of liquefaction for a given fines content, N_{60}, and τ_{av}/σ_o is determined from a plot of N_{60} versus τ_{av}/σ_o. If the coordinates (N_{60}, τ_{av}/σ_o) lie above the appropriate fines-content curve, the soil will liquefy under an earthquake of magnitude 7.5. Correction factors have been suggested by Seed *et al.* [1983] to yield curves for earthquakes with magnitudes other than 7.5.

The procedure does not account for the duration of shaking during the earthquake.

2.2.4 liquefaction probability

Liao *et al.* [1987] proposed a probabilistic method to evaluate the liquefaction potential using a regression analysis of SPT data from 278 sites where liquefaction was observed to occur. They worked with two models: one, termed the **CSR** (for cyclic stress ratio) model (Fig. 1), is similar to that of Seed *et al.* [1984]; the other, termed the **source model**, makes use of earthquake load parameters, viz magnitude and epicentral distance. The liquefaction demarcation curve of Seed *et al.* [1984] corresponds approximately to a 50% probability for the occurrence of liquefaction as formulated by the CSR model.

The major advantage of the work of Liao *et al.* is that the liquefaction potential of soils can be cast into probabilistic terms. Thus, one can construct a classification scheme where, for example, the letter H (for high) used by Youd and Perkins [1978] can be associated with a specific probability for liquefaction; one that is greater than 50%.

3 REGIONAL SEISMICITY

The eastern United States is an intraplate region with normally a moderate level of seismic activity. Historically there have been very large earthquakes, but these have been sporadic and few in number. Nonetheless, the severity of these big earthquakes and the fact that the energy is dispersed over very large areas, makes the subject of seismic activity an important one.

Western New York experiences the arrival of seismic waves from many sources. For the purposes of the following discussion, we will distinguish between "local sources" (within the New York State and southern Canada) and "distant sources" (anywhere else in the eastern United States).

3.1 Local Seismicity

Examination of the seismic activity in New York State and adjacent areas during the early 1970s (Sbar and Sykes, 1977) showed that, at least for this period, central New York, much of the Adirondacks and neighboring areas of Pennsylvania were essentially aseismic. The active areas were restricted to four zones: a zone from Boston to central New Hampshire, a zone from Kirkland Lake (Ontario) to northern New York, a cluster of activity centered on the towns of Attica and Dale in western New York, and a region northeast of Quebec City (La Malbaie). Of the two regions in New York State, the Adirondack zone is more active presently than is the area around Attica. Historically, this may not have been true.

Of particular interest to this project is the seismic activity located in western New York region. The major event was at Attica on August 12, 1929. This had an intensity of VIII (MM) (Coffman and Von Hake, 1973; Smith, 1962), but there has been a tendency to lower the original estimates to VII (Fox and Spikes, 1977) or to a magnitude of 5.2 (Sykes, 1978). Nonetheless, the event was felt over an area of 130,000 km^2 and did considerable damage (Fletcher and Sykes, 1977). There have been two more recent earthquakes, January 1, 1966 and June 13, 1967, each with an intensity of VI. A study of these by Hermann [1978] indicated that the depths were shallow, on the order of 2 to 3 km, suggesting that the 1929 event was also shallow. The suggestion was made by Hermann that the shallow depth would explain the relatively large amount of destruction given the relatively weak nature of the earthquake. Similar observations were made in connection with the New Madrid earthquakes of 1811 and 1812 (Hermann, 1978).

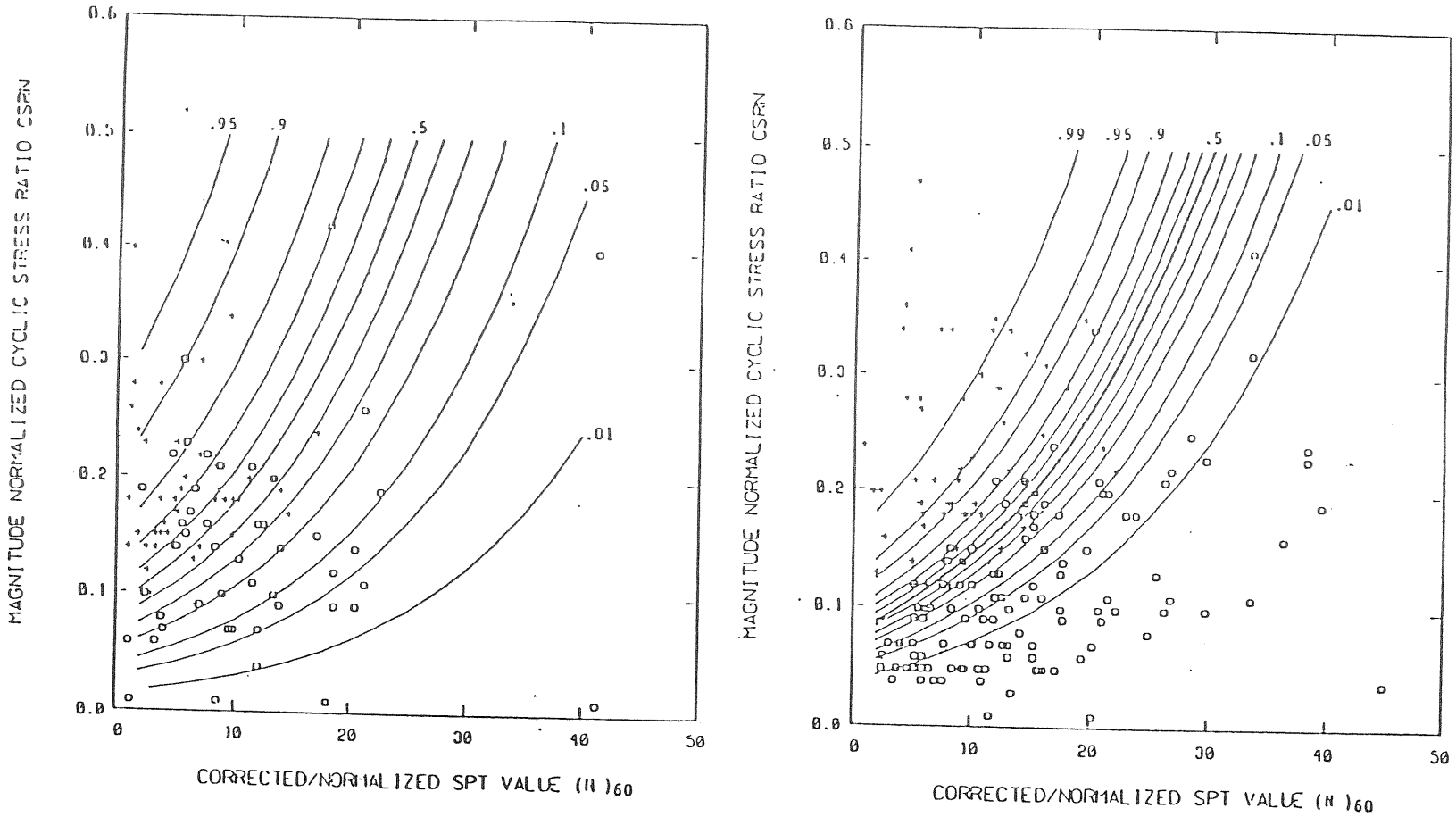

a) silty sands

b) clean sands

Figure 1. Probability of liquefaction determined from the N_{60} values using the magnitude normalized CSR model (after Liao et al 1987)

The study region we selected for study is sufficiently small (less than eleven square miles) that the seismicity within it is difficult to evaluate given the current state of knowledge for earthquakes in and near New York State. However, the existing earthquake records for New York State, which cover the past 300 years, are probably the best source to gauge the seismicity of the area. Veneziano and Van Dyck [1984] and Mitronovas and Nottis [1984] in their reports on the seismicity of New York have compiled a record of earthquake events, and an earthquake catalogue for New York State. Their record clearly indicates the future risk that prevail for the region due to moderate earthquakes.

Earthquakes in Pan-America, the western United States, Japan, and China are presently used as the basis for evaluation of earthquake hazards. It is essential to be aware of the characteristics of possible earthquake hazards in the eastern United States compared to the well documented western ones in order to realistically interpret, judge and apply the various evaluation techniques. Hays [1984] has compiled such a comparison.

The W 125th Street fault in Manhattan could be disregarded as a possible source of ground shaking according to the conclusions of both Hays [1984] and Mitronovas and Nottis [1984].

3.2 Distant Seismicity

Major historical earthquakes in the eastern United States generally are spatially restricted. Events with intensities greater than or equal to VIII have occurred in Quebec (La Malbaie), the zone from northern New York to Kirkland Lake, Boston, New Madrid, Charleston, Attica and Massena, and a few other, apparently isolated events. Looking at this distribution (Acharya, 1980), Western New York is rather centrally located, with important seismic activity to the northeast and to the southwest. Even though the distances are large, the efficient transfer of energy from the epicenters over long distances in the eastern United States makes these large earthquakes of extreme importance to the estimation of risk for the population centers of New York.

4 STUDY AREAS

For this initial survey of the liquefaction potential in New York State, two areas were chosen. The criteria used for the selection were: 1) that the areas have a substantial population density, 2) they should have geologically young sediments, 3) a ground water table close to the surface, and 4) a history of geotechnical exploration from which to draw the information necessary for the liquefaction analysis. The reasons for choosing these criteria will be made clear in subsequent sections. Two areas were identified: one in the upper part of Manhattan, New York City and the other in the waterfront sections of Buffalo.

4.1 Manhattan

The geology of southeastern New York is among the most complicated in the state. Structural features of this region include unconformities and disconformities; several kinds of folds; and normal, reverse, and thrust faults.

The stratigraphic sequence found in Manhattan includes rocks of the oldest known type, the Grenville formation, to unconsolidated glacial deposits of Pleistocene age. Manhattan Schist is a pelitic Schist of Middle to Upper Ordovician age and is the most abundant type of rock found in Manhattan. Inwood Limestone underlies the Manhattan Schist and is found in a belt which runs roughly between Clinton and Second Avenues, south of 34th Street. Gneissic rocks of the Precambrian Fordham Series are found between the Inwood Limestone and the East River.

All of the rock formations on Manhattan have undergone folding. Most of the folding occurred during three major periods of geologic disturbance in Precambrian, Postordovicic, and Postdevonic times. Faulting is commonly associated with regional folding. Two major faults in Manhattan are located north of Central Park, and have a general northwest to southeast direction of strike. The larger of these two faults, the 125th Street Fault, runs from the south end of 125th Street, through the northern tip of Central Park, to the north end of Ward's Island. The smaller of the two faults runs roughly parallel to the 125th Street Fault in the Harlem River basin.

4.2 Buffalo

The western part of New York State lies on the edge of the Appalachian Basin. The surface rocks are Paleozoic limestones, dolomites, with abundant shales, and some locally important sandstones. The sedimentary rocks do not form a continuous Paleozoic sequence (the Lower Ordovician is missing, for example), but all the sedimentary rocks are conformable, and there has been little tectonic deformation. There is a general regional dip of about 40 ft. per mile.

North of Lake Ontario, the crystalline basement rocks outcrop. Bedrock in the study area typically consists of Hamilton Group limestone and ranges in depth from 0 to 60 ft. (City of Buffalo, Division of Planning, map: "City of Buffalo Rock Elevations").

Unconsolidated deposits within the study area are highly variable due to the complex stratigraphy of surficial deposits and alteration of natural soils by extensive excavation, dredging, and fill operations. Naturally occurring soils are heterogeneous, but the stratigraphy of unconsolidated deposits can be generally characterized as follows: compact to dense clayey glacial till overlain by red-brown very soft to medium stiff varved clay, overlain by a grey-brown stiff varved silt/clay. Gradational variations are present throughout the entire area and some units are not ubiquitous due to diverse glaciation patterns. Well to poorly sorted sand, and/or gravel seams and lenses are interbedded among units at many locations. Rather thick deposits of loose fine sands exist at locations in the vicinities of the Buffalo River and Lake Erie shorelines indicating the presence of buried alluvial/glaciofluvial channels and ancient beach deposits. The groundwater table is shallow, generally at depths a few feet below grade.

Sites which have undergone construction operations are atypical of the area. Soils at many of these sites have been disturbed by construction of inland waterways to facilitate shipping commerce in the mid to late 1800's. A network of inland waterways, canals, and slips were built in the areas presently known as the Black Rock and Buffalo harbors. Filling of these waterways began in the early 1900's as alternate transportation systems were implemented. Landfilling was also performed in order to make development of swampy areas possible. In addition to filling of inland areas, the original Lake Erie shoreline has been extended 600 - 800 ft. west of its natural position (Goldberg-Zoino Associates, 1984). The waterfront edge is currently being extended toward the Lake by diked disposal area projects undertaken by the U.S. Army Corps of Engineers, Buffalo District.

4.3 Geotechnical Data

The data which were used for the liquefaction analysis came from two types of sources: drilling done by governmental agencies and geotechnical investigations done by private engineering companies at the request of local builders. In general, the data for Manhattan came primarily from the public sector while the Buffalo study drew largely from the data collected by private engineering companies.

4.3.1 Upper Manhattan

A total of 3,308 borehole logs covering the period from 1940 to 1986 were collected mainly from two agencies. Approximately ninety five percent of the borehole logs contained the soil descriptions, data on ground water level, and N values. The ground water level at this particular site is very close to the ground surface. Thus, in nearly all the boreholes drilled at this site, casings were used to support the sides of the hole.

One complication appeared during the evaluation of the geotechnical data collected for parts of Manhattan. This concerns those areas, typically along the Hudson and East Rivers, where new land was created by adding fill to the river banks. The material in these reclaimed sections can extend to depths of as much as 20 ft.. The geotechnical data for these areas are very suspect, and, even if they are of good quality, it is still difficult to make reliable estimates of the liquefaction potential because, at present, there is a complete lack of understanding and practical experience with the behavior of this type of material under earthquake conditions.

A review of the borehole logs revealed that about 60% of the near surface materials (within depths of less than 50 ft.) can be classified as silty-sand and sandy-silt, both of which are potentially liquefiable.

The quality of the data in over 75% of the boreholes appeared to be exceptionally good. Most of the N values, however, were obtained from non-standard tests and had to be corrected.

4.3.2 Buffalo

The data collected for the Buffalo study area consists of approximately 2,500 borehole logs from about 90 sites. An extensive preliminary literature search was performed using the National Center for Earthquake Engineering Research (NCEER) Information Services Office and by use of the on-line computer database GEOREF. Historical records documenting local effects of past regional seismic events were reviewed at the Buffalo Historical Society and State University of New York at Buffalo libraries. Extensive data were also collected with the assistance of Empire Soils Investigations Inc., an engineering/consulting firm located in Blasdell, New York. Many other local agencies have also contributed to the data base.

5 LIQUEFACTION MAPPING

5.1 Mapping Methodology

The selected study areas lie within an isoseismal area. A realistic design earthquake magnitude cannot be reliably extractable from whatever is known so far of the seismicity of New York State. The liquefaction evaluation procedures used in this project do not involve design magnitude of earthquakes. The maximum surface acceleration (amax) values are used in the compilation. Therefore, the design earthquake magnitude can be taken as any arbitrary value, since its influence is taken as uniform for the region.

For the region, a 7.5 magnitude (M) will be assumed so that Seed's criteria plots can be applied. The maximum surface acceleration (amax) is the critical factor and is related to the M value. Empirical relationships were established (Seed *et al.*, 1983) based on actual field liquefaction records between maximum ground acceleration (amax), epicentral distance (R) and earthquake magnitude (M). However, such relationships cannot be applied to the study region with both M and R unpredictable and with no applicable field liquefaction data available.

The contribution by Algermissen *et al.* [1982] deals with the peak ground acceleration at sites underlain by rock in New York City. Since the present study area coincides with that of Algermissen *et al.*, their plots of maximum ground acceleration as a function of exposure period for the New York City area are directly applicable.

From their relations, amax has a 90% non exceedence value of approximately 0.18 *g* over a 50 year period. Earthquakes of (MMI) intensity VI are possible in New York State and these could generate maximum surface accelerations up to 0.15 *g* (McCann *et al.*, 1980). Therefore, a value of amax = 0.15 *g* is not unrealistic in evaluating the liquefaction potential of the areas described in this study.

The following methodology was adopted for deriving the liquefaction potential maps for the two selected sites.

- Each borehole log was inspected and those containing N values less than 15 at depths of less than 50 ft. were selected for detailed evaluation.
- A latitude-longitude grid system was used to reference each site.
- The relevant data - N values, hammer characteristics, ground water elevation, depth of the borehole, thickness of the soil layers, soil classification (including the fines content), and geographic location - were entered into a standard spread sheet program.
- The lowest N value for each layer was selected and then corrected to the equivalent standard N_e value using equation (2). The N_{60} value was evaluated using equation (4).
- A maximum acceleration, a_{max} = 0.15 *g*, was selected for both the Manhattan and Buffalo sites based on earthquake records compiled by Algermissen *et al.* [1982] and McCann *et al.* [1980].
- The probability of liquefaction was obtained by using the critical stress ratio method of Liao *et al.* [1987]. An average bulk unit weight of 110 lbs/ft.^{3} was assumed.

5.2 Liquefaction Maps

The maps were produced for an earthquake of magnitude 7.5 and a peak ground acceleration 0.15 *g*. It is necessary that suitable scaling factors are used when evaluating the liquefaction potential for different magnitudes.

Each of the two sites investigated presented special problems. The results of our preliminary analysis are presented below.

5.2.1 Upper Manhattan

Fig. 2 shows the liquefaction potential map generated for upper Manhattan. In view of the great uncertainties involved in the estimation of the liquefaction potential, the final calculated values were grouped into three categories and these are the zones shown in Fig.2. The categories are arbitrary but they were selected to be consistent with much of the previous work in liquefaction potential mapping.

H---------high; probability of liquefaction > 50%

M---------moderate; probability of liquefaction 10 - 50%

L---------low; probability of liquefaction < 10%

Approximately 1/2 of the study area has a high to moderate probability of liquefaction. The high risk areas are adjacent to the shore of the Harlem River. The area generally to the north-west of Second Avenue has a low probability of liquefaction and does not appear to have any significant risk of ground failure.

Even though Ward's and Randall's Islands were included in the study area, they have not been evaluated because of a lack of SPT values.

5.2.2 Buffalo

The analysis of the Buffalo region has not progressed to the same degree as the study of Manhattan. The data for the latter became available at a much later date than the Manhattan data. Our examination of the Buffalo data are more qualitative and the evaluations have been based more on the geological nature of the soils identified in the borehole logs. The quantitative evaluation of the Buffalo data is continuing.

Fig. 3 shows a preliminary liquefaction potential map of the waterfront area of Buffalo. Two areas on Kelly Island, an industrialized section of the waterfront, show high probabilities for liquefaction. These areas contain deposits of very loose silty-sands.

6 DATABASE DESIGN

As part of the study of the liquefaction potential of New York State, a comprehensive data base system was designed and largely implemented. The purpose of the data base was to store the large number of bore hole data which were accumulated during the investigation of that area of Manhattan bounded by 145th and 96th Streets (East-West), and the Hudson and East Rivers (North-South), as well as the central part of Buffalo. The total number of soil and SPT values accumulated from bore hole investigations are on the order of 20,000 for Manhattan alone.

A data base system serves several purposes. Two are of prime importance for this project: 1) storage of the collected data for future use, and 2) the ability to retrieve selected values for the evaluation of the liquefaction potential of the two areas in question. Since it is not possible to foresee future uses for these data, the data base has been designed in a very general manner allowing easy addition of future applications.

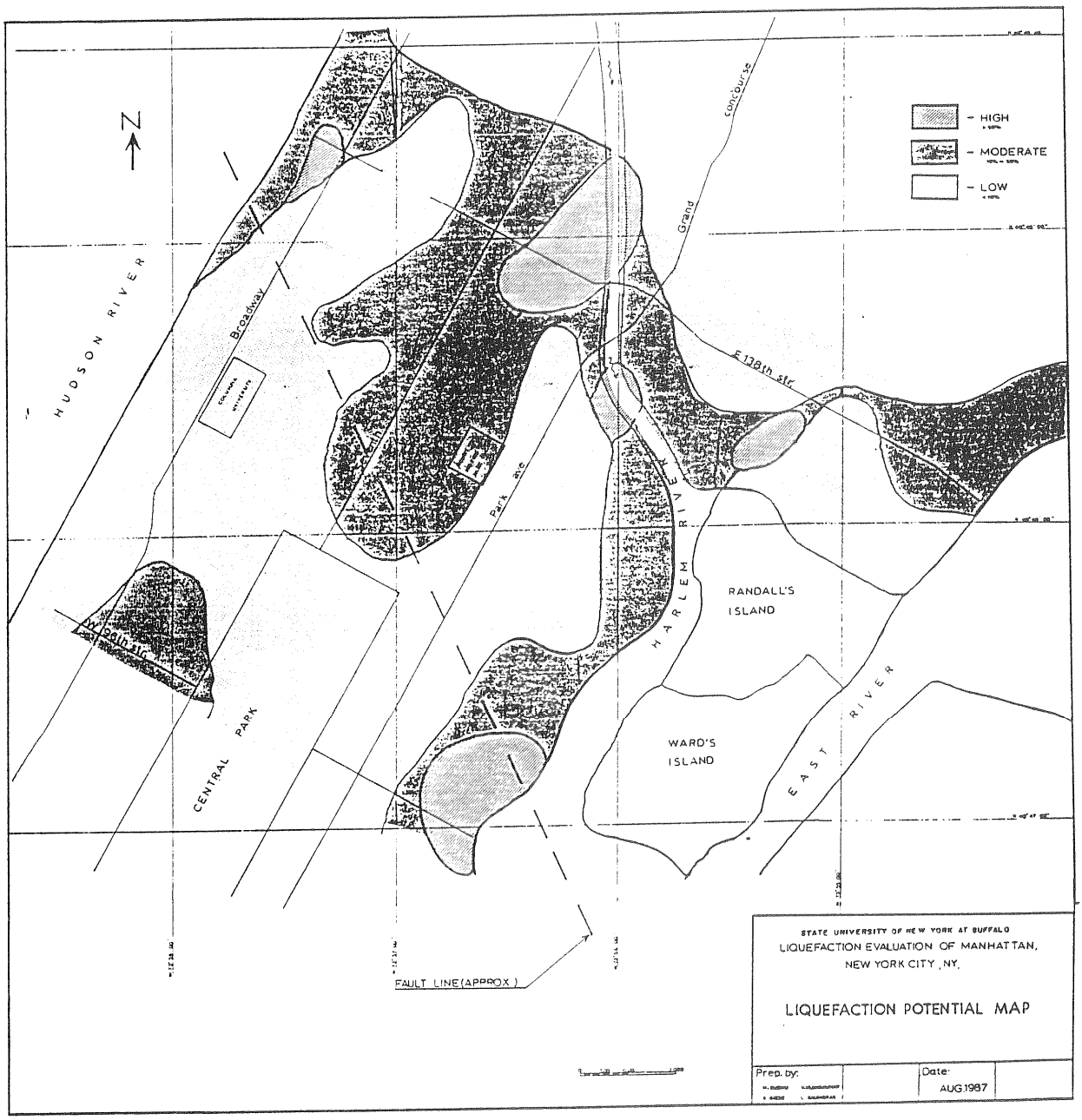

Figure 2. Liquefaction Potential Map
(Upper Manhattan Study Area)

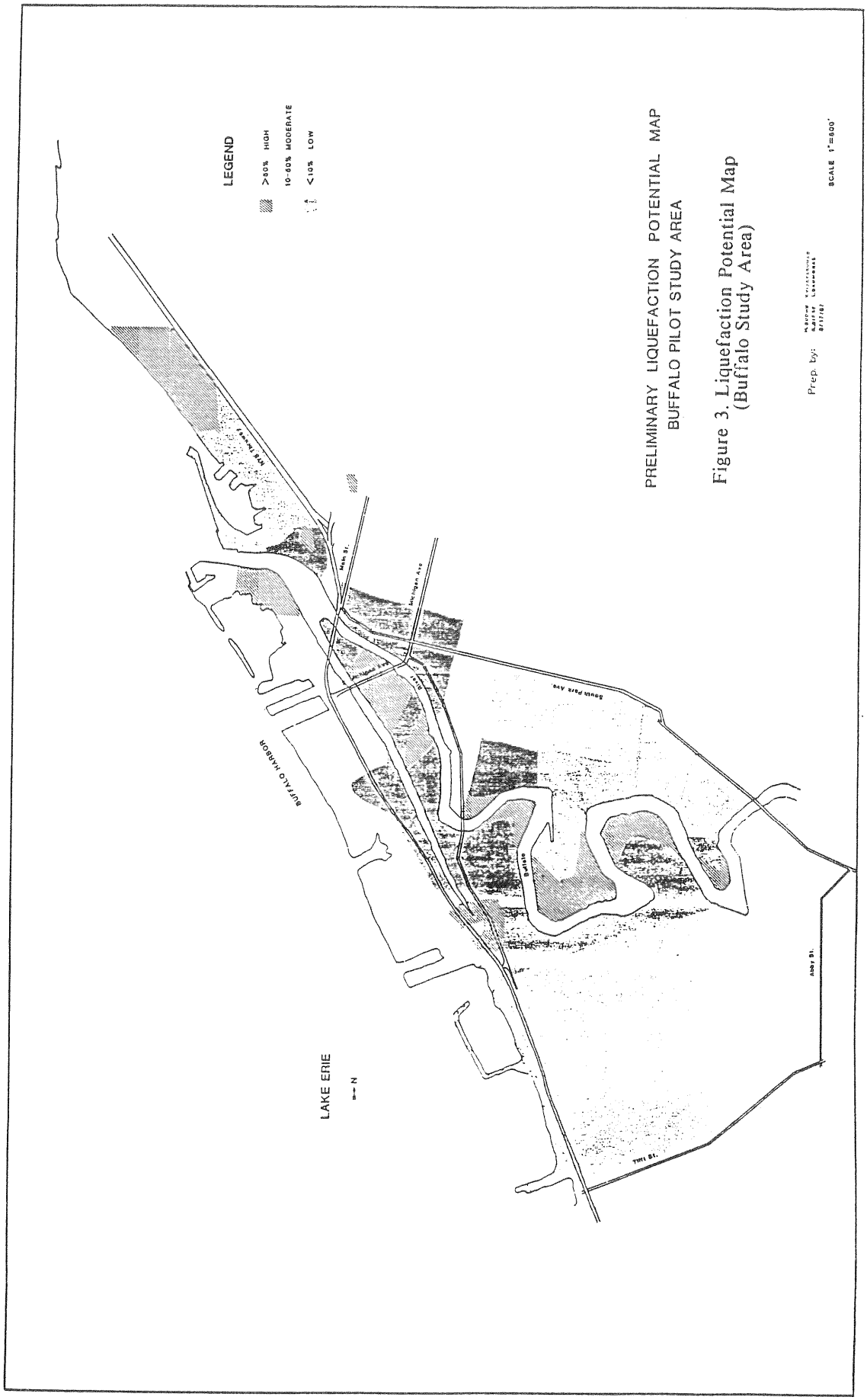

Figure 3. Liquefaction Potential Map
(Buffalo Study Area)

Most of our effort during this first year has gone into designing and implementing the data base code. There remain several major tasks-

1. We have created a minimal data base which is used primarily for testing the program; it contains too few bore hole records to serve any practical purpose. Continued work on the data base will focus largely on adding information to the data base so that we will be able to manipulate any of the thousands of pieces of information which we have collected to date.

2. We have spent little time working on the code necessary for the subsequent analysis of the bore hole data. A major effort will be made to create the software necessary to completely analyze the bore hole data of the two regions for liquefaction potential.

3. We will modify the program so that it will be capable of a more flexible graphics output, both to the monitor screen and to a printer/plotter.

4. Design ways in which the data base could be made accessible to a wider group of users. A dial-up access is one such mechanism.

7 CONCLUSIONS

Liquefaction potential maps of two heavily populated urban areas in New York State - upper Manhattan and central Buffalo - have been assembled from subsurface borehole data. The liquefaction potential has been determined by a method which is partly empirical and partly statistical and assumes an earthquake of magnitude 7.5 with a peak ground acceleration of 0.15 *g*. Given an event of this magnitude and surface acceleration, soils adjacent to the Harlem River in Manhattan and along the Buffalo waterfront would be highly susceptible to liquefaction

Many parts of the two study areas, especially those bordering water, are reclaimed land formed by infilling with assorted debris. It was not possible to evaluate the liquefaction potential of these areas since we have no historical record of how this type of artificial deposit will behave when subjected to earthquake stresses. One would suspect that this type of artificial fill would be likely to amplify earthquake induced ground motions and to shift the frequency spectrum of the motions to longer periods.

The liquefaction potential maps are not intended to suggest that presently existing structures in areas which are identified as being underlain by highly liquefiable soils are at risk since such an evaluation is beyond the scope of the present study. The maps provide useful information for: 1) preliminary structural design considerations, 2) planning of emergency procedures, and 3) the assessment of land use.

The geotechnical data base which is being assembled in connection with this project should be expanded to take in larger sections of heavily populated areas in New York State

8 LIMITATIONS

The liquefaction potential maps presented here were zoned into categories of high, medium, and low liquefaction potential. The zoning criteria however were relative and adopted as per the opinion of the authors. These maps have some critical limitations with regard to their interpretation or actual use. The important limitations are :

1. The liquefaction evaluation procedure involved correlations made using data for outer areas in the nations and abroad and not from the region of study.

2. The established empiricisms specify a percentage of silt and clay content, whereas the assessment of these quantities at each site was based on the qualitative classifications of the soils. Clean sand or silt layers were not observed near the surface within the study area. Rather, a mixture of gravels, sands, silts, and clays are common - the effects of which are not taken into account in the evaluation procedure. It should be noted that such effects have the tendency of reducing the liquefaction potential, making the results of the present study conservative.

Veneziano, D. and J. Van Dyck (1984) "Analysis of Eastern United States Seismicity on a One-Degree Grid: Incompleteness, Recurrence Rates, and Non-Stationarity". Electric Power Research Institute, Palo Alto, California, 149 pp.

Youd, T. L., and S. N. Hoose (1977) "Liquefaction Susceptibility and Geologic Setting", Proceedings of the Sixth World Conference on Earthquake Engineering, V. 3, Prentice Hall, Inc., Englewood Cliffs, New Jersey, 2189-2194.

Youd, T. L., and M. Perkins (1978) "Mapping Liquefaction Induced Ground Failure Potential," Journal of the Geotechnical Engineering Division. ASCE 104 (GT4):433 - 446.

Youd, T. L., and J. B. Perkins (1985) "Map Showing Liquefaction Susceptibility in San Mateo County, California," Miscellaneous Investigations Series Map I -1257-G, U. S. Geological Survey, Menlo Park, California.

Youd, T. L., J. C. Tinsley, D. M. Perkins, E. J. King, and R. F. Preston (1978) "Liquefaction Potential Map of San Fernando Valley, California." in Proceedings of the Second International Conference on Microzonation for Safety Construction - Research and Applications, V. 1, National Science Foundation, Washington, D.C., 268-278, 1980.

LIQUEFACTION OF GLACIOMARINE SEDIMENTS DURING THE 1727 EARTHQUAKE IN NEWBURYPORT, MASSACHUSETTS

Martitia P. Tuttle, Leonardo Seeber and Lauren Bradley
Lamont-Doherty Geological Observatory
Palisades, New York 10964

ABSTRACT

In Newburyport, Massachusetts, liquefaction and ground failure inferred from the reported effects of the 1727 (Mfa = 5.0) earthquake can be attributed to specific geologic-hydrologic conditions. Data from exposures, boreholes, and radar profiles reveal an irregular bedrock surface overlain by glacial till, ice-contact and glaciomarine deposits. The ice-contact deposits form a northwest trending ridge (upland). Adjacent to the ridge, well-sorted and thixotropic glaciomarine sand fills bedrock lows and are capped by glaciomarine clay (lowlands). Groundwater entering through the ice-contact deposits becomes artesian in the clay-capped glaciomarine sand. These conditions prevail along the southern flank of the upland where the 1727 liquefaction effects were concentrated. A high concentration of deformation structures have been observed in the ice-contact and glaciomarine deposits in Newburyport. Some of these structures could have formed by ground shaking during earthquakes. Conditions similar to those in Newburyport are likely to exist elsewhere along the New England coast from Boston to northern Maine where glaciomarine clays overlie sands. An understanding of the conditions in Newburyport that led to liquefaction and ground failure during the relatively small 1727 earthquake, can help us assess the liquefaction potential in coastal New England. Efforts continue to identify deformation structures that formed as a result of the 1727 earthquake. In addition, preliminary *in situ* testing of the engineering properties of materials is scheduled for October, 1987.

INTRODUCTION

Liquefaction causing permanent secondary deformation in unconsolidated sediments has been reported for several earthquakes in the eastern U.S. Reports of these earthquakes indicate that (1) moderate earthquakes can cause various types of ground failure, (2) liquefaction induced by earthquakes tends to be localized and variable in its effects over short distances, suggesting a strong geological control of site response, and (3) large earthquakes are likely to leave a record of their effects in sediments that are susceptible to liquefaction. Thus, characteristics of liquefaction and ground failure caused by historic earthquakes and the timing of large prehistoric earthquakes may be retrieved by studying deformation features in unconsolidated sediments. Evidence of prehistoric earthquakes has been found in the epicentral areas of the 1886 Charleston, South Carolina [Obermeier et. al., 1985] and the 1811-1812 New Madrid, Missouri [Russ, 1979] earthquakes, the two large historic events known to have caused liquefaction in the eastern United States. Other earthquakes that may have caused liquefaction in the Northeast include the 1663 and 1944 St. Lawrence Valley, the 1727 and 1755 Massachusetts, and 1884 New York City events. The 1727 Massachusetts earthquake is one of the better documented cases of earthquake-induced liquefaction and ground failure in the glaciated Northeast. It provides the opportunity to characterize earthquake-induced deformation in glacial sediments, to perhaps recognize prehistoric earthquakes

in glacial sediments in Newburyport and elsewhere in the Northeast, to identify the geologic-hydrologic conditions that led to liquefaction during the relatively small 1727 event, and therefore to improve assessments of seismic risk in the region.

EFFECTS OF THE 1727 NEWBURYPORT EARTHQUAKE

The Newburyport area was settled in the early 1600s. The original landing was on high ground along the Parker River. Settlement started there and spread north toward the Merrimack River. Homes were built on the deltaic uplands, cattle was grazed in the lowlands, and the marshes were harvested for hay. The mouth of the Merrimack River provided an ideal harbor and became a thriving port, known as Newburyport. By the time of the 1727 earthquake the Newburyport area was sparsely settled. Numerous earthquakes were felt between 1635 and 1845, the larger being the 1638, 1727 and 1755 events. According to historical reports, the 1727 earthquake (felt-area magnitude, Mfa = 5.0; maximum intensity, Imax = VII) caused the following effects in the Newburyport area : (1) upland was locally changed to quagmire, (2) places in the marsh lowland were elevated, becoming too dry to support native grasses, (3) in at least ten places in the clay lowlands, water and sand issued from 0.3- to 0.6-meter-wide "chasms" depositing, in one case, 16 to 20 "cartloads" of fine sand on the ground surface, and (3) also in the clay lowlands, new springs opened and others went dry (Figure 1) [Coffin, 1845; Perley, 1891; Currier, 1906; and Boston Edison, 1976; Betty Knight, personal communication 1986]. These reports indicate that liquefaction of sediments occurred in both the uplands and the lowlands. In the uplands, liquefaction caused quick conditions and in the lowlands, it may have initiated a lateral spread. Similar effects were reported southeast of Boston in Scituate Massachusetts, during the 1755 (Mfa = 5.5) Cape Ann earthquake [Boston Edison, 1976].

SURFICIAL GEOLOGY OF THE NEWBURYPORT AREA

In the Newburyport area, an irregular bedrock surface (ranging from +50 m to at least -32 m elevation) is overlain by till and ice-contact and glaciomarine deposits [Chute and Nichols, 1941; Sammel, 1967; Edwards, 1987]. The town itself is built on an ice-contact delta confined to a narrow northwest-trending belt (Figure 1). The delta was deposited by glacial meltwater in a subaqueous marine environment about 13,000 yrs B.P.; its location was controlled by bedrock topography, sea level and crustal rebound [Edwards, 1987]. The linear shape of the delta supposedly reflects the position of the ice-front at the time of delta formation. The delta forms a ridge (upland) 20 to 30 m above present sea level and is surrounded by clay lowlands at about 10 m above sea level. Cross-sections of pre-existing borehole data [Sammel, 1967; and Delaney and Gay, 1981] drawn (NE-SW) perpendicular to the long dimension of the delta suggest that a sequence of clay overlying sand occurs along both flanks of the delta (Figure 2). The sand unit overlies till and is restricted to bedrock lows adjacent to the delta. The clay unit is widely distributed and onlaps bedrock highs and the flanks of the delta up to approximately 15 m elevation. The delta (20 m elevation in this area) is comprised primarily of sand and gravel and serves as the recharge area for local aquifers [Delaney and Gay, 1981]. Distal and lateral portions of the delta are characteristically finer-grained.

Glaciomarine clay has been mapped along the coast from Quincy, south of Boston, to northern Maine, where it is known as the Presumscott Formation

Figure 1. Surficial geology map of the Newburyport, Massachusetts area. [modified from Sammell, 1967; and Edwards, 1987]. Effects of the 1727 earthquake were reported in the deltaic uplands, clay lowlands and marsh lowlands. Note the line of section drawn perpendicular to the trend of the delta (Figure 2). $ indicates the location of our subsurface investigation (Figure 3) . Approximate locations of historic effects of the 1727 earthquake: (See text for references.)

S = "... it brake the ground in the common ... and there is from 16 to 20 loads of fine sand thrown out ..."

J = "... it broke out in more than 10 places in ye town in ye clay lowlands, blowing up ye sand some more, some less ..."

B= "... the very first shock opened a new spring by my father Samuel Bartlett's house in the meadow ..."

K = "... this spring was discovered the day after the earthquake; the spring had not been there before ..."

U = "... some upland was changed to quagmire..."

M = "... marshland was raised up, being afterward too dry for its native grass to grow ...".

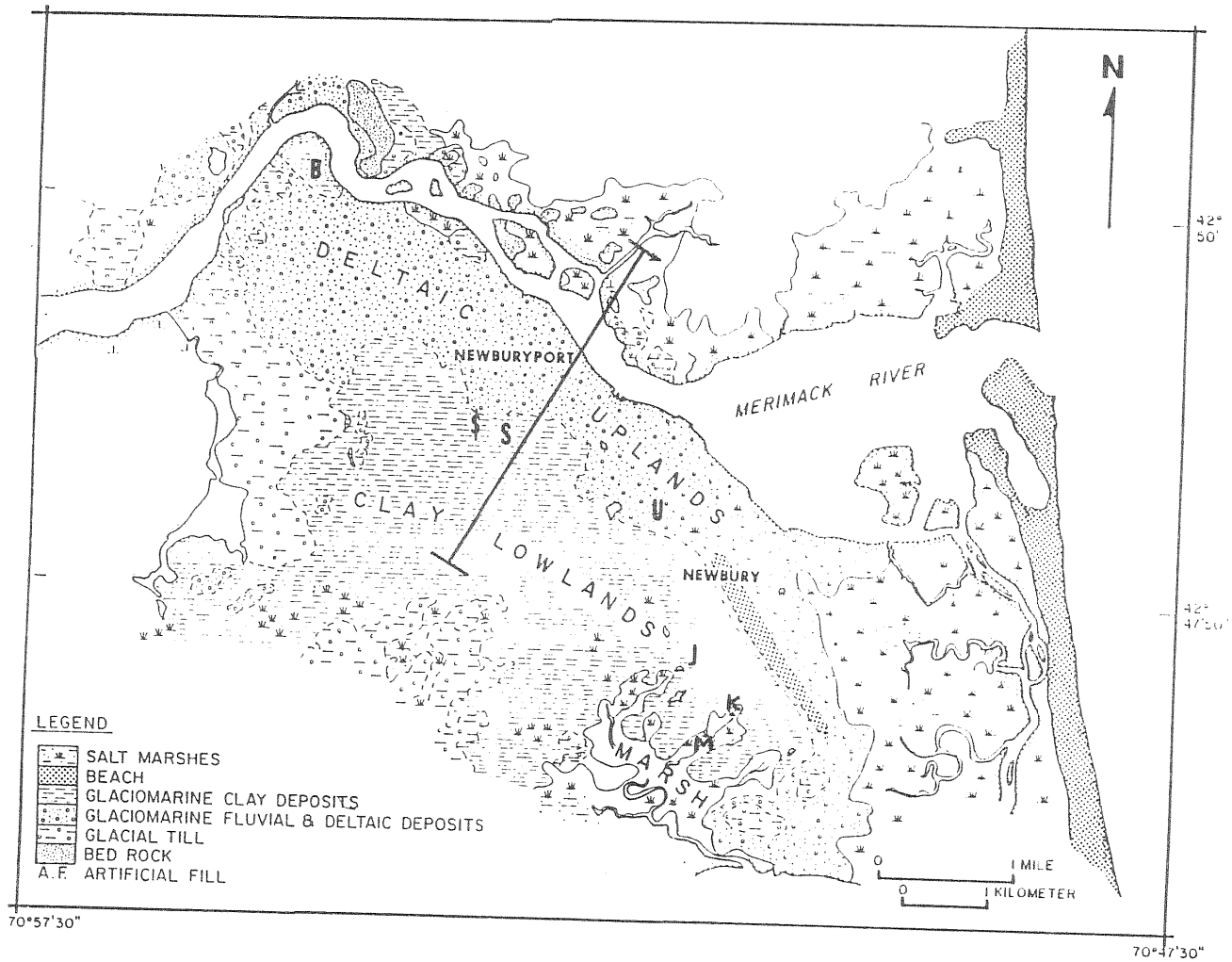
N
DELTAIC
NEWBURYPORT
MERIMACK RIVER
CLAY
LOWLANDS
UPLANDS
NEWBURY
MARSH
42°
50'
42°
47'30"
70°57'30"
70°47'30"
LEGEND
SALT MARSHES
BEACH
GLACIOMARINE CLAY DEPOSITS
GLACIOMARINE FLUVIAL & DELTAIC DEPOSITS
GLACIAL TILL
BED ROCK
A.F. ARTIFICIAL FILL
0 1 MILE
0 1 KILOMETER

Figure 1.

CROSS SECTION OF NEWBURYPORT DELTA BASED ON BOREHOLE DATA

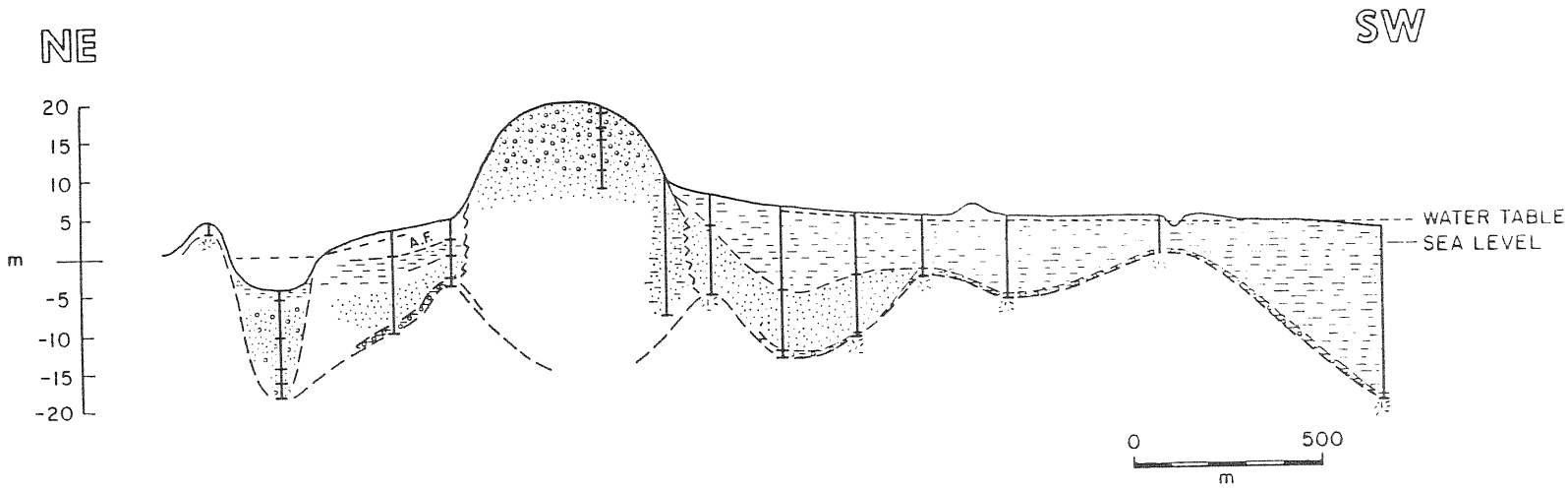

Figure 2. Cross section of the Newburyport delta based on pre-existing borehole data [Sammel, 1967; and Delaney and Gay, 1981]. To either side of the delta, glaciomarine clays are underlain by sand possibly derived from the delta and deposited in the adjacent bedrock lows. The delta serves as a recharge area for local aquifers. Ground water becomes artesian in the clay-capped glaciomarine sand possibly contributing to their liquifaction susceptibility. See Figure 1 for location of the cross section and for legend of symbols.

[Bloom, 1960; and Kaye, 1976]. This regionally distributed clay is thought to represent deposition during a marine incursion accompanying retreat of the late Wisconsin marine-based glacier; the clay was not deposited south of Quincy because isostatic depression was not great enough there to cause submergence [Hanson, 1984]. Occurrences of well-sorted sand beneath the clay has been described in Maine and New Hampshire, as well as in Massachusetts [Bloom, 1960 and 1963; Smith, 1984; and Oldale, 1964]. Like similar glaciomarine sequences recognized elsewhere along the New England Coast, the fining-upward sequence of the Newburyport lowlands probably represents deposition of subaqueous outwash following retreat of the marine-based glacier [Smith, 1984]. Since its distribution is retricted to bedrock lows adjacent to the delta, the sand that is overlain by clay was probably derived from the ice-contact delta as lateral support for the delta was removed during retreat of the ice margin. Most likely, the overlying clay was rock flour deposited at some distance from the glacier. The deposition of clay in this area may reflect the retreat of the ice-front farther inland. West and north of Newburyport, clay is overlain by sand, silt and peat deposited during subsequent marine regression caused by crustal rebound [Edwards, 1987].

GEOLOGIC-HYDROLOGIC CONDITIONS LEADING TO LIQUEFACTION

A site where reportedly the ground opened and water and sand were discharged at the surface during the 1727 earthquake has been approximately located at about 10 m elevation on the fringe of the clay lowland and adjacent to the southwestern flank of the Newburyport delta (Figure 1). A subsurface investigation in this area, consistent with borehole data mentioned above, reveals an irregular bedrock surface overlain first by thixotropic sand and then by relatively impermeable clay (Figure 3). The clay is interlaminated and is 1 to 2 meters thick. The sand is very fine- to medium-grained and is 2 to 4 meters thick. The thixotropic sand typically occurs beneath a thin transition zone between the clay and sand. The lower boundary of the sand conforms with the irregular bedrock surface; whereas, the upper boundary is roughly horizontal. The overlying clay is fairly uniform in thickness and onlaps bedrock highs. Groundwater in the thixotropic sand is artesian and rises in boreholes when the boundary between the sand and clay deposits is pierced.

The deposits in the Newburyport lowlands are similar in stratigraphic relationships, grain-size distribution and relative thickness to deposits that have liquefied during other modern earthquakes. However, the 1727 earthquake is on the lower end of the scale of earthquakes that have caused liquefaction. Liquefaction usually occurs during large earthquakes [National Research Council, 1985]. For example, in the central Mississippi Valley, liquefaction and ground failure of late Wisconsin braided stream and meander belt deposits capped by clay-rich overbank deposits occurred during the large 1811 New Madrid (Imax=XI) and 1895 Charleston (Imax = VIII) earthquakes but not during numerous moderate earthquakes (Imax=VII) including the 1895 , 1903, 1909, 1923, 1927, and 1968 events [Obermeier, 1984]. In Newburyport, overpressured conditions and/or internal structure of the sediments, may have made the sediments especially susceptible to earthquake-induced liquefaction. If initial pore pressures in the sand were high at the time of the earthquake, only a minimal reduction in effective stress would be required to cause liquefaction. The internal structure of the sand may have played a role in its liquefaction. An honey-combed structure, where grains are arranged in crude arches, is common in sands that have been deposited from suspension and is susceptible to

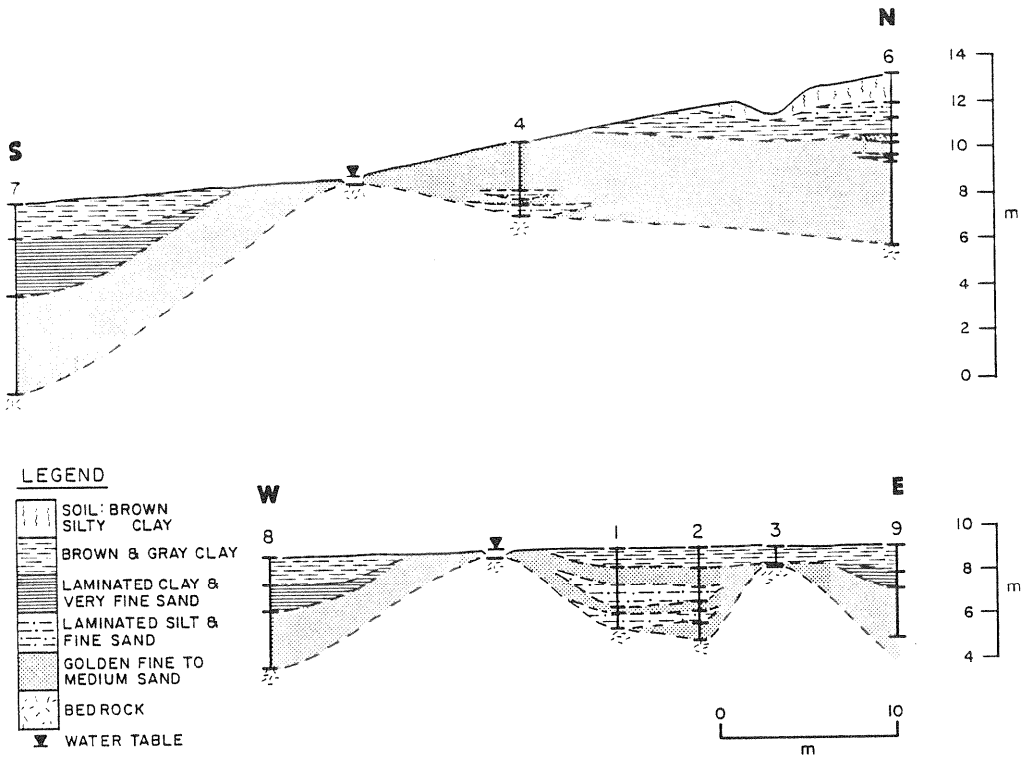

Figure 3. Cross sections of subsurface data acquired in an area where ground fissuring and sand venting occurred during the 1727 earthquake. Top soil has been removed from most of the site. An irregular bedrock surface is overlain by thixotropic sand capped by clay. Ground water in the sand is artesian creating overpressured conditions in the sand.

collapse when subjected to vibration or shock. Most likely, the sediments existed in an apparent stable condition, hovering just below the failure criteria. Only some triggering phenomena such as an earthquake was needed to initiate the progressive loss of strength within the sediments.

DEFORMATION STRUCTURES IN GLACIOMARINE SEDIMENTS

A reconnaissance of sand-and-gravel pits, excavations and stream-channel exposures within a 20-km radius centered on the 1727 mesoseismal area has revealed a high concentration of deformation structures in coarse-grained, proximal as well as fine-grained, distal glaciomarine deposits in Newburyport. Basically, four types of deformation structures were observed including clastic dikes of various shapes and sizes, water escape structures, recumbent folds, and contorted bedding.

The clastic dikes occur near the surface of the delta and range from simple to complex in both configuration and in sedimentary character. The simple clastic dikes have one primary trunk, widened towards the top and are filled with one-type of material. In one case, the filling material, composed of gravel and coarse sand cemented with clay, formed an apron above the feature. Except for the cementing clay, the filling was coarser grained than the overlying or surrounding material. Lateral injection features were associated with this clastic dike. In another case, the material filling the feature was comprised of sand and cobbles and was very similar to material in the upper-most layer in the deltaic sequence from which it was probably derived. The upper-most layer was overlain by an organic soil buried by fill. A plug of gray, silty material was observed above the feature and within the cobbly layer. The silty material thinned laterally away from the feature. Similar material was not observed above or beside the clastic dike. Both normal and thrust faulting was associated with this feature. In the two cases decribed above, 2 to 3 m of the total height and 0.5 to 1 m of the apparent width were exposed. Other simple clastic dikes are much smaller, on the order of mm in width. The complex clastic dikes appear to be confined and oriented vertically at depth but fan out near the ground surface at about 3 m. The fans range in size from 1 to 4 m across and are comprised of distinctly different materials including clay, sand and gravel. Water escape structures occur in delta sediments both at depth and near the ground surface. Those occurring at depth within the pile are truncated by overlying layers of delta sediments; those structures occurring near the ground surface extend into the overlying layers. In one case, deformation appeared to extend into an overlying loess deposit; in another case, deformation may have extended into the modern soil. Recumbent folds are common in fine sands on the northern flank of the delta. The axes of the folds are roughly parallel to the long dimension of the delta and perpendicular to the slope. Contorted bedding occurs in glaciomarine silt and clay deposits adjacent to the northern flank of the delta. Deformation is usually confined within 0.5 to 3 m sediment packages. However, in one instance, the boundary between packages was deformed above a clastic sill composed of well-sorted sand.

Stratigraphic relationships indicate that some of the structures are syndepositional, in particular the recumbent folds in sand exposed on the flanks of the delta, contorted bedding within packages of glaciomarine silts and clays, and dewatering structures that have been truncated by subsequent layers. Other structures such as clastic dikes and dewatering structures that extend into overlying layers clearly postdate deposition. In several cases, a superposition of structures suggests a series of deformational events. Although syn-

depositional structures can be attributed to rapid sedimentation and slumping of unstable materials, it is harder to explain post-depositional structures by ordinary sedimentary processes. In glacial sediments elsewhere in the Northeast, deformation structures that post-date deposition have been attributed to periglacial processes, to collapse of unstable sediments, and to dewatering and differential compaction of subjacent sediments [Schafer, 1968; Black, 1983; and Schafer et. al., 1987]. Whether they were formed syn- or post-depositionally, many of the Newburyport structures could also have been caused by earthquakes. Earthquakes have been recognized as one possible mechanism for the formation of recumbent-folded deformed cross-bedding, contorted bedding, dewatering structures and clastic dikes [Lowe, 1975; Sims, 1975; Allen, 1982; Allen and Banks, 1972; Morner, 1985; and El-Isa and Mustafa, 1986]. An earthquake origin has been hypothesized for similar structures described elsewhere in the Northeast including (1) sand diapirs and thixotropic features in glacial sediments in northern New York within the St. Lawrence Seismic Zone [Coates, 1975] and (2) clastic dikes in glaciofluvial sediments in eastern Connecticut located about 30 to 40 km from the Moodus earthquake source area [Thorson et. al., 1986]. However, considering the numerous ways in which the structures in Newburyport could have formed, it is not possible at this time to attribute any of them to historic or pre-historic earthquakes. Structures that fit the descriptions of effects of the 1727 earthquake (clastic dikes and dewatering structures near the ground surface that cut or deform post-glacial deposits) are the most likely to be earthquake-induced. Absolute ages of these structures are not yet known but could help to establish the timing and origin of their formation.

MODEL OF LIQUEFACTION AND GROUND FAILURE DURING THE 1727 EARTHQUAKE

Considering that during shaking, pore pressure in clay-capped sand would rise above the already overpressured conditions, the geologic-hydrologic conditions that exist along the flank of the delta seem ideal for liquefaction and ground failure to occur during earthquakes. We hypothesize that ground shaking in Newburyport could cause the overpressured, thixotropic sand to liquefy, resulting in loss of its strength and weight-bearing capacity. No longer supported by the underlying sand, the clay would founder or slide laterally down dip from bedrock highs and from the axis of the delta. Liquefied sand could then find routes to the surface where the clay deposit is weakened by extension or along the base of the clay to its onlap contact with the delta. Liquefaction and quick conditions could also occur in delta sediments where fine-grained, distal deposits could form perched water-tables. This scenario could account for the various types of ground failure described in historical reports of the 1727 earthquake including both changes in topography and expulsion of sand through fissures in the clay lowlands, transformation of upland into quagmire, and perhaps also for the formation of some of the deformation structures recently observed in the deltaic deposits as well as the silt and clay deposits flanking the delta.

CONCLUSION

Although 1727 earthquake-induced deformation structures have yet to be identified, some of the key factors that probably allowed liquefaction and ground failure to occur during the relatively small event include (1) the irregular

bedrock surface, (2) the sedimentary characteristics (grain-size distribution, thickness, stratigraphic relationship and age) of the glaciomarine deposits and (3) the overpressured ground-water conditions within these deposits. Further study including subsurface investigations and testing of the engineering properties of materials are needed to constrain our model. Characterization of the geologic-hydrologic conditions that led to ground failure during the 1727 earthquake, can help us recognize similar conditions elsewhere in coastal New England.

BIBLIOGRAPHY

Allen, J.R.L., and N.L. Banks, An Interpretation and Analysis of Recumbent-Folded Deformed Cross-Bedding, Sedimentology, Elsevier Publishing Company, Amsterdam, 257-283, 1972.

Allen, J.R.L., Sedimentary Structures: Their Character and Physical Basis, Elsevier Publishing Co., Amsterdam, 663 p., 1982.

Black,R.F., Pseudo-Ice-Wedge Casts of Connecticut, Northeastern United States, Quaternary Research 20,74-89, 1983.

Bloom, A.L., Late Pleistocene Changes of Sea Level in Southwestern Maine: Augusta, Maine, Maine Geol. Survey, Dept. Econ. Dev., 143 p., 1960.

Bloom, A.L., Late-Pleistocene Fluctuations of Sea Level and Postglacial Crustal Rebound in Coastal Maine, Am. Jour. of Science, 261, 862-879, 1963.

Boston Edison Company, Historical Seismicity of New England, BE-S67601, 641 p., 1976.

Chute, N.E., and R.L. Nichols, Geology of the Coast of Northeastern Massachusetts, Commonwealth of Massachusetts, Bulletin No. 7, 47 p., 1941.

Coates, D.R. (ed.)., Quaternary Deformed Sediments of the St. Lawrence Lowland as an Index of Seismicity, Report to New York State Atomic and Space Development Authority, 268 p., 1975.

Coffin, J., A Sketch of the History of Newbury, Newburyport, and West Newbury, 1635-1845, Samuel Drake, 1845.

Currier, J.J., History of Newburyport, Massachusetts, Currier, 766 p., 1906.

Delaney, D.F., and F.B. Gay, Hydrologic Data of the Lower Merrimack River Basin, Massachusetts, from Concord River, Lowell to Plum Island, Newburyport, U.S.G.S. Open File Report 81-1185, 1981.

Edwards, G.B., and R.N. Oldale, Late-Quaternary Paleodeltas of the Merrimack River, Western Gulf of Maine (Abs.), 22nd Annual Meeting of the Geological Society of America, Northeastern Section, Abstracts with Programs, p. 12, 1987.

El-Isa, Z.H., and H. Mustafa, Earthquake Deformation in the Lisan Deposits and Seismotectonic Implications, Geophys. J. R. Astr. Soc., 86, 413-424, 1986.

Hanson, L.S., Quaternary Geology and Geomorphology, in Geology of the Coastal Lowlands, Boston to Kennebunk, Maine, 76th Annual Meeting, N.E.I.G.C., I36-I46, 1984.

Kaye, C.A., Outline of Pleistocene Geology of the Boston Basin, in Cameron, B. ed., Geology of Southeastern New England, a guidebook for field trips; 68th Annual meeting N.E.I.G.C., Princeton, New Jersey, Science Press, 46-63, 1976.

Lowe, D.R., Water escape structures in coarse-grained sediments, Sedimentology, 22, 157-204, 1975.

Morner, N., Paleoseismicity and Geodynamics in Sweden, Tectonophysics, 117, 139-153, 1985.

National Research Council (U.S.), Committee on Earthquake Engineering Liquefaction of Soils During Earthquakes, National Academy Press, 240 p., 1985.

Obermeier, S.F., Liquefaction Potential in the Central Mississippi Valley, in Gori, P.H. and Hays, W.W., eds., Proceedings of the Symposium on "The New Madrid Seismic Zone", U.S.G.S. Open-File Report 84-770, 391-446, 1984.

Obermeier, S.F., G.S. Gohn, R.E. Weems, R.L. Gelinas, and M. Rubin, Geologic Evidence for Recurrent Moderate to Large Earthquakes near Charleston, South Carolina, Science, 227, 408-411, 1985.

Oldale, R.N., Surficial Geology of the Salem Quadrangle, MA, U.S. Geological Survey Geologic Quadrangle Map GQ-271, 1964.

Perley, S., Historic Storms of New England, The Salem Press Publishing and Printing Co., Salem 1891.

Russ, D.P., Late Holocene Faulting and Earthquake Recurrence in the Reelfoot Lake area, northwestern Tennessee, Geological Society of America Bulletin, Part 1, 90, 1013-1018, 1979.

Sammel, E.A., Water Resources of the Parker and Rowley River Basins, Massachusetts, U.S.G.S. Hydrologic Investigations, Atlas HA-247, 1967.

Schafer, J.P., Periglacial features and pre-Wisconsin weathered rock in the Oxford-Waterbury-Thomaston area, Western Connecticut, in New England Intercollegiate Geological Conference, Guidebook No. 2 for fieldtrips in Connecticut, B-2, 1-5, 1968.

Schafer, J.P., S.F. Obermeier, and, J.R. Stone, On the Origin of Wedge Structures in Southern New England, (Abs.), 22nd Annual Meeting of the Geological Society of America, Northeastern Seciton, Abstracts with Programs, p.55, 1987.

Sims, J. D., Earthquake-induced structures in sediments of Van Norman Lake, San Fernando, California, Science, 182, 161-163, 1972.

Smith, G.W., Glaciomarine Sediments and Facies Associations, Southern York County, Maine, in Geology of the Coastal Lowlands, Boston to Kennebunk, Maine, 76th Annual Meeting N.E.I.G.C., 352-369, 1984.

Thorson, R.M., W.S. Clayton, and L. Seeber, Geologic Evidence for a Large Prehistoric Earthquake in Eastern Connecticut, Geology, 14, 463-467, 1986.

EARTHQUAKE-INDUCED LIQUEFACTION FEATURES IN THE COASTAL SOUTH CAROLINA REGION

Stephen F. Obermeier, Robert E. Weems, and Robert B. Jacobson
U.S. Geological Survey
National Center
Reston, Virginia 22092

ABSTRACT

Features interpreted to be earthquake-induced sand blows of Holocene age have been discovered throughout much of the coastal region in South Carolina and in the southeastern extremity of North Carolina. Nearly all these sand blows presently are manifested as filled craters.

Interpretation of an earthquake origin for the craters is based on independent lines of evidence: (1) the filled craters have a morphology consistent with historical descriptions and photographs of sand blows produced by the Charleston, South Carolina earthquake of 1886; (2) the filled craters occur near or along the crests of Pleistocene beach ridges, which is a setting that corresponds with the geologic-topographic setting of the most abundant craters produced by the 1886 earthquake; (3) filled craters are especially abundant at sites reported in 1886; and (4), the filled craters have sedimentary relations that are consistent only with a suddenly applied, strong, short-lived, upward-directed hydraulic force which, on the topographically high beach ridge crests could reasonably have been produced only by earthquake-induced liquefaction.

The craters generally formed in episodes long-separated in time. Radiocarbon ages show that at least three prehistoric, liquefaction-inducing earthquakes have taken place within the past 7200 years near Charleston. Ages of some craters far from Charleston differ from ages near Charleston. Insufficient data have been collected to determine if all crater ages far from Charleston differ from ages near Charleston.

Both the diameter and relative abundance of pre-1886 craters are greater in the vicinity of Charleston (particularly in the 1886 meisoseismal zone) than elsewhere along the coastal regions of South Carolina and southeastern North Carolina, although the susceptibility of the widespread beach deposit sites to earthquake-induced liquefaction is approximately the same throughout this area. These data indicate that, in this coastal region, the strongest earthquake shaking during the Holocene has taken place repeatedly near Charleston.

INTRODUCTION

The strongest historic earthquake in the southeastern United States took place in 1886 near Charleston, South Carolina. The meizoseismal zone (encompassing Modified Mercalli intensity-X effects) was about 35 km wide and 50 km long (Bollinger, 1977),

and the estimated body-wave magnitude (m_b) was between 6.6 and 7.1 (Nuttli, 1983). The potential for a future earthquake with the strength of the 1886 earthquake is a major concern in engineering design in the Southeast. The concern is reinforced by a 300-year historical record of continuing weak seismic activity near Charleston. The source of the earthquakes in the Charleston area remains unidentified, and seismotectonic hypotheses are widely disparate despite many geologic, geophysical, and seismic studies during the past decade. No faults or fault systems have been identified that fully explain the large 1886 Charleston earthquake or the other smaller, historic earthquakes which have occurred throughout much of South Carolina (Hays and Gori, 1983; Dewey, 1985; Science News, 1986). Because direct evidence of seismotectonic conditions is lacking and because the historic earthquake record is too limited to provide a dependable basis for estimating the frequency of moderate to strong earthquakes, we undertook a search for pre-1886 sand blows. Liquefaction-induced features, particularly sand blows, were a commonplace effect of the 1886 earthquake within the meizoseismal zone, causing us to first search that area. The initial discovery of pre-1886 sand blows was reported by Gohn and others (1984) and Obermeier and others (1985). The study was next extended throughout much of coastal South Carolina (Obermeier and others, 1986) and more recently into southeastern North Carolina.

Current results of the search are illustrated on Figure 1. Figure 1 shows (1) the approximate boundary of the 1886 Charleston earthquake meizoseismal zone, (2) areas conspicuous in 1886 for development of sand blows (described as "craterlets" by Dutton, 1889), and (3) the sites of pre-1886 sand blows that we have discovered. The unshaded part of Figure 1 encompasses the principal area searched for sand blows; in this area, the sediments are predominantly of marine origin. Fluvial deposits were searched only locally along the Edisto River.

None of the pre-1886 sand blows have any expression on the ground surface that is discernible by on-site examination or on airphotos. The sand blows are seen only where exposed in walls of excavations at least 1.5 m in depth; generally, sand-blow exposures have been found in drainage ditches and borrow pits. At most sites shown on Figure 1, at least three or four sand blows are exposed within a few hundred meters of one another. The following section focuses on the geologic setting in which these sand blows are found and on criteria for interpreting their earthquake origin.

EARTHQUAKE-INDUCED LIQUEFACTION FEATURES

Earthquake Criteria

Identification of an earthquake origin for the features we have observed depends primarily on eliminating (non-earthquake) artesian springs as an alternate mechanism. Other mechanisms that must be eliminated include liquefaction induced by ocean wave pounding, ground disruption by trees and landslides, compaction-induced dewatering, and physical and chemical weathering.

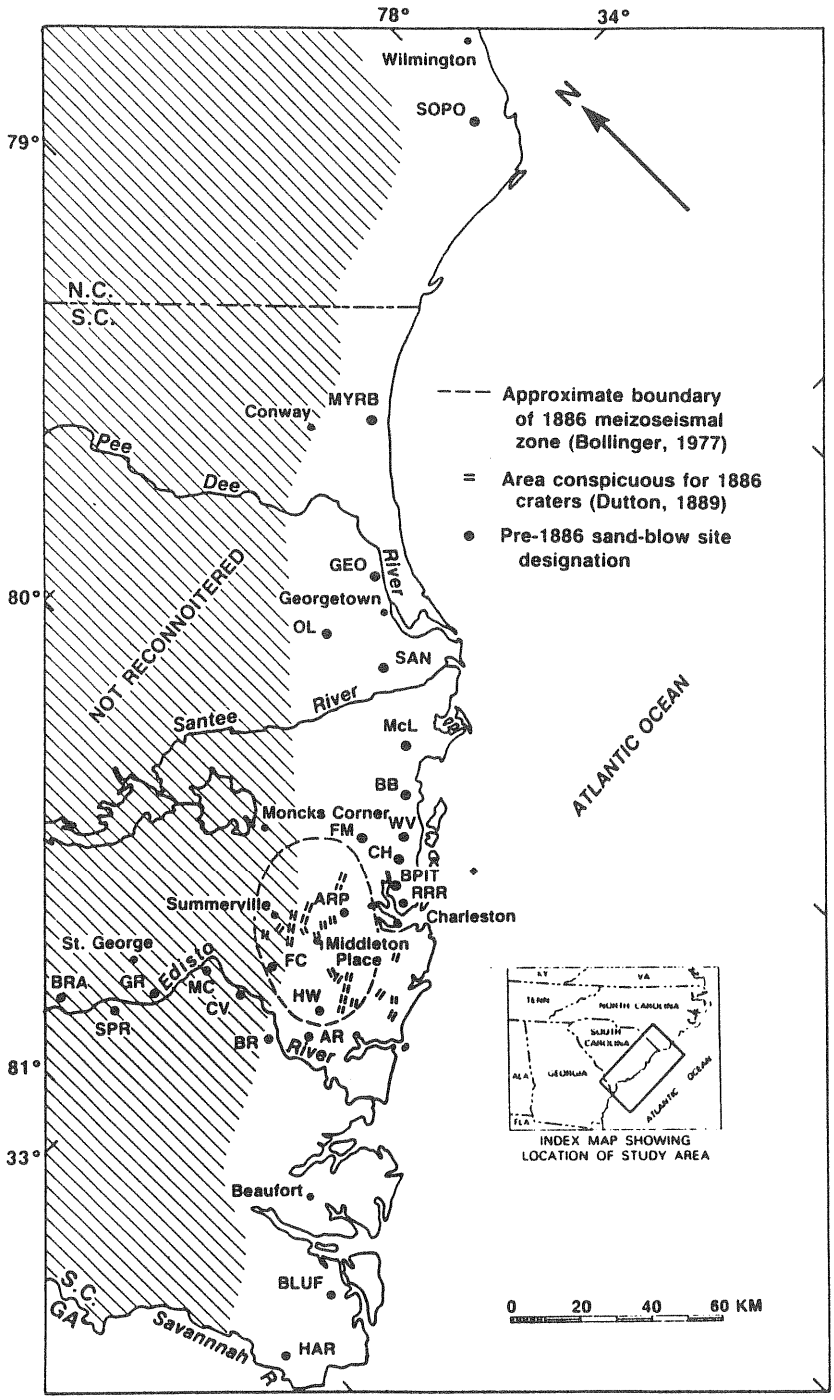

Figure 1. Map showing pre-1886 sand-blow sites. Region without shading is made up predominantly of marine sediments younger than about 240,000 years. Shading denotes region of older marine sediments. Younger fluvial sediments occur locally. All sand-blow sites in unshaded region are in marine-related deposits, and all sites in region with shading are in fluvial deposits. Numerous sites discovered in 1886 meizoseismal zone are not shown because of lack of space.

Geologic criteria we have developed for interpreting that features are sand blows having an earthquake origin generally consist of four elements:

1. The features must have sedimentary characteristics that are consistent with an earthquake-induced liquefaction origin: that is, there is evidence of (a) an upward directed, strong hydraulic force that was (b) suddenly applied and (c) was of short duration.
2. The features have sedimentary characteristics that are consistent with historically-documented observations of earthquake-induced liquefaction processes.
3. The features are in groundwater settings where a suddenly applied, strong hydraulic force of short duration could not be reasonably expected except from earthquake-induced liquefaction. In particular, these settings must be extremely unlikely sites for artesian flowing springs.
4. Similar features must occur at multiple sites (within a few kilometers of one another), in similar geologic and groundwater settings. Where evidence of age is present, it should support the interpretation that the features formed in one or more discrete, short episodes that individually affected a large area and that were separated by long time periods during which no such features formed.

As fewer of these criteria are satisfied, the confidence in an earthquake origin generally diminishes.

Geologic Setting

In South Carolina, the coastal region is known locally as the "low country" because it has low local relief (1 to 3 m) and low elevation (0 to 30 m) and because vast expanses of swamp and marshland are under water much of the year. Most of the Carolina low country is covered by a 5- to 10-m-thick blanket of unconsolidated Quaternary marine and fluvial deposits, which lies on semilithified Tertiary sediments (McCartan and others, 1984). The Quaternary sediments primarily occur as a series of six well-defined, temporally discrete, interglacial beaches and associated back-barrier and shelf deposits that form belts subparallel to the present shoreline. The oldest beach deposits are farthest inland and at the highest altitudes; younger beach deposits are progressively closer to the ocean and at lower altitudes.

Figure 1 shows the approximate inland limits of the marine-related deposits (beach, shelf, and open-sound back barrier) designated as Q3 by (McCartan and others, 1984). Q3 deposits are about 200,000 to 240,000 years old (Szabo, 1985) and are present about 20 to 40 km inland from the modern coast. The part of Figure 1 containing units Q1, Q2, and Q3 of McCartan and others (1984) is shown without shading. The search for sand blows was generally restricted to these units because older deposits have such a low susceptibility to liquefaction (due to weathering and deep ground water) that the likelihood of forming sand blows during the Holocene and late Pleistocene has been extremely low.

The geologic setting most frequently associated with recognizeable earthquake-induced liquefaction features is the crest or flank of a Pleistocene beach ridge, where a thin cover of lay-bearing sand or humate-rich soil overlies well-sorted, clean sand (i.e., containing no silt or clay). According to first hand observations of effects of the 1886 earthquake by Earl Sloan, "these craterlets are found in greatest abundance in belts parallel with (beach) ridges and along their anticlines" (Peters and Herrmann, 1986). A schematic cross-section through a typical low-country beach ridge, such as the ridges described by Sloan, is shown in Figure 2. To a much lesser extent, sand blows have been found in fluvial and back-barrier sediments.

Types of Features

At the great majority of sites on Figure 1, we observed the "craterlet" (or crater) type of sand blow, which was the type most abundantly produced by the 1886 earthquake. At a small number of sites, there is evidence for a second type of sand blow, in which the earthquake-induced features formed as deposits vented to the surface, often through a tabular fissure, leaving a relict sand mound. At a few sites, there is evidence for earthquake-induced oscillating ground movement on a liquefied stratum and for earthquake-induced lateral spreads (landslides of great lateral extent which formed on nearly level ground far from any scarps downslope or upslope).

Sand blows--Only the crater type of sand blow is discussed because of the abundance of this type and because of the difficulty generally attendant in attributing an earthquake origin to the vented-sand-mound type of feature.

Almost all of the pre-1886 craters had an original morphology and size comparable to the 1886 craters described by Dutton (1889); however, today the craters are filled with sediment. All filled sand blow craters share many common sedimentary structures and sequences in fill sedimentation, which are illustrated in Figure 3. The figure shows a soil horizon cut by an irregular crater, which is filled with stratified to massive (nonstratified) and graded sediments; five layers (identified on the figure) are characteristically present. Materials within the craters are sand and clasts from the Bh (humate-rich B horizon), B-C, and C horizons, and sand from depths much below the exposed C horizon. In a pre-1886 filled crater, the Bh horizon that developed on the in-filled sediment generally is much thinner than the Bh horizon of the laterally adjacent, undisturbed soil. With increasing age, the Bh horizon on the filled crater becomes thicker, more clay rich, and has better developed soil structure.

Interpreted phases in the formation of the filled sand-blow craters include the following: (1) after earthquake-induced liquefaction at depth, a large hole is excavated at the surface by the violent upward discharge of the liquefied mixture of sand and water; (2) accumulation of a sand rim around the hole by continued expulsion of liquefied sand and water after the violent discharge; (3) churning of sand, soil clasts, and water in the

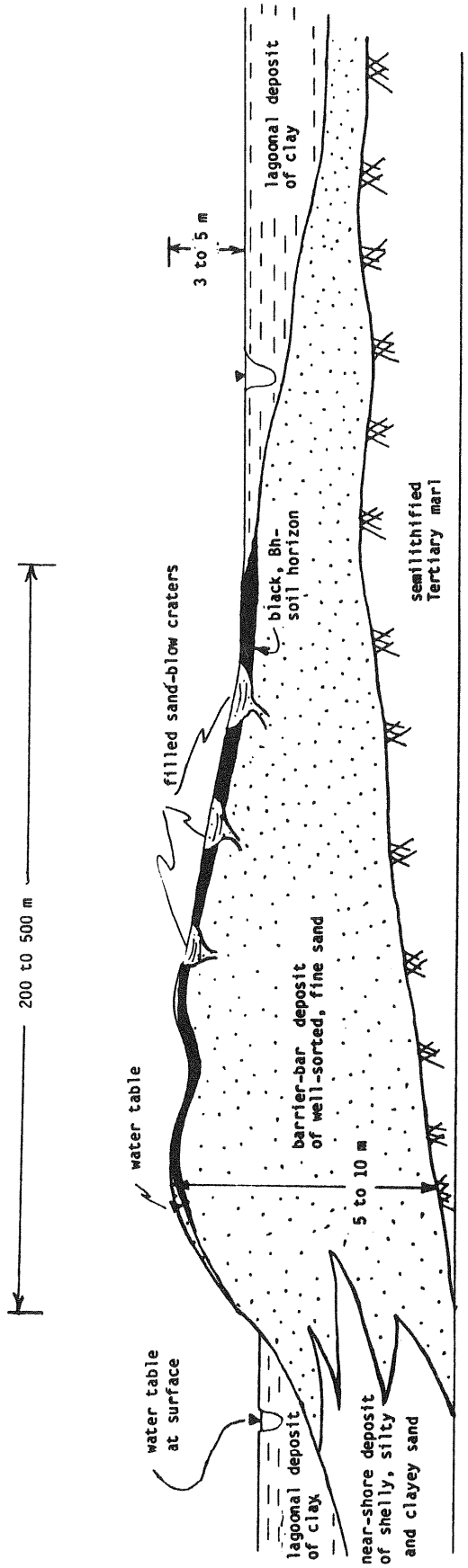

Figure 2. Schematic cross section of representative Pleistocene barrier showing sediment types, groundwater table location, filled sand-blow craters, and Bh-soil horizons.

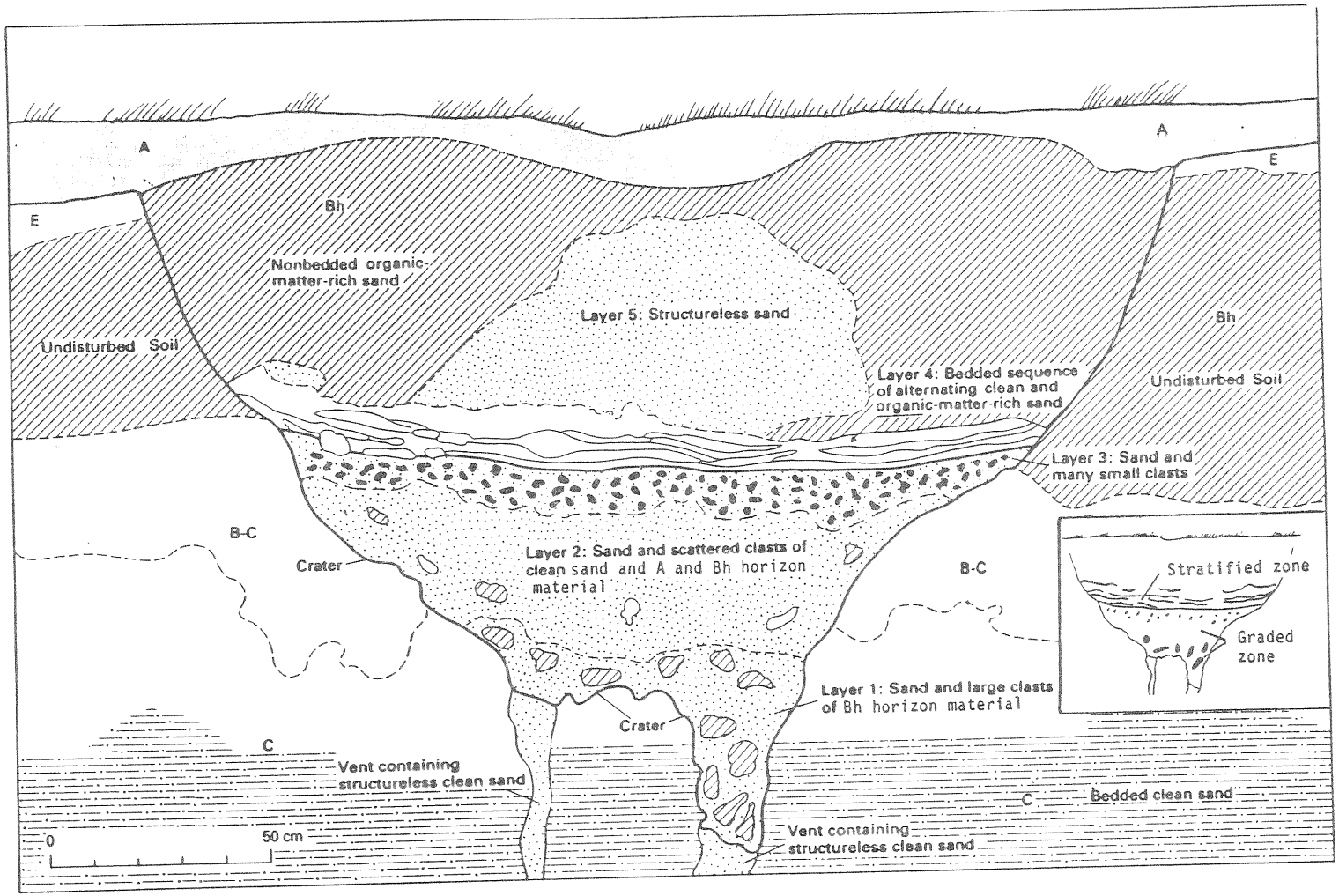

Figure 3. Schematic cross section of representative filled sand-blow crater. Letters correspond to soil horizon designations. Filled crater in this figure significantly predates 1886 earthquake, based on thickness of Bh horizon in the filled crater.

lower part of the bowl, followed by settling of the larger clasts and formation of the graded-fill sequence; and (4) filling of the crater from adjacent surface materials to form the thin stratified-fill sequence, during the weeks to years after the eruption. In the craters predating the 1886 eathquake, the sand blanket ejected from the crater is indistinguishable in the field from the surface and near-surface (A, E, and Bh) soil horizons, because the blanket has been incorporated into these soil horizons.

We infer that the craters were formed by a short-lived process because of the presence of friable clasts of Bh- and C-horizon soil in the graded zone, and because of the very sharp boundary between the graded and layered zones (i.e., the contact between layers 3 and 4). We interpret that the force was strong and upward directed because many of the large clasts in layer 1 have clearly been rounded by tumbling in a fluidized bed. Where multiple craters occur along the topographically highest part of a beach ridge, and where multiple craters appear to have formed at the same time (on the basis of similar soil profiles or similar radiocarbon dates), then all four geologic criteria are satisfied for interpreting an earthquake origin. This interpretation of origin is strongly reinforced by historical accounts of the general morphology and geologic setting where the craters formed, and by our discovery of craters where they were reported by first-hand accounts (Peters and Herrmann, 1986) to be plentiful in 1886 (at sites HW and ARP on Fig. 1).

Reverse shears--Along the flanks of some Pleistocene beaches, reverse shears in association with liquefaction features also were probably formed by earthquakes. The shears generally occur near the crests and on ground sloping less than 1 percent. Shear displacements commonly range from 1 to 4 cm. These slopes are so gentle and the possibility of high artesian pressures is so remote that gravity-induced slumping is virtually impossible. Reverse shears of earthquake origin have also been found on level ground. At one site (site RRR on Fig. 1), for example, reverse shears dipping in opposite directions formed about 10 m apart in the stratum that liquefied during shaking, and sand blows with vents traceable to this liquefied stratum formed between the shears; the only possible mechanism that could have formed the opposite dipping shears was alternating directions of ground motion on the liquefied stratum.

Reverse shears can occur also as isolated features, but they are generally found in association with sand blows. In many filled craters there is a reverse shear near the edge of the crater. The shear is invariably located on the downslope side of the crater, and the shear cuts otherwise undisturbed soil horizons and underlying sediments. The shear formed prior to venting because the vent is not cut by the shear. At some sites, the shears along crater edges could have formed only in response to earthquake-induced lateral spread movement because the shears are traceable into and along the bedding of the stratum that liquefied. At these sites, gravity-induced (non-earthquake)

slumping was precluded by low slope angles and high frictional strength of the sand materials. Only rarely is an exposure sufficiently deep to show that the shear goes into a stratum that liquefied, and thus an earthquake origin cannot be confidently assigned at all sites. However, we are of the opinion that these reverse shears along crater edges are strongly indicative of an earthquake origin, even where they have formed on gently sloping ground (less than 2 percent) as much as 5 m below the beach crest.

Lateral spreads are much more difficult to locate than sand blows because they were not nearly as commonplace as sand blows. In addition, lateral spreads generally formed in wet areas, near streams, in which the regional water table is so high as to preclude drainage and expose outcrops, even with ditching.

Confidence in Interpretation of Origin

Features at all sites shown on Figure 1 are interpreted to be of earthquake origin, although the confidence level differs for various sites. Sites where we have greatest confidence are those where the following features occur: (1) craters have formed on topographically high beach ridge crests; (2) ground oscillation shears have formed in opposite directions; (3) lateral spreads have formed which could not be gravity-induced, and have shears traceable into a liquefied stratum; or (4), shattered ground (indicating forceful injection) is cut by numerous sand-filled dikes in settings where high artesian pressures could not have been involved. Sites of highest confidence include the following: HAR, BLUF, BR, AR, HW, ARP, RRR, CH, FM, WV, McL, SAN, OL, and SOPO.

All other sites on Figure 1 are filled craters that are more than several meters below the crests of beach ridgesor are on fluvial teraces (where groundwater conditions are not well known), causing the confidence level to be lower. Some craters at site MYRB have reverse shears, however, which makes an earthquake origin very probable.

Elimination of all sites from Figure 1 except those in which we have highest confidence does not affect our interpretation of Holocene seismic activity (discussed below).

AGES OF CRATERS

Craters are generally the only features for which radiocarbon ages related to earthquake ages can be generated, because other liquefaction-related features are not found in association with preserved organic matter. Three methods have been used to bracket the times of crater formation (Weems and others, 1986): (1) radiocarbon ages of woody material (tree limbs or pine bark) that fell into the open crater soon after crater formation; (2) dating of roots sheared off at the edge of the crater (pre-dating crater crater formation), and dating of roots that grew into the stratified fill portion of the crater (post-dating crater formation) and (3) dating of clasts of Bh material that fell into the graded fill zone of the crater. The first method yields a

highly accurate age for the time of earthquake occurrence, whereas the other two yield a broad range of possible ages. Sufficient data have been collected at site HW (near Charleston) to show that at least three pre-1886 earthquakes produced sand blows within within the past 7200 years. Radiocarbon dating of pine bark in a crater at site ARP (also near Charleston) independently verifies the middle of these three events. The only definitive statement about earthquake recurrence that can presently be made is that, near Charleston, there have been at least four sand-blow-producing (m_b probably >5.5) earthquakes within the past 7200 years (including the 1886 event). Highly accurate ages of crater formation have been obtained from sites far from Charleston, however, that differ from ages near Charleston, thereby suggesting that the craters far from Charleston emanated from epicentral regions far from Charleston. Insufficient radiocarbon ages have been determined from liquefaction features throughout the Carolina coastal region to define epicentral regions of separate earthquakes. At many sites far from Charleston, there are at least two generations of craters that are long separated in time of formation.

HOLOCENE EARTHQUAKE SHAKING

Methodology

Measurement of the size and number of craters at each site shown on Figure 1 provides a means to estimate the relative severity of shaking that has affected the coastal region during the Holocene. The methodology for estimating shaking intensity is based on the premise that the number and size of liquefaction features is greatest where earthquake shaking is strongest, for a fixed geologic setting, liquefaction susceptibility, and depth to water table. The condition of a fixed geologic setting is met almost ideally. Most sites shown in the unshaded area of Figure 1 are in Pleistocene beach deposits (units Q2 and Q3 of McCartan and others, 1984) of approximately the same thickness lying on Tertiary marl that is rock-like with respect to transmission of seismic energy; such sites provide a narrow range of geologic settings. Thus, bedrock shaking, which has been amplified to produce liquefaction in the near-surface sediments, has almost certainly been amplified comparably at many places throughout the coastal region.

The condition of a uniform liquefaction susceptibility is also almost certainly satisfied at the widely scattered sites on Figure 1. Source-stratum sands typically are loose (based on limited Standard Penetration data and numerous observations of ease of augering) and have about the same thickness. Moreover, the thickness and properties of non-liquefiable sediments overlying the source stratum lie within a narrow range. It is also a certainty that reoccurrences of liquefaction does not greatly diminish the ability to produce numerous large craters in the loose sands that are typical of the Carolina coastal region. (This is verified by the observation that, at site HW, there are large numbers of large craters that formed in each of at least three generations of Holocene earthquakes, with each generation widely spaced in time.) Thus, at sites in beach deposits on

Figure 1, liquefaction susceptibility is generally high and has not have been greatly reduced by a previous occurrence of liquefaction.

Depth to the water table, the other major variable, is uniformly very shallow and has been shallow throughout the Holocene as evidenced by the depth of the Bh horizon (see Fig. 3). The maximum depth of the seasonal water table is marked very nearly by the base of the Bh horizon, which is the zone of accumulation of organic matter and forms above the limit of vertical infiltration of water. Throughout the coastal region, the base of the Bh (generally 0.6 to 1 m below land surface) is nearly coincident with the present-day water table. Radiocarbon ages from the basal Bh horizon are 5 to 10 thousand years at site HW (Weems and others, 1986, p. 7). Because these ages are mean residence times of organic matter in a dynamic system with continuing vertical infiltration of younger organic matter, some of the organic matter has been there even longer. Furthermore, below the base of the Bh horizon, these soils lack measureable (> 0.1 percent) organic carbon and any evidence of prior oxidization or illuviation that indicates vadose conditions have extended below the present base of the Bh horizon during the Holocene. In summary, it can be concluded that the water table has been very shallow throughout the Holocene over wide areas of the Carolina Coastal Plain.

Shaking Intensity

Figure 4 shows the relative number of pre-1886 craters and the ranges of crater diameters for selected areas along the coast. Four clases of crater diameters are shown: small, medium, large, and huge. These diameters are the maximum widths exposed in the ditch walls. The relative number is the measure of the number of craters per unit area found in the setting most susceptible to earthquake-induced liquefaction. The relative numbers constitute a semi-quantitative index of crater density based on our exploration of numerous drainage-ditch networks throughout the region. A relative number of 1000 has been arbitrarily assigned to the area encompassed by the 1886 meizoseismal zone. Based on this, a value of about 10 is appropriate for the area north of the Santee River; this is equivalent to stating that there are approximately one percent as many craters north of the Santee River as in the 1886 meizoseismal zone.

Both the relative number and crater diameter are greatest within the 1886 meizoseismal zone. Both decrease with distance from the 1886 meizoseismal zone, although the shape of their associative curves remains about the same. The relationships are consistent with the conclusion that the distribution represents a variation in exposure to strong earthquake shaking. Based on this line of reasoning, we conclude that pre-1886 Holocene shaking has been strongest in the approximate area of the 1886 meizoseismal zone. North of the Santee River, shaking has been much weaker. Intermediate shaking has taken place between Charleston and the Santee River, and also between Beaufort and the Savannah River.

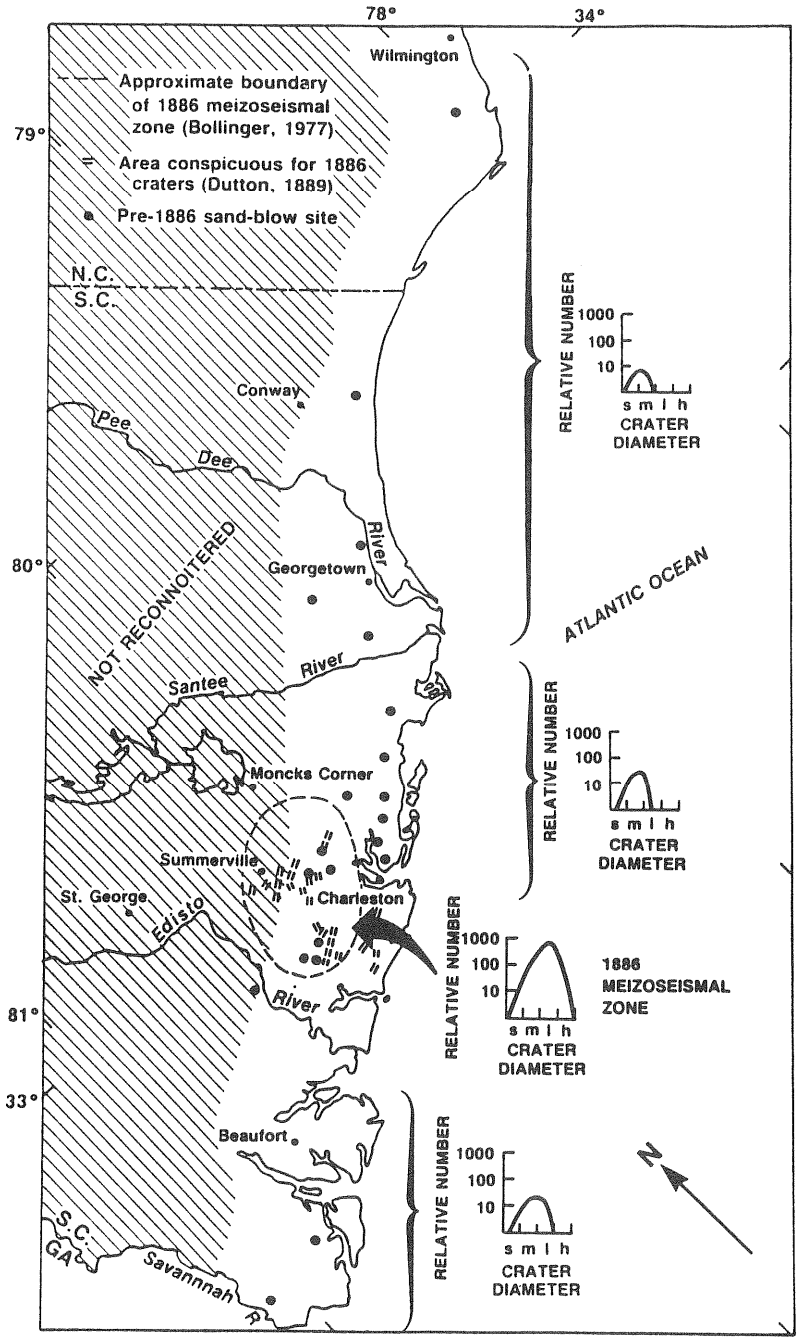

Figure 4. Relative number of filled craters and crater diameters for pre-1886 sand blows at sites on marine-related sediments. The relative number is a scaling based on comparison with abundance of craters in the 1886 meizoseismal zone, which has an arbitrary value of 1000. Crater diameters are small (s, less than 1 m), medium (m, 1-2 m), large (l, 2-3 m), and huge (h, greater than 3 m). Some sites in 1886 meizoseismal zone are not shown in Figure 1; all other sites on this figure are also shown on Figure 1.

Confidence in this interpretation is moderate to high for the area between Charleston and Wilmington, because of the hundreds of kilometers of ditches we searched. Our confidence is high for the 1886 meizoseismal zone, and moderate to high for the area between Beaufort and the Savannah River. Our confidence is not nearly as high for the area between the Beaufort and the Edisto River, and in the area southeast of the 1886 meizoseismal zone; this lower confidence is caused by the limited number of ditches and pits available for inspection.

Whether or not the pre-1886 Holocene shaking in the 1886 meizoseismal zone is associable with earthquakes stronger than the 1886 event can be resolved only by further radiocarbon ages for craters at sites far beyond the 1886 meizoseismal zone.

CONCLUSIONS

1. At least three prehistoric liquefaction-inducing earthquakes have taken place within the past 7200 years, near Charleston. Different ages of craters have been obtained far from Charleston, suggesting more epicenters exist far from Charleston.
2. Preliminary data indicate that Holocene earthquake shaking has been stronger near Charleston than elsewhere along the coast of South Carolina and the coast of southeastern North Carolina.

ACKNOWLEDGEMENTS

This study was acomplished only with the generous assistance of many people and many organizations. The field-intensive nature of the study required permission to work at sites scattered throughout South Carolina. Numerous people who assisted are not listed below. We especially thank Messrs. Don McConaughy and Jack Lacy, Westvaco Corporation; Mr. James Ralston, International Paper Company; Messrs. J. G. McGavin II, and M. B. Walden, Union Camp Corporation. We also thank Prof. Joyce Bagwell and Baptist College of Charleston for generously permitting us to use their facilities.

The research was supported by the U.S. Nuclear Regulatory Commission under Agreement Number RES-82-001.

REFERENCES

Bollinger, G.A., 1977, Reinterpretation of the intensity data for the 1886 Charleston, South Carolina, earthquake, in Rankin, D.W., ed., Studies related to the Charleston, South Carolina, earthquake of 1886-A preliminary report: U.S. Geological Survey Professional Paper 1028, p. 17-32.

Dewey, J.W., 1985, A review of recent research on the seismotectonics of the Southeastern seaboard and an evaluation of hypotheses on the source of the 1886 Charleston, South Carolina, earthquake: U.S. Nuclear Regulatory Commission, Washington, D.C., NUREG/CR-4339, 44 p.

Dutton, C.E., 1889, The Charleston earthquake of August 31, 1886: U.S. Geological Survey Ninth Annual Report 1887-88, p. 203-528.

Gohn, G.S., Weems, R.E., Obermeier, S.F., and Gelinas, R.L., 1984, Field studies of earthquake-induced liquefaction-flowage features in the Charleston, South Carolina area: preliminary report: U.S. Geological Survey Open-File Report 84-670, 26 p.

Hayes and Gori, eds., 1983, Proceedings of Conference XX, A workshop on "The 1886 Charleston, South Carolina, earthquake and its implications for today": U.S. Geological Survey Open-File Report 83-843, 502 p.

McCartan, L., Lemon, E.M., Jr., and Weems, R.E., 1984, Geologic map of the area between Charleston and Orangeburg, South Carolina: U.S. Geological Survey Miscellaneous Investigations Map I-1472, scale 1:250,000.

Nuttli, O.W., 1983, 1886 Charleston, South Carolina, earthquake revisited, in Hays, W.W., and Gori, P.L., Proceedings of Conference XX, A workshop on "The 1886 Charleston, South Carolina, earthquake and its implications for today": U.S. Geological Survey Open-File Report 83-843, p. 44-50.

Obermeier, S.F., Gohn, G.S., Weems, R.E., Gelinas, R.L., and Rubin, M., 1985, Geologic evidence for recurrent moderate to large earthquakes near Charleston, South Carolina: Science, v. 227, p. 408-411.

Obermeier, S.F., Jacobson, R.B., Powars, D.S., Weems, R.E., Hallbick, D.C., Gohn, G.S., and Markewich, H.W., 1986, Holocene and late Pleistocene(?) earthquake-induced sandblows in coastal South Carolina: Proceedings of the third U.S. National conference on earthquake engineering, Earthquake Engineering Research Institute, v. 1, p. 197-208.

Peters, K.E., and Herrmann, R.B., compilers and eds., 1986, First-hand observations of the Charleston earthquake of August 31, 1886, and other earthquake materials: South Carolina Geological Survey, Bulletin 41, 116 p.

Science News, 1986, A century after the Charleston earthquake: v. 129, no. 17, April 26, 1986, p. 263.

Szabo, B.J., 1985, Uranium-series dating of fossil corals from marine sediments of southeastern United States Coastal Plain: Geological Society of America Bulletin, v. 96, p. 398-406.

Weems, R.E., Obermeier, S. F., Pavich, M.J., Gohn, G.S., Rubin, M., Phipps, R.L., and Jacobson, R.B., 1986, Evidence for three moderate to large prehistoric Holocene earthquakes near Charleston, South Carolina: Proceedings of the third U.S. National conference on earthquake engineering, Earthquake Engineering Research Institute, v. 1, p. 197-208.

OBSERVATIONS OF SOIL LIQUEFACTION IN THE NEW MADRID SEISMIC ZONE

Steven G. Wesnousky, Eugene S. Schweig, & Silvio K. Pezzopane
Center for Earthquake Research and Information
Memphis State University
Memphis, Tennessee 38152

ABSTRACT

The great 1811-12 New Madrid earthquakes produced extensive liquefaction which is still very much in evidence today. Visible as a myriad of light-colored and irregular shapes against the dark brown soils of the Mississippi embayment, sands liquefied and extruded during the 1811-12 earthquakes are readily recognized both in the field and on aerial photographs. The extent of surficial liquefaction deposits produced by the 1811-12 earthquakes has been well established via both field studies and air photo analyses. Liquefaction deposits are most concentrated in a zone approximately 20-50 km wide that strikes southwestward about 150 km along the western edge of the Mississippi River from near New Madrid, Missouri to Marked Tree, Arkansas. Extruded sands account for more than 25% of the surface deposits in much of this area, and excavations show the sand deposits reaching to more than a meter in thickness. It is certain that the occurrence today of similar sized earthquakes in the New Madrid region would produce equally destructive liquefaction. However, few data exist to bear upon how often events similar to 1811-12 recur, or whether such earthquakes can be expected elsewhere in the Central United States. Statistical analysis of historical seismicity cannot confidently address these questions due to the relative brevity of recorded history. But clues to the past occurrence of large earthquakes may be recorded in the geology, and application of paleoseismologic techniques may be the key to determining the expected location and occurrence rate of large earthquakes in the area. Ongoing flood control efforts by the Army Corps of Engineers have resulted in an extensive system of major drainage ditches throughout the New Madrid Seismic Zone. The most recently excavated drainages provide an opportunity to look for liquefaction features that possibly predate the 1811-12 sequence and to examine the mechanics of liquefaction in the vertical dimension. Several drainages have thus far been examined. Exposed stratigraphy is generally composed of fine to medium grained alluvial sands alternating with clay beds. Exposures are limited to a depth of about 3 meters by the water table, and the source of liquefied sands is below this level in each case. Exposures examined show that impermeable clay layers play a controlling role in the liquefaction process by limiting the vertical flow of sands, as evidenced by sills of sand extending more than 5 meters from the central pipe beneath impermeable clay layers. Cross-cutting relationships indicate at least several phases of sand injection, but evidence of liquefaction prior to the 1811-12 earthquakes has not been observed. This preliminary work shows that the preexisting and growing network of drainages

provide perhaps the most viable opportunity to examine the mechanics of liquefaction and to search for paleoseismic evidence of large pre-1811 earthquakes within the Mississippi embayment.

INTRODUCTION

The great 1811-12 New Madrid earthquakes produced extensive liquefaction which is still very much in evidence today. Visible as a myriad of light-colored and often irregular shapes against the dark brown soils of the Mississippi embayment, sands liquefied and extruded during the 1811-12 earthquakes are still readily recognized both in the field and on aerial photographs. No systematic study of the geological effects of the earthquake were undertaken immediately after the earthquakes. Consequently, understanding of the extent, magnitude, and style of liquefaction produced by the earthquakes results from compilations of graphic accounts of contemporaries whom witnessed the events and later studies of evidence registered in the geologic record. Our intent here is not to duplicate those efforts. Rather, we will limit ourselves to a brief synopsis of work bearing on liquefaction which took place during 1811-12 as a basis for discussing the potential that still exists to further the understanding of liquefaction processes and seismic hazard in the Mississippi embayment through further study of the geologic record.

THE NEW MADRID SEISMIC ZONE

Seismological Characteristics

The New Madrid Seismic Zone strikes about 175 km in a northeasterly direction through the Mississippi embayment, from near Memphis, Tennessee in the south to Cairo, Illinois in the north (Figure 1.) The seismic zone is not expressed on the ground surface by an active and mappable fault zone, though subtle evidence of tectonic warping and faulting of recent sediments have been reported in a limited region which overlies the seismic zone (e.g. Usher, [1837]; McGee, [1892]; Russ, [1979], [1982]; Stearns, [1979]). Nonetheless, reviews of isoseismal data and secondary ground deformations resulting from the New Madrid earthquakes lend strong support to assertions that the New Madrid Seismic Zone was indeed the source of the displacements which produced the 1811-12 New Madrid earthquakes (Nuttli, [1973]). Isoseismals show that the 1811-12 sequence of earthquakes were arguably the largest seismic disturbance in the contiguous United States during historical time (Figure 2). The magnitude and extent of observed ground deformations are consistent with such an argument.

Contemporary Accounts of Liquefaction Phenomena during 1811-12

Initial reports of ground deformations and damage during the earthquakes are primarily the result of eyewitness accounts of local inhabitants. Several compilations of such material have been published since 1811-12 (e.g. Mitchell, [1815]; Fuller, [1912]; Penick, [1981]). Though personal accounts of the earthquakes are often and understandably biased toward

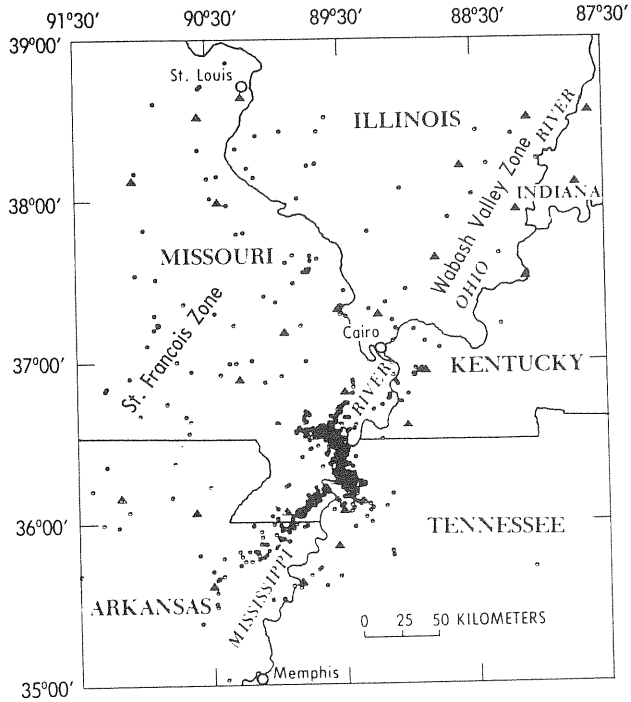

Figure 1. The location of the New Madrid Seismic Zone is clearly delineated by this plot of earthquake epicenters and extends from south of Cairo, Illinois to northwest of Memphis, Tennessee [Figure taken directly from Stauder, 1982].

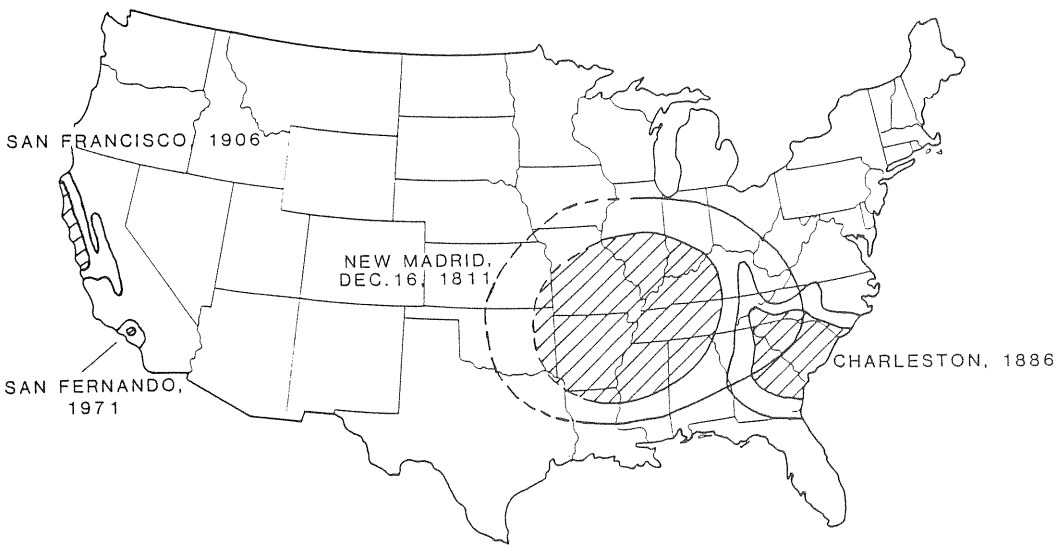

Figure 2. Isoseismals of Modified Mercalli VI and VII for four major United States earthquakes. Regions sustaining MM VII shaking or greater are hachured [adapted from Rankin, 1977].

the sensational, compilations of those accounts leave no doubt regarding the extensive nature of liquefaction during 1811-12. Perusal of the accounts provides evidence of major liquefaction phenomena, including extensive ground fissuring, the ejection of sand, water, and other debris through fissure systems, the settling of extensive tracts of land below the water-table, and numerous landslides along the bluffs that border the Mississippi river. Evidence of the style, magnitude, and extent of liquefaction that took place in 1811-12 is also provided by geologic studies subsequent to the earthquakes.

Geologic Accounts of Liquefaction Phenomena

Sir Charles Lyell was among the first geologists to visit and provide a graphic description of liquefaction phenomena as recorded in the geologic record (Lyell, [1849]; Fuller, [1912]). Lyell recorded the still relatively fresh evidence of fissuring, sand blows, landslides, and 'sunken' lands. A number of other descriptions of geologic deformations that occurred during the 1811-12 earthquake were reported during the century after the earthquake. Among them, Usher, [1837] and McGee, [1892] cited evidence for doming and uplift of young alluvial sediments in the New Madrid region. The first work to systematically document the style, extent, and magnitude of deformations resulting from the New Madrid earthquakes is Fuller's [1912] synthesis of prior accounts of the earthquakes and report of his own geological traverses across the region nearly 100 years after the event. Fuller's work shows liquefaction during 1811-12 was pervasive within a zone ranging from 20 to 50 km wide extending northeasterly for a distance of about 150 km from near Memphis, Tennessee in the south to New Madrid, Missouri in the north (Figure 3). Fuller concluded that fissuring of the ground surface was the most common and widespread form of liquefaction phenomena within this zone. He cited contemporary accounts indicating fissures reaching to 5 mile in length and 600-700 feet in width. His study of landforms showed that the fissures commonly produced the down-faulting of narrow blocks to 5 or 6 feet or more, and were generally limited to the portion of the zone south of New Madrid, within the broad flat alluvial bottoms of the Mississippi and St. Francis drainage basins. The creation of fissures was often accompanied by the ejection of water, sand, mud, and gas. Ejecta commonly was produced through sandblows, leaving distinct patches of sand reaching diameters of 100 feet or more for circular varieties, or lengths of 200 feet and breadths of 25-50 feet for the linear varieties. In other cases, the amount of ejecta was sufficient to cover tracts of land many miles in extent by sand and water 3 to 4 feet in thickness and depth, respectively. Local settling or warping of alluvial deposits due to ground shaking also resulted in flooding of tracts of land miles in extent and, in turn, the widespread destruction of forest lands. Fuller [1912] also corroborated eyewitness accounts of extensive landslide failures by observing the scars of landslides still well preserved and concentrated along the set of bluffs that border the eastern edge of the Mississippi River between New Madrid, Missouri and Cairo, Illinois. Contemporary and geologic accounts thus show that essentially every type of liquefaction failure that has been observed during recent

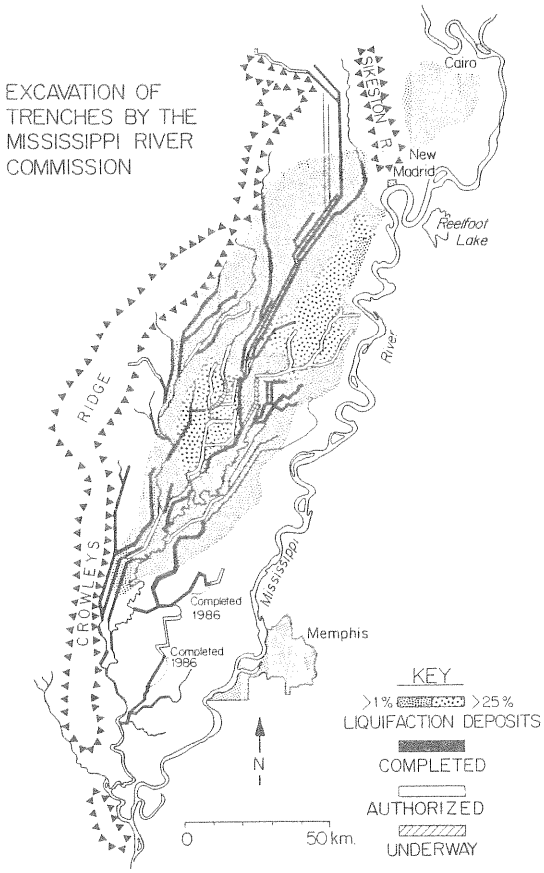

Figure 3. Aerial photography and field studies (Fuller, 1912; Heyl and McKeown, 1978; Obermeier, 1984) show liquefaction phenomena were pervasive during 1811-12 in the region extending from near Cairo, Illinois to northwest of Memphis, Tennessee. Areas where liquefaction deposits still comprise $\geq$ 1% and $\geq$ 25% of the ground cover are shaded and stippled, respectively. The region of liquefaction south of New Madrid encompasses the St. Francis drainage basin which empties into the Mississippi River south of Memphis. It is this region which Fuller (1912) referred to as the 'St. Francis Sunk Lands'. For purposes of flood control and land reclamation, the U.S. Army Corps of Engineers have excavated an extensive network of drainage channels. The channels which range from completed (black) to underway (hachured), and authorized (open) for excavation in the near future, total 100's of kilometers in length, are generally several or more meters in depth, and are 10's of meters wide. Excavation of these channels provides kilometers of new exposure each year which is ideal for examining the geologic record of liquefaction within the St. Francis Sunk Lands.

earthquakes was pervasive over a region measured in 1000's of square kilometers during 1811-12. Indeed, liquefaction phenomena reported for other large earthquakes within the contiguous United States during historical time appear pale in comparison to that registered during the New Madrid earthquakes.

During the last decade, investigators have used aerial photography to reexamine the extent of liquefaction during the 1811-12 earthquakes. Jibson and Keefer [1984] examined landslide deposits along the bluffs that run along the eastern edge of the Mississippi River between about New Madrid, Missouri and Memphis, Tennessee. They concluded that the majority of landslides in evidence were produced by shaking during 1811-12, and that the entire extent of bluffs remains extremely susceptible to landsliding during earthquakes. Heyl and Mckeown's [1978] and Obermeier's [1984] recent use of aerial photography generally confirmed Fuller's conclusions regarding the extent of liquefaction in 1811-12 (Figure 3). Of considerable interest, the above zone of concentrated liquefaction deposits overlies the zone of microearthquakes which define the New Madrid Seismic Zone (Figures 1 and 3).

Potential for Further Study

It is thus evident from reports of the 1811-12 earthquakes that deposits of the Mississippi embayment are extremely prone to liquefaction. The New Madrid region is a vastly different place than it was in 1811-12. Characterized by a population measured in the thousands in 1811-12, the number of people living within the zone characterized by strong ground motions in 1811-12 now measures in the millions. In that regard, we may be certain that the recurrence of earthquakes similar to those in 1811-12 would produce equally extensive liquefaction and, in turn, immense losses to property and life. However, there are few data which bear upon how often events similar to 1811-12 occur, or whether such earthquakes can be expected to occur elsewhere in the Central United States as well. For example, Nava and Johnston [1985] recently estimated the average repeat time of New Madrid-type earthquakes to equal about 600 years, but their estimate was based on the extrapolation of instrumentally recorded data reaching back only 10 years and historical records for the period after 1811. A similar value of repeat time for large earthquakes in the region was also put forth by Russ [1982], based primarily on geomorphic study of displaced and deformed near-surface sediments exposed along Reelfoot Fault. That estimate, however, was limited because it could not be certain whether or not the discrete displacements registered in the trench were due to earthquakes equivalent in size and origin to the New Madrid earthquakes. The widespread liquefaction phenomena recorded so well in the stratigraphy of the Mississippi embayment represent an excellent opportunity to further address the question of seismic potential in the Mississippi embayment.

Recent studies in Charleston, South Carolina have shown the potential value that geological study of liquefaction effects may play in under-

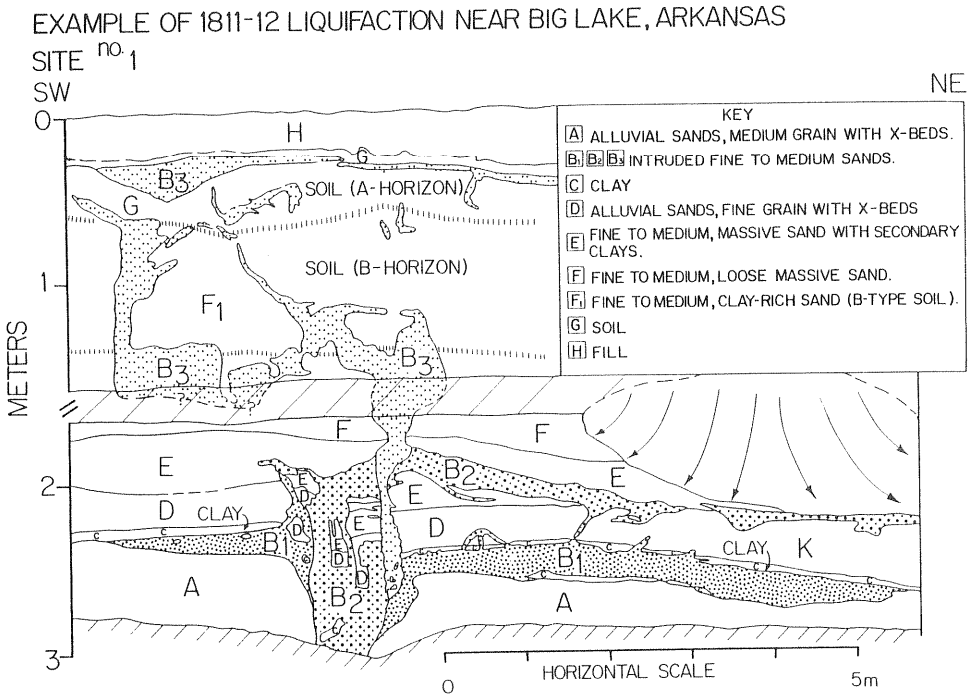

Figure 4. Trench log demonstrates excellent exposure of liquefaction phenomena afforded by channels recently excavated by the Army Corps of Engineers. Three episodes of sand injection are evident at this site. (stippled units B_1, B_2, and B_3). Note that the competent clay (unit C) and clay-rich (unit E) layers inhibited the upward propagation of liquefied sand, as evidenced by the intruded sills of liquefied sand that underly the respective units.

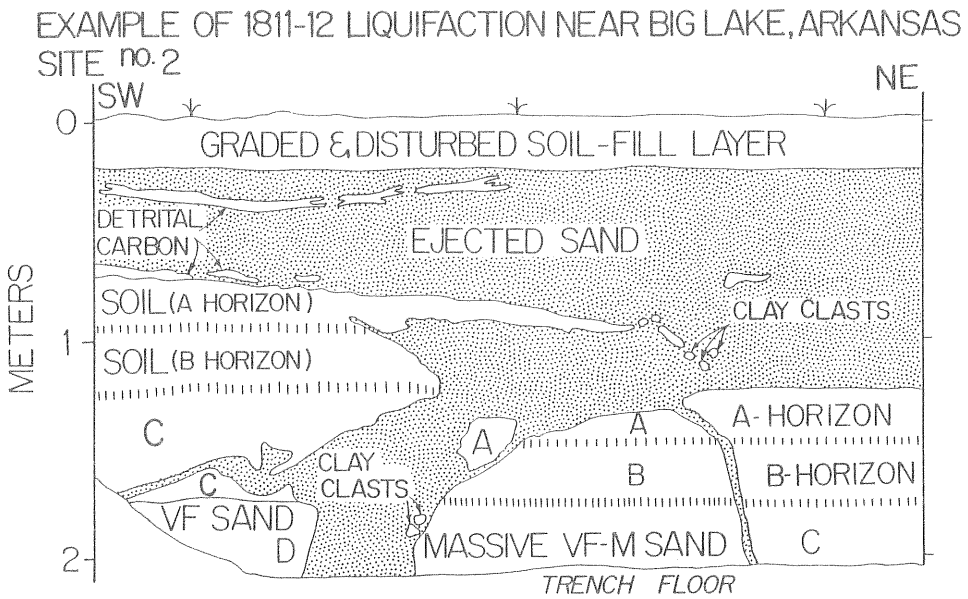

Figure 5. A second example of liquefaction exposed near Big Lake, Arkansas shows the extrusion of sand through soil horizons, resulting in an overlying deposit of sand up to 1m thick.

standing the prehistoric record of large earthquakes in a region (Obermeier et al., [1985]; Talwani and Cox, [1985]. As yet, a systematic examination of liquefaction phenomena with the purpose of identifying deformation due to prehistoric earthquakes within the Mississippi embayment has not been implemented. Ongoing flood control efforts by the U.S. Army Corps of Engineers has resulted in an extensive system of major drainage channels throughout the New Madrid Seismic Zone (Figure 3). The most recently excavated channels provide an excellent opportunity to search for liquefaction features that possibly predate the 1811-12 sequence and to examine the mechanics of liquefaction in cross-section as well. Thus far, we have examined several sites along these channels on a reconnaissance basis. Though evidence of earthquakes prior to 1811-12 has not been observed, the resulting logs of exposed sediments show the excellent exposure of liquefaction phenomena afforded by the Corp's channels.

Logs of 2 exposures examined near Big Lake, Arkansas are shown in Figures 4 and 5. At site no. 1 (Figure 4) the exposed stratigraphy consists of thick soil horizons underlain by fine to medium grained alluvial sands alternating with clay beds. The logs clearly shows that impermeable clay layers play a controlling role in the liquefaction process by limiting the vertical flow of sands, as evidenced by sills of sand (stippled) that extend from the central pipe to a distance of 5 or meters horizontally beneath impermeable clay layers. Cross-cutting relationships further indicate several phases of sand injection (Figure 4). In this case, the liquefied sand was primarily limited to injection into dikes and sills in the subsurface. Site no. 2 (Figure 5) shows the cross-section of a sand blow or fissure that shows apparent extension of about 50 cm and from which extruded sands reached to about a 1 meter thickness. The exposures are limited to between 2-3 meters depth by the water table at both site no 1 and 2, and the source of liquefied sands is below this level in each case. Though evidence of any liquefaction prior to the 1811-12 earthquakes has not been observed in this brief reconnaissance, our work shows that the preexisting and growing network of drainage channels provide perhaps the most viable and economical opportunity to systematically examine the mechanics of liquefaction and to search for evidence of large earthquakes prior to 1811-12 within the Mississippi embayment. This resource currently remains untapped.

REFERENCES CITED

Fuller, M.L., 1912, The New Madrid Earthquake, *U.S. Geological Survey Bulletin* **494**, 118 p.

Heyl, A., and McKeown, F., 1978, Preliminary seismotectonic map of central Mississippi valley and environs, U.S. Geological Survey Miscellaneous Field Studies Map MF-1011.

Jibson, R. and Keefer, D., 1984 Earthquake-induced landslide potential for the central Mississippi Valley, Tennessee and Kentucky, *U.S. Geological Survey Open-file Report* **84-770**, p. 353-390.

Lyell, Charles, 1849, A second visit to the United States, v. **2**: New York, Harper and Brothers, 287 p.

McGee, W.J., 1892, A fossil earthquake [abs.]: *Geological Society of America Bulletin*, v. **4**, p. 411-415.

Mitchell, S.L., 1815, A detailed narrative of the earthquakes which occurred on the 16th day of December, 1811: Trans. Lit. and Philos. Soc. New York, v. **1**, p. 281-307.

Nuttli, O.W., 1973, The Mississippi Valley earthquakes of 1811 and 1812 intensities, ground motion and magnitudes: *Seismological Society of America Bulletin*, v.**63**, no. 1, p. 227-248.

Obermeier, S., 1984, Liquefaction potential for the central Mississippi Valley, *U.S. Geological Survey Open-file Report* 84-770, p. 391-446.

Obermeier, S., Gohn, G., Weems, R., Gelinas, R., and Rubin, M., 1985, Geologic evidence for recurrent moderate to large earthquakes near Charleston, South Carolina, *Science*, v. **227**, p. 408-411.

Penick, J., 1981, The New Madrid earthquakes of 1811-12: Columbia, Mo., The University of Missouri Press, 181 p.

Rankin, D.W., 1977, Studies related to the Charleston, South Carolina, earthquake of 1886 - introduction and discussion, *U.S. Geological Survey Professional Paper*, **1028**, p. 1-16.

Russ, D.P., 1979, Late Holocene faulting and earthquake recurrence in the Reelfoot Lake area, northwestern Tennessee, *Geological Society of America Bulletin*, **90**, p. 1013-1018.

Russ, D.P., 1982, Style and significance of surface deformation in the vicinity of New Madrid, Missouri, *U. S. Geological Survey Professional Paper* **1236-H**,p. 94-114.

Stauder, W., 1982, Present-day seismicity and identification of active faults in the New Madrid seismic zone, *U.S. Geological Survey Professional Paper* **1236**, p.20-30.

Stearns, R.G., 1979, Recent vertical movement of the land surface in the Lake County uplift and Reelfoot Lake basin areas, Tennessee, Missouri, and Kentucky: *U.S. Nuclear Regulatory Commission NUREG/CR - 0874*, 37 p.

Talwani, P., and Cox, J., 1985, Paleoseismic evidence for recurrence of earthquakes near Charleston, South Carolina, *Science*, v. **229**, p. 379-381.

Usher, F.C., 1837, On the elevation of the banks of the Mississippi in 1811: *Silliman's Journal (American Journal of Science, First Series)*, v. **31**, p. 291-294.

APPENDIX A
EDITOR'S NOTES

These *Proceedings* contain short papers of nearly 40 invited oral presentations made at the Symposium *Earthquake Hazards, Ground Motions, Soil Liquefaction and Engineering Practice in Eastern North America* that was held by NCEER at the Sterling Forest Conference Center, Tuxedo, N.Y., during October 20-22, 1987.

The sequence of papers in the *Proceedings* differs only in minor aspects from the sequence of presentations given at the Symposium. Respective editorial comments are:

Session 1 and 2 in the Symposium are sequentially reversed from Topic 1 and 2 in the *Proceedings*. This was for merely logistic reasons. It was the convenor's intent to start the meeting with the theme *Seismic Hazards Assessment vs. Engineering Paractice* to emphasisze the connectedness and juxtaposition of engineering and earth-science issues in this Symposium. The printed *Proceedings* restore this emphasis.

Three of the invited speakers could not attend the Symposium; however, G. Atkinson forwarded a written version which is included here with the topic for Session 3. A. Cornell's intended contribution to Session 5 was unavailable since he had to cancel attendance at the Symposium on a very short notice.

Referring to the individual topics or sessions we note:

(1) Topic 1 (Session 2) covers the theme *Seismic Hazards Assessment vs. Engineering Practice*. Two papers from Session 2 were unavailable (C.Stepp and I.Idriss). Where available, we have used the abstract.

(2) All papers for the Topic 2 (Session 1), *Tectonics and Seismicity of Eastern North America,* are reproduced in the *Proceedings*..

(3) All papers given at Session 3, *Seismic Sources, Attenuation, and Ground-Motion Estimates* are included. G. Atkinson's paper not given at the symposium session is added.

(4) All papers given at Session 4, *Geological Site Effects and Soil Liquefaction,* are included.

(5) Written submissions were not requested from the panel members of the Panel Discussion of Session 5: *The Eastern Dilemma: Moderate Seismic Hazard vs. High Catastrophic Potential*. The panel discussion was intentionally not taped or transcribed, and no formal notes were taken. The reader of the introductory program notes for this session (see Appendix B) can easily infer why this omission was intentional: to facilitate a frank and open discussion of the loaded issue of rare but potentially catastrophic events in the eastern parts of North America. The discussion was not strictly limited to this issue, but certainly centered on it. The panel members and participating Symposium attendees needed to have the assurance that little they had to say, and wanted to say, had to remain unsaid just because speakers would

later be held to their assessments when these would appear in print. Some of the information provided was of delicate nature, some of it was expressed with strong hesitations because of the large uncertainties involved; others expressed strong personal biases that few wanted to see printed. As regrettable as this loss of documentation for posteriority may appear for those who could not attend the Symposium, and as unfortunate as it may be in general to have no record at all of this remarkable session, it was a calculated risk. Most of what was said was well suited for print. However, few panelists volunteered written notes for inclusion into the *Proceedings*. I thank D.G. Friedman and T. Statton for their efforts.

The editor/convenor considered summarizing the essence of this panel discussion, but found it virtually impossible to convey the messages without the risk of doing injustice to the panelists' contributions. In the future, I hope that times and public attitudes will change sufficiently to allow for discussion of delicate or risky topics publicly and for the transcription of them for preservation. Such documentation will be needed for educating the public and knowledge transfer.

The questions posed to the panel of Session 5 were: (1) can large earthquakes occur in regions of eastern North America where we have no knowledge of their occurrence in the past? (2) Can presently existing or discussed model codes and associated engineering principles effectively mitigate against the very rare, largest possible eastern North American earthquakes ? The answers that emerged were: (1) we cannot exclude the possibility of large earthquakes in regions with previously unreported occurrences, but their occurrence is not very likely. (2) Proposed and existing codes probably cannot mitigate very effectively against the largest events. However even inadequate codes would tend to help greatly to reduce the worst damage if they only were in effect long enough before a major catastrophic event. A long lead time is necessary for codes, even when increasingly rigorously enforced, to protect significant numbers of structures.

The most frequently expressed fear was that no codes at all may be adopted or become effective, if highly conservative codes would be proposed that attempted to protect against the unlikely largest events. Large events are earthquakes with magnitudes of $M \geq 7$ that may recur at some location only every 1,000 to 10,000 years. Codes may instead aim to protect against the more likely 50- or 100- year events with magnitudes M=4 to 6, depending on locality. It was surmised that very conservative codes would be perceived by the public as economically prohibitive, whether that perception is correct or not. This perception may change after a catastrophic event, which then may provide the occasion to introduce an updated more conservative code, as has been the case in almost all earthquake-prone countries or states after catastrophic events that exceeded seismic loads defined in previous, less conservative guidelines. It was perceived mostly by U.S. members and less strongly by the Canadian experts, that in the eastern parts of North America the public is reluctant to accept the costs of even moderate preventive measures. This attitude may persist until it is reversed by a potentially costly experience, for instance one that would be generated by a modern occurrence or recurrence of the 1886 Charleston, S.C., or a 1811/12 New Madrid, MO., type earthquake sequence. Urban regions in eastern North America could be affected by such an event where historically none has occurred, but may have occurred in prehistoric Holocene times, although this fact or possibility may not be sufficiently recognized.

It was felt that at present a useful strategy would be to get reasonable minimum seismic codes adopted by local and regional authorities, especially of urban entities close to suspected or proven seismogenic features. Such codes introduce communities to the concept of preparedness for the seismic hazards associated with the more frequent events, such as those that have occurred in the region in historic times, but may not be remembered by the modern society. This concept applies for instance for the more active regions of the eastern U.S (clearly for the central U.S around the New Madrid seismic zone, but also perhaps for Boston and New York City). It is necessary to adopt codes that protect against magnitude 5 to 6 events, or say those that are likely to be experienced with a probability of at least 10% in 50 years (corresponding to an event recurring with near-certainty about every 500 years).

Other scientific, technical and societal issues emerged from the often lively and frank discussions during times set aside after the formal presentations of each session. In fact this Symposium was characterized by sustained exchanges of information and opinions, especially between seismologists, engineers, geotechnical experts, and risk-, damage- and insurance experts that perhaps can only be fully appreciated by those who participated. We have no assurance, but expect, that the results and fruits from these discussions will soon emerge in pending research work, building codes, insurance policies, and -foremost- in good engineering judgement applied to future structures and rehabilitation of existing ones. It is impossible to convey here the multitude of constructive ideas that were exchanged, both publicly and on the side lines of this highly stimulating Symposium. The short written *Proceedings* contributions are but a faint shadow of the lively discussions, but hopefully still convey some of the urgency of the issues.

I express my sincere thanks to the participants for their contributions; to the administrative staff at Lamont-Doherty Geological Observatory, especially Linda Murphy, who prepared most of the meeting details, logistics, and preparation of the programs, abstracts and *Proceedings*; to the staff of the Sterling Forest Conference Center for providing hospitable facilities; to the NCEER staff at SUNY/Buffalo, especially Jane Stoyle, for accomplishing production of the *Proceedings* in a remarkably short time; and to the main sponsors of NCEER (the National Science Foundation and the Research Foundation of the State University of New York) for providing the support that enabled this Symposium to be convened.

Klaus H. Jacob
Palisades, N.Y., December 1987.

APPENDIX B

PROGRAM FOR THE NCEER SYMPOSIUM:

SEISMIC HAZARDS, GROUND MOTIONS, SOIL-LIQUEFACTION AND ENGINEERING PRACTICE IN EASTERN NORTH AMERICA.

OCTOBER 20 - 22, 1987
STERLING FOREST CONFERENCE CENTER, TUXEDO, NEW YORK

Day 1, Tuesday - Oct. 20, AM

8:15 AM: Welcome by K. Jacob

8:30 AM: Technical Session 1: Tectonics and Seismicity of Eastern North America*

1. M. ZOBACK: In situ stress, crustal strain and seismicity in eastern North America
2. K. EVANS: Crustal stresses and seismic potential in the northern Appalachian basin: The application of stress maps to hazard assessment
3. J. ADAMS: Seismicity, crustal stresses and seismotectonics in eastern Canada
4. L. SEEBER: Seismicity and tectonics of the eastern U.S.
5. J. ARMBRUSTER: Seismicity and seismic zonation along the Appalachians and the Atlantic Seaboard based on intensity data
6. J. EBEL: The seismicity of the northeastern U.S.
7. A. JOHNSTON: Seismotectonics of the central U.S.
8. G. BOLLINGER: Seismotectonics of the Virginia seismic zones
9. K. COPPERSMITH: Estimating maximum earthquakes in the central and eastern United States
10. D.VENEZIANO: Probabilistic assessment of seismicity using earthquake catalogs

10:25-12:15 AM: Extended Discussion of all Topics of Technical Session 1
Moderators: C. Stepp and K. Jacob

*Note that this represents Topic 2 in the *Proceedings*.

Day 1, Tuesday - Oct. 20, PM

1:30 PM: Technical Session 2: Seismic Hazards Assessment vs. Engineering Practice**

1. P. BASHAM: Seismic hazards assessment and seismic codes for eastern Canada
2. D. PERKINS: Seismic hazards maps for the U.S.: Present use and research objectives
3. C. STEPP: On probabilistic seismic hazard methodology for critical industrial facilities in the eastern United States
4. J. P. SINGH: Current trends in seismic zonation
5. I.M. IDRISS: Site response: Research issues vs. engineering practice
6. G. NORDENSON: Are current seismic codes realistic for earthquake resistant design in the eastern U.S.?
7. M. SHINOZUKA: Earthquake vs. wind risks to buildings and structures in the eastern U.S.
8. C. SCAWTHORN: Approximation of earthquake losses for a major earthquake near a large eastern U.S. urban center
9. R. WHITMAN: Thoughts re seismic building code: Reqirements for ENAM

3:20 - 5:00 PM: Extended Discussion of all Topics of Technical Session 2
Moderators: P.Basham and P. Gergely

7:30 - ? PM: Open Evening Discussion

** Note that this represents Topic 1 in the *Proceedings*.

Day 2, Wednesday - Oct. 21, AM

8:30 AM: Technical Session 3: Seismic Sources, Attenuation, and Ground-Motion Estimates

1. D. BOORE: Quantitative ground motion estimates
2. J.G. ANDERSON: How important is attenuation for characterization of ground motions?
3. F. WU: Source and attenuation studies in northeastern North America
4. A. PAPAGEORGIOU: Comparison of predictions of ground motion and special response parameters at hard rock sites in eastern North America with recorded data from intraplate earthquakes around the world
5. J. NABELEK: Source properties of the Goodnow N.Y. earthquake
6. D. WEICHERT: The Nahanni earthquakes
7. P. SOMERVILLE: Earthquake source and ground motion characteristics in eastern North America
8. J. BARKER: Modeling Ground-Motion Attenuation in eastern North America
9. R. HERRMANN: Strong motion studies in the central U.S.
10. R. McGUIRE: Issues in estimating ground motion for ENA
11. G. ATKINSON†: Implications of eastern ground motion characteristics for seismic hazrd assessment in eastern North America

10:20-12:15 AM: Extended Discussion of all Topics of Technical Session 3
Moderators: K. Jacob and F. Wu

† Was unable to attend.

Day 2, Wednesday - Oct. 21, PM

1:30 PM: Technical Session 4: Geological Site Effects and Soil-Liquefaction

1. R. DOBRY: Some basic aspects of soil liquefaction during earthquakes
2. A. ROGERS: Prediction of site response based on geologic conditions
3. C. SOYDEMIR, Liquefaction criteria for New England: A design engineers overview
4. C. COSTANTINO and C. MILLER: Geotechnical soil properties in the greater NYC metropolitan region
5. M. BUDHU: The liquefaction potential of soils in portions of upper Manhattan and of Buffalo
6. M. TUTTLE: Liquefaction of glaciomarine sediments during the 1727 earthquake in Newburyport, Massachusetts
7. S. OBERMEIER: Earthquake-induced liquefaction features in the coastal South Carolina region

8 S. WESNOUSKY: Observations of soil liquefaction in the New Madrid seismic zone

3:20-5:00 PM: Discussion: The importance of site effects and the potential for soil liquefaction in ENAM
Moderators: I. Idriss and R. Whitman

7:30 - ? Open evening discussion

Day 3: Thursday - Oct. 22. AM

8:30 AM: Technical Session 5 (Discussion): The Eastern Dilemma: Moderate Seismic Hazard vs. High Catastrophic Potential

Some regions in eastern North America may be capable of rare but quite large (New Madrid, Charleston, St. Lawrence River, Grand Banks or Baffin Bay type) earthquakes that can effect large regions. Can codes and engineering measures in eastern North America effectively attempt to mitigate against losses from these rare but potentially widely damaging events, or not? Should they? Does consideration of risk for any single site (or structure), versus integrated risk and economic effects for entire (populated) regions lead to different approaches for formulating mitigation measures ? What measures other than building codes are needed?

Moderators of Panel Session: R. Ketter and C. Scawthorn
Panelists and their assigned topics:

A. Cornell†: Probabilistic Estimates
P. Basham: Canada
R. Whitman: Boston and Massachussetts
G. Nordenson: New York City (Buildings)
T. Statton New York State/New Jersey
T. O'Rourke: Life-lines general, Pipelines
W. Haid and C. Costantino: NY City Subways and Transportation Systems
L. Reiter: Nuclear Powerplants
G. Fox: Bridges
J. Hinton: Communication Systems
D. G. Friedman: Insurance Issues

1:00-1:40 PM: **Bus Ride from Sterling Forest to Lamont-Doherty Geological Observatory, Palisades N.Y**

1:40-3:00 PM: **Visit of the NCEER ground-motion instrumentation facility at L-DGO**

† Was unable to attend.

APPENDIX C

Partial Discussion Notes from Session 5:
"The Eastern Dilemma: Moderate Seismic Hazard vs. High Catastrophic Potential"

T. Statton
"Some Thoughts Regarding the State of Earthquake Mitigation in the Eastern U.S."

D. G. Friedman:
"Uses of Earthquake Information in an Insurance Operation"

Some Thoughts Regarding the State of Earthquake Mitigation in the Eastern U.S.

Thomas C. Statton
Woodward-Clyde Consultants
Wayne, New Jersey

Elements of society have become impassioned in their quest for a "risk free" existence. Seat belts, emission controls, and the search for contaminants in the parts per billion range are now commonplace. The hazards that such controls seek to regulate, even when poorly understood, are real in that their consequences are wholly manifest within the life span and memory of individuals.

In contrast, earthquake hazards in areas such as the northeastern United States can only be postulated and characterized through historical information and scientific reasoning obscure to the public. Instrumented mannequins and laboratory rats find their equivalents in controversial estimates of crustal strain, rupture mode, and maximum magnitude. The long recurrence times relative to the human life span result in a low awareness of seismic hazard. While seismic hazard may exceed that for "parts per billion" compounds, the occurrence of large earthquakes is so infrequent in the northeastern U.S. that society has forgotten that they can and will occur.

The manifestation of our "now" consciousness can be examined as it relates to the New York metropolitan area. Common wisdom in this area recognizes seismic hazard as a phenomenon endemic to California, Alaska, Mexico City, and perhaps a few other foreign locations. A small earthquake (M=4) in southeastern New York in 1985, which caused surprise and alarm to some local residents, is only dimly recollected today and is regarded as a curiosity. It most certainly was not a trigger for recognition of a significant greater hazard.

Local building codes also illustrate the lack of concern for seismic hazard. While criteria exist for the design of access, egress, lighting, and ventilation, the potential for seismic loading is unaddressed. This reflects society's perception of local seismic hazard, whether it is accurate or not.

Historical and recent seismic data offer a firmer foundation for evaluating the seismic hazard in the New York metropolitan area. For example, during 1986 about fifty small earthquakes were detected and located in this region. Most events were so small they were unnoticed by the public, and simply joined the archives of previous occurrences.

Larger earthquakes have, however, occurred in the past. An earthquake of about magnitude 5 occurred in the New York City vicinity in 1884. The possibility, and inevitability, of similar events in the future seems to have been lost on local building commissions and planners. Uncertainty exists in estimates of their frequency (every 100 yrs, 150 yrs, 200 yrs?), but earthquakes of this size represent a lower bound to the maximum magnitude to be expected in this region.

Prudence suggests that "Round 1" be declared over. Recognition of a lower bound to maximum magnitude is a sufficient cause for action. The fragility of our surroundings to seismic loading from the lower bound earthquake should be studied. Typical buildings, transportation and utility lifelines, and critical life support systems should be examined in light of the ground motions produced by such an event. Both education and legislation are required, but the tools and examples of their application are available.

With the first round over, and before the second round begins, the scientific and engineering communities should take stock of the recent accomplishments, and fulfill the responsibilities that squarely reside with them. Such responsibilities include the promotion of educational programs addressing public awareness of earthquake hazard, and evaluation and tightening of design codes for construction and rehabilitation of buildings and critical facilities. We wish to avoid the situations that occurred during the 1971 San Fernando earthquake: an ambulance rendered useless beneath the ruins of its car-port, collapsed overpass structures. These images should become the focus of our actions.

USES OF EARTHQUAKE INFORMATION IN AN INSURANCE OPERATION

D.G. Friedman
The Travelers Insurance Company
Hartford, Connecticut

Information needs about the natural hazards (earthquakes, storms) vary by type of activity such as emergency preparedness, hazard mitigation, structural engineering and insurance. For an insurance operation there is a need for much information because the natural hazards can greatly affect the activities of a large multiple line company that insures hundreds of thousands of lives and properties that are unevenly spread across hazard prone areas of the United States. A company's aggregate exposure in insurance lines that are vulnerable to effects of the geophysical and atmospheric perils can range from hundreds of millions to billions of dollars.

To provide this coverage and manage the risk, an insurer has information needs pertaining to the casualty and damage producing potential of these perils to its particular books of business. In many cases, the classical actuarial procedure of using loss experience in a few recently past years does not provide an adequate estimate of present risk to the company's current portfolio. This is because of small sample statistical problems inherent in attempting to analyze infrequent or rare events that may or may not have occurred in a short period of years. Even in a high hazard area the frequency of highly damaging geophysical or atmospheric events is small. When a small sampling period is used, the risk estimates can be biased by the chance occurrence (or non-occurrence) of one of the infrequently occurring large damage producing events during the short time interval. A much longer sampling period is needed to obtain a realistic estimate of the frequency and severity of the damage producing earthquakes or storms.

Use of a longer sequence of past years increases the likelihood of obtaining a more representative measure of the expected frequency, severity and location of these geophysical and atmospheric events relative to the spatial array and density of insured lives and property (elements-at-risk) in the exposed portfolio. However advantages of a longer sampling period are negated by the reduced applicability of the loss experience which rapidly decays in usefulness with age. Major reasons for this decay are the significant changes over time in the portfolio: Number of insured elements-at-risk, their geographical distribution and loss vulnerabilities. Consequently, a more useful measure of current risk to the 1987 portfolio of business in the San Francisco area, for example, is not what happened to 1906 population and buildings but what the estimated effects would be if there was a present day recurrence of the 1906 earthquake acting upon the currently insured elements-at-risk.

However, insurance decisions involving the impact potential of earthquakes and storms to an insurance portfolio must be made on a day-to-day basis. It is not practical to wait until some poorly defined time in the future, perhaps years away, when more appropriate natural hazard risk information may become available. Decisions must be made without delay using whatever pertinent background data that may be at hand. Unfortunately, the amount of available useful information is usually small. This is especially true at the present time with respect to the earthquake hazard in the central and eastern United States.

To provide management with the most useful available material for decision-making purposes, it has been useful for some insurance companies to obtain a better understanding of the mechanism that produces natural disasters. This background knowledge assists in identifying major influencing factors and how they interact to occasionally create large

damage producing situations (natural disasters). This information is provided to the insurance decision-maker to supplement risk assessment results obtained using standard actuarial techniques.

Two important measures of risk to an insurance portfolio are expected average annual loss and catastrophe producing potential of the insured "natural hazard" perils. Average annual loss is an indicator of the "pure premium" needed in the rate to cover the perils. Catastrophe potential is a measure of the tendency for casualties or damage caused by these perils to be clustered in both space and time, that is, many losses occurring as a result of a single geophysical or atmospheric event.

Estimation of the average annual loss and catastrophe producing potential of earthquakes and storms depends upon the interactions of a large number of contributing factors. It is not possible to completely define, quantify and model all of them and their complicated interactions that at times lead to the creation of a natural disaster. However, some insurance companies have gained useful insights by working with a mathematical approximation involving some of the more important ones. These are:

1. Physical characteristics of the earthquake or storm that leads to the generation of a geographical pattern of strong ground motion for an earthquake or high winds for a storm such as a hurricane. Physical characteristics of an earthquake include its magnitude, type of faulting, location and length of rupture, direction and speed of rupture, and depth of the energy release. For a hurricane, the shape, size and internal gradient in the high wind pattern is determined by the storm's intensity (central barometric pressure), overall storm size, its rate of movement, and the direction and curvature of its path relative to the coastline.

2. Local influences that affect the severity of the event at a given location. For earthquakes, it is the local ground and water table conditions that can influence the duration and severity of ground motion of various wave lengths. For a hurricane, local influences on the observed maximum wind speed associated with the passage of a hurricane are topography, rural versus urban environments, types and location of windbreaks such as trees and other obstacles to the wind.

3. Vulnerability of elements-at-risk in an exposed insurance portfolio to loss or damage when ground motion of an earthquake at a specific location attains a given level of severity and duration or when wind attains a given speed during the passage of a hurricane. Vulnerability of buildings to damage depends upon such things as their type, age, height, local exposure, type and quality of construction.

4. Number, type, and geographical distribution of the insured elements-at-risk in an insurance portfolio.

Damage production of earthquakes and hurricanes is very sensitive to the relative positioning of the earthquake's geographical pattern of strong ground motion (or the spatial distribution of high wind accompanying the inland passage of a hurricane) upon the haphazard geographical array of the exposed elements-at-risk in the affected area. There are usually a very large number of possible overlappings of these ground motion patterns or high wind patterns upon the spatial array of the elements-at-risk. Each different overlapping can produce a different loss potential. The physical characteristics of the earthquake or hurricane (such as the important combination of the event's intensity and

location) determines the positioning, size, shape and internal gradients of these ground motion and wind speed patterns. The particular positioning of these patterns upon the spatial distribution and density of the insured elements-at-risk determines the earthquake's (or hurricane's) damage producing potential. This potential can vary widely in magnitude depending upon the positioning of the pattern even though the physical characteristics of the event (earthquake or hurricane) are held constant. Probabilities of occurrence of each of the simulated overlappings must be consistent with the known seismological and climatological conditions in the hazard prone area.

Each insurer, either implicitly or explicitly, takes account of the interaction of the four above mentioned factors in estimating the loss producing potential of earthquakes and hurricanes to its books of business that are vulnerable to these particular perils. There is a wide range in the depth of analysis among insurers that is used to estimate earthquake or hurricane damage potential. It ranges from a brief qualitative consideration to the utilization of mathematical modeling and computer simulation techniques to estimate the economic impact of each of the many possible overlappings of earthquake ground motion or hurricane wind patterns on a geographical array of insured properties.

One company which developed its computerized simulation modeling procedures for the earthquake and hurricane hazards in the mid-1960's, has continuously updated the models over the past two decades by incorporating new research findings in the physical sciences (seismology, meteorology, climatology) and engineering that pertain to the damage producing potential of these perils. The models provide an analysis vehicle for translating this new information and knowledge into an insurance context for determining its implications to the insurance operation.

For the California earthquake hazard, the original model in the 1960's of this company generated and superimposed the geographical patterns of Modified Mercalli intensity upon a computerized mapping of the insured elements-at-risk. Vulnerability relationships provided a means of estimating the damage potential of the simulated earthquake. Currently, in addition to using the Modified Mercalli pattern, the model also computes the loss potential based upon the generation and mathematical superposition of the geographic pattern of ground motion represented by spectral acceleration or spectral velocity of given wave length depending upon the building type that is exposed. It incorporates a measure of the estimated effect of strong motion duration as a function of the earthquake's moment magnitude. Consideration also is given to the additional increments of damage potential to the exposed portfolio caused by possible differences in the direction and speed of faulting during an earthquake and the effect of the probable pattern of aftershock earthquakes following a great event.

For the earthquake hazard in the central and eastern United States, much less work has been done to estimate the loss producing potential to exposed books of insured business. There are information needs for an insurance operation in each of the four categories: Earthquake characteristics (and the resultant effects of the spatial pattern of strong ground motion and the duration); local ground condition influences upon ground motion at a given location: vulnerability relationships between typical types of buildings in the central and eastern United States and their susceptibility to damage for a given level of ground motion severity, duration, and wave length; and inventories of all building (insured and uninsured) by location, type and other characteristics. These inventories are needed by an insurer to estimate the possible damaging impact of other earthquake induced perils in addition to the direct earthquake (shake) coverage such as fire-following-earthquake. Other lines of insurance are also directly or indirectly affected by the occurrence of a moderate or great magnitude earthquake. These include worker's compensation, general liability, fire, automobile, life and medical.

APPENDIX D

PARTICIPANTS AND GUESTS
Address List

Adams, John
613-995-5519
Geological Survey of Canada
Observatory Crescent
Ottawa, Ontario K1A 0Y3
Canada

Anderson, John G.
619-534-2424
Inst. of Geophys. & Planet. Physics, A-025
University of California, San Diego
La Jolla, CA 92093

Armbruster, John
914-359-2900
Lamont-Doherty Geological Observatory
Palisades, NY 10964

Atkinson, Gail M.††
519-741-0757
125 Dunbar Road South
Waterloo, Ontario N2L 2E8
Canada

Barker, Jeff
607-777-2512
Department of Geological Sciences
SUNY at Binghamton
Binghamton, NY 13901

Barstow, Noël†
914-687-9150
Rondout Associates
P.O. Box 224
Stone Ridge, NY 12484

Basham, Peter
613-995-0904
Geophysics Division
Geological Survey of Canada
Building #7
Observatory Crescent
Ottawa, Ontario K1A 0Y3
Canada

Bollinger, G.A.
703-961-6729
Seismological Observatory
Virginia Polytechnic Institute
and State University
Blacksburg, VA 24060

Boore, David
415-329-5616
U.S. Geological Survey
345 Middlefield Road, MS977
Menlo Park, CA 94025

Budhu, M.
716-636-2016
Department of Civil Engineering
212 Engineering West R-8
SUNY at Buffalo
Buffalo, NY 14260

Busby, Bob†
914-359-2900
Lamont-Doherty Geological Obsevatory
Palisades, NY 10964

Chu, Jean†
914-359-2900
Lamont-Doherty Geological Observatory
Palisades, NY 10964

Coppersmith, Kevin J.
415-957-9557
Geomatrix Consultants
One Market Plaza
Spear Street Tower #717
San Francisco, CA 94105

Costantino, Carl J.
212-690-8145
Department of Civil Engineering
City College of New York
New York, NY 10031

Dargush, Andrea†
716-636-3391
NCEER
SUNY at Buffalo
Red Jacket Quadrangle
Buffalo, NY 14261

Dobry, Ricardo
518-276-6934
Dept. of Civil Engineering
Rensselaer Polytechnic Institute
Troy, NY 12180

Ebel, John
617-899-095
Weston Observatory/Boston College
381 Concord Road
Weston, MA 02193

Ekström, Göran†
914-359-2900
Lamont-Doherty Geological Observatory
Palisades, NY 10964

Estabrook, Chuck†
914-359-2900
Lamont-Doherty Geological Observatory
Palisades, NY 10964

Evans, Keith
914-359-2900
Lamont-Doherty Geological Observatory
Palisades, NY 10964

Friedman, Don G.
203-277-3488
Director, Natural Hazards Program
The Travelers Insurance Co.
Corporate Strategy and Research, 6 PB
One Tower Square
Hartford, CT 06183

Gergely, Peter
607-255-4217
Department of Civil Engineering
Cornell University
Ithaca, NY 14853

Haid, William
718-330-3986
Division Director
Civil Engineering Design Division
New York Transit Authority
370 Jay Street
Brooklyn, NY 11201

Herrmann, Robert B.
314-658-3120
Dept. of Earth and Atmospheric Sciences
St. Louis University
St. Louis, Missouri 63103

Hinton, John
201-829-3872
Earthquake Damage Restoration
Bell Communications Research
435 South Street
Morristown, NJ 07960

Idriss, I. M.
714-835-6886
Woodward-Clyde Consultants
203 No. Golden Circle Drive
Santa Ana, CA 92705

Jacob, Klaus
914-359-2900
Lamont-Doherty Geological Observatory
Palisades, NY 10964

Johnson, Douglas H.†
914-359-2900
Lamont-Doherty Geological Observatory
Palisades, NY 10964

Johnston, Arch C.
901-454-2007
Center for Earthquake Research
Memphis State University
Memphis, TN 38152

Kelleher, John†
202-357-7356
Program Director
Seismol. & Deep Earth Structure Program
Division of Earth Sciences
National Science Foundation
Washington, DC 20550

Ketter, Robert L.
716-636-3001
Director, NCEER
SUNY-Buffalo
115 Red Jacket Quadrangle
Buffalo, NY 14260

Lerner-Lam, Arthur†
914-359-2900
Lamont-Doherty Geological Observatory
Palisades, NY 10964

McGuire, Robin K.
303-278-9800
President
RISK Engineering Inc.
5255 Pine Ridge Road
Golden, CO 80403

Miller, Charles A.
212-690-6741
Department of Civil Engineering
City College of New York
New York, NY 10031

Mueller, Chuck
415-853-5917
U.S. Geological Survey
345 Middlefield Road
Menlo Park, CA 94025

Nabelek, John
503-754-2757
College of Oceanography
Oregon State University
Corvallis, OR 97331

Nordenson, Guy J. P.
212-481-1119
OVE ARUP
115 East 27th Street
New York, NY 10016

Obermeier, Stephen F.
703-648-6791
U.S. Geological Survey
National Center, MS 926
12201 Sunrise Valley Drive
Reston, VA 22092

O'Rourke, Thomas
607-255-6470
School of Civil & Environmental Engineering
Cornell University
Hollister Hall
Ithaca, NY 14853-3501

Pacheco, Xavier†
914-359-2900
Lamont-Doherty Geological Observatory
Palisades, NY 10964

Papageorgiou, Apostolos
518-266-6331
Department of Civil Engineering
Rensselaer Polytechnic Institute
Troy, NY 12180-3590

Park, Jeffrey†
203-432-3150
Dept. of Geology & Geophysics
Kline Geology Laboratory
P.O. Box 6666
Yale University
New Haven, CT 06511

Perkins, D. M.
303-236-1616
U. S. Geological Survey
Denver Federal Center
Box 25046, Stop 966
Denver, CO 80225

Pomeroy, Paul†
914-687-9150
Rondout Associates
P.O. Box 224
Stone Ridge, NY 12484

Reiter, Leon
303-492-7626
U.S. Nuclear Regulatory Commission
P-1114)
Washington, D.C. 20555

Rogers, Albert M.
303-236-1585
U.S. Geological Survey
Branch of Geologic Risk Assessment
Box 25046, MS 965
Denver Federal Center, MS 966
Denver, CO 80225

Scawthorn, Charles
415-495-5431
Senior Manager of R & D
D & A Division
EQE Incorporated
595 Market Street, 18th Floor
San Francisco, CA 94105

Seeber, Leonardo
914-359-2900
Lamont-Doherty Geological Observatory
Palisades, NY 10964

Shinozuka, Masanobu
212-280-3892)
Dept. of Civil Engineering
632 SW Mudd Building
Columbia University
New York, NY 10027

Simpson, David W.†
914-359-2900
Lamont-Doherty Geological Observatory
Palisades, NY 10964

Singh, J. P.
415-222-5700
President
Geospectra Engineers and Geoscientists
3095 Atlas Road/Ste 213
Richmond, California 94806

Somerville, Paul G.
818-449-7650
Woodward-Clyde Consultants
566 El Dorado Street
Pasadena, CA 91101

Soydemir, Cetin
617-492-6460
Haley and Aldrich, Inc.
238 Main Street
P.O. Box 60
Cambridge, MA 02142

Statton, C. Thomas
201-785-0700
Woodward-Clyde Consultants
c/o 201 Willowbrook Boulevard
Wayne, NJ 07470

Stepp, J. Carl
415-855-2103
Director, Seismology Program Office
EPRI
3412 Hillview Avenue
P.O. Box 11412
Palo Alto, CA 94303

Thurber, Cliff†
914-359-2900
Lamont-Doherty Geological Observatory
Palisades, NY 10964

Turkstra, Carl J.†
718-643-8958
Dept. of Civil Engineering
Polytechnic Institute
333 Jay Street
Brooklyn, NY 11201

Tuttle, Martitia
914-359-2900
Lamont-Doherty Geological Observatory
Palisades, NY 10964

Um, Junho†
914-359-2900
Lamont-Doherty Geological Observatory
Palisades, NY 10964

Vanmarcke, Erik H.†
609-452-5896
School of Engineering& Appl. Sci., Room E311
Princeton University
Princeton, NJ 08544

Veneziano, Daniele
617-253-7199
Dept. of Civil Engineering, Room 1-382
Massachusetts Inst. of Technology
Cambridge, MA 02139

Weichert, Dieter
604-356-6433/6500
Geological Survey of Canada
Pacific Geoscience Center
P. O. Box 6000
Sidney, British Columbia V8L 4B2
Canada

Wesnousky, Steven
901-454-2007
Center for Earthquake Research
Memphis State University
Memphis, TN 38152

Whitman, Robert V.
617-253-7127
Dept. of Civil Engineering, Room I-342
Massachusetts Institute of Technology
77 Massachusetts Ave.
Cambridge, MA 02139

Wu, Francis T.
607-777-2512
Department of Geological Sciences
SUNY, Binghamton
Binghamton, NY 13901

Zerva, Aspasia†
212-690-6741
Department of Civil Engineering
City College of New York
New York, NY 10031

Zoback, Mark
415-723-9438
Stanford University
Geophysics Dept.
Mitchell Building, Room 366
Stanford, CA 94305

† Guest only
†† Was unable to attend

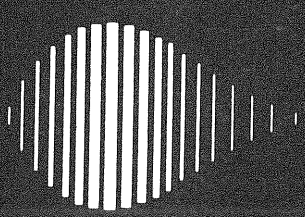

National Center for Earthquake Engineering Research
State University of New York at Buffalo